

General Disclaimer

One or more of the Following Statements may affect this Document

- This document has been reproduced from the best copy furnished by the organizational source. It is being released in the interest of making available as much information as possible.
- This document may contain data, which exceeds the sheet parameters. It was furnished in this condition by the organizational source and is the best copy available.
- This document may contain tone-on-tone or color graphs, charts and/or pictures, which have been reproduced in black and white.
- This document is paginated as submitted by the original source.
- Portions of this document are not fully legible due to the historical nature of some of the material. However, it is the best reproduction available from the original submission.

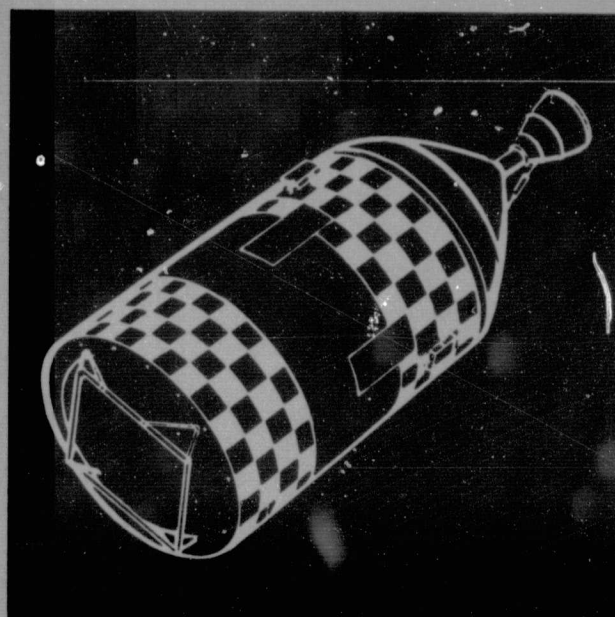
MCR-75-270
NAS8-30746

NASA CR-144029
Not on Record
12-31-75

Final
Report

October 1975

Space Tug Thermal Control Follow-On



(NASA-CR-144029) SPACE TUG THERMAL CONTROL
FOLLOW-ON Final Report (Martin Marietta
Corp.) 312 p HC \$9.75 CSCL 22B

N76-23346

Unclass

G3/18 41190



MARTIN MARIETTA

MCR-75-270
Contract NAS8-30746

Final
Report

October 1975

**SPACE TUG THERMAL
CONTROL FOLLOW-ON**

Prepared for:
George C. Marshall Space Flight Center
Marshall Space Flight Center, Alabama 35812

Prepared by:
Terry L. Ward
Program Manager

MARTIN MARIETTA CORPORATION
Box 179
Denver, Colorado 80201

FOREWORD

This document was prepared by the Martin Marietta Corporation under Contract NAS8-30746, "Space Tug Thermal Control Follow-On". This effort was accomplished for the National Aeronautics and Space Administration, George C. Marshall Space Flight Center under the technical direction of the Structures and Propulsion Laboratory, Thermal Engineering Branch with Mr. James H. Wise serving as Technical Monitor.

The work described herein was performed over the period of 6 May 1974 to 22 October 1975.

The work of the following major contributors is acknowledged:

J. Michael Connolly
Jim C. Neuman

CONTENTS

	<u>Page</u>
I. INTRODUCTION	1
II. SUMMARY	2
APPENDIX A	A-1 thru A-55
APPENDIX B	B-1 thru B-116
APPENDIX C	C-1 thru C-123

I. INTRODUCTION

The Space Tug Thermal Control Follow-On program was conducted to further explore some of the thermal control concepts proposed for use in Space Tug in a breadboard test program. The objectives of the test program were to demonstrate the thermal control capabilities of a louver/battery configuration and a thermal conditioning panel/heat pipe radiator configuration. An additional objective was added to model the header pipe and radiator of the second test and correlate the analysis with the test results.

These three objectives were achieved and are reported separately within the three appendices of this report.

II. SUMMARY

The louver/battery test was conducted to demonstrate the louver's ability to control the Tug battery temperature and also compare actuator mechanisms. Two flight type louver assemblies were procured and tested. Each of these assemblies were actuated by bimetallic springs. Results of this test were compared with a Martin Marietta built louver assembly which was actuated by a fluidic actuator. Each unit exhibited similiar effective emittances and performance when full open and closed. The bimetallic units function well throughout the testing while fluidic actuator exhibited a sluggish response.

The heat pipe radiator/thermal conditioning panel test was conducted to demonstrate the performance of an all heat pipe thermal control system. The radiator and thermal conditioning panel were provided GFP for this test. The two units were connected together thermally via a procured fixed conductance heat pipe. Steady-state and transient tests were performed with all test articles performing flawlessly. The major conclusion drawn from this test was that physical interfaces between the test articles should be minimized. Bolted and clamped joints for such a design result in Δt s that reduce the system capability to reject heat. The test demonstrated the radiators capability to reject the design heat loads at design environments and also demonstrated the capability to reject heat loads at lower than the design cold case environment. Appendix B discusses the test program and results.

The development of an integrated thermal model of the radiator, header pipe, and thermal conditioning panel provided the means to evaluate the above test results. The analysis of heat pipe systems in steady-state and transient conditions has recently been a state-of-the-art problem. While the results of the analysis indicate that system performance can be obtained with confidence, the analysis is sensitive individual pipe performance and interface conductances. Appendix C presents the analysis results and overall conclusions.

REPRODUCIBILITY OF THE
ORIGINAL PAGE IS POOR

Test
Report

October 1975

**BATTERY/LOUVER
SYSTEM**

MARTIN MARIETTA CORPORATION
Box 179
Denver, Colorado 80201

CONTENTS

	<u>Page</u>
I. INTRODUCTION	A-1
II. SUMMARY	A-2
III. TEST DESCRIPTION AND OBJECTIVES	A-3
IV. BIMETALLIC ACTUATED LOUVER SYSTEM TEST ARTICLE	A-4
V. FLUID ACTUATED LOUVER SYSTEM TEST ARTICLE	A-13
VI. TEST FACILITIES AND DATA RECORDERS	A-23
VII. THERMAL MODEL DESCRIPTION	A-26
VIII. TEST RESULTS AND MODEL CORRELATION	A-27
IX. CONCLUSION	A-54
X. REFERENCES	A-55

Figure

A-1	Bimetallic Actuated Louver System Module	A-5
A-2	Louver System Attached to Baseplate	A-6
A-3	Component Simulator Blocks and Fluid Loop	A-7
A-4	Completed Bimetallic Actuated Test Article with Cover-On	A-8
A-5	Bimetallic Actuated Test Article Thermocouple Location	A-10
A-6	Bimetallic Actuated Test Article Mounted in Chamber	A-12
A-7	Fluid Actuated Louver System Test Article	A-14
A-8	Viking Fluid Actuator	A-16
A-9	Viking Fluid Actuator Schematic	A-17
A-10	Actuator Stroke Versus Steady State Actuator Temperature	A-18
A-11	Fluid Actuated Test Article Thermocouple Location	A-20
A-12	Fluid Actuated Test Article Mounted in Chamber	A-22
A-13	Data Acquisition System	A-25
A-14	Bimetallic Actuated Test Articles Baseplate Temperature for 15 W Power, 273.3°K Cover	A-29
A-15	Bimetallic Actuated Test Article Baseplate Temperature for 15 W Power, 287.6°K Cover	A-30

A-16	Bimetallic Actuated Test Article Baseplate Temperature for 30 W Power, 354.4°K Cover	A-31
A-17	Bimetallic Actuated Test Article Baseplate Temperature for 30 W Power, 272.2°K Cover	A-32
A-18	Bimetallic Actuated Test Article Baseplate Temperature for 30 W Power, 288.6°K Cover	A-33
A-19	Bimetallic Actuated Test Article Baseplate Temperature for 45 W Power, 254.4°K Cover	A-34
A-20	Bimetallic Actuated Test Article Baseplate Temperature for 45 W Power, 272.1°K Cover	A-35
A-21	Bimetallic Actuated Test Article Transient Baseplate Temperature for 0 W Power	A-36
A-22	Bimetallic Actuated Test Article Transient Baseplate Temperature for 20 W Power	A-37
A-23	Bimetallic Actuated Test Article Transient Baseplate Temperature for 45 W Power	A-38
A-24	Fluid Actuated Test Article Baseplate Temperature for 0 W Power, 261.8°K Cover	A-40
A-25	Fluid Actuated Test Article Baseplate Temperature for 5 W Power 170.1°K Cover	A-41
A-26	Fluid Actuated Test Article Baseplate Temperature for 7.5 W Power, 172.1°K Cover	A-42
A-27	Fluid Actuated Test Article Baseplate Temperature for 10 W Power, 190.6°K Cover	A-43
A-28	Fluid Actuated Test Article Baseplate Temperature for 15 W Power, 199.6°K Cover	A-44
A-29	Fluid Actuated Test Article Baseplate Temperature for 20 W Power, 210.3°K Cover	A-45
A-30	Fluid Actuated Test Article Baseplate Temperature for 30 W Power, 228.9°K Cover	A-46
A-31	Fluid Actuated Test Article Baseplate Temperature for 35 W Power, 238.9°K Cover	A-47
A-32	Fluid Actuated Test Article Transient Baseplate Temperature for Case 1	A-49
A-33	Fluid Actuated Test Article Transient Component Power for Case 1	A-50
A-34	Fluid Actuated Test Article Transient Blade Angle for Case 1	A-50
A-35	Fluid Actuated Test Article Transient Cover Temperature for Case 2	A-51
A-36	Fluid Actuated Test Article Transient Baseplate Temperature for Case 2	A-52
A-37	Fluid Actuated Test Article Transient Blade Angle for Case 2	A-53
A-38	Fluid Actuated Test Article Transient Cover Temperature for Case 2	A-53

Table

A-1	Summary of Bimetallic Actuated Louver System Test	
	Article Characteristics	A-9
A-2	Bimetallic Actuated Test Article Thermocouple	
	Locations	A-11
A-3	Summary of Fluid Actuated Louver System Test	
	Article Characteristics	A-15
A-4	Fluid Actuated Test Article Thermocouple Locations . . .	A-21
A-5	6x15 ft Vacuum Chamber Facility	A-24
A-6	Summary of Steady State Tests Using the	
	Bimetallic Actuated Test Article	A-28
A-7	Cover Heating Environment Used for Transient Cases . .	A-28
A-8	Summary of Steady State Tests Using the Fluid	
	Actuated Test Article	A-39

I. INTRODUCTION

Application of a louver system to thermal control of typical space tug components is desirable for many reasons. They are particularly useful because of high reliability, a semi-passive nature requiring no electrical power, and their ability to readily compensate for a change in the component power dissipation on the spacecraft environment.

Interior louvers are even more reliable and predictable than exposed louvers because they are unhampered by the complex effects of solar impingement and direct exposure to the space environment. However, the heat rejection is reduced by the addition of the cover which acts as a radiation shield to the environment. The choice to use covered louvers on the tug was based on the thermal and mission requirements. The heat dissipation of typical tug components, with the exception of the fuel cell, are within the control range of covered louvers with moderate surface areas.

II. SUMMARY

Two louver systems were tested to demonstrate their thermal control capabilities as applied to spacecraft components. Both louver systems are of the interior type and differ primarily in the way the blades are actuated. System 1 uses bimetallic spiral wound springs while System 2 uses a fluidic actuator developed for the Viking thermal switch.

The primary objective of both series of tests was to demonstrate the louver systems capability of maintaining thermal control of typical spacecraft components. Both steady-state and transient environmental conditions were simulated along with various component power dissipations. A post test model correlation was then carried out to verify the analytical techniques and to establish interior louver system operational characteristics.

III. TEST DESCRIPTION AND OBJECTIVES

Two covered louver systems were tested in a thermal vacuum environment in order to establish the operational characteristics of covered louver systems and to verify the analytical modeling techniques. The primary difference between the two louver systems tested was the way in which the blades were actuated. Louver System 1 used the more conventional bimetallic spiral wound actuators while Louver System 2 used a fluidic actuator built by Martin Marietta for use on the Viking thermal switch.

Each louver system was subjected to a series of tests designed to demonstrate the capability of the louver system to maintain the thermal control of a simulated tug component. Both steady-state and transient conditions were simulated. Steady-state tests were performed by supplying a constant power input to the component simulator while maintaining the louver cover at a fixed temperature. Transient simulation consisted of varying the power supplied to the lower cover consistent with an absorbed environmental flux typical of a tug earth orbital mission.

IV.

BIMETALLIC ACTUATED LOUVER SYSTEM TEST ARTICLE

Photographs of the bimetallic louver system taken during the test article fabrication are shown in Figures A-1 through A-4. Table A-1 gives physical characteristics of the test article. The louver system is composed of two 20.32x40.64 cm (8x16 in.) flight-type thermal controller modules designed and built by Northrop Electronics Division, Palos Verdes Peninsula, California.

Each module consists of 16 highly polished aluminum blade halves bonded together to form eight louver blades. The eight louver blades are controlled in place by four bimetallic actuator elements housed in the center channel of the lower system. The shaft end of each louver blade fits into a nylon spool in the center of each bimetallic element. The elements respond to a temperature change of the baseplate via a radiation coupling through slots in the bottom of the housing. The actuator is designed to produce 90° of blade rotation over the temperature range of 288.9°K to 302.8°K (60°F to 85°F).

The modules were fastened to a 45.72x45.72 cm (18x18 in.) baseplate using low conductance nylon screws. The baseplate was 0.32 cm (1/8 in.) aluminum. Two aluminum blocks weighing a total of 6.41 kg (14.14 lb) provided the thermal mass for the component simulator. The blocks were bolted directly to the baseplate using a thermal heatsink compound to ensure a good contact. Heater tape was attached to the blocks to simulate an evenly distributed component power input. A fluid loop utilizing GH_2 was also attached to the blocks to provide for cooling the test article. This was necessary to establish initial temperatures at the start of each test. Guard heaters were put on the copper tubes to control the heat flow from the test article during testing.

The cover also measured 45.72x45.72 cm (18x18 in.) and was made from 0.16 cm (1/16 in.) thick aluminum. It was stood off from the baseplate using six teflon blocks measuring 1.27 cm ($\frac{1}{2}$ in.) square by 6.35 cm ($2\frac{1}{2}$ in.) long. Heater tape was used to provide up to 100 W of power to control the cover temperature.

The baseplate and both sides of the cover were painted with 3 M Black Velvet paint ($\epsilon \approx 0.90$). The entire assembly, with the exception of the cover, was wrapped with 20 layers of aluminized Mylar, each being separated by a layer of netting.

Instrumentation used on the assembly consisted of 24 Type E chromel/constantan thermocouples located as shown in Figure A-5. These thermocouples are tabulated in Table A-2. In addition to temperature measurement, voltage and current measurements were made for each of the heaters. These included the simulated component heater, the cover heater, and the fluid loop guard heaters. A photograph of the louver assembly mounted in the chamber is shown in Figure A-6.

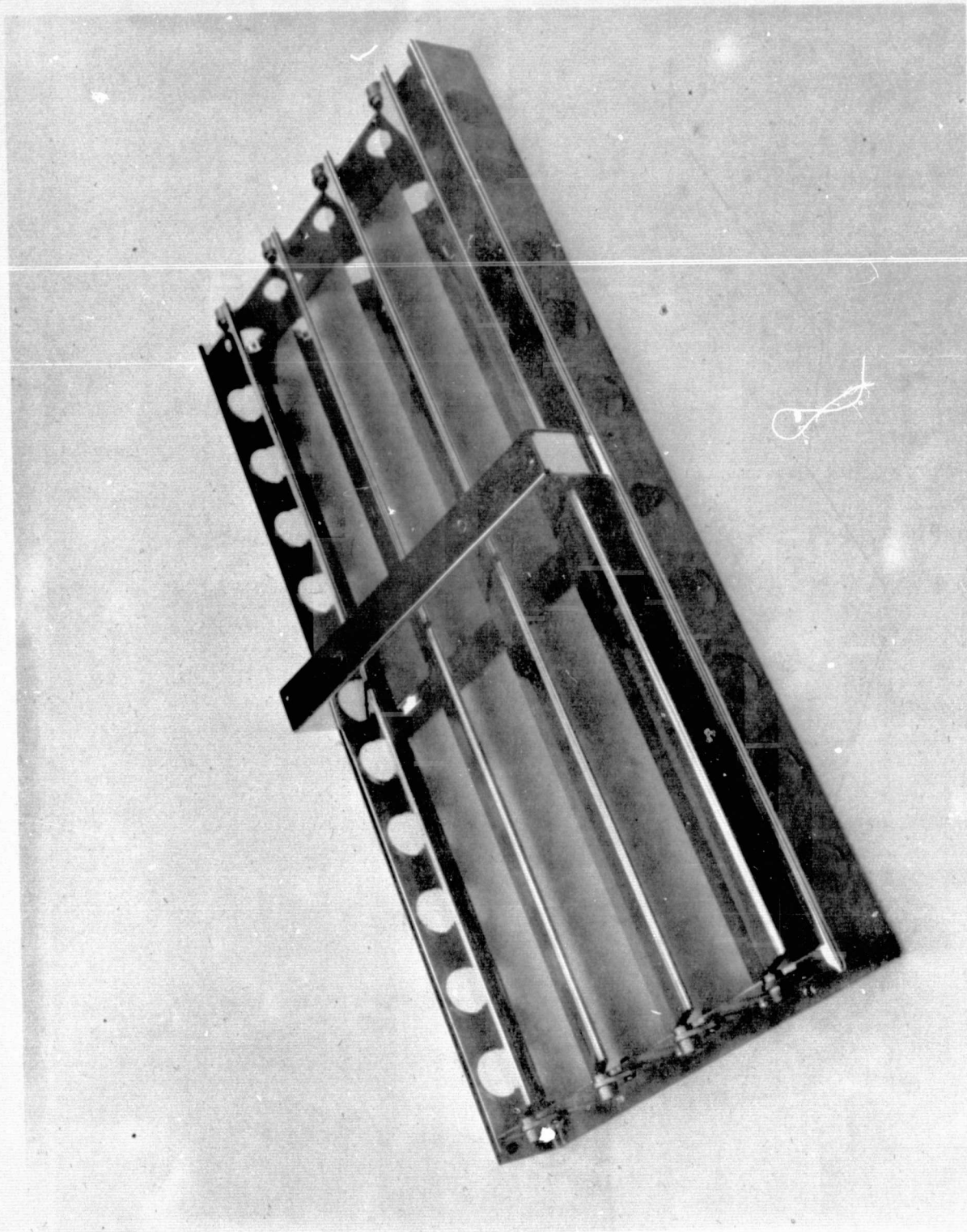


Figure A-1

Figure A-1 Bimetallic Actuated Lower System Module

REPRODUCIBILITY OF THE
ORIGINAL PAGE IS POOR

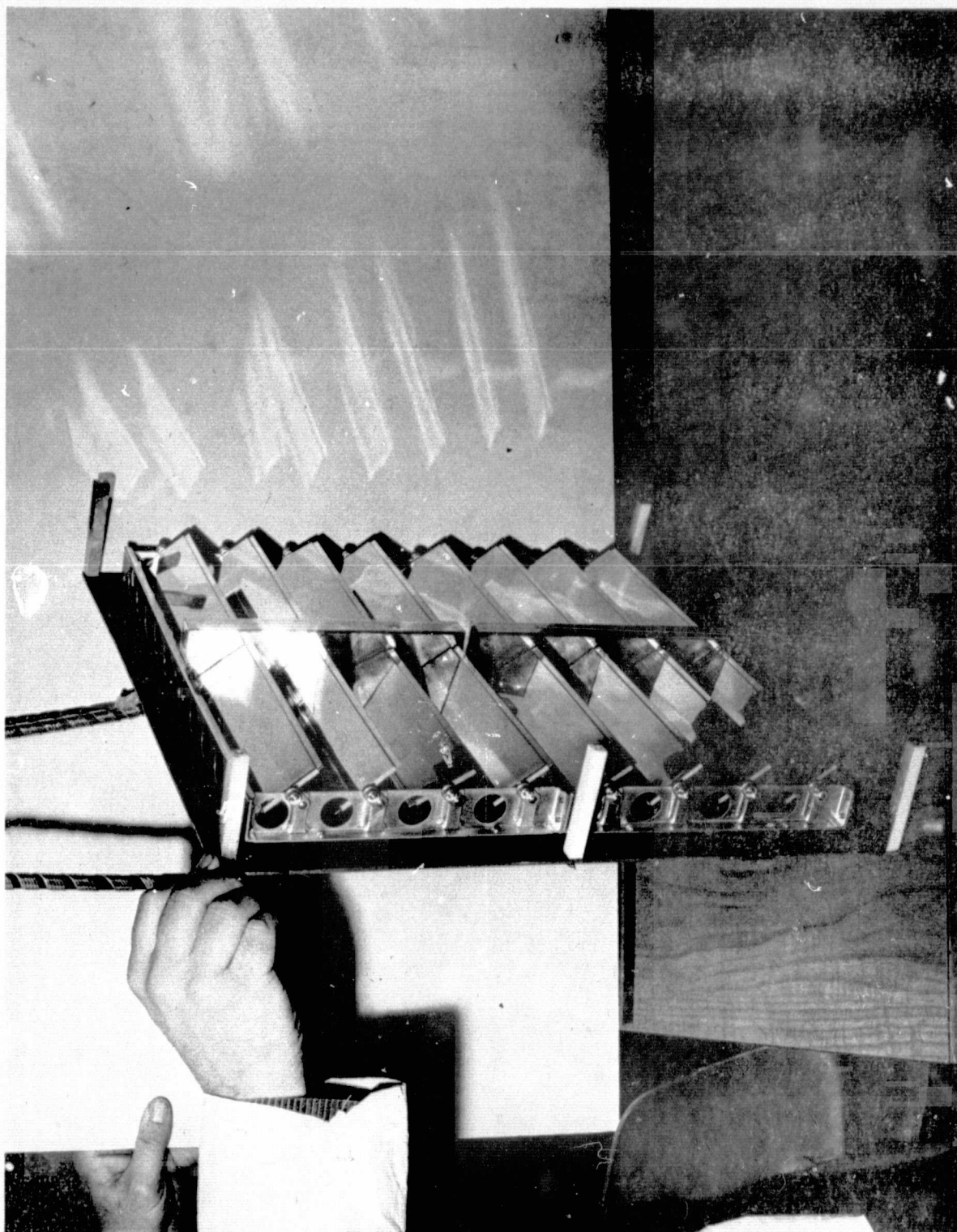


Figure A-2 Lower System Attached to Baseplate

Figure A-2

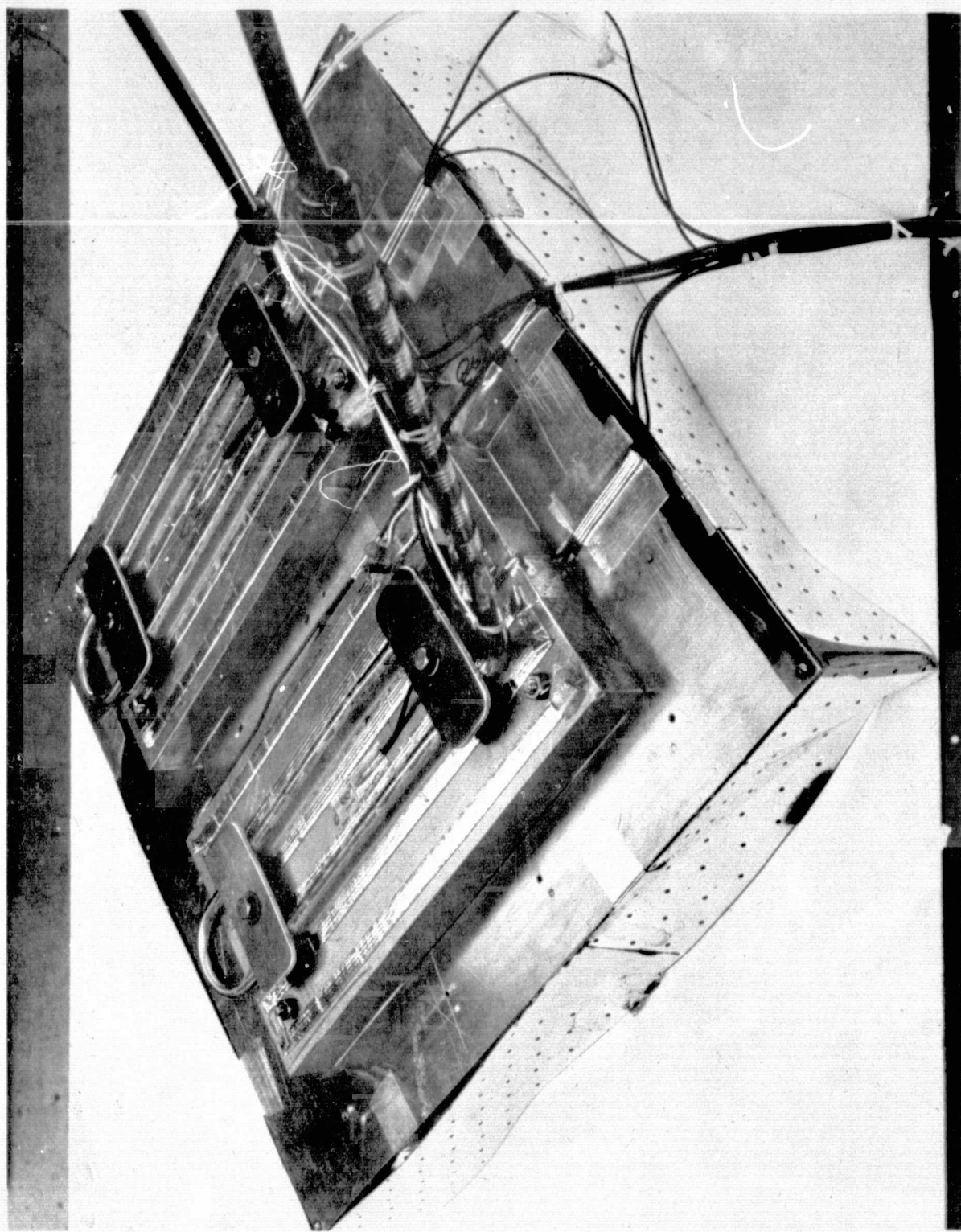


Figure A-3

Figure A-3 Component Simulator Blocks and Fluid Loop

REPRODUCIBILITY OF THE
ORIGINAL PAGE IS POOR



Figure A-4 Completed Bimetallic Actuated Test Article with Cover Installed

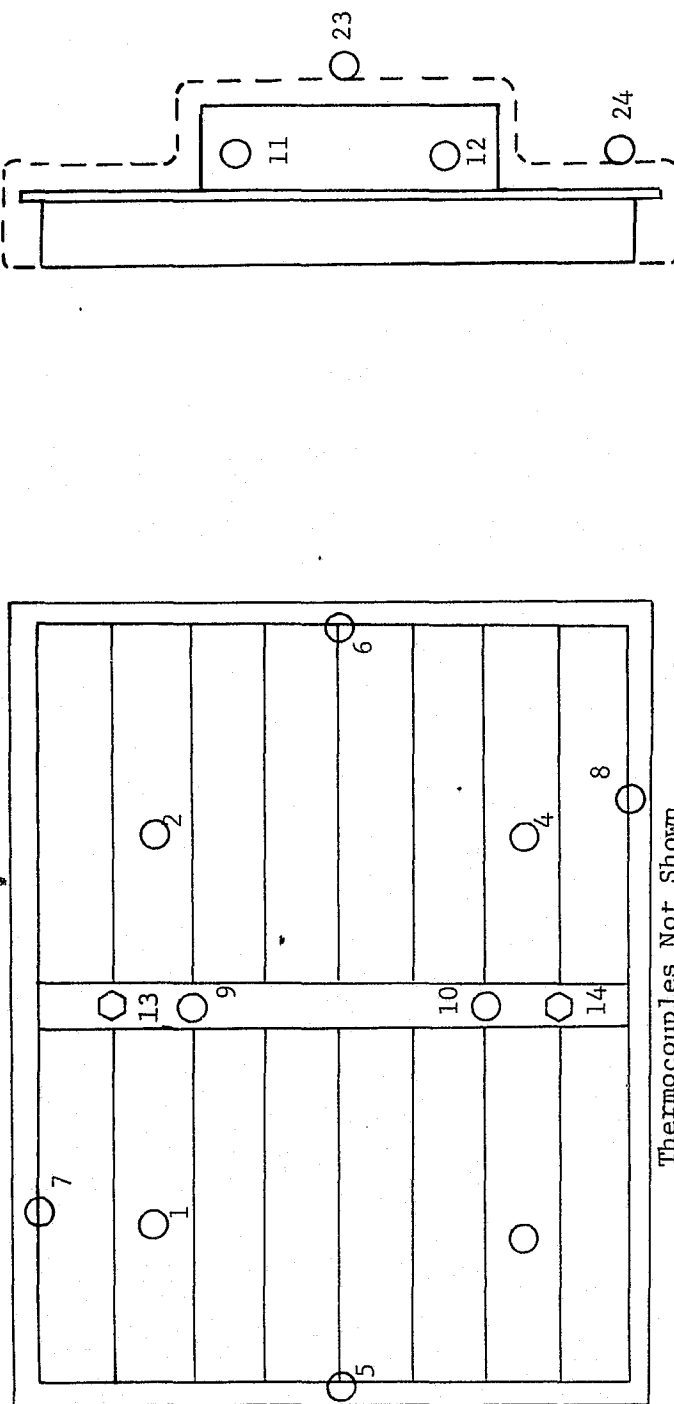
Figure A-4

A-8

REPRODUCIBILITY OF THE
ORIGINAL PAGE IS POOR

Table A-1
*Summary of Bimetallic Actuated Louver Test
Article Characteristics*

Item	Characteristics
Louver System	Two Northrop flight-type thermal controller modules
Dimensions	20.3x40.6x4.9 cm (8.00x16.00x1.93 in.) per module
Blades	Polished aluminum, $\epsilon \approx 0.06$, 8 per module 18.3x4.9 cm (7.20x1.93 in.)
Actuators	Spirally wound bimetallic element; four per module
Weight	0.27 kg (0.6 lb) per module
Baseplate	Aluminum
Dimensions	45.7x45.7x0.32 cm (18.0x18.0x0.125 in.)
Coating	3M Black Velvet paint, $\epsilon \approx 0.90$
Area	Total 0.209 m ² (2.250 ft ²) eff. Radiating 0.149 m ² (1.602 ft ²)
Weight	1.84 kg (4.05 lb)
Component Simulator	Two aluminum blocks 15.2x30.5x2.5 cm (6.0x12.0x1.0 in.) each
Weight	3.495 kg (7.705 lb) each
Cover	Aluminum
Dimension	45.7x45.7x0.16 cm (18x18x0.063 in.)
Coating	3M Black Velvet paint, $\epsilon \approx 0.90$ (both sides)
Insulation	20 Alternate layers of perforated aluminumized Mylar and tissue glass



Legend:

- T/Cs 15 through 18 located on External Cover
- T/Cs 19 through 22 located on Guard Heaters
- T/Cs Located underneath Bimetallic Elements

Figure A-5 Bimetallic Actuated Test Article Thermocouple Locations

Figure A-5

Table A-2
Bimetallic Actuated Test Article Thermocouple Locations

T/C Number	Location
1	Baseplate
2	Baseplate
3	Baseplate
4	Baseplate
5	Frame Side (Inside)
6	Frame Side (Inside)
7	Frame End (Inside)
8	Frame End (Inside)
9	Actuator Center Channel
10	Actuator Center Channel
11	Component Simulator
12	Component Simulator
13	Baseplate underneath Actuator Element
14	Baseplate underneath Actuator Element
15	Cover
16	Cover
17	Cover
18	Cover
19	Guard Heater
20	Guard Heater
21	Guard Heater
22	Guard Heater
23	Outside Insulation
24	Outside Insulation

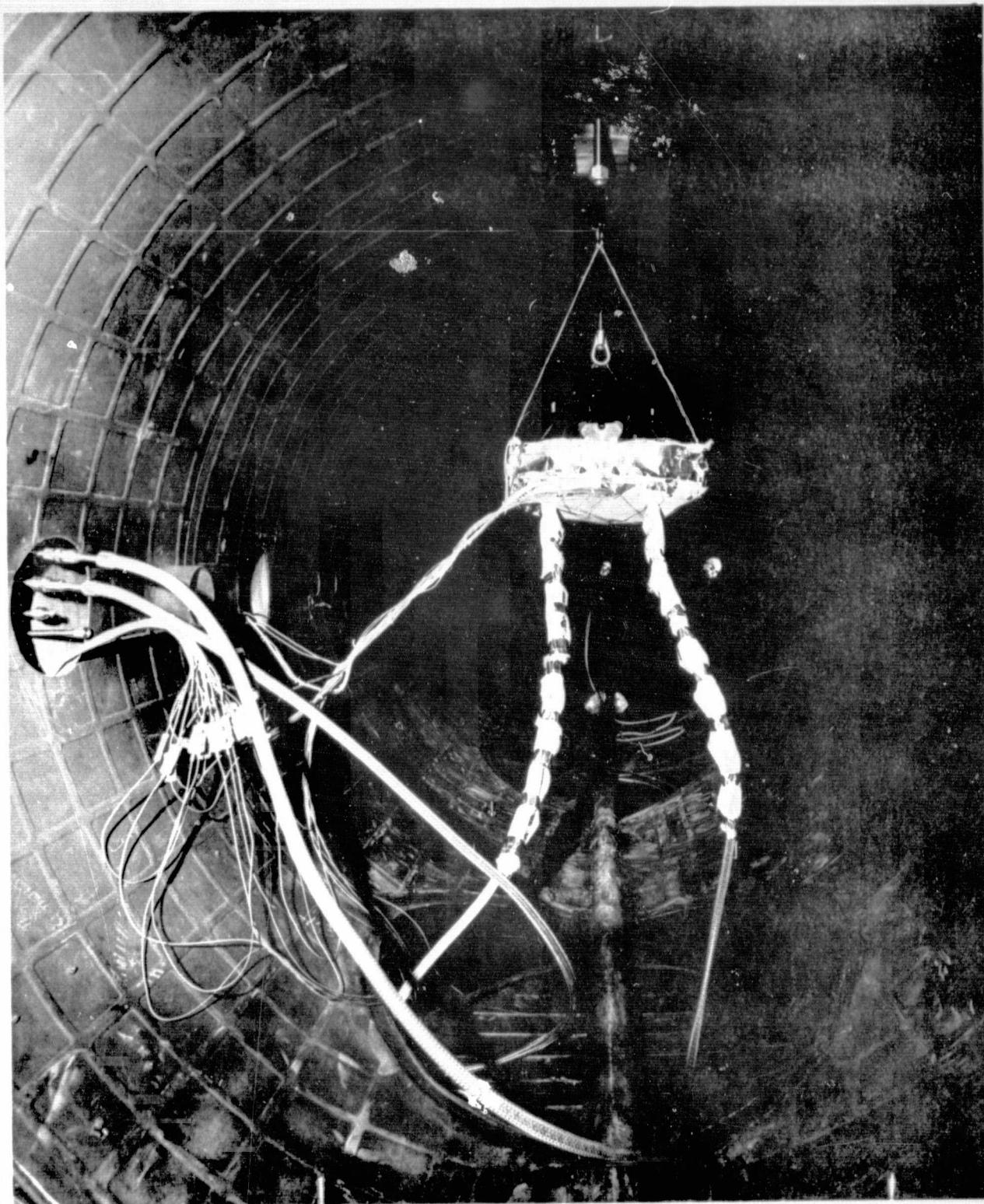


Figure A-6 Bimetallic Actuated Test Article Mounted in Chamber

V. FLUID ACTUATED LOUVER SYSTEM TEST ARTICLE

The fluid actuated louver system test article is shown in Figure A-7 which was a photograph taken during disassembly of the test article after completion of the test. The radiation characteristics of both louver systems are quite similar. That is, they have the same number of blades, approximately the same radiating area, and the same optical properties. The major distinction between the two systems is the blade actuation mechanism. Table A-3 gives the physical characteristics of the test article. The actual louver system was built by Martin Marietta in 1970 and was based on a louver design used on the Mariner spacecraft.

A photograph of the fluid actuator used for the test is shown in Figure A-8. The actuator was developed by Martin Marietta for the Viking program to actuate the Viking lander thermal switch. A schematic of the actuator is shown in Figure A-9. The rack and pinion gear mechanism which controls the louver blade rotation is powered by the actuator. The actuator utilizes the vapor pressure of Freon-12 as the pressure agent. For a given temperature, the vapor pressure of Freon is constant and thus permits the actuator bellows to stroke without pressure loss due to volume increase. A single rod transmits the actuator motion to the rack and pinion mechanism. The actuator is bolted through footpads that are integral to the actuator body to the component side of the louver baseplate. In addition, thermal grease was applied to the bolted joints to provide good heat transfer from the baseplate. The actuator body is a stainless steel pressure chamber which is divided into two sections by metallic bellows. The bellows serve as flexible barriers to retain the Freon and were sized to provide the spring force to close the thermal contacts on the Viking thermal switch.

The actuator was designed to transmit motion to the output shaft over a temperature range of 275°K (34°F) to 286.1°K (55°F). The desirable operating range for the louver system was 288.7°K (60°F) to 302.5°K (85°F) which would require that the activation temperature range of the actuator be modified. However, after evaluating the modification alternatives available, which included introducing a noncondensable pressurized gas into the bellows or adding an external pressurization mechanism to the housing, the decision was made to test the assembly at the design temperature range of the Viking actuator. Bench tests of the actuator by itself and attached to the louver system were performed to establish the relationship between actuator temperature and output shaft stroke. The results of this test, shown in Figure A-10, indicate a very linear relationship between the actuator temperature and output shaft movement.

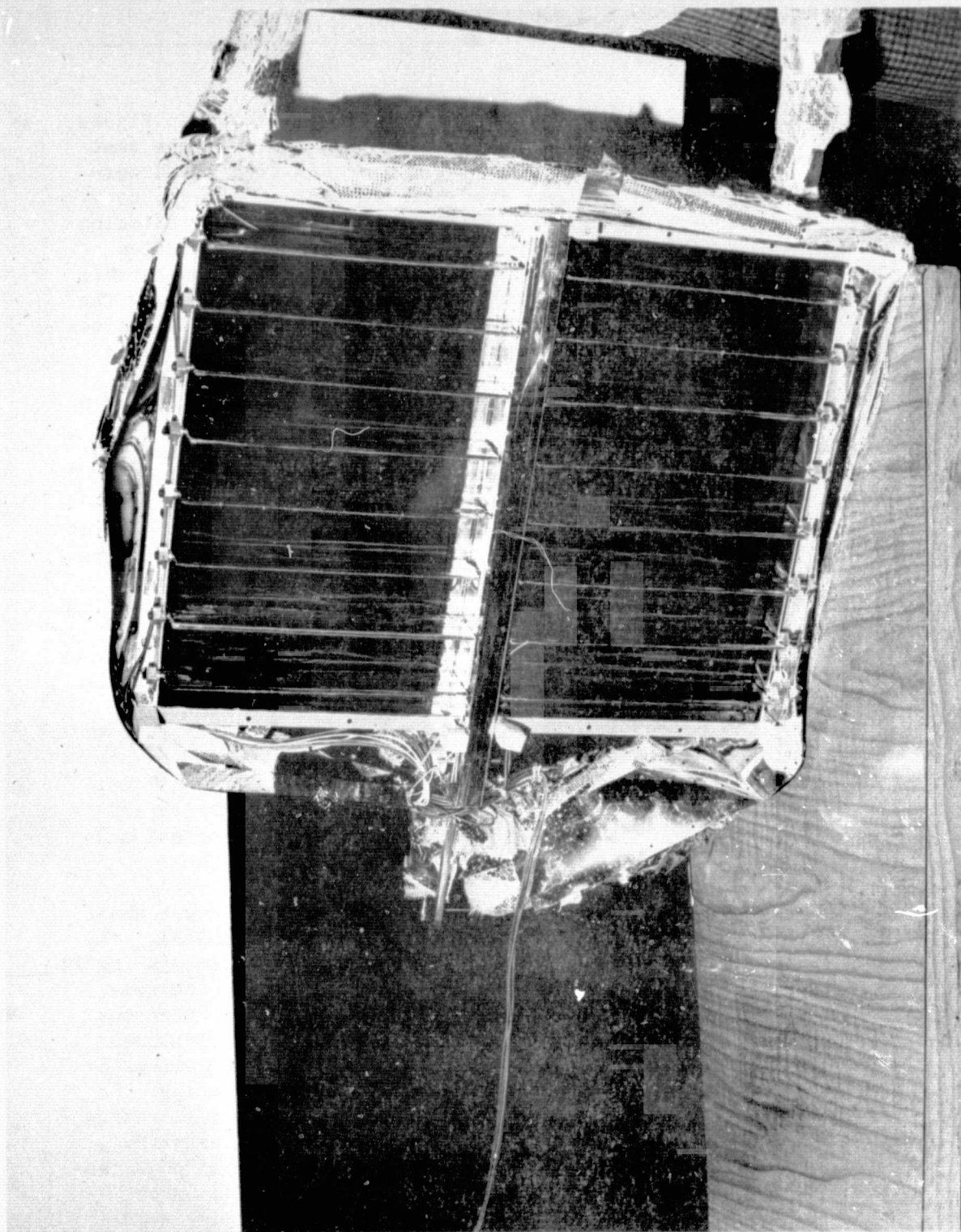


Figure A-7

Figure A-7 Fluid Actuated Lower System Test Article

Table A-3

Summary of Fluid Actuated Louver System Test Article Characteristics

Item	Characteristics
Louver System	Basic Mariner louver system design built by Martin Marietta and modified to allow blade positioning by a rack and pinion gear mechanism.
Dimensions	36.0x48.6x4.8 cm (14.7x19.125x1.90 in.)
Blades	16 Aluminum-type H 45-1119 20.96x4.67 cm (8.25x1.84 in.)
Blade Coating	Aluminized polyester tape, 3M Company designation Y8437, $\epsilon \approx 0.06$
Actuator	Viking thermal switch actuator built by Martin Marietta. Weight 0.91 kg (2.0 lb), dimensions 38 cm long, 3.81 cm dia (15x1.5 in.).
Weight	1.23 kg (2.71 lb)
Baseplate	Aluminum
Area	Total 0.195 m ² (2.01 ft ²) Eff. Radiating 0.165 m ² (1.78 ft ²)
Weight	1.64 kg (3.62 lb)
Coating	3M Black Velvet paint, $\epsilon \approx 0.09$
Component Simulator	Aluminum block with integral fluid loop
Dimensions	48.5x36.8x1.3 cm (19.1x14.5x0.5 in.)
Weight	4.88 kg (10.75 lb)
Cover	
Dimensions	46.8x36.8x0.16 cm (19.125x14.5x0.063 in.)
Coatings	3M Black Velvet paint, $\epsilon \approx 0.90$ both sides
Insulation	20 alternate layers of perforated aluminized Mylar and tissue glass

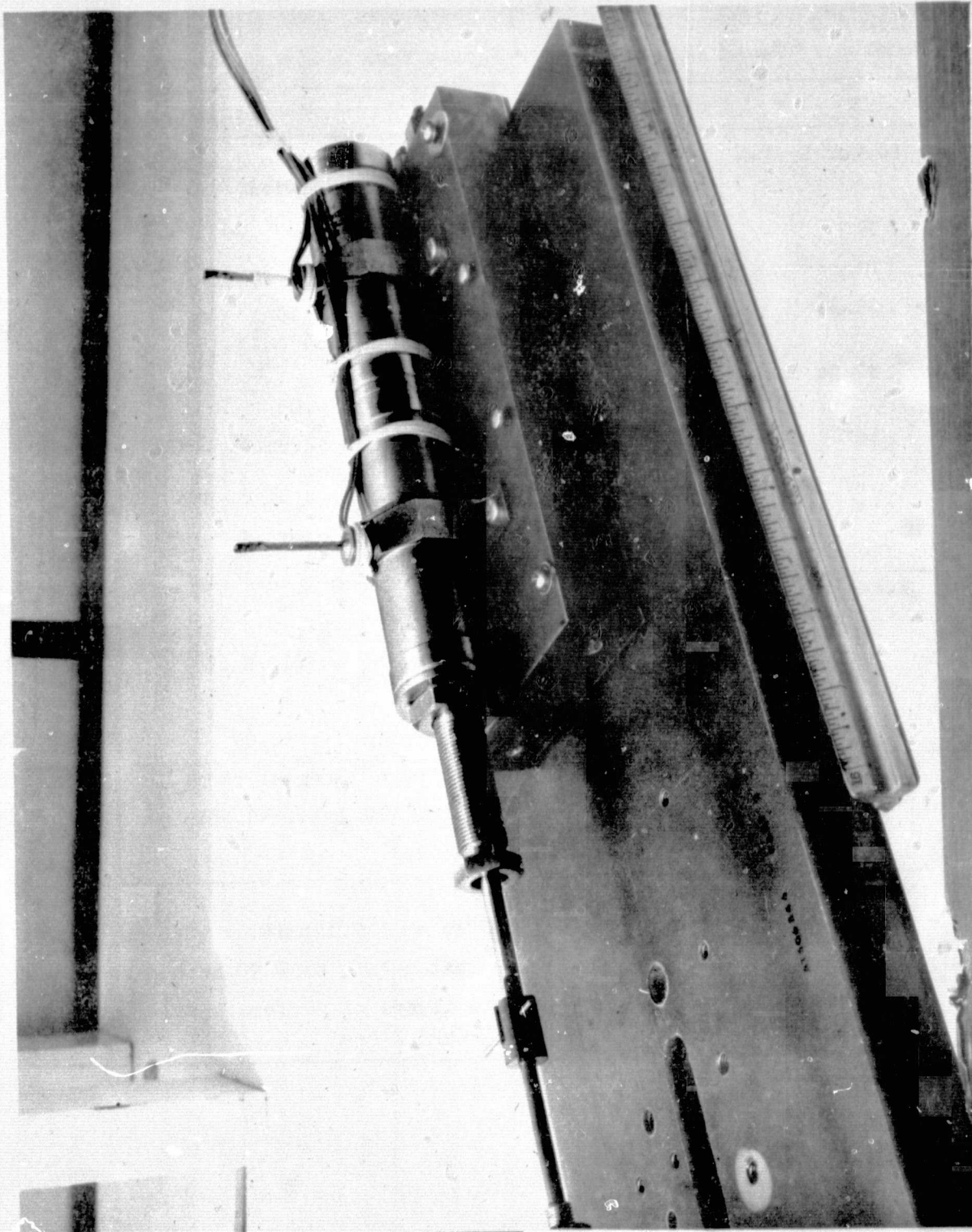


Figure A-8 Viking Fluid Actuator

Figure A-8

Figure A-9

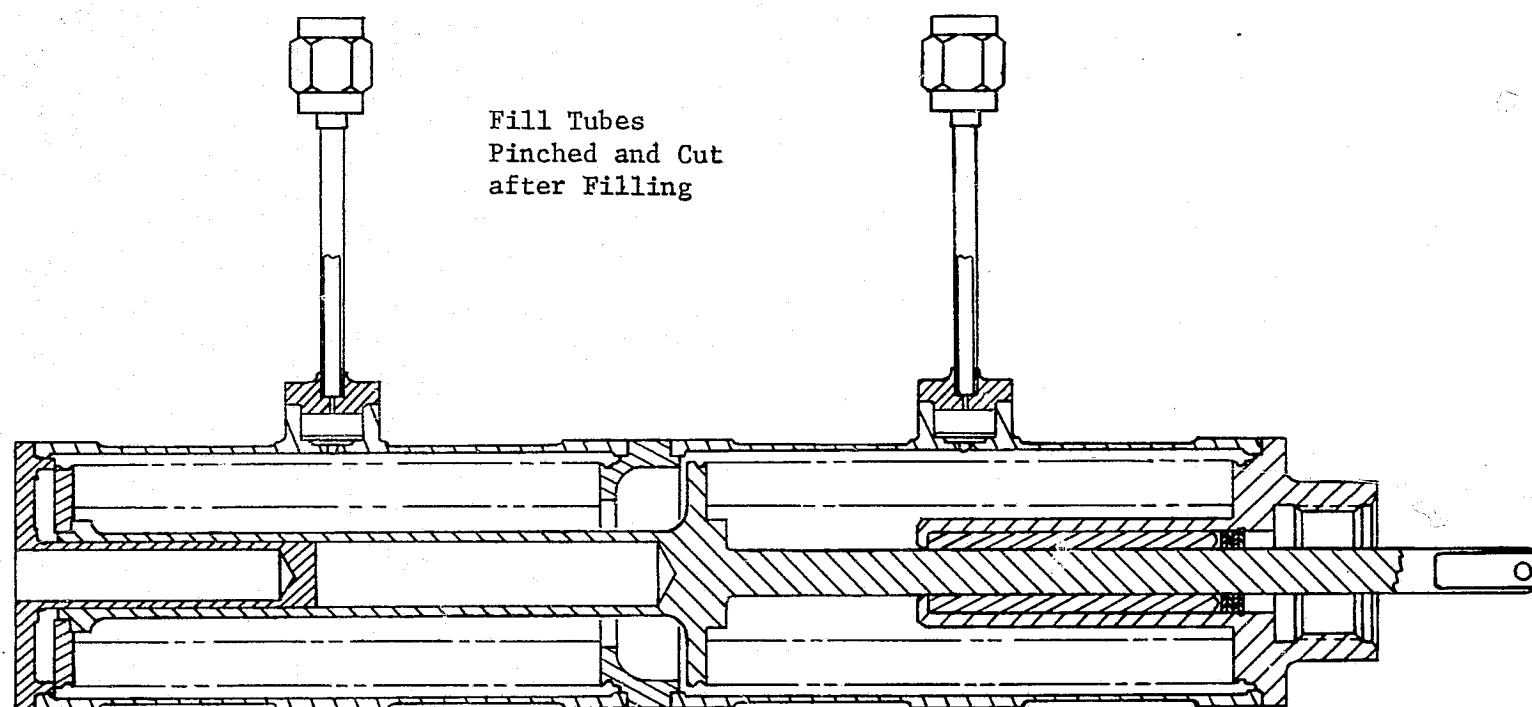
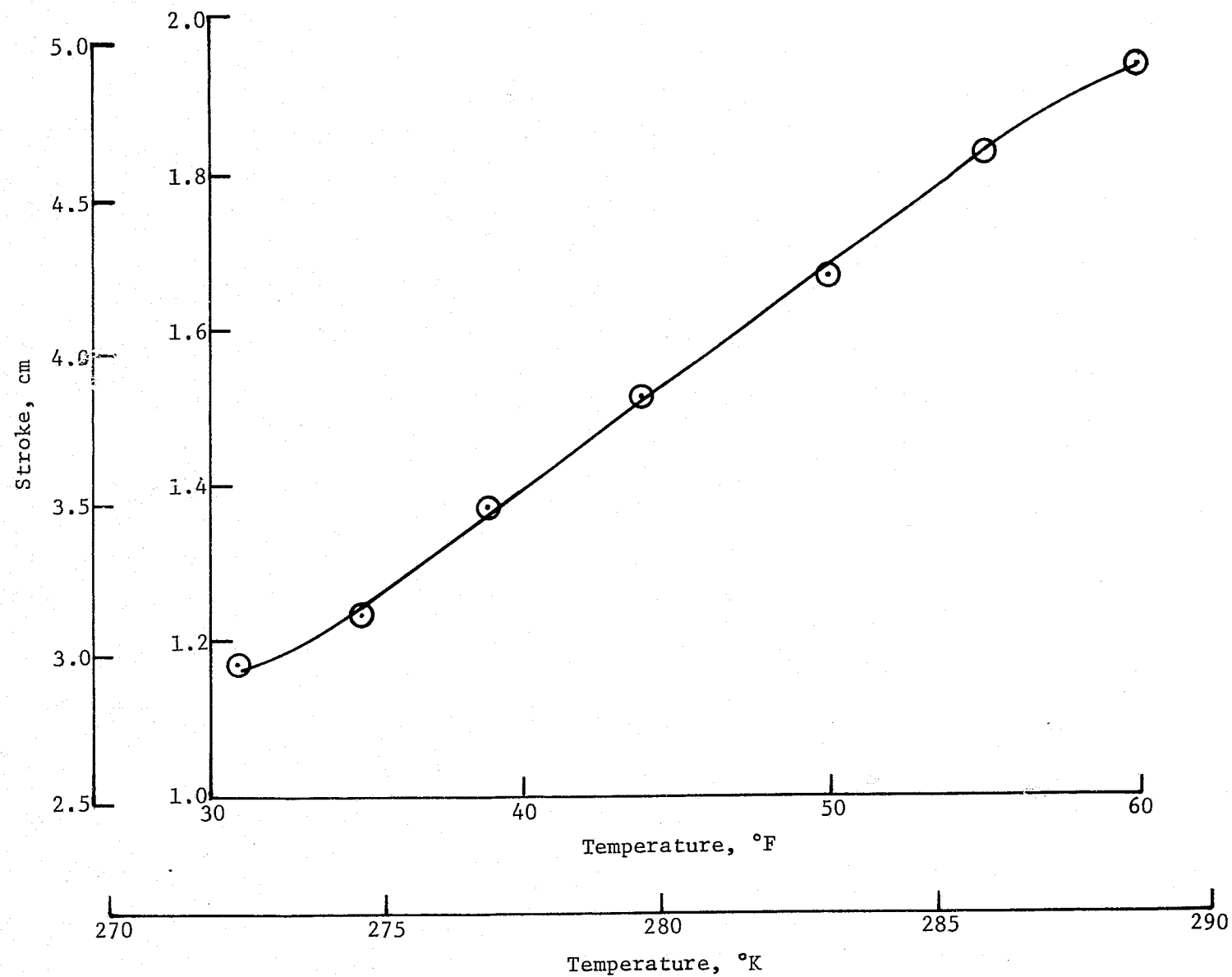


Figure A-9 Viking Fluid Actuator Schematic

Figure A-10

*Figure A-10 Actuator Stroke Versus Steady State Actuator Temperature*

The louver system instrumentation is shown in Figure A-11 and tabulated in Table A-4. In addition to the test article temperature and power measurements, a potentiometer was attached to an extra pinion gear to record the blade rotation produced by the actuator. The paint coating and insulation system were identical to those used on the bimetallic louver system test article. An aluminum plate with an integral fluid loop was fabricated to provide both the simulated component mass and enable cooling to establish initial temperatures. A photograph of the test article mounted in the chamber is shown in Figure A-12.

Figure A-11

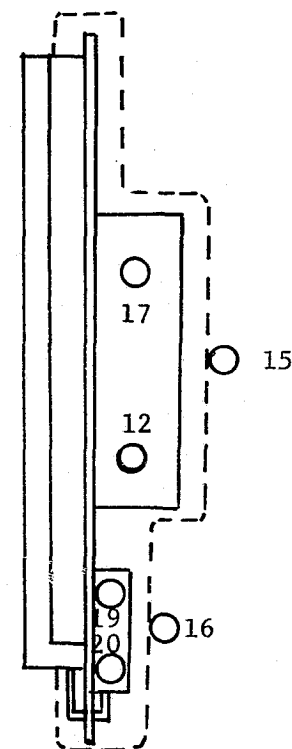
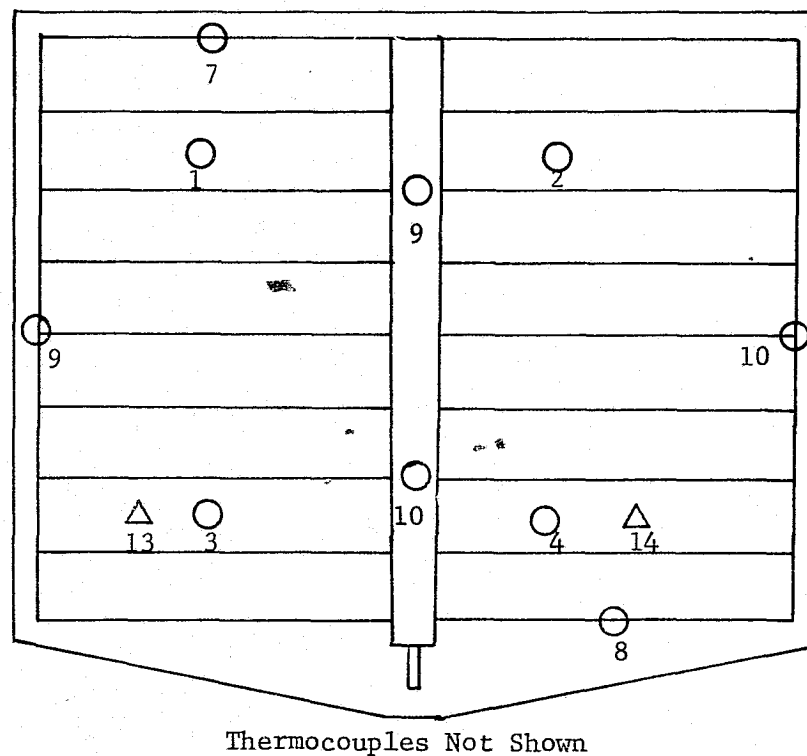


Figure A-11 Fluid Actuated Test Article Thermocouple Location

Table A-4
Fluid Actuated Test Article Thermocouple Locations

TC Number	Location
1	Baseplate
2	Baseplate
3	Baseplate
4	Baseplate
5	Guard Heater
6	Guard Heater
7	Frame End (Inside)
8	Frame End (Inside)
9	Frame Side (Inside)
10	Frame Side (Inside)
11	Guard Heater
12	Guard Heater
13	Louver Blade
14	Louver Blade
15	Outside Insulation
16	Outside Insulation
17	Component Simulator
18	Component Simulator
19	Baseplate underneath Actuator
20	Actuator
21	External Cover
22	External Cover
23	External Cover
24	External Cover

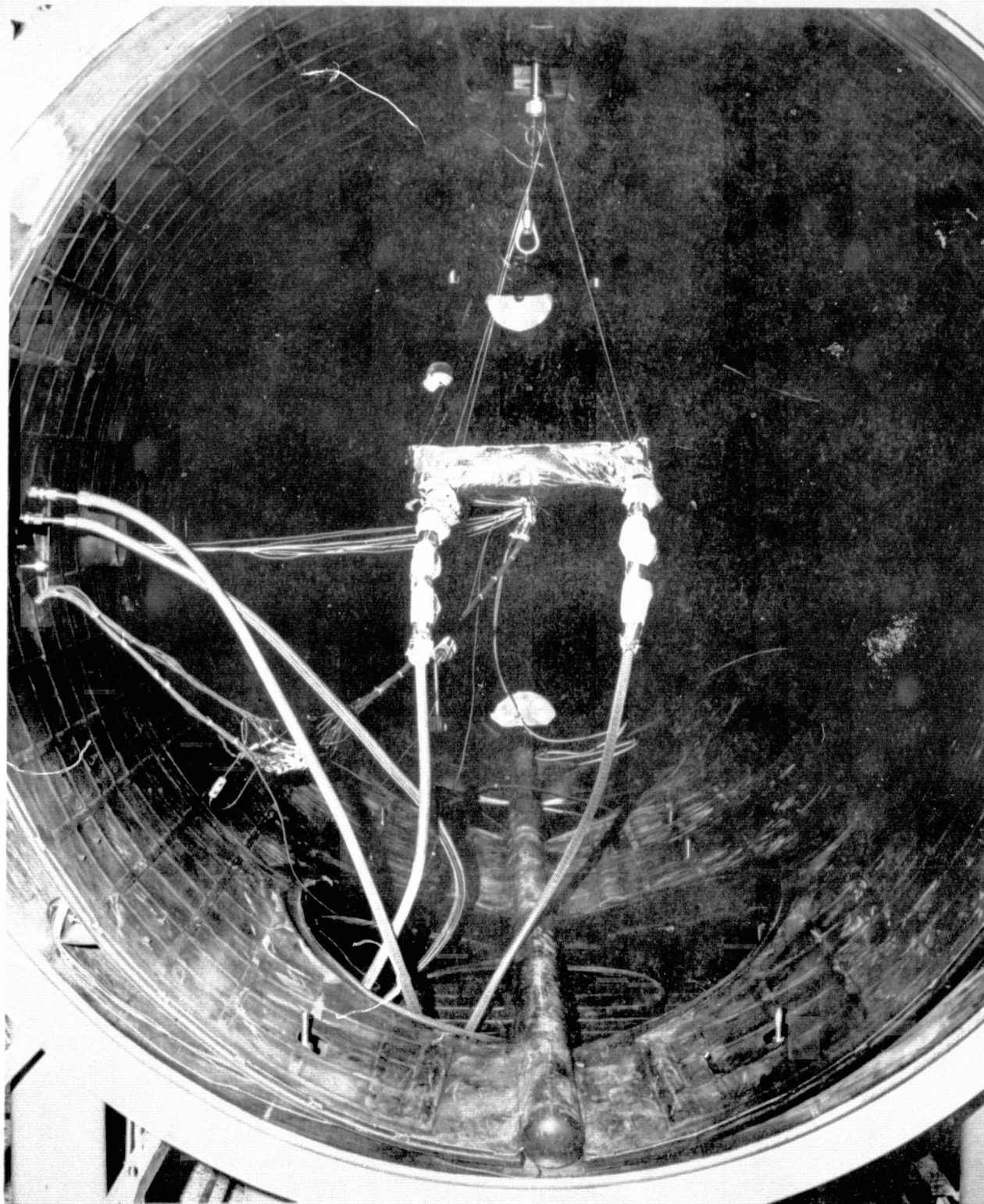


Figure A-12 Fluid Actuated Test Article Mounted in Chamber

VI. TEST FACILITIES AND DATA RECORDERS

Photographs of the test articles mounted in the 6x15 thermal vacuum chamber are shown in Figures A-6 and A-12. The test articles are suspended by low conductance stainless steel wire attached to the teflon cover mounting blocks. Guard heaters and insulation were used to prevent heat leaks from the inlet and outlet tubes to the fluid loops.

A description of the thermal vacuum facility is presented in Table A-5. A photograph of the data acquisition systems is shown in Figure A-13. A Bristol strip chart recorder with a temperature range from 61°K (-350°F) to 672°K (750°F) was used to record thermocouple data. This wide temperature range was necessary because the next standard recorder scale, 144°K (-200°F) to 478°K (400°F), would not be adequate to record temperatures on the outer insulation. The accuracy of the temperature readings was $\pm 1.4^{\circ}\text{K}$ ($\pm 2.5^{\circ}\text{F}$). Heater power which included two guard heaters, a cover heater, and a baseplate heater for both test articles was individually controlled using Varac controllers.

Table A-5 6x15 ft Vacuum Chamber Facility

Nominal Chamber Size	6 ft in diameter by 15.5 ft long
Maximum Test Specimen Size	5 ft in diameter by 11 ft long
Ultimate Pressure	1×10^{-8} torr
Pumping System	<p>Roughing -</p> <p>Portable cart capable of pumping the chamber to 5×10^{-5} torr. Cart contains a cold trap and a 650 CFH booster pump backed up with a 60 CFM compound pump.</p> <p>Hi-vacuum -</p> <p>Ion/titanium sublimation system with net pumping speed in excess of 24,000 liters/sec</p>
Cold Wall	<p>LN₂ cooled -</p> <p>99% optically dense shroud capable of absorbing a heat load of 26,000 Btu/hr</p>
Solar Simulation	<p>Target volume -</p> <p>1 sun - 42 in. diameter by 60 in. long</p> <p>2.5 sun - hexagonal, 30 in. across flats by 30 in. long</p> <p>Intensity -</p> <p>1 sun - 1400 W/m² nominal with a range of 1250 W/m² to 1600 W/m²</p> <p>2.5 sun - 3500 W/m² nominal with a range of 2000 W/m² to 4500 W/m²</p>

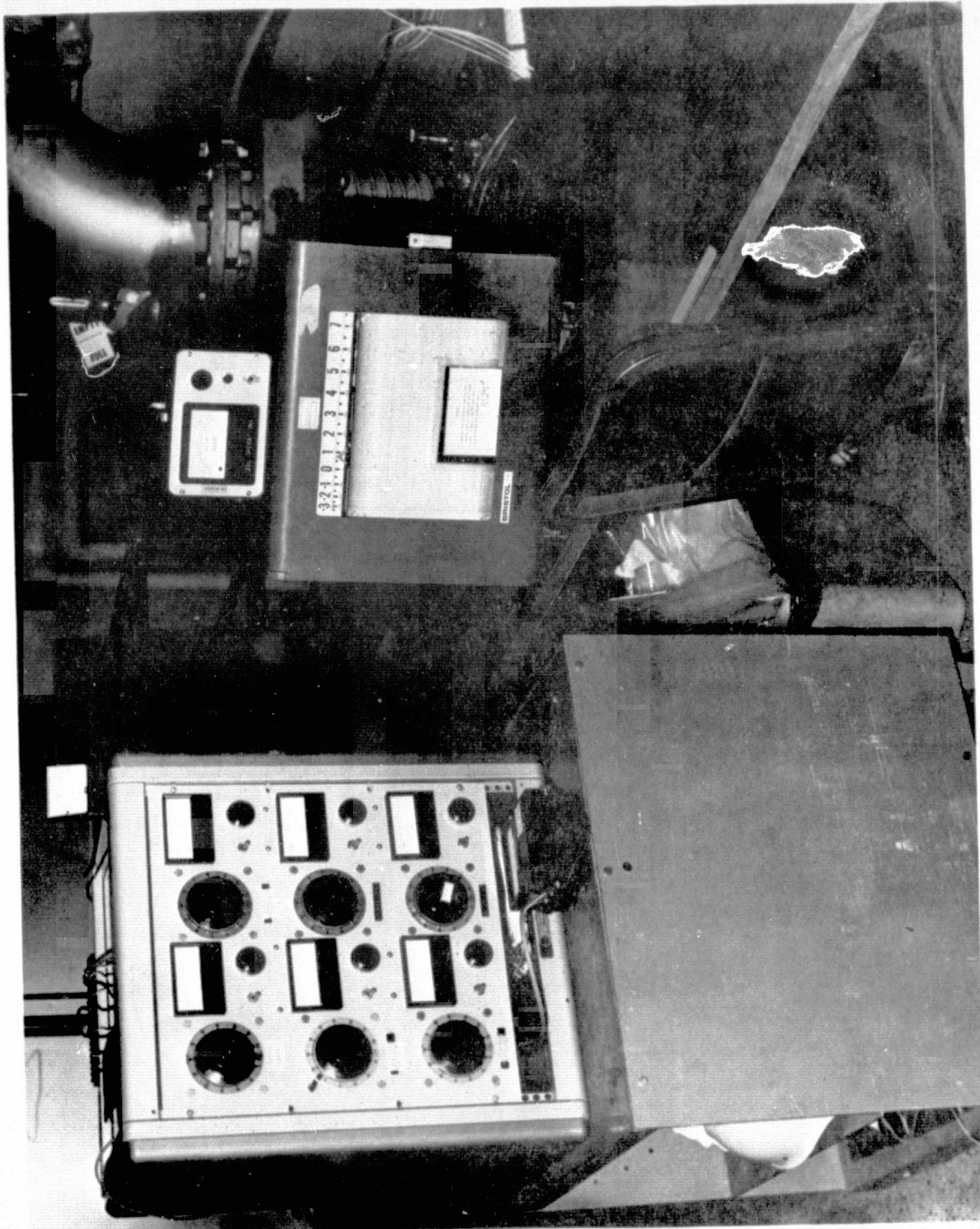


Figure A-13 Data Acquisition System

Figure A-13

REPRODUCIBILITY OF THE
ORIGINAL PAGE IS POOR

VII. THERMAL MODEL DESCRIPTION

A thermal network model was constructed for each louver system test article for use in the MITAS (Ref 1) thermal analyzer. The models were used for both steady state and transient model correlations. The effective emittance of the baseplate as a function of blade angle was calculated using a computer program (Ref 2) which characterizes a covered louver system with a diffuse base and specular blades. The effective emittance is the radiation interchange factor from the baseplate to the cover and takes into account the blockage of the louver blades. In the case of the bimetallic louver system, the effective emittance values were adjusted to account for the holes in the frame to lighten the assembly.

The louvered area of each baseplate was modified to account for the blockage of the actuator housing and the frame. The model also simulated radiation from the baseplate to the cover through the unlouvered portion of each baseplate. Conduction through the teflon standoffs as well as heat leaks through the multilayer insulation were modeled.

Test data input to both models consisted of the power applied to the component simulator heater and the cover temperature. The cover temperature was used as a boundary condition. However, the heat input necessary to hold the cover at the test data temperature was calculated and compared to the cover power test data. An array of blade angle versus baseplate temperature taken from Northrop data for the bimetallic louver system was input into the model. A blade angle, measured directly from the potentiometer, versus time array was put in the model for the fluid actuated test article.

VIII. TEST RESULTS AND MODEL CORRELATION

The results of the testing and model correlation for the steady state test using the bimetallic louver system test article are summarized in Table A-6. The table gives the heater power applied to the simulated component the final test data for the cover power and temperature, the final baseplate temperature test data reading, the model baseplate temperature correlation, as well as the figure number which shows the model correlation and test data for the baseplate temperature versus time. As shown in the plots of the baseplate temperature history, the actual test data was tabulated from approximately two to five hours depending on the duration of the particular test. The last test data value for the cover temperature was used to project the transient simulation out to 10 hours at which time a true steady state solution was simulated. The extended transient simulation indicates the steady state temperature which would have been obtained had the actual test been allowed to continue.

The baseplate temperature results of the transient tests using the bimetallic louver system are shown in Figures A-21 through A-23 for 0, 20, and 45 W of component power respectively. The power supplied to the cover corresponds to an absorbed environmental flux (Ref 3) given in Table A-7.

Table A-6
Summary of Steady State Tests Using the Bimetallic Actuated
Test Article

Component Power	Cover Power	Cover Temperature		Baseplate Temperature				Baseplate Temperature
				Test		Model		
W	W	°K	(°F)	°K	(°F)	°K	(°F)	Figure No.
15.0	43.3	273.3	(32.0)	297.9	(76.2)	297.6	(75.7)	A-14
15.0	57.7	287.6	(57.7)	303.7	(86.7)	304.6	(88.2)	A-15
30.0	14.3	254.4	(-2.0)	305.0	(89.0)	302.7	(84.8)	A-16
30.0	28.2	272.2	(30.0)	309.1	(96.3)	310.5	(98.9)	A-17
30.0	43.7	288.6	(59.5)	319.9	(115.8)	318.8	(113.8)	A-18
45.0	0.0	254.4	(-2.0)	312.5	(102.5)	313.2	(103.7)	A-19
45.0	13.1	272.1	(29.7)	322.0	(119.6)	321.3	(118.4)	A-20

Table A-7 Cover Heating Environment Used for Transient Cases

Time, hr	Absorbed Flux	
	W/cm ²	(Btu/hr-ft ²)
0.000	1.695E-02	(53.767)
0.135	1.079E-02	(34.203)
0.269	5.139E-03	(16.294)
0.404	2.002E-03	(6.348)
0.538	7.951E-04	(2.521)
0.592	6.069E-04	(1.924)
0.592	6.069E-04	(1.924)
0.673	6.135E-04	(1.945)
0.807	1.712E-03	(5.429)
0.942	4.269E-03	(13.537)
1.022	6.557E-03	(20.792)
1.022	6.557E-03	(20.792)
1.076	8.396E-03	(26.620)
1.211	1.299E-02	(41.214)
1.345	1.811E-02	(57.407)
1.480	1.998E-02	(63.349)
1.608	1.696E-02	(53.767)
	Average	8.467E-03 (26.842)

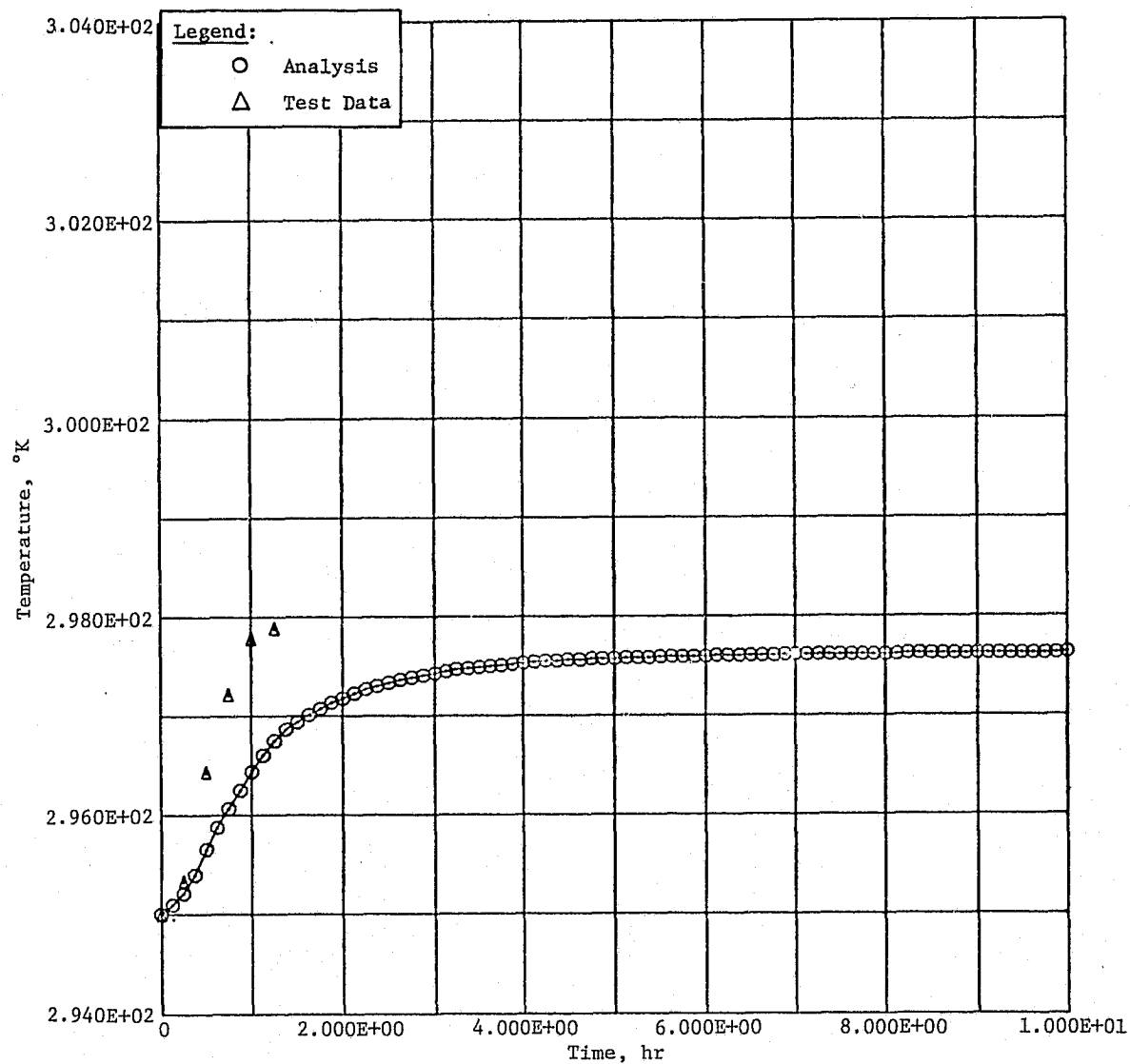


Figure A-14
Bimetallic Actuated Test Article Baseplate Temperature for
15 W Power, 273.3°K Cover

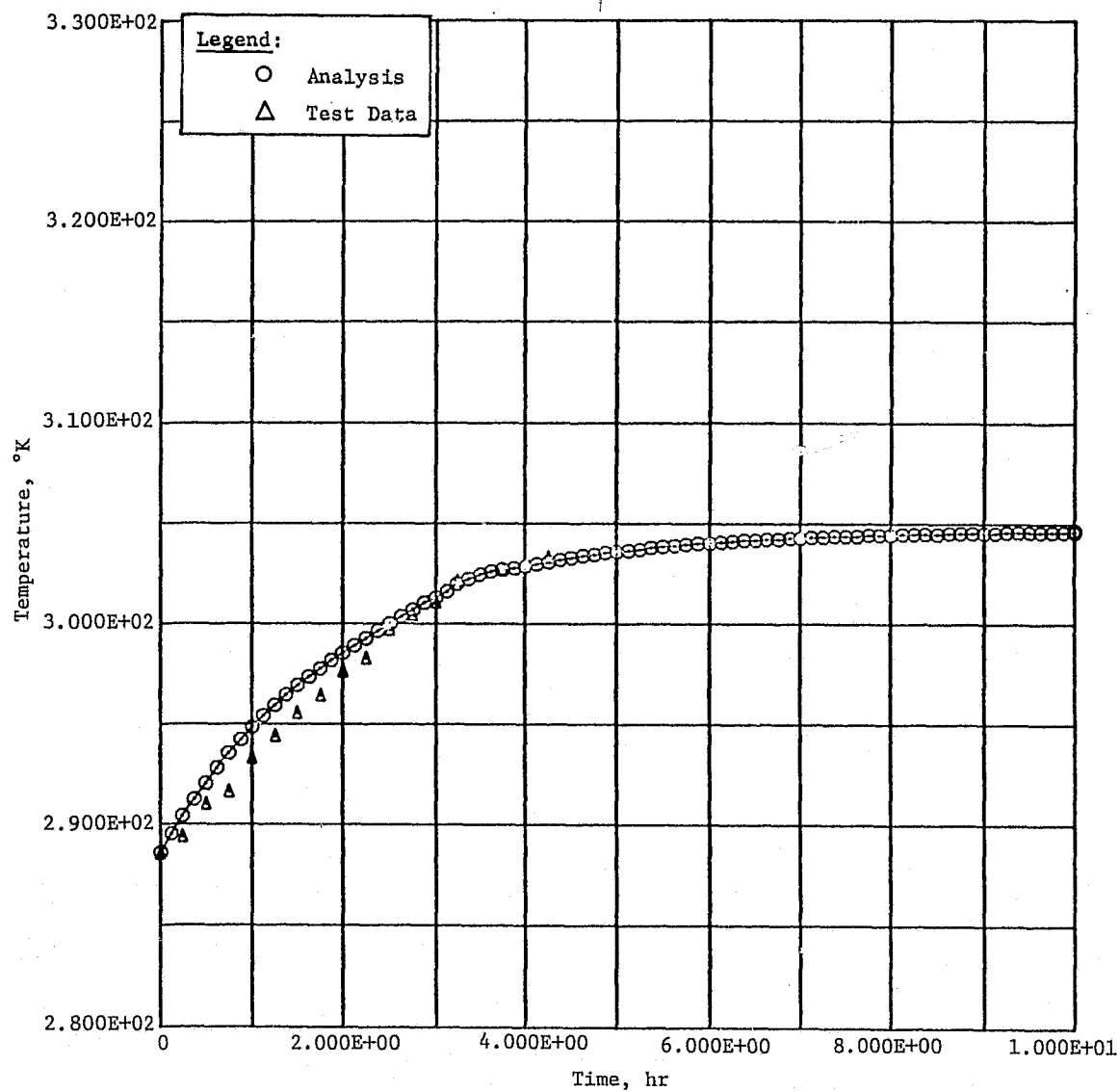


Figure A-15
 Bimetallic Actuated Test Article Baseplate Temperature for
 15 W Power, 287.6°K Cover

REPRODUCIBILITY OF THE
 ORIGINAL PAGE IS POOR

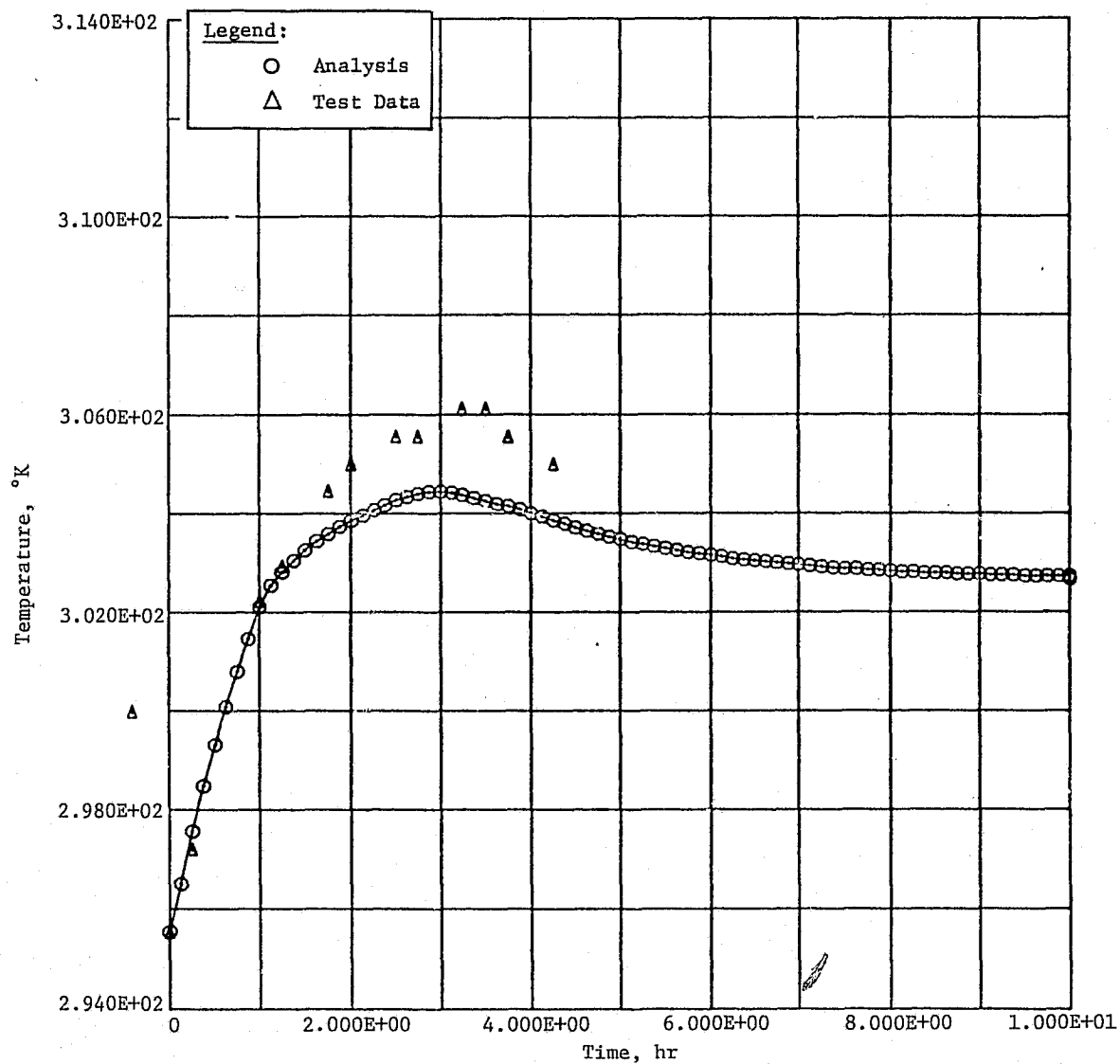


Figure A-16
Bimetallic Actuated Test Article Baseplate Temperature for
30 W Power, 254.4°K Cover

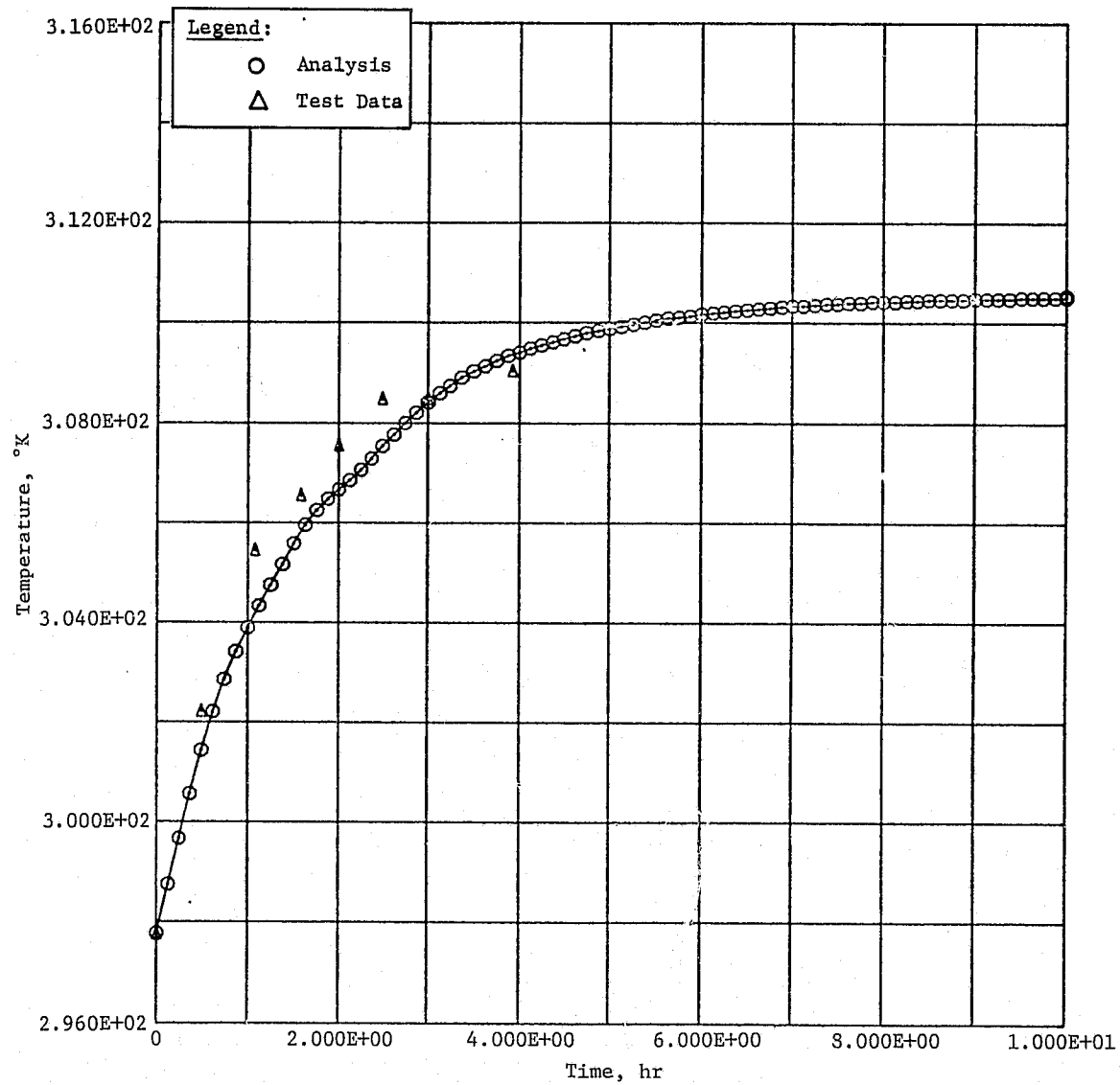


Figure A-17
 Bimetallic Actuated Test Article Baseplate Temperature for
 30 W Power, 272.2°K Cover

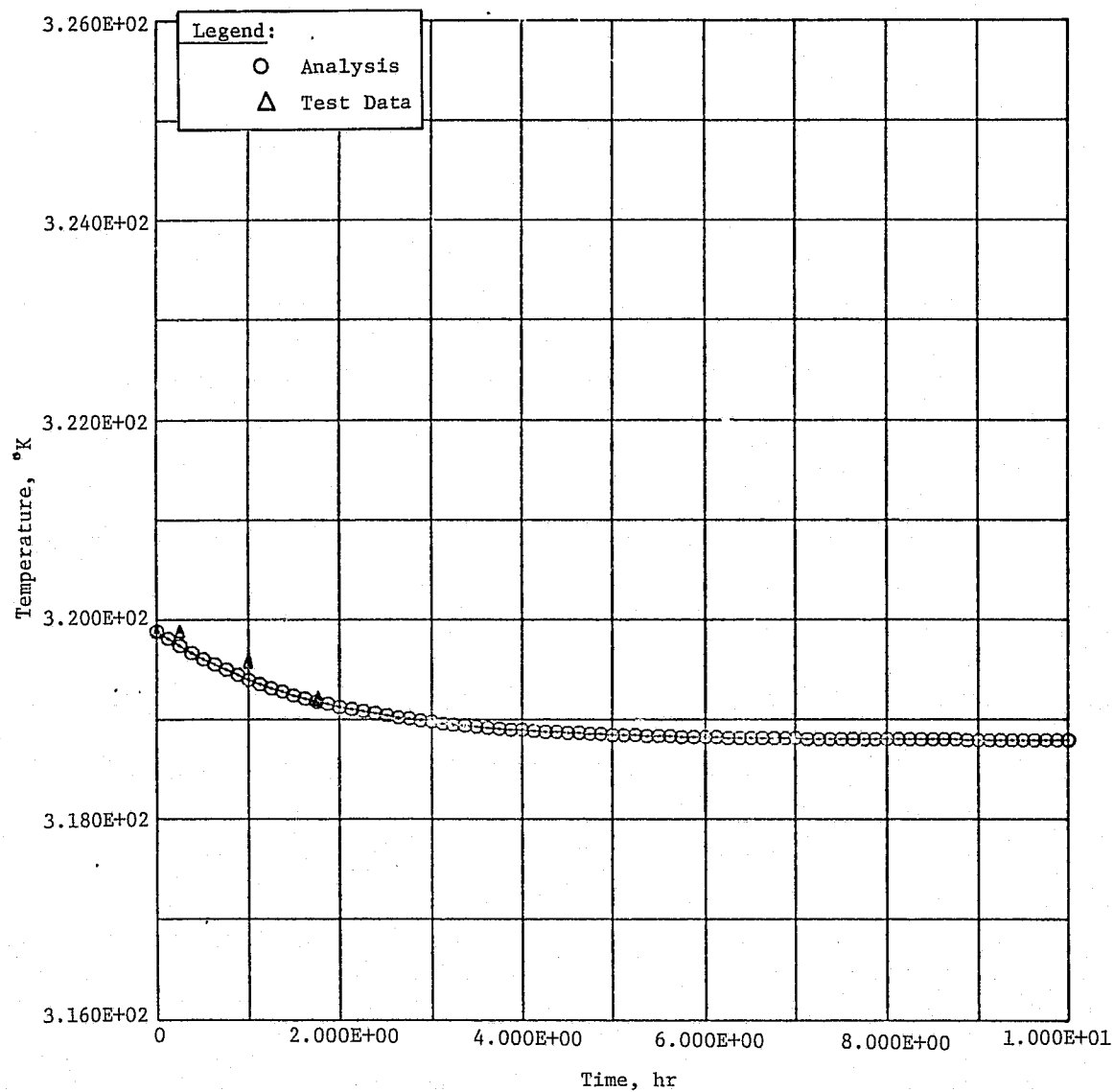


Figure A-18
Bimetallic Actuated Test Article Baseplate Temperature for
30 W Power, 288.6°K Cover

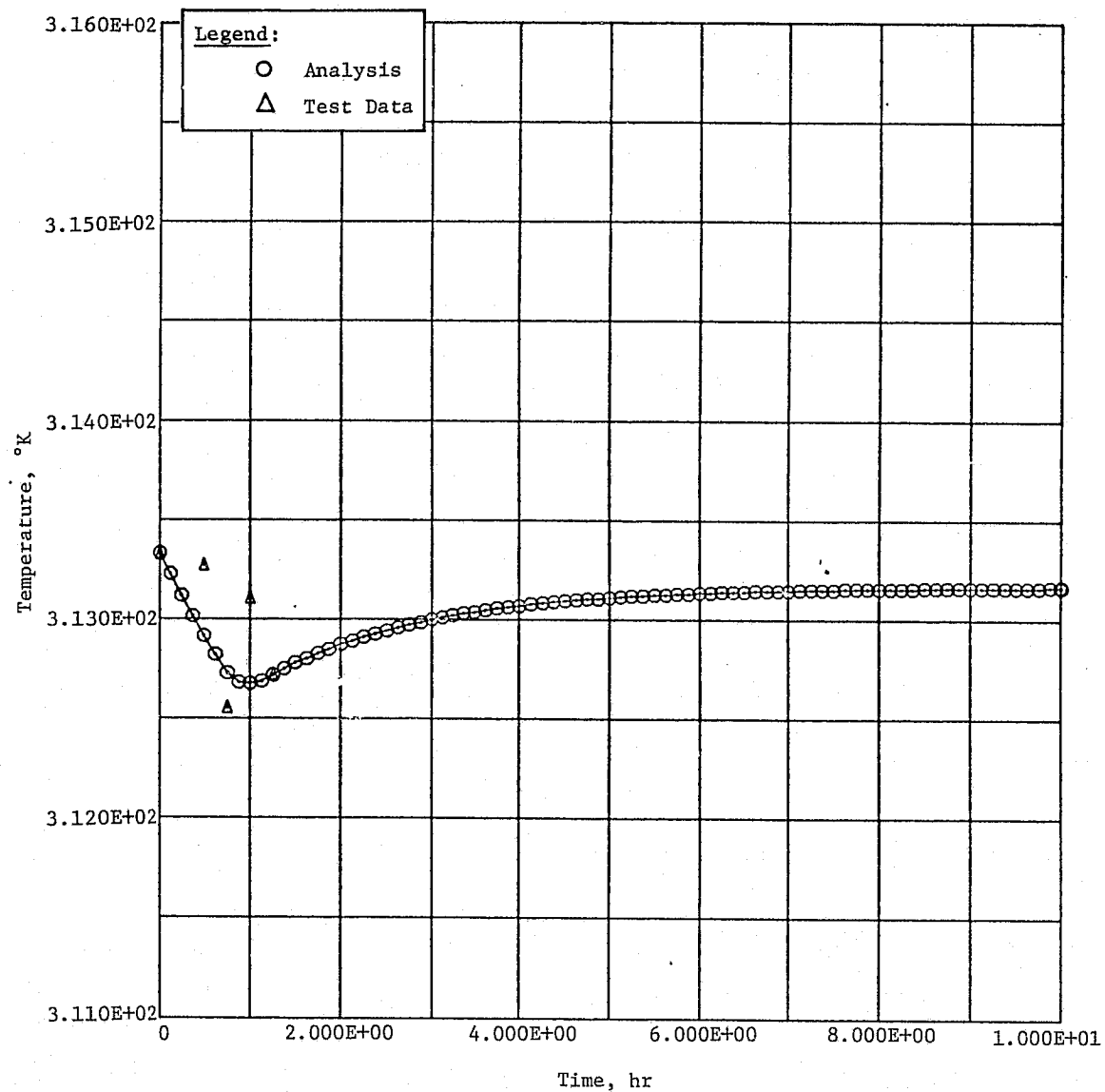


Figure A-19
 Bimetallic Actuated Test Article Baseplate Temperature for
 45 W Power, 254.4°K Cover

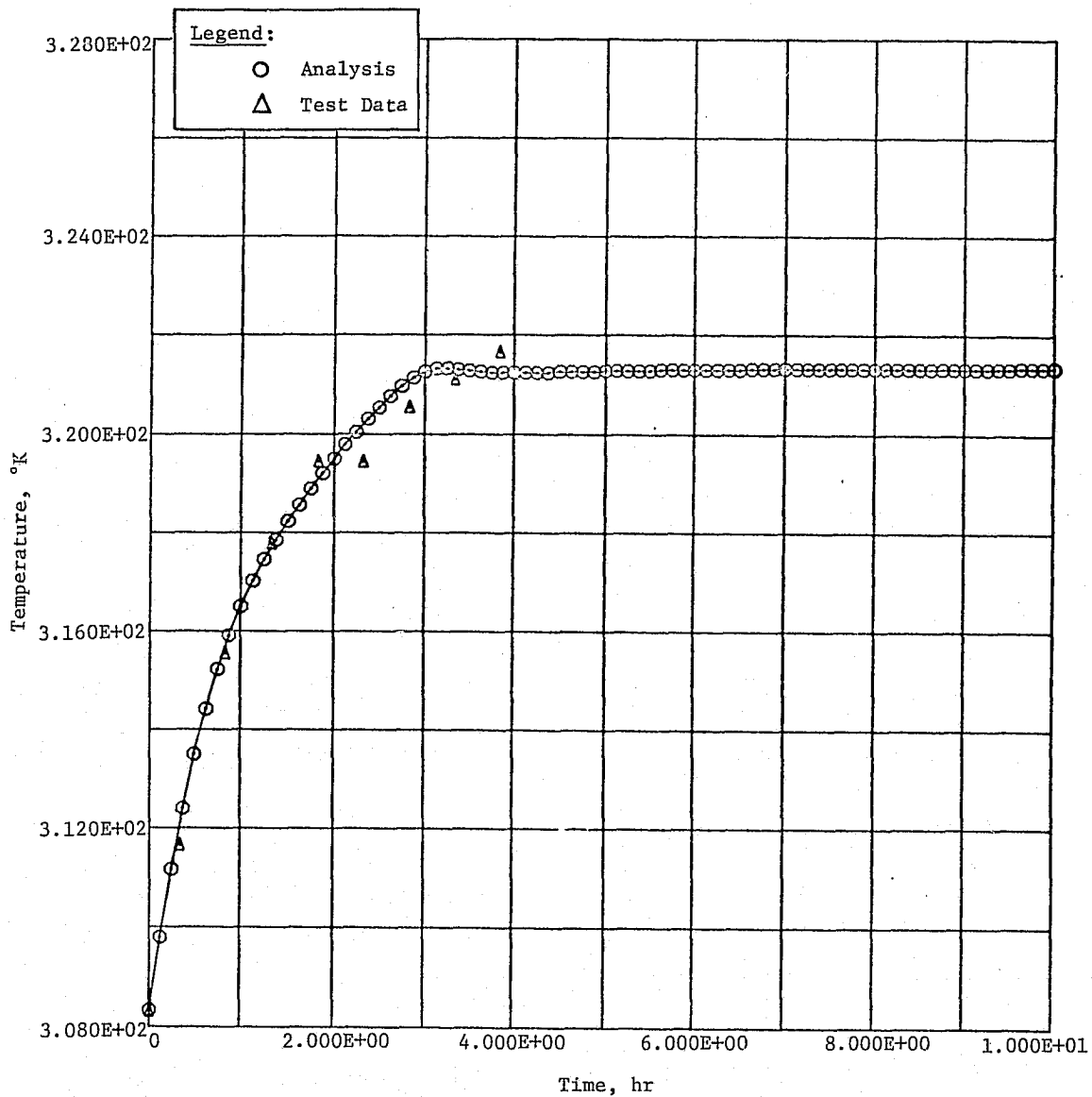


Figure A-20
Bimetallic Actuated Test Article Baseplate Temperature for
45 W Power, 272.1°K Cover

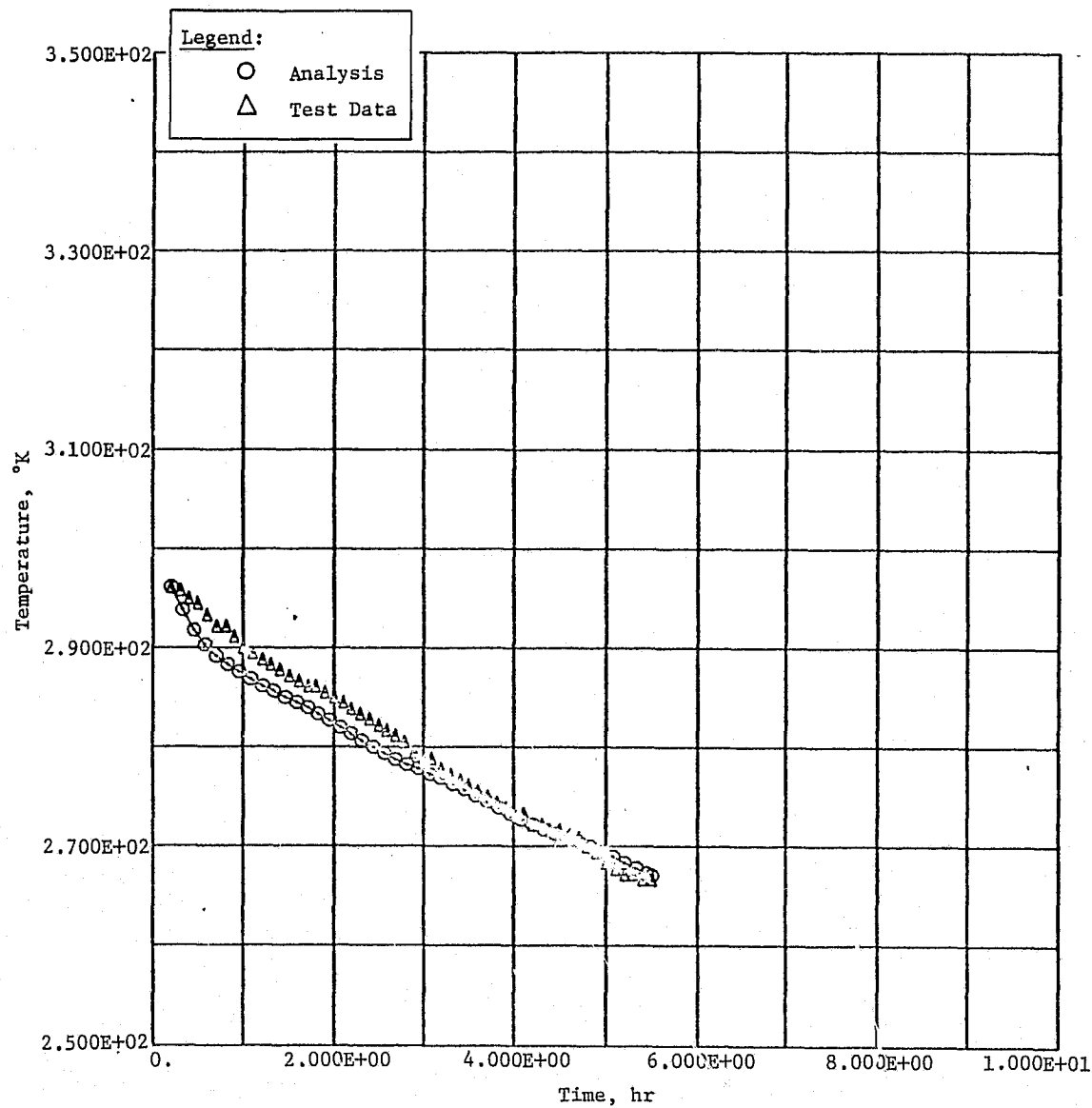


Figure A-21
 Bimetallic Actuated Test Article Transient Baseplate
 Temperature for 0 W Power

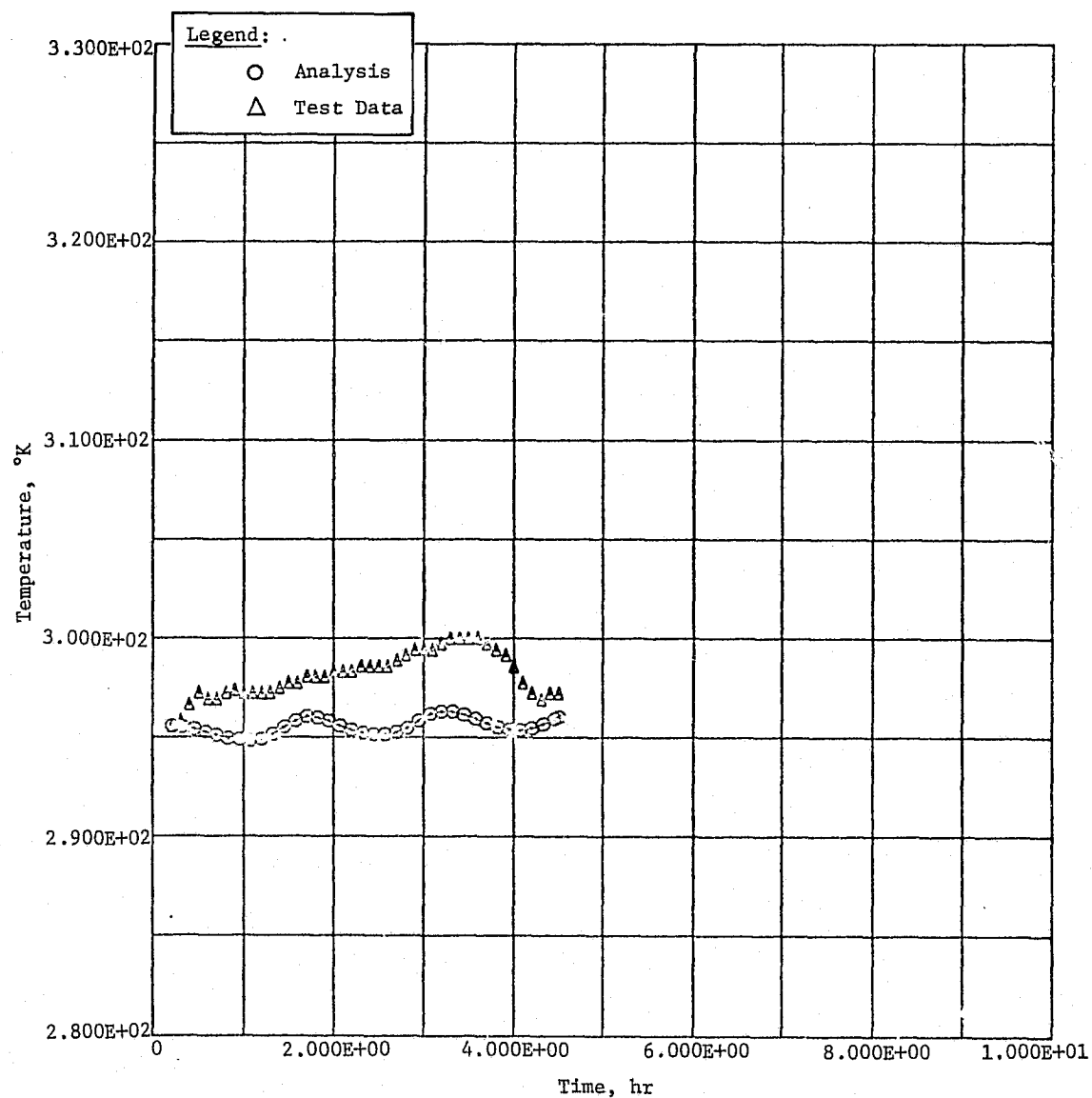


Figure A-22
Bimetallic Actuated Test Article Transient Baseplate
Temperature for 20 W Power

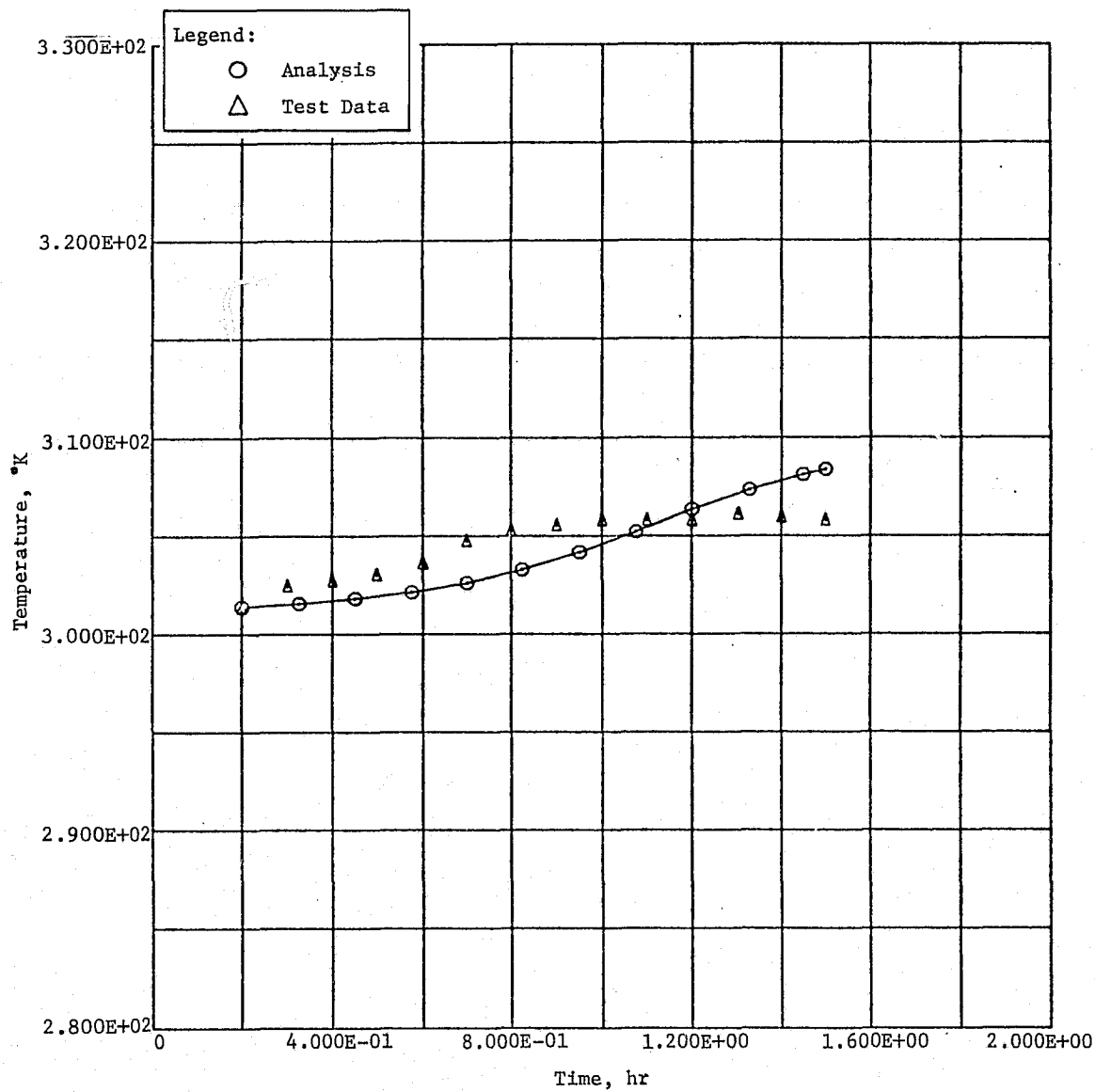


Figure A-23
 Bimetallic Actuated Test Article Transient Baseplate
 Temperature for 45 W Power

REPRODUCIBILITY OF THE
 ORIGINAL PAGE IS POOR

The results of the steady state cases using the fluid actuated louver system test article are summarized in Table A-8. The baseplate temperature model correlation and test data plots extend only to the end of the actual test. Further simulation using the model (past the duration of the test) could not be performed because test data only was used for the blade position. An analytical model of the actuator position as a function of baseplate temperature was attempted based on the steady state curve fit of the actuator temperature versus stroke relationship shown in Figure A-10. However, in the covered louver system test, even though the actuator housing temperature indicated a particular blade position based on Figure A-10, the measured blade position would not correspond to this value. This was probably due to a difference between the Freon vapor temperature and the housing temperature because of the relatively inefficient gas conduction mechanism necessary to head the Freon vapor. Once the vapor temperature started to respond to the change in housing temperature, the housing temperature had exceeded the control range and resulted in driving the actuator from one extreme to the other. The influence of cover temperature on the baseplate was minimized by not applying power to the cover in an attempt to gain control of the actuator.

Table A-8 Summary of Steady State Tests Using the Fluid Actuated Test Article

Component Power	Cover Power	Cover Temperature	Baseplate Temperature				Baseplate Temperature
W	W	°K (°F)	Est		Model		Figure No.
		°K (°F)	°K (°F)	°K (°F)	°K (°F)	°K (°F)	
0.0	45.0	261.8 (11.3)	264.2 (15.5)	265.3 (17.6)			A-24
5.0	0.0	170.1 (-153.8)	249.6 (-10.8)	251.7 (-7.0)			A-25
7.5	0.0	172.1 (-150.3)	256.8 (2.3)	258.0 (4.4)			A-26
10.0	0.0	190.6 9-117.0)	260.6 (9.0)	262.6 (12.6)			A-27
15.0	0.0	199.6 (-100.8)	273.5 (32.3)	272.3 (30.2)			A-28
20.0	0.0	210.3 (- 81.5)	277.4 (39.3)	277.5 (39.5)			A-29
30.0	0.0	228.9 (- 48.0)	283.3 (50.0)	281.8 (47.2)			A-30
35.0	0.0	238.9 (- 30.0)	292.8 (67.0)	289.2 (60.5)			A-31

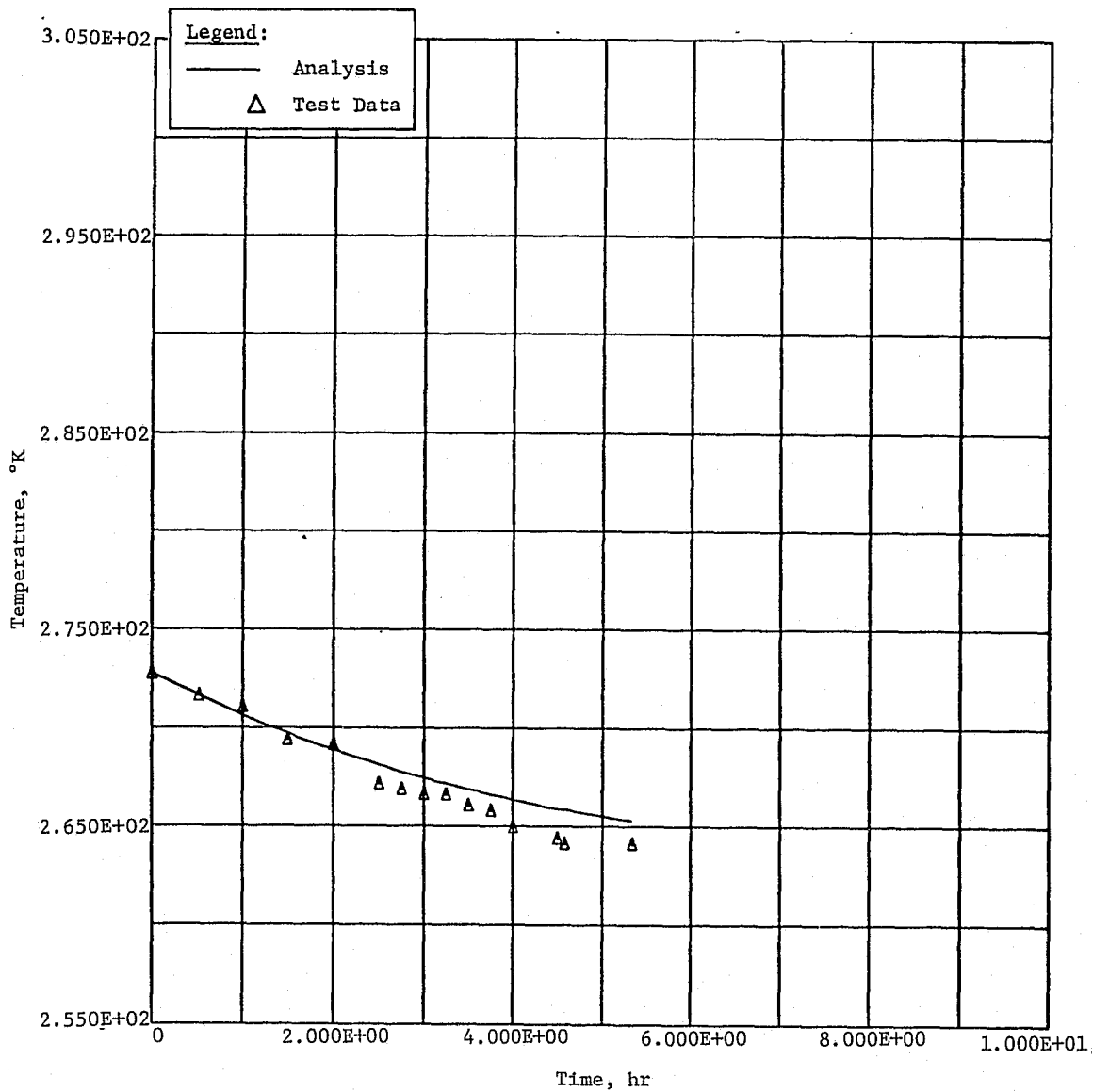


Figure A-24
Fluid Actuated Test Article Baseplate Temperature for
0 W Power, 261.8°K Cover

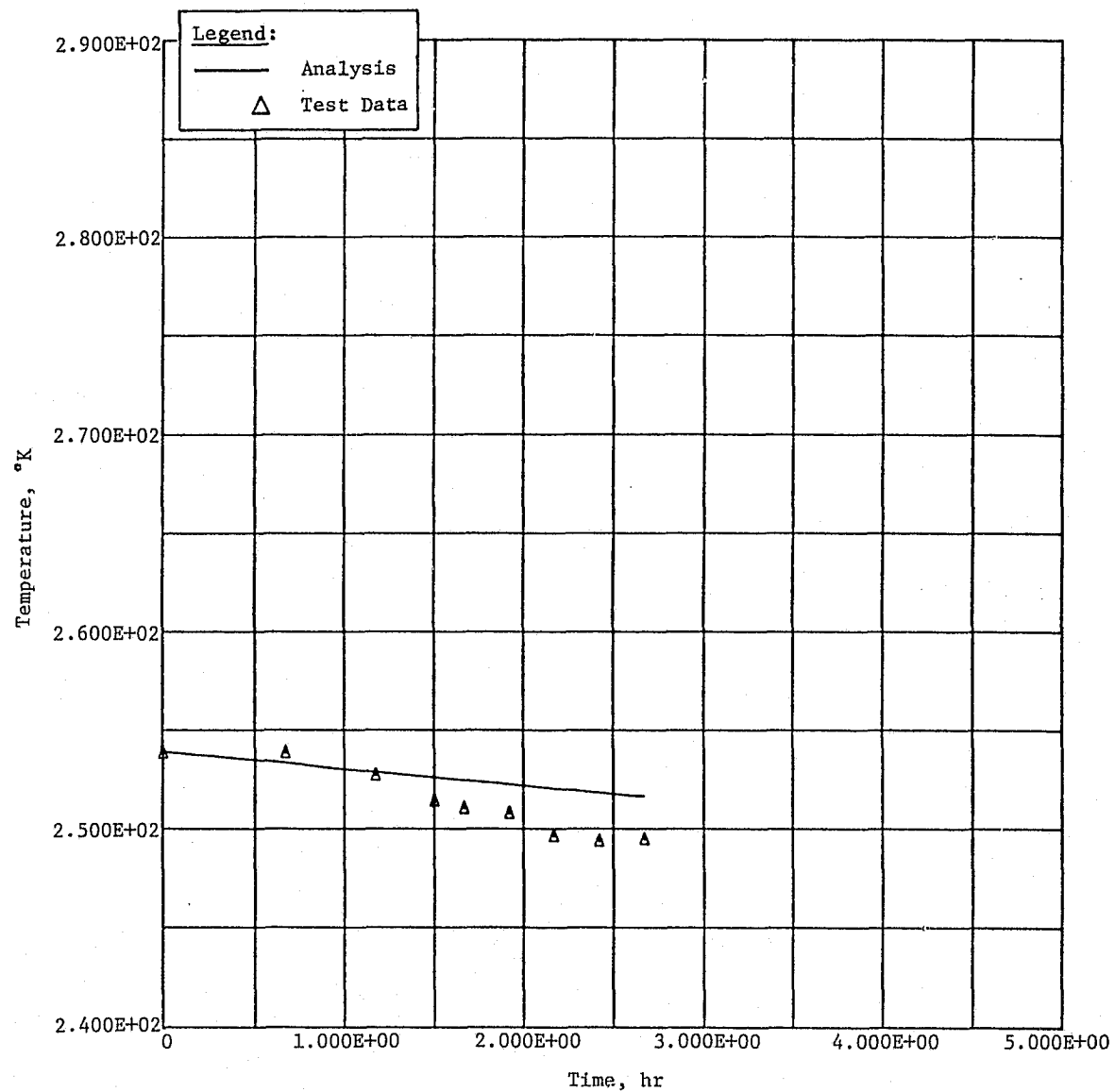


Figure A-25
Fluid Actuated Test Article Baseplate Temperature for
5 W Power, 170.1°K Cover

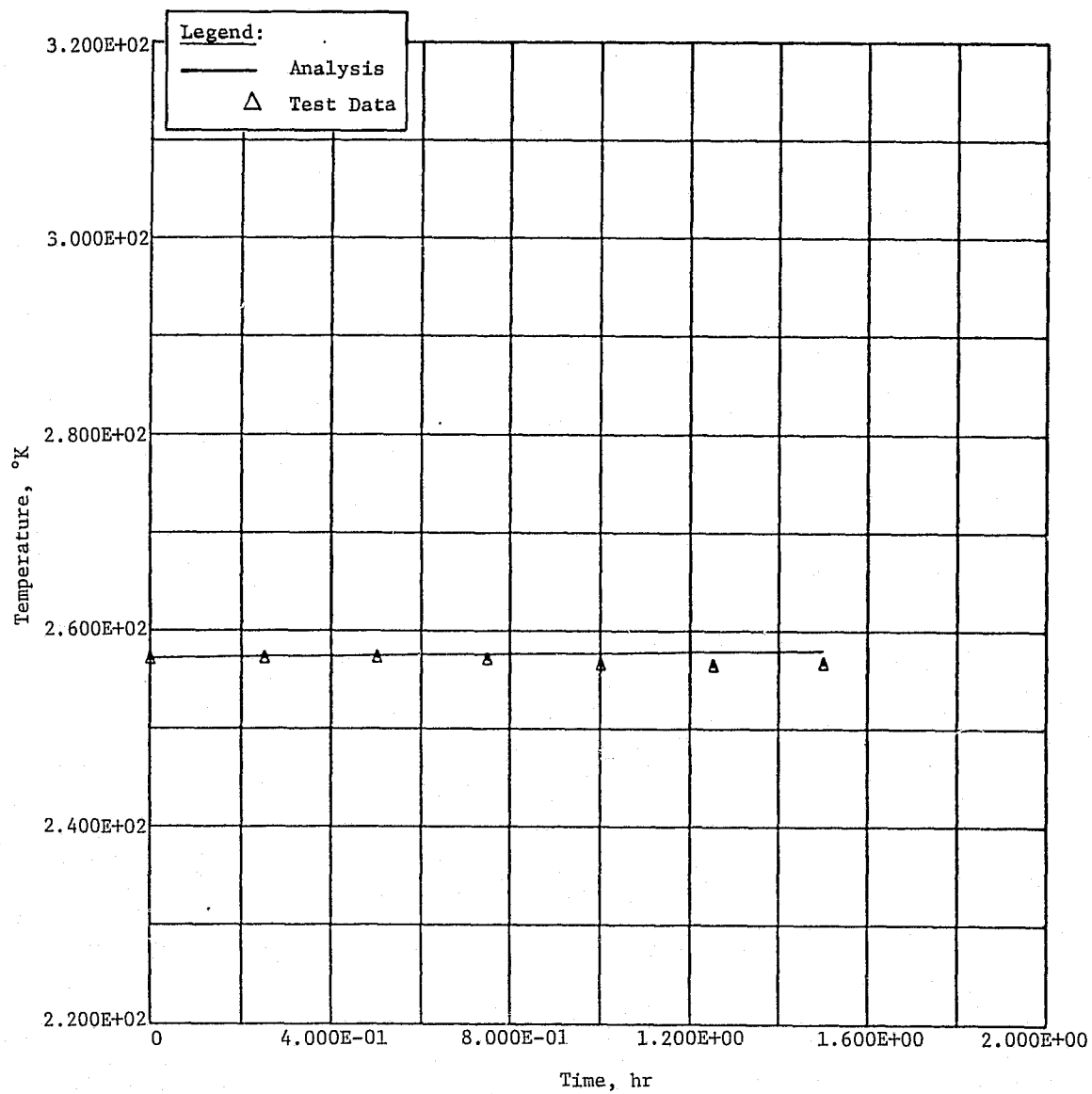


Figure A-26
Fluid Actuated Test Article Baseplate Temperature for
7.5 W Power, 172.1°K Cover

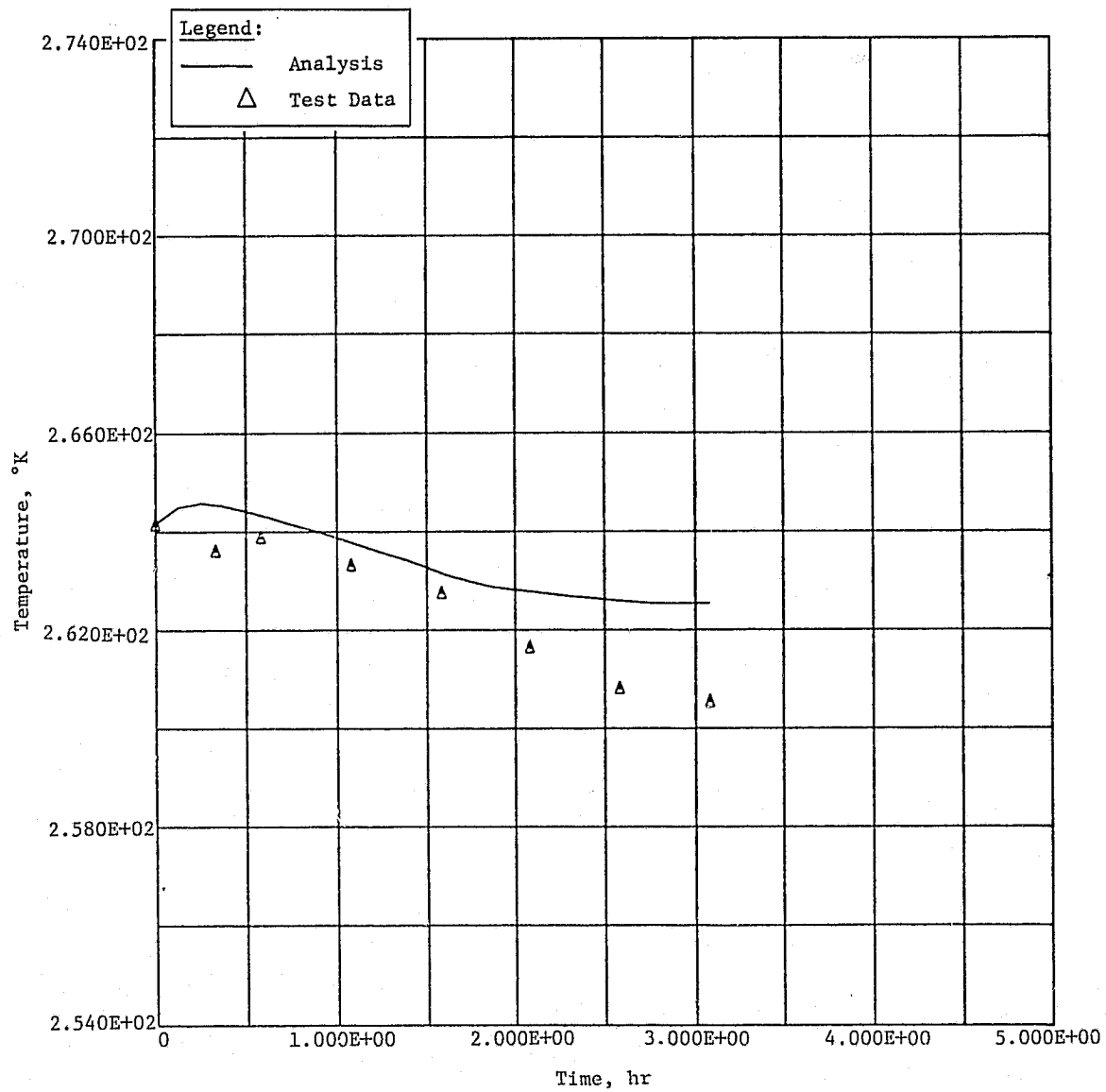


Figure A-27
Fluid Actuated Test Article Baseplate Temperature for
10 W Power, 190.6°K Cover

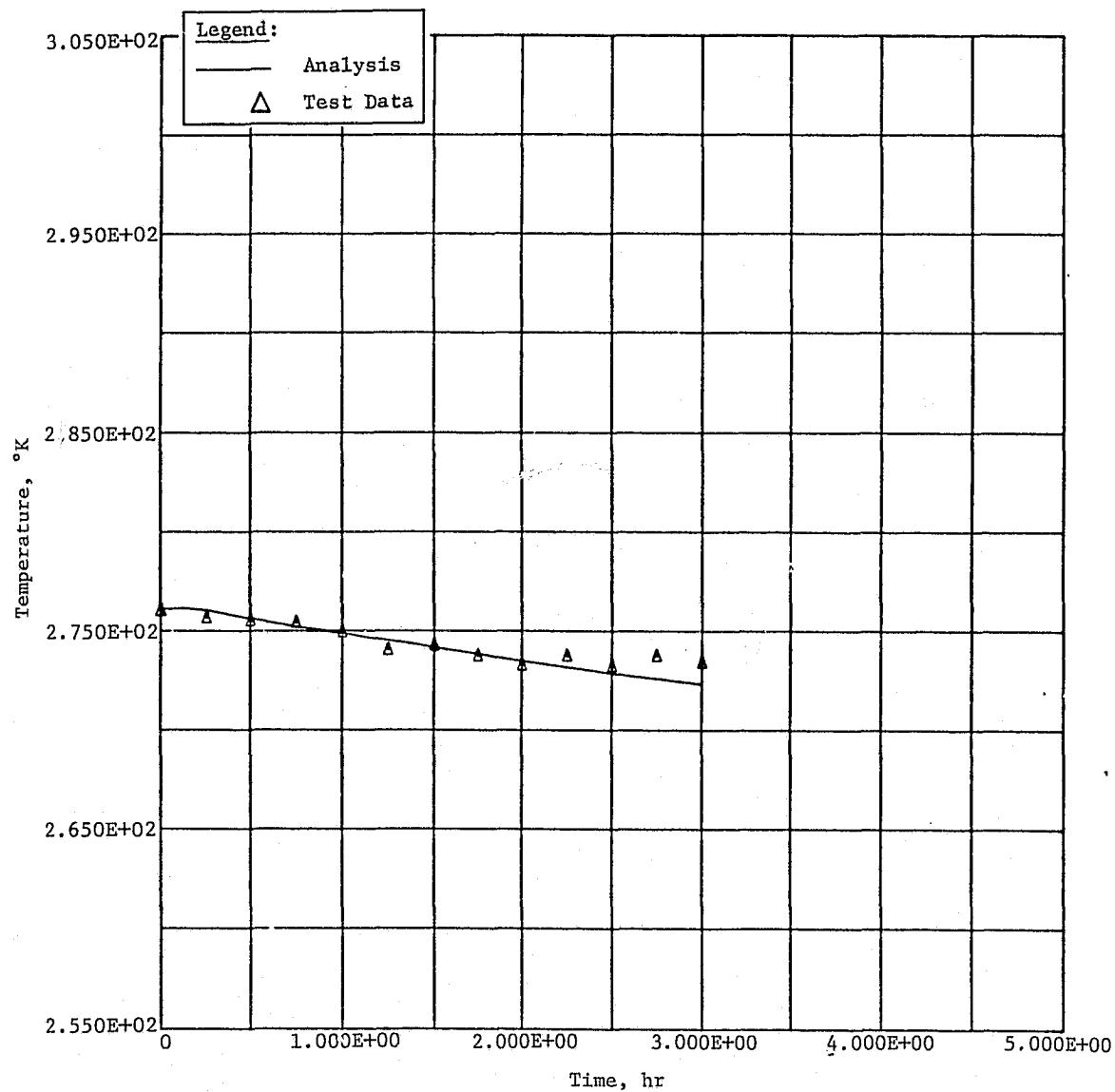


Figure A-28
Fluid Actuated Test Article Baseplate Temperature for
15 W Power, 199.6°K Cover

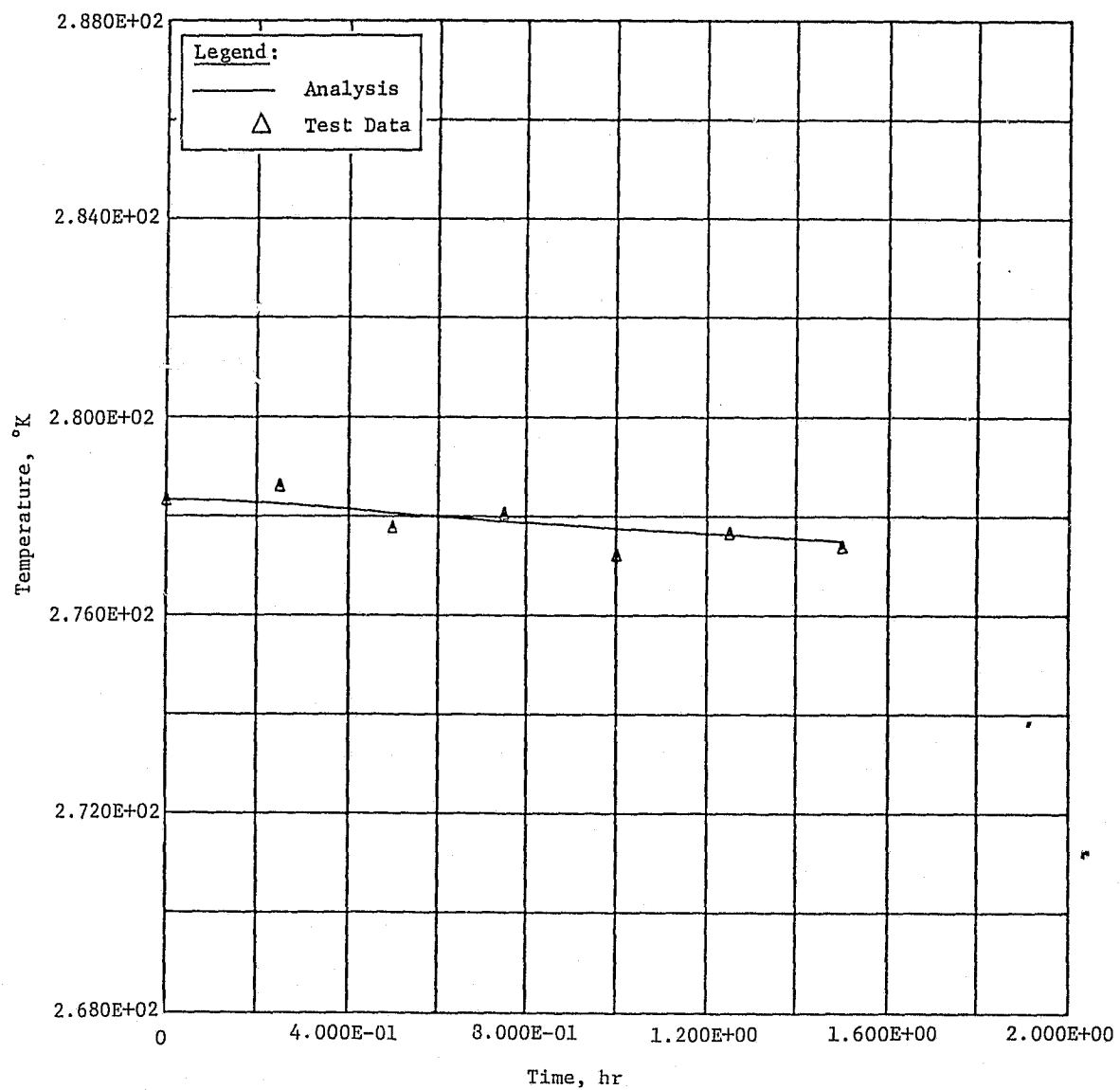


Figure A-29
Fluid Actuated Test Article Baseplate Temperature for
20 W Power, 210.3°K Cover

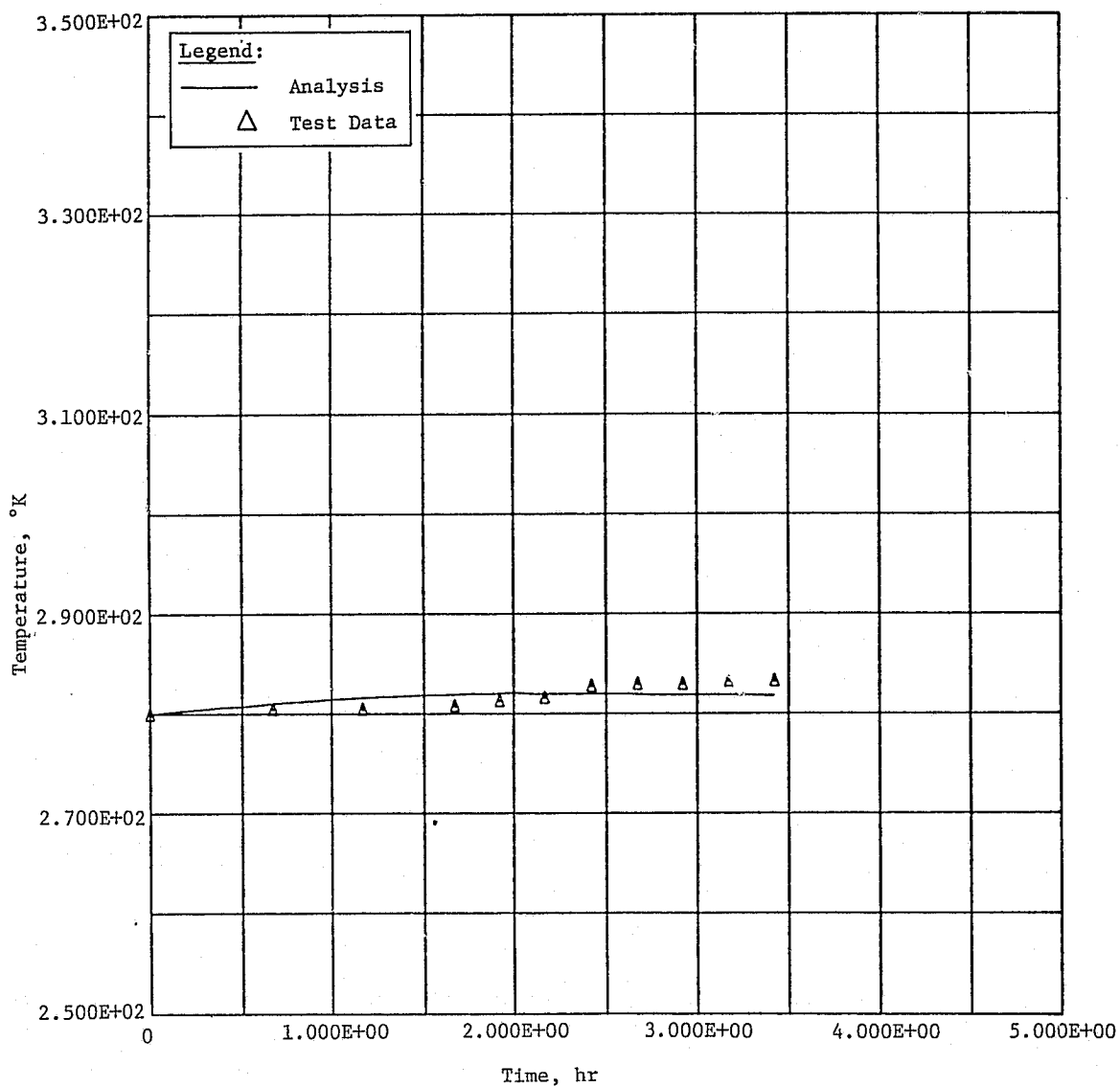


Figure A-30
Fluid Actuated Test Article Baseplate Temperature for
30 W Power, 228.9°K Cover

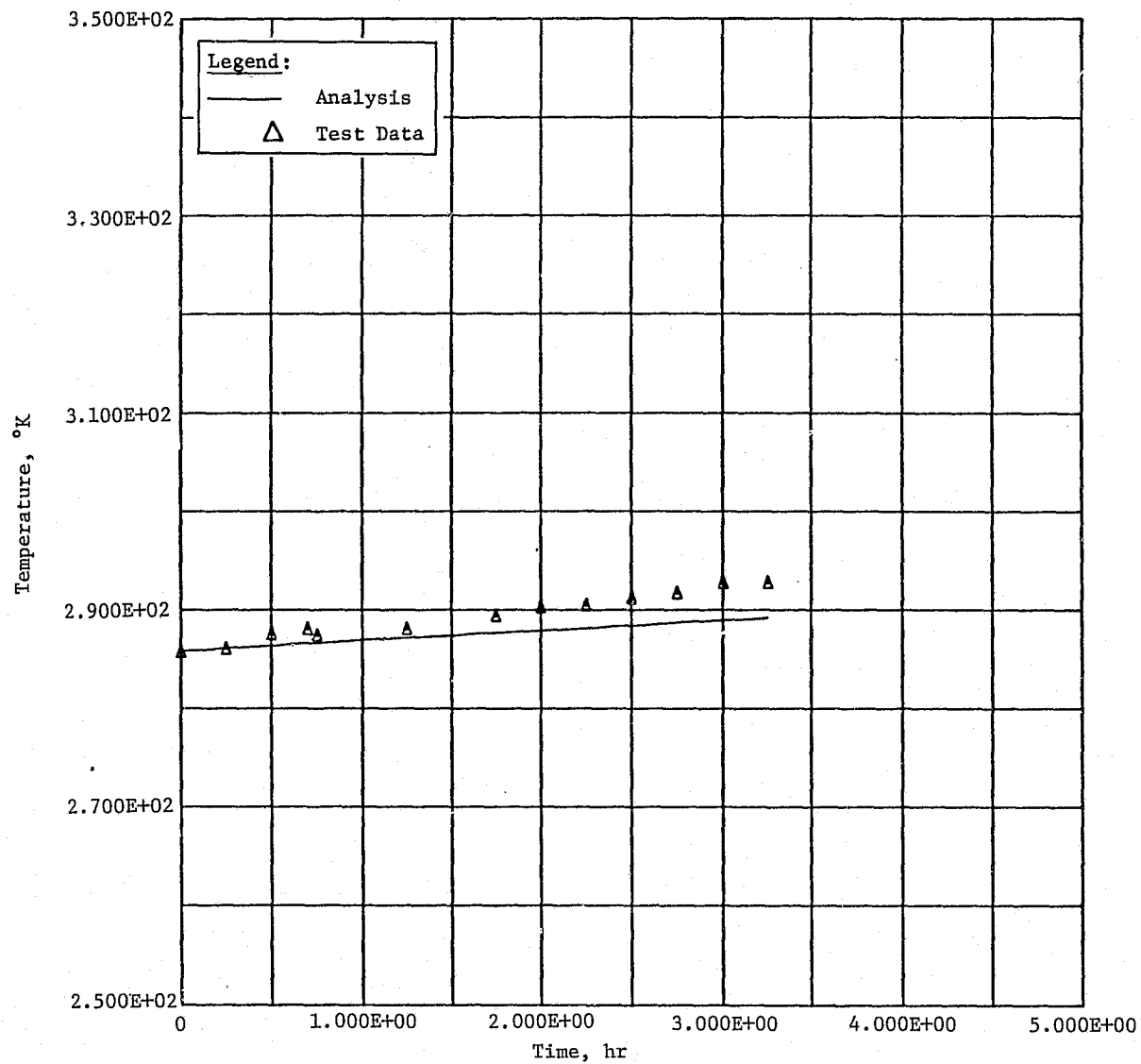


Figure A-31
Fluid Actuated Test Article Baseplate Temperature for
35 W Power, 238.9°K Cover

7

Two transient tests were simulated for the fluid-activated louver system. Case 1 involved continually varying the input power to the simulated component with no power to the cover. The baseplate temperature model prediction and test data for this case is shown in Figure A-32. The power to the base, blade angle, and cover temperature all versus time are shown in Figures A-33, A-34, and A-35 respectively. Transient Case 2 involved applying a constant 10 W of power to the simulated component and imposing the time varying environmental flux given in Table A-7 to the cover. Baseplate temperatures for Case 2 are given in Figure A-36. The blade angle and cover temperature test data for this case are given in Figures A-37 and A-38 respectively.

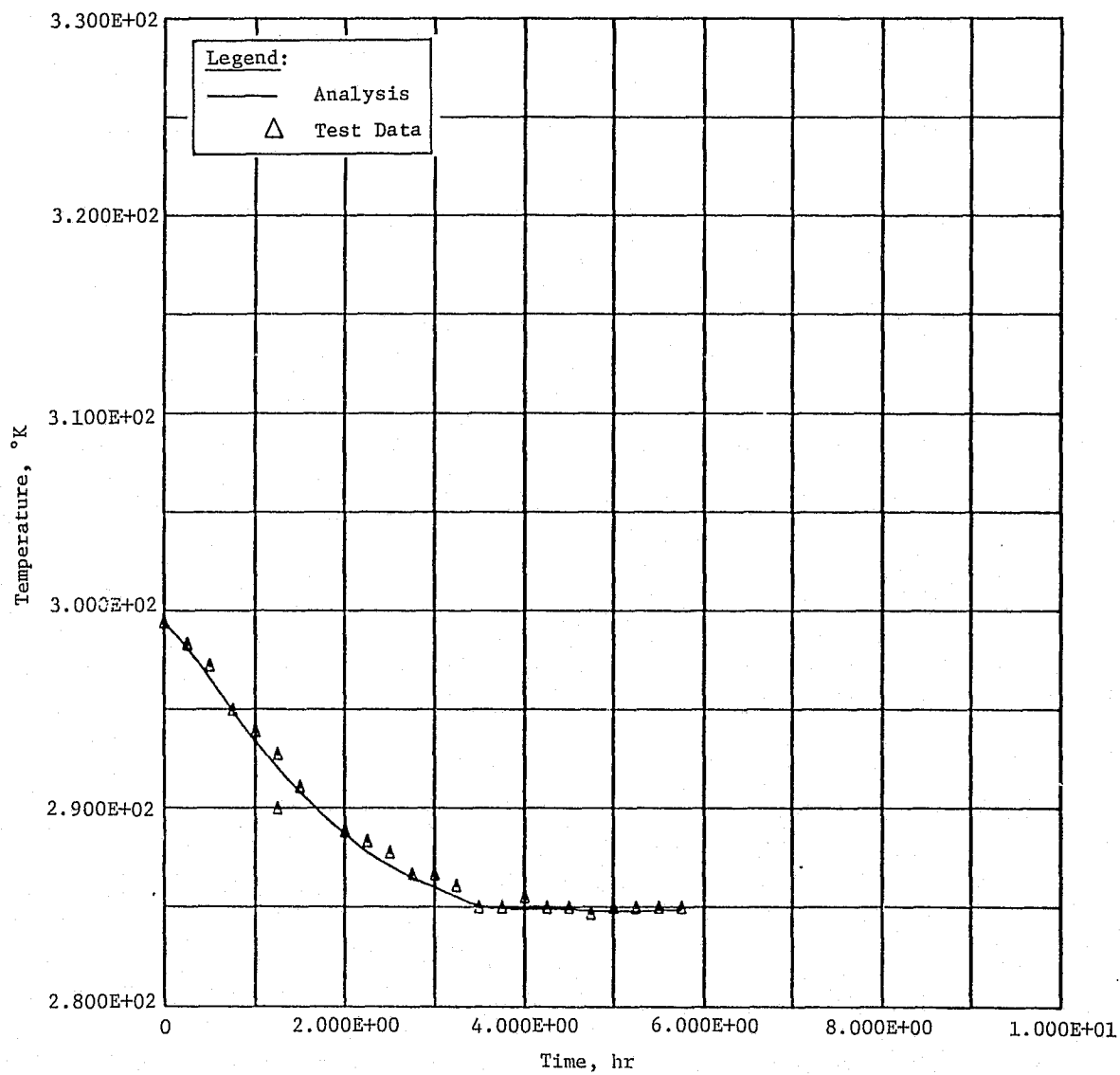


Figure A-32
Fluid Actuated Test Article Transient Baseplate
Temperature for Case 1

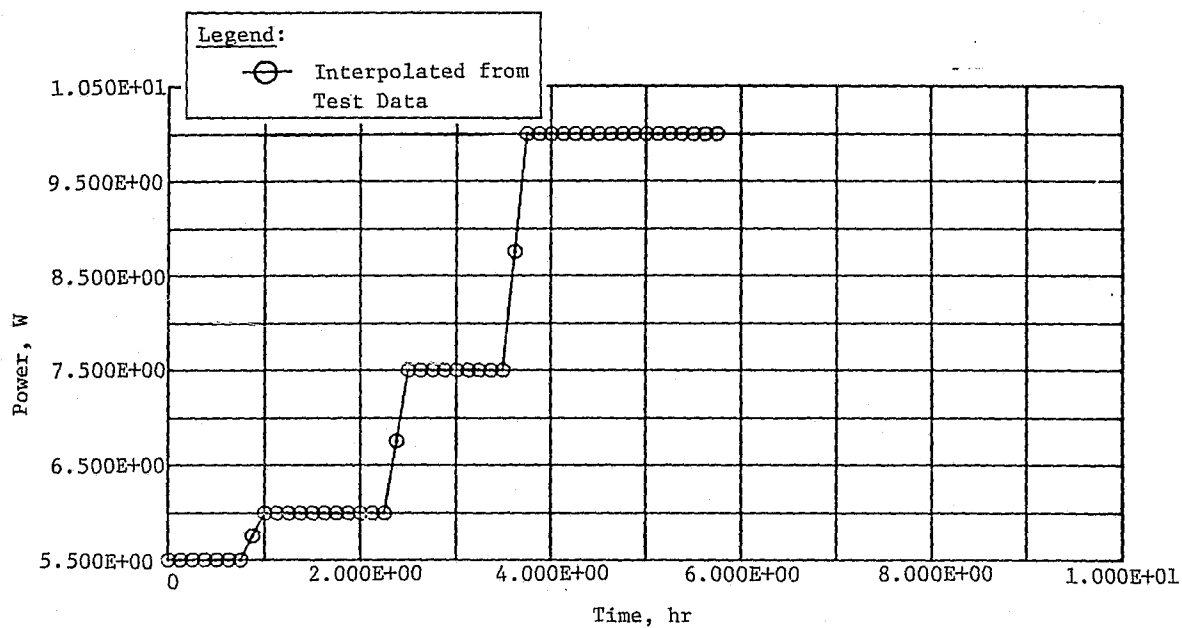


Figure A-33
Fluid Actuated Test Article Transient Component Power for Case 1

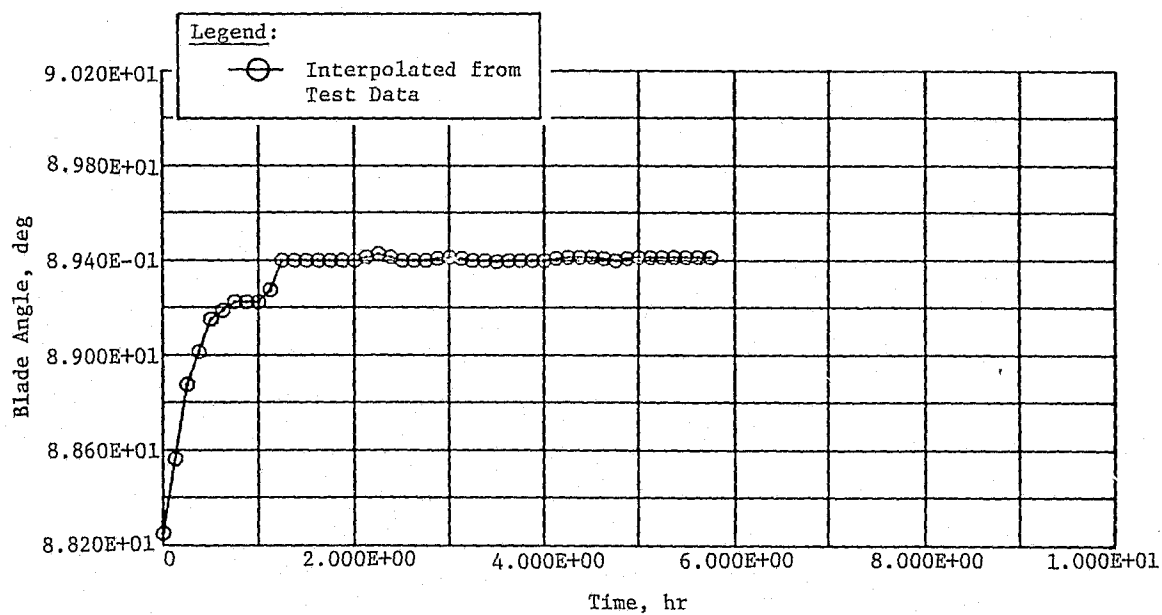


Figure A-34
Fluid Actuated Test Article Transient Blade Angle for Case 1

Figure A-35

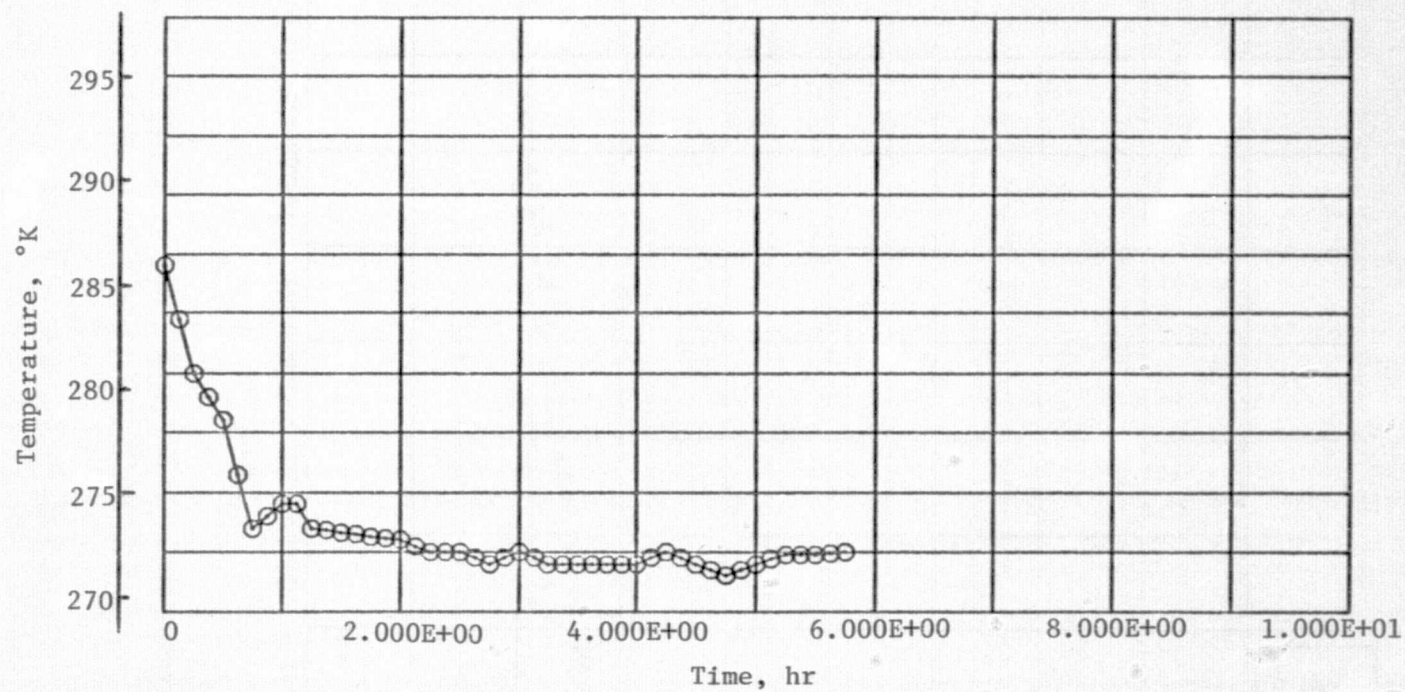


Figure A-35
Fluid Actuated Test Article Transient Cover Temperature for Case 1

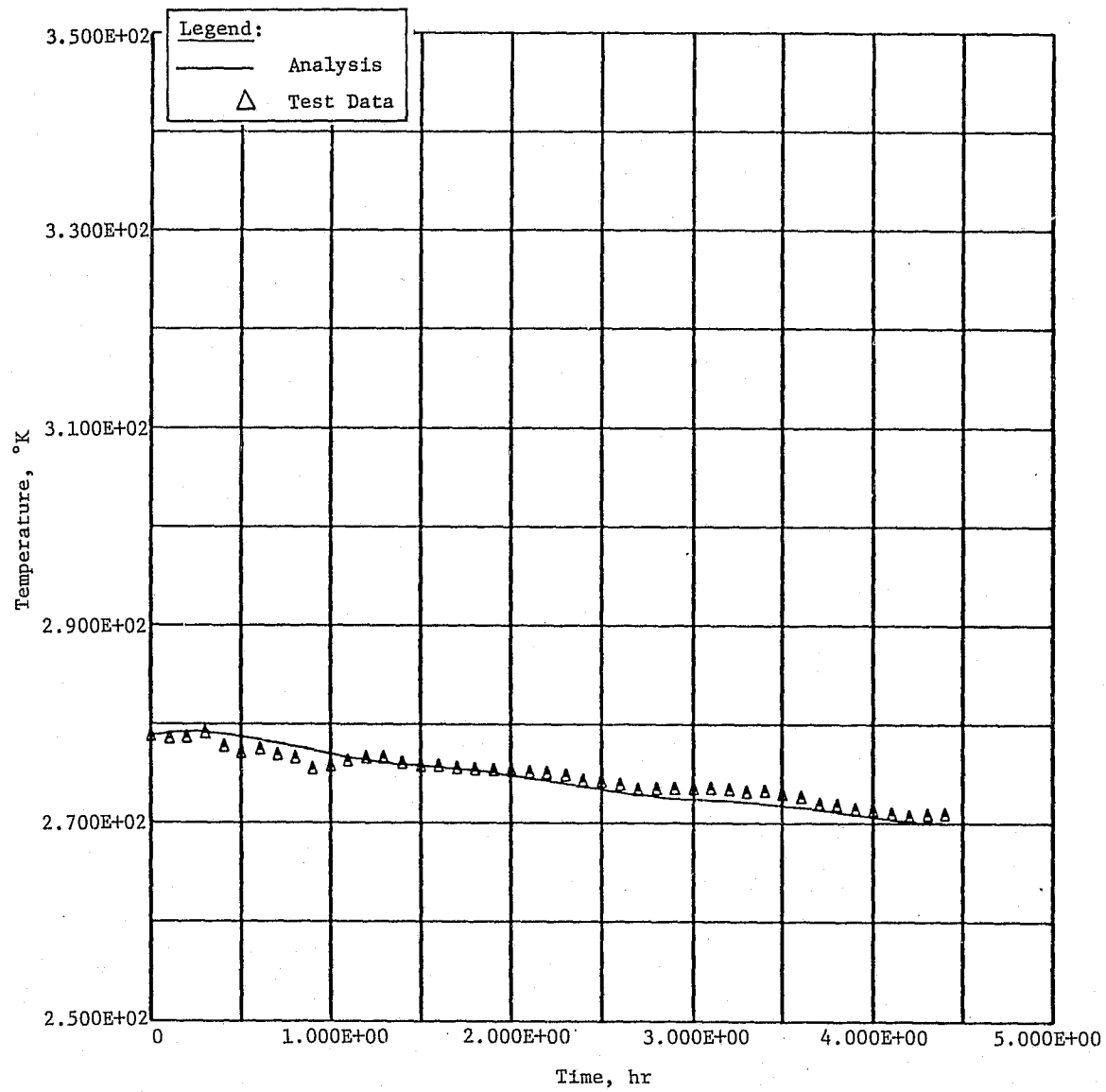


Figure A-36
Fluid Actuated Test Article Transient Baseplate
Temperature for Case 2

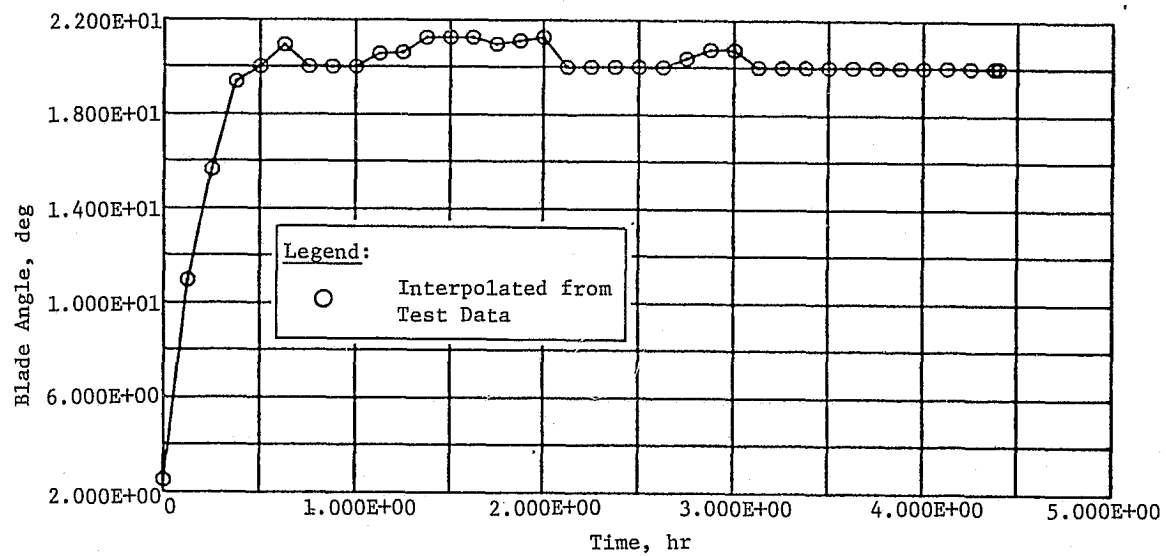


Figure A-37
Fluid Actuated Test Article Transient Blade Angle for Case 2

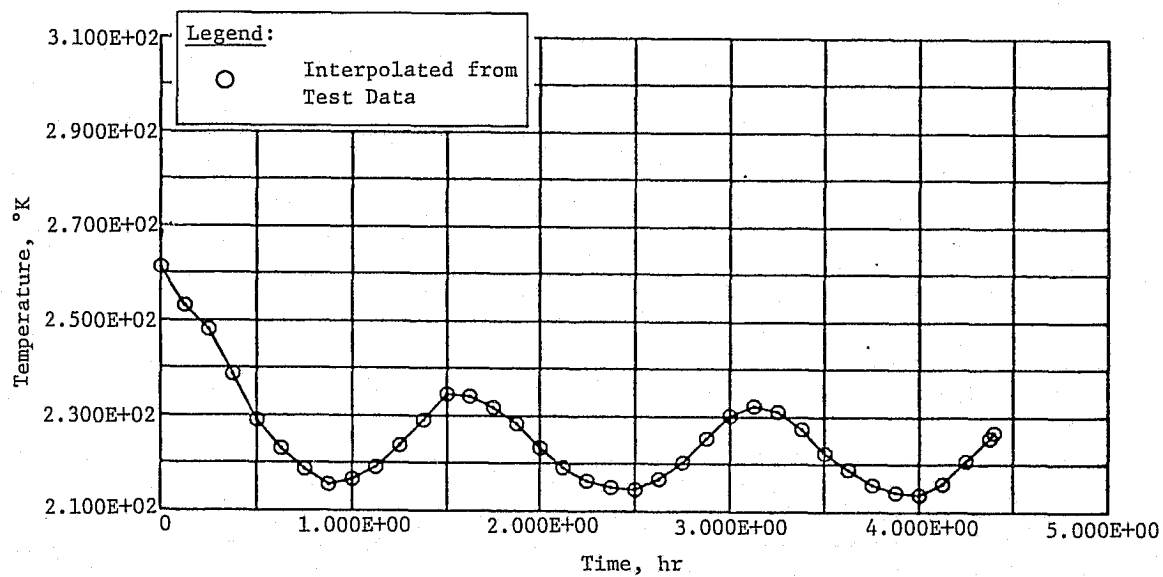


Figure A-38
Fluid Actuated Test Article Transient Cover Temperature for Case 2

IX.

CONCLUSION

The results of both louver system steady state and transient tests indicate the condition when component thermal control can be maintained. The analytical models developed to correlate the test data are capable of predicting the operational characteristics of an interior louver system. The bimetallic actuated louver system operated as expected. It was able to maintain component temperatures below 305°K (90°F) while dissipating 15 W of power to a cover at a temperature of approximately 289°K (60°F) or dissipating 30 W to a cover at approximately 256°K (0°F). Also there was no detectable time lag between component baseplate temperature and the blade response.

The operation of the fluid actuated louver system test article was affected by the actuator design. The desirable operating temperature range of the louver system had to be lowered to be compatible with the actuator temperature range. This had an adverse affect on the capability of the louver system to reject heat because the radiation heat transfer mechanism depends on the absolute temperature level of the radiating bodies. This can be easily corrected in the actuator design by either using a different fluid or by pressurizing the existing Freon actuator with about 10 psi of GN_2 or He. A more critical characteristic of the actuator was the significant time lag involved for the actuator to respond to a temperature change of the component. This was attributed to the relatively slow heating of the Freon actuator vapor. This did not effect the original Viking thermal switch application of the actuator because the response to temperature change was not a critical factor. However, when response to temperature change is critical, such as the louver system, then this type of actuator may not be adequate.

X.

REFERENCES

1. R. J. Conner, *et. al*: *Martin Marietta Thermal Analysis System (MITAS)*. MDS-SPLPD-71-FD238. Martin Marietta Corporation, Denver, Colorado, June 1971.
2. J. F. Parmer and D. L. Buskirk: *Thermal Control Characteristics of Interior Louver Panels*. ASME Paper 67-HT-64.
3. J. H. Wise: "Environments Pursuant to Contract NAS8-30746". GFP Memorandum EP44(74-139), National Aeronautics and Space Administration, Marshall Space Flight Center, Huntsville, Alabama, June 11, 1974.

Test
Report

October 1975

**HEAT PIPE
RADIATOR/THERMAL
CONDITIONING PANEL**

MARTIN MARIETTA CORPORATION
Box 179
Denver, Colorado 80201

CONTENTS

	<u>Page</u>
I. INTRODUCTION	B-1
II. SUMMARY	B-3
III. OBJECTIVE	B-4
IV. TEST DESCRIPTION	B-5
A. Test Article Description	B-6
B. Test Control and Instrumentation	B-18
C. Chamber Installation	B-24
V. TEST FACILITY	B-29
VI. TESTING	B-34
A. Hot Case Tests, 238.66°K Shroud	B-34
B. Cold Case Tests, 194.29°K Shroud	B-65
C. Transient Tests	B-82
D. 144°K Shroud Testing	B-93
VII. CONCLUSIONS	B-110
VIII. REFERENCES	B-111
ATTACHMENT A	B-112 thru B-116

Figure

B-1	Integrated Heat Pipe Systems	B-1
B-2	Heat Pipe Radiator Panel	B-7
B-3	Heat Pipe Radiator Panel	B-8
B-4	Heat Pipe Radiator Thermocouple Locations	B-10
B-5	Radiator Header Heat Pipe	B-12
B-6	Header Heat Pipe and Thermal Conditioning Panel	B-13
B-7	Header Heat Pipe and Thermal Conditioning Panel	B-14
B-8	Radiator Header Pipe Thermocouple Locations	B-15
B-9	Thermal Conditioning Panel Thermocouple and Heater Zone Locations	B-16
B-10	Thermal Conditioning Panel with Five Heater Zones of 200 W Capability	B-17
B-11	Environmental Shroud Used as a Radiator Sink	B-19
B-12	Radiator Shroud	B-20
B-13	Thermal Conditioning Panel Control Circuit	B-21
B-14	Control Panel with Digital Potentiometers	B-22
B-15	Instrumentation and Control System	B-23
B-16	Chamber Installation Schematic	B-25
B-17	Preliminary Chamber Installation	B-26
B-18	Header Pipe and Feeder Tube Installation Closeup	B-27
B-19	Final Chamber Installation	B-28
B-20	6x15 Ion/Titanium Sublimation Vacuum Chamber	B-30
B-21	Portable Gas Heat Exchanger	B-32
B-22	Portable Gas Heat Exchanger	B-33
B-23	Test 1, Hot Case, 100.1 W	B-35
B-24	Test 1, Hot Case, 100.1 W	B-36
B-25	Test 1, Hot Case, 200.26 W	B-37
B-26	Test 1, Hot Case, 200.26 W	B-38
B-27	Test 1, Hot Case, 299.88 W	B-39
B-28	Test 1, Hot Case, 299.88 W	B-40
B-29	Test 1, Hot Case, 380.96 W	B-41
B-30	Test 1, Hot Case, 380.96 W	B-42
B-31	Test 1, Hot Case, 200.23 W	B-43
B-32	Test 1, Hot Case, 200.23 W	B-44
B-33	Test 1, Hot Case, Thermal Conditioning Panel	B-45
B-34	Test 1, Hot Case, Header Heat Pipe	B-46
B-35	Test 1, Hot Case, Radiator Heat Pipe No. 1	B-47
B-36	Test 1, Hot Case, Radiator Heat Pipe No. 2	B-48
B-37	Test 1, Hot Case, Radiator Heat Pipe No. 3	B-49
B-38	Test 1, Hot Case, Radiator Heat Pipe No. 4	B-50
B-39	Test 1, Hot Case, Radiator Heat Pipe No. 5	B-51
B-40	Test 1, Hot Case, Radiator Heat Pipe No. 6	B-52
B-41	Test 1, Hot Case, Skin	B-53
B-42	Test 1, Hot Case, Average Shroud	B-54
B-43	Test 1, Hot Case, Thermal Conditioning Panel	B-55
B-44	Test 1, Hot Case, Header Heat Pipe	B-56
B-45	Test 1, Hot Case, Radiator Heat Pipe No. 1	B-57

B-46	Test 1, Hot Case, Radiator Heat Pipe No. 2	B-58
B-47	Test 1, Hot Case, Radiator Heat Pipe No. 3	B-59
B-48	Test 1, Hot Case, Radiator Heat Pipe No. 4	B-60
B-49	Test 1, Hot Case, Radiator Heat Pipe No. 5	B-61
B-50	Test 1, Hot Case, Radiator Heat Pipe No. 6	B-62
B-51	Test 1, Hot Case, Radiator Skin Temperature	B-63
B-52	Test 1, Hot Case, Shroud	B-64
B-53	Test 2, Cold Case, 200.39 W	B-66
B-54	Test 2, Cold Case, 200.39 W	B-67
B-55	Test 2, Cold Case, 398.27 W	B-68
B-56	Test 2, Cold Case, 398.27 W	B-69
B-57	Test 2, Cold Case, 499.92 W	B-70
B-58	Test 2, Cold Case, 499.92 W	B-71
B-59	Test 2, Cold Case, Thermal Conditioning Panel	B-72
B-60	Test 2, Cold Case, Header Heat Pipe	B-73
B-61	Test 2, Cold Case, Radiator Heat Pipe No. 1	B-74
B-62	Test 2, Cold Case, Radiator Heat Pipe No. 2	B-75
B-63	Test 2, Cold Case, Radiator Heat Pipe No. 3	B-76
B-64	Test 2, Cold Case, Radiator Heat Pipe No. 4	B-77
B-65	Test 2, Cold Case, Radiator Heat Pipe No. 5	B-78
B-66	Test 2, Cold Case, Radiator Heat Pipe No. 6	B-79
B-67	Test 2, Cold Case, Radiator Skin Temperature	B-80
B-68	Test 2, Cold Case, Shroud	B-81
B-69	Test 3, Transient Environment, Thermal Conditioning Panel	B-83
B-70	Test 3, Transient Environment, Header Heat Pipe	B-84
B-71	Test 3, Transient Environment, Radiator Heat Pipe No. 1	B-85
B-72	Test 3, Transient Environment, Radiator Heat Pipe No. 2	B-86
B-73	Test 3, Transient Environment, Radiator Heat Pipe No. 3	B-87
B-74	Test 3, Transient Environment, Radiator Heat Pipe No. 4	B-88
B-75	Test 3, Transient Environment, Radiator Heat Pipe No. 5	B-89
B-76	Test 3, Transient Environment, Radiator Heat Pipe No. 6	B-90
B-77	Test 3, Transient Environment, Radiator Skin Temperature	B-91
B-78	Test 3, Transient Environment, Shroud	B-92
B-79	Test 4, 144°K Shroud, 599.28 W	B-94
B-80	Test 4, 144°K Shroud, 599.28 W	B-95
B-81	Test 4, 144°K Shroud, 400 W	B-96
B-82	Test 4, 144°K Shroud, 400 W	B-97
B-83	Test 4, 144°K Shroud, 499.84 W	B-98
B-84	Test 4, 144°K Shroud, 499.84 W	B-99
B-85	Test 4, Thermal Conditioning Panel	B-100
B-86	Test 4, Header Heat Pipe	B-101
B-87	Test 4, Radiator Heat Pipe No. 1	B-102

B-88	Test 4, Radiator Heat Pipe No. 2	B-103
B-89	Test 4, Radiator Heat Pipe No. 3	B-104
B-90	Test 4, Radiator Heat Pipe No. 4	B-105
B-91	Test 4, Radiator Heat Pipe No. 5	B-106
B-92	Test 4, Radiator Heat Pipe No. 6	B-107
B-93	Test 4, Radiator Skin Temperature	B-108
B-94	Test 4, Shroud	B-109

Table

B-1	Thermal Conditioning Panel/Heat Pipe Radiator Test Summary	B-5
B-2	Planned Thermal Conditioning Panel/Heat Pipe Radiator Test Summary	B-6
B-3	Thermocouple Comparison	B-9
B-4	Instrumentation Summary	B-18
B-5	Operating Characteristics for the Solar-Thermal/Vacuum Chamber	B-29
B-6	Additional Capabilities of the Solar-Thermal/Vacuum Chamber	B-31
B-7	Nomenclature Used for All Data Presentation	B-34

I. INTRODUCTION

The application of heat pipes to thermal control of satellites has grown significantly in recent years. In most cases the heat pipe was used only as a transport medium. This test was intended to demonstrate the ability of an integrated heat pipe system to collect, transport, distribute, and control heat from the source to the sink. This method can result in significant weight reductions while improving the system performance and reliability if the heat pipes perform as required.

The ability to control a system of this nature requires the use of variable conductance heat pipes (VCHP). The VCHP has been, and still remains, the pacing item for the development and flight of an integrated heat pipe system. Configuration (a) of Figure B-1 was tested.

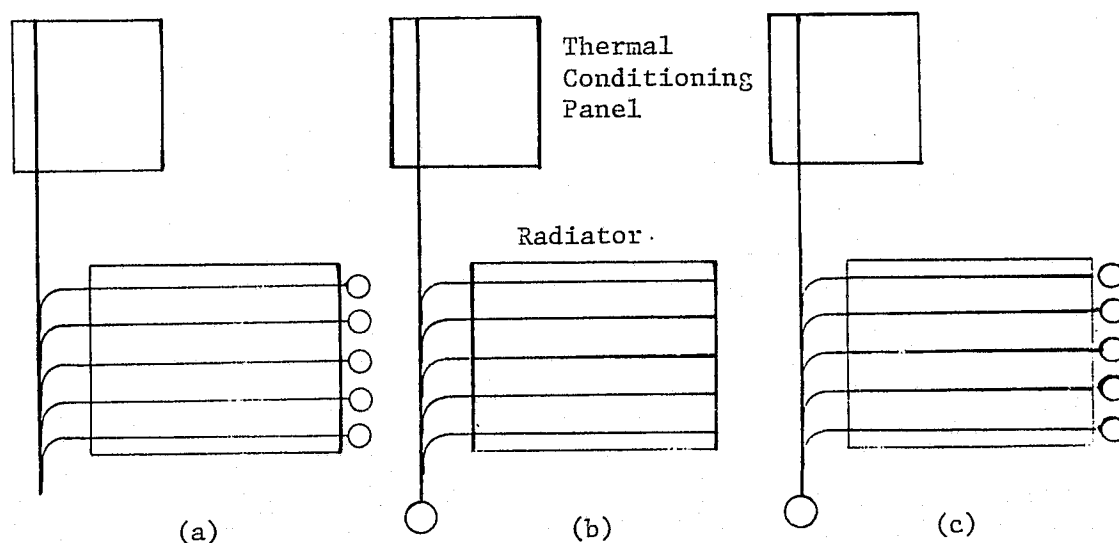


Figure B-1 Integrated Heat Pipe Systems

Each of the systems shown in Figure B-1 uses a collector panel called a thermal conditioning panel. This panel has integral heat pipes enabling the application of nonuniform heating while controlling the temperature differential over the panel to a small value. For low heat loads, this panel would provide three of the four functions presented above.

Additional rejection capability can be achieved with large heat loads by adding a separate radiator with integral control capability in the radiator feeder pipes, in the header pipe, or both.

Our original plan was to test configuration (c) (Figure B-1); however, performance problems were experienced with the government furnished property (GFP) header pipe. Hence, configuration (a) was tested. We accomplished this by procuring a fixed conductance header pipe. To facilitate installation into the chamber, the header pipe had a 90° bend in the adiabatic section of the heat pipe.

II.

SUMMARY

Testing of the heat pipe radiator/thermal conditioning panel was conducted in the 6x15 thermal vacuum chamber at Martin Marietta's Space Simulation Laboratory. Three series of tests were conducted to demonstrate the system capability. This was the first series of vacuum testing of the radiator which performed flawlessly throughout the test program. The design of the radiator and the thermal conditioning panel was limited to 324.8°K because ammonia was used as the working fluid in each unit. This resulted in the test plan being modified to perform an additional series of testing to further demonstrate the radiator capabilities.

III. OBJECTIVE

The overall objective of the Space Tug Thermal Control Follow-On contract was to experimentally demonstrate that the thermal control subsystem concepts selected and defined in Phase I of the contract were viable, to obtain data for refining analytical models, and to optimize concept configurations and performance.

The objective of this test was to demonstrate and measure the performance of an integrated heat pipe thermal control system. The special test objectives were to:

- 1) Measure performance of the system under a constant thermal environment on the radiator at constant heat loads to the thermal conditioning panel to obtain steady-state results. Hot and cold radiator environments were tested.
- 2) Measure the performance of the system under a cyclic thermal environment with a constant heat load to the thermal conditioning panel.

IV. TEST DESCRIPTION

These objectives (Sec. III) were accomplished by conducting the testing consistent with the radiator and thermal conditioning panel design requirements. The upper temperature limit of 324.8°K required a modification to the original test plan to avoid over temperature of the thermal conditioning panel. Table B-1 summarizes the tests that were conducted. Table B-2 presents the original test plan summary.

*Table B-1
Thermal Conditioning Panel/Heat Pipe Radiator Test Summary*

	Testing Conducted			
	1	2	3	4
1. Type of Test	Transient to Steady-State	Transient to Steady-State	Cyclical 1.5 hr Period	Transient to Steady-State
2. Conditioning Panel Heating Level, W	100	200	200	600
	200	400	400	400
	300	500		500
	380			
	200			
3. Radiator Sink Temperature, °K	Constant 238.66	Constant 194.29	Cyclical 238.7 to 194	Constant 144.29
4. Simulated Flight Environment	Hot Environment	Cold Environment	Orbital Cyclical	Colder Environment

Table B-2

Planned Thermal Conditioning Panel/Heat Pipe Radiator Test Summary

	Test		
	1	2	3
1. Type of Test	Transient to Steady-State	Transient to Steady-State	Cyclic, with 1.5-hr Period
2. Conditioning Panel Heating Level, W	100	200	200
	200	400	400
	300	600	600
	400	800	
	200	1000	
3. Radiator Sink Temperature, °K	Constant 238.66	Constant 194.29	Cyclic, 238.7 to 194
4. Simulated Flight Environment	Hot Environment Orbit	Cold Environment Orbit	Variable Environment Orbit

The first two series of tests were conducted at steady-state shroud temperatures of 238.7°K and 194.3°K while varying the power to the levels shown until the temperatures achieved steady-state. The third series of testing was conducted at constant power levels while varying the shroud temperature in a sine wave manner between 238.7 and 194.3°K with a 90 min period. The fourth series of testing was conducted at a shroud temperature of 144.3°K at three power levels.

A. TEST ARTICLE DESCRIPTION

1. Heat Pipe Radiator

The radiator panel (Figures B-2 and B-3) is an aluminum panel comprised of six variable conductance feeder heat pipes. The evaporator section of each pipe is bent 90° from the condenser to permit attachment to the header pipe. The radiator is 1.22 by 1.83 m (4 by 6 ft) with a total radiating area of 2.23 m² (24 ft²) excluding the heat pipe and reservoir areas which extend beyond the radiator panel. The feeder pipes used ammonia as the working fluid and nitrogen as the noncondensable control gas.

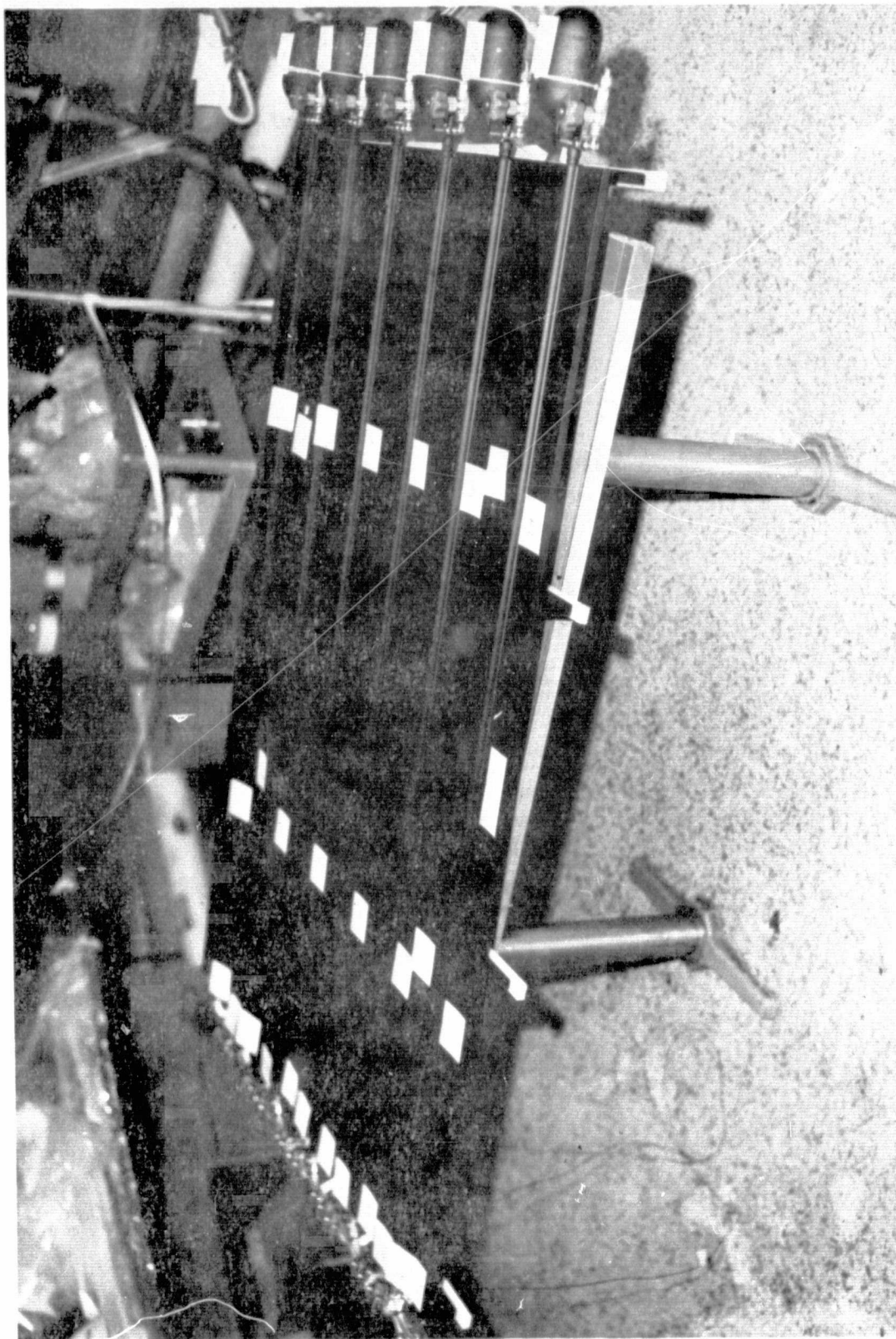


Figure B-2

Figure B-2 Heat Pipe Radiator Panel

B-7

REPRODUCIBILITY OF THE
ORIGINAL PAGE IS POOR

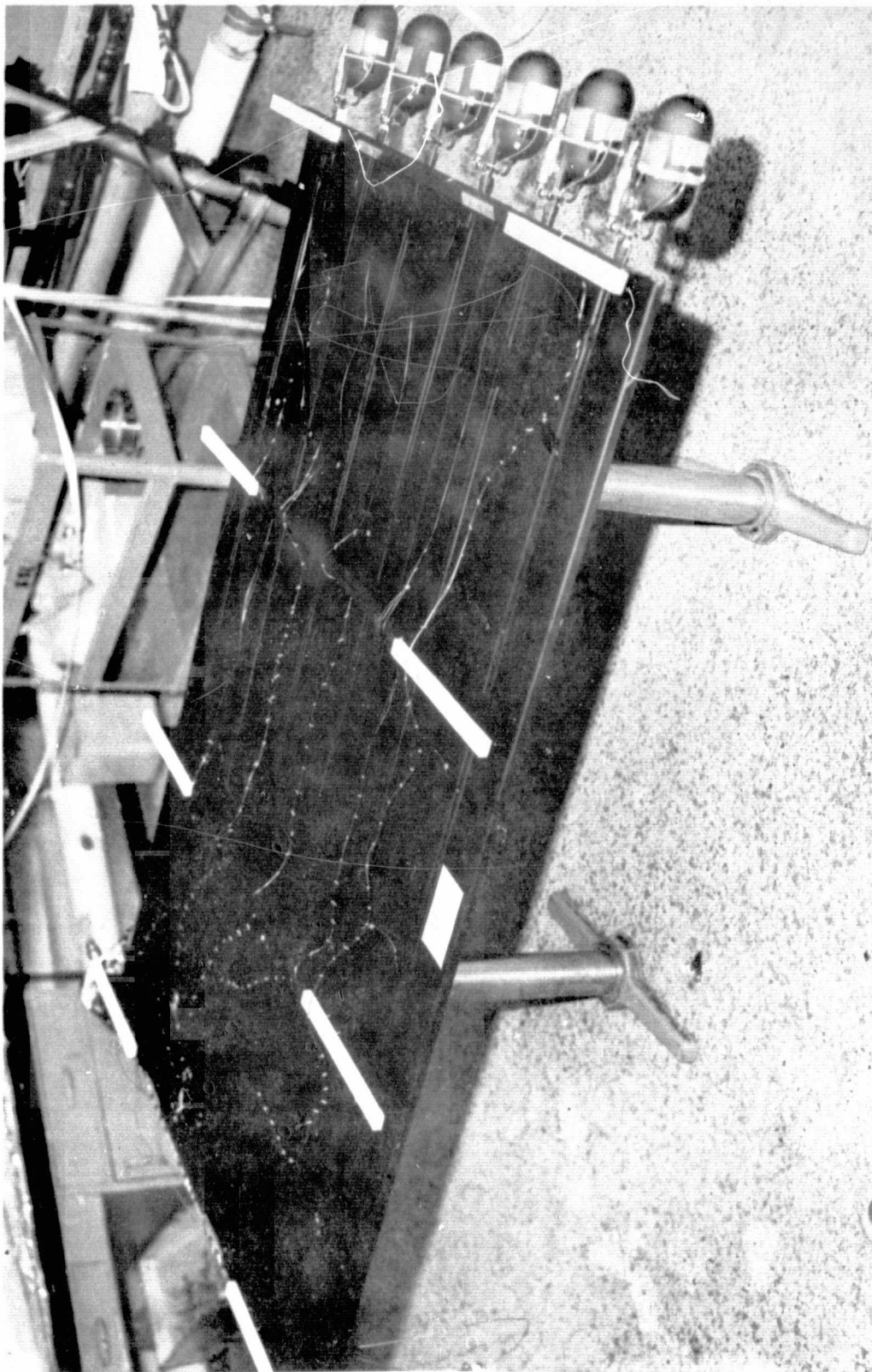


Figure B-3 Heat Pipe Radiator Panel

Figure B-3

B-8

REPRODUCIBILITY OF THE
ORIGINAL PAGE IS POOR

The radiator panel was developed for NASA-MSFC under contract NAS8-29905 by Grumman Aerospace Corporation. The radiator was then supplied GFP to Martin Marietta for this test program. Reference 1 describes the design, build, and test of the radiator.

The radiator panel was received with 38 copper-constantan thermocouples installed on the radiator. An attempt was made to use these thermocouples but proved impractical due to the facility instrumentation capabilities and cost of supporting hardware. The laboratory is setup to use chromel-constantan thermocouples. The use of copper constantan would have required the modification of the recorders, chamber feedthroughs, connecting wiring, etc. The modifications and unnecessary cost items associated with using the existing thermocouples were avoided by installing thermocouples compatible with the existing instrumentation system.

The radiator was instrumented with chromel-constantan thermocouples (Figure B-4). The thermocouple locations agree with the present thermocouple locations with some deletions and additions. A total of 34 thermocouples were installed. Table B-3 presents, for information purposes, a comparison of the thermocouples installed by Grumman versus those installed for this series of tests.

Table B-3
Thermocouple Comparison

GAC	MM	GAC	MM	GAC	MM	GAC	MM
1	NI	11	5	21	15	31	27
2	NI	12	NI	22	17	32	28
3	1	13	7	23	18	33	29
4	2	14	8	24	19	34	30
5	NI	15	9	25	20	35	31
6	3	16	10	26	21	36	32
7	NI	17	11	27	22	37	33
8	NI	18	12	28	23	38	34
9	4	19	13	29	24		
10	NI	20	14	30	25		

Notes: 1) NI - Not installed

2) Thermocouples 6, 16, and 26 do not have corresponding GAC thermocouples.

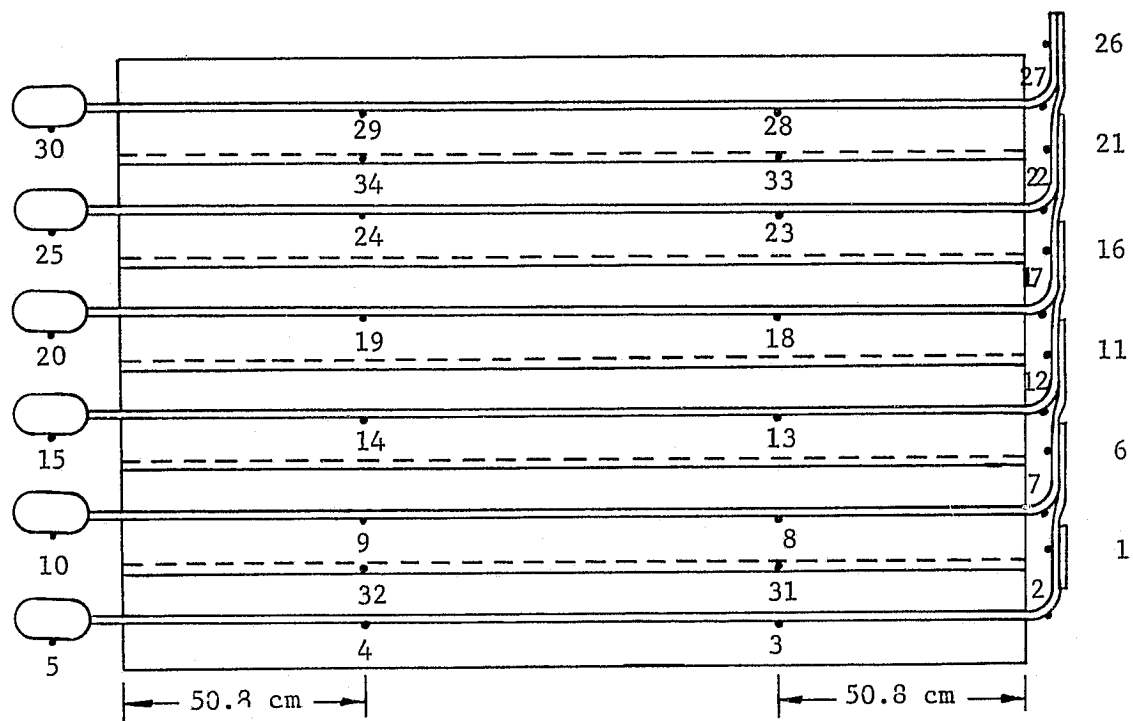


Figure B-4 Heat Pipe Radiator Thermocouple Locations

After installing the thermocouples, an insulation blanket was assembled from 20 layers of vented aluminized Mylar with nylon netting separators. The blanket was sized to drape over the radiator sides and the reservoir end to form an enclosure with the flat plate shroud. A second 20-layer blanket was fabricated for completing the enclosure at the header pipe end of the radiator.

2. Header Heat Pipe

The header heat pipe was purchased from Isothermics Incorporated. This pipe (Figures B-5, B-6, B-7 and B-8) was designed to carry a 1-kW load using Genetron 31-114 as the working fluid. The pipe was made of copper with mounting provisions integral to the design. The pipe was designed for use in a 1 g environment and does not include a wick internal to the pipe.

Fifteen thermocouples were installed on the header pipe as shown in Figure B-8. Thermocouples 10 through 15 were matched with radiator thermocouples 1, 6, 11, 16, 21, and 26 respectively.

The header pipe was checked out at Isothermics before shipment to Denver. Attachment A presents the data resulting from that checkout.

3. Thermal Conditioning Panel (TCP)

The thermal conditioning panel was developed for NASA-MSFC by Donald W. Douglas Laboratories under contract NAS8-28639. The panel was government furnished property (GFP) supplied to Martin Marietta by MSFC. References 2 and 3 describe the design, build, and test of the panel. The panel was designed as an isothermal panel with 12 heat pipes between 2 aluminum panels. Ammonia was used as the working fluid.

The thermal conditioning panel (TCP) was instrumented (Figure B-9) with 11 thermocouples. In addition, five heater zones of 200 W capability each were added (See Figure B-10). All heater zones were controllable over the 200 W range. A heater tape 0.95 cm (0.375 in.) wide was applied to the TCP covering the entire area of each zone.

The application of heat to the panel agreed with the recommended 0.31 W/cm^2 (2 W/in.^2). Removal of the applied heat load at the header pipe interface was accomplished at a flux density of 0.66 W/cm^2 (5.56 W/in.^2). This appears to be consistent with previous testing conducted under the original build and test contract to Donald W. Douglas Laboratories.

A 20-layer aluminized Mylar blanket was fabricated to provide an insulated enclosure for the TCP and the header pipe evaporator section. This blanket was installed after chamber installation of the TCP.

Figure B-5
B-12

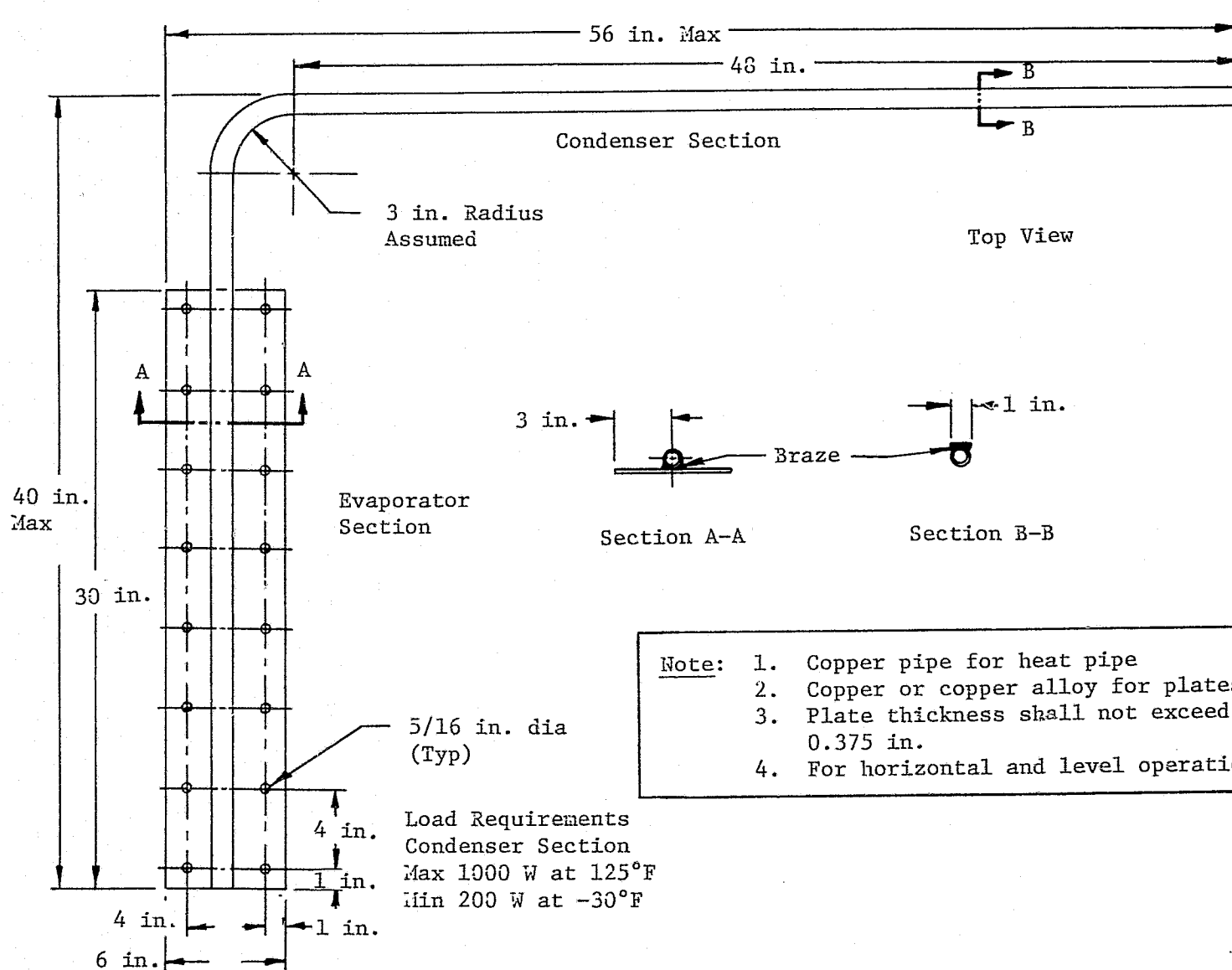


Figure B-5 Radiator Header Heat Pipe



Figure B-6 Header Heat Pipe and Thermal Conditioning Panel

REPRODUCIBILITY OF THE
ORIGINAL PAGE IS POOR

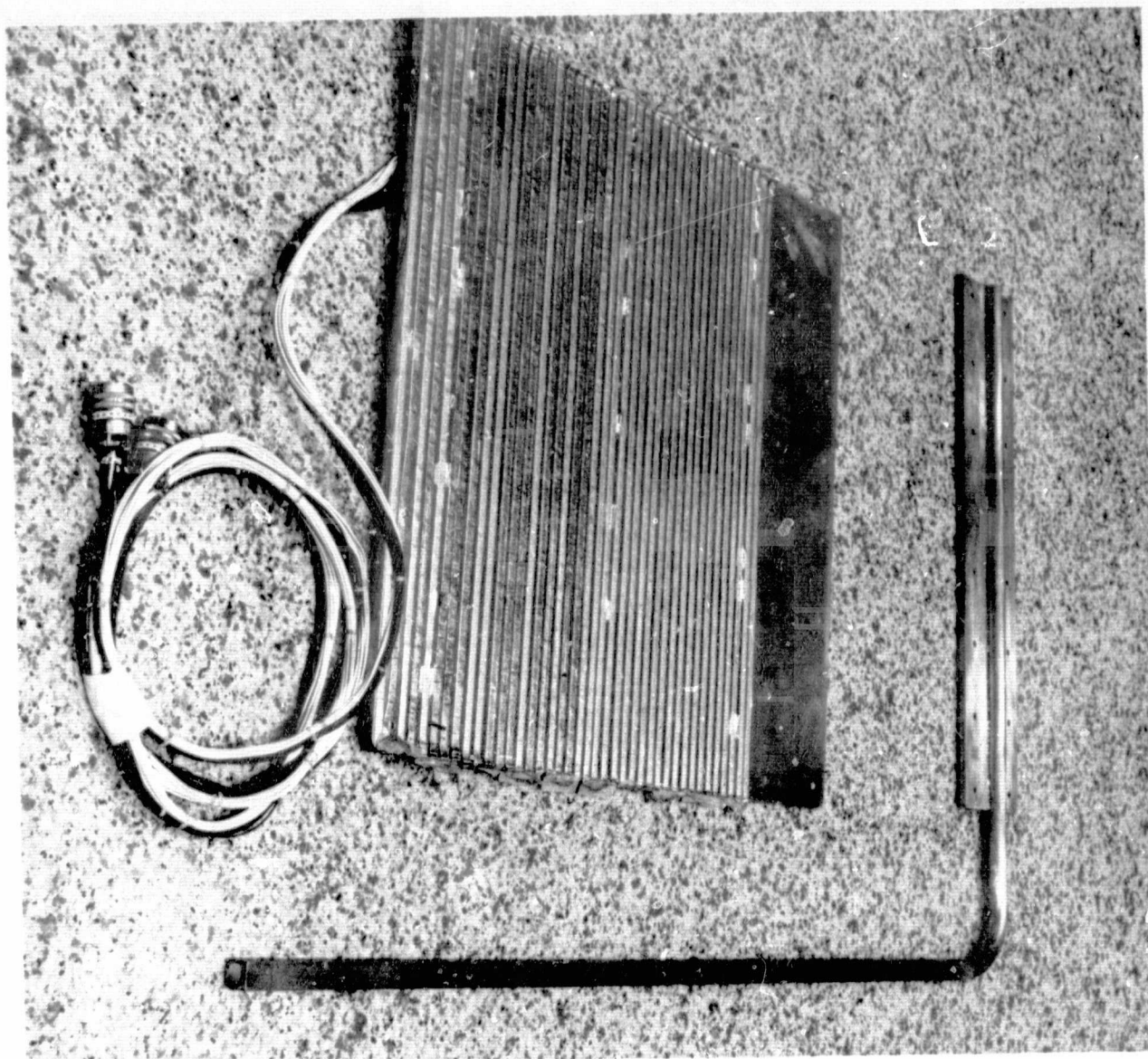
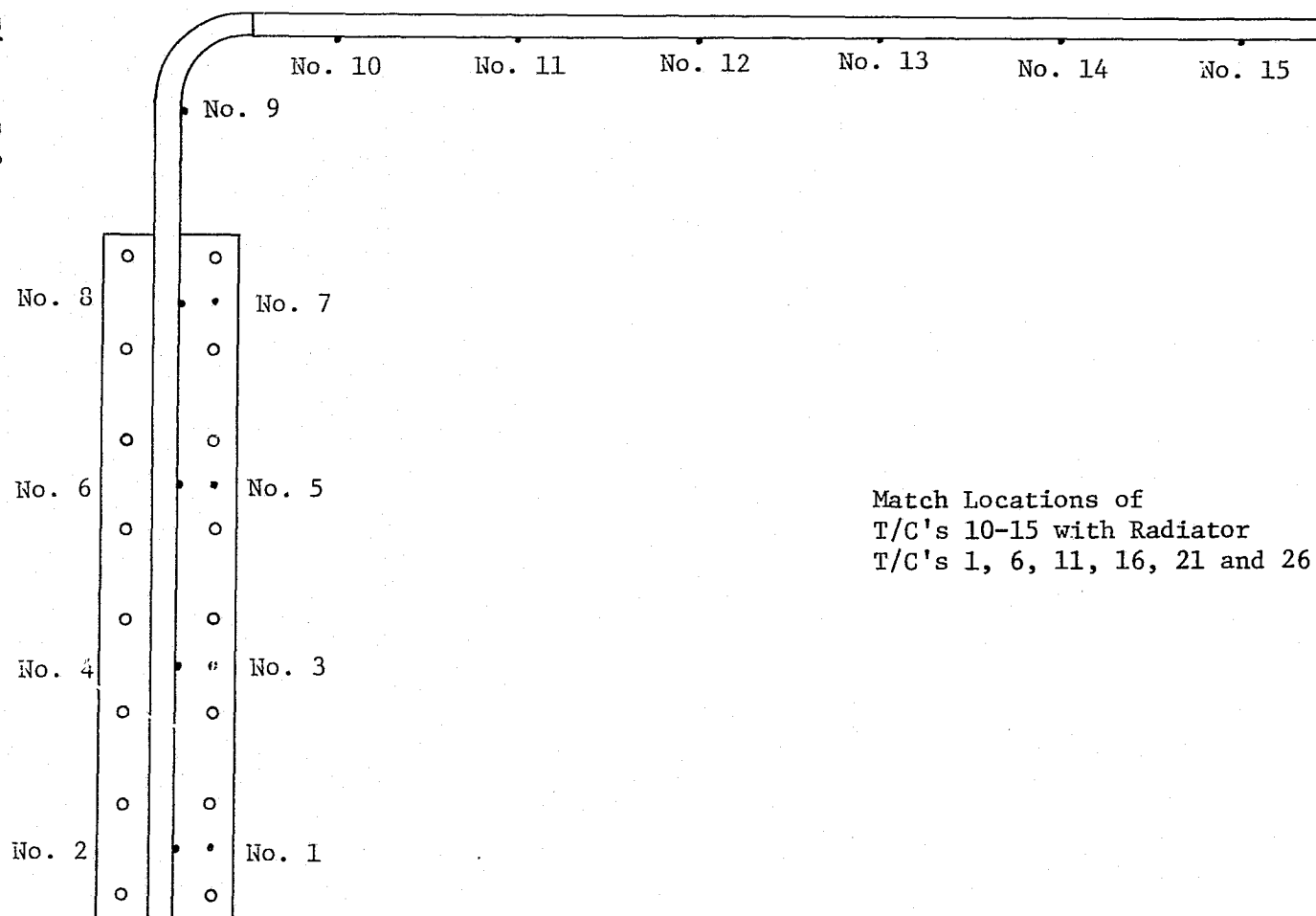


Figure B-7 Header Heat Pipe and Thermal Conditioning Panel

Figure B-8



Match Locations of
T/C's 10-15 with Radiator
T/C's 1, 6, 11, 16, 21 and 26

B-15

Figure B-8 Radiator Header Pipe Thermocouple Locations

B-16

Figure B-9

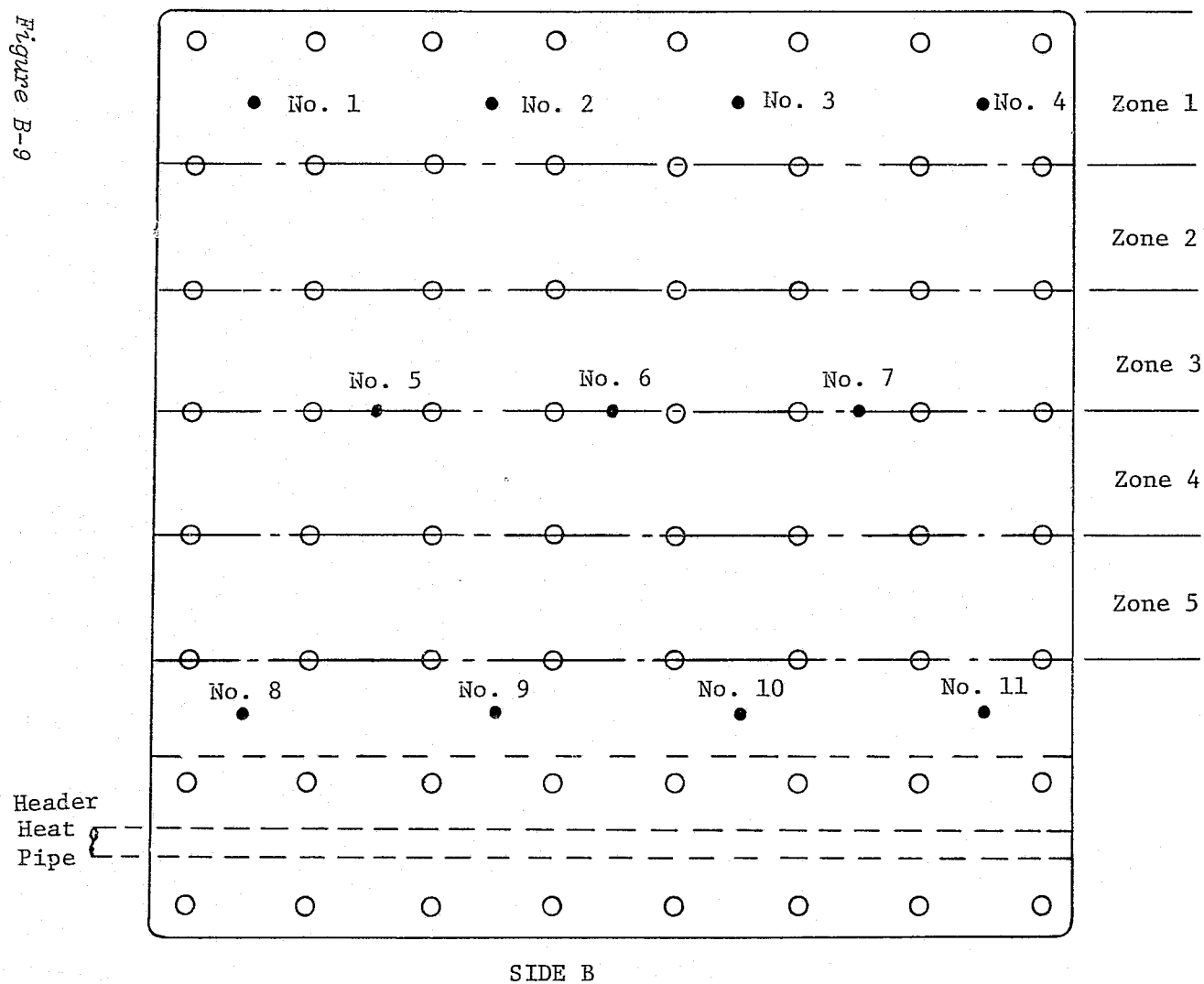


Figure B-9 Thermal Conditioning Panel Thermocouple and Heater Zone Locations

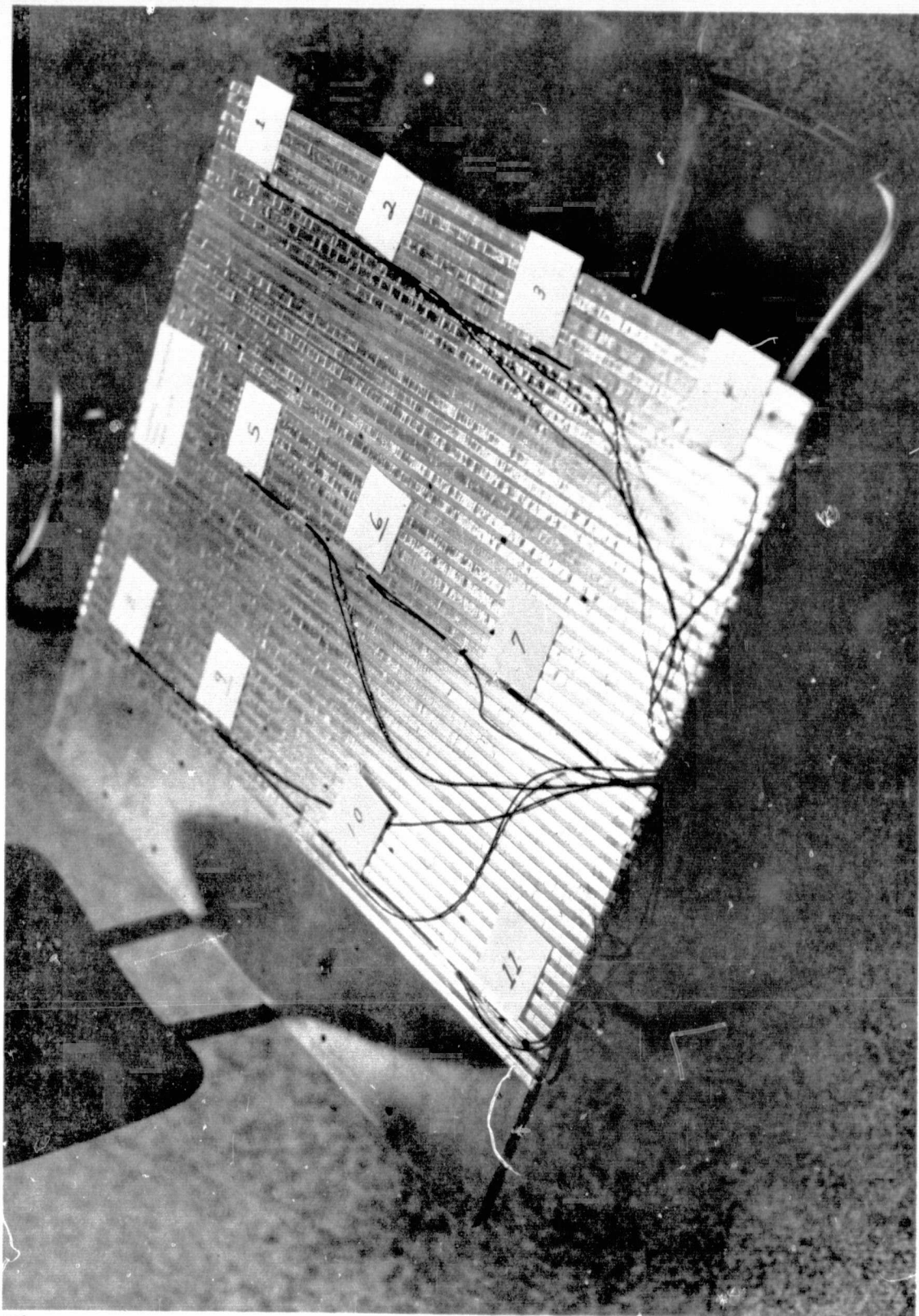


Figure B-10

Figure B-10 Thermal Conditioning Panel with Five Heater Zones of 200 W Capability

4. Environmental Shroud

A flat shroud (Figure B-11) was used in this test as the radiator radiation sink. The shroud was 122x213 cm (48x84 in.) and was instrumented with 10 thermocouples (Figure B-12). The shroud was required to enable meeting the 1.5-hr environmental temperature cycle. The chamber shroud would not respond fast enough over the required temperature range in the 1.5-hr cycle time. The flat shroud was insulated on the chamber side to avoid cooling down the present chamber shroud. This minimized the heat load on the gas heat exchanger system used to control the shroud temperature.

B. TEST CONTROL AND INSTRUMENTATION

The heater control of the test was accomplished by using an existing regulated dc power supply and control panel shown schematically in Figure B-13. Figure B-14 shows the control panel including digital potentiometers for controlling each zone. Voltage and current measurements were obtained by selecting the desired channel and recording the appropriate meter outputs. Figure B-15 shows the overtemperature controller on top of the control panel which was wired to interrupt power to the heaters on the TCP when it exceeded 324.8°K. Also shown are the multi-point recorders used in recording the data. The data were recorded manually on summary sheets during the test.

The number of thermocouples and heaters was quantized to be consistent with previous testing and to provide data consistent with the overall test objectives. Table B-4 summarizes the instrumentation requirements for each test article and the chamber shroud.

Table B-4
Instrumentation Summary

Item	Thermocouples	Heaters
Radiator	34	
Header Pipe	15	
Thermal Conditioning Panel	11	5
Shroud	<u>10</u>	—
Total	70	5

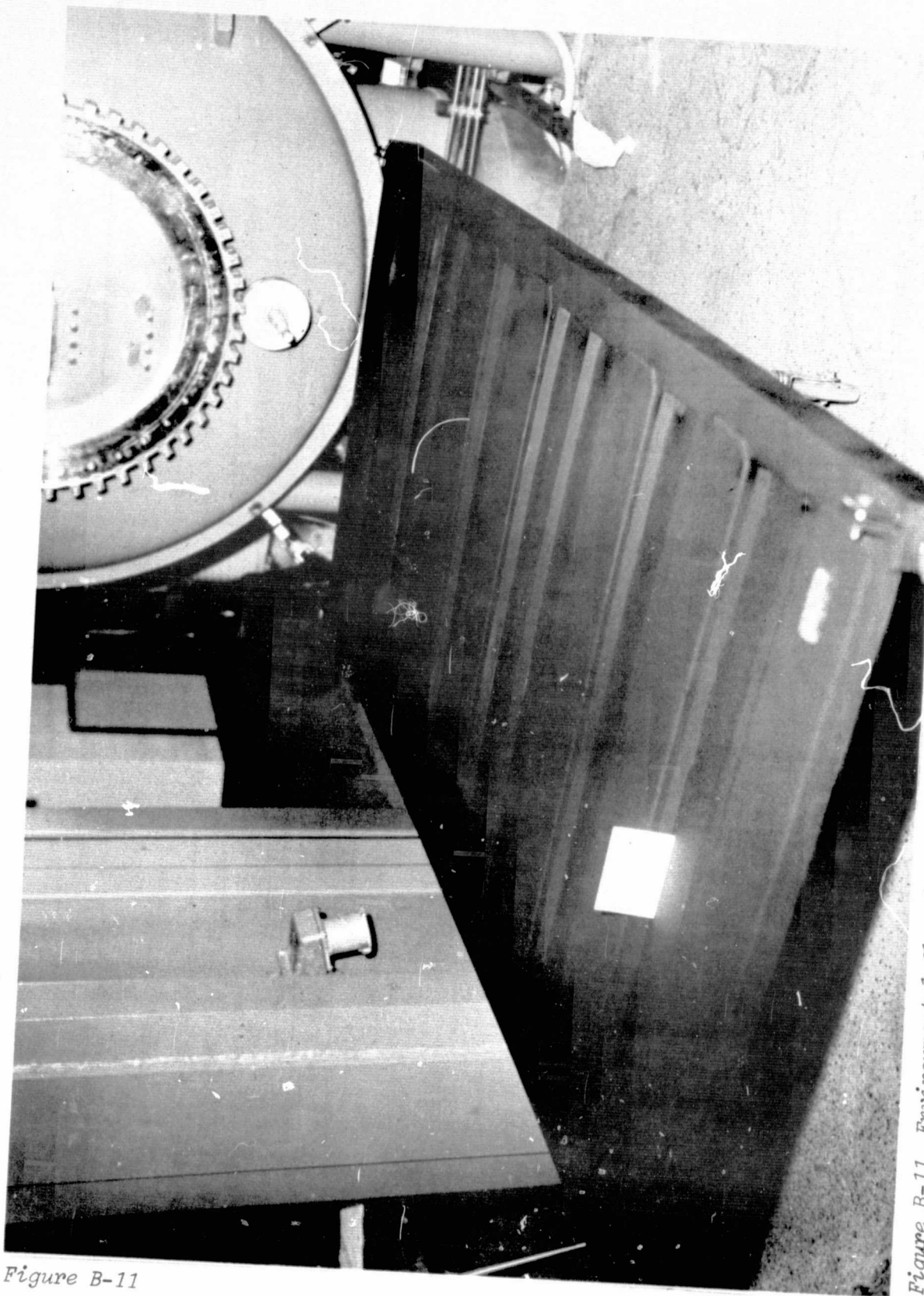
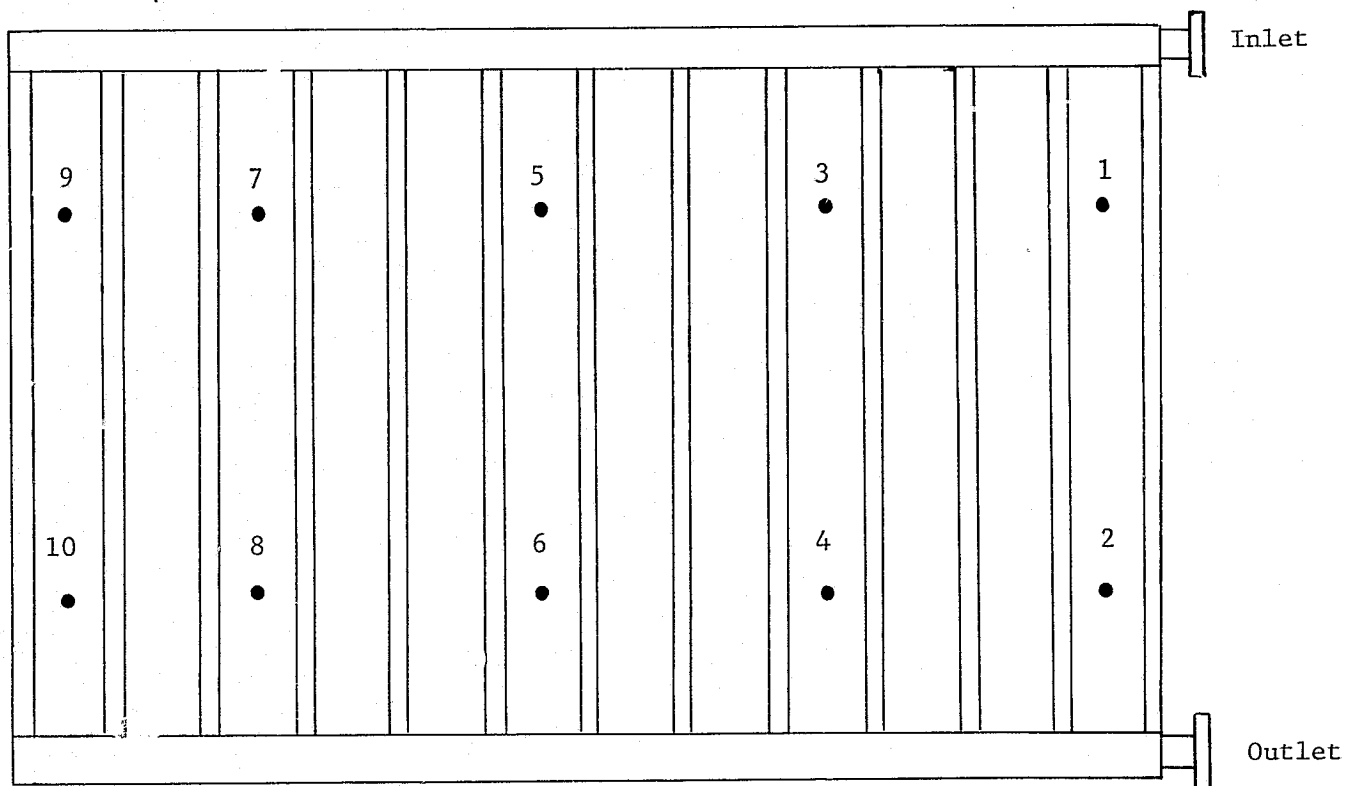


Figure B-11

Figure B-11 Environmental Shroud Used as a Radiator Sink

B-20

Figure B-12



Legend:

• Thermocouple Locations

Note: Temperature, °K

Figure B-12 Radiator Shroud

Figure B-13

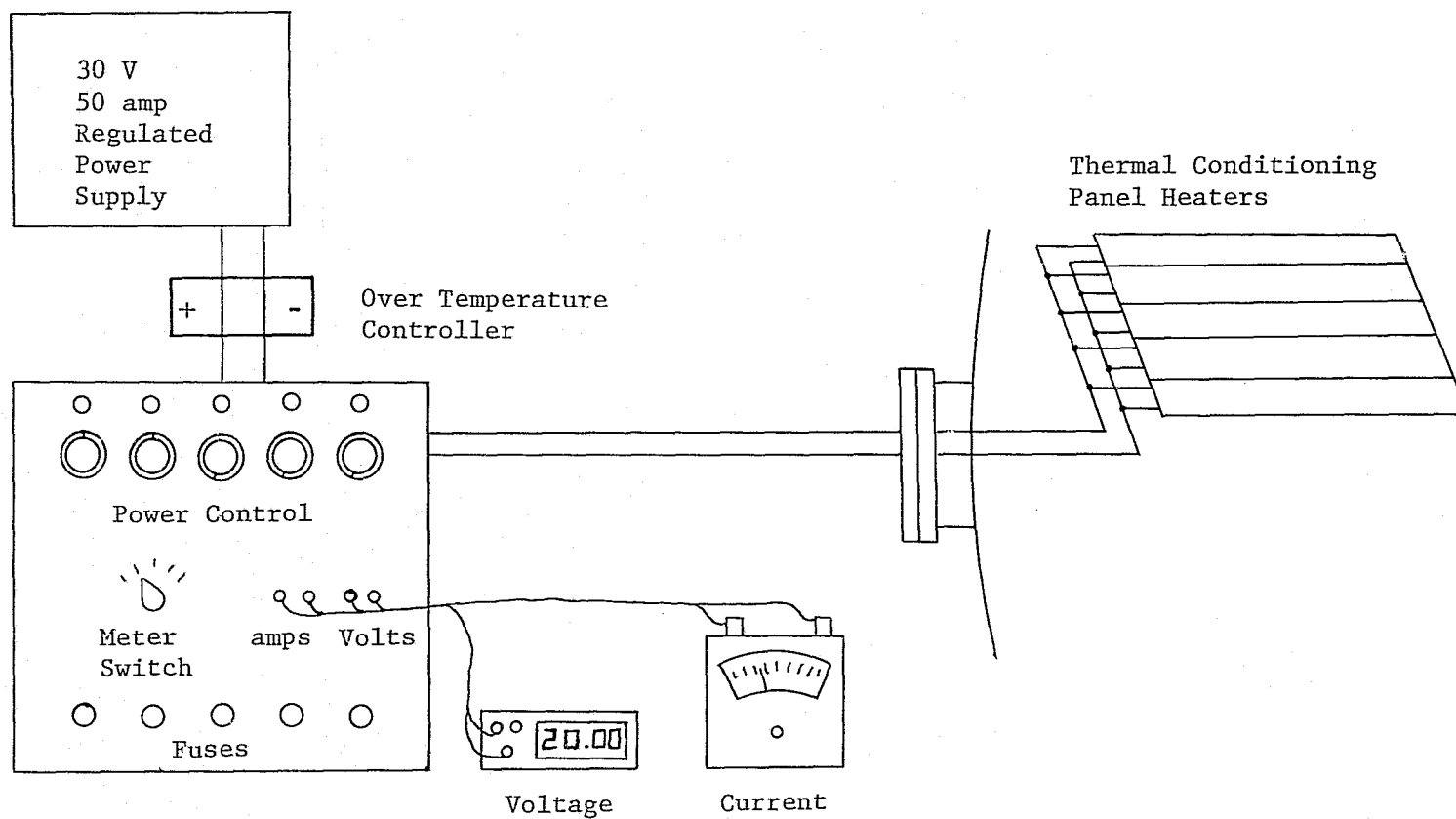


Figure B-13 Thermal Conditioning Panel Control Circuit

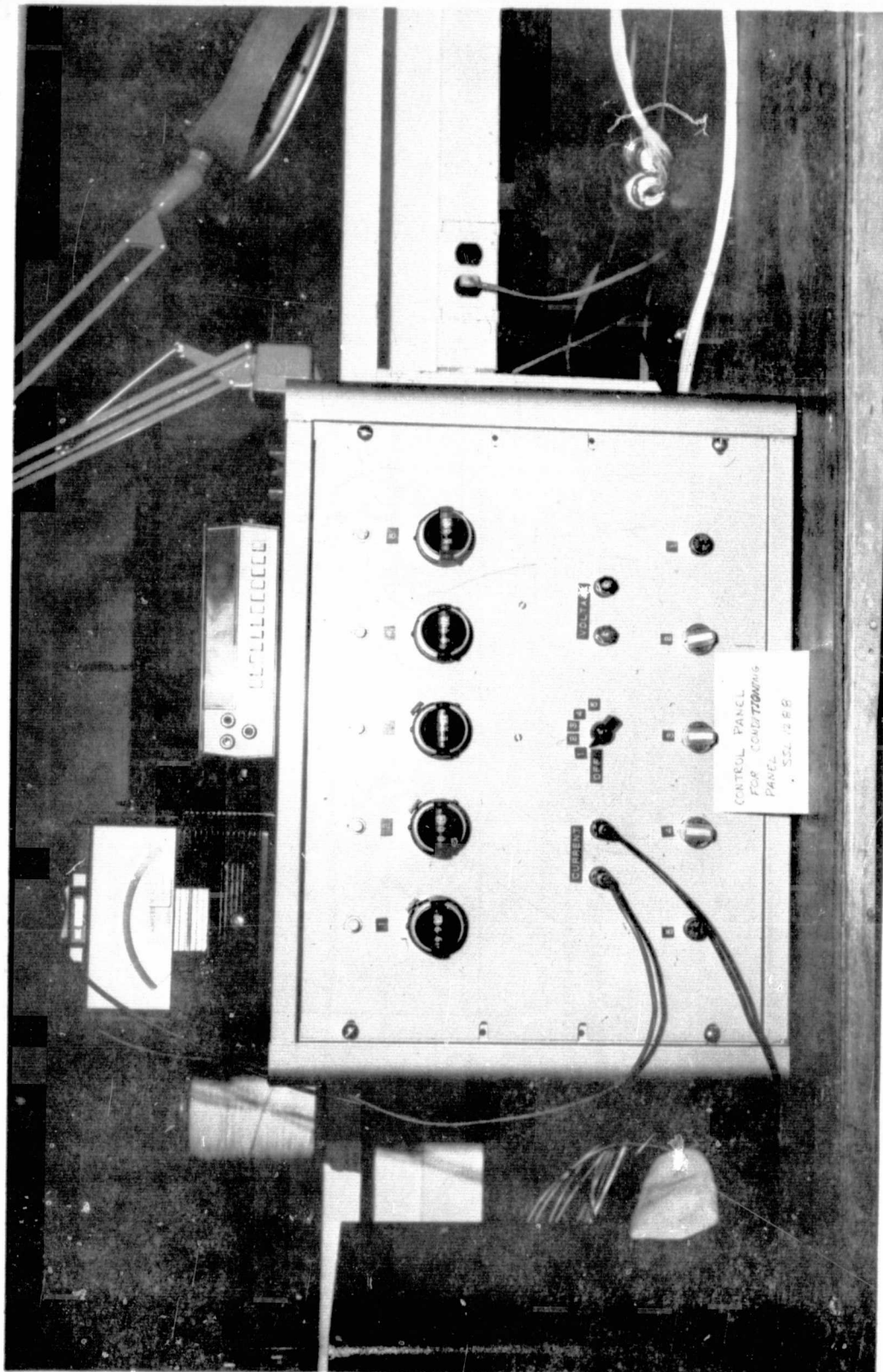


Figure B-14 Control Panel with Digital Potentiometers

Figure B-14

B-22

REPRODUCIBILITY OF THE
ORIGINAL PAGE IS POOR



Figure B-15

Figure B-15 Instrumentation and Control System

B-23

REPRODUCIBILITY OF THE
ORIGINAL PAGE IS POOR

The thermocouple data were recorded on 24-channel recorders. The radiator data required two recorders and permitted recording the TCP temperatures on the second recorder. The header pipe and shroud data were recorded on separate recorders. The heater power was recorded manually on separate data sheets. The accuracy of thermocouple recording was $\pm 1.4^{\circ}\text{K}$ ($\pm 2.5^{\circ}\text{F}$).

C. CHAMBER INSTALLATION

The three subassemblies were installed in the chamber as shown schematically in Figure B-16.

The radiator and thermal conditioning panel were suspended from the aluminum frame shown in Figure B-17. Figures B-2 and B-3 show the teflon blocks used to suspend the radiator. The header heat pipe condenser mounting surface was greased with a DC 29 heat sink compound before clamping to the radiator feeder pipes. The same compound was used to interface between the header pipe and the TCP before bolting the two units together (See Figure B-18).

The radiator, header pipe, and TCP were then leveled to ensure proper heat pipe operation. The shroud was installed 6.5 cm (4 in.) below the radiator completing the piping installation. After conducting a controls and instrumentation checkout, the radiator and shroud were enclosed by an insulation blanket comprised of 20 layers of 1/2 mil-vented double aluminized Mylar with nylon netting separators. This created an enclosure between the radiator and the shroud and minimized the influence of the chamber upon the test.

Figure B-19 shows the final installation with the TCP and line insulation installed. The radiator/shroud blanket is not visible in the figure.

Figure B-16

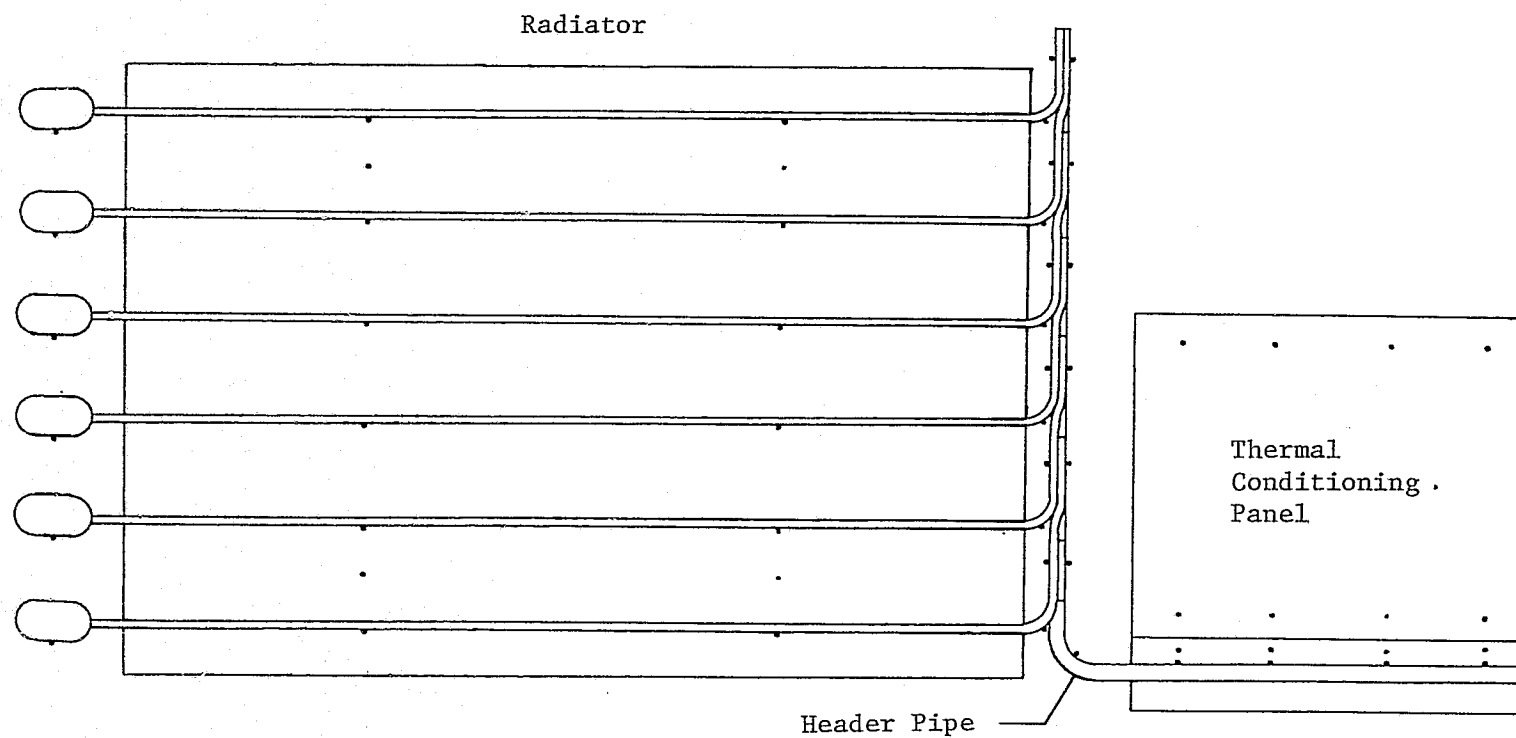


Figure B-16 Chamber Installation Schematic

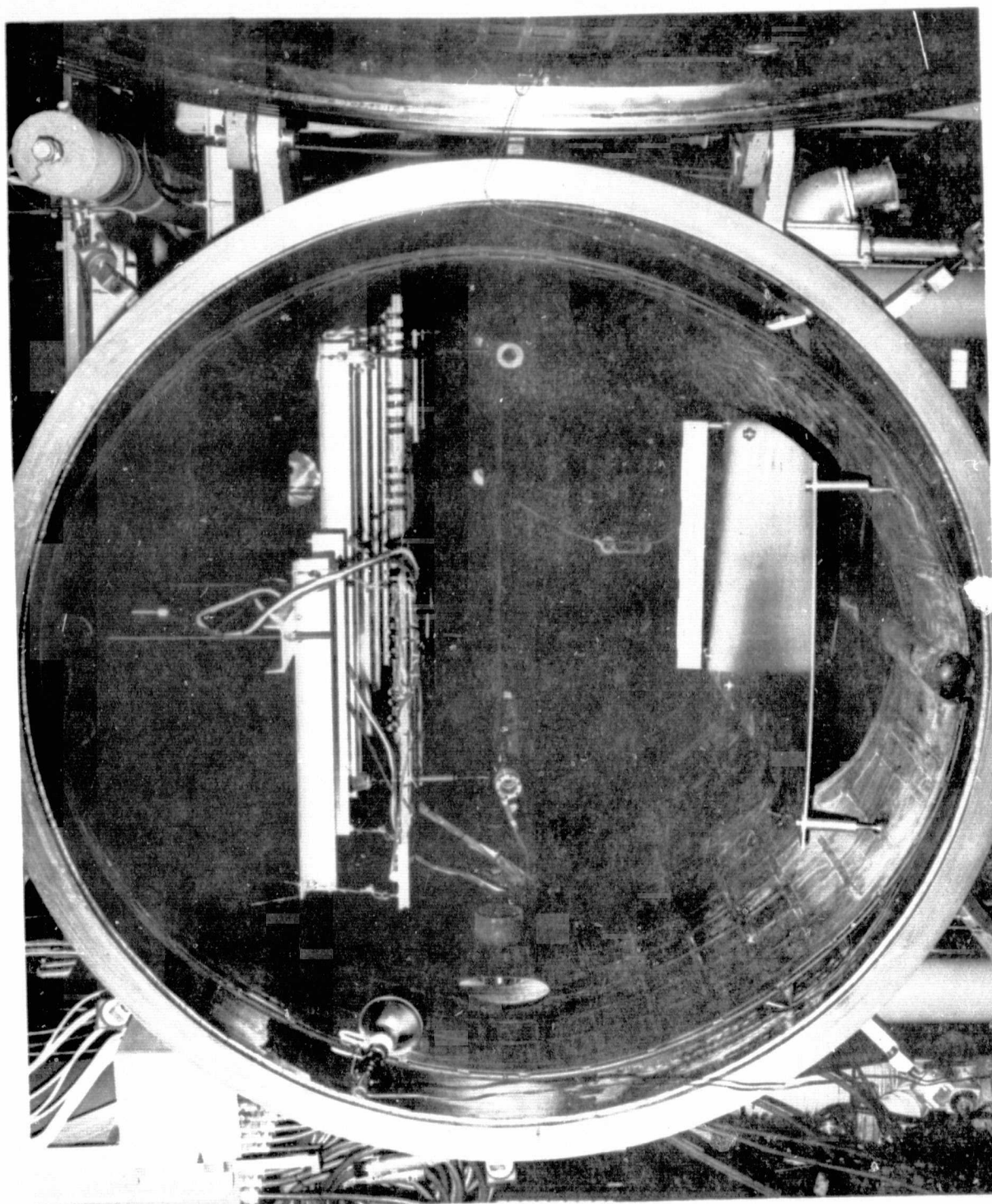


Figure B-17 Preliminary Chamber Installation

Figure B-17

B-26

REPRODUCIBILITY OF THE
ORIGINAL PAGE IS POOR

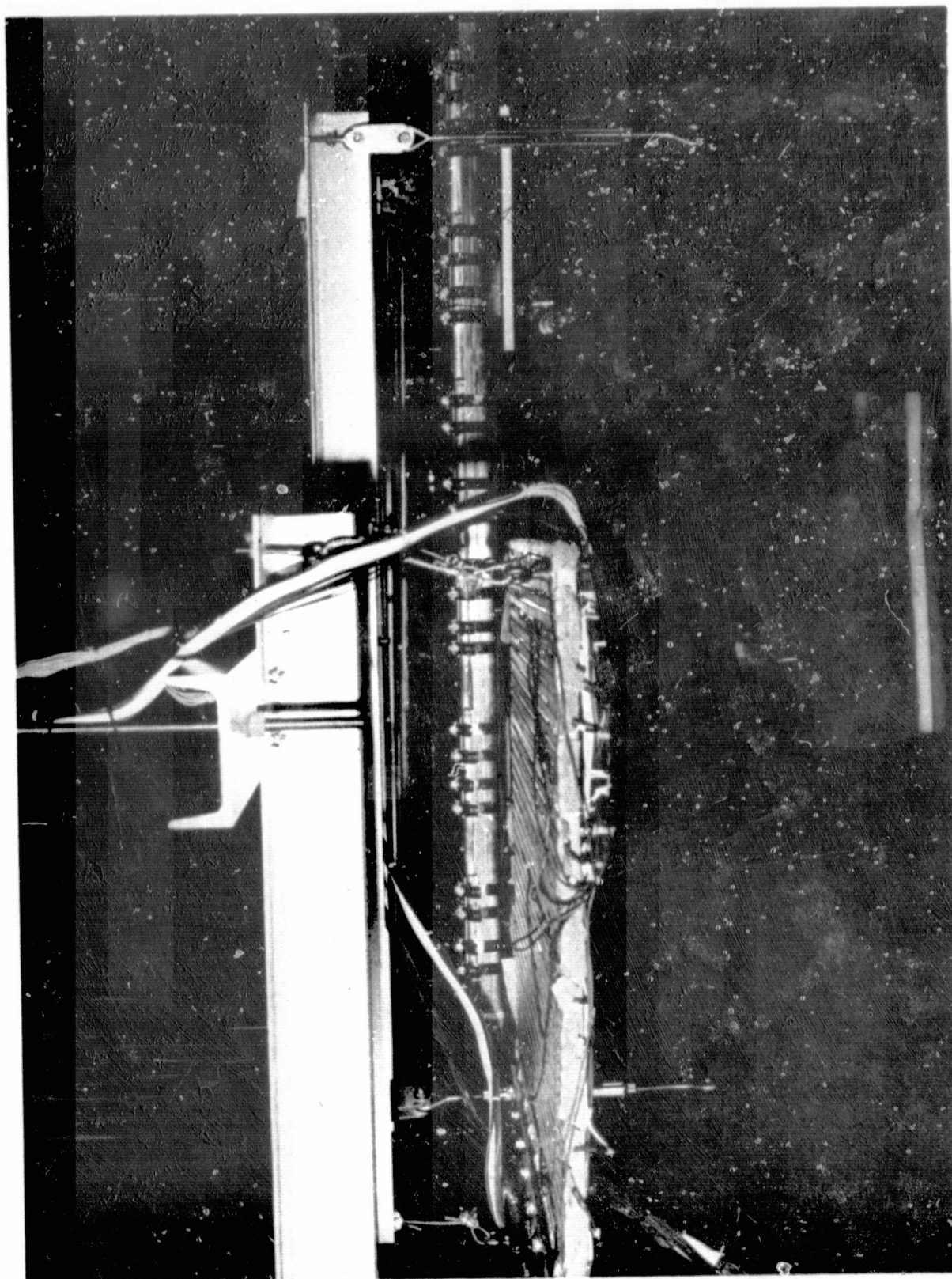


Figure B-18

Figure B-18 Header Pipe and Feeder Tube Installation Closeup

B-27

REPRODUCIBILITY OF THE
ORIGINAL PAGE IS POOR

C-2

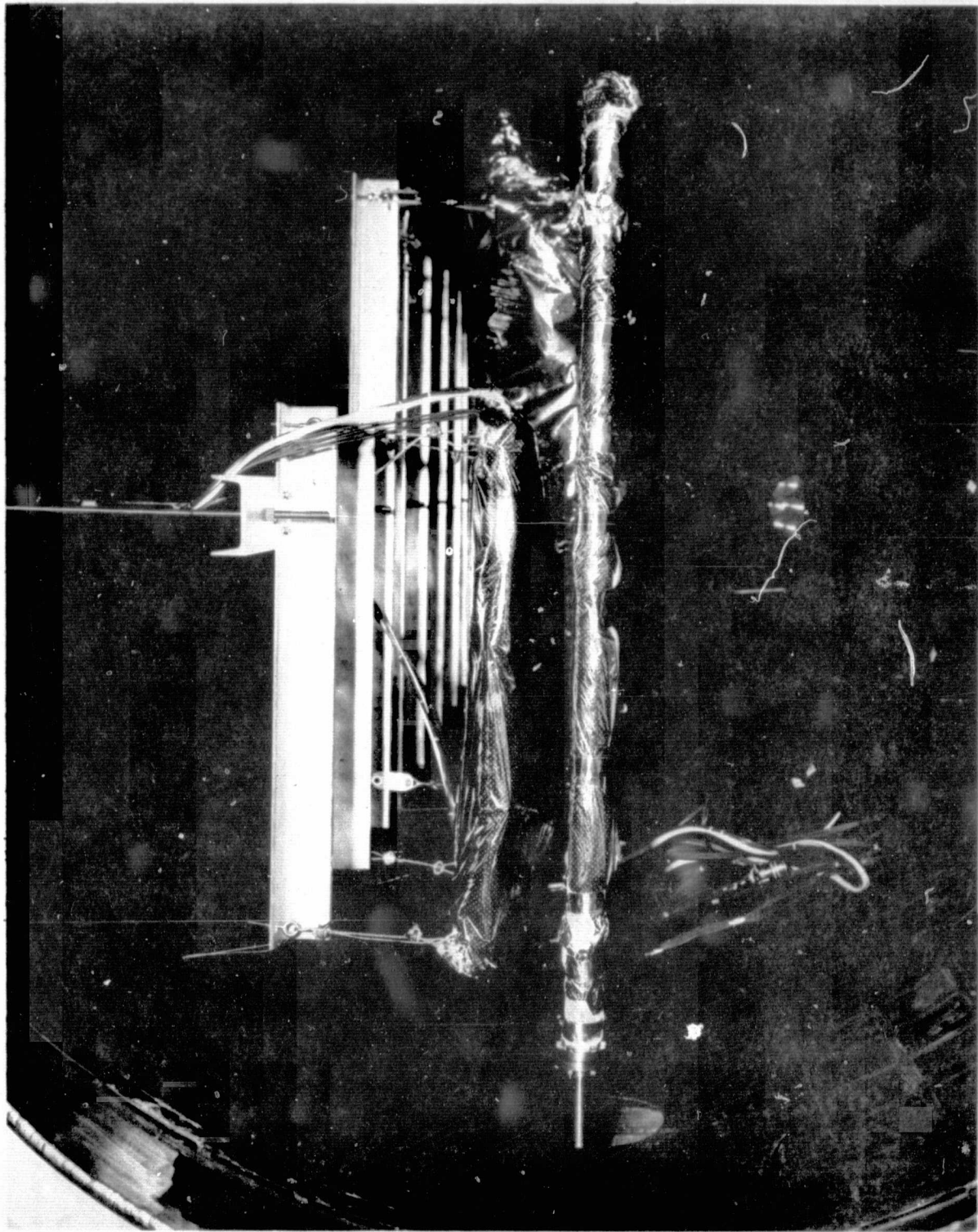


Figure B-19

B-28

Figure B-19 Final Chamber Installation

REPRODUCIBILITY OF THE
ORIGINAL PAGE IS POOR

V. TEST FACILITY

A 6x15-ft ion/titanium sublimation-pumped chamber capable of attaining a vacuum level of 10^{-8} torr with a pumping speed of 50,000 liters/sec was used during the conditioning panel/heat pipe radiator tests (See Figure B-20).

The operating characteristics of the 6x15-ft solar-thermal/vacuum chamber, based on both design specifications and actual test data, are shown in Table B-5.

Table B-5
Operating Characteristics of the Solar-Thermal/Vacuum Chamber

Nominal Chamber Size	Six ft O.D. x 15 ft 6 in. long
Ultimate Pressure	1×10^{-8} torr
Pumping System	<p><u>Roughing</u> Portable cart capable of pumping the chamber to 5×10^{-5} torr. Cart contains a cold trap and 650-cfm booster pump backed up with a 60-cfm compound pump.</p> <p><u>High Vacuum</u> Bulk titanium subliminator with LN_2 cooled substrate with an <i>intrinsic</i> pumping speed of 50,000 liters/sec at 1×10^{-7} torr. Ion pumps are capable of pumping 1400 liters/sec of air with a noble gas load capability of 20% relative to air for argon.</p>
Chamber Feedthroughs	<p><u>Instrumentation</u> 300 chromel/constantan thermocouples.</p> <p><u>Power</u> 24 channels, each with a capability of 28 Vdc at a maximum current of 10 amps. Eight feedthroughs with a 100-amp capacity.</p>

Additional capabilities of the 6x15-ft solar-thermal/vacuum chamber, which are available, but were not required to support the proposed test program, are shown in Table B-6.

REPRODUCIBILITY OF THE
ORIGINAL PAGE IS POOR

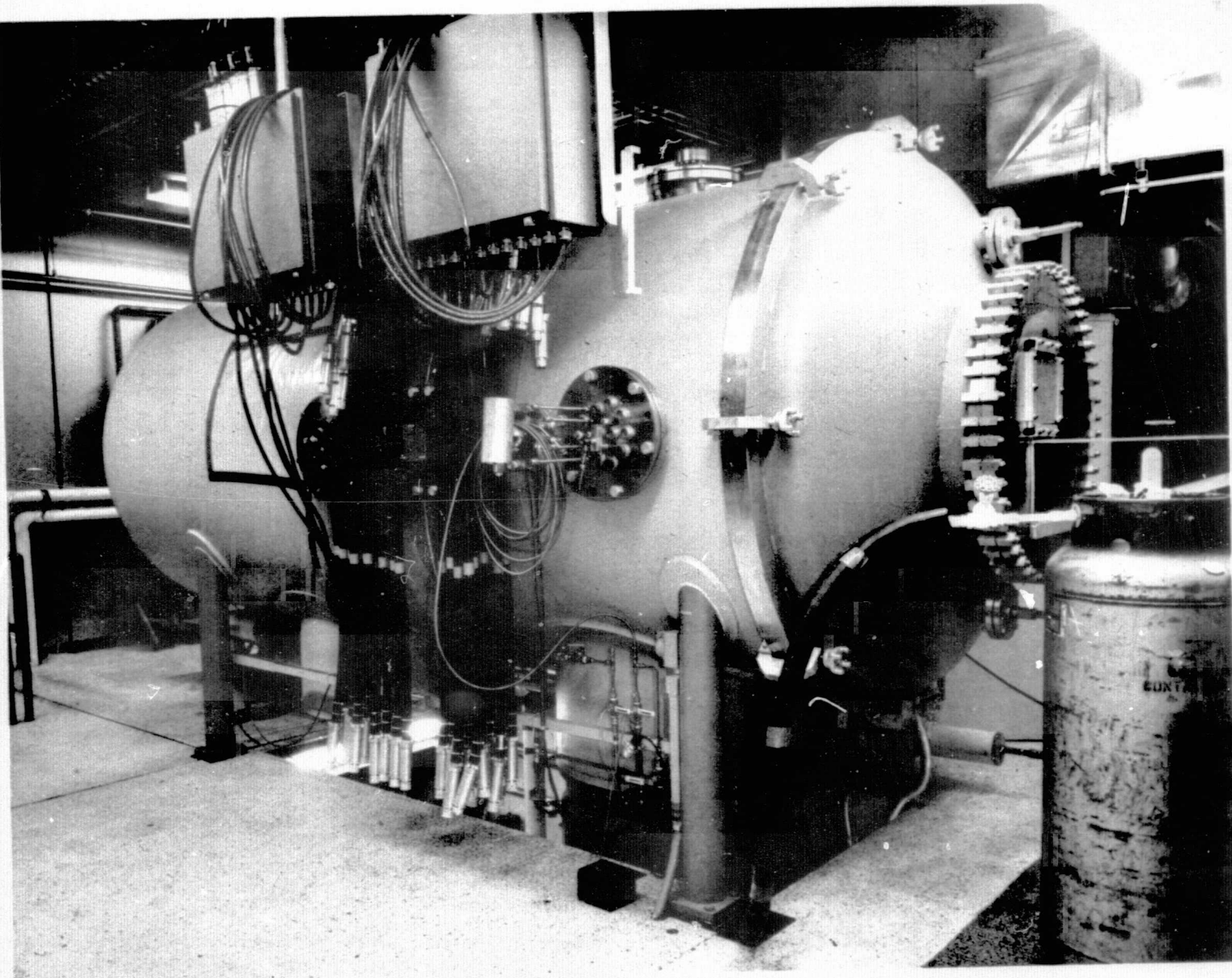


Figure B-20 6x15 Ion/Titanium Sublimation Vacuum Chamber

Figure B-20

B-30

Table B-6
Additional Capabilities of the Solar-Thermal/Vacuum Chamber

<u>Solar Simulation</u>	
Intensity	One to 2.5 solar constants (1400 to 4000 W/m ²).
Uniformity	± 5% over a 4-cm ² area in a plane perpendicular to the axis of the beam.
Spectral Range	0.5 to 2.7 μ
Spectral Match	Filtered xenon with a close match to the Johnson curve.
<u>Residual Gas Analysis</u>	Continuous scanning of the mass spectrum from 1 to 500 AMU or any portion thereof.

Temperature control of the shroud was obtained by using the portable gas heat exchanger shown in Figures B-21 and B-22. The unit uses gaseous nitrogen forced through a closed loop which is controlled to the desired temperature. Liquid nitrogen is used for cooling and a 10 kW heater is used for heating. An electronic controller is used to control the system by manual or automatic setpoint inputs. The system is capable of controlling the output gas temperature between 116 and 339°K (-250 and 150°F) while subjected to heat loads up to 10 kW.

Standard Operating Procedures (SOPs) govern the operation and protection of both the test specimen and the test facility. Specific test requirements are integrated into these SOPs through a controlled release system. The facility is operated by certified operators who have a thorough knowledge of vacuum technology and test techniques.

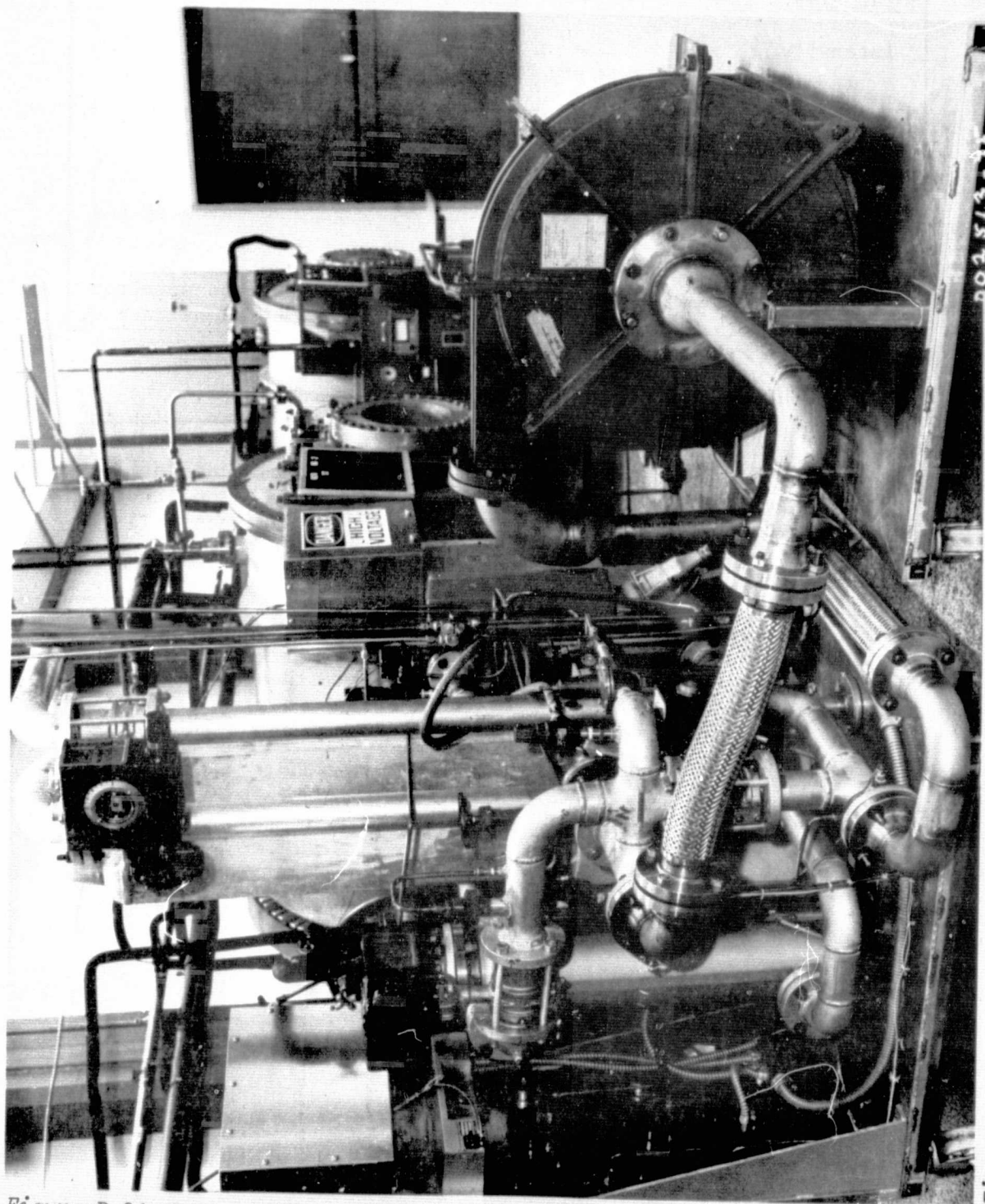


Figure B-21

B-32

Figure B-21 Portable Gas Heat Exchanger

REPRODUCIBILITY OF THE
ORIGINAL PAGE IS POOR

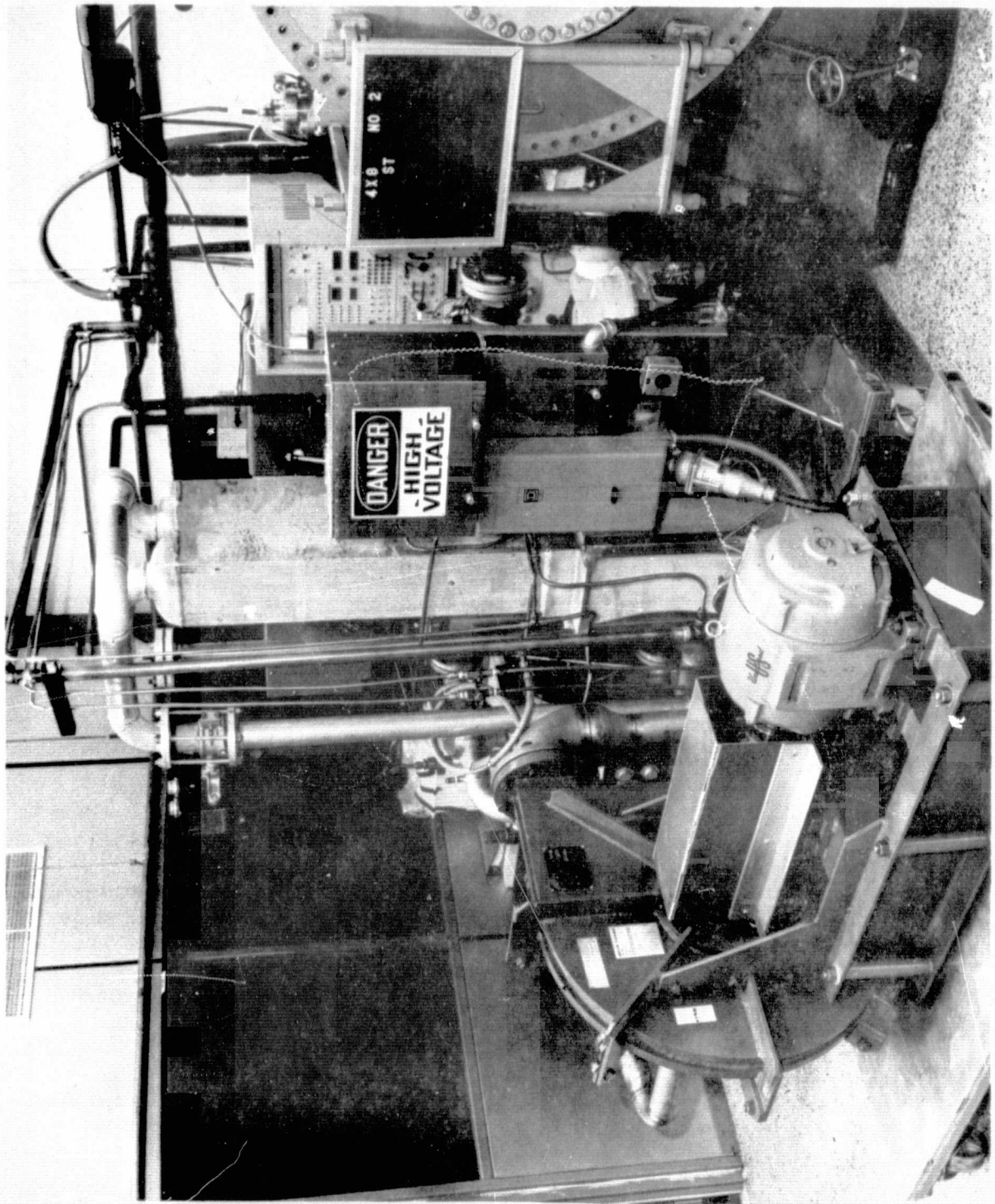


Figure B-22

Figure B-22 Portable Gas Heat Exchanger

B-33

REPRODUCIBILITY OF THE
ORIGINAL PAGE IS POOR

VI. TESTING

The data presentation for all of the testing used the following nomenclature shown in Table B-7.

Table B-7 Nomenclature Used for All Data Presentation

Thermocouple Designation	Test Hardware	Reference, Figure
T	Thermal Conditioning Panel	B-10
H	Header Pipe	B-9
R	Radiator	B-4
S	Shroud	B-13
Note: The shroud temperatures were presented as average values since the variation in temperature over the shroud was 5°K.		

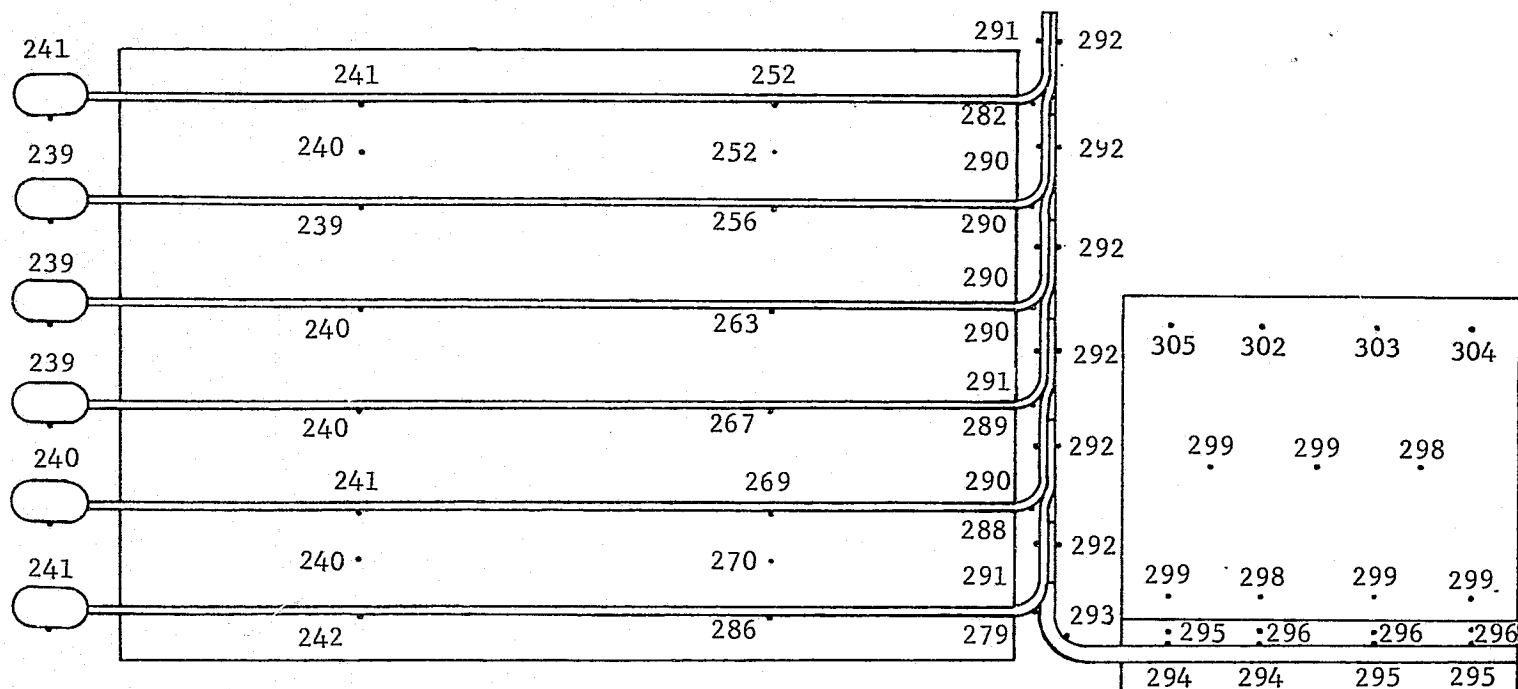
TEST 1, HOT CASE, 238.66°K SHROUD

Testing of the radiator/thermal conditioning panel was performed from 16 April to 24 April 1975 beginning with the hot case. For this series of testing the shroud was held at 238.7°K (-30°F) and heat was applied to the thermal conditioning panel (Table B-7) until steady-state was achieved. The planned 400 W test was reduced to the 380 W level to avoid over temperature of the thermal conditioning panel. The steady-state and transient data obtained from the tests are presented in Figures B-23 through B-52.

Figures B-23 through B-32 summarize the test data by location on the test hardware for the five power levels at steady state conditions. Figures B-33 through B-52 present temperature histories from the same runs showing the transient response of the system to varying power loads for constant environment temperatures.

The thermal conditioning panel exhibited a maximum of 8°K ΔT (Table B-7) over the panel. The header pipe exhibited ΔT s ranging from 3°K at 100 W to 8°K at 380 W. The two 200 W runs both exhibited a 5.5°K ΔT .

Figure B-23

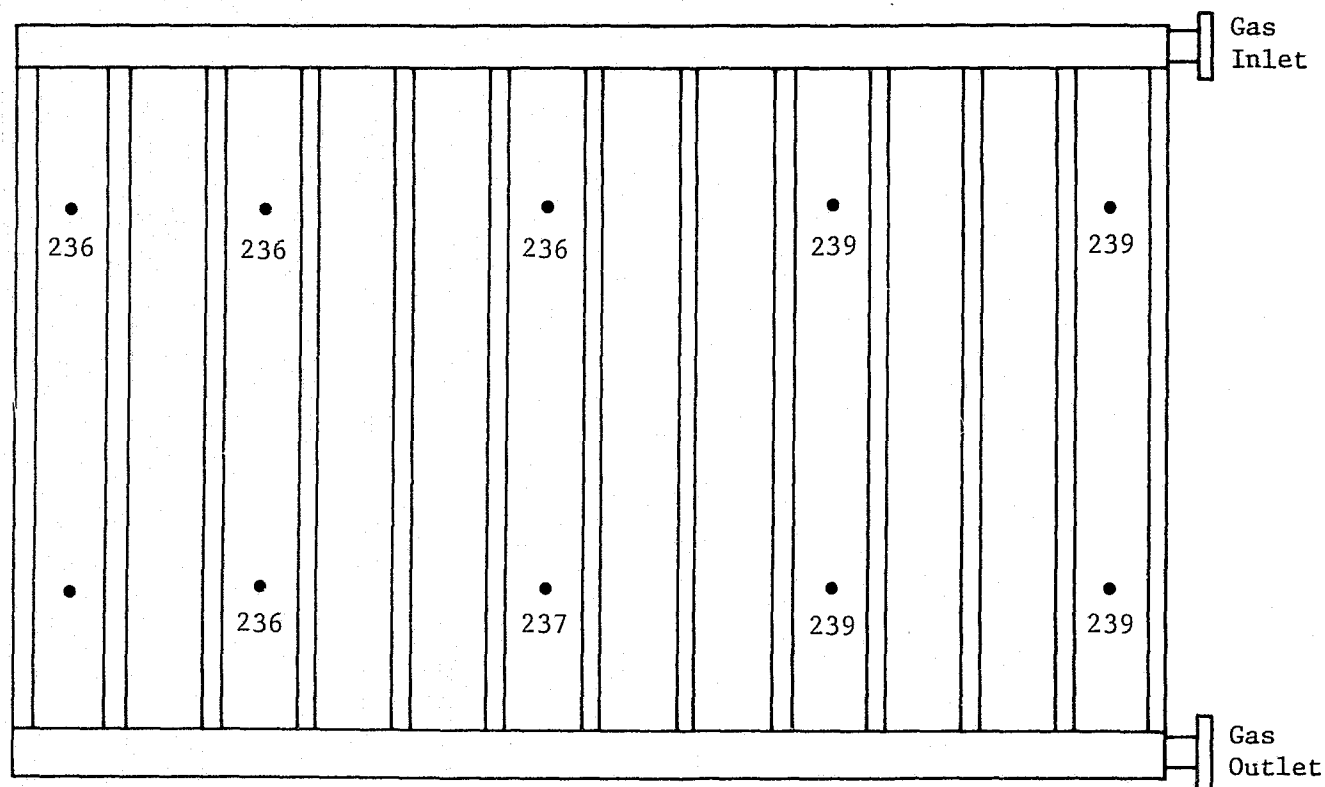


Legend:

• Thermocouple Locations

Note: Temperature, °K

Figure B-23 Test 1 Hot Case, 100.1 W

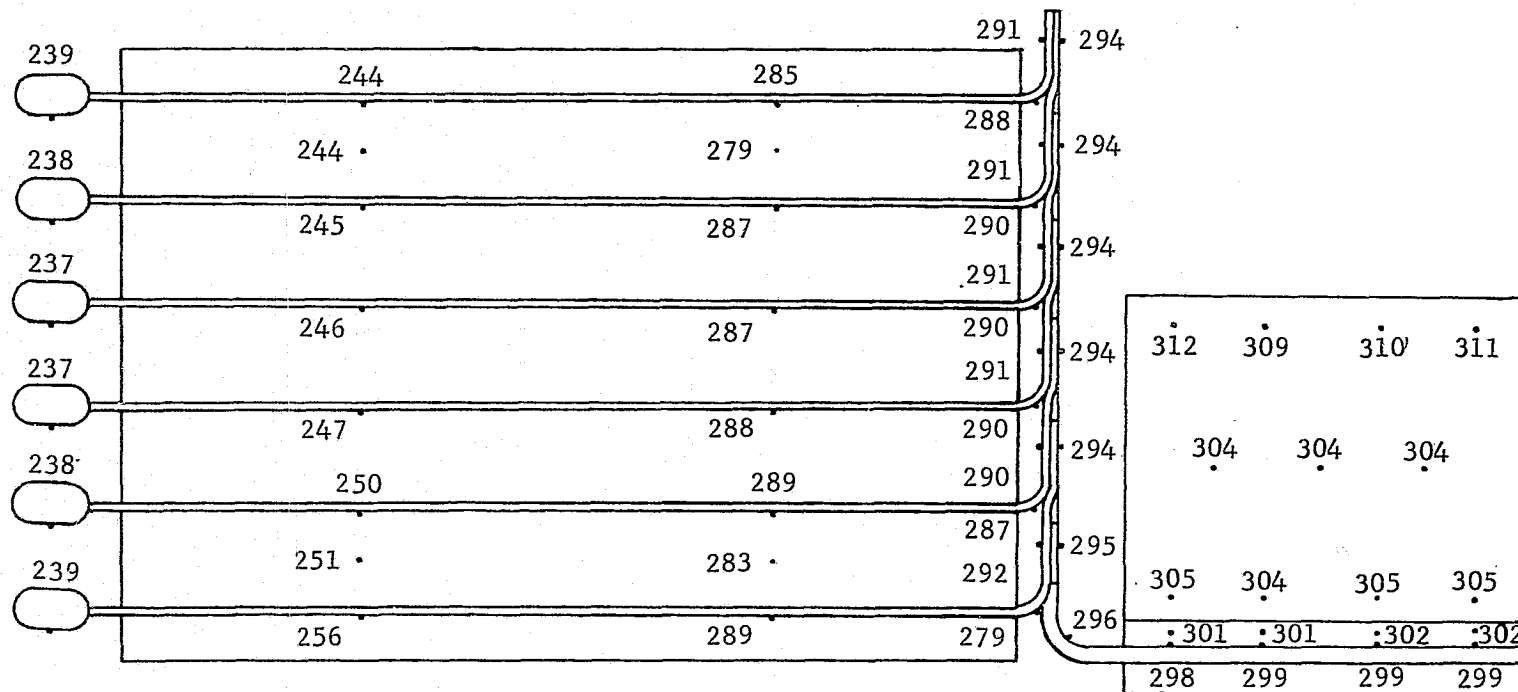
Legend:

Thermocouple Locations

Note: Temperature, °K

Figure B-24 Test 1 Hot Case, 100.1 W

Figure B-25

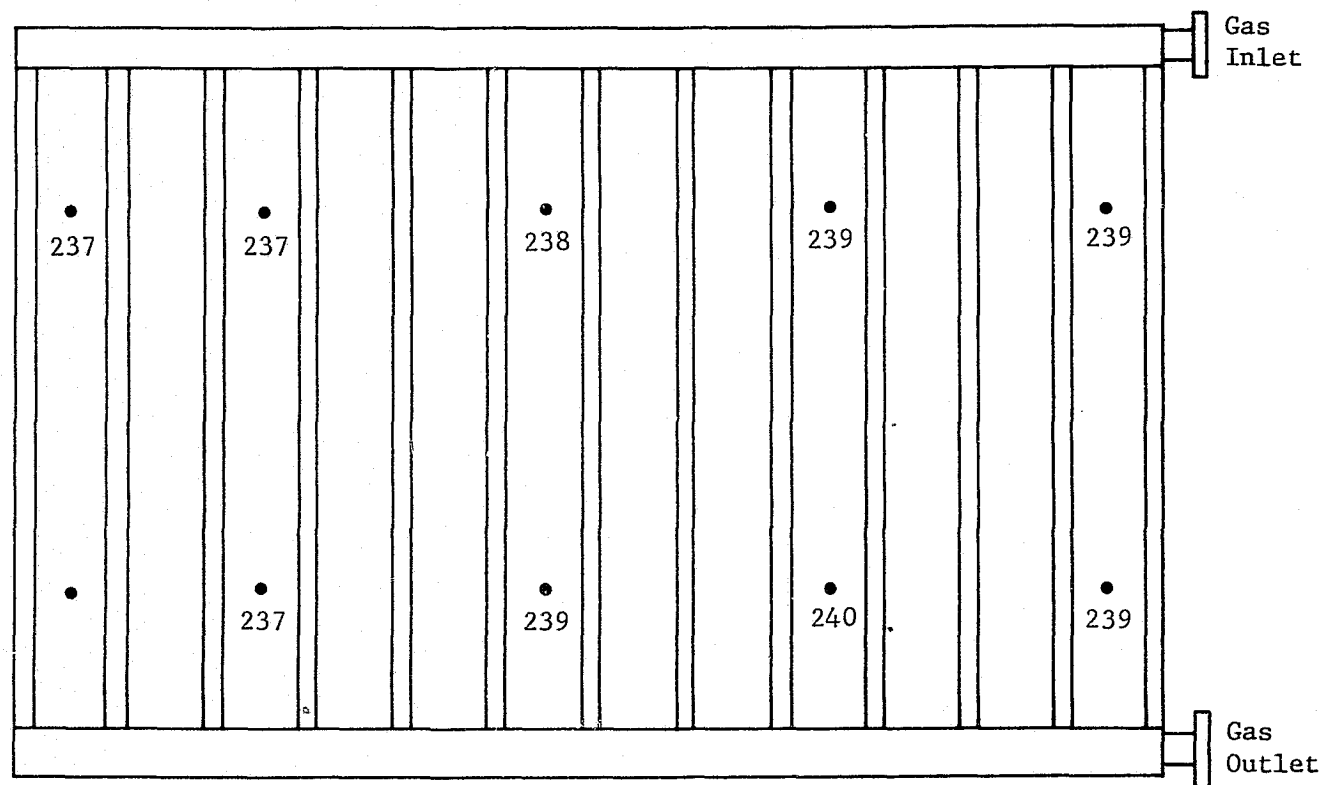


Legend:

• Thermocouple Locations

Note: Temperature, °K

Figure B-25 Test 1 Hot Case, 200.26 W

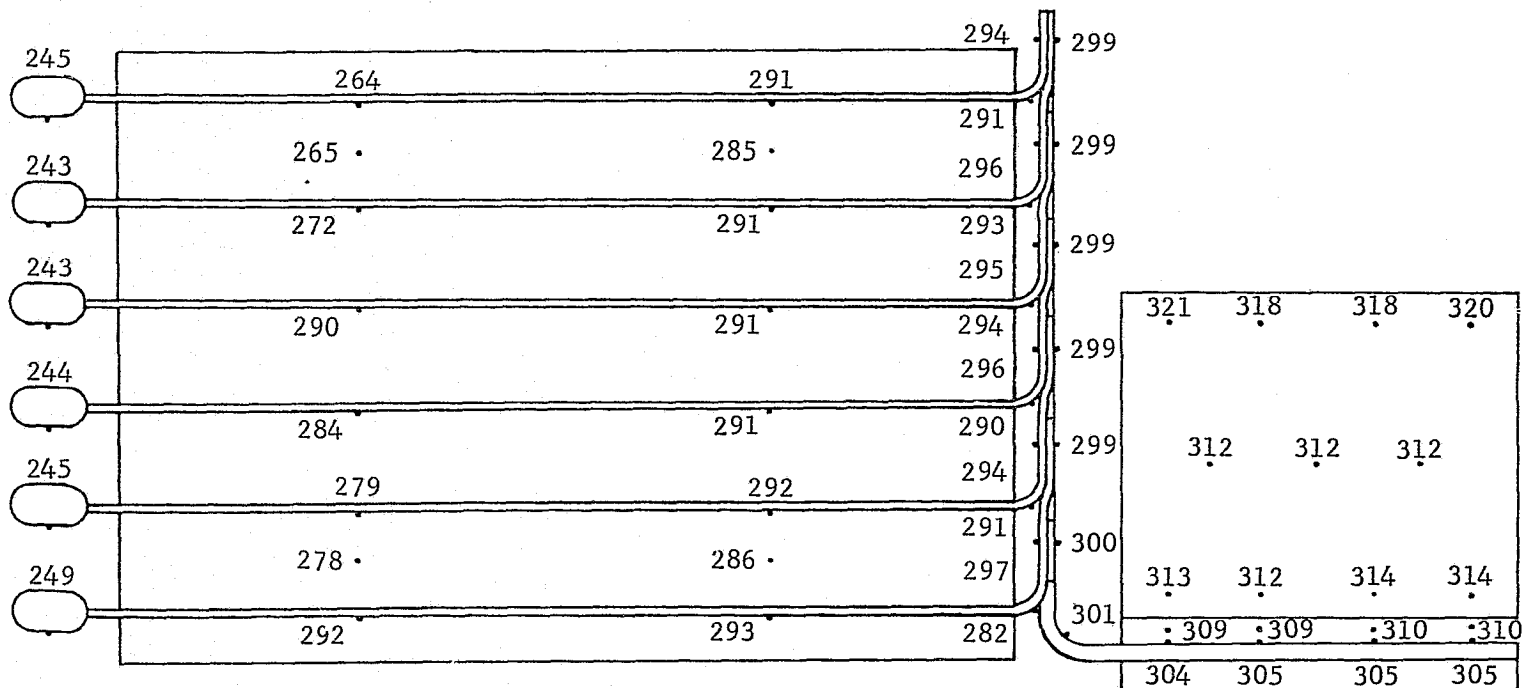
Legend:

Thermocouple Locations

Note: Temperature, °K

Figure B-26 Test 1 Hot Case, 200.26 W

Figure B-27



Legend:

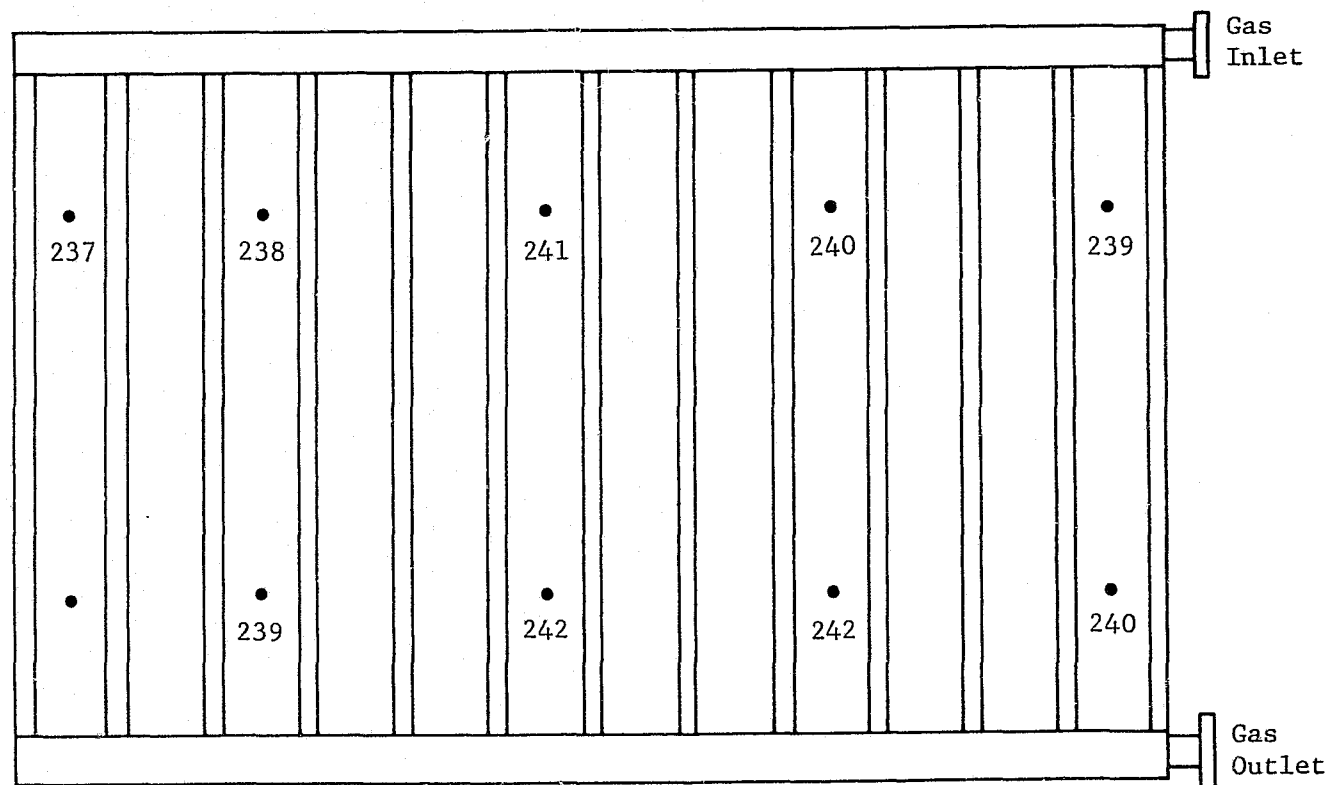


Thermocouple Locations

Note: Temperature, °K

Figure B-27 Test 1 Hot Case, 299.88 W

B-40
Figure B-28



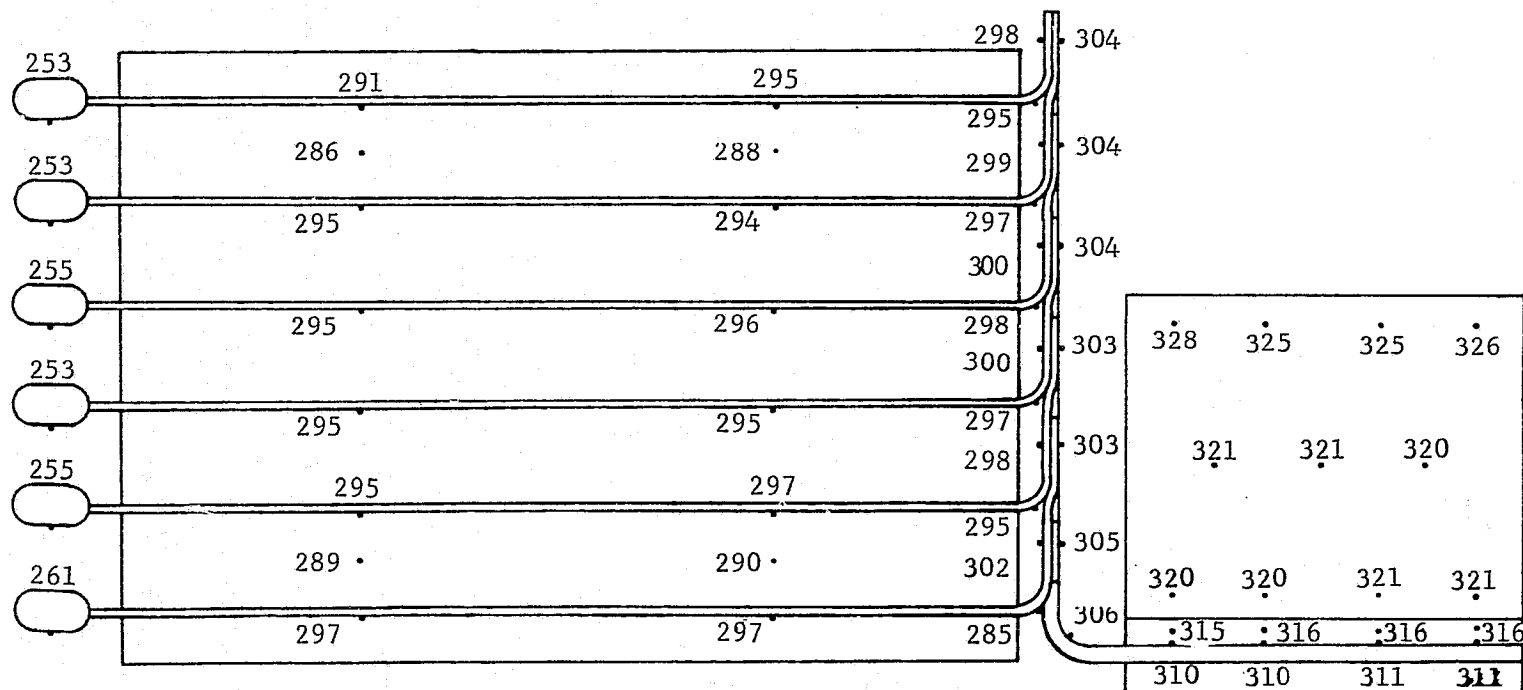
Legend:

• Thermocouple Locations

Note: Temperature, °K

Figure B-28 Test 1 Hot Case, 299.88 W

Figure B-29



Legend:



Thermocouple Locations

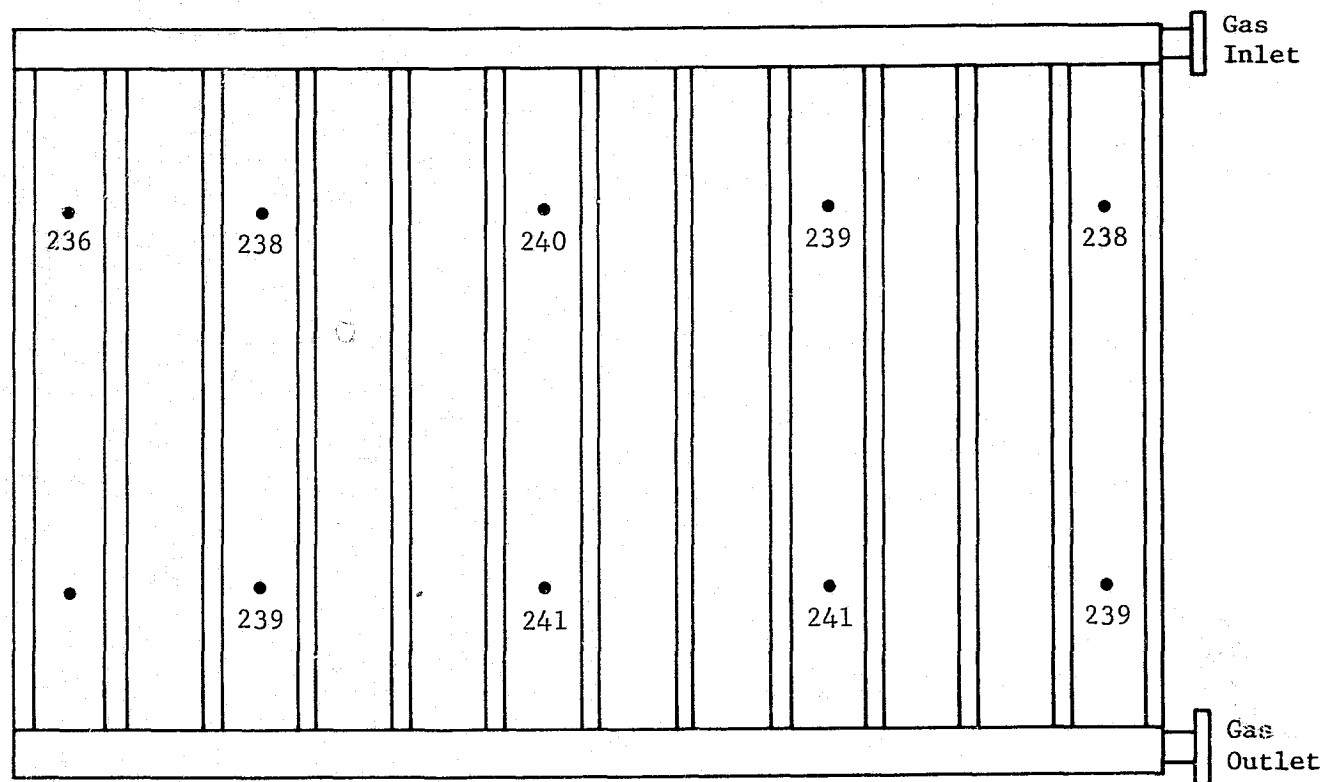
Note: Temperature, °K

B-41

Figure B-29 Test 1 Hot Case, 380.96 W

B-42

Figure B-30



Legend:

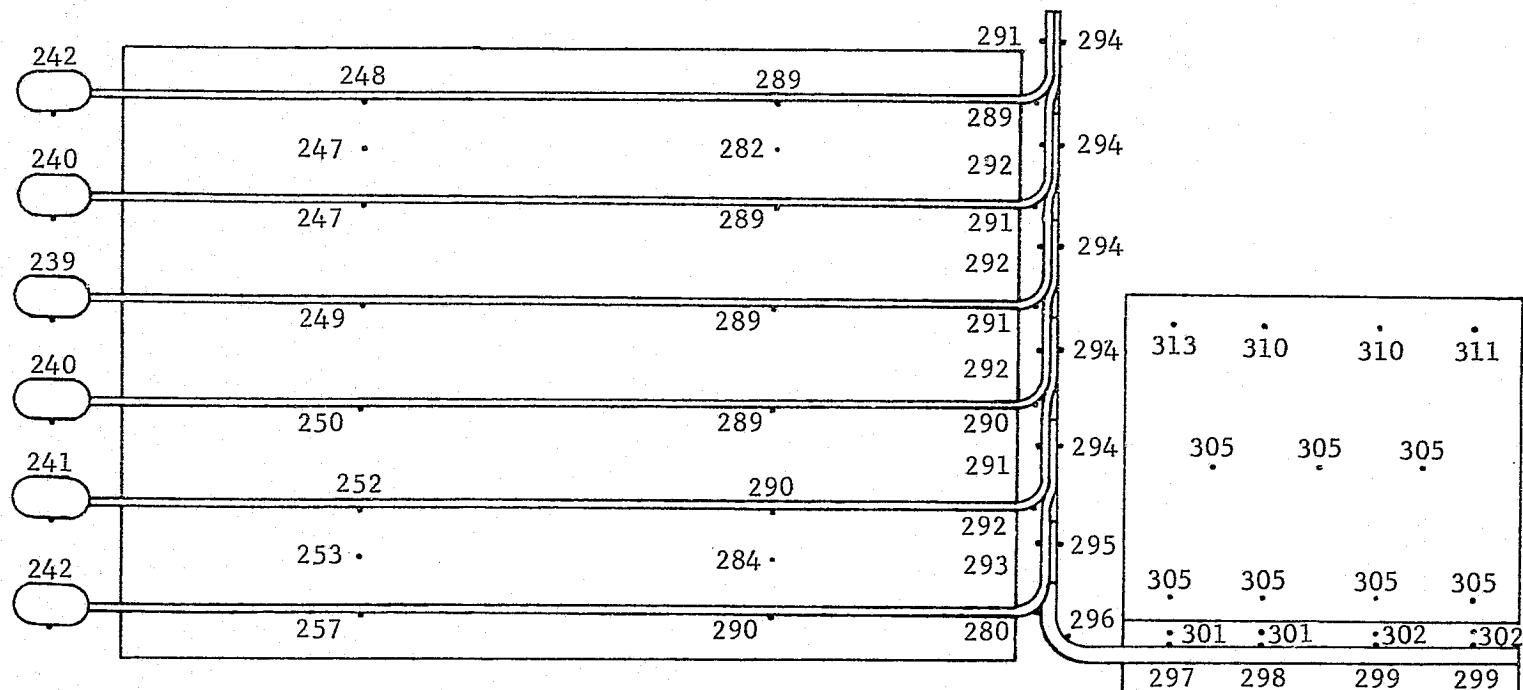


Thermocouple Locations

Note: Temperature, °K

Figure B-30 Test 1 Hot Case, 380.96 W

Figure B-31

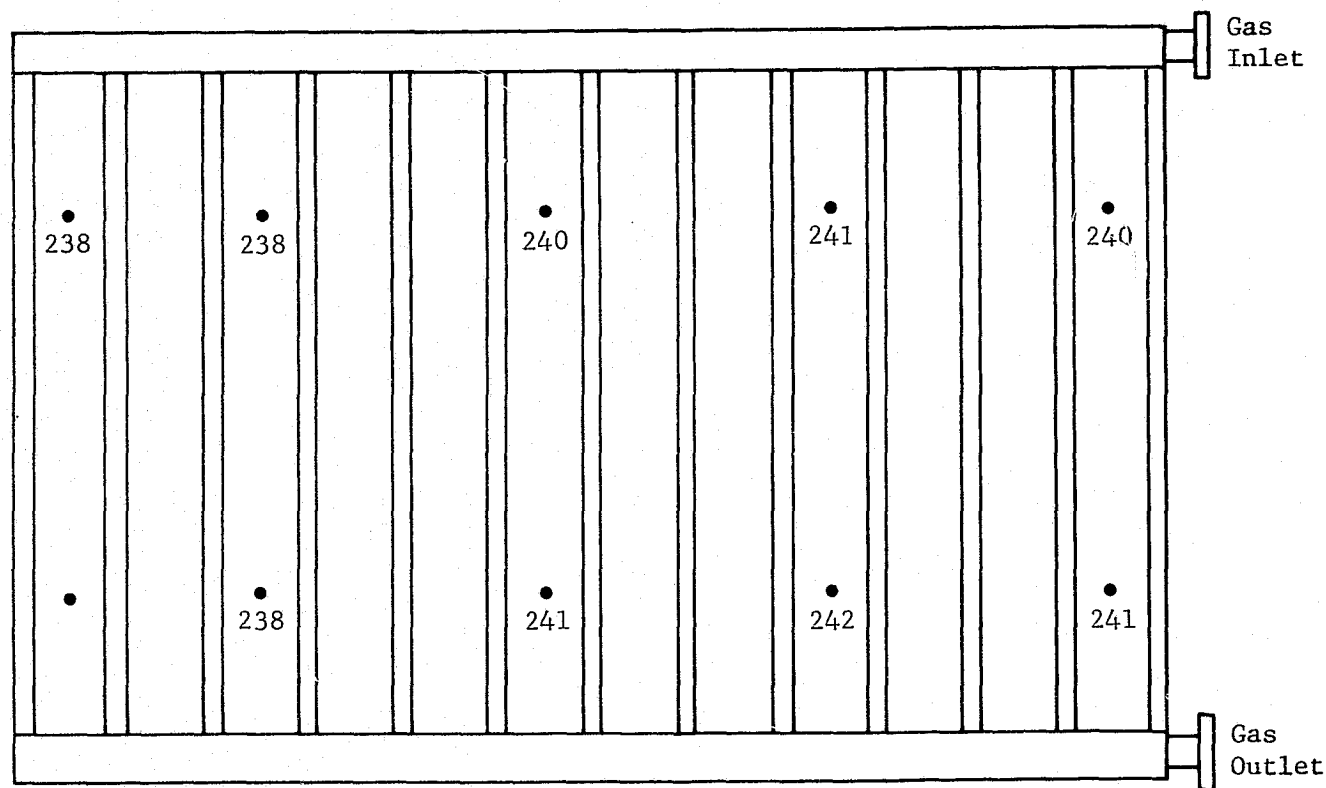


Legend:

• Thermocouple Locations

Note: Temperature, °K

Figure B-31 Test 1 Hot Case, 200.23 W

Legend:

• Thermocouple Locations

Note: Temperature, °K

Figure B-32 Test 1 Hot Case, 200.23 W

REPRODUCIBILITY OF THE
ORIGINAL PAGE IS POOR

Figure B-33

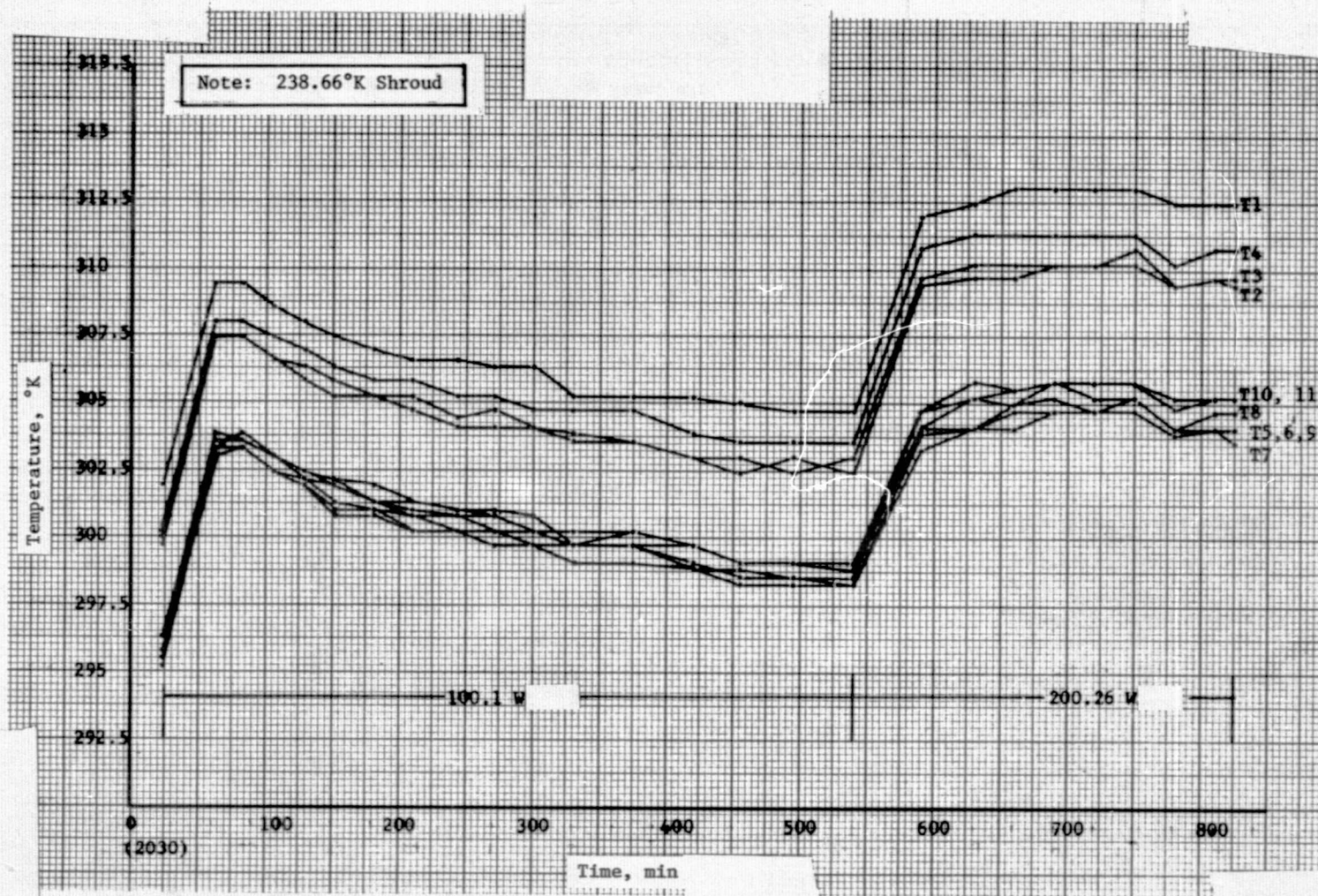


Figure B-33 Test 1 Hot Case Thermal Conditioning Panel

B-46

Figure B-34

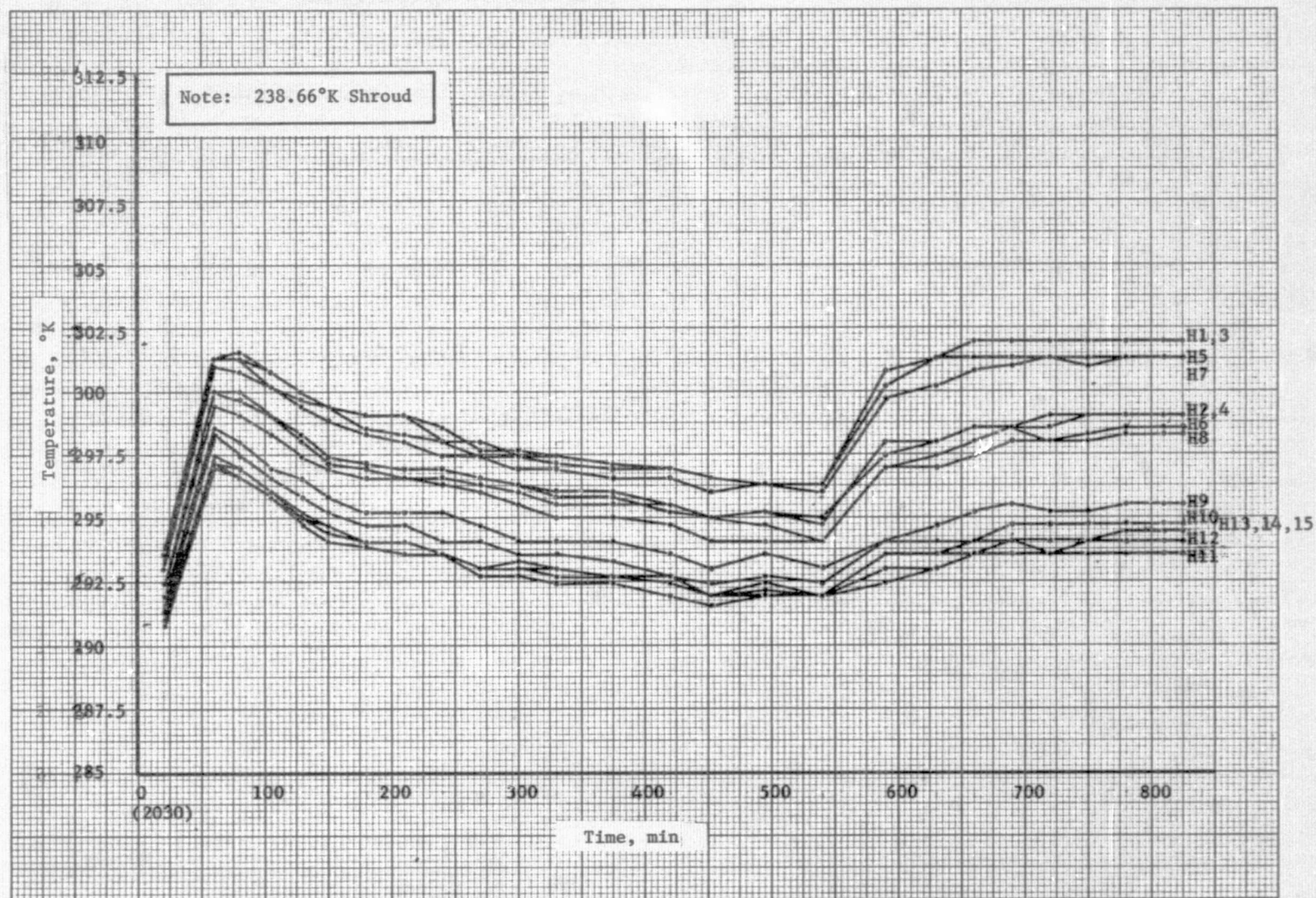
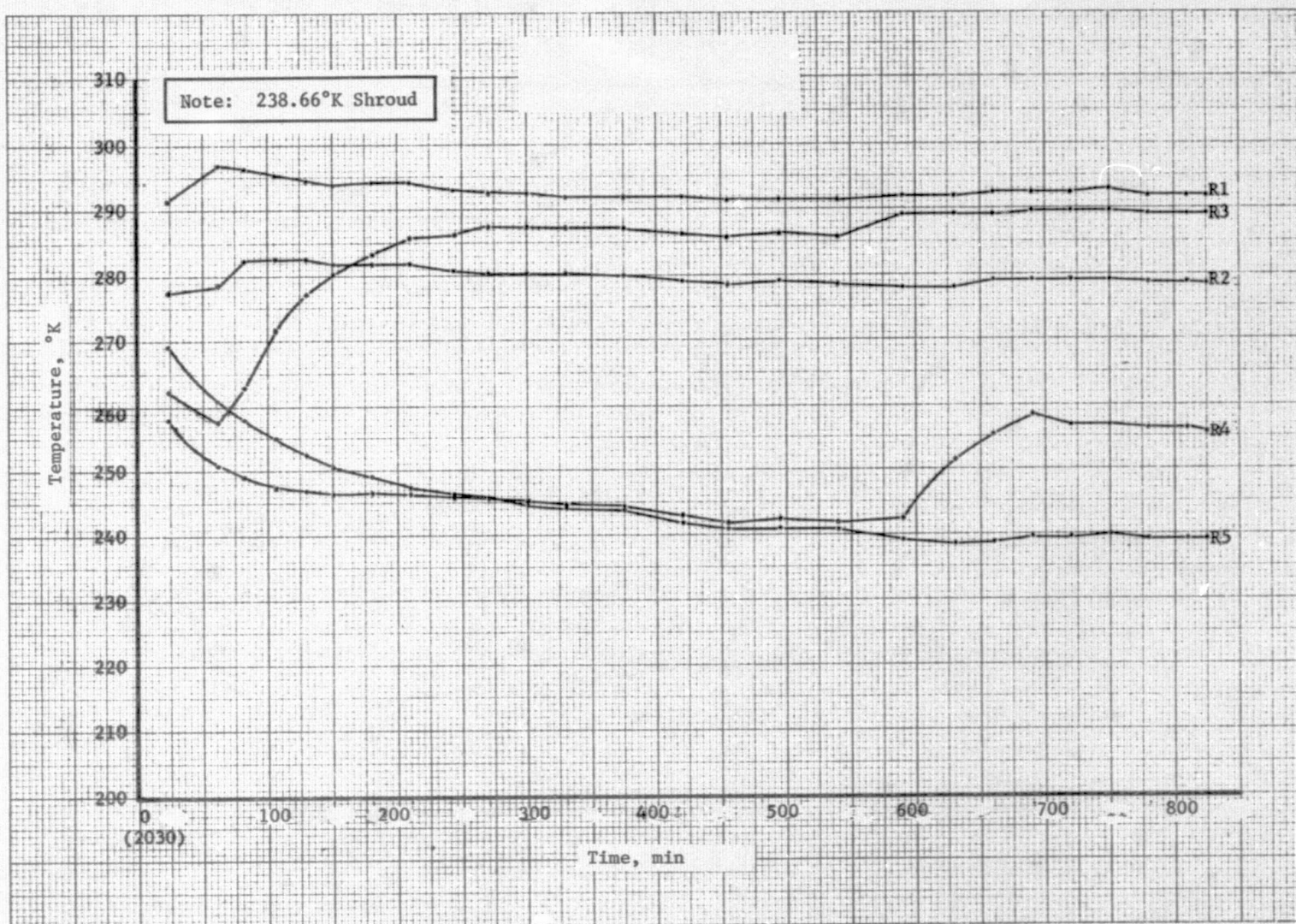


Figure B-34 Test 1 Hot Case Header Heat Pipe

REPRODUCIBILITY OF THE
ORIGINAL PAGE IS POOR

Figure B-35



B-47

Figure B-35 Test 1, Hot Case Radiator Heat Pipe No. 1

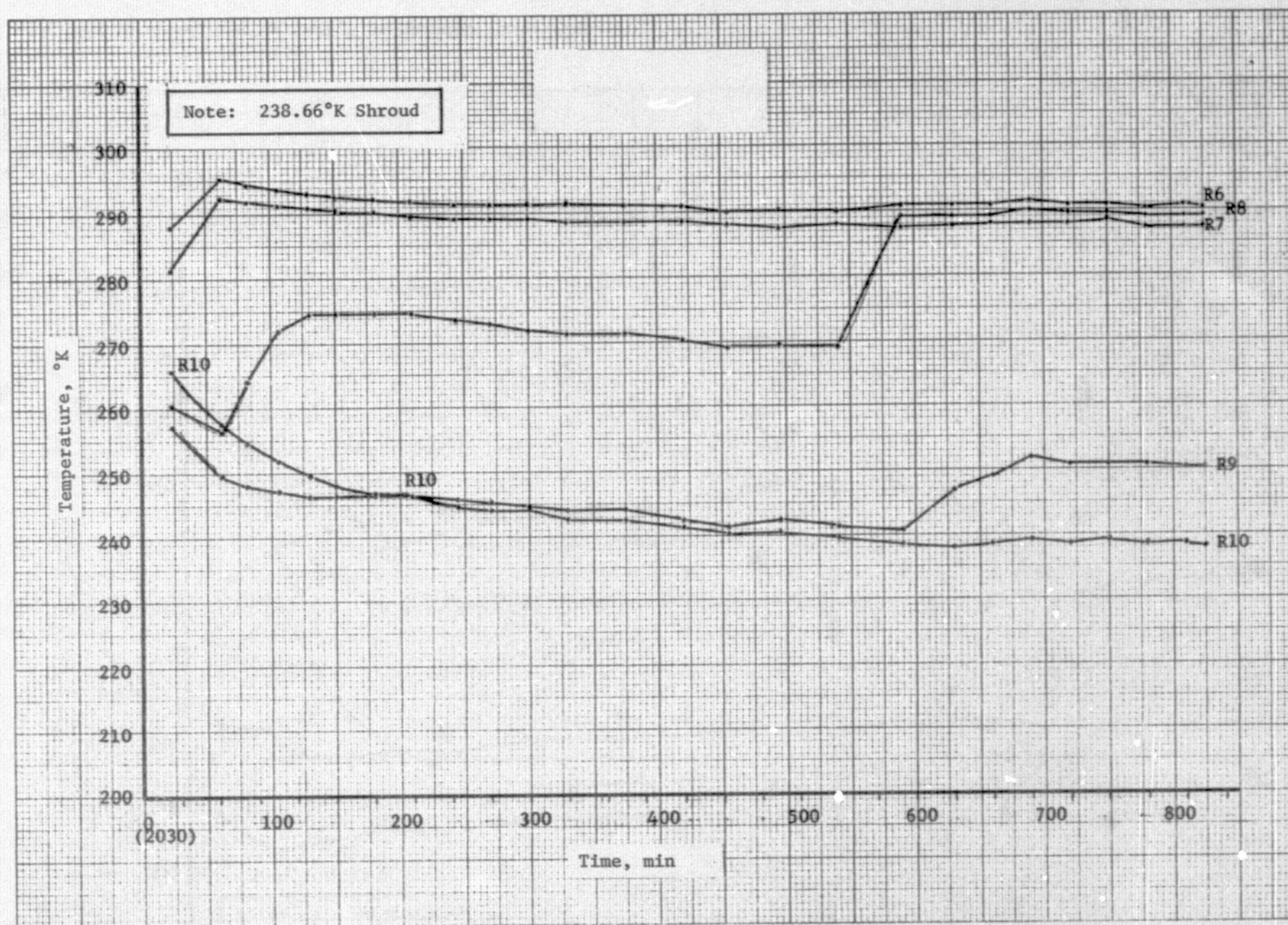
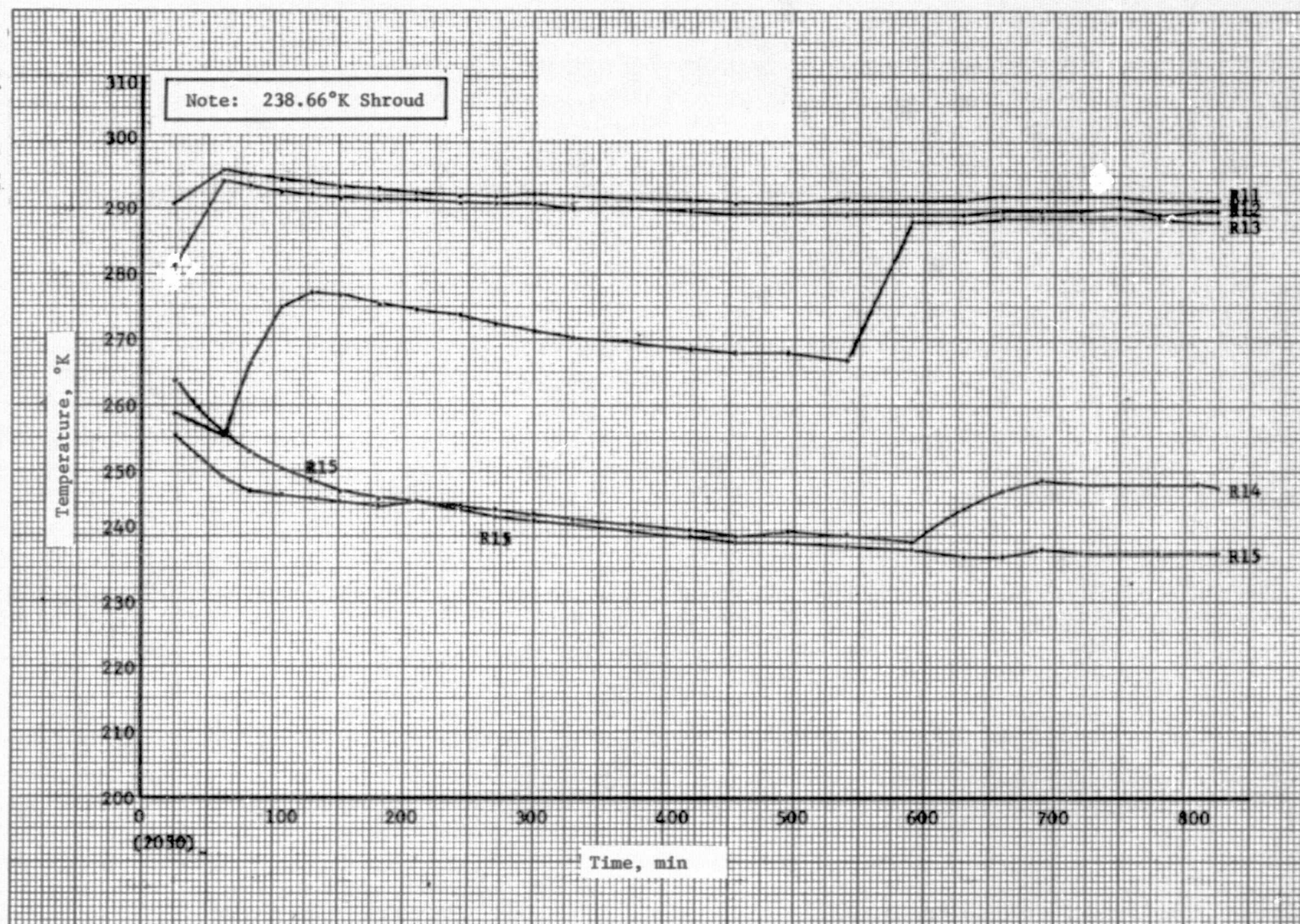


Figure B-36 Test 1, Hot Case Radiator Heat Pipe No. 2

Figure B-37



B-49

Figure B-37 Test 1, Hot Case Radiator Heat Pipe No. 3

Figure B-38
B-50

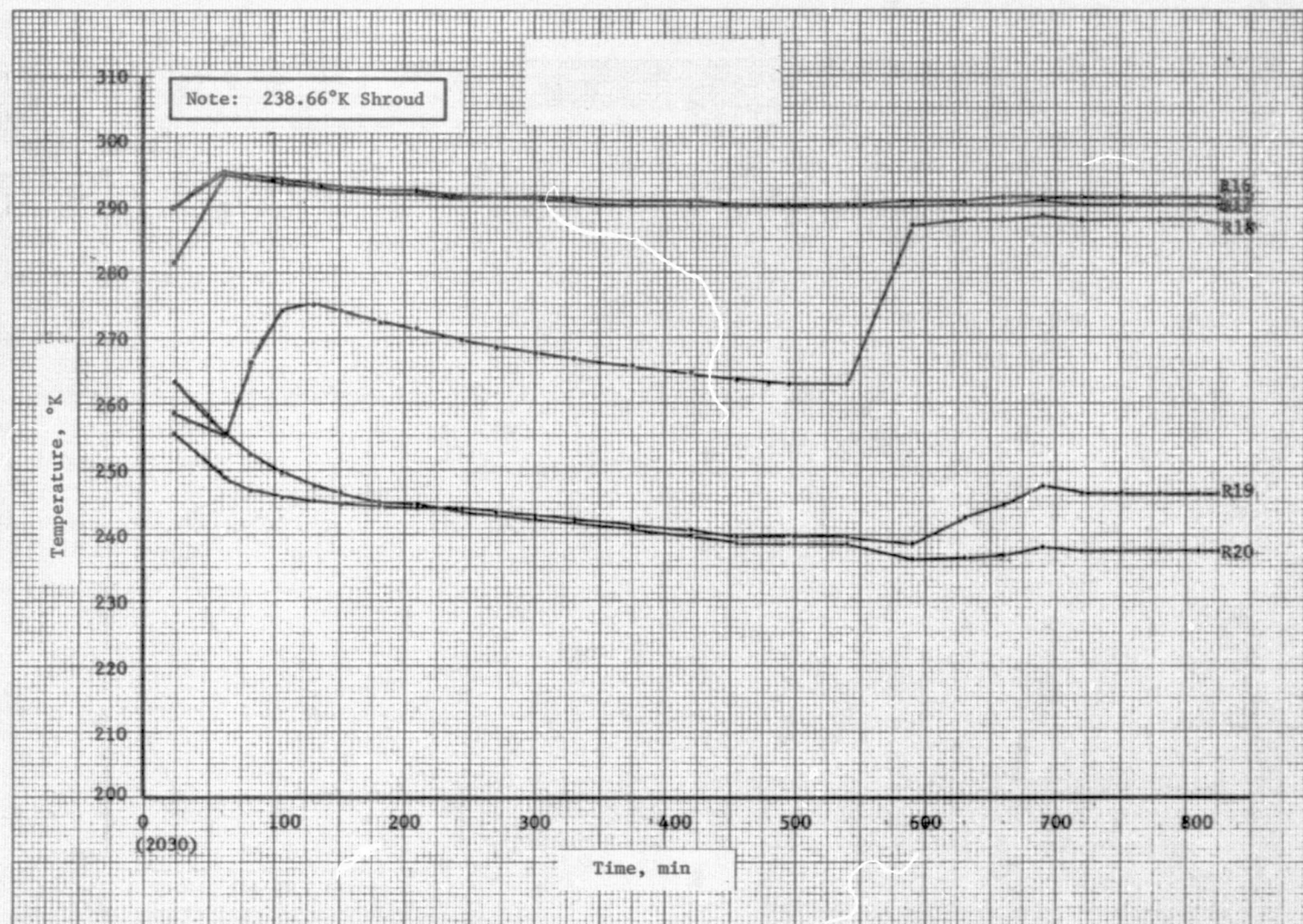


Figure B-38 Test 1, Hot Case Radiator Heat Pipe No. 4

REPRODUCIBILITY OF THE
ORIGINAL PAGE IS POOR

Figure B-39

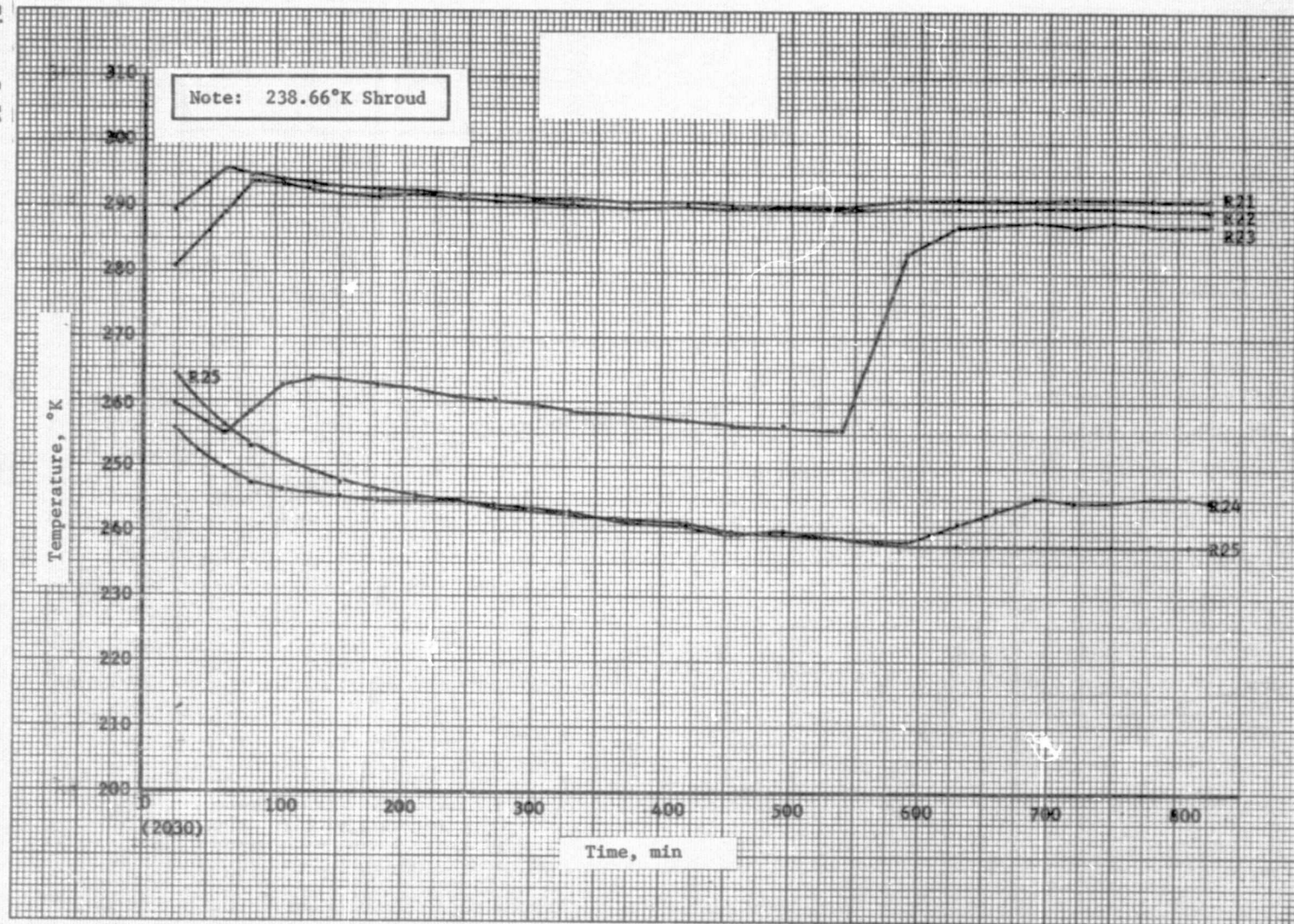


Figure B-39 Test 1, Hot Case Radiator Heat Pipe No. 5

Figure B-40
B-52

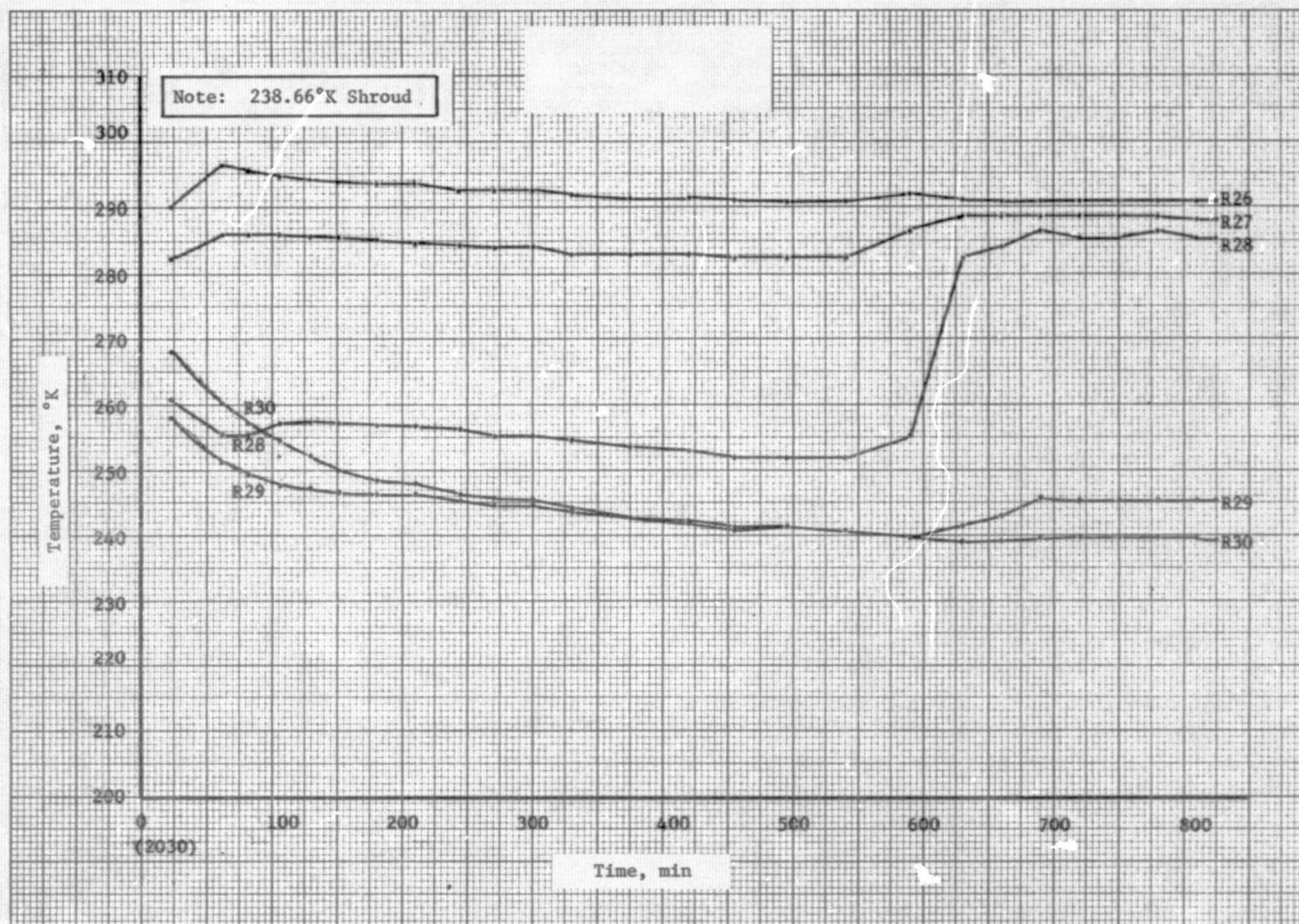


Figure B-40 Test 1, Hot Case Radiator Heat Pipe No. 6

Figure B-41

B-53

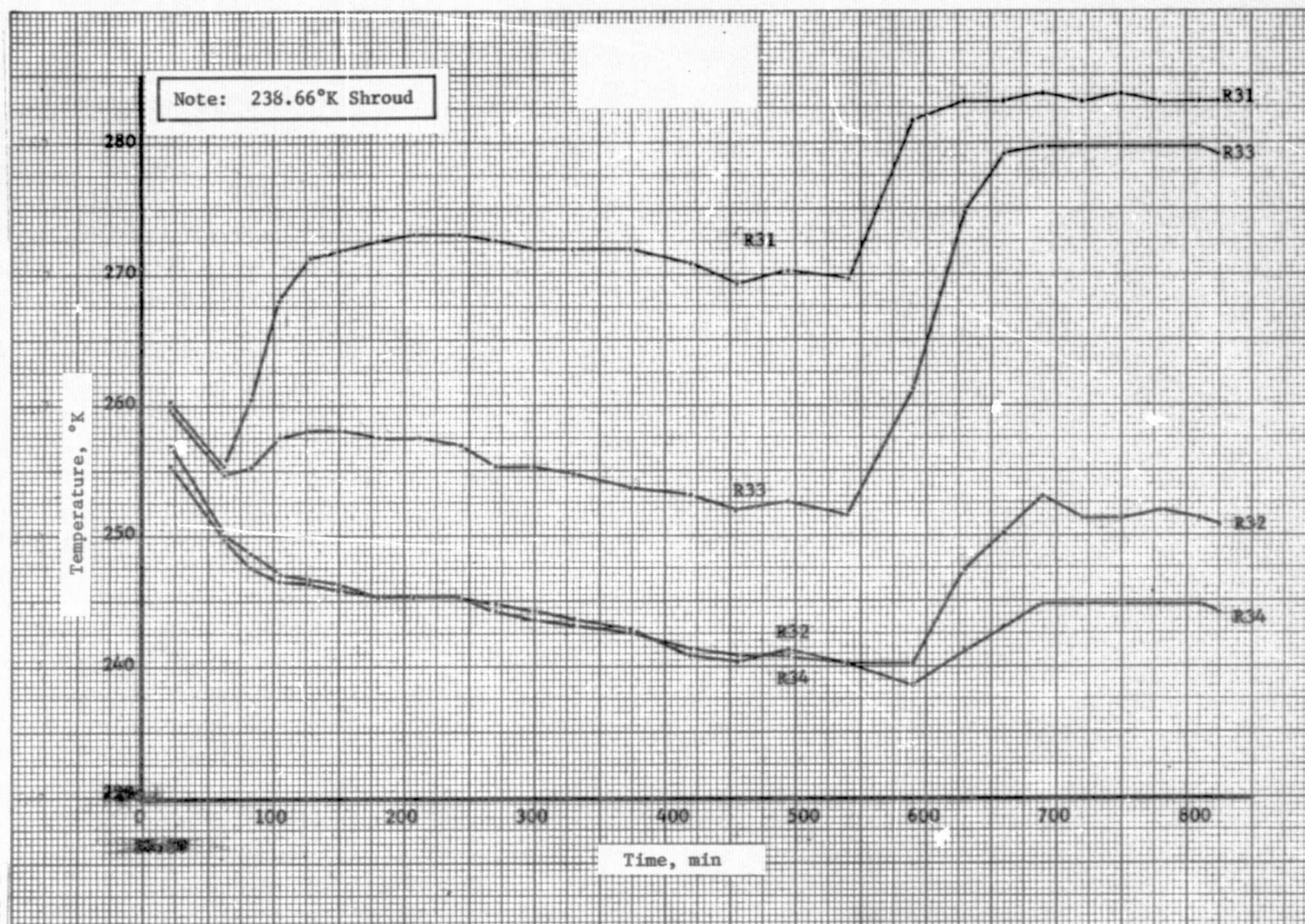


Figure B-41 Test 1, Hot Case Skin

Figure B-42
B-54

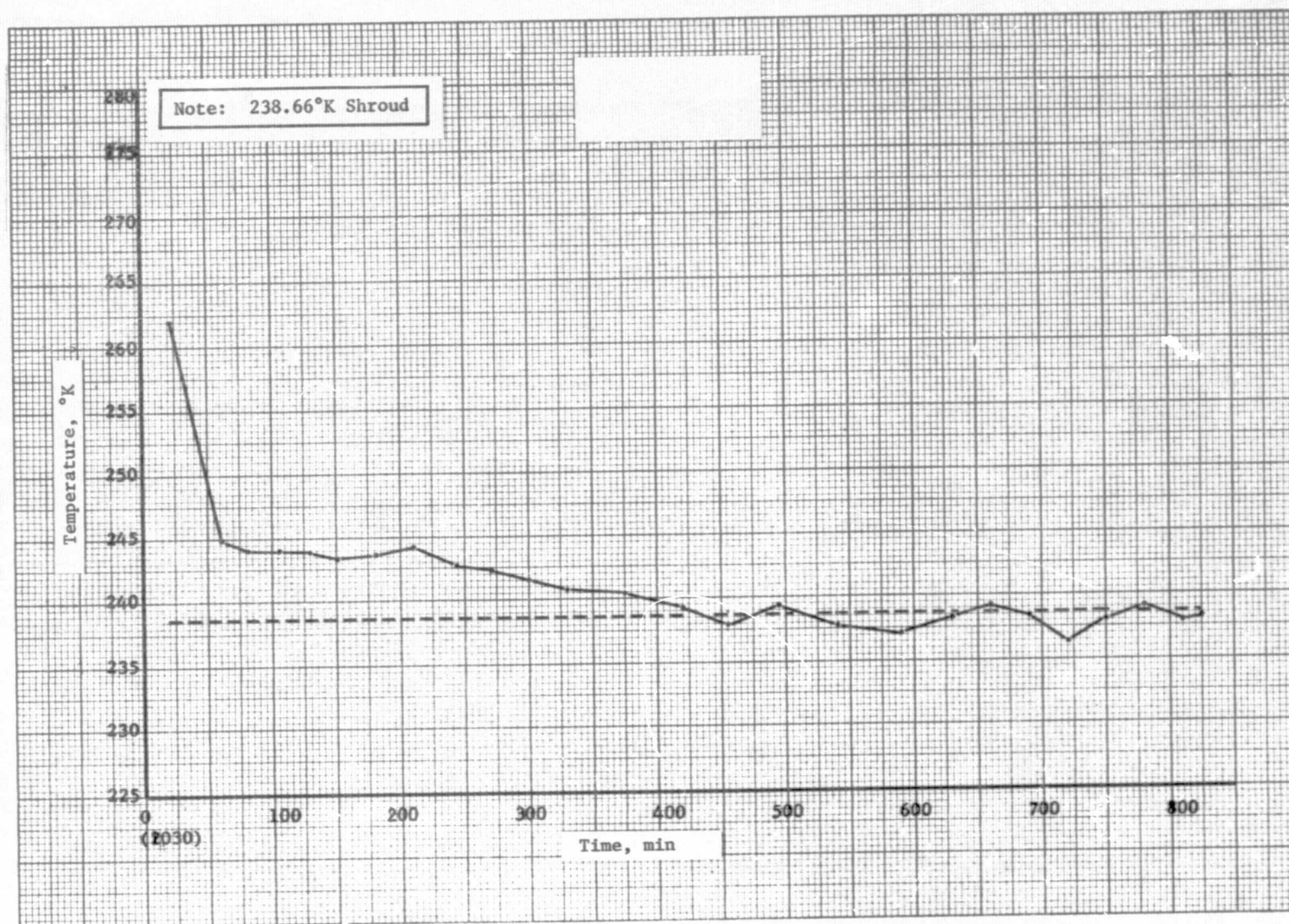
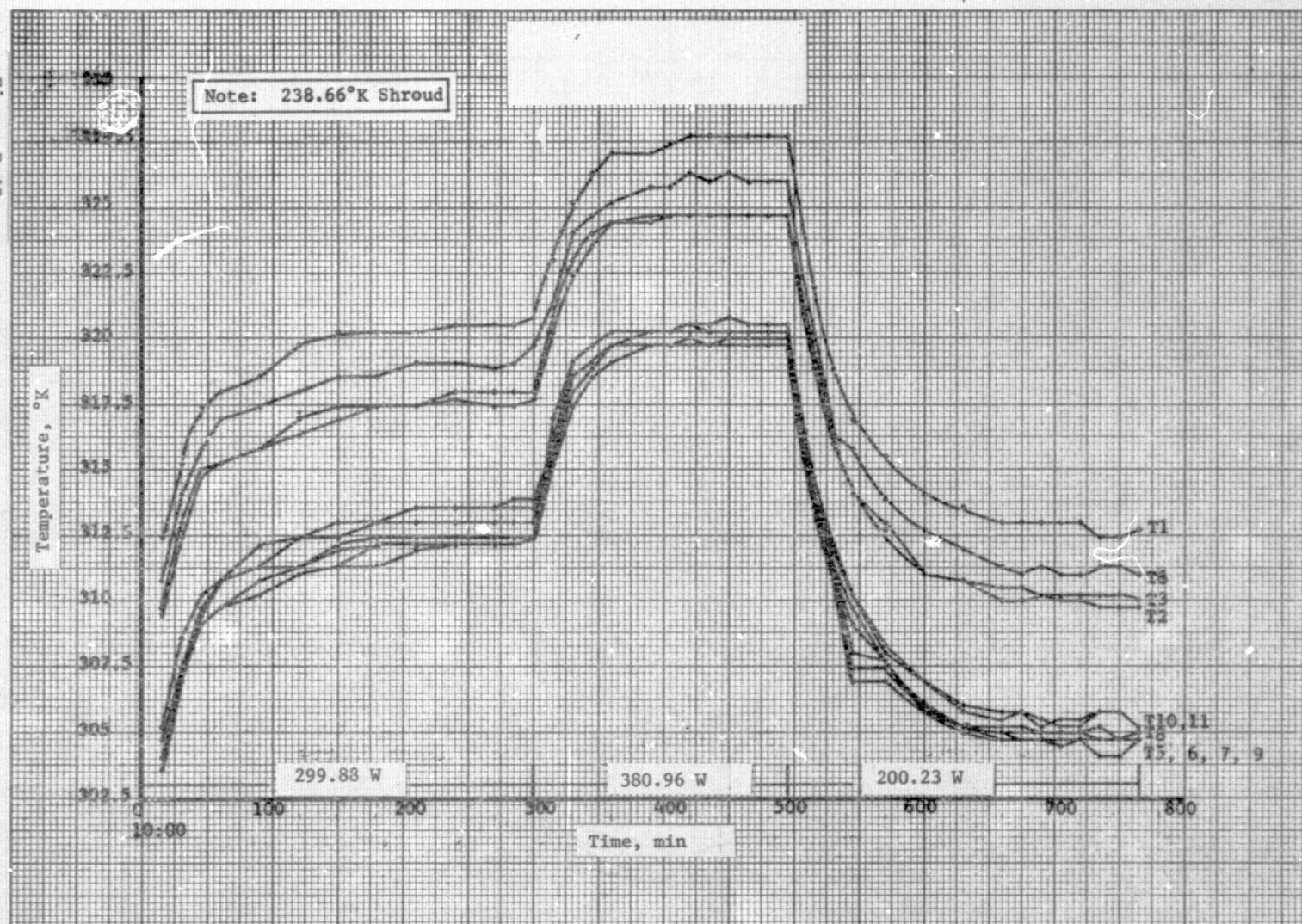


Figure B-42 Test 1, Hot Case Average Shroud

Figure B-43



B-55

Figure B-43 Test 1, Hot Case Thermal Conditioning Panel

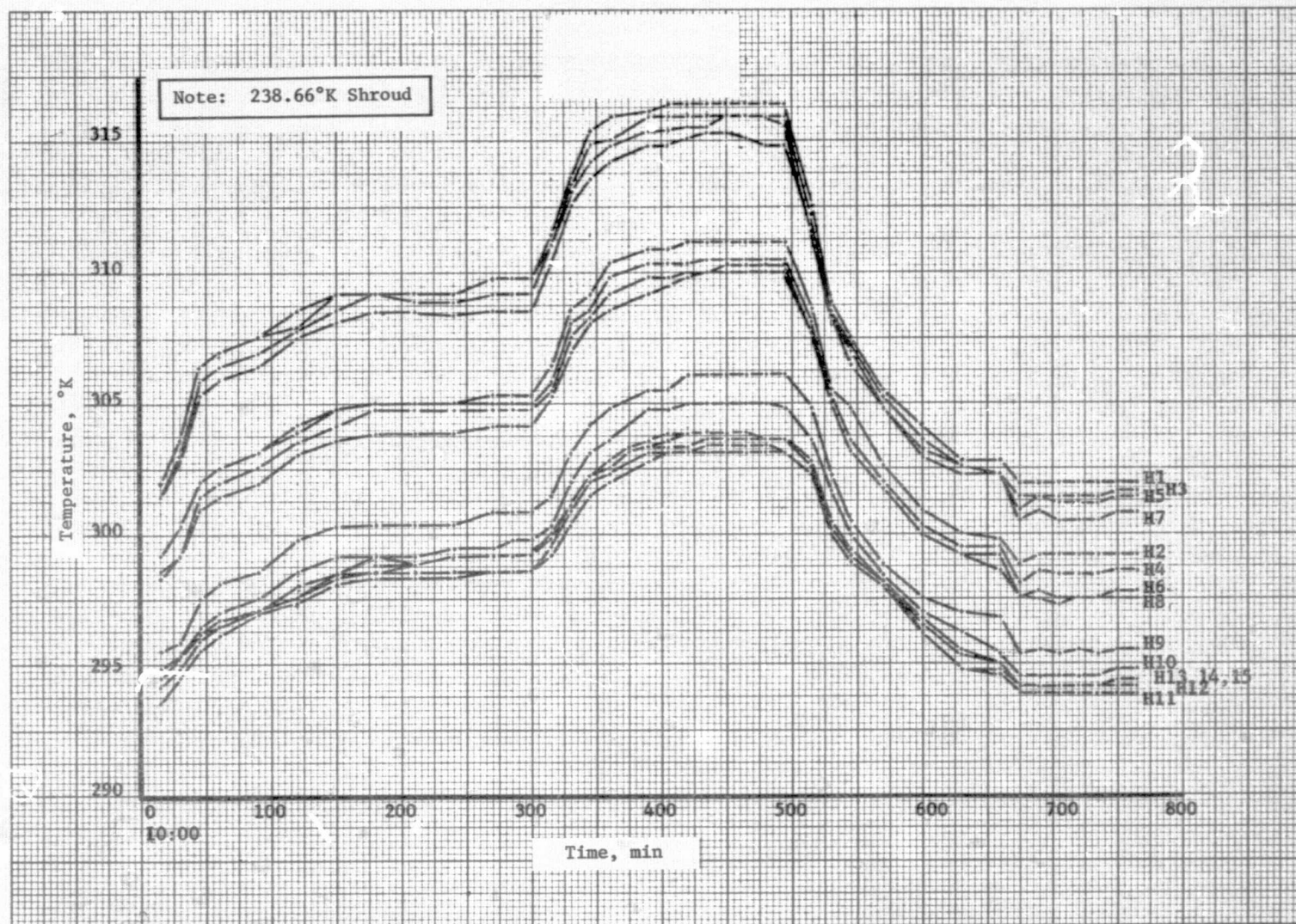
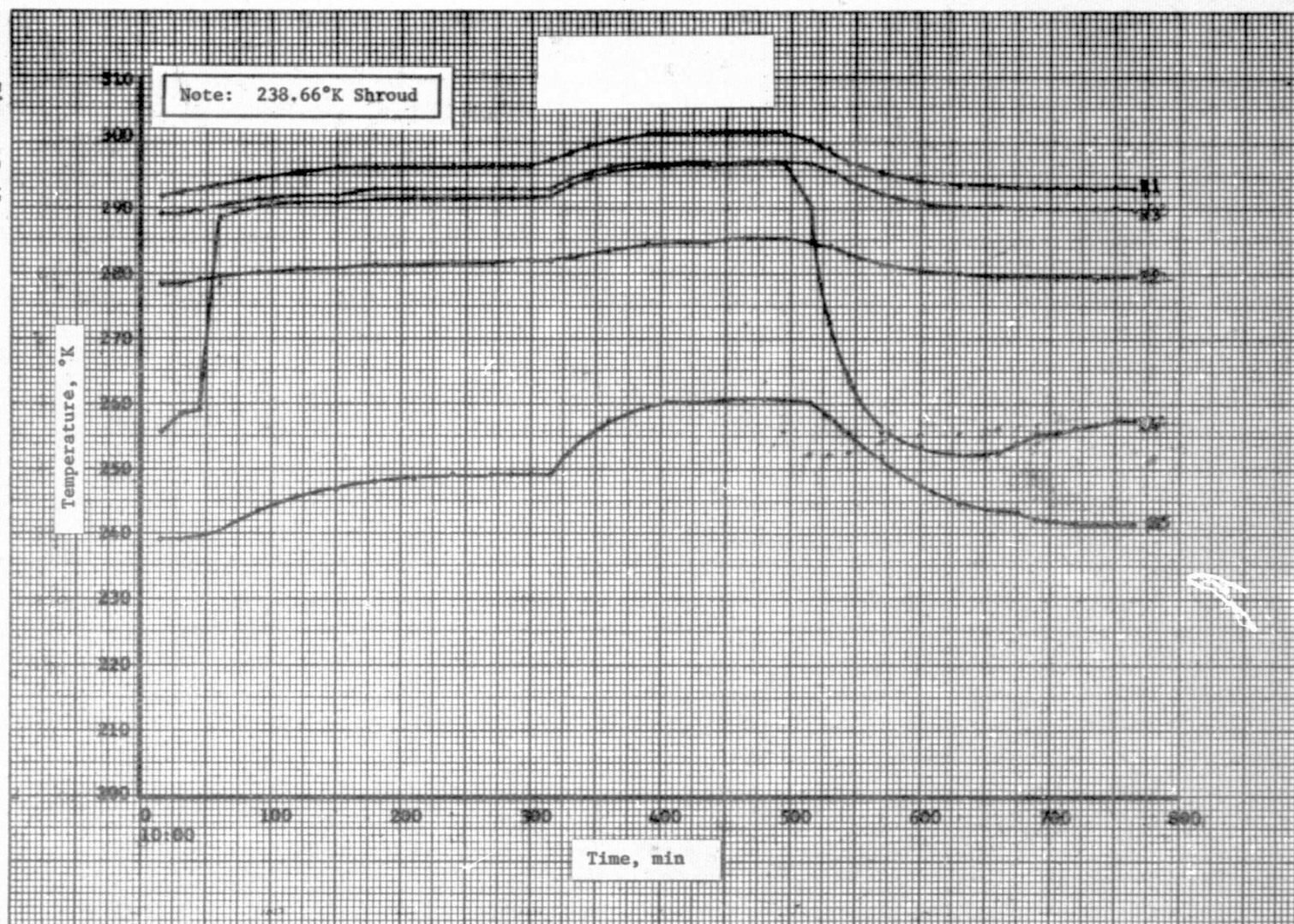


Figure B-44 Test 1, Hot Case Header Heat Pipe

Figure B-45



B-57

Figure B-45 Test 1, Hot Case Radiator Heat Pipe No. 1

Figure B-46
B-58

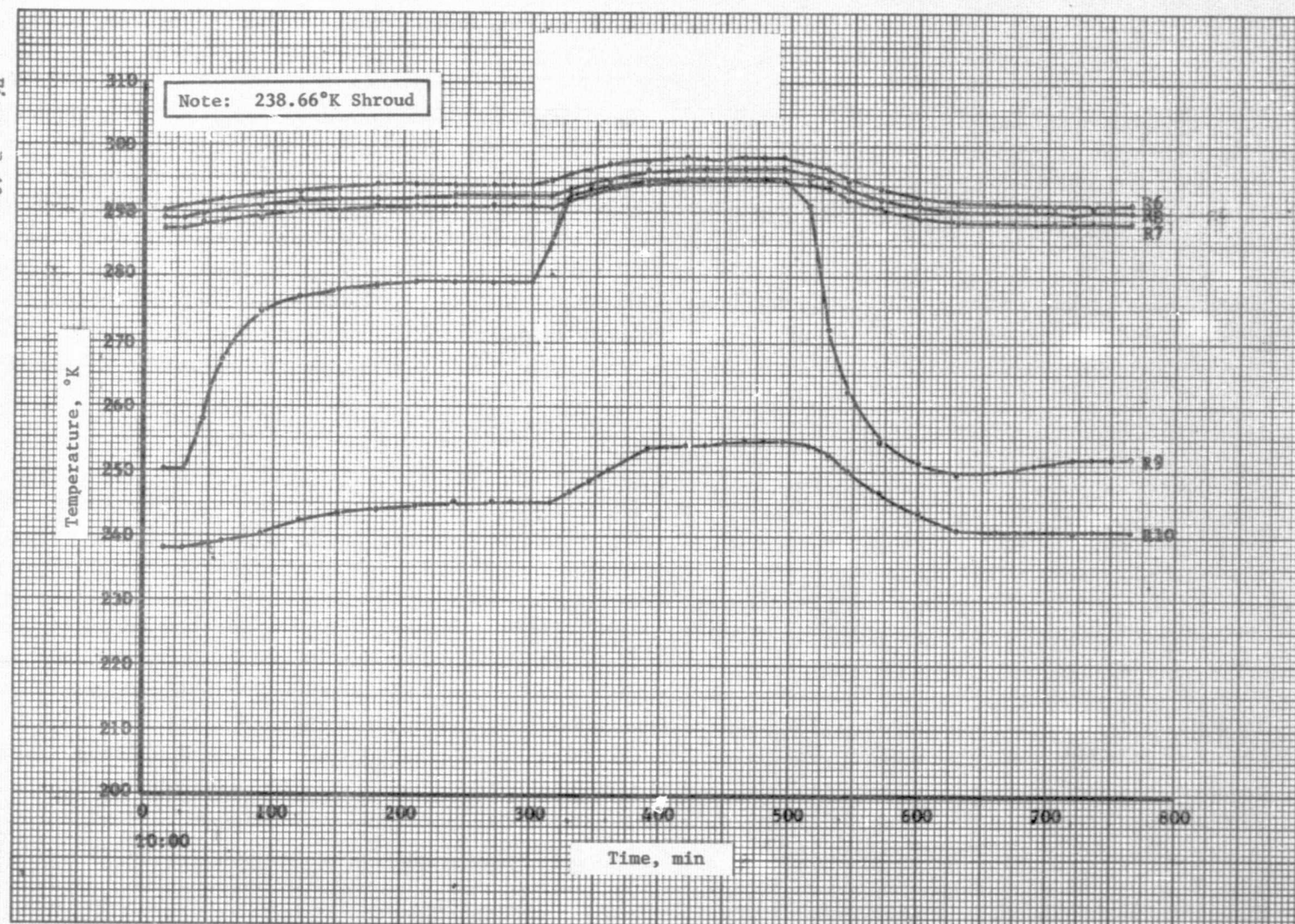
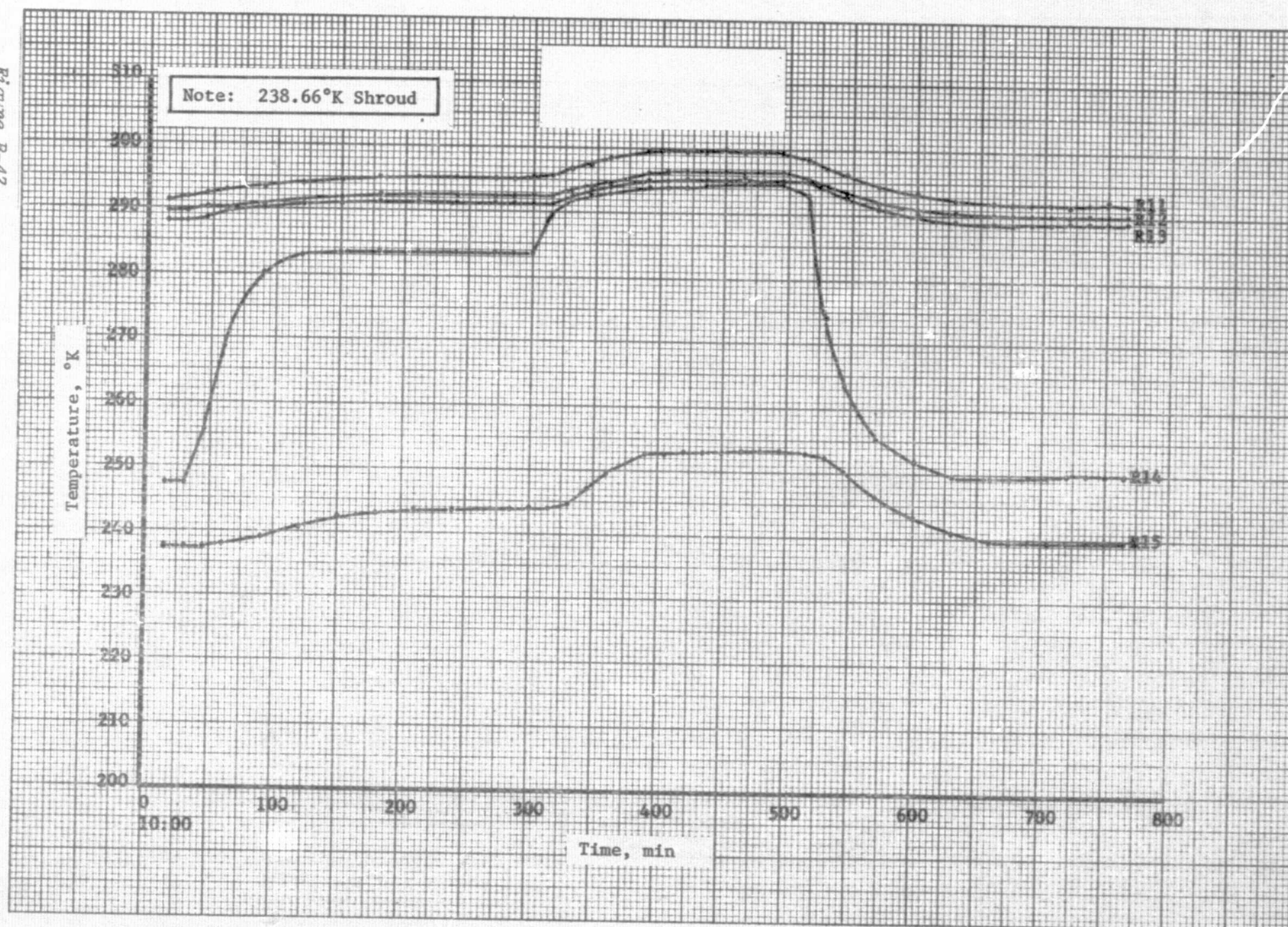


Figure B-46 Test 1, Hot Case Radiator Heat Pipe No. 2

Figure B-47



B-59

Figure B-47 Test 1, Hot Case Radiator Heat Pipe No. 3

Figure B-48
B-60

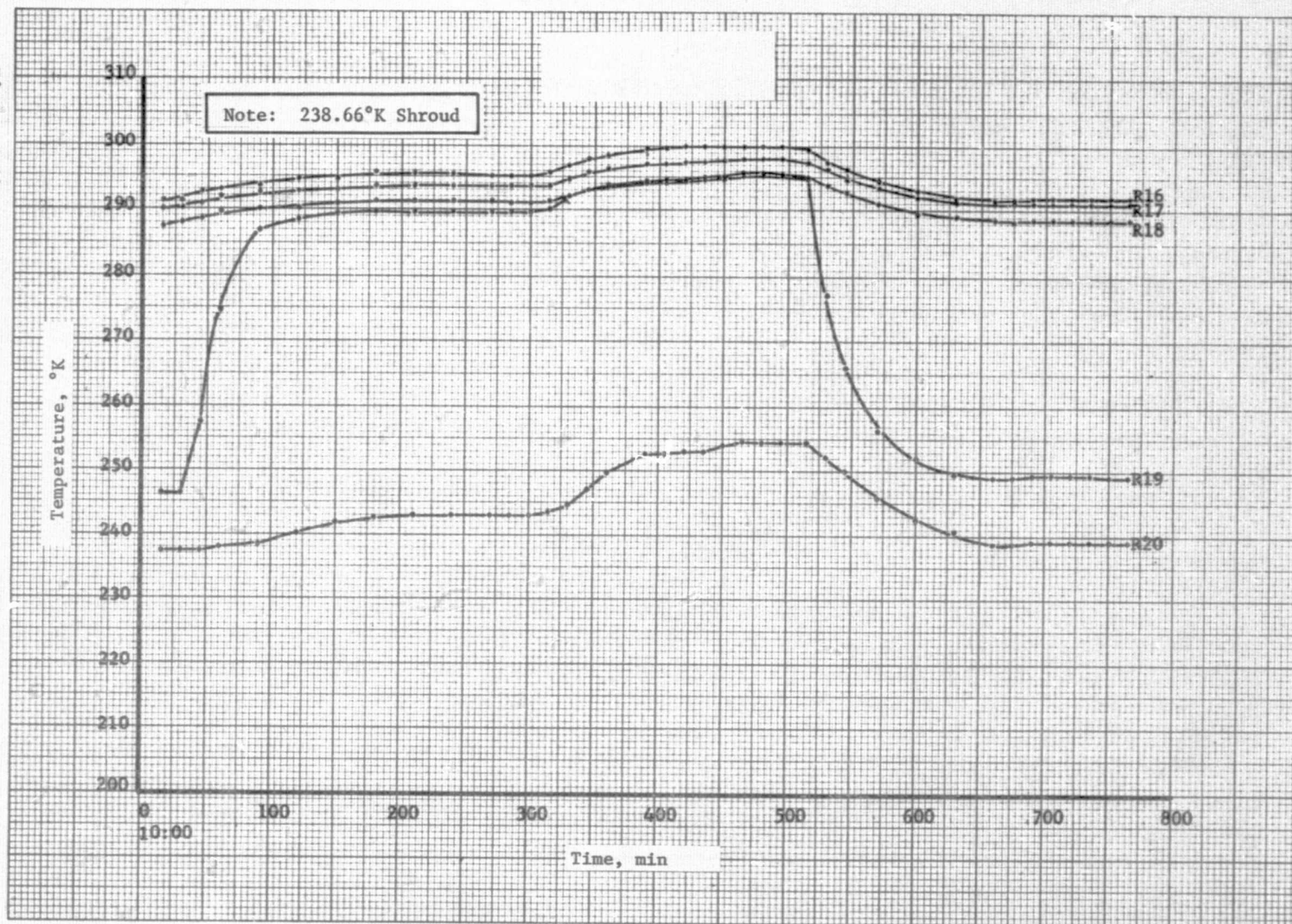
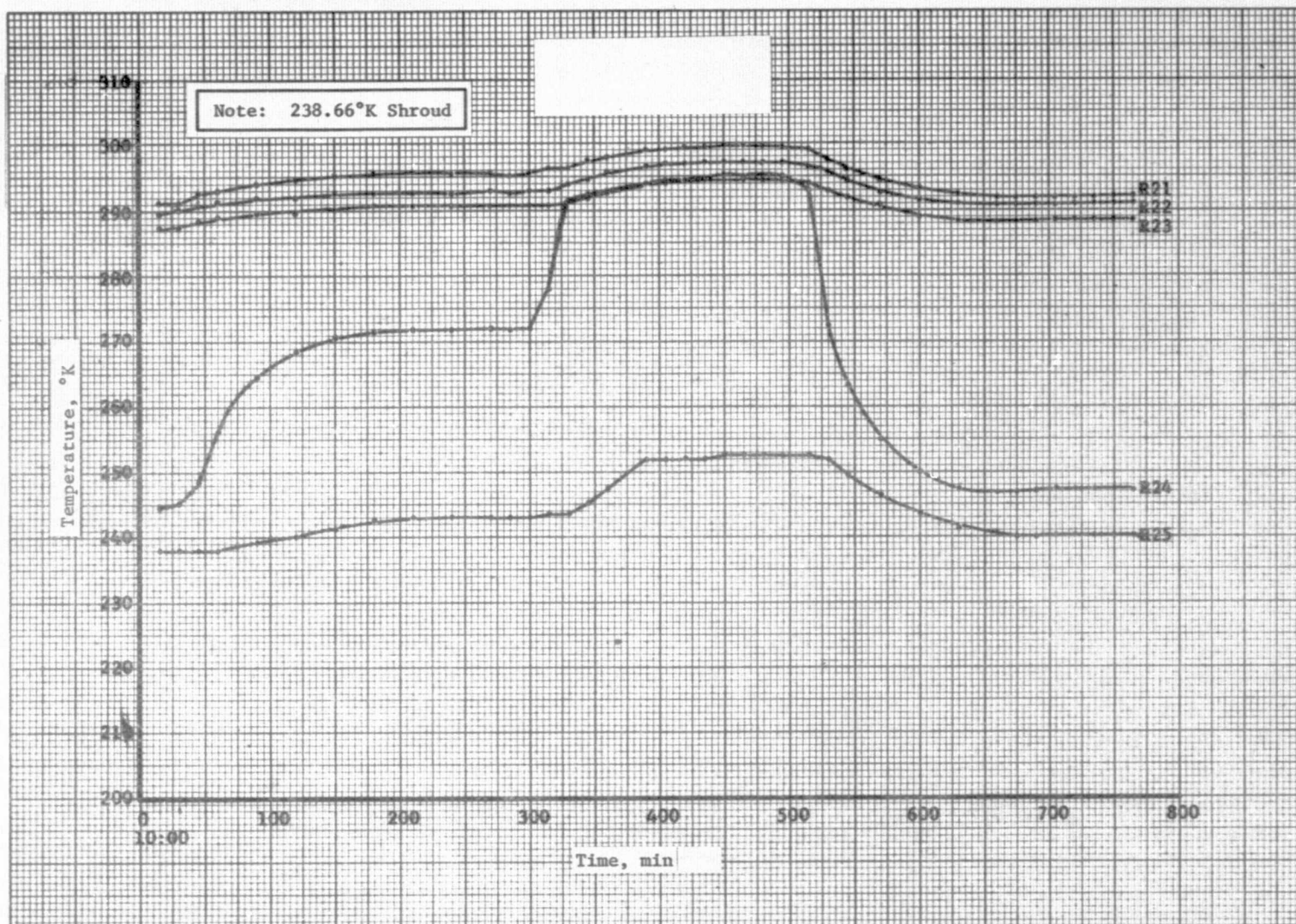


Figure B-48 Test 1, Hot Case Radiator Heat Pipe No. 4

Figure B-49



B-61

Figure B-49 Test 1, Hot Case Radiator Heat Pipe No. 5

Figure B-50
B-62

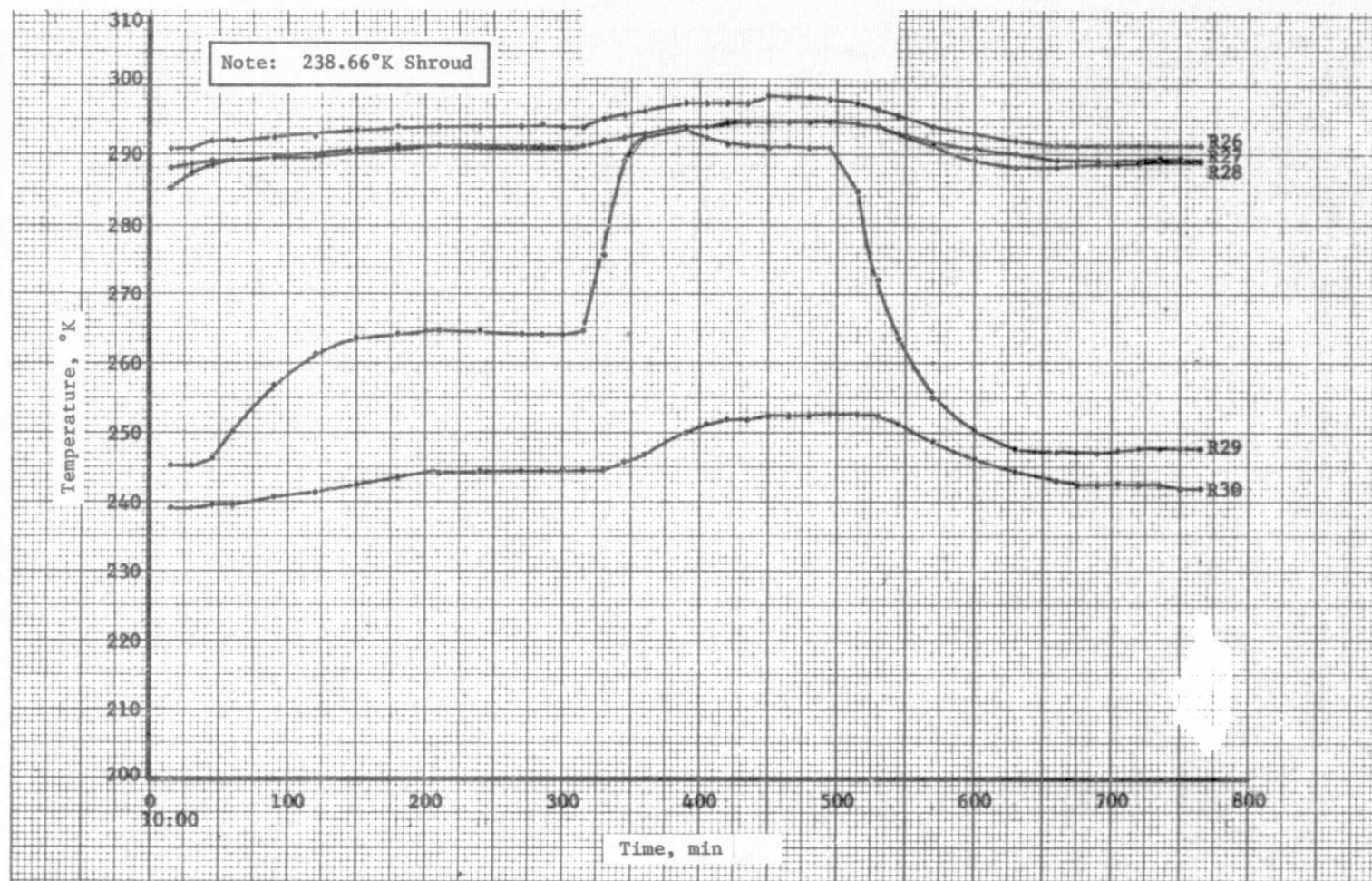


Figure B-50 Test 1, Hot Case Radiator Heat Pipe No. 6

REPRODUCIBILITY OF THE
ORIGINAL PAGE IS POOR

Figure B-51

B-63

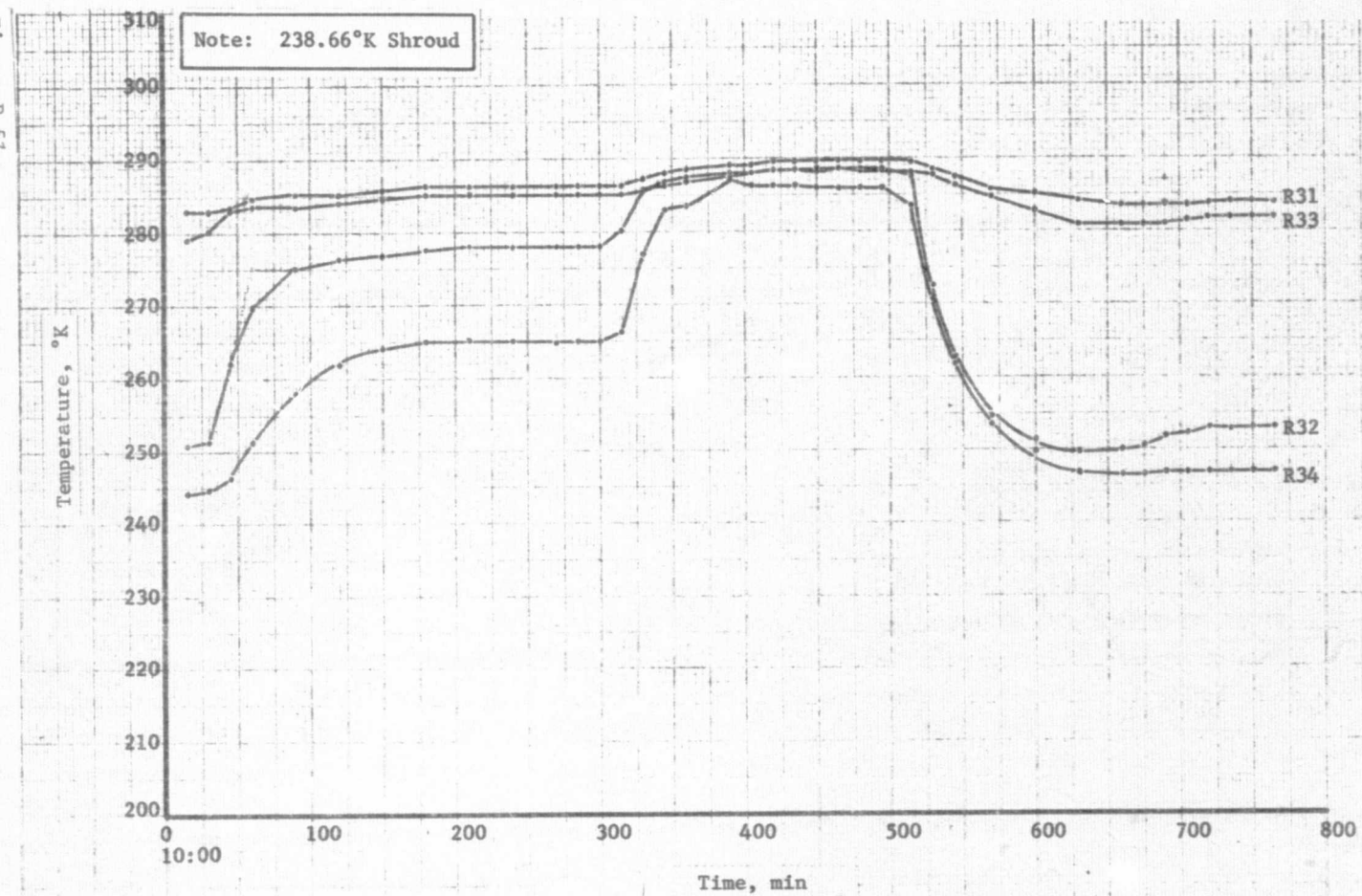


Figure B-51 Test 1, Hot Case Radiator Skin Temperature

B-64
Figure B-52

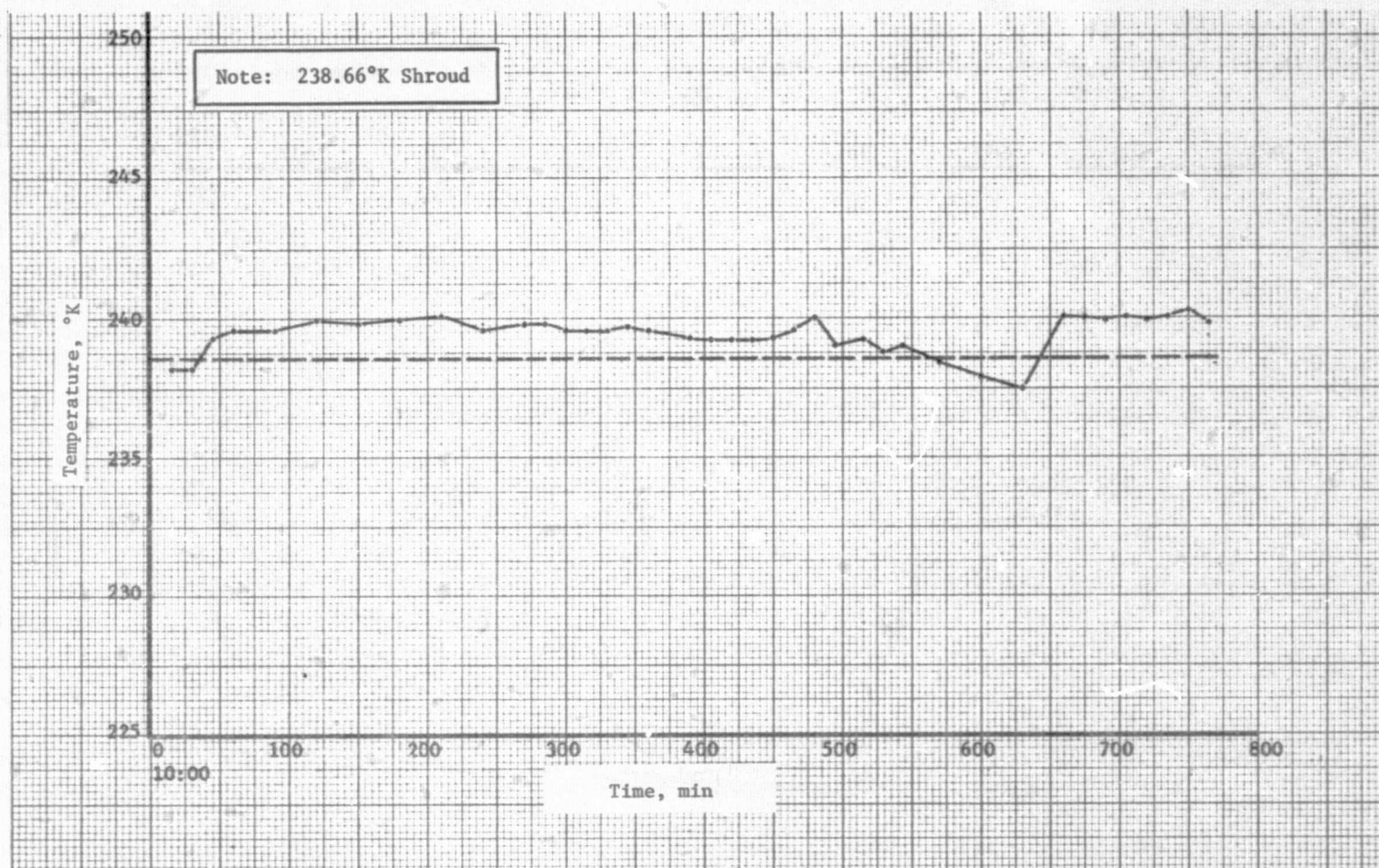


Figure B-52 Test 1, Hot Case Shroud

The radiator data clearly shows the front movement throughout this test series as exemplified by Figures B-35 and B-45 by thermocouples R3 (Table B-7) and R4. Thermocouple R2 was observed during the test to read lower than R3. This thermocouple (Figure B-4) was located on the adiabatic section of feeder tube 1. After removing the radiator from the chamber it appeared that this thermocouple had become detached from the tube and was very likely influenced by the shroud temperature. The radiator skin temperature shown in Figures B-41 through B-51 show the expected trends including a nonuniform front location in the feeder tubes. This was anticipated since the evaporator section of feeder pipe 6 is only 15.24 cm (6 in.) long compared with the 30.48 cm (12 in.) length of the other 5 pipes.

The shroud temperatures are presented as average values in the transient plots and as individual temperatures by location in the steady-state summaries. Thermocouple S-10 (Table B-7) failed to yield data comparable with the other shroud temperature and is not presented in any of the data summaries. The average temperature plots are based upon the nine thermocouples for each plot. No attempt was made to correct the problem on the S-10 thermocouple due to the time required to remove the insulation blankets and the potential requirement of removing the shroud from the chamber before corrective action could be performed. After completing the test, this thermocouple was found to be detached from the panel.

B. TEST 2 COLD CASE 194.29°K SHROUD

Cold case testing of the system was continued after completing the hot case by reducing the shroud temperature to 194.3°K (-110°F). The 200 and 400 W power levels were accomplished without difficulty after increasing the power to 600 W over the temperature of the thermal conditioning panel was achieved. At that point the test plan was modified to three power levels; 200, 400 and 500 W. The 600, 800, and 1000 W tests were deleted. In place of the two deleted tests a colder shroud temperature test was added by agreement with the COR, Mr. Jim Wise.

The data derived from the cold case testing are presented in Figures B-53 through B-68. Figures B-53 through B-58 present the steady-state results by location on the test hardware for the three power level tests. Figures B-59 through B-68 present temperature histories from these runs showing the transient response from a changing power load at a constant shroud temperature.

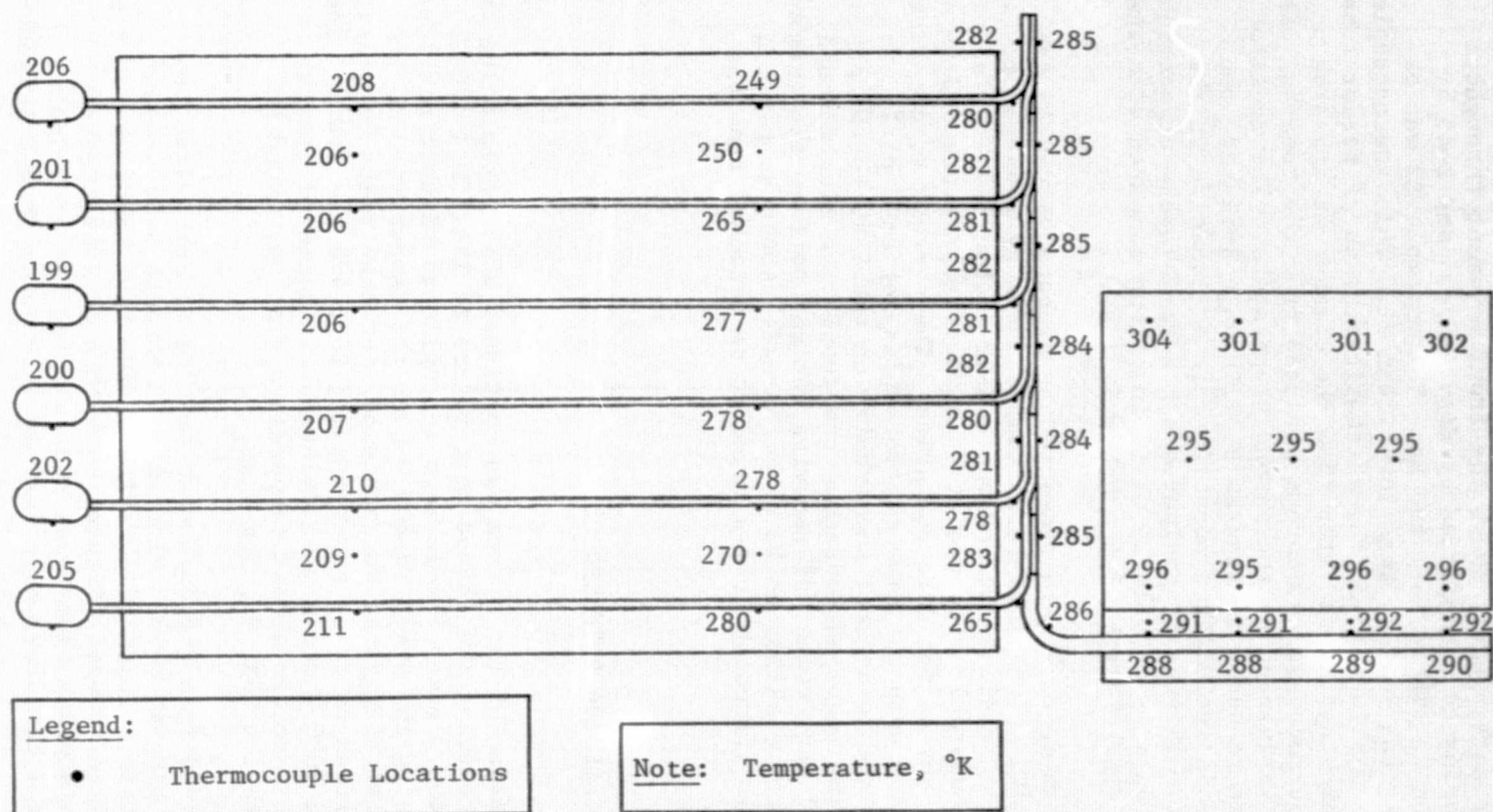


Figure B-53 Test 2 Cold Case, 200.39 W

Figure B-54

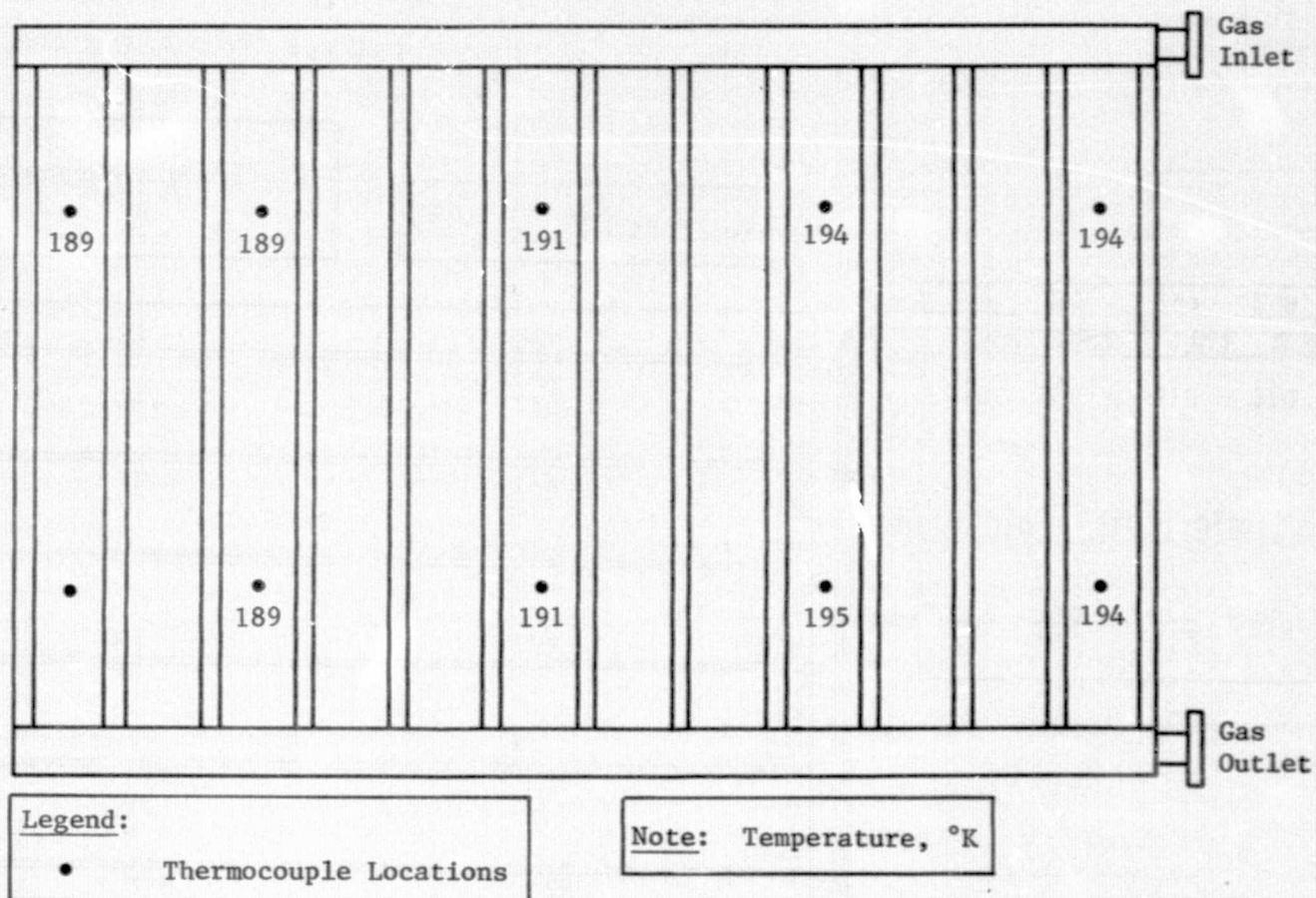
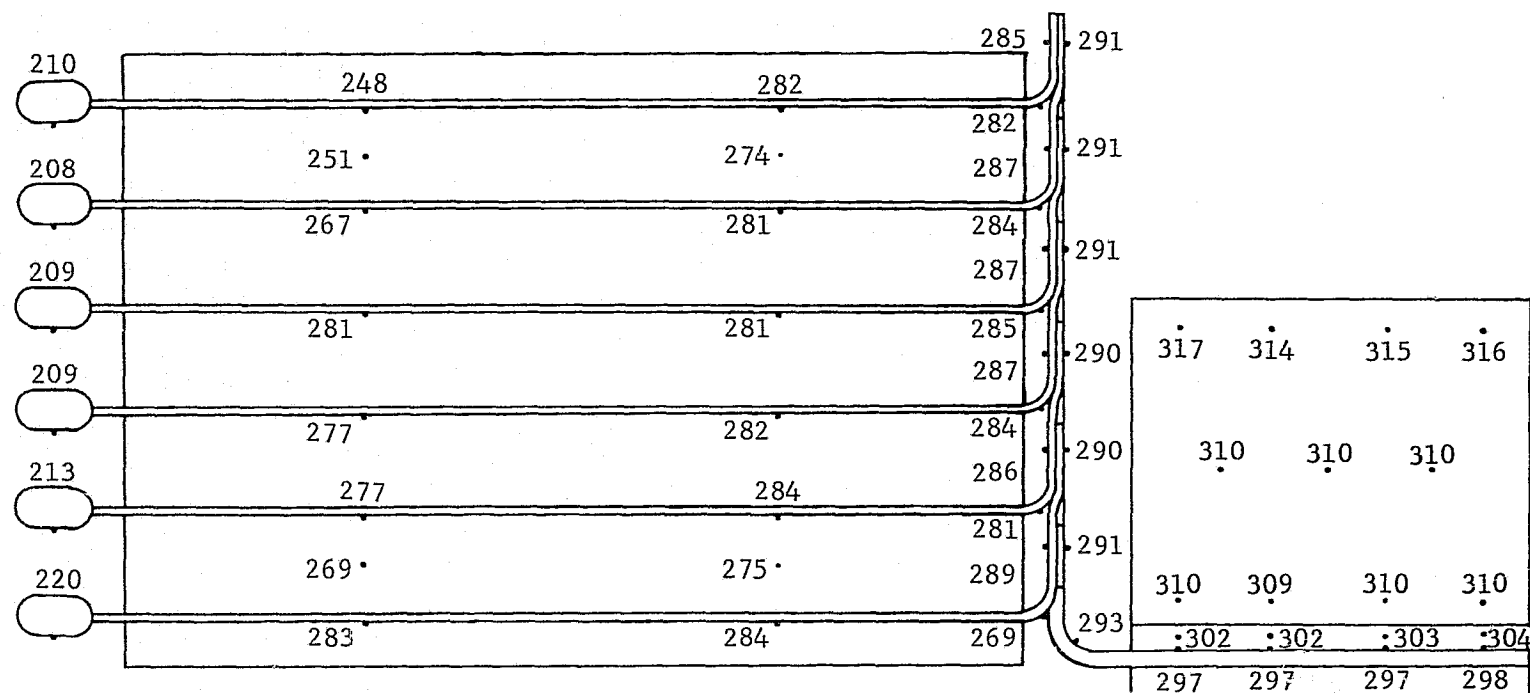


Figure B-54 Test 2 Cold Case, 200.39 W

Figure B-55



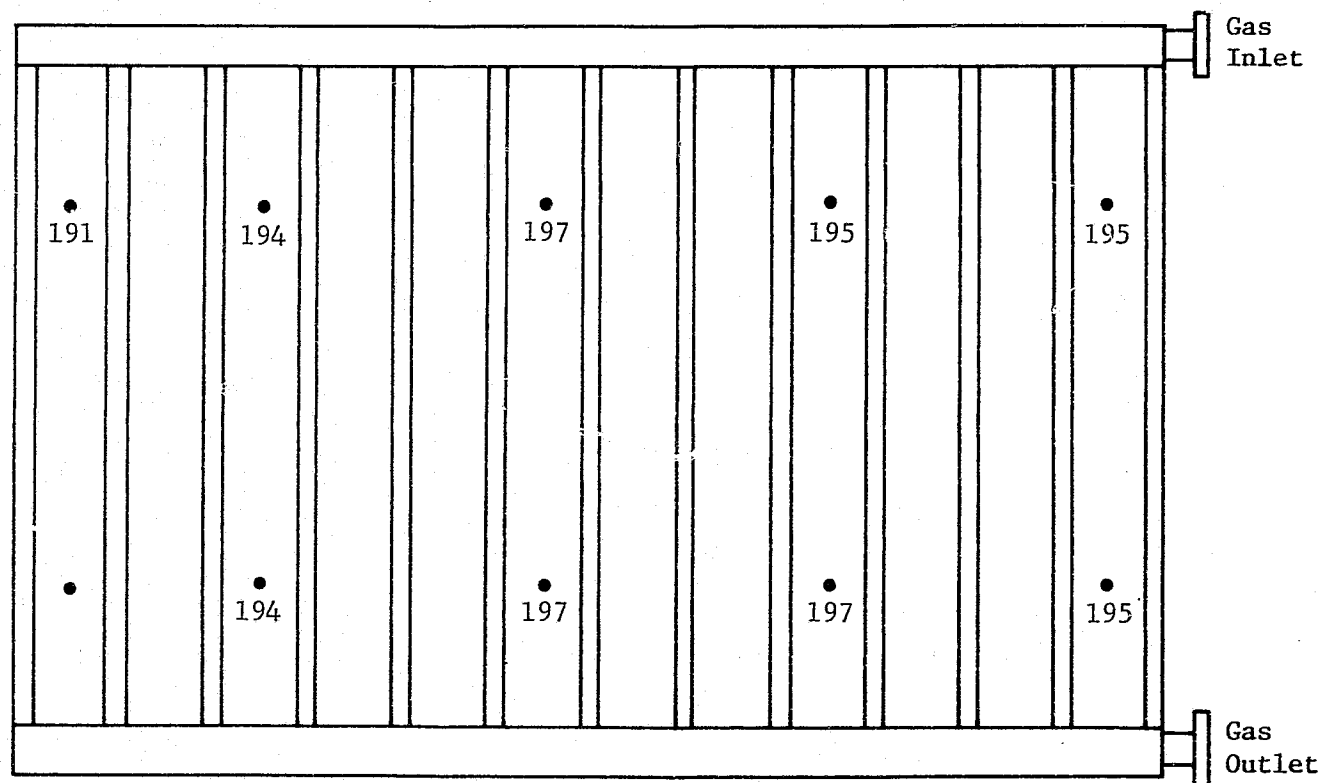
Legend:

• Thermocouple Locations

Note: Temperature, °K

Figure B-55 Test 2 Cold Case, 398.27 W

Figure B-56



Legend:

• Thermocouple Locations

Note: Temperature, °K

Figure B-56 Test 2 Cold Case, 398.27 W

Figure B-57
B-70

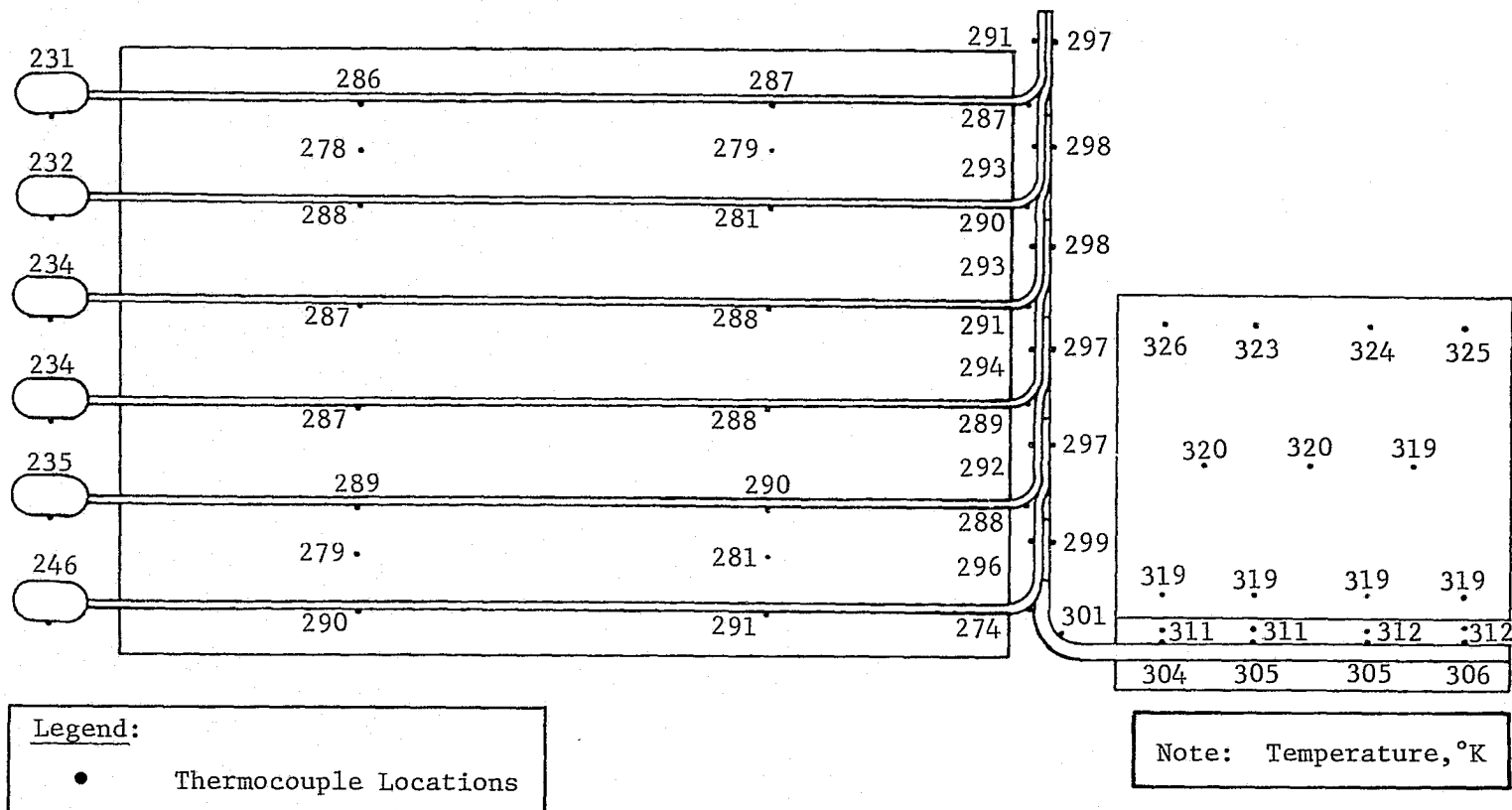
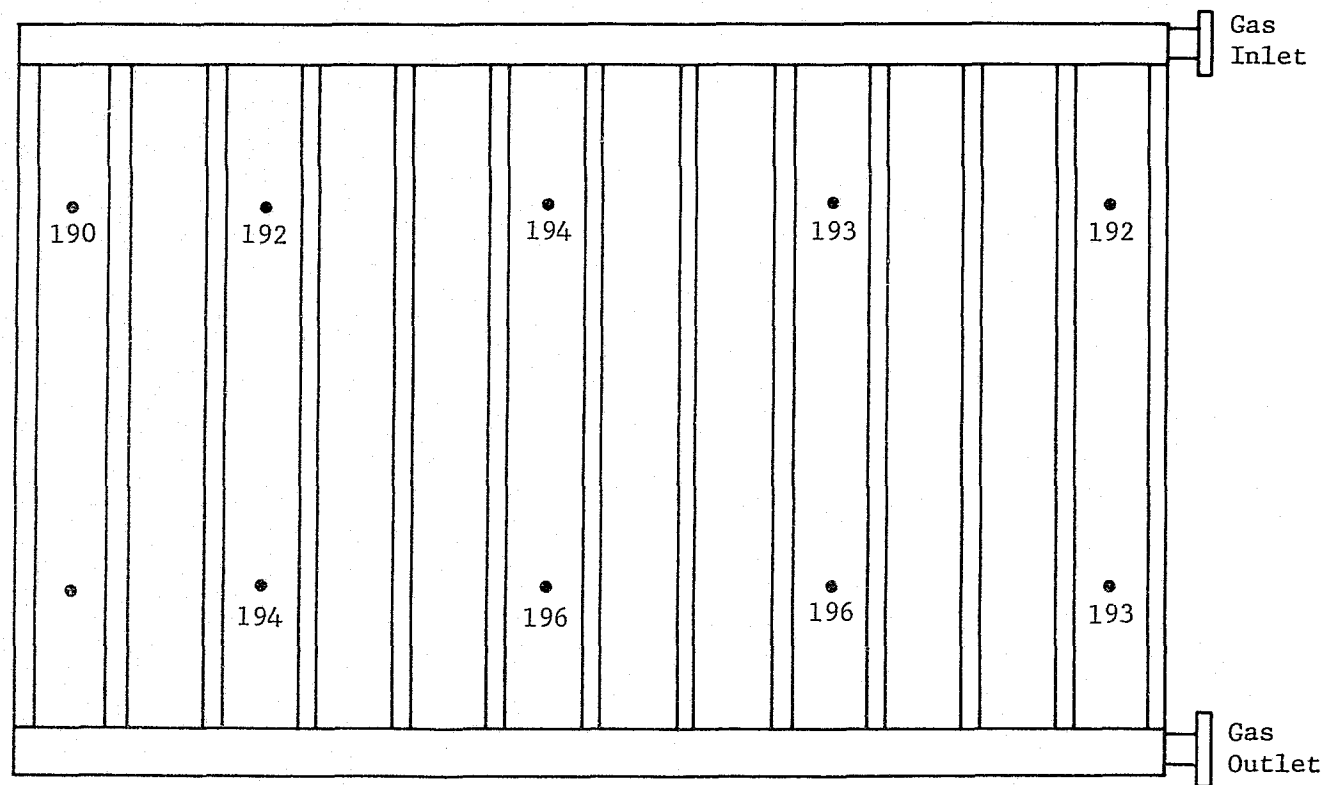


Figure B-57 Test 2 Cold Case, 499.92 W

Figure B-58



Legend:

• Thermocouple Locations

Note: Temperature, °K

Figure B-58 Test 2 Cold Case, 499.92 W

Figure B-59
B-72

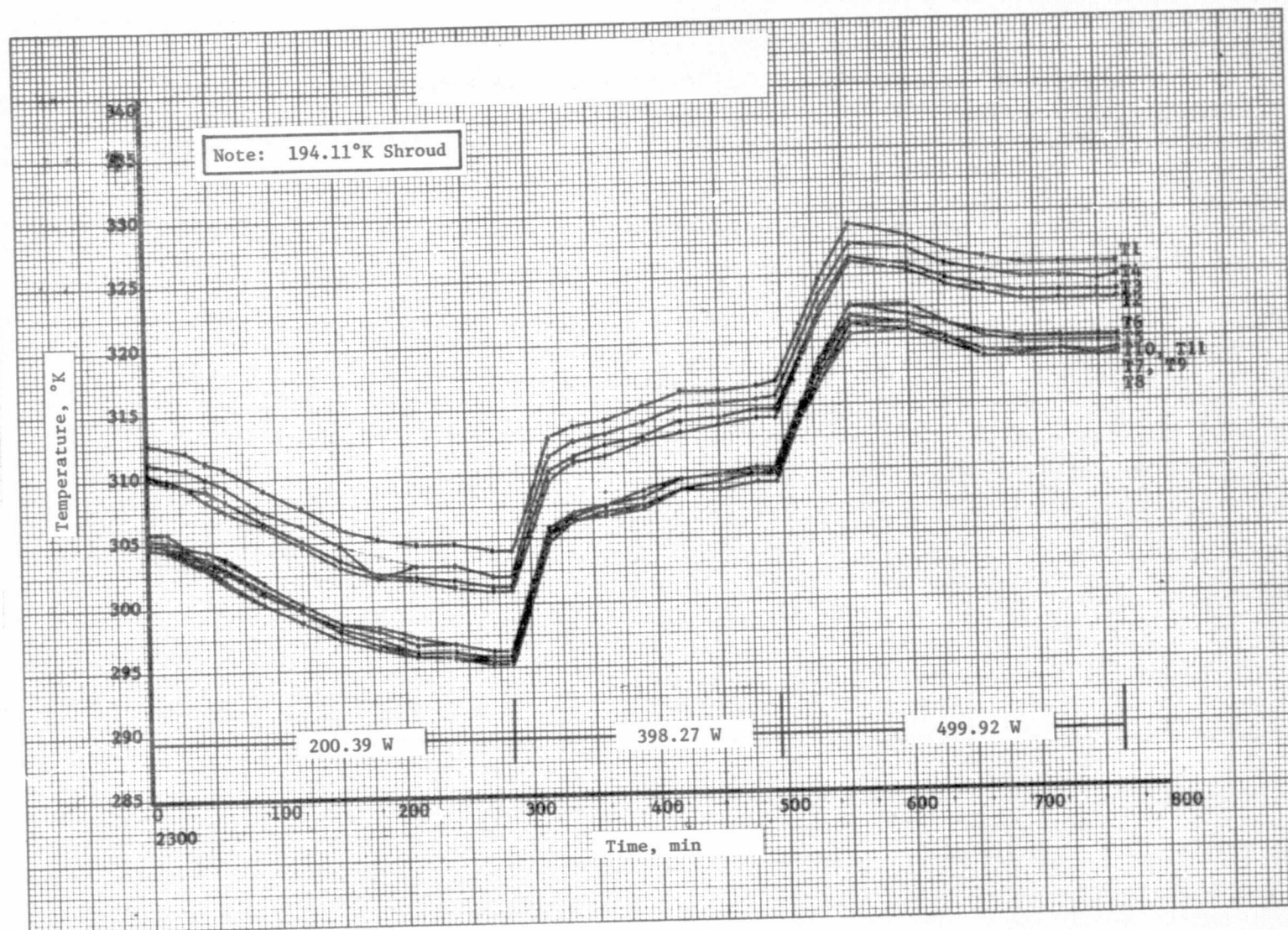


Figure B-59 Test 2, Cold Case Thermal Conditioning Panel

REPRODUCIBILITY OF THE
ORIGINAL PAGE IS POOR

Figure B-60

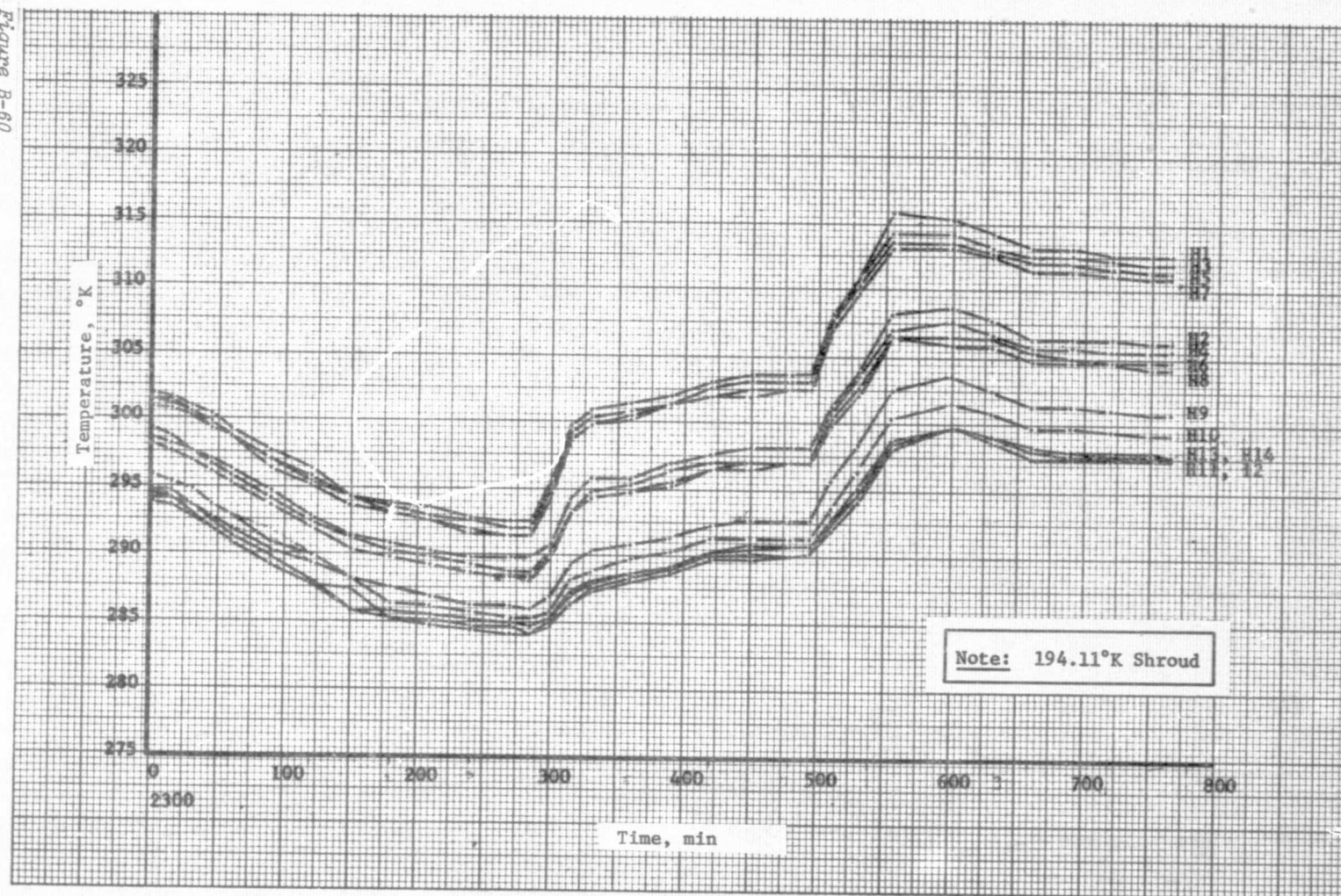


Figure B-60 Test 2, Cold Case Header Heat Pipe

Figure B-61
B-74

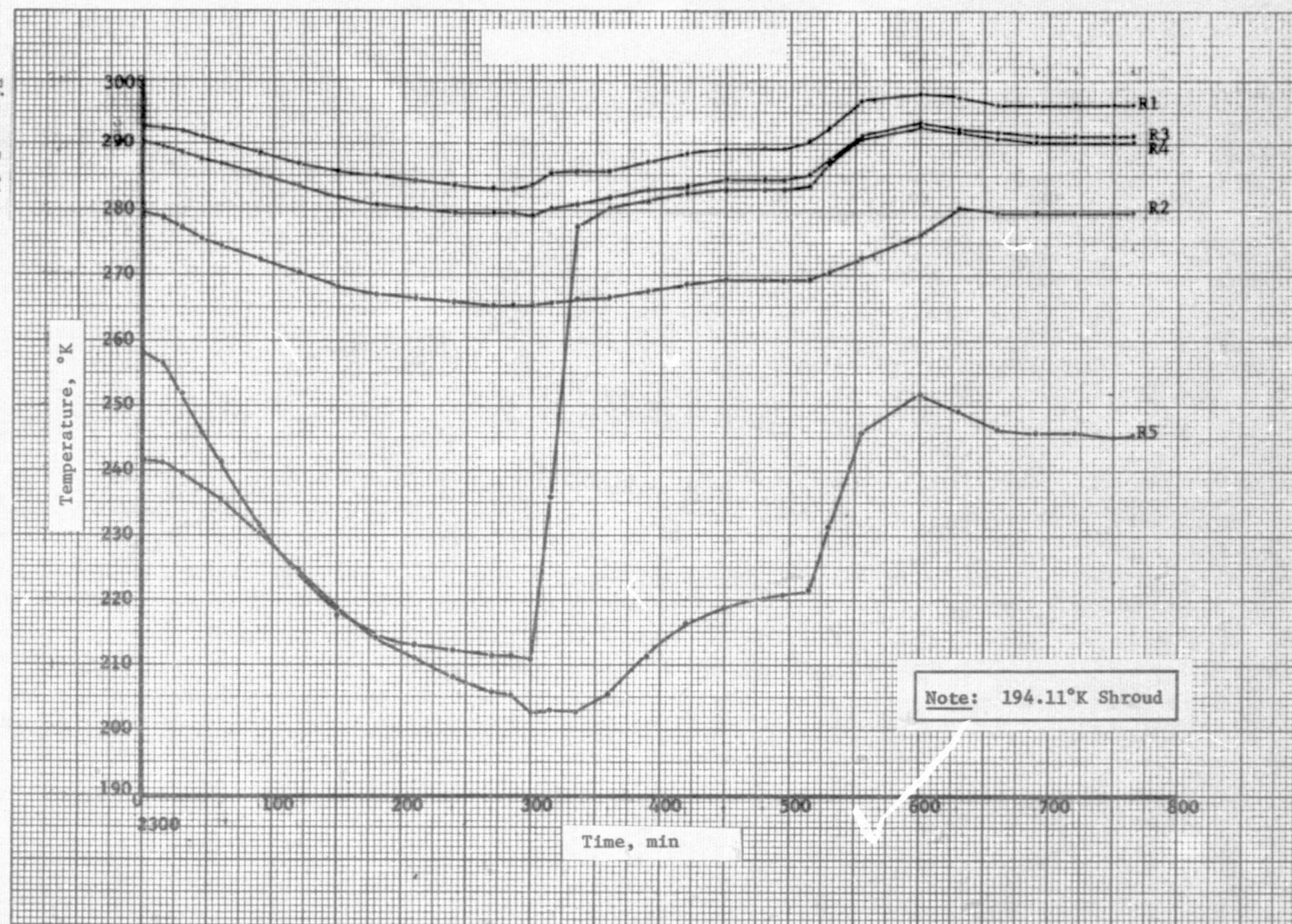
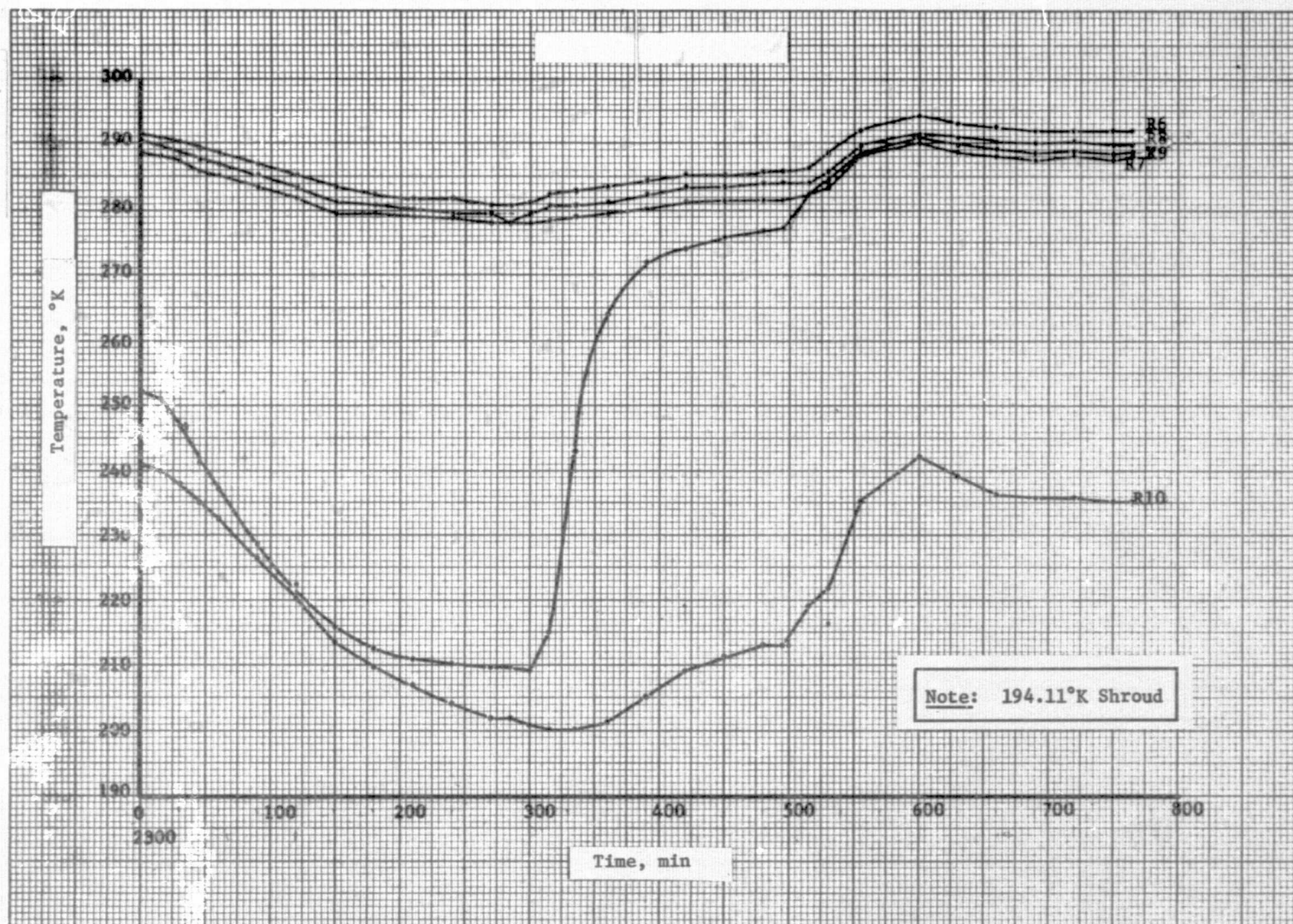


Figure B-61 Test 2, Cold Case Radiator Heat Pipe No. 1

Figure B-62



B-75

Figure B-62 Test 2, Cold Case Radiator Heat Pipe No. 2

B-76

Figure B-63

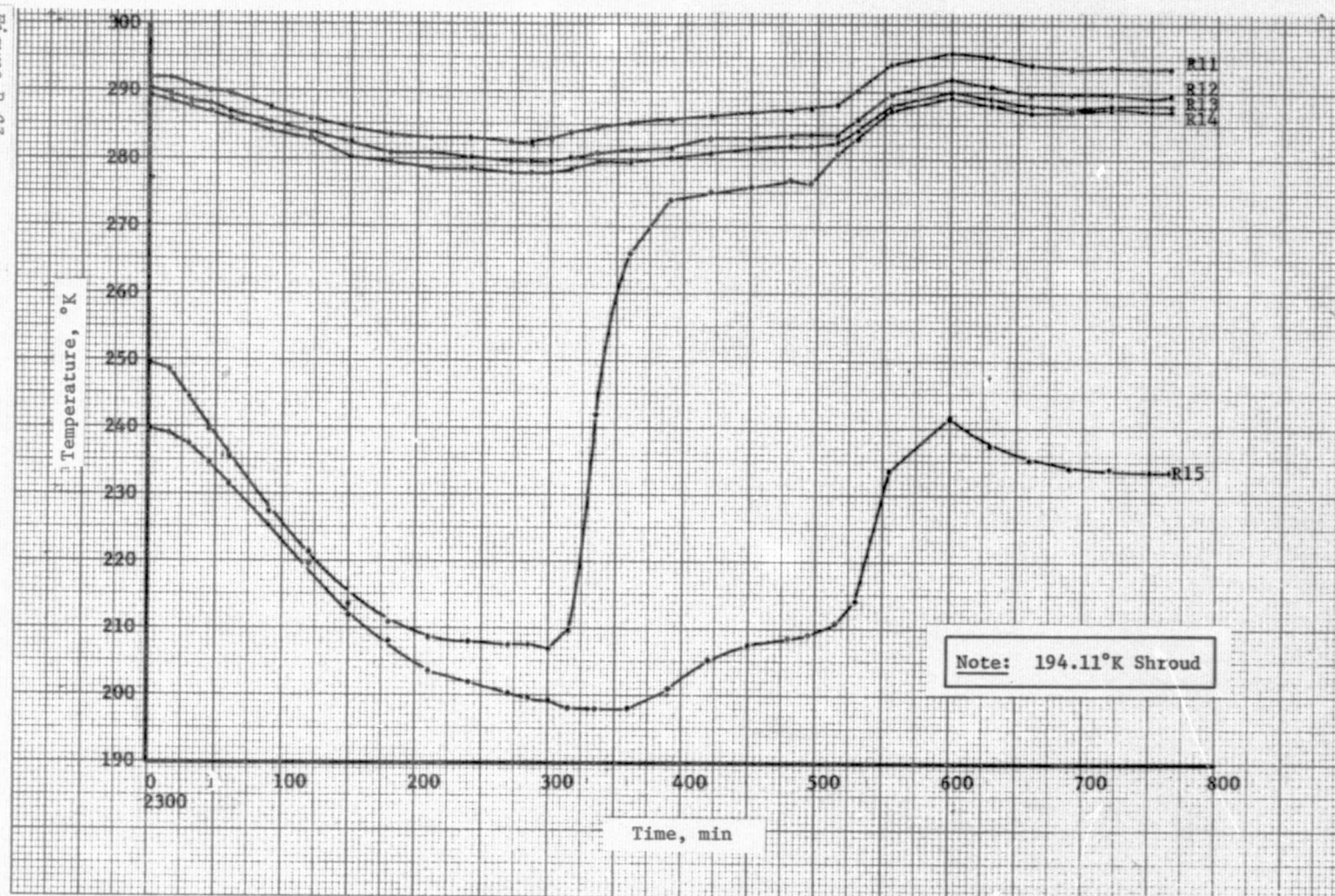


Figure B-63 Test 2, Cold Case Radiator Heat Pipe No. 3

REPRODUCIBILITY OF THE
ORIGINAL PAGE IS POOR

Figure B-64

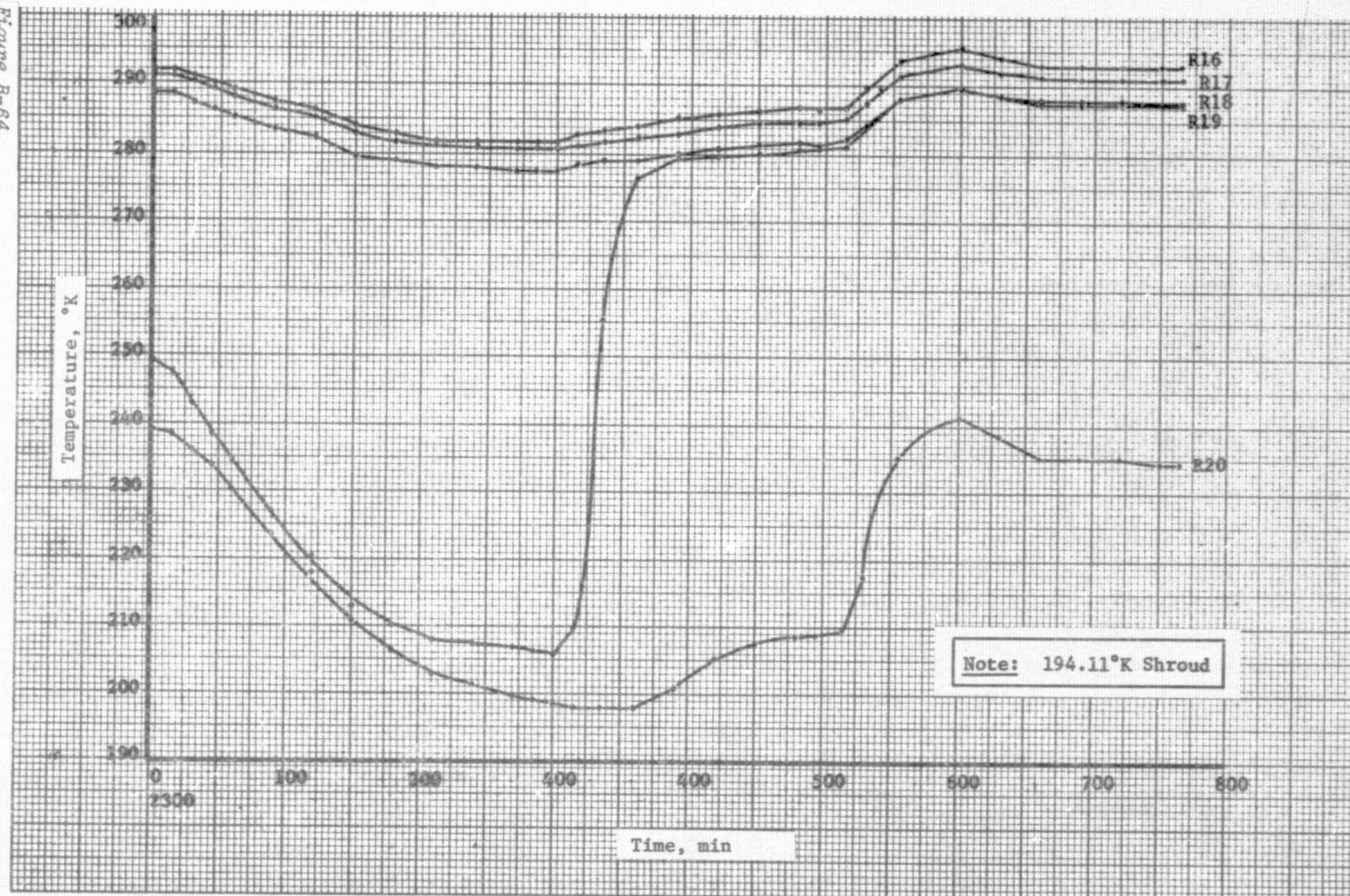


Figure B-64 Test 2, Cold Case Radiator Heat Pipe No. 4

Figure B-65
B-78

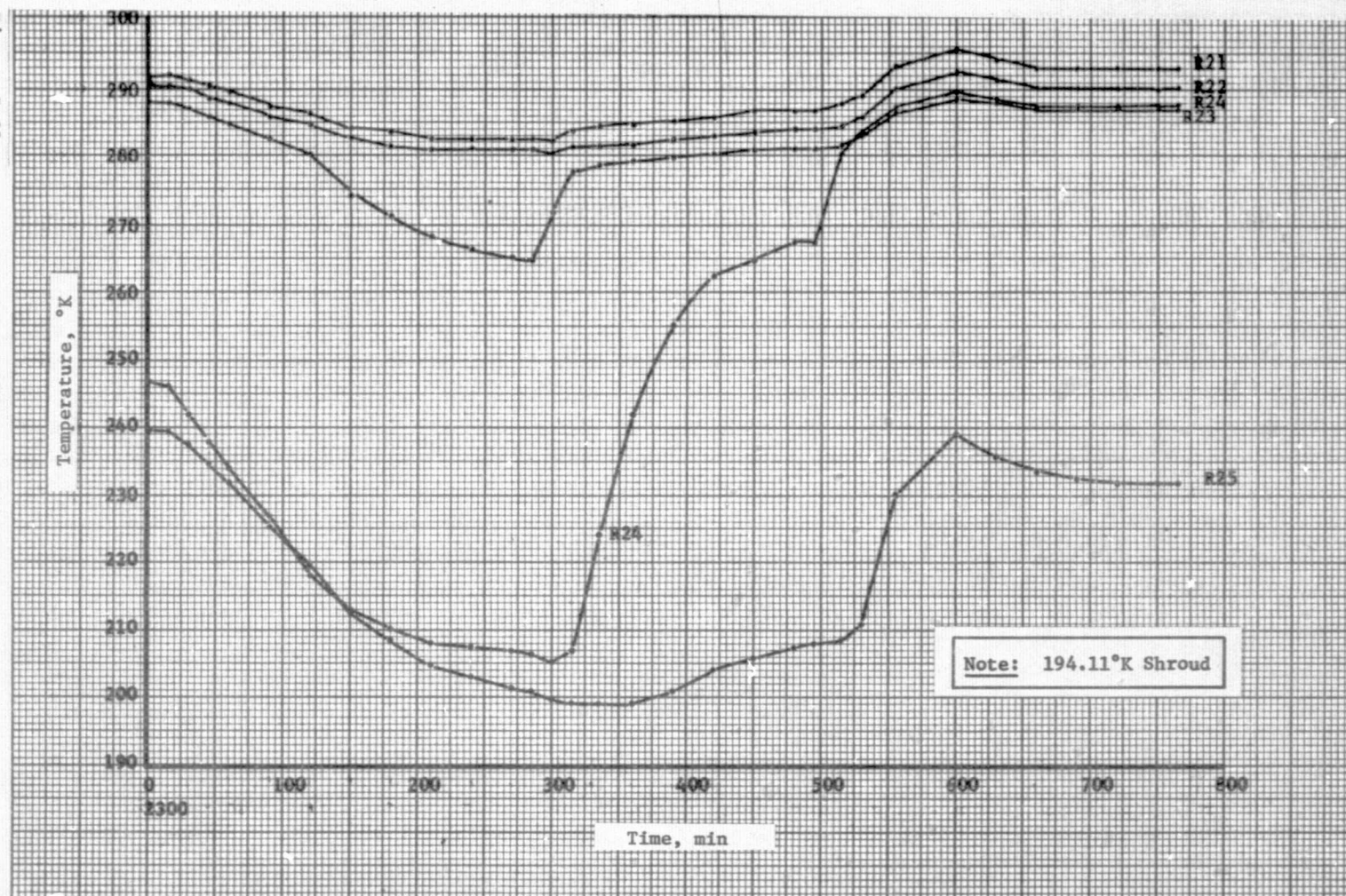
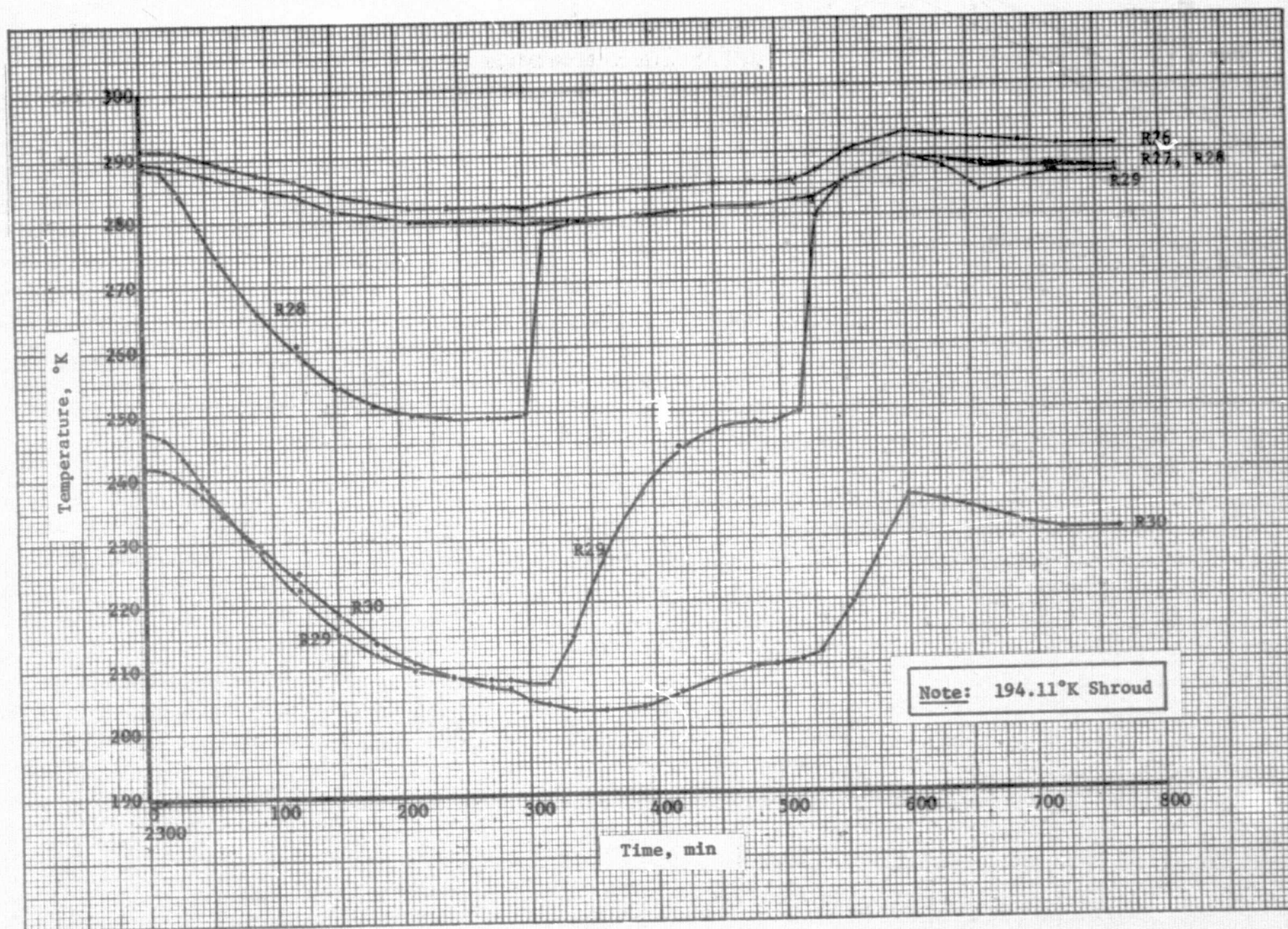


Figure B-65 Test 2, Cold Case Radiator Heat Pipe No. 5

Figure B-66



B-79

Figure B-66 Test 2, Cold Case Radiator Heat Pipe No. 6

Figure B-67
B-80

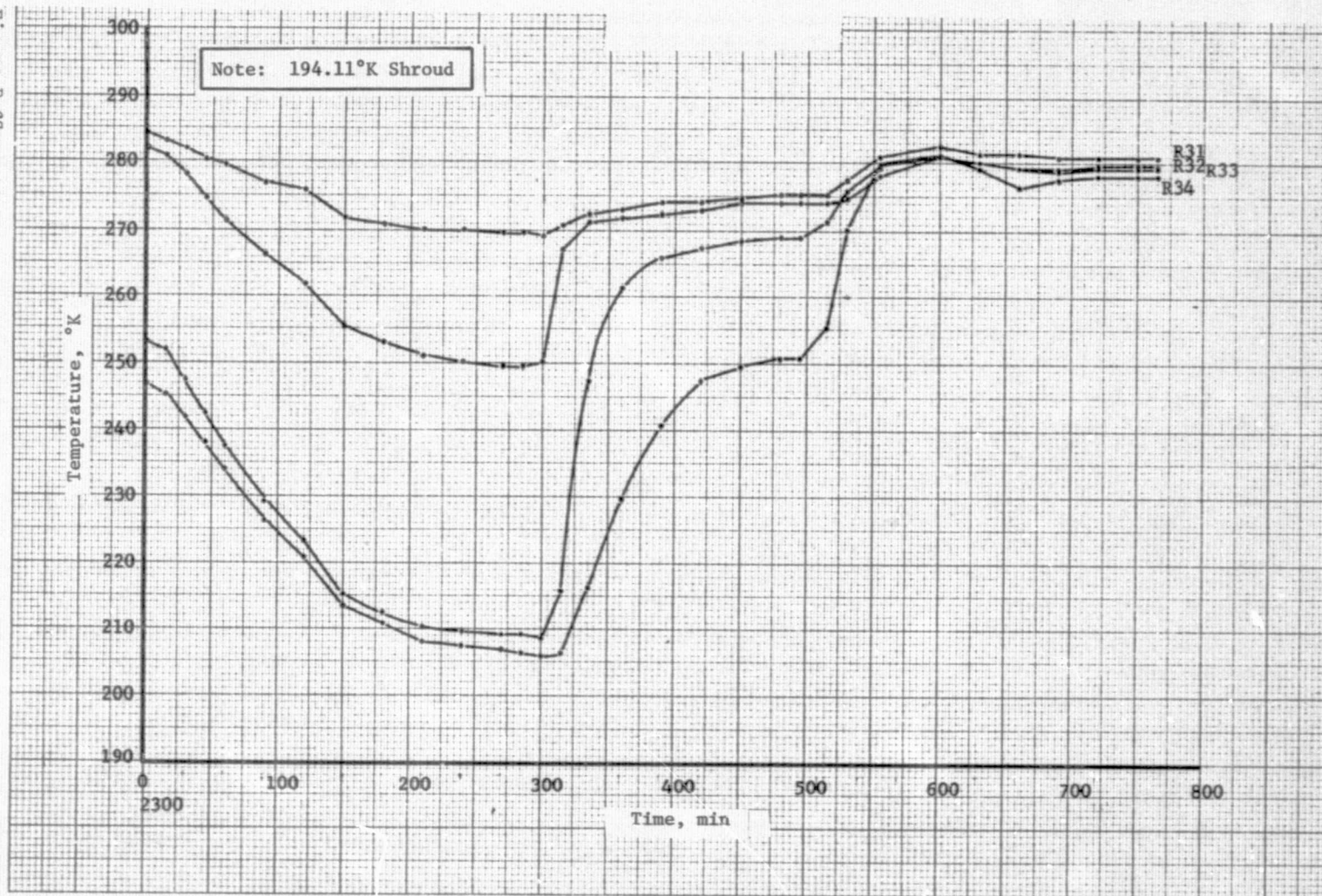


Figure B-67 Test 2, Cold Case Radiator Skin Temperature

REPRODUCIBILITY OF THE
ORIGINAL PAGE IS POOR

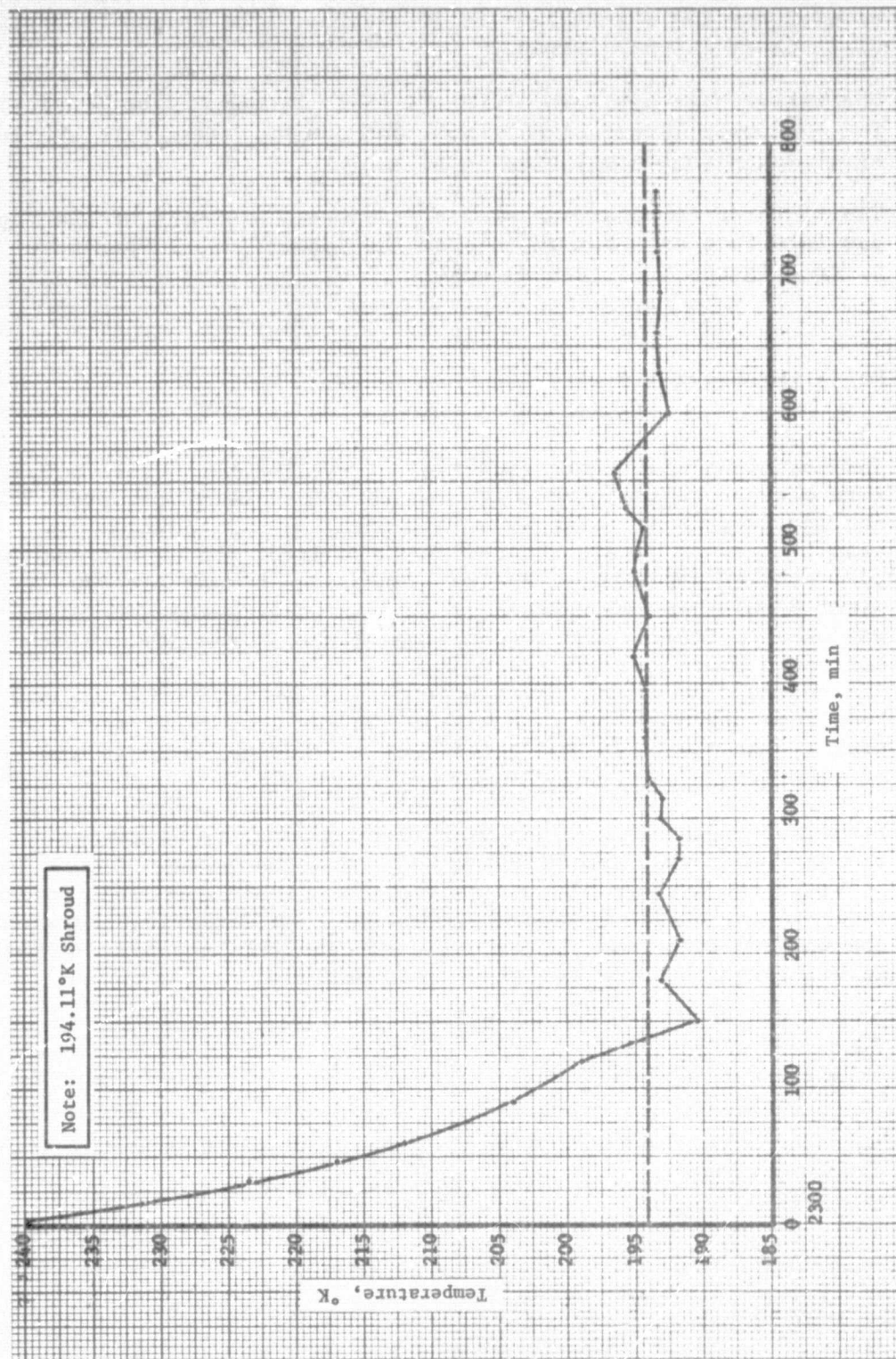


Figure B-68

Figure B-68 Test 2, Cold Case Shroud

The thermal conditioning panel exhibited a maximum of 9°K ΔT over the panel at 200 W. The 400 and 500 W runs both resulted in 8°K ΔT . This agreed with hot case results for the 400 W condition, however the 200 W results were 1°K higher. The reason for this discrepancy is unexplained.

The header heat pipe exhibited ΔT s of 4, 7, and 9°K respectively for the power levels of 200, 400, and 500 W. These data are in agreement with the hot case results.

The radiator temperatures show a pronounced movement of the vapor/gas interface as shown in each of the feeder tube temperature plots (Figures B-61 through B-66).

C. TRANSIENT TESTS

The transient tests were conducted by cycling the shroud temperature between the hot and cold case shroud temperatures 238.7°K and 194.2°K , in a cosine wave form with a 90 min period. Two transient tests were conducted as a result of the over temperature problem experienced during the cold case test series. A minor problem was encountered in the gas heat exchanger which was used to control the shroud temperature. This problem was corrected by increasing the vent area of the unit eliminating the choked flow conditions in the vent. Two sets of transient runs were conducted as a result of the gas heat exchanger problem, however only the second set of runs was reduced and presented.

Figures B-69 through B-78 present the temperature histories of the data that resulted from the 200 and 400 W tests. Figure B-78 presents the average shroud temperature. The unconnected points indicate the desired temperature curve. The comparison between the desired curve and the actual curve was within a few degrees Kelvin throughout the transient test series.

Figure B-69

B-83

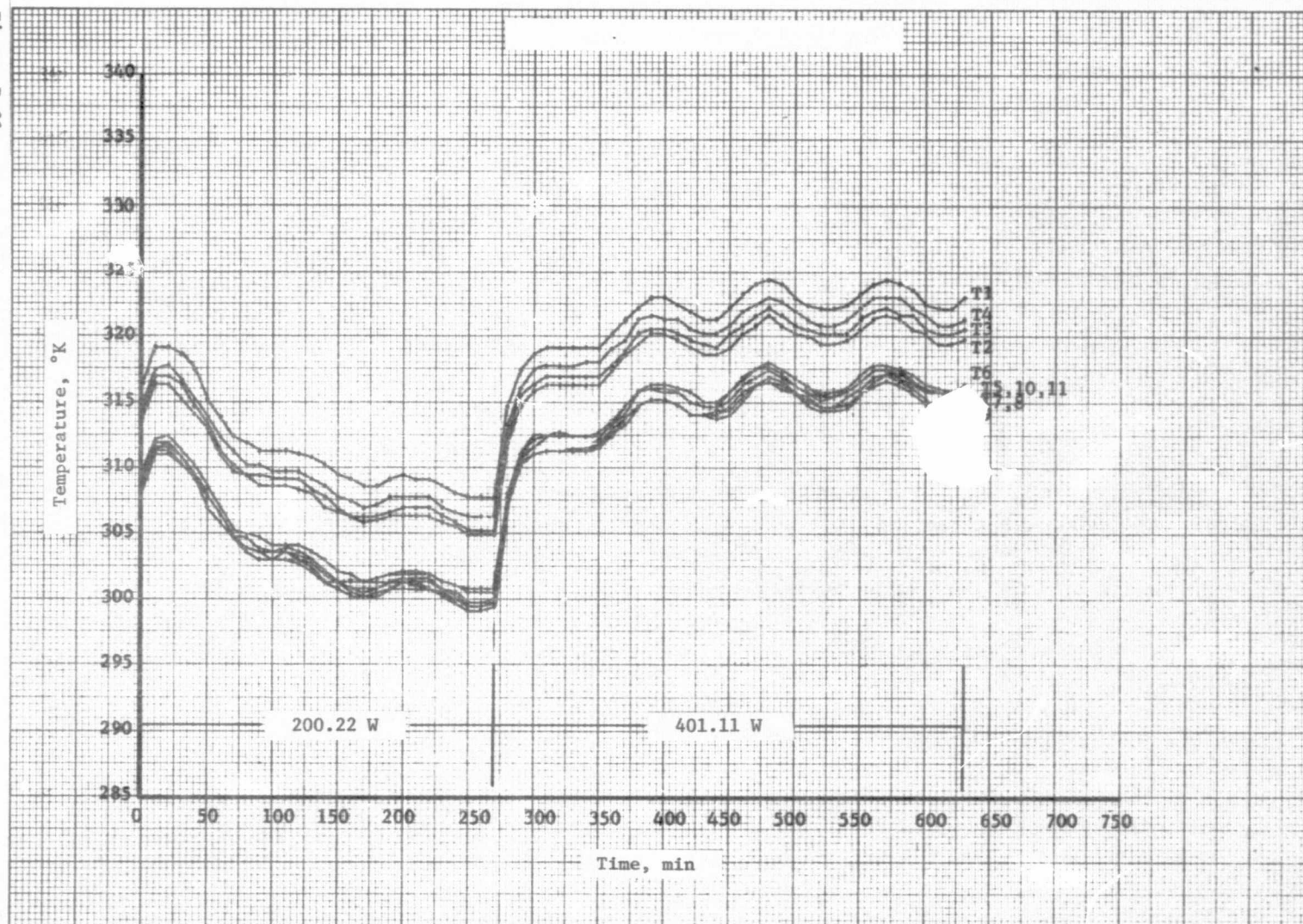


Figure B-69 Test 3 Transient Environment Thermal Conditioning Panel

Figure B-70
B-84

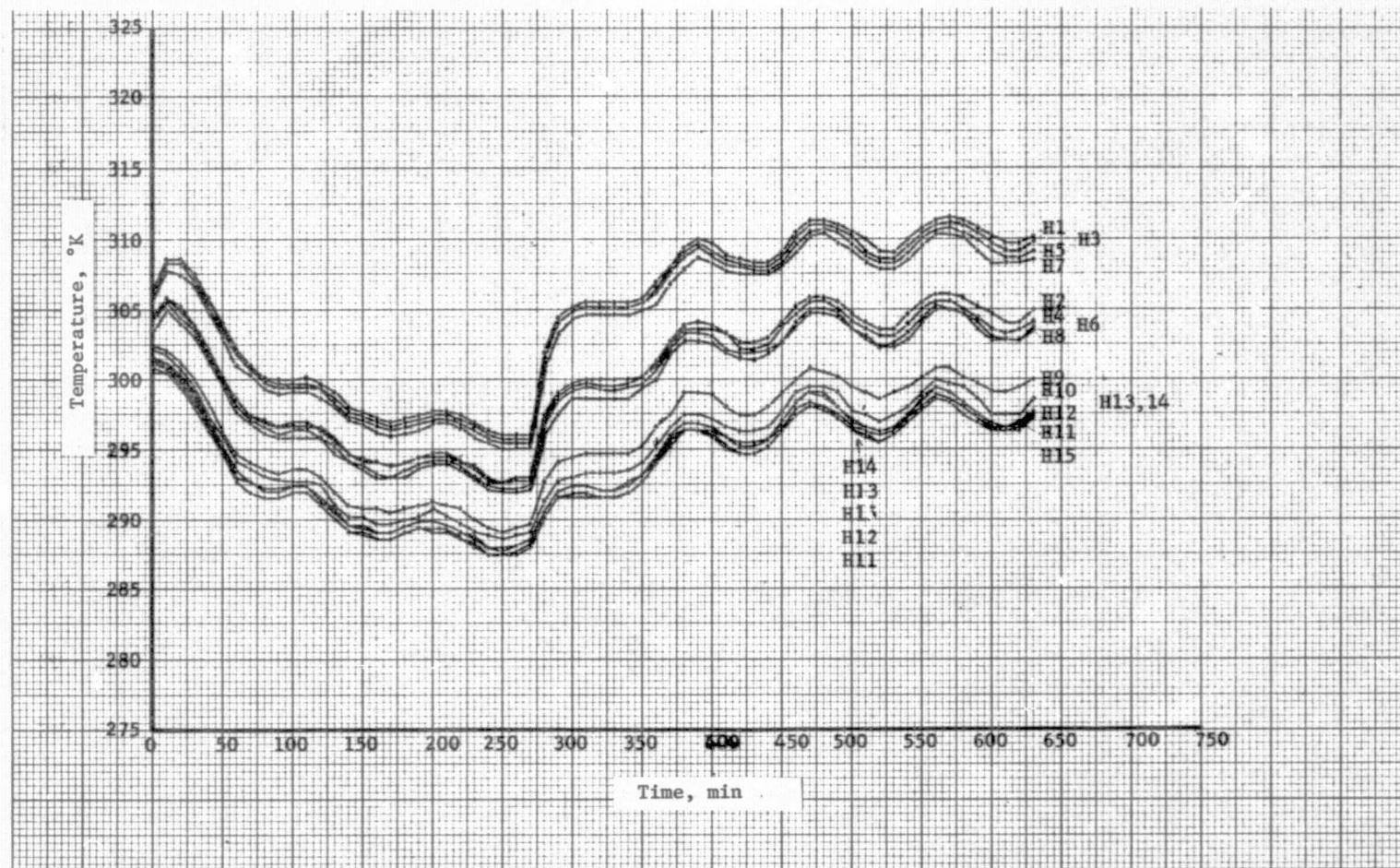


Figure B-70. Test 3, Transient Environment Header Heat Pipe

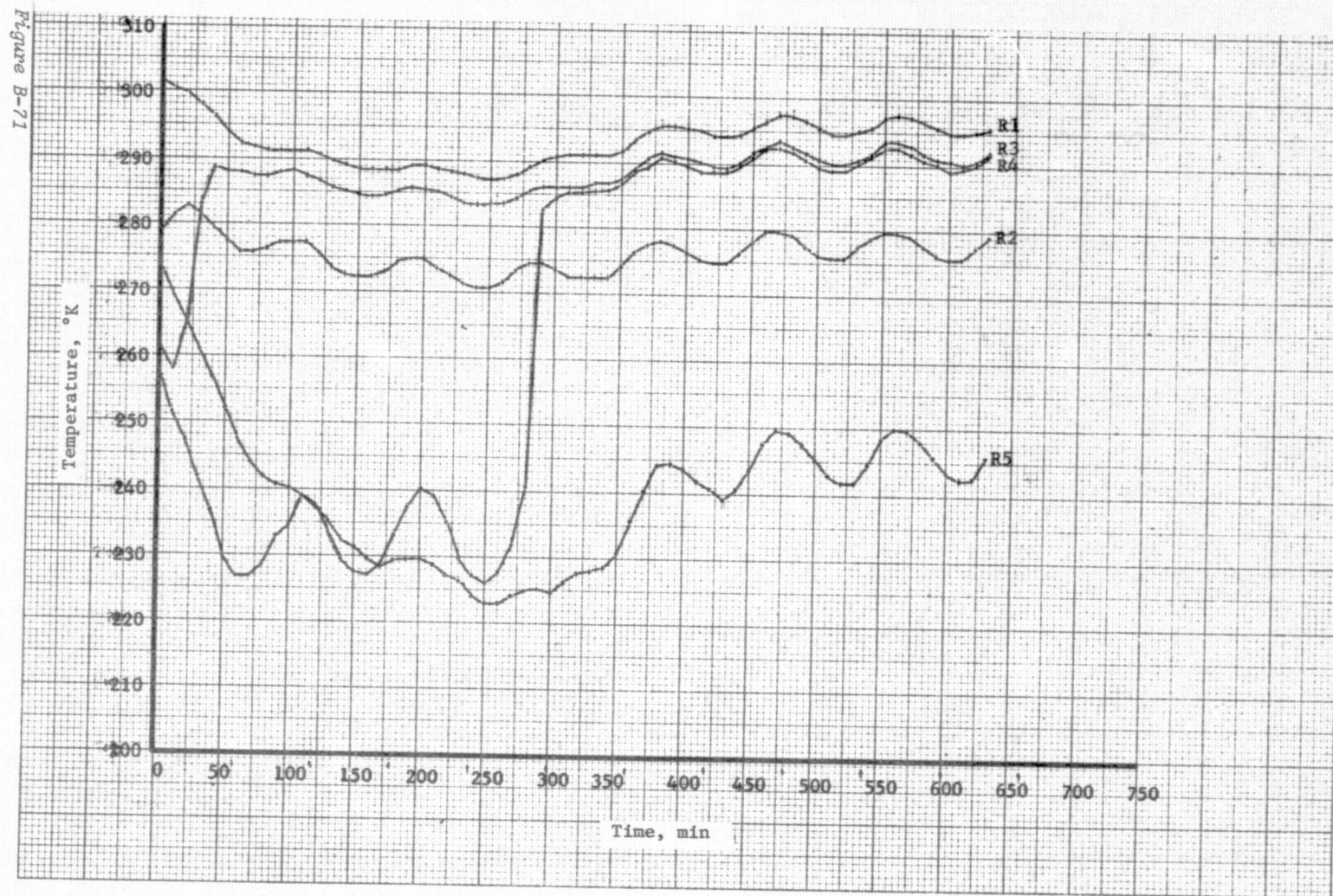


Figure B-71 Test 3, Transient Environment Radiator Heat Pipe No. 1

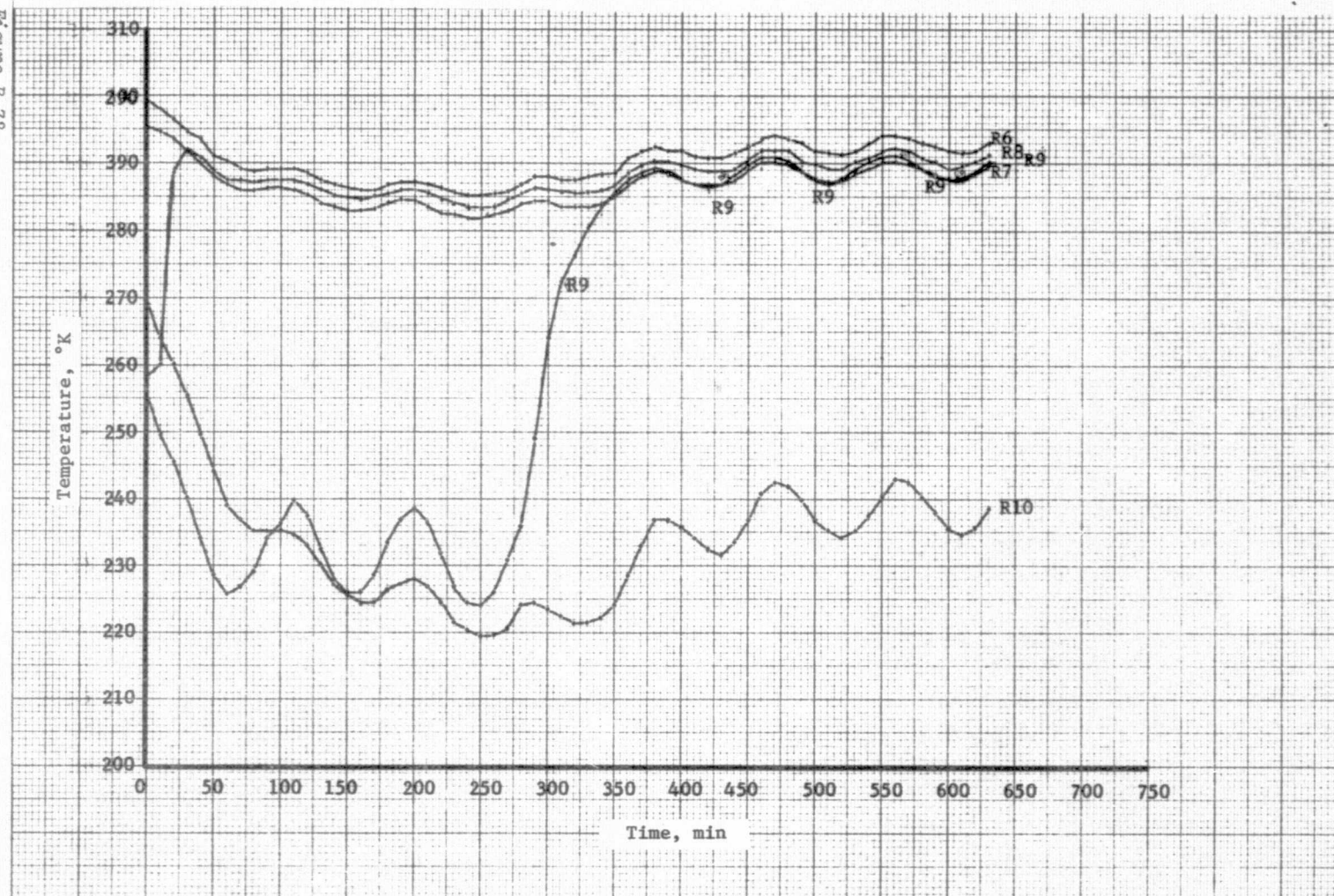
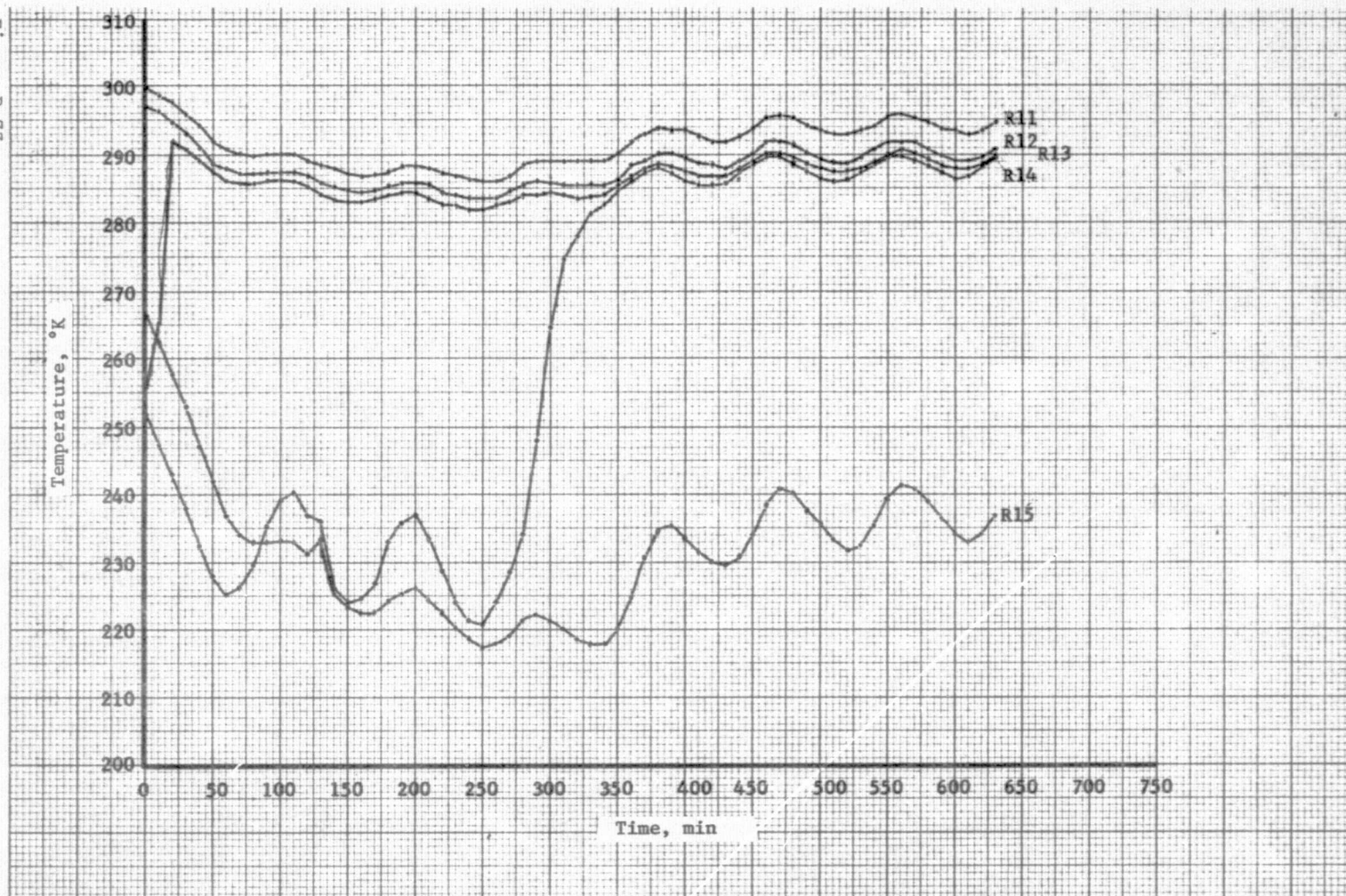


Figure B-72 Test 3, Transient Environment Radiator Heat Pipe No. 2

Figure B-73



B-87

Figure B-73 Test 3, Transient Environment Radiator Heat Pipe No. 3

B-88
Figure B-74

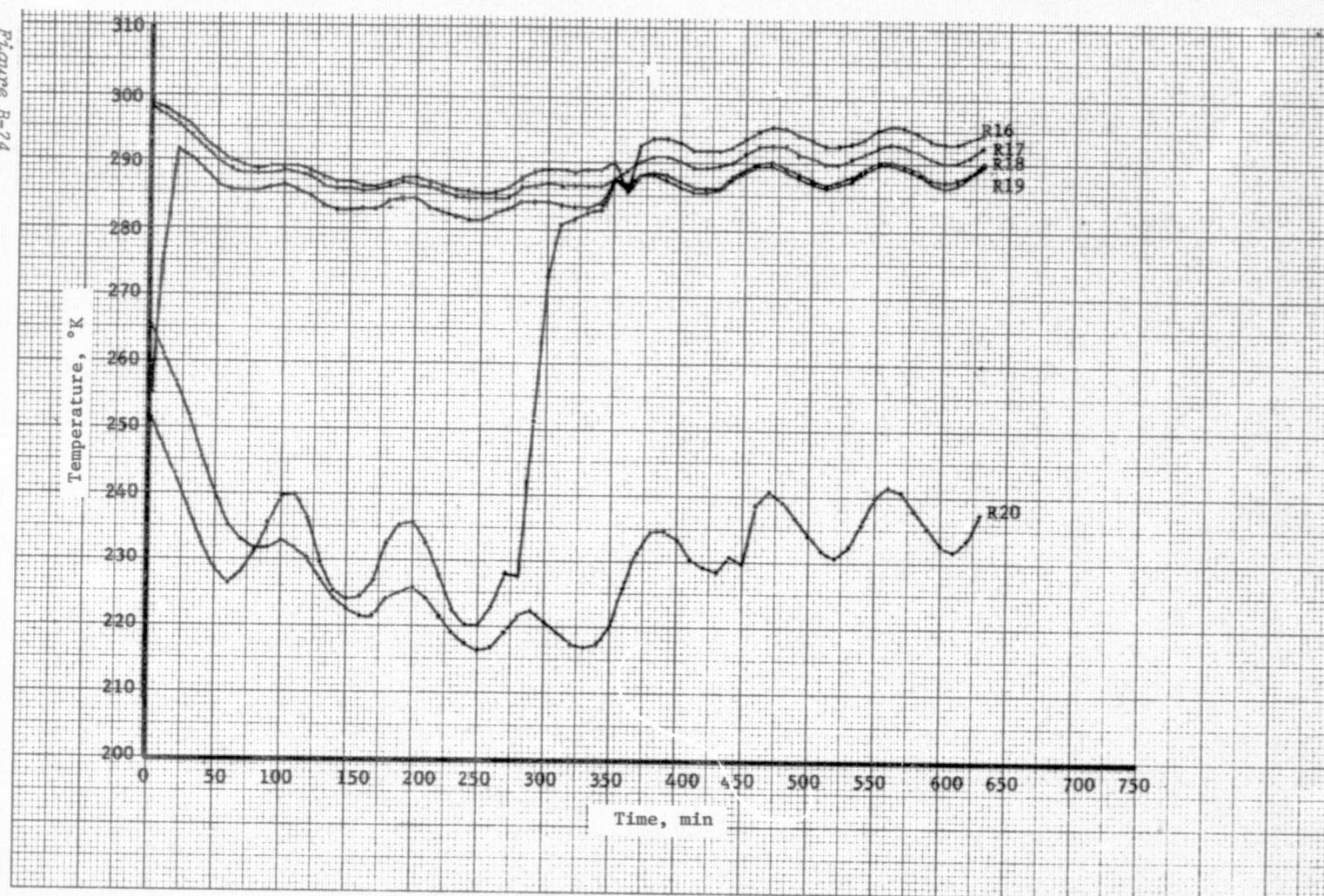
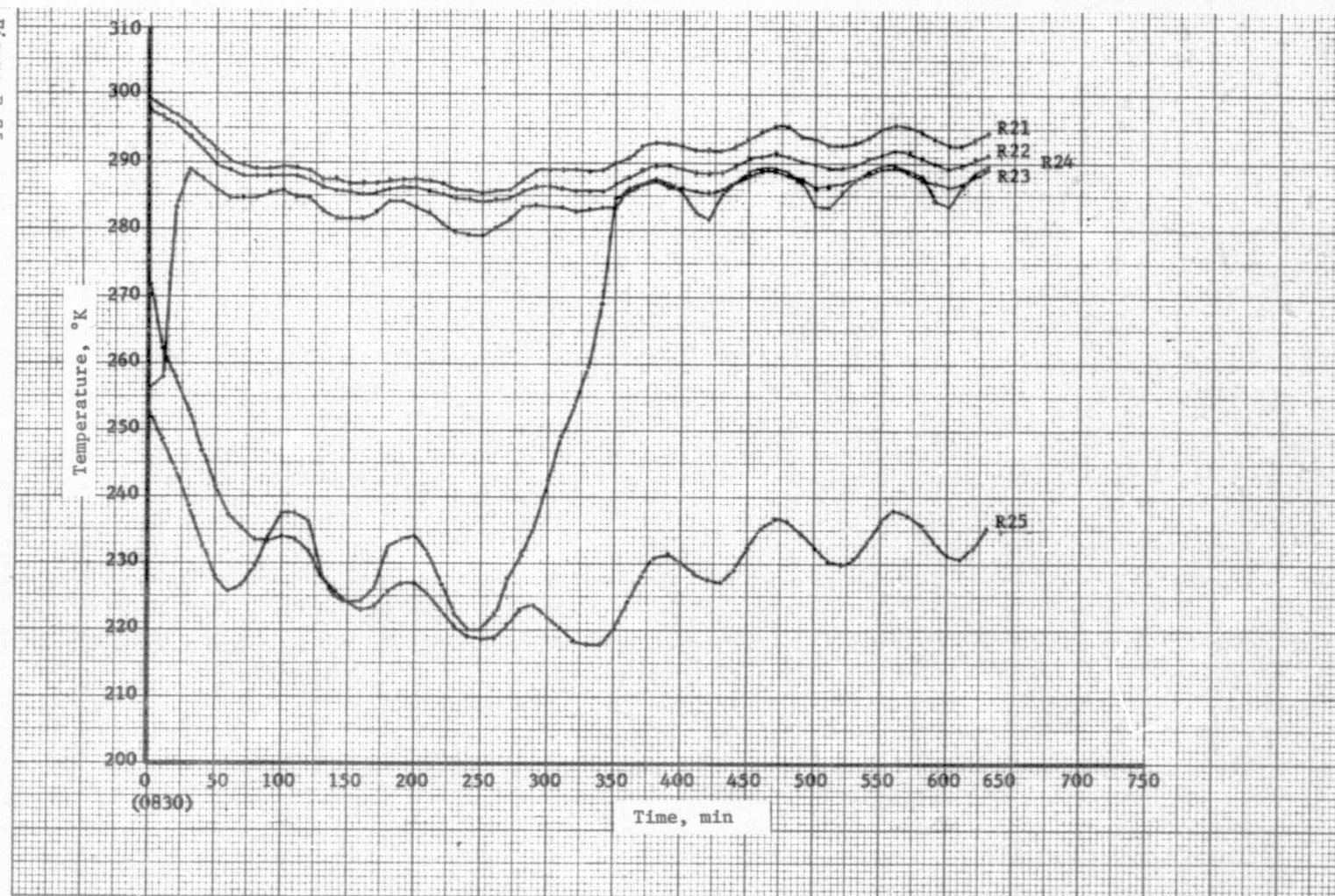


Figure B-74 Test 3, Transient Environment Radiator Heat Pipe No. 4

Figure B-75



B-89

Figure B-75 Test 3, Transient Environment Radiator Heat Pipe No. 5

Figure B-76
B-90

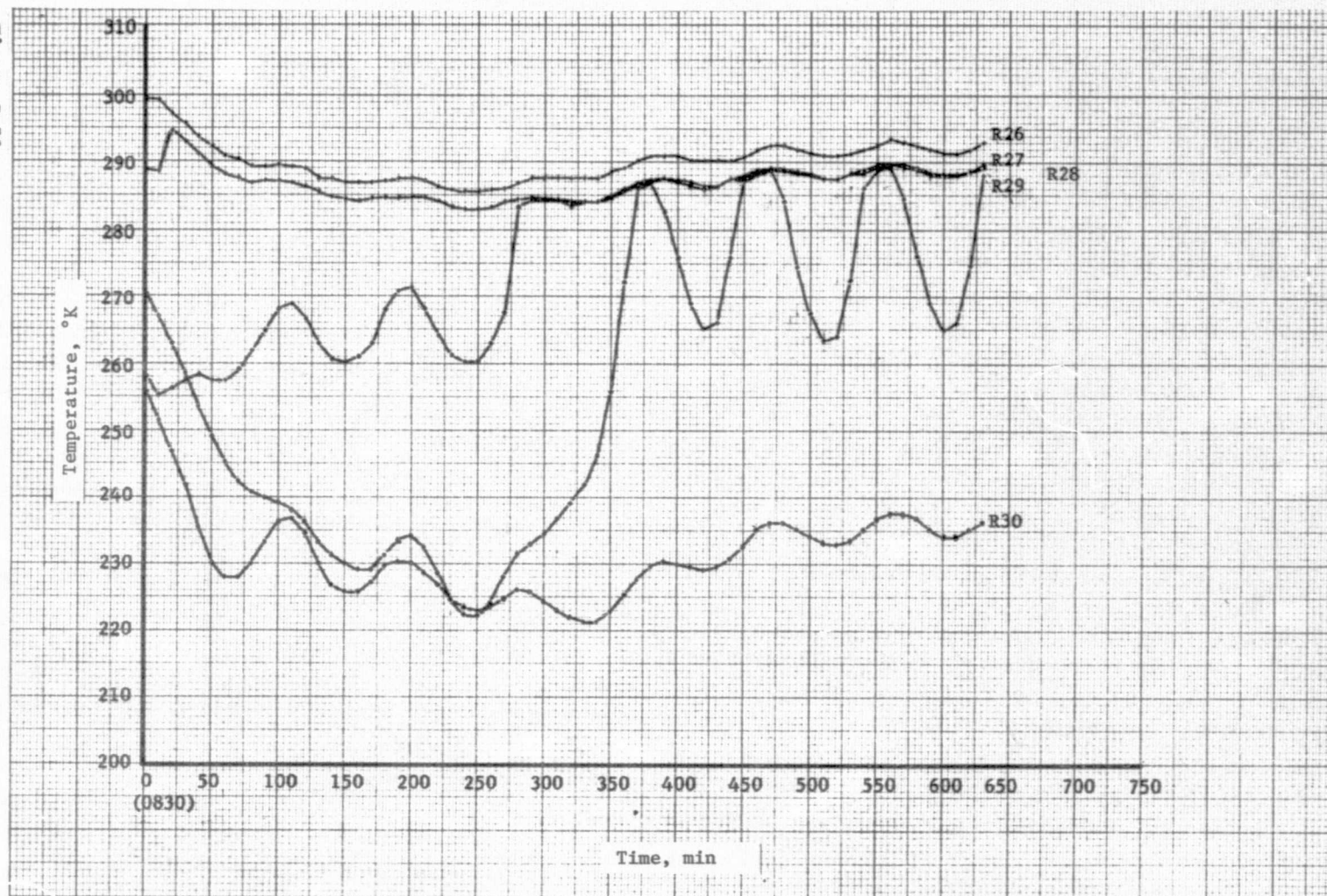
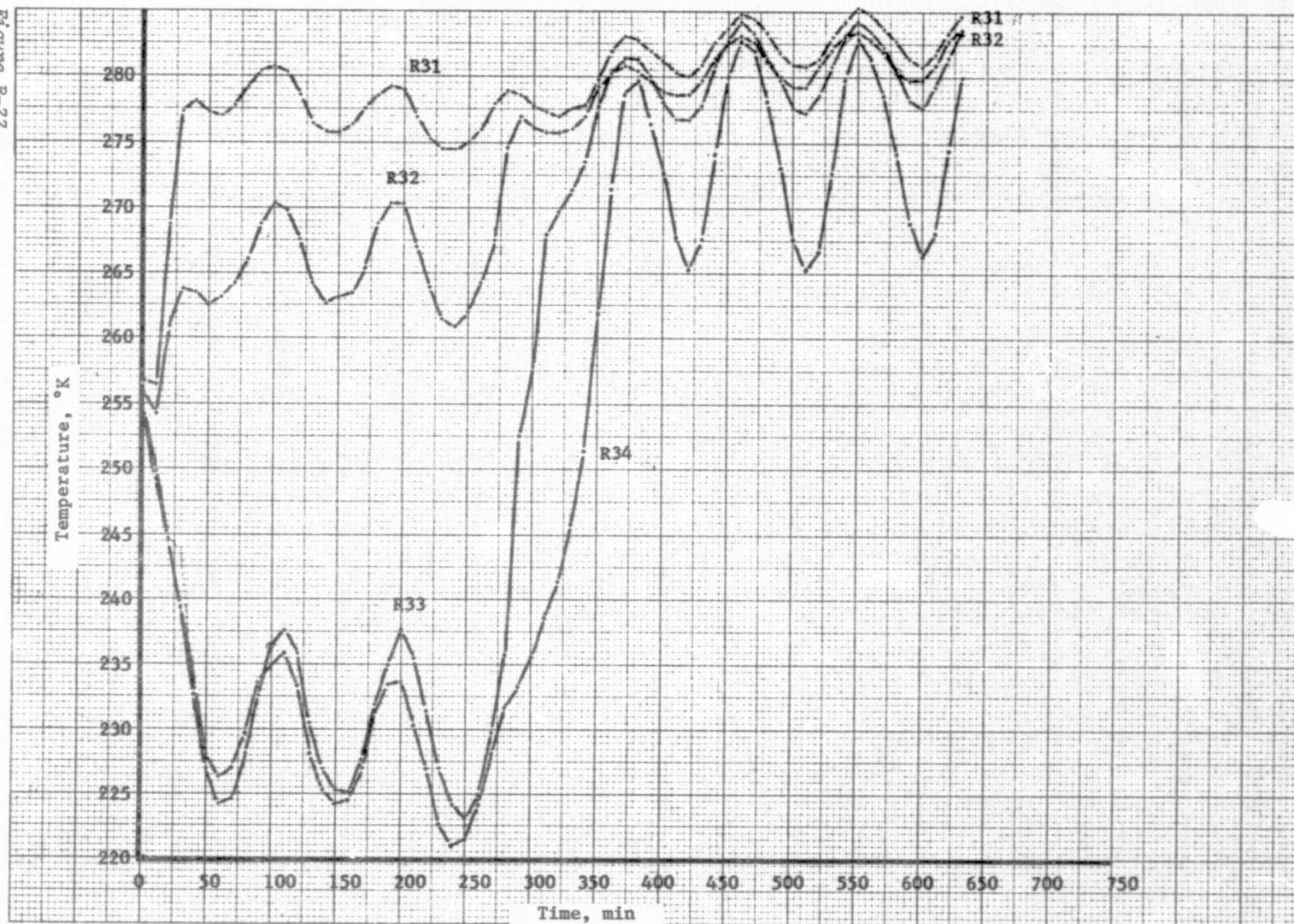


Figure B-76 Test 3, Transient Environment Radiator Heat Pipe No. 6

REPRODUCIBILITY OF THE
ORIGINAL PAGE IS POOR

Figure B-77



B-91

Figure B-77 Test 3, Transient Environment Radiator Skin Temperature

B-92

Figure B-78

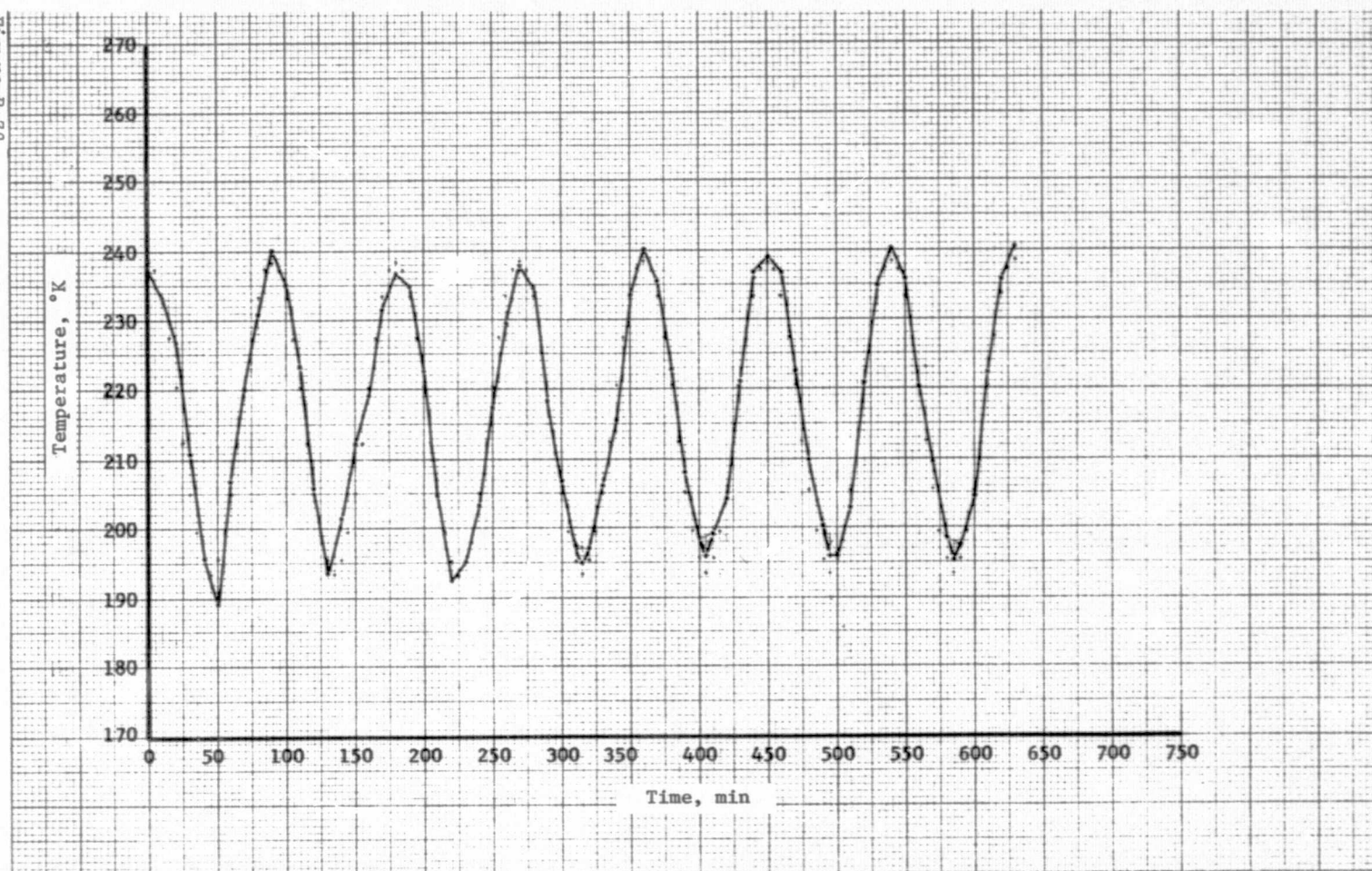


Figure B-78 Test 3, Transient Environment Shroud

D. 144°K SHROUD TESTING

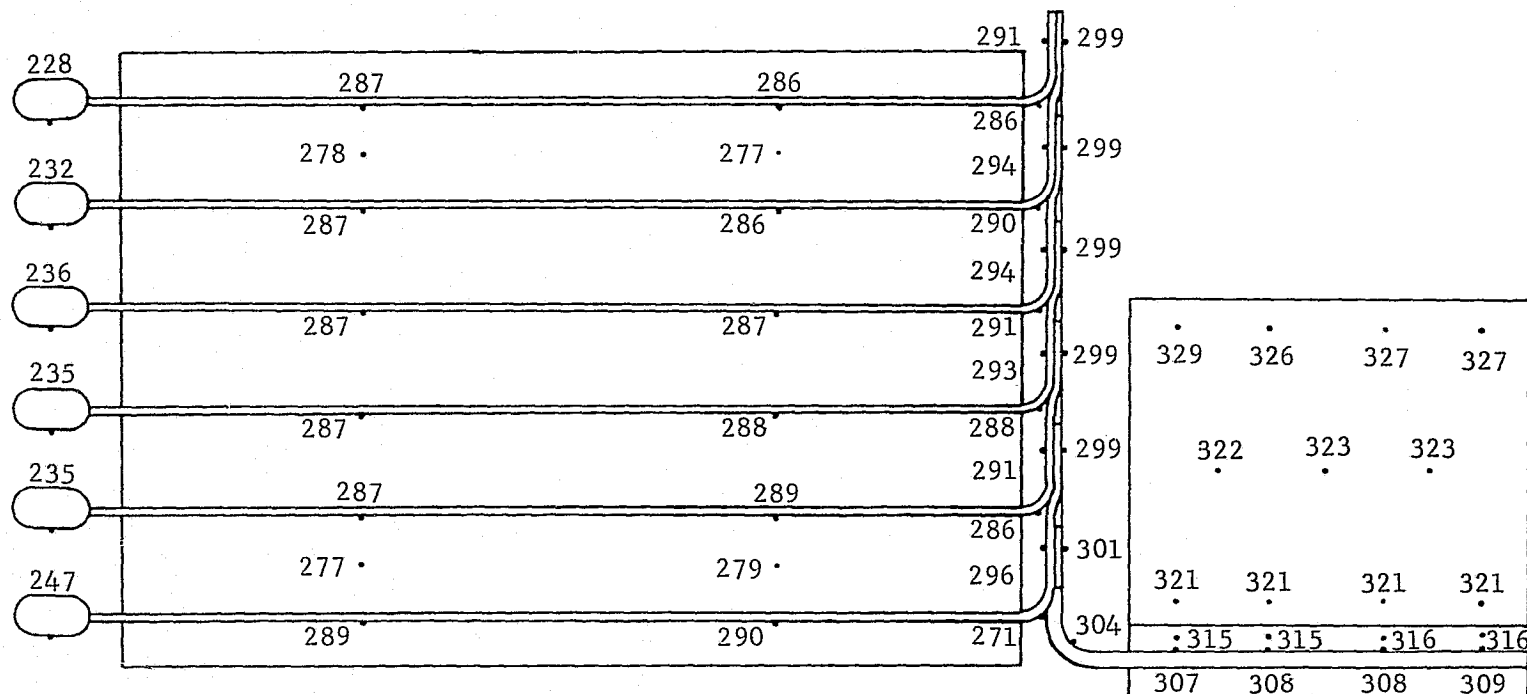
The 144°K shroud testing was conducted to obtain additional cold case performance data instead of the testing that could not be conducted under the original plan. This test exceeded the cold case design environment for the radiator and was compensated for by increasing the load to be dissipated.

Three power levels 400, 500, and 600 W were tested, however the lower load was terminated before achieving steady-state. The 400 W load test was terminated early as the reservoir temperature continued to drop below the freezing point of ammonia, the feeder pipe working fluid. The power level was increased to 500 W and the test continued until steady-state was achieved.

This test demonstrated the capability of the radiator to operate in a significantly colder environment (144°K versus 194°K). The response of the radiator to changing load for this environment was also obtained. Figures B-79 through B-84 show the temperatures obtained for this series of testing by location on the test hardware. Figures B-85 through B-94 show the temperature histories of the data.

B-94

Figure B-79



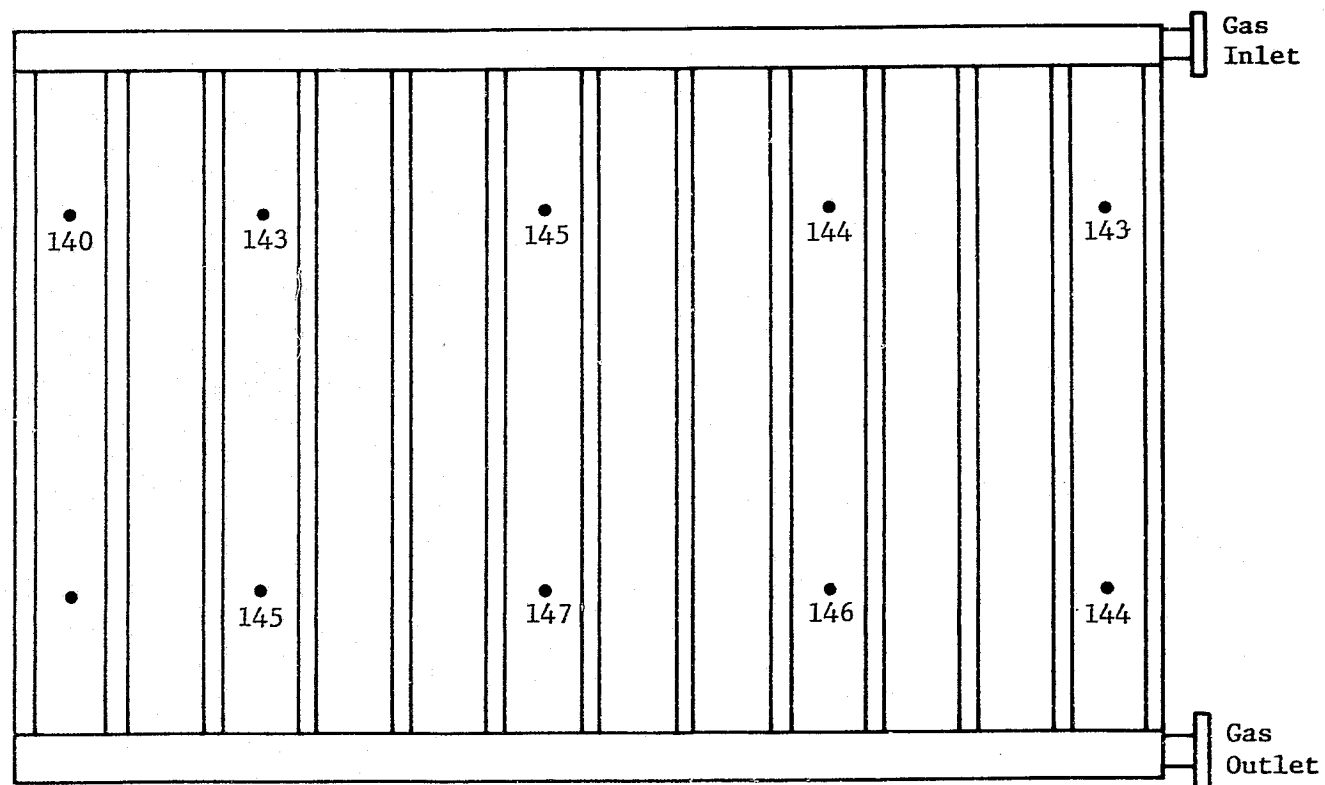
Legend:

• Thermocouple Locations

Note: Temperature, °K

Figure B-79 Test 4 144°K Shroud, 599.28 W

Figure B-80



Legend:

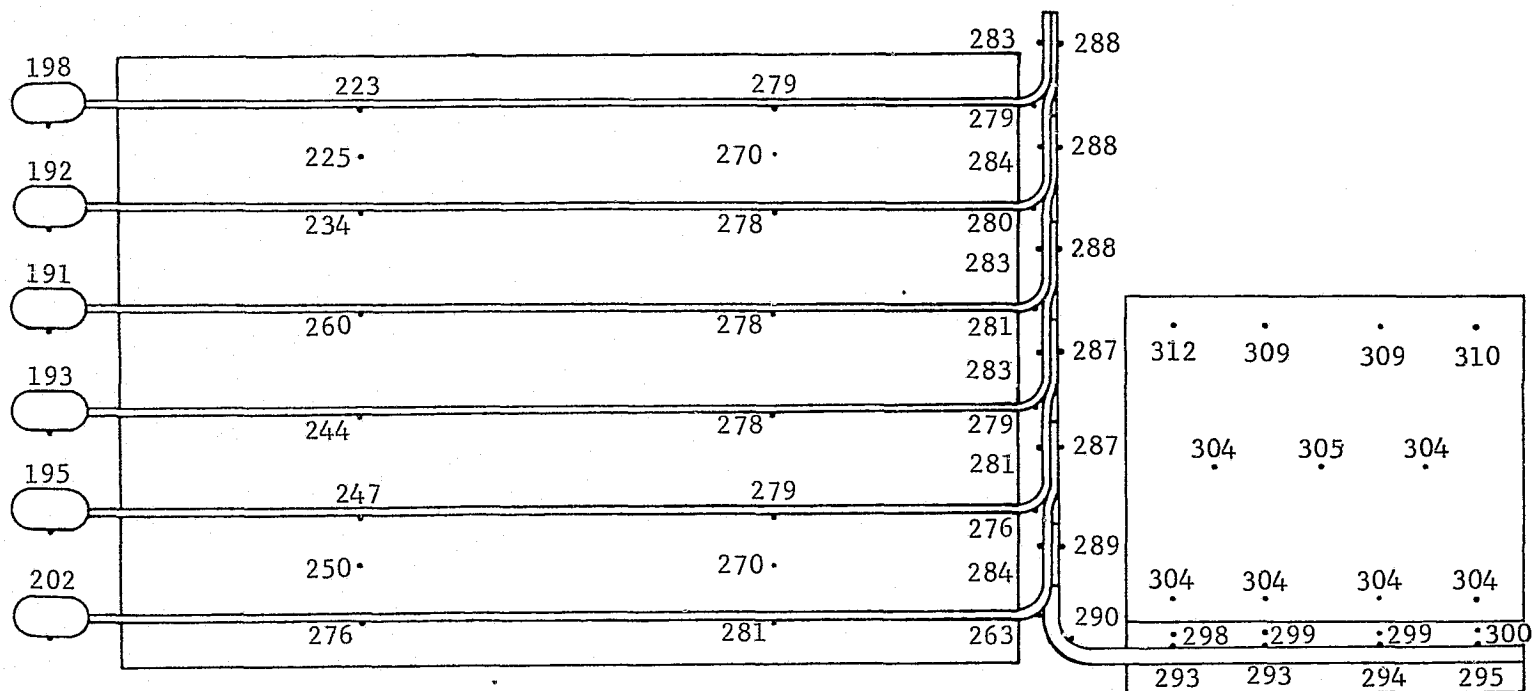
• Thermocouple Locations

Note: Temperature, °K

Figure B-80 Test 4 144°K Shroud, 599.28 W

B-96

Figure B-81



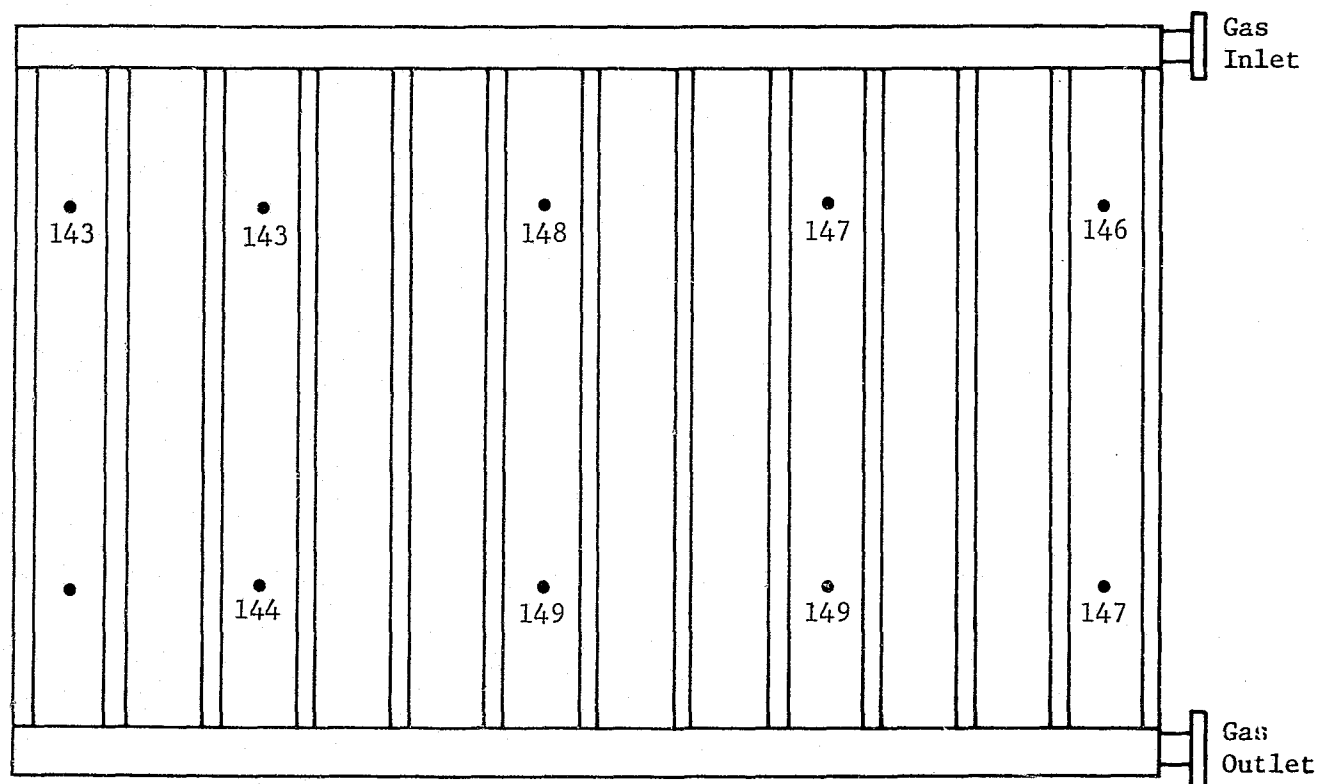
Legend:

• Thermocouple Locations

Note: Temperature, °K

Figure B-81 Test 4 144°K Shroud, 400 W

Figure B-82



Legend:



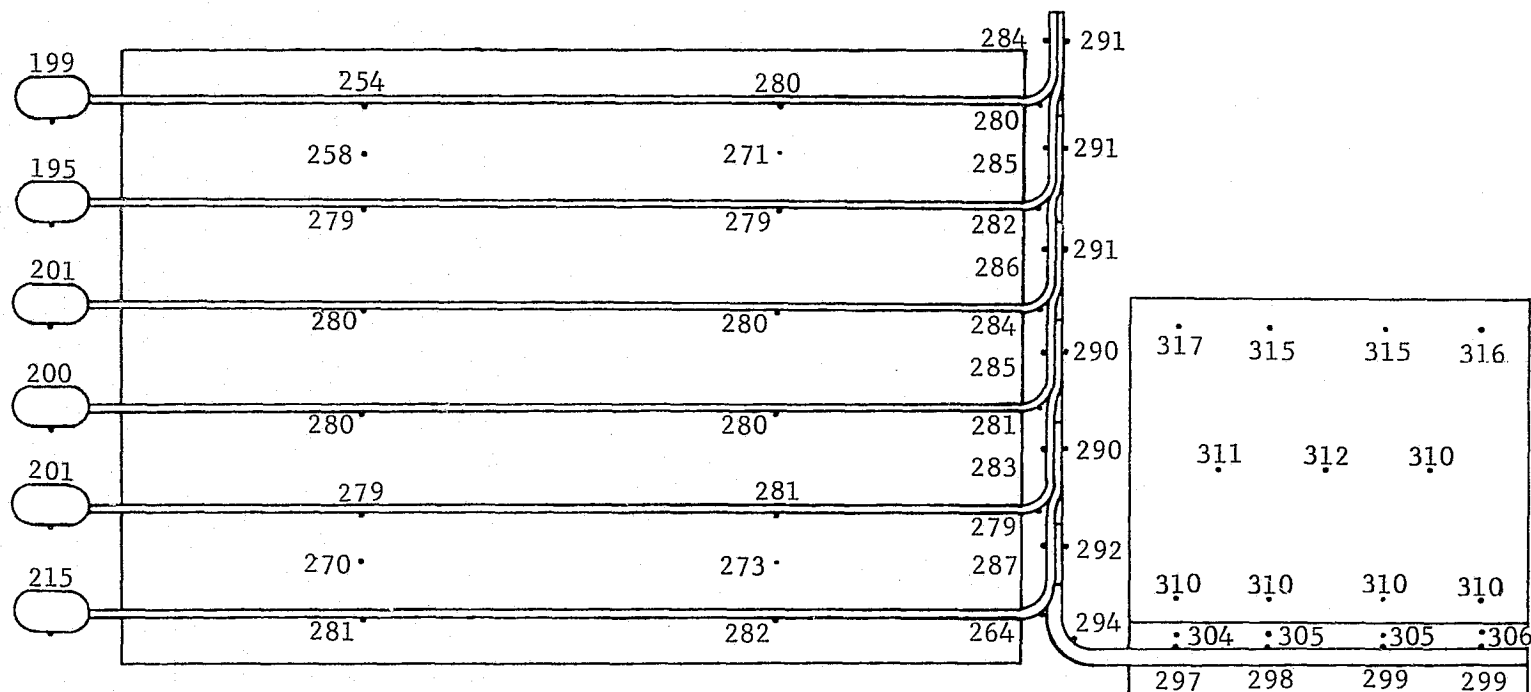
Thermocouple Locations

Note: Temperature, °K

Figure B-82 Test 4 144°K Shroud, 400 W

B-98

Figure B-83



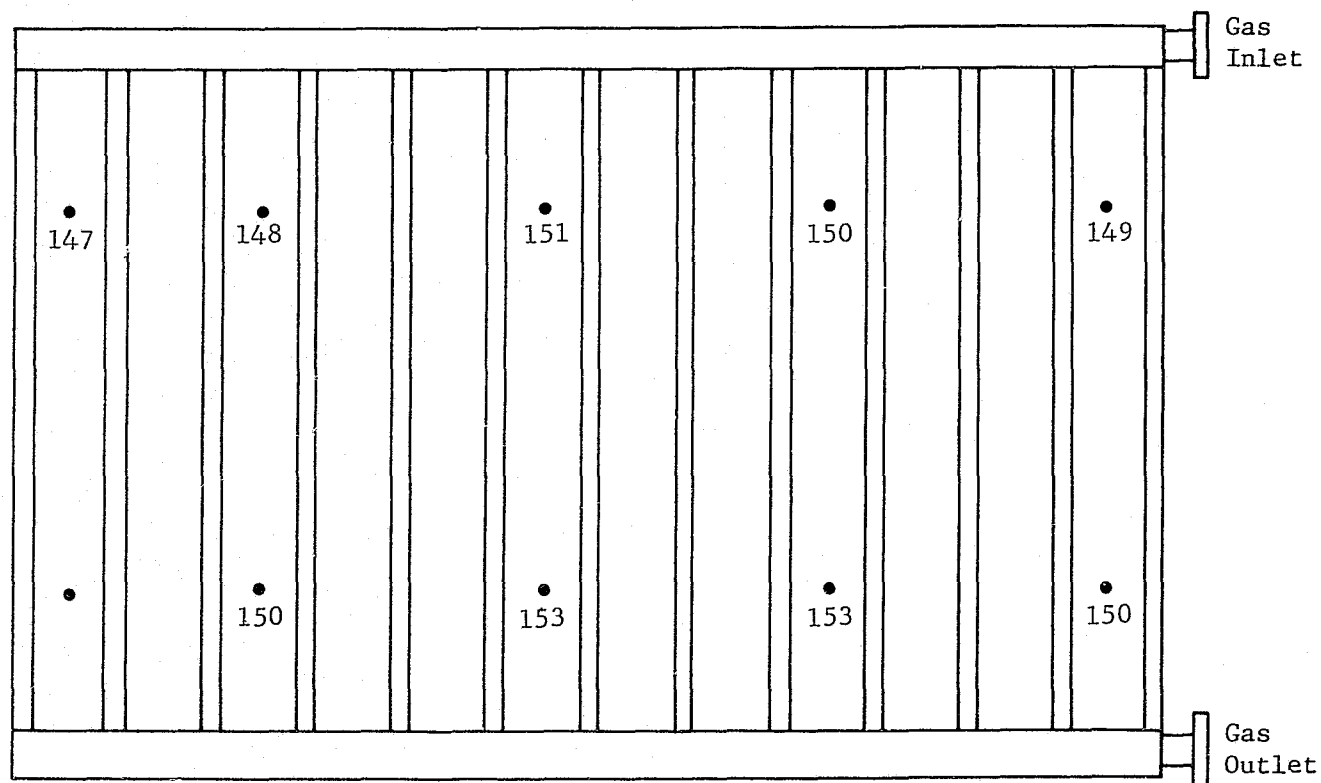
Legend:

• Thermocouple Locations

Note: Temperature, °K

Figure B-83 Test 4 144°K Shroud, 499.84 W

Figure B-34



Legend:



Thermocouple Locations

Note: Temperature, °K

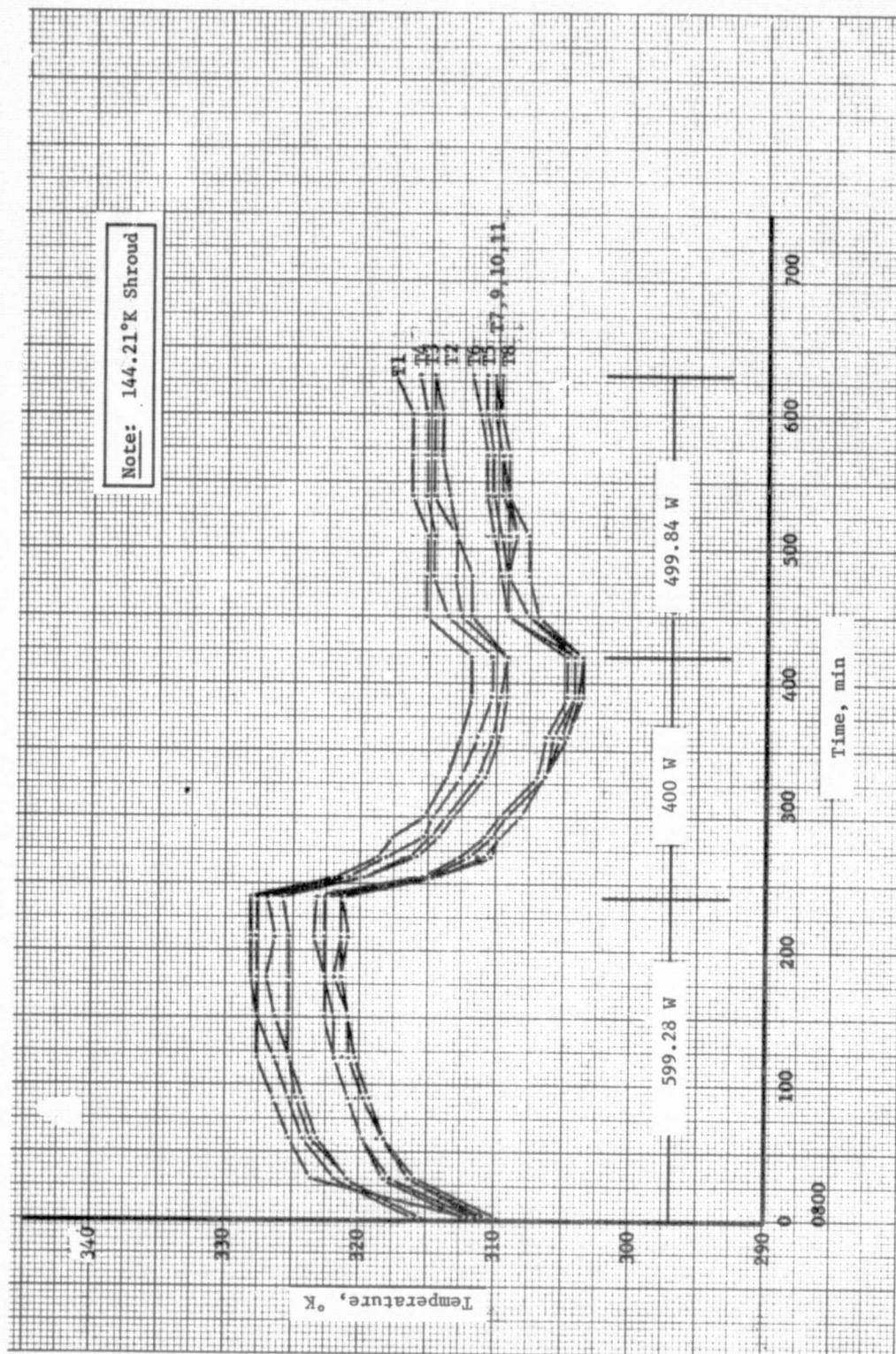


Figure B-85

B-100

Figure B-85 Test 4, Thermal Conditioning Panel

REPRODUCIBILITY OF THE
ORIGINAL PAGE IS POOR

Figure B-86

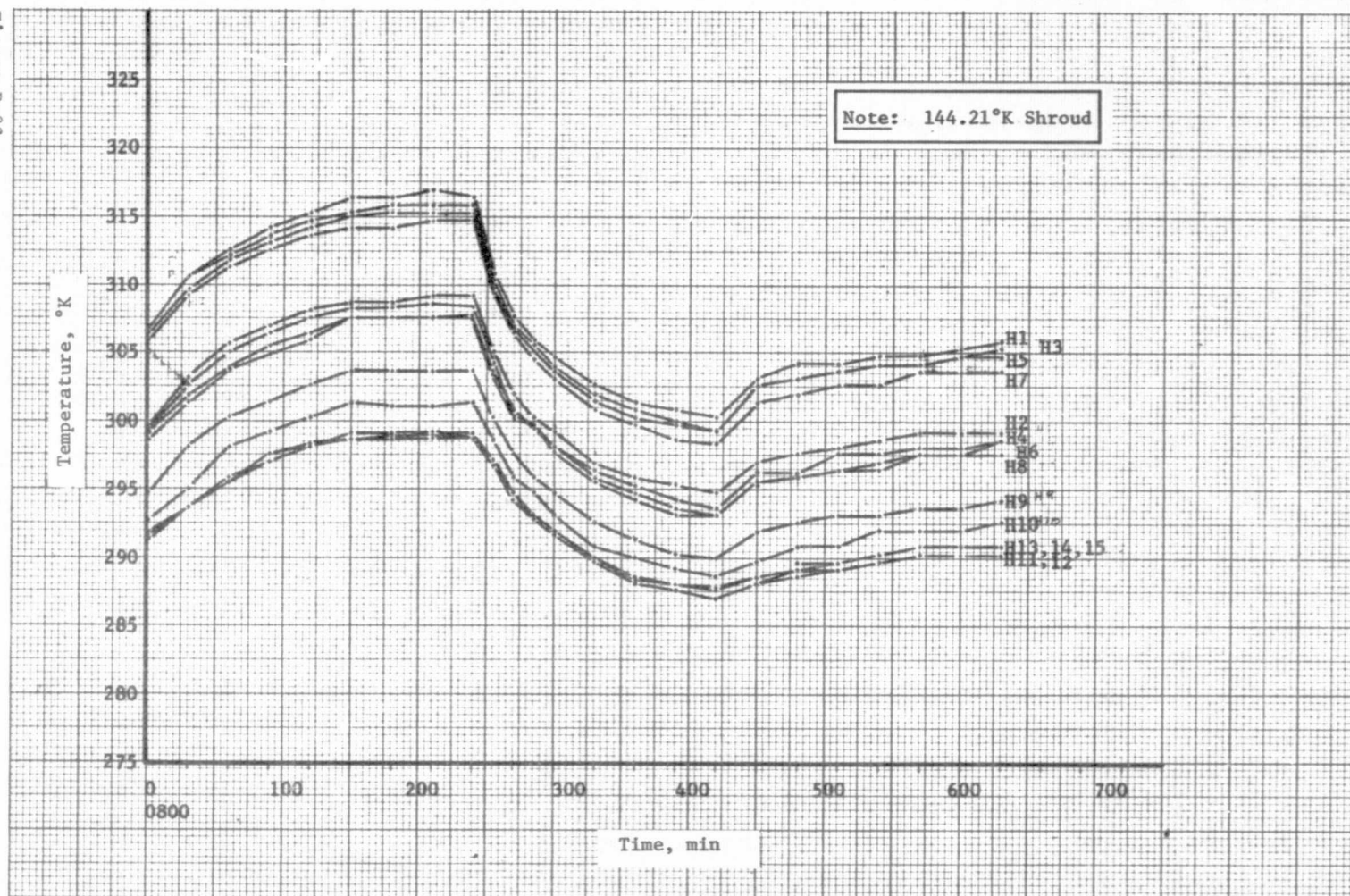


Figure B-86 Test 4, Header Heat Pipe

Figure B-87
B-102

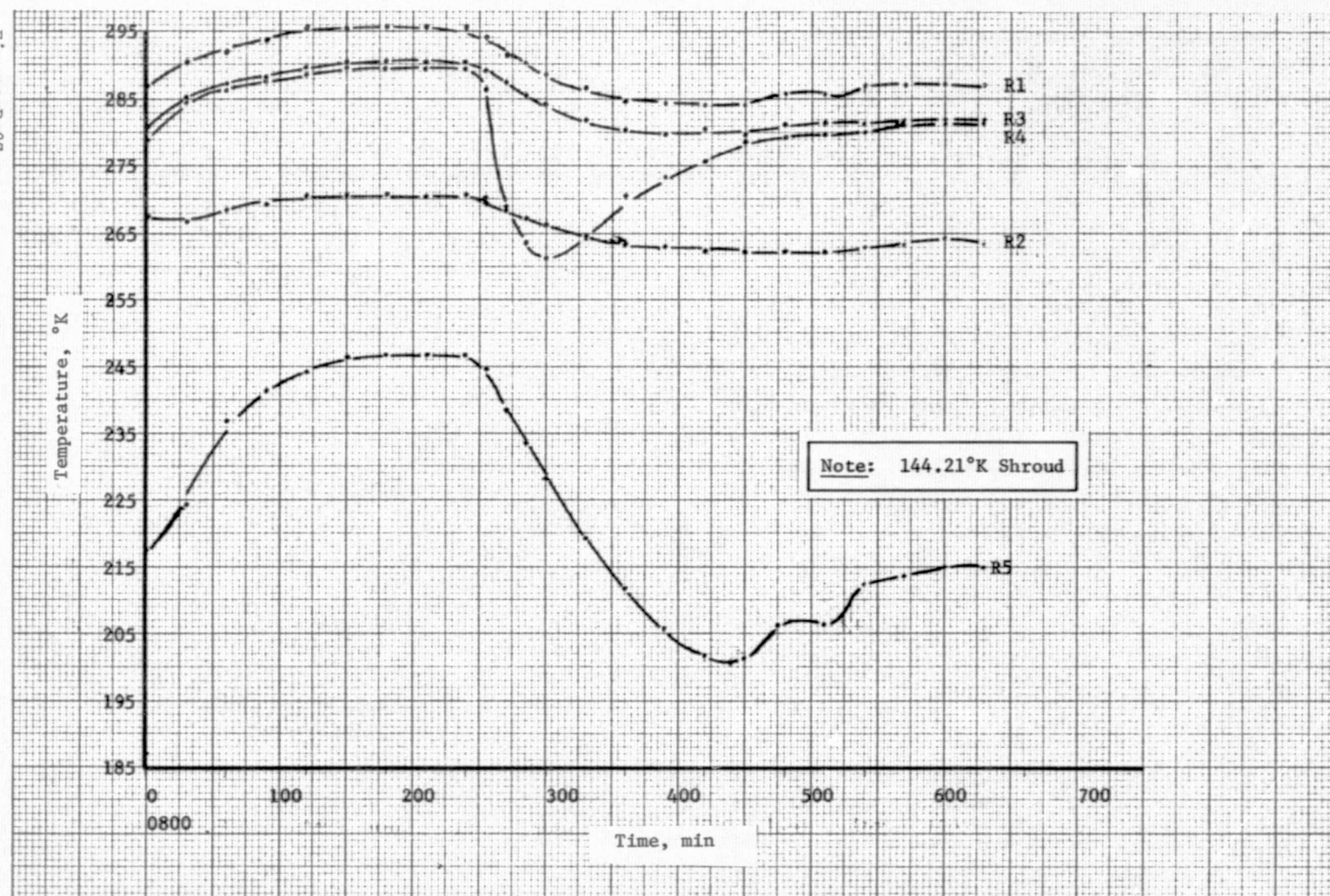
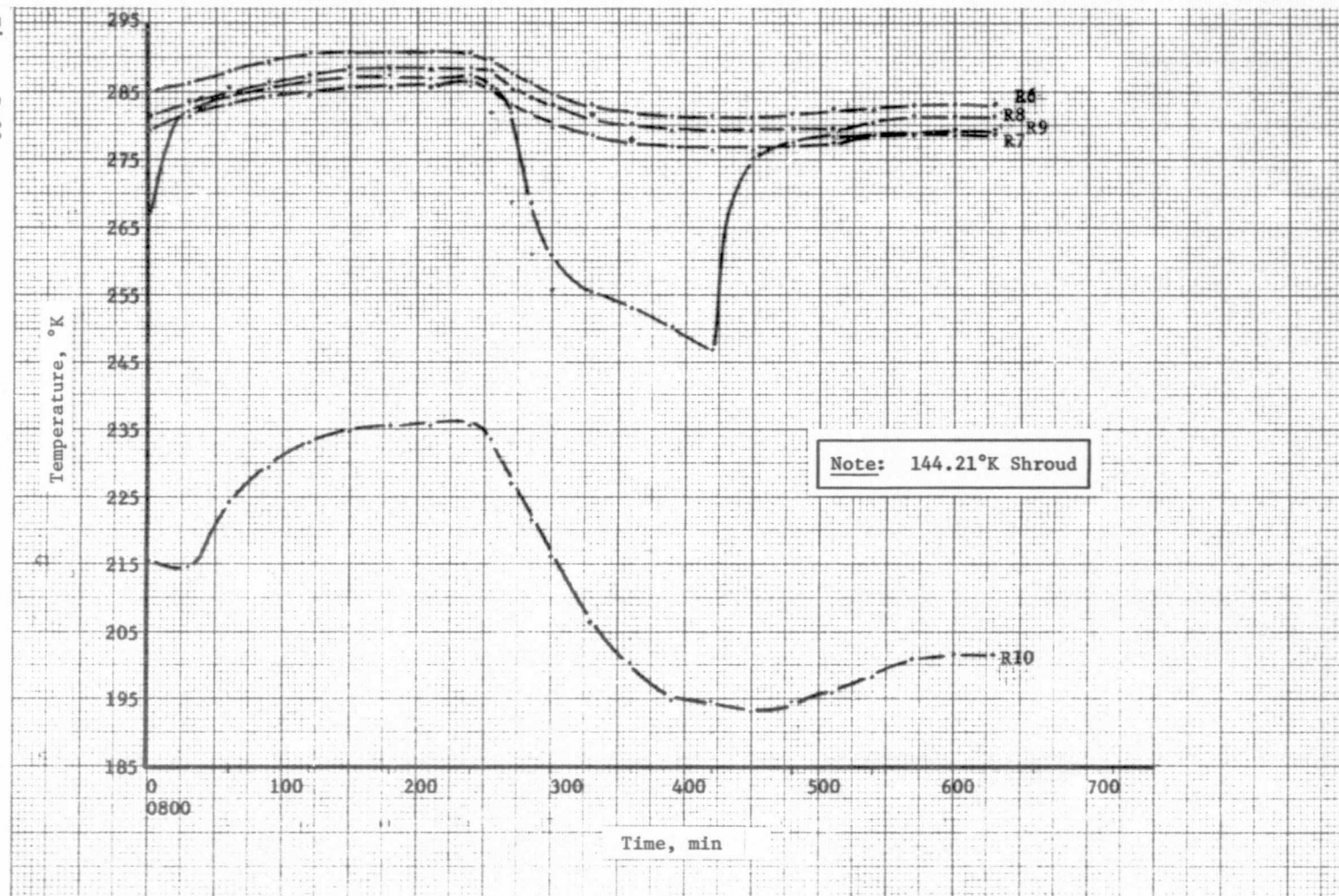


Figure B-87 Test 4, Radiator Heat Pipe No. 1

Figure B-88



B-103

Figure B-88 Test 4, Radiator Heat Pipe No. 2

Figure B-89
B-104

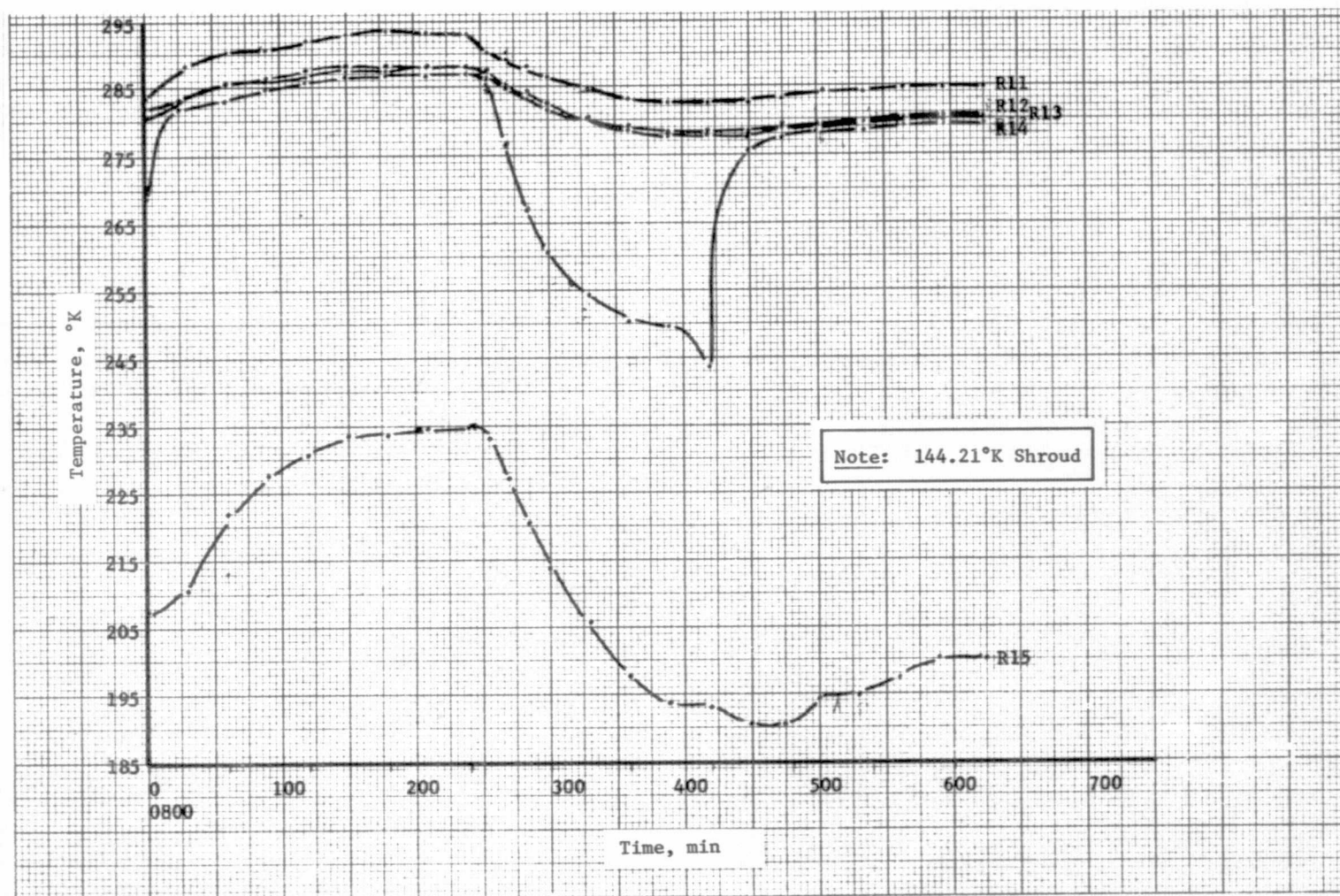
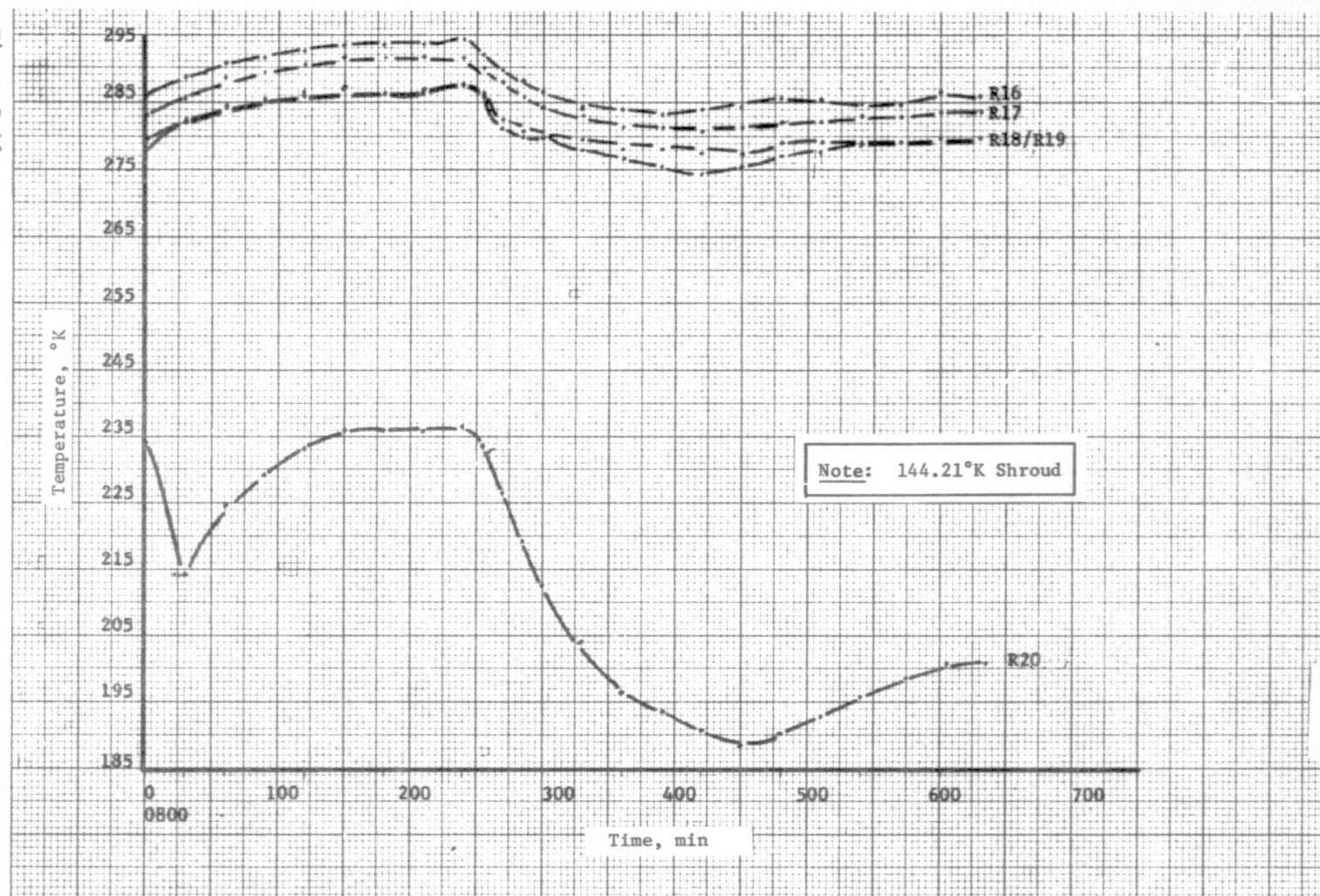


Figure B-89 Test 4, Radiator Heat Pipe No. 3

REPRODUCIBILITY OF THE
ORIGINAL PAGE IS POOR

Figure B-90



B-105

Figure B-90 Test 4, Radiator Heat Pipe No. 4

B-106
Figure B-91

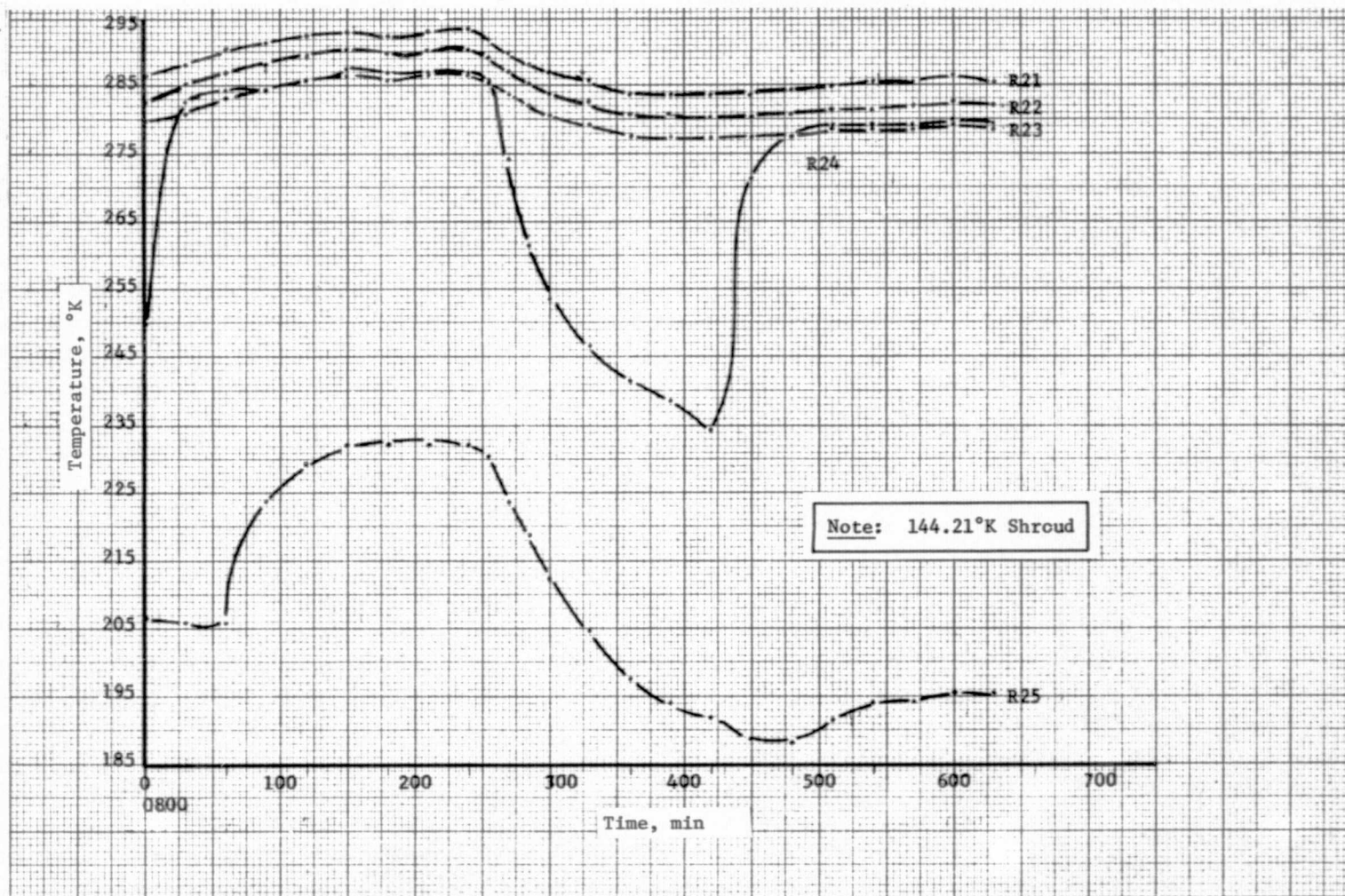


Figure B-91 Test 4, Radiator Heat Pipe No. 5

Figure B-92

B-107

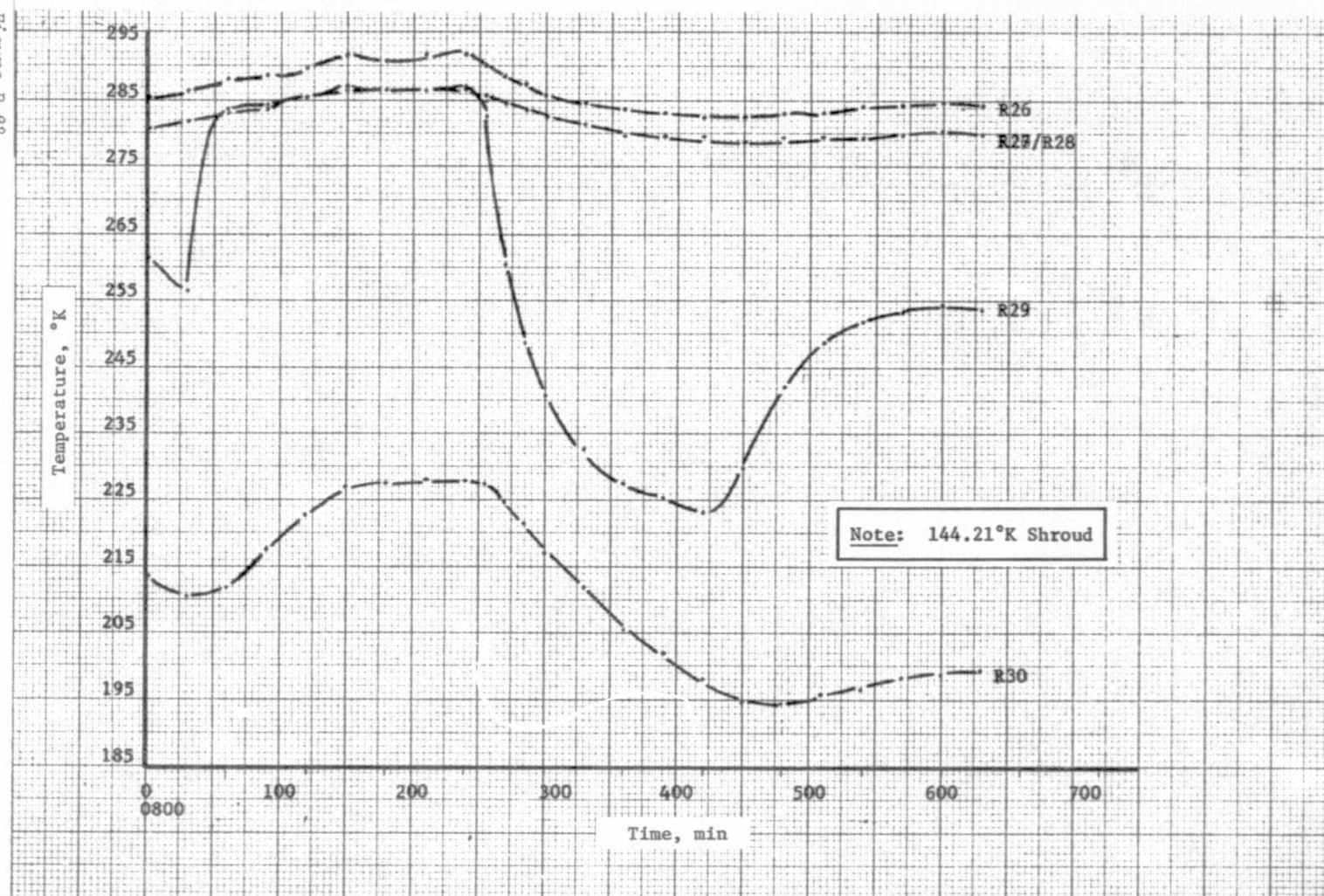


Figure B-92 Test 4, Radiator Heat Pipe No. 6

Figure B-93
B-108

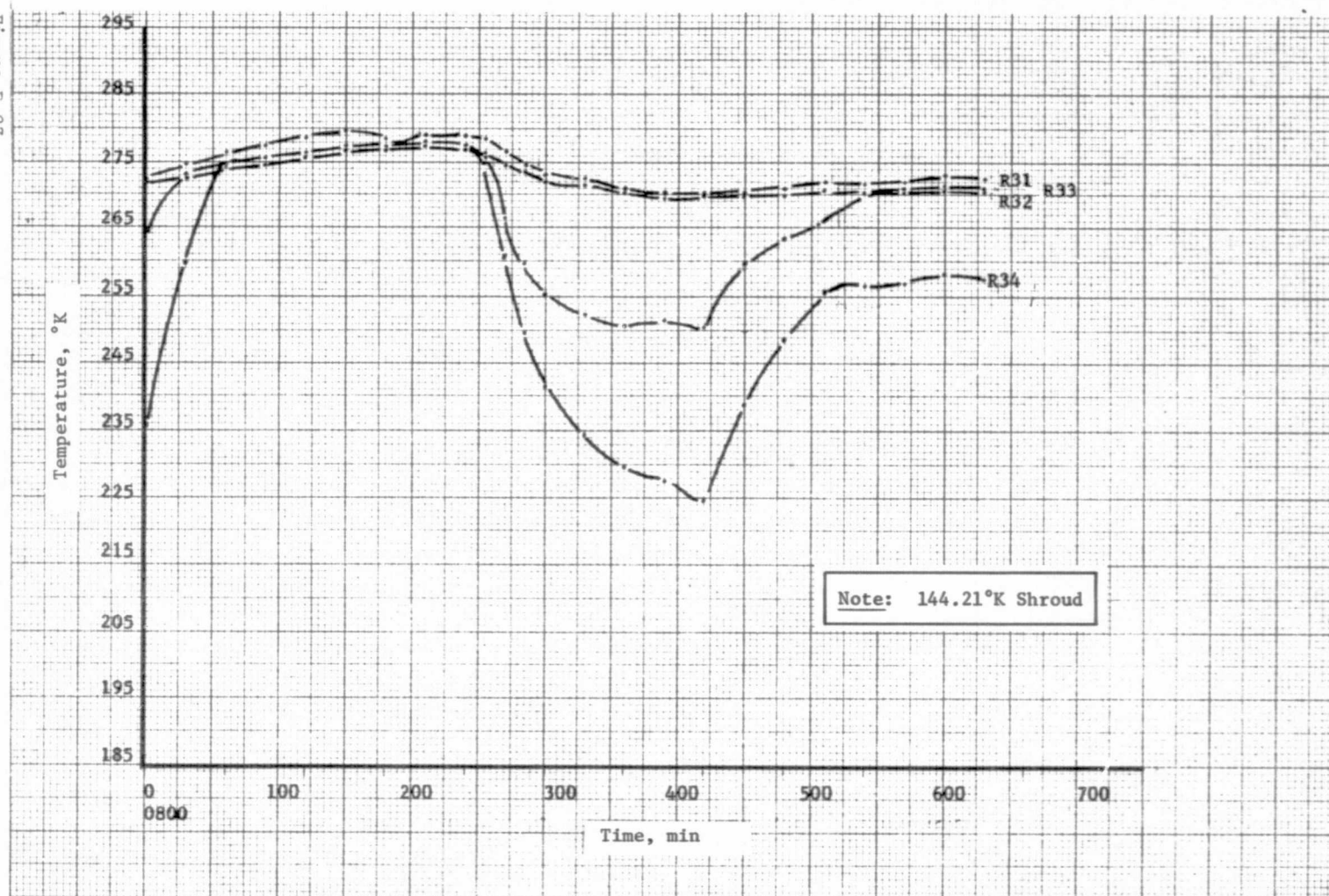
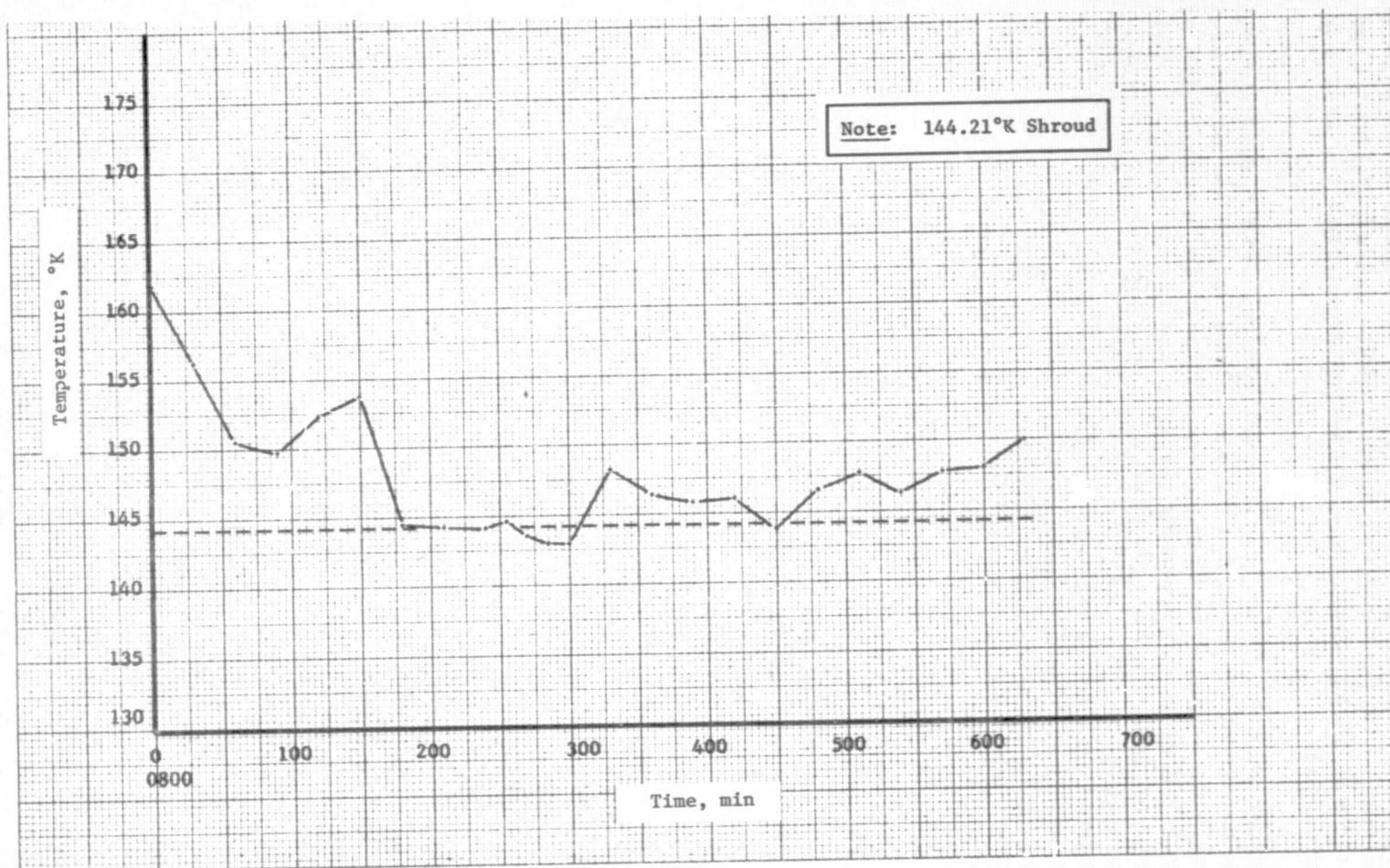


Figure B-93 Test 4, Radiator Skin Temperature

REPRODUCIBILITY OF THE
ORIGINAL PAGE IS POOR

Figure B-94



B-109

Figure B-94 Test 4, Shroud

VII. CONCLUSIONS

The heat pipe radiator/thermal conditioning panel demonstrated that an all heat pipe thermal control system can satisfy future spacecraft thermal control needs. While all of the heat pipes performed as expected, one conclusion drawn from the test was significant.

The use of heat pipes in a thermal control system should minimize the number of physical interfaces between pipes and other equipment. Each interface introduces a ΔT into the system which will result in a lower system performance per unit of weight. This test was intended to integrate two existing heat pipe systems and demonstrate their operational capability. Three interface ΔT 's resulted in connecting the two major test articles. Specific thermal control applications should consider making the header pipe or its equivalent an integral part of the collector device. One or two of the system interfaces can be avoided improving overall system performance.

VIII. REFERENCES

1. F. Edelstein: *Deployable Heat Pipe Radiator*. DHPR-75-13, (Contract NAS8-29905). Grumman Aerospace Corporation, April, 1975.
2. E. W. Saaski: *Heat Pipe Thermal Conditioning Panel*. Executive Summary Report, MDC G4422, (Contract NAS8-28639). Donald W. Douglas Laboratories, September, 1973.
3. E. W. Saaski: *Heat Pipe Thermal Conditioning Panel, Detailed Technical Report*. MDC G4421, (Contract NAS8-28639). Donald W. Douglas Laboratories, September, 1973.



March 4, 1975

Martin Marietta Aerospace
Denver Division
P.O. Box 2371
Denver, Colorado 80201

Attention: Terry Ward

Dear Terry:

Enclosed please find a copy of our test report and lab data sheet concerning the heat pipe we manufactured for you.

We did not know exactly how the pipe would be interfaced with heat source and sink. We assumed that the heat input would be uniform over the 30 inch evaporator and that the heat output would be uniform over the 48 inch condenser. Tests were run level and horizontal. It was decided to verify the upper load requirement and assume that the lower loads would be acceptable.

If you have any questions regarding the report or data, please feel free to call me at any time.

Very truly yours,

ISOTHERMICS, INC.

Robin Rhodes
Project Engineer

RR/dss
Enclosure

PRECEDING PAGE BLANK NOT FILMED

ATTACHMENT A

March 3, 1975

TO: R. Rhodes
FROM: C. Wyman
SUBJECT: Testing of Martin Marietta Pipe MO 5114

1. Test Set Up

- A. Thermocouples No. 1 to 8 are mounted on the evaporator plane in the first and third; bolt holes from each end.

Thermocouples No. 9 and 10 are mounted on the heat pipe in the evaporator section.

Thermocouples No. 11 and 12 are mounted on the heat pipe on the 90° bend.

Thermocouples No. 13 to 16 are mounted on the condenser plate.

B. Heaters

Two heater wires were attached to the evaporator plate outside the bolt holes. Each heater measured 20 ohms resistance.

C. Insulation and Cooling

Evaporator section was covered with two layers of 2 in. fiberglass. The condenser section was cooled by evaporation of a refrigerant.

Tests 1 and 2, R-113 refrigerant used.
Tests 3 to 10, R-11 refrigerant used.

D. Pipe Set Up Level and Horizontal

- E. Load Evaporator - each heater had 20 ohms resistance.
Voltage varied current measured.
Watts calculated using I^2R .

2. Results

Over all pipe conductance $\frac{\text{Watts}}{^\circ\text{F Rise}}$ $\frac{\text{Watts}}{\text{T evaporator} - \text{T condenser}}$

Test No.	T Evaporator	T Condenser	I	Watts	Pipe Conductance
1 & 2	138.2	130.1	3	360.0	44.4
3	105.9	91.4	3.6	518.4	36.1
4 & 5	107.4	89.1	4.0	640.0	34.96
6, 7, & 8	121.0	93.8	5.0	1000.0	36.76
9 & 10	122.4	94.3	5.5	1210.0	44.6
Note: Temperatures in $^\circ\text{F}$					

10 Tests at five sets of conditions

One and two used R-113 cooling - insufficient cooling capacity

Three changed to R-11 for cooling - uneven temperature on condenser, indicated that R-113 was insulating portions of the condenser. Ran approximately $\frac{1}{2}$ hr to stability. R-11 attached Silicone insulation on the t/c's (condenser).

Four and five R-11 uniform condenser temperatures restored.

Six, seven and eight R-11 cooling excellent operation at 100% power requirement.

Nine and ten R-11 cooling - 210 W beyond requirement, tests terminated.

Note: Due to time factor and lack of equipment, the low limit (-30°F) could not be verified.

Conclusions:

1. Pipe is capable of meeting high end requirements.
2. Overall pipe conductance based on the five conditions tested is 38.9 W per $^\circ\text{F}$ rise.

No. = TC in B11 Holes Large Plate

Condenser En
R-113 used to Remove He
R-11 U

Heaters Outside B11 Holes 26.2 each

B-116

REPRODUCIBILITY OF THE
ORIGINAL PAGE IS POOR

Post-Test
Analysis
Report

October 1975

**HEAT PIPE
RADIATOR/THERMAL
CONDITIONING PANEL**

MARTIN MARIETTA CORPORATION
Box 179
Denver, Colorado 80201

CONTENTS

	<u>Page</u>
I. INTRODUCTION	C-1
II. SUMMARY	C-2
III. MODEL DESCRIPTION	C-3
IV. MODEL CORRELATIONS	C-6
A. Steady-State Correlations	C-6
B. Transient Correlations	C-28 thru C-36
V. CONCLUSIONS	C-37
VI. REFERENCES	C-38
ATTACHMENT 1	C-39 thru C-70
ATTACHMENT 2	C-71 thru C-123

Figure

C-1	Heat Pipe Radiator Thermal Model Mode Diagram	C-4
C-2	Heat Pipe Model	C-5
C-3	Hot Case Steady-State, 100.1 W	C-7
C-4	Hot Case Steady-State, 100.1 W	C-8
C-5	Hot Case Steady-State, 200.23 W	C-9
C-6	Hot Case Steady-State, 200.23 W	C-10
C-7	Hot Case Steady-State, 299.88 W	C-11
C-8	Hot Case Steady-State, 299.88 W	C-12
C-9	Hot Case Steady-State, 380.96 W	C-13
C-10	Hot Case Steady-State, 380.96 W	C-14
C-11	Hot Case Steady-State, 200.26 W	C-15
C-12	Hot Case Steady-State, 200.26 W	C-16
C-13	Cold State Steady-State, 200.39 W	C-18
C-14	Cold State Steady-State, 200.39 W	C-19
C-15	Cold Case Steady-State, 398.27 W	C-20
C-16	Cold Case Steady-State, 398.27 W	C-21
C-17	Cold Case Steady-State, 499.92 W	C-22
C-18	Cold Case Steady-State, 499.92 W	C-23
C-19	144°K Shroud Steady-State, 499.84 W	C-24

C-20	144°K Shroud Steady-State, 499.84 W	C-25
C-21	144°K Shroud Steady-State, 599.28 W	C-26
C-22	144°K Shroud Steady-State, 599.28 W	C-27
C-23	Header Heat Pipe	C-29
C-24	Radiator Heat Pipe No. 1	C-30
C-25	Radiator Heat Pipe No. 2	C-31
C-26	Radiator Heat Pipe No. 3	C-32
C-27	Radiator Heat Pipe No. 4	C-33
C-28	Radiator Heat Pipe No. 5	C-34
C-29	Radiator Heat Pipe No. 6	C-35

Table

C-1	Contact Conductances	C-5
-----	--------------------------------	-----

I. INTRODUCTION

The analysis of the heat pipe radiator/thermal conditioning panel test results was performed to demonstrate the ability of predicting multi-heat pipe system thermal performance. The test data from Appendix B was compared with the model results for both steady-state and transient conditions. To accomplish this comparison a 112 node thermal model of the header pipe and radiator was developed. Steady-state and transient runs were made and the results compared with the test data.

The predicted results agreed with the test results both in heat rejection and temperature. The most difficult task in the analysis was matching the front location in the individual feeder pipes on the radiator.

The complexity of this analysis is significant when compared with the analysis of previous radiator systems using a pumped fluid. The number of variables introduced by the variable conductance heat pipes over-shadows those of the pumped fluid systems. While the pumped fluid radiators have been designed and analyzed for over ten years, heat pipe radiators are relatively new and their analytical techniques have not achieved the maturity of other thermal control systems and techniques.

Over the past two years, Martin Marietta has devoted an IR&D task to the development of these analytical techniques and has verified the techniques for several fixed and variable conductance heat pipe designs including one radiator system. The analysis described in this report was the first data correlation attempted for an axial grooved variable conductance heat pipe.

II. SUMMARY

The heat pipe radiator thermal model correlations with the test data demonstrated that heat pipe systems can be modelled as a part of an overall system thermal model. The predicted results agreed very well with the test data for all steady-state and transient runs.

The added complexity of modelling heat pipes and including them in a thermal model is significant. The predictability of the front location in a variable conductance pipe represents the most difficult task. In general the predicted front locations appeared to be within 10 cm (approximately 5% of total length) of the actual location on the average with the maximum error being 30 cm (approximately 15% of total length).

Future applications of these techniques and improvements in heat pipe modelling will provide even better results as heat pipe applications to spacecraft increase. The results indicate that heat pipe analytical techniques are now achieving the maturity of techniques developed for analyzing other thermal control devices such as pumped fluid systems.

REPRODUCIBILITY OF THE
ORIGINAL PAGE IS
GUARANTEED

III. MODEL DESCRIPTION

The thermal analysis of the radiator/TCP test was accomplished using a 112 node thermal model of the system. The radiator contained 60 nodes, the header heat pipe 16 nodes, and the shroud 36 nodes.

The radiator model was divided into 10 nodes per feeder heat pipe. Each pipe contained one evaporator node, one transport node, six condenser nodes, one reservoir node and one vapor node. The header pipe consisted of four evaporator plate nodes, four evaporator nodes, one transport node, six condenser nodes, and one vapor node. Figure C-1 presents the nodal breakdown of the radiator and header pipes. Each of the heat pipes were modelled in the same general manner as shown in Figure C-2 for feeder pipe 1 on the radiator.

The evaporator of each feeder pipe was connected with the appropriate header condenser node via a contact conductance. The contact conductance was calculated based upon the test ΔT and the predicted heat load per pipe. Five steady-state runs (three hot case and two cold case) were used to determine the values shown in Table C-1.

The average values in Table C-1 were used in the model to obtain the predicted performance presented later in the test.

Heat was applied to the header evaporator plate uniformly over the four-plate nodes based upon the measured heat loads from each test. An attempt was made to model the thermal conditioning panel (TCP) as a single node and apply the heat load at this point. This did not yield reasonable results due to a variation in the apparent contact conductance between the plate and TCP. This variation is attributed primarily to variation in temperature on the TCP under the plate. Since this temperature distribution was not measured in the test, the proper conductance value was unobtainable from the model or test data.

Since this was the first attempt to checkout the axial groove pipe simulation, problems with the axial groove logic in the subroutines were anticipated. Initially low ΔT s were obtained for the feeder pipes. A match of feeder pipe ΔT s was obtained by reducing the tube to vapor conductances by a factor of 18.6. The original conductance calculation did not account for conducting through a liquid layer in the area of vaporization or condensation. A brief literature search revealed that a liquid layer of approximately 0.00254 cm (0.001 in.) yields the appropriate conductance in series with the radial conductance of the tube (ref 1). Furthermore, Reference

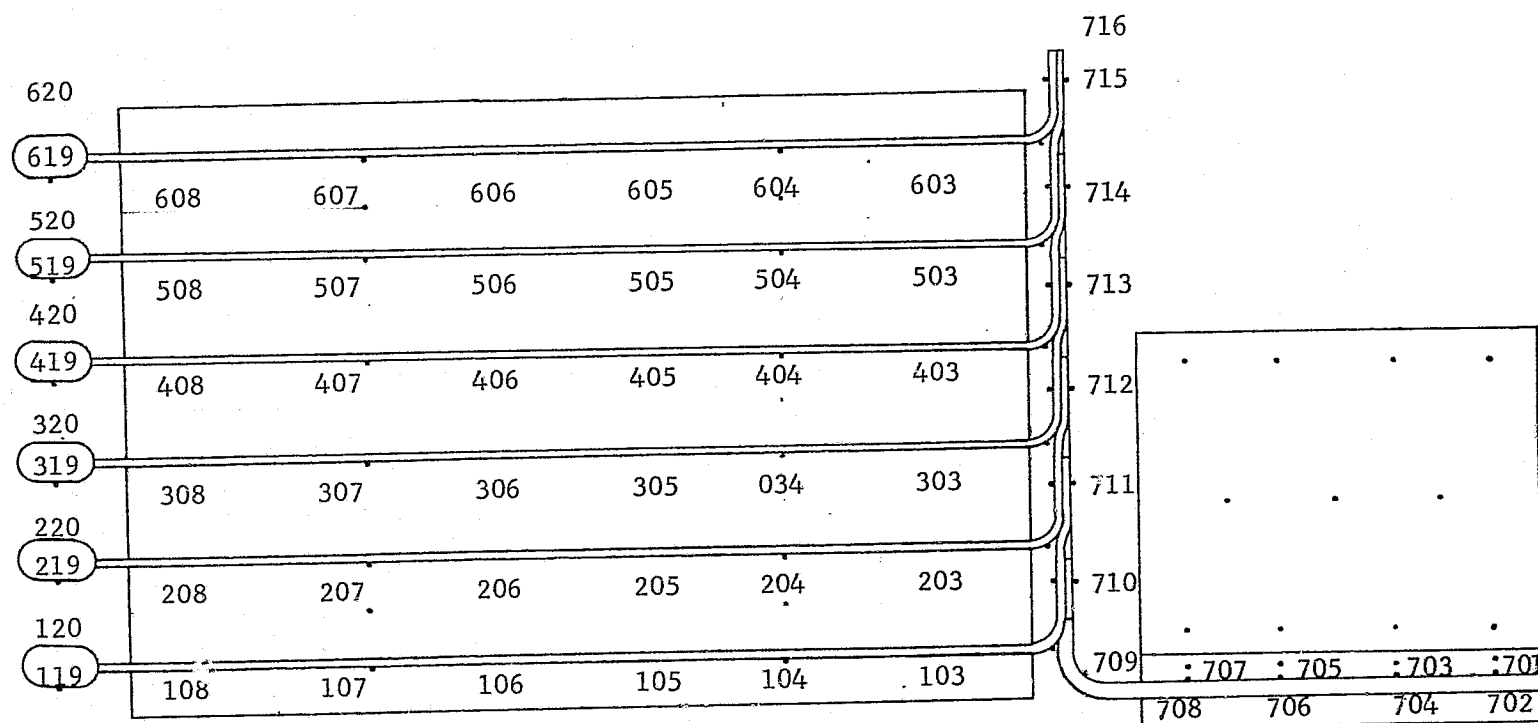


Figure C-1 Heat Pipe Radiator Thermal Model Mode Diagram

1 states that the vaporization in the evaporator occurs in the vicinity of the meniscus attachment line while condensation in the condenser occurs primarily on the fin ends. For the results discussed later, a constant radial conductance for both the evaporator and condenser sections was used.

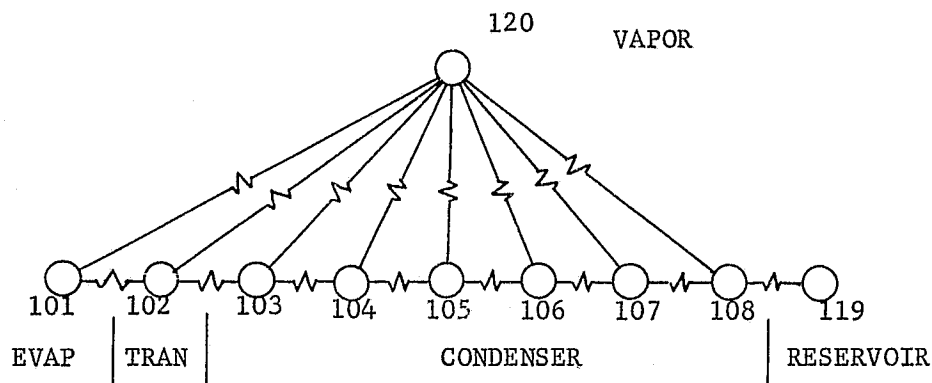


Figure C-2 Heat Pipe Model

Table C-1 Contact Conductances

	Pipe 1	Pipe 2	Pipe 3	Pipe 4	Pipe 5	Pipe 6
$\bar{G} \frac{W}{^\circ K}$	10.26	10.73	9.38	7.07	8.69	7.29
Standard Deviation $\frac{W}{^\circ K}$	1.69	1.90	1.99	1.65	0.79	1.97

The early runs further indicated that using the gas load of 0.0135 lb_m of nitrogen (Ref 2) did not yield the proper gas front location. The model assumes flat front theory with tube conduction. This was not sufficient in locating the front until the gas load was reduced by 6%. The reduced load was within the loading accuracy according to Grumman Aerospace Corporation ($\pm 10\%$). The actual gas weight is very difficult to weigh and the load was determined by the perfect gas equation. Some diffusion effects are also likely; however, this effect was considered to be small.

NOTED: DOCUMENT OF THE
ORIGINAL PAGE IS FOR

IV. MODEL CORRELATIONS

Model correlations with the test data yielded good agreement for the steady-state and transient runs both in temperature and front location. The discussion of the model results are presented first for the steady-state cases followed by the transient runs.

A. STEADY-STATE CORRELATIONS

1. Hot Case

All of the hot case test runs were simulated by the model and the results are presented in Figures C-3 through C-12. Each of the six feeder heat pipes' temperatures are plotted versus node location superimposing the test temperatures for direct comparison with the model results. The 100 W hot case is presented in Figures C-3 and C-4. The front locations for pipes 3 and 4 were in excellent agreement with test while pipes 5 and 6 predicted fronts 10 and 15 cm, respectively beyond the locations indicated by test. Pipes 1 and 2 predicted fronts 25 and 15 cm inside those indicated by test. This run yielded the most significant front location errors of the hot case analyses.

In reviewing all of the data one should bear in mind that the reservoir temperatures were set to the measured test temperature with one exception. The thermocouple on reservoir 1 was loose and did not yield accurate test data. Its reading was adjusted to a more reasonable value.

The 200 W case is presented in Figures C-5 and C-6. The temperature predictions were in excellent agreement with test as were the front locations. The 300 W case is shown in Figures C-7 and C-8. Pipes 1, 4 and 6 were in excellent agreement with test while pipes 2, 3, and 5 showed errors in front location 20, 12, and 17 cm, respectively, beyond that indicated by test. The 380 W case is shown in Figures C-9 and C-10. This case resulted in excellent agreement for the first 5 pipes with pipe 6 predicting the front inside of that indicated by test by 32 cm. The 200 W test was repeated to show repeatability of results which also showed repeatability of the model. The data is presented in Figures C-11 and C-12.

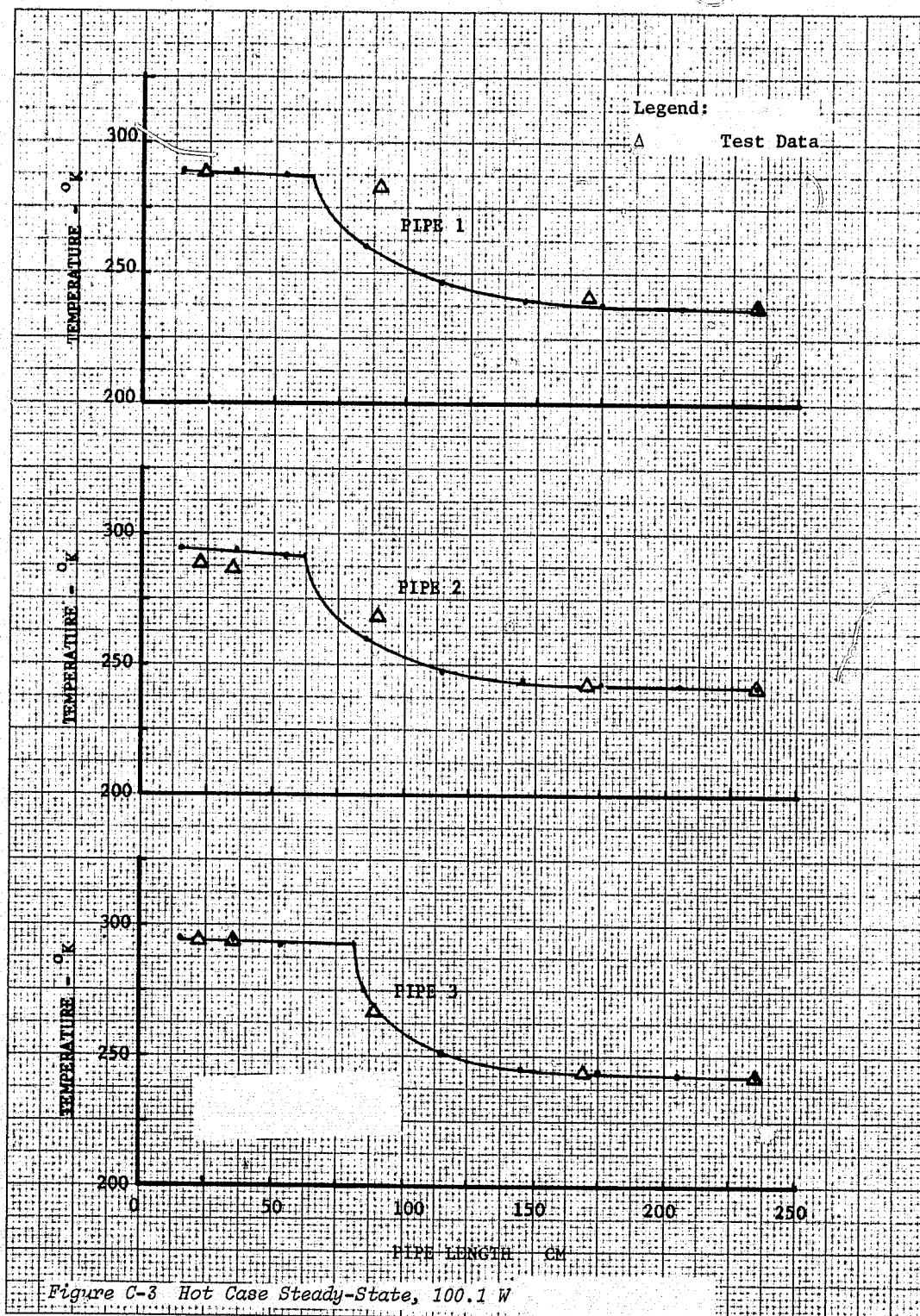
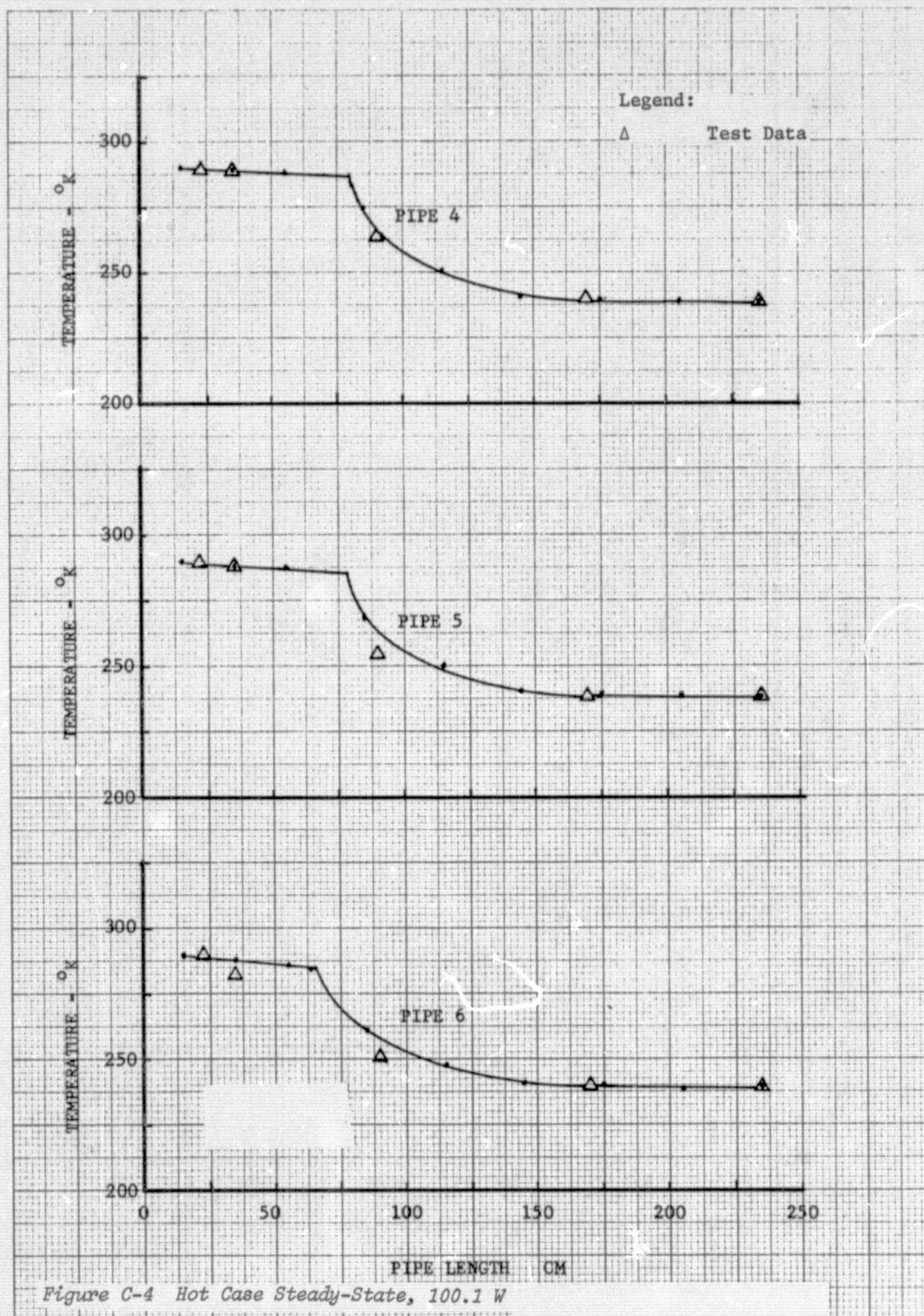
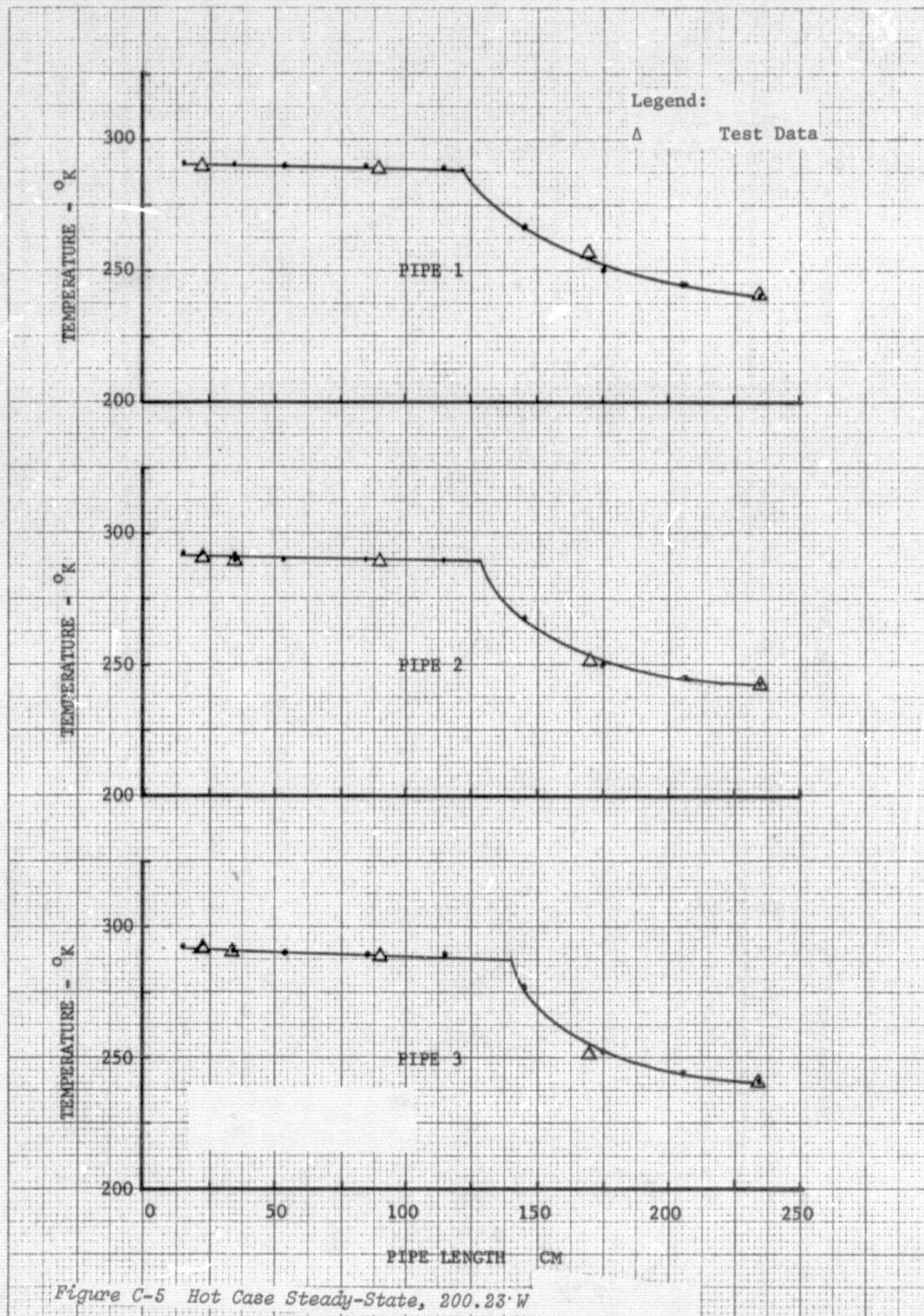


Figure C-3 Hot Case Steady-State, 100.1 W





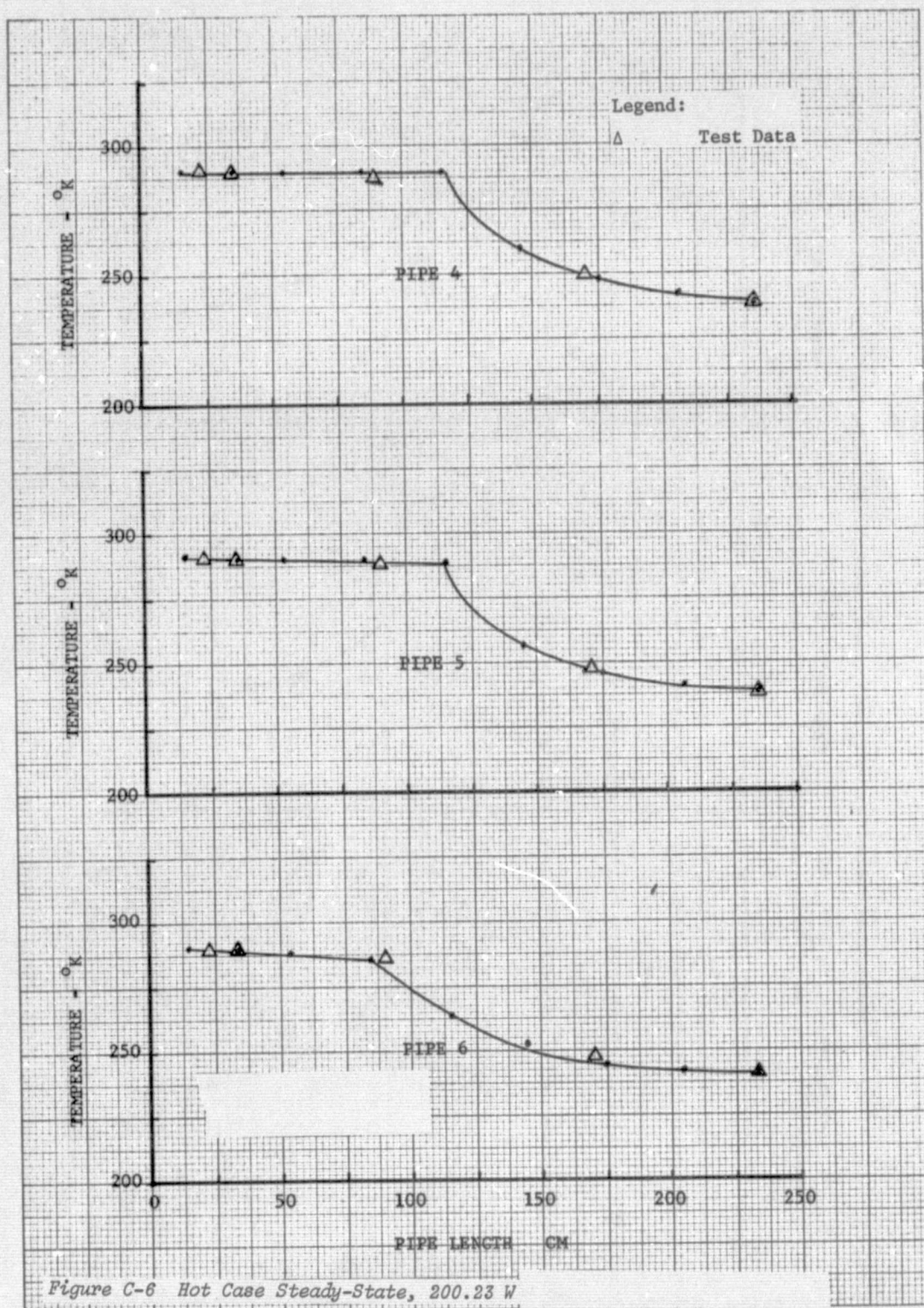


Figure C-6 Hot Case Steady-State, 200.23 W

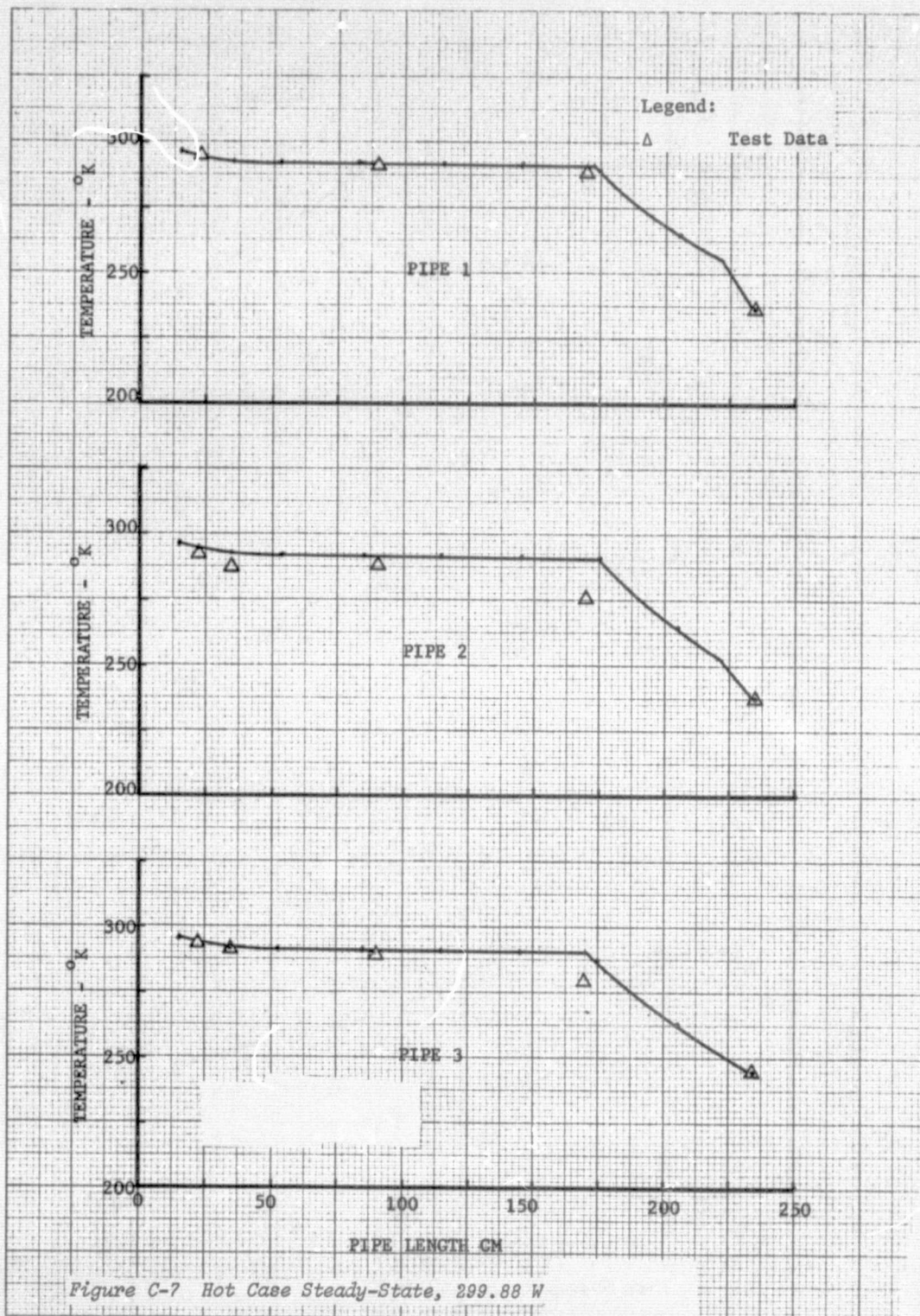
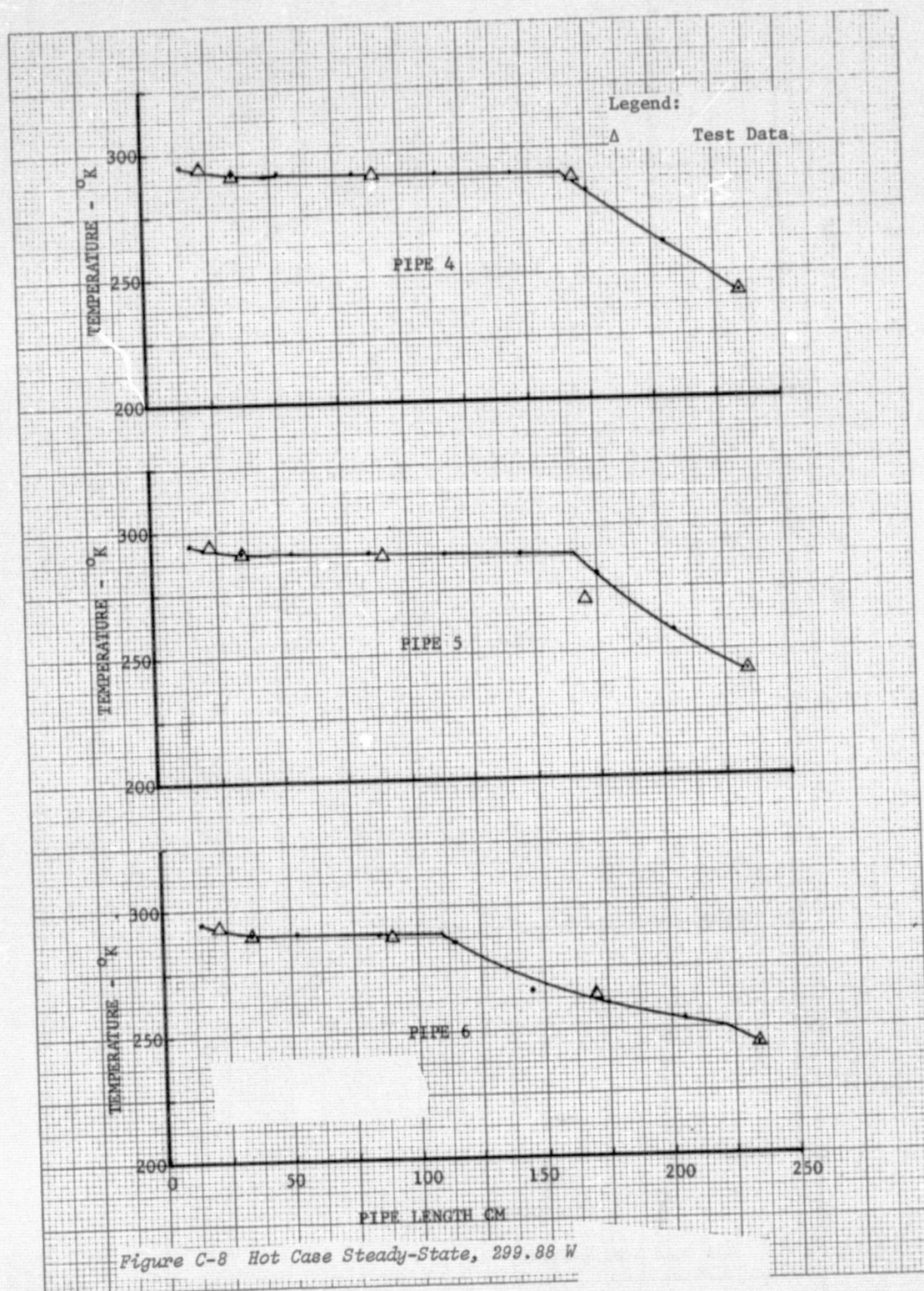


Figure C-7 Hot Case Steady-State, 299.88 W



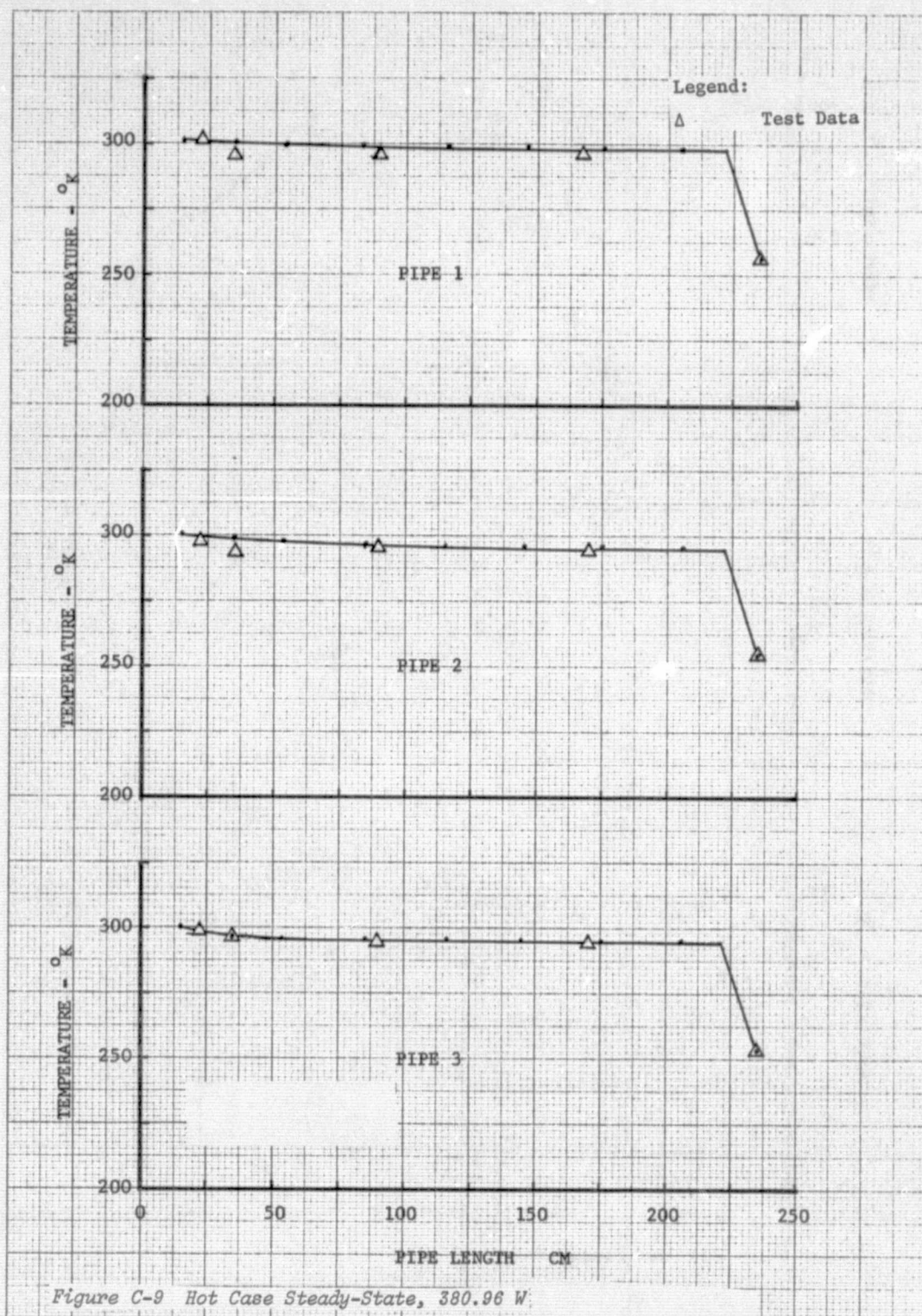
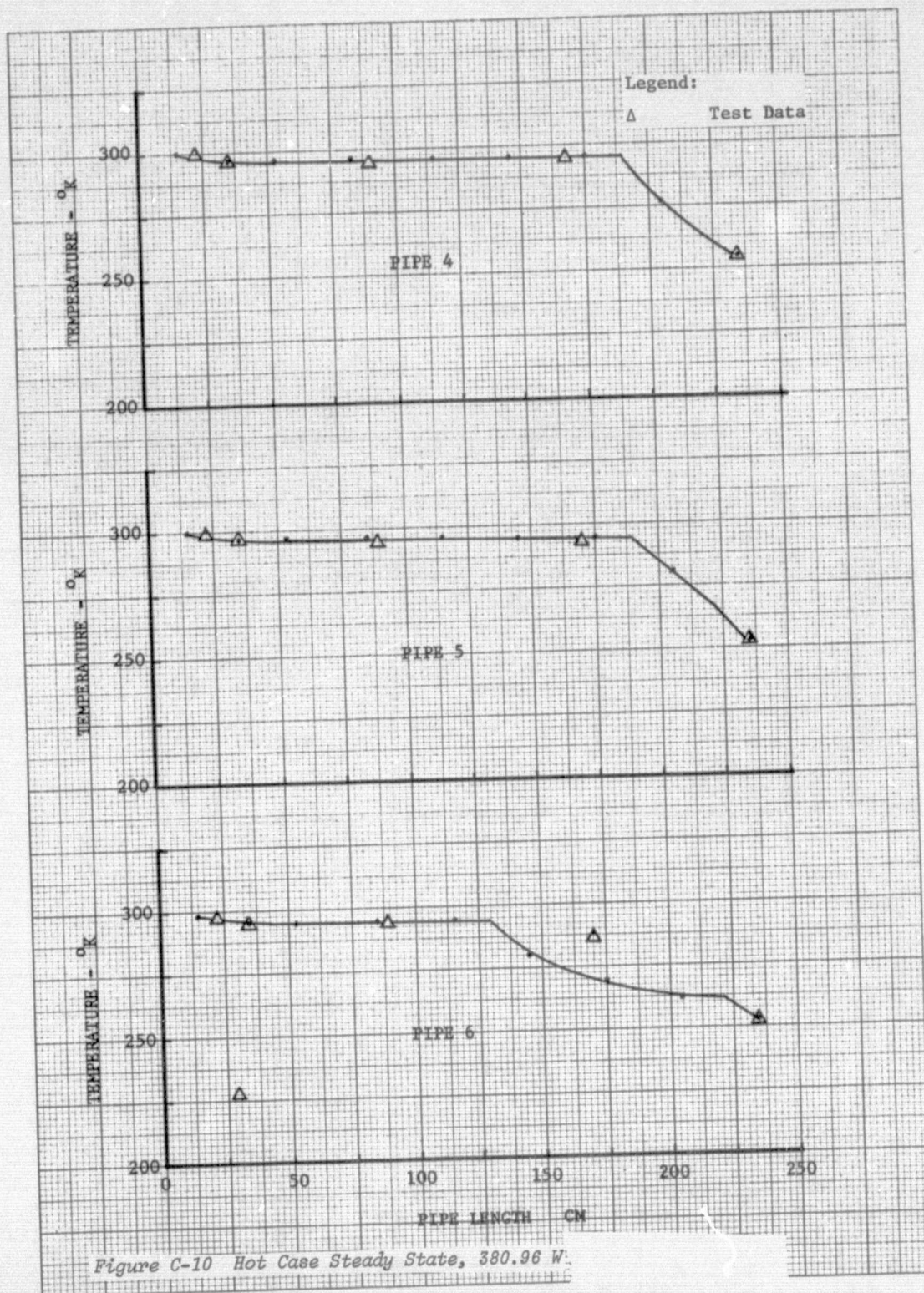


Figure C-9 Hot Case Steady-State, 380.96 W



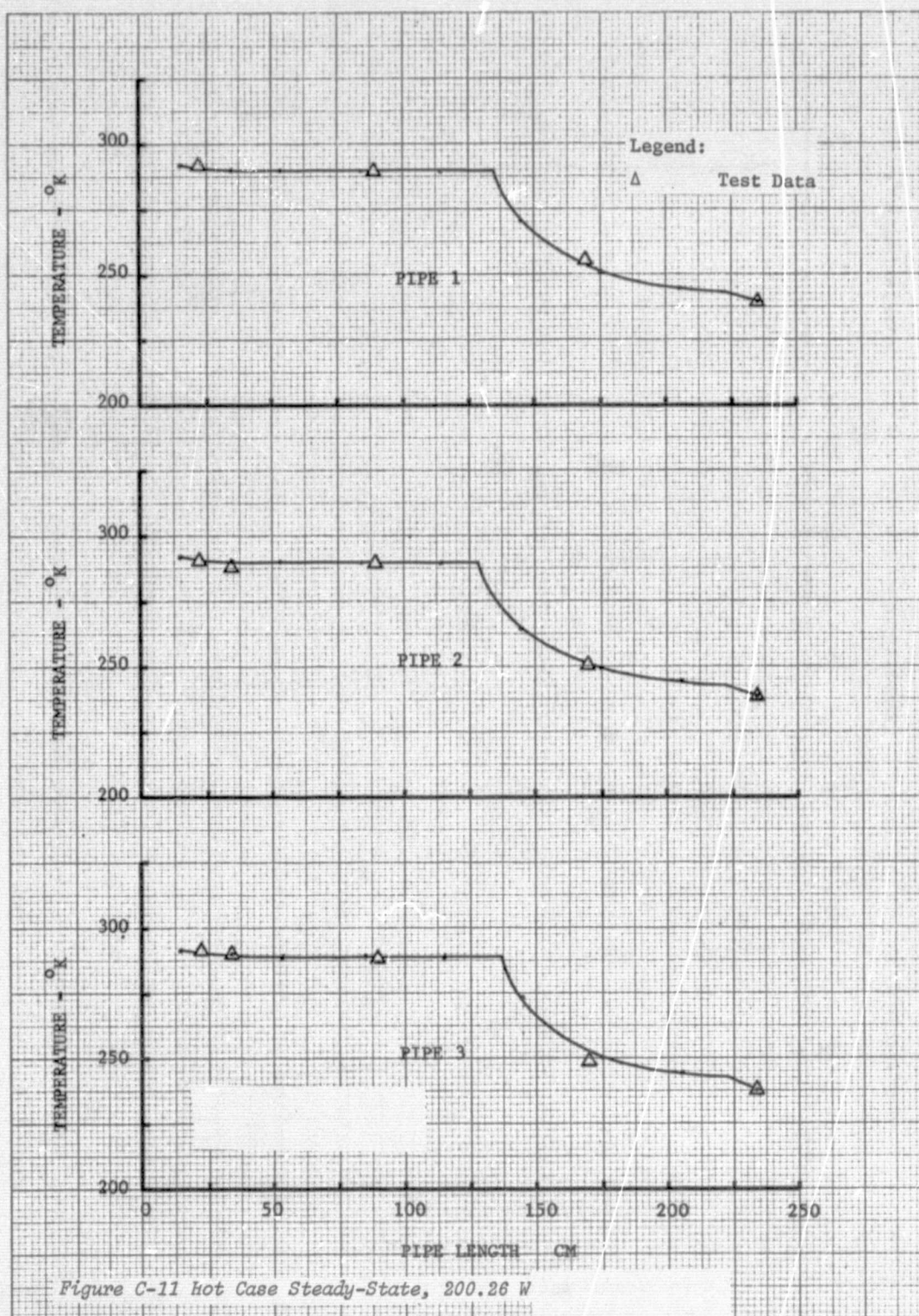
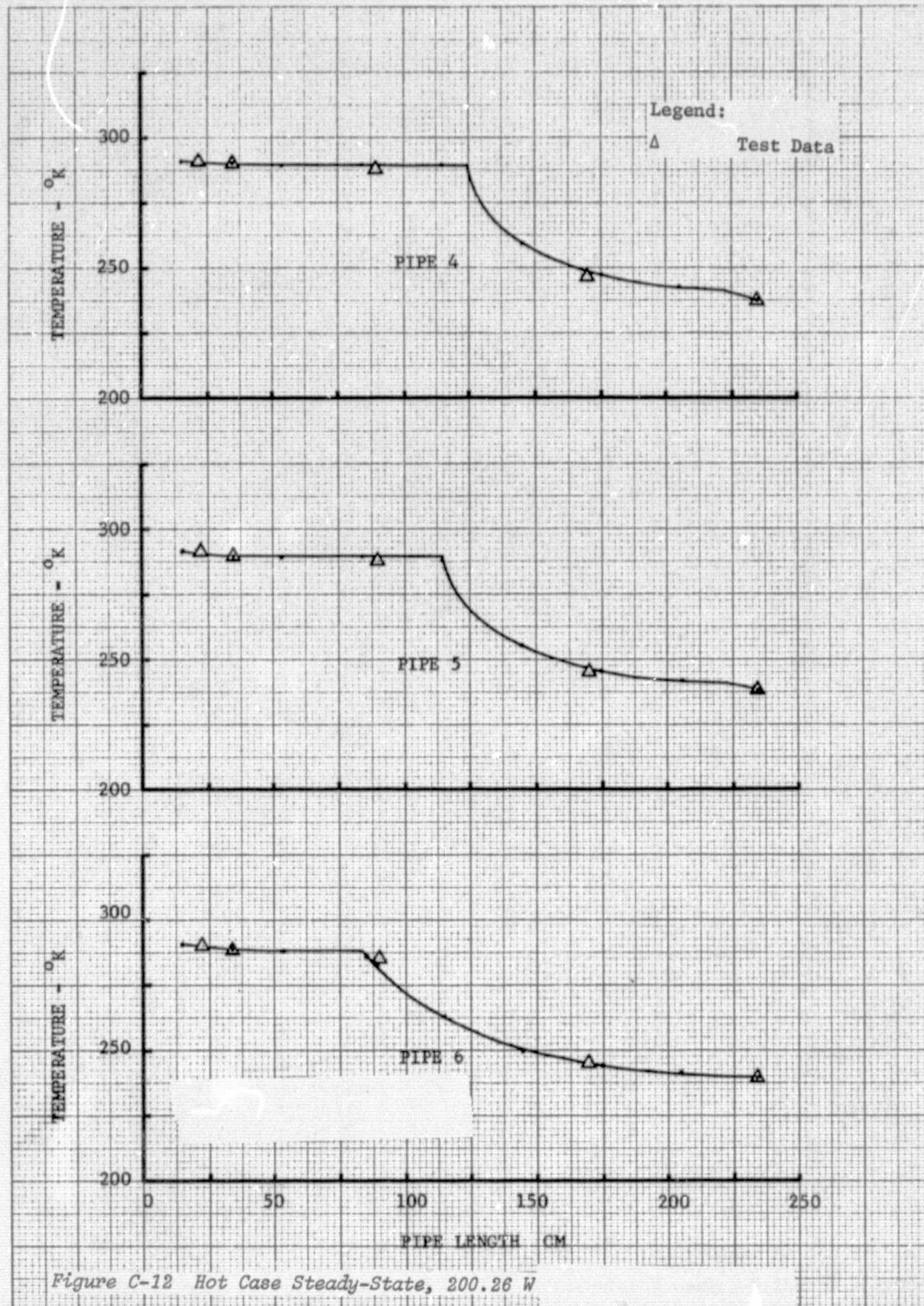


Figure C-11 Hot Case Steady-State, 200.26 W



2. Cold Case

The cold gas correlations are summarized in Figures C-13 thru C-18. Figures C-13 and C-14 present the 200 W case. The model predicted temperature and front locations very well for this case. Pipe 5 presented approximately 10 cm error in front location. The 400 W case, Figures C-15 and C-16, resulted in slightly larger front location errors, 17 cm for pipe 2, 10 cm for pipe 3, 5 cm for pipe 5, and 15 cm for pipe 6. The 500 W case, Figures C-17 and C-18, gave very good results for the first 5 pipes with the sixth pipe showing a significant error in front location.

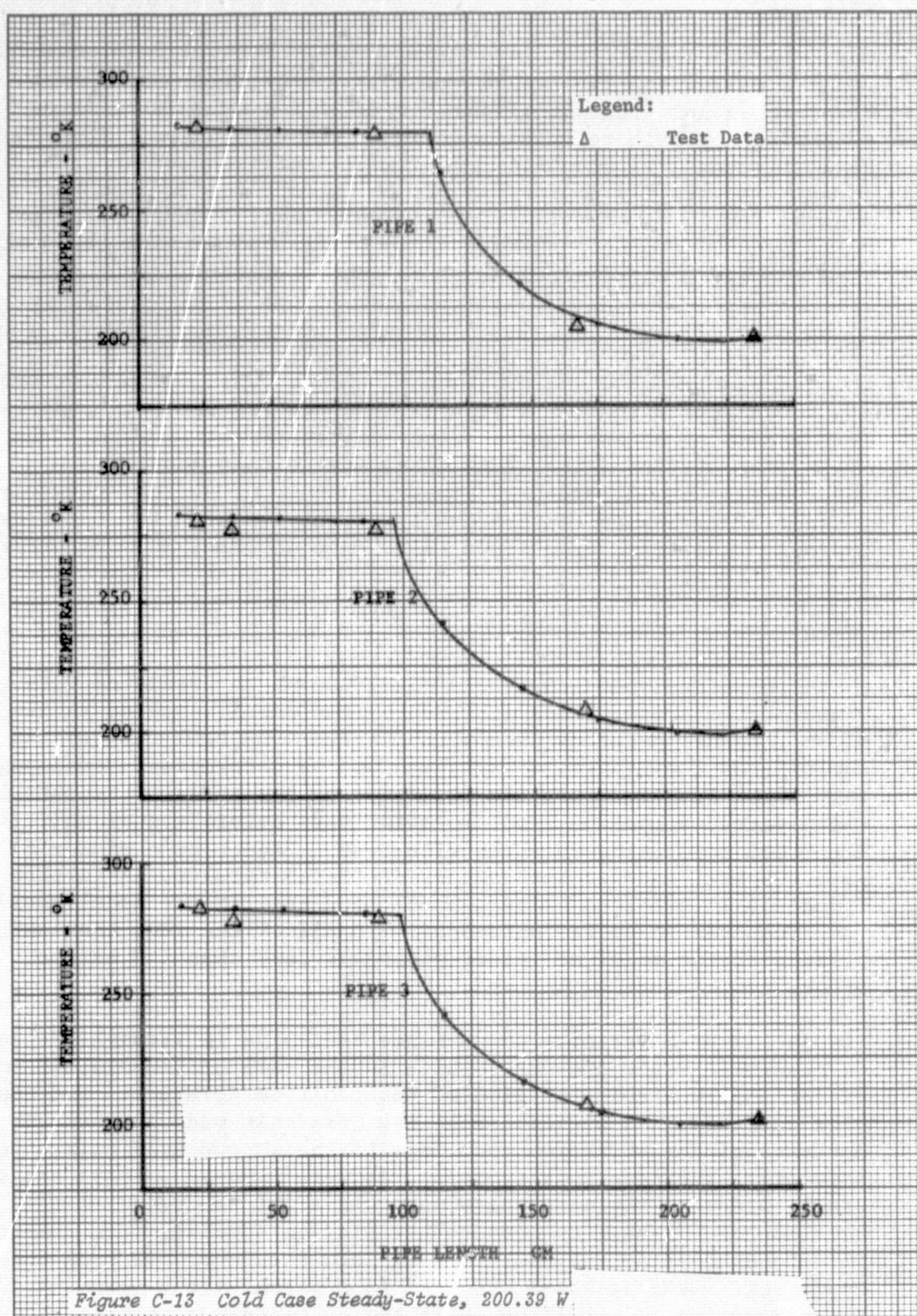
3. 144°K Shroud

The 144°K shroud 500 and 600 W cases showed nearly excellent agreement with test. The 500 W case is shown in Figures C-19 and C-20. Temperature agreement was excellent for the first 5 pipes. The sixth pipe predicted the front 22 cm inside that indicated by test. Figures C-21 and C-22 present the 600 W data and show excellent agreement in temperature and front location for the first 5 pipes. The sixth pipe appeared to have at least a 30 cm error in front location.

4. Discussion

As shown in the above data general agreement in predicted versus measured temperatures was achieved by the model. Due to the lack of sufficient number of thermocouples from the test the precise location of the vapor gas front can not be determined. Assuming that the temperature profile indicated by the model is reasonable the apparent errors in front location were determined by shifting the model prediction to agree with test. Feeder pipe number 6 gave the most inconsistent set of predicted results. A further reduction in gas load below the -6% load used in the model would have resulted in poorer agreement. In all of the runs the energy balance of the model at steady-state was less than 1 W maximum error.

Simulation of a variable conductance heat pipe is strongly dependent on reservoir vapor pressure, which in the case of ammonia, is an exceptionally strong function of reservoir temperature. The complex geometry in the vicinity of the reservoir made an accurate estimate of the radiation couplings to the shroud difficult. Consequently, the reservoir temperatures were imposed in this analysis in order to minimize these unknowns. All the steady-state runs contained logic to compute a radiation coupling from reservoir to shroud based on the heat leaking into the reservoir from the condenser. Several cases resulted in apparent front movement into the reservoirs, a condition which the model is not capable of simulating. When the average radiation couplings for the runs with the front not influencing the reservoir were used between the reservoirs and shroud, predicted temperatures within 2°K resulted for the 500 W 144°K shroud case.



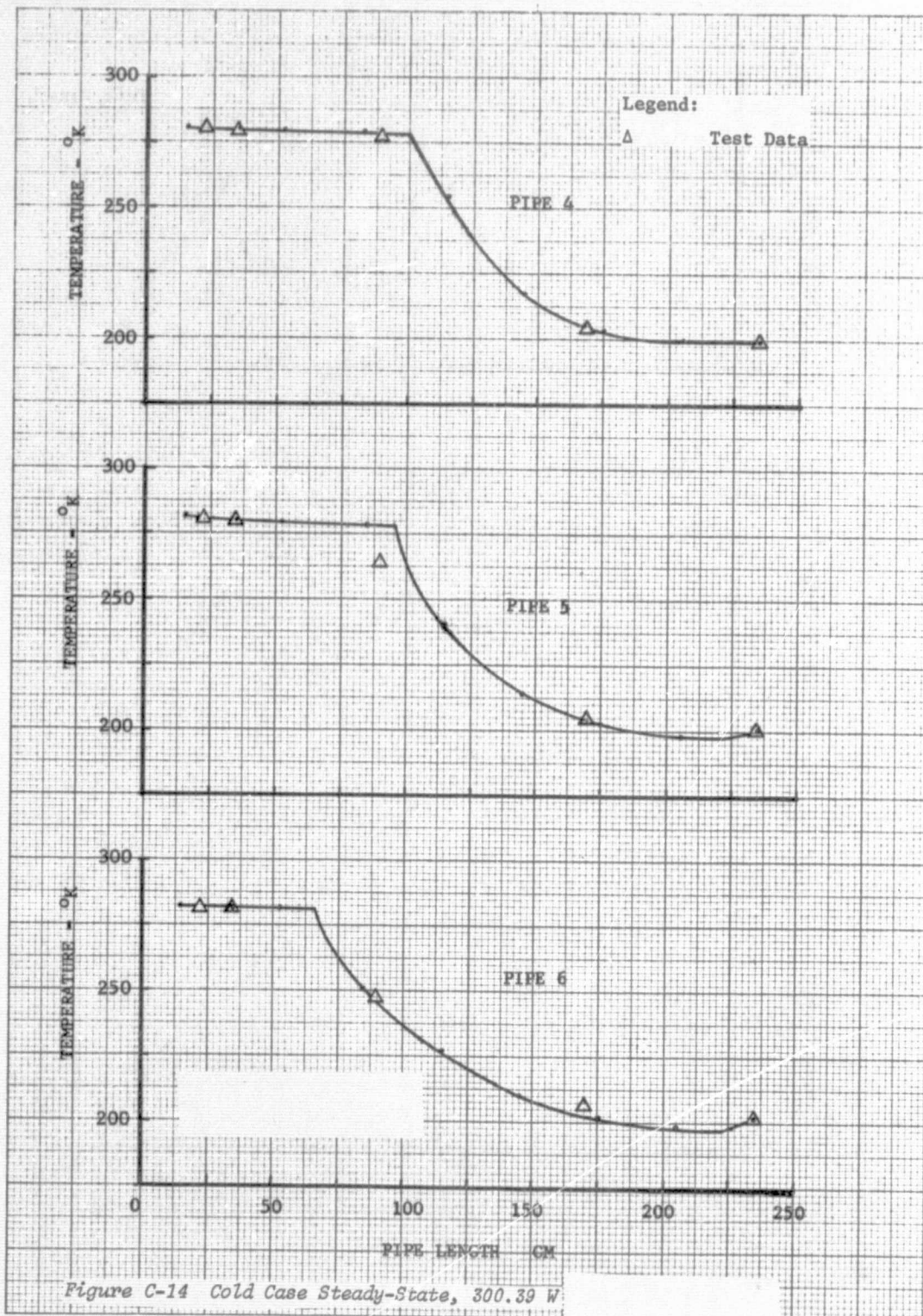


Figure C-14 Cold Case Steady-State, 300.39 W

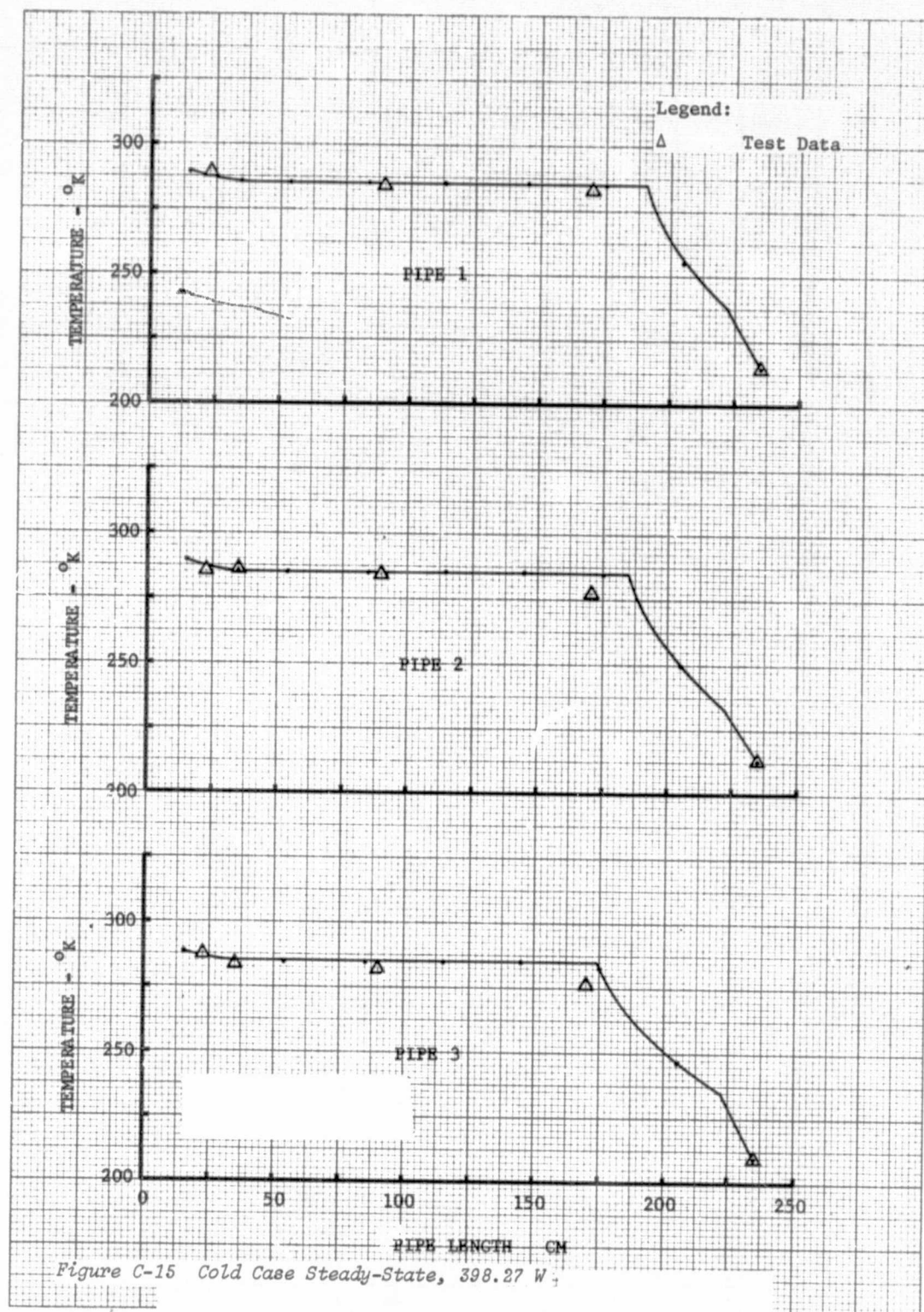
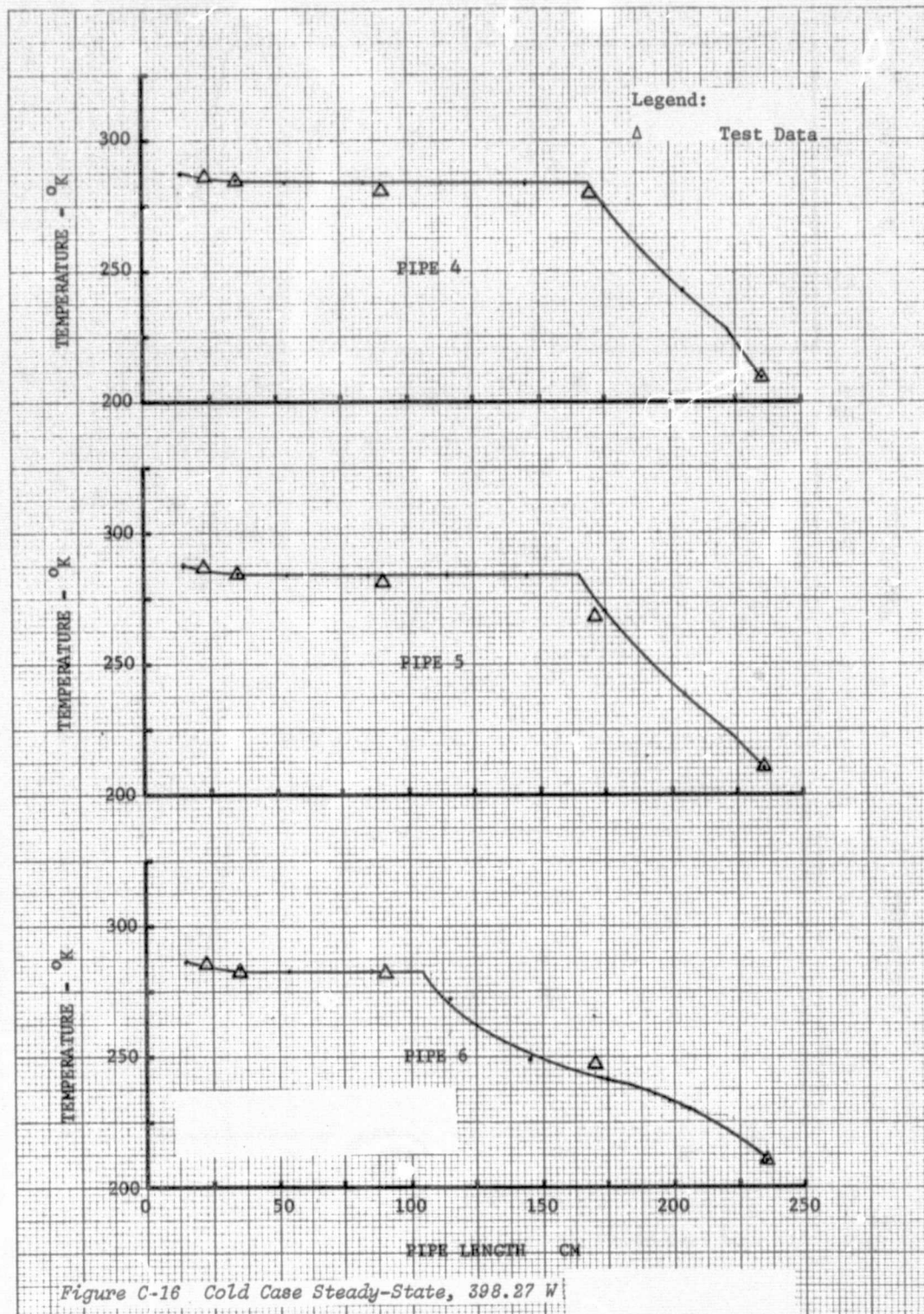


Figure C-15 Cold Case Steady-State, 398.27 W.



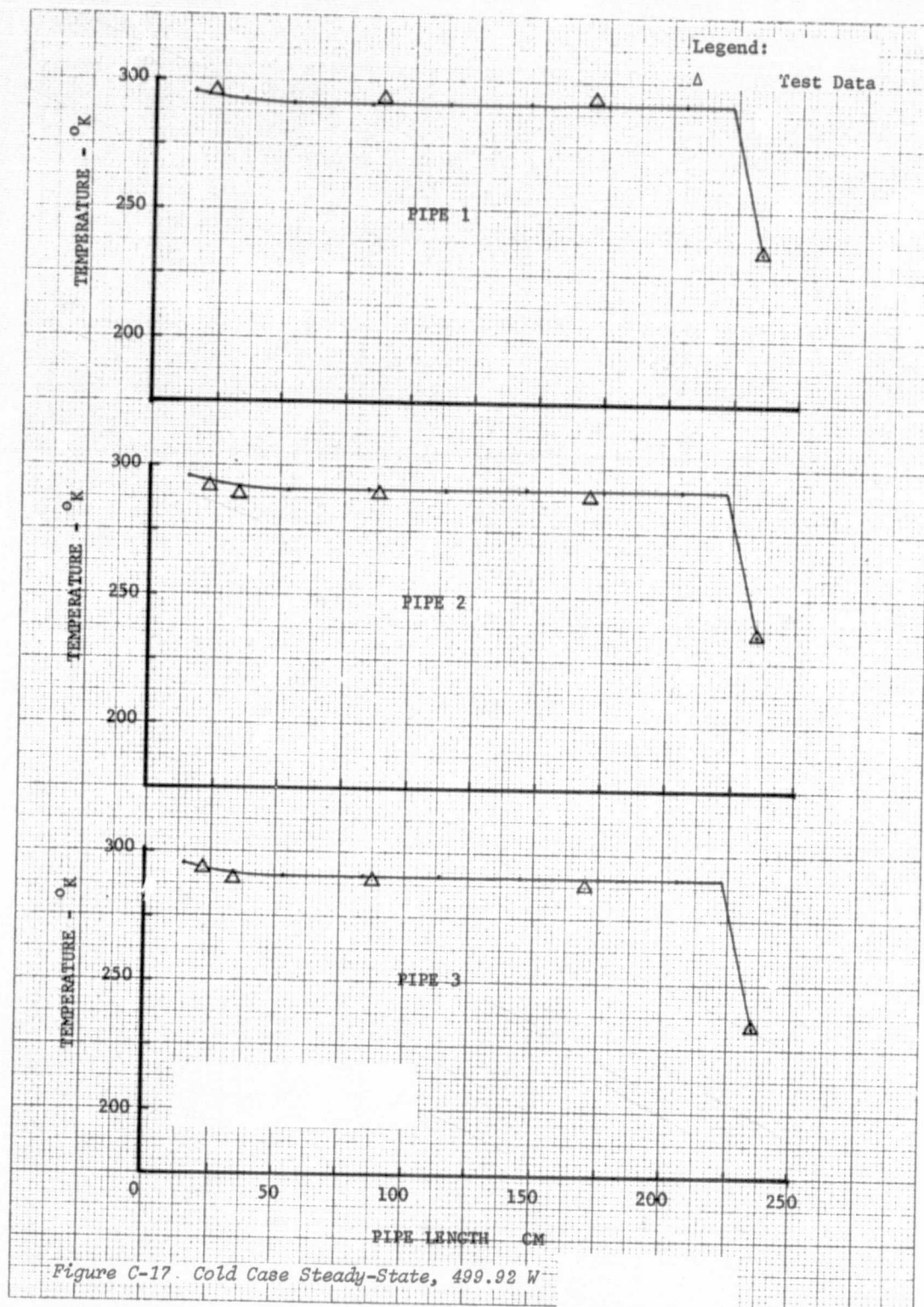


Figure C-17. Cold Case Steady-State, 499.92 W

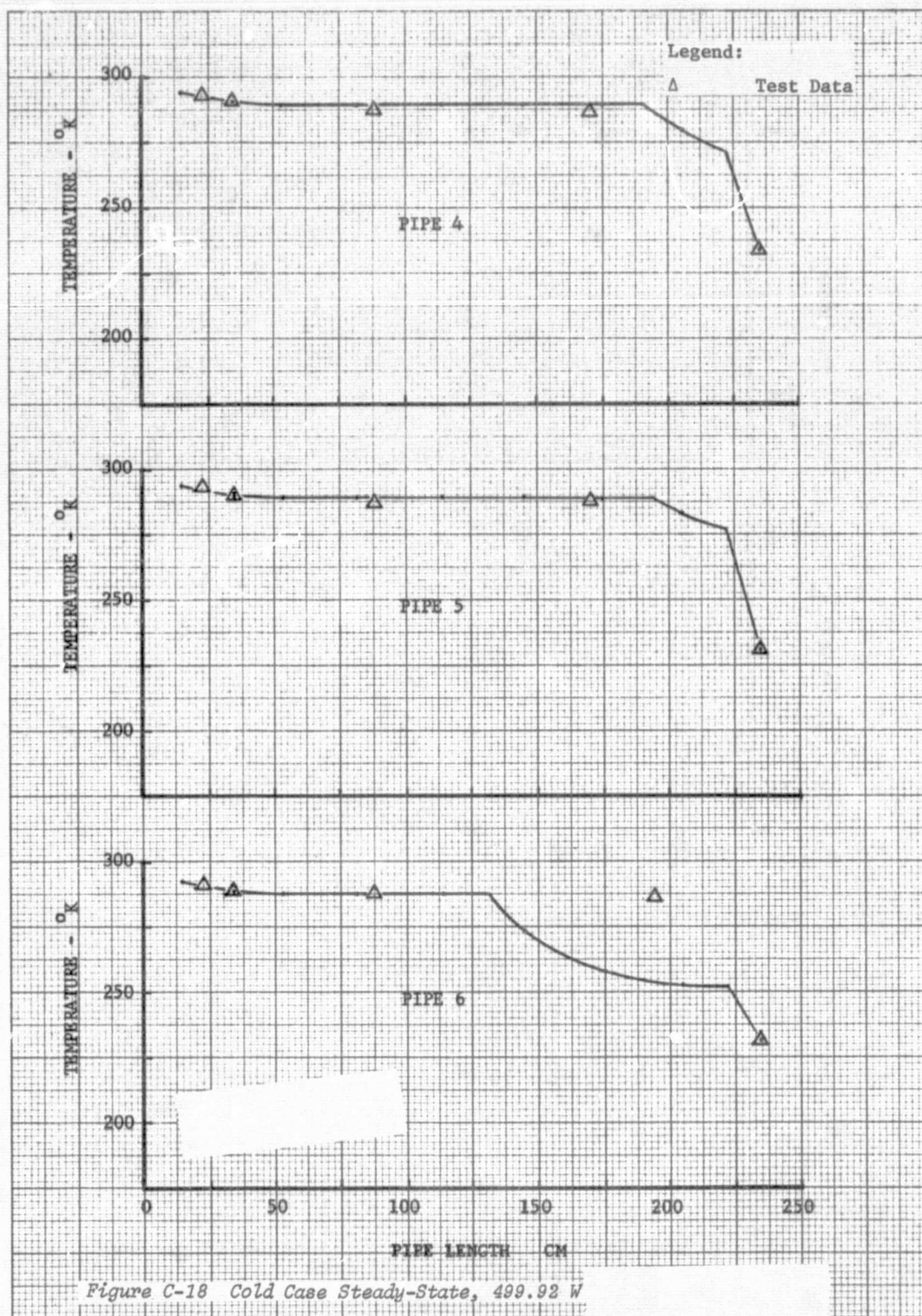
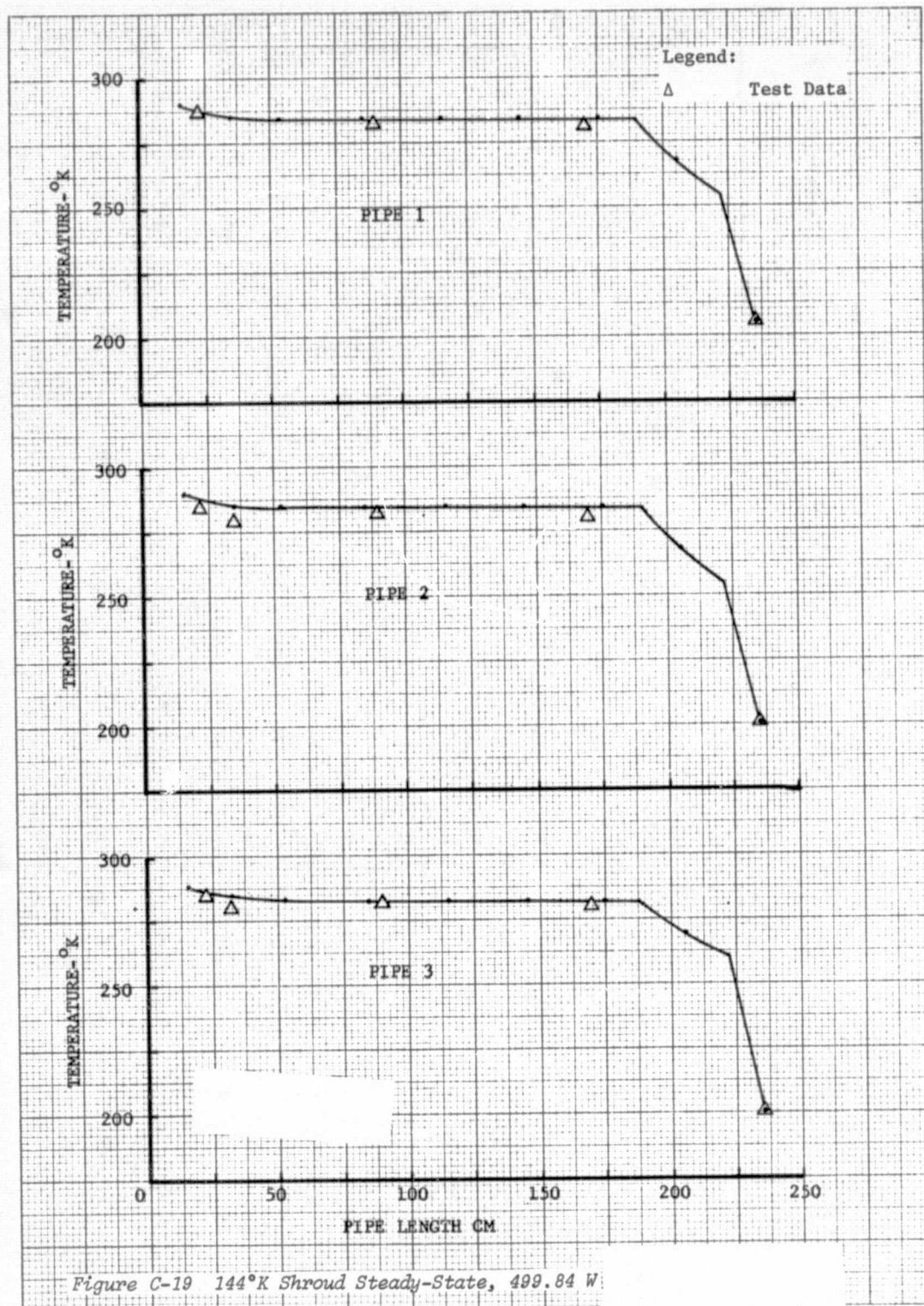
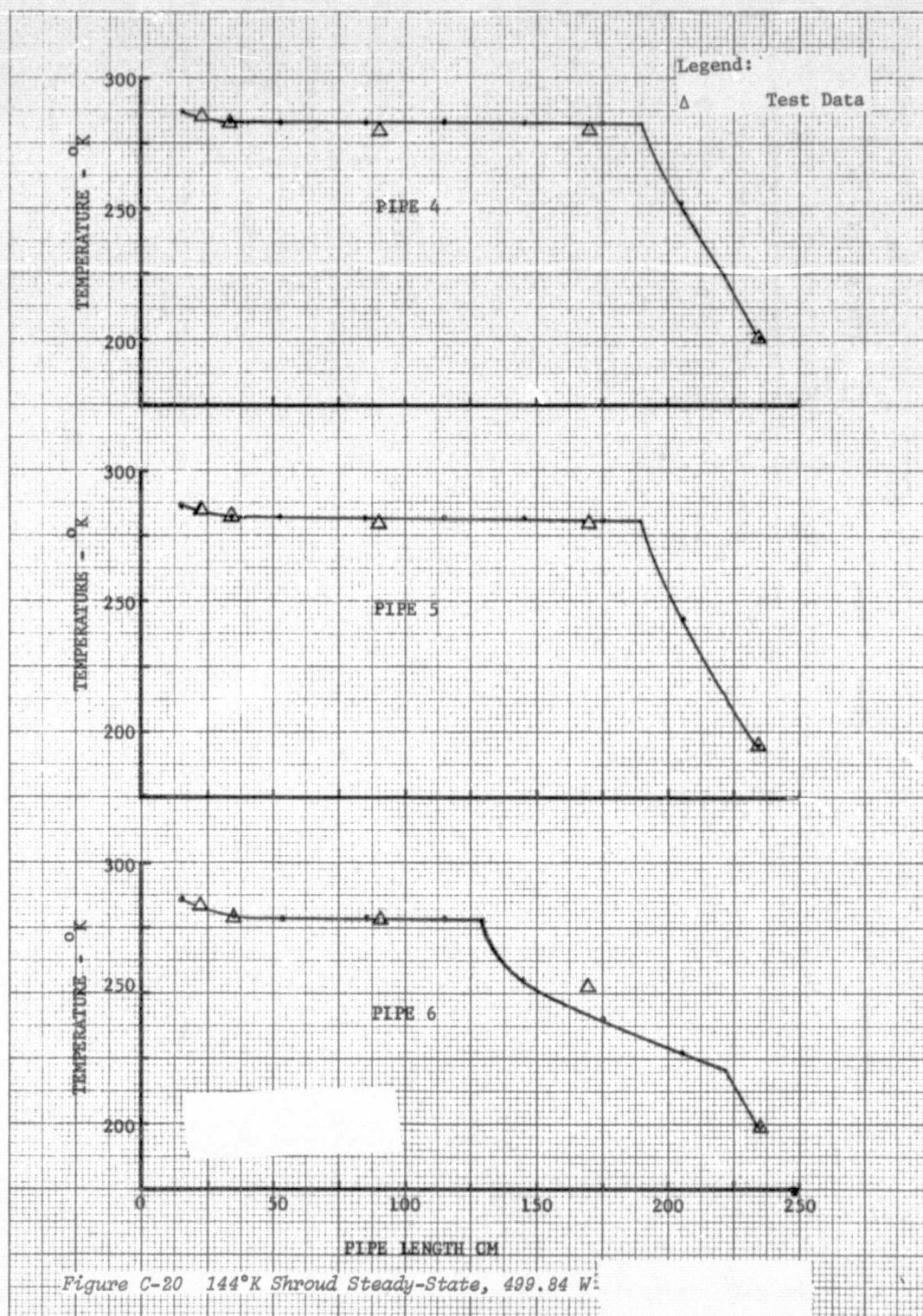
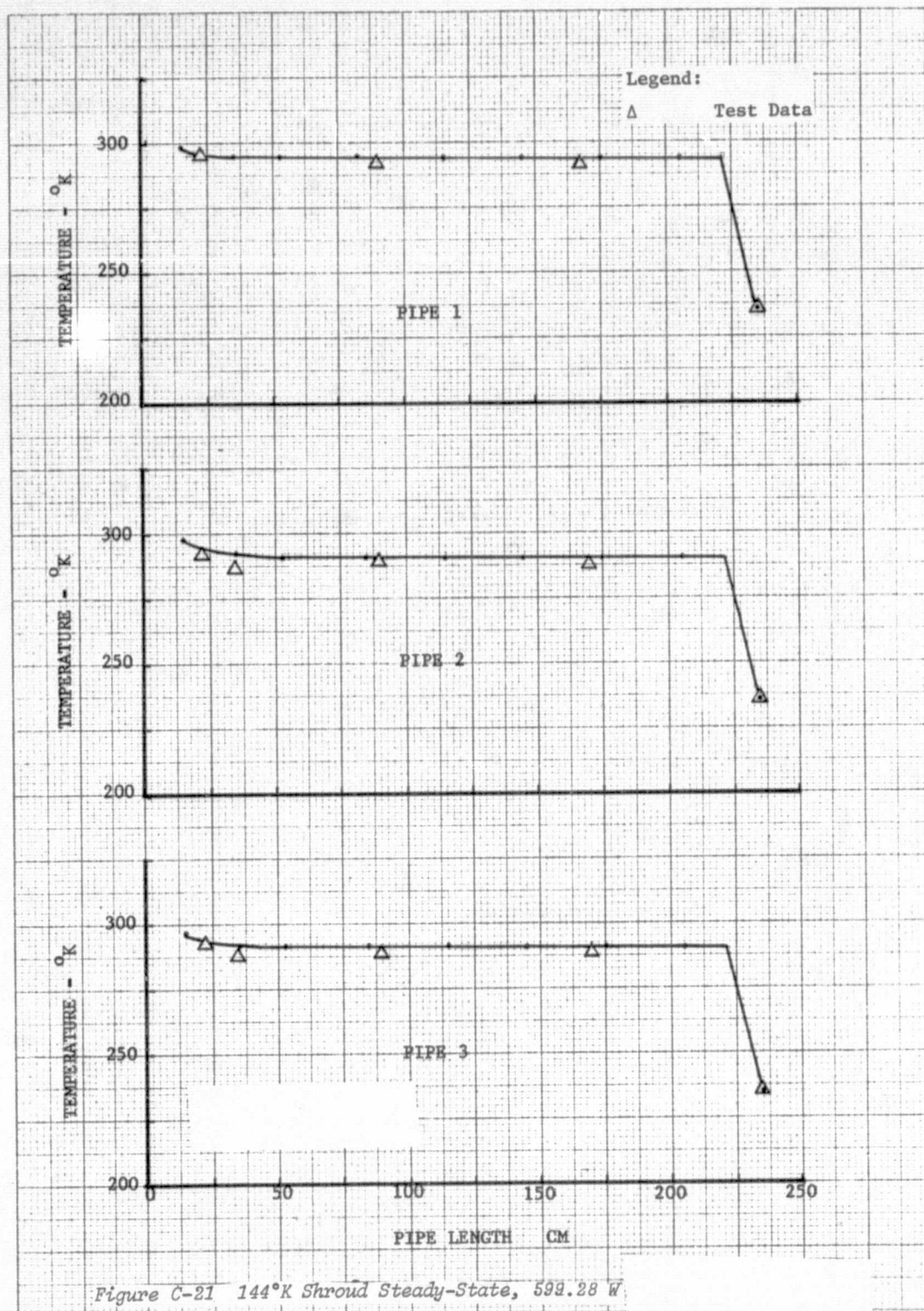


Figure C-18 Cold Case Steady-State, 499.92 W







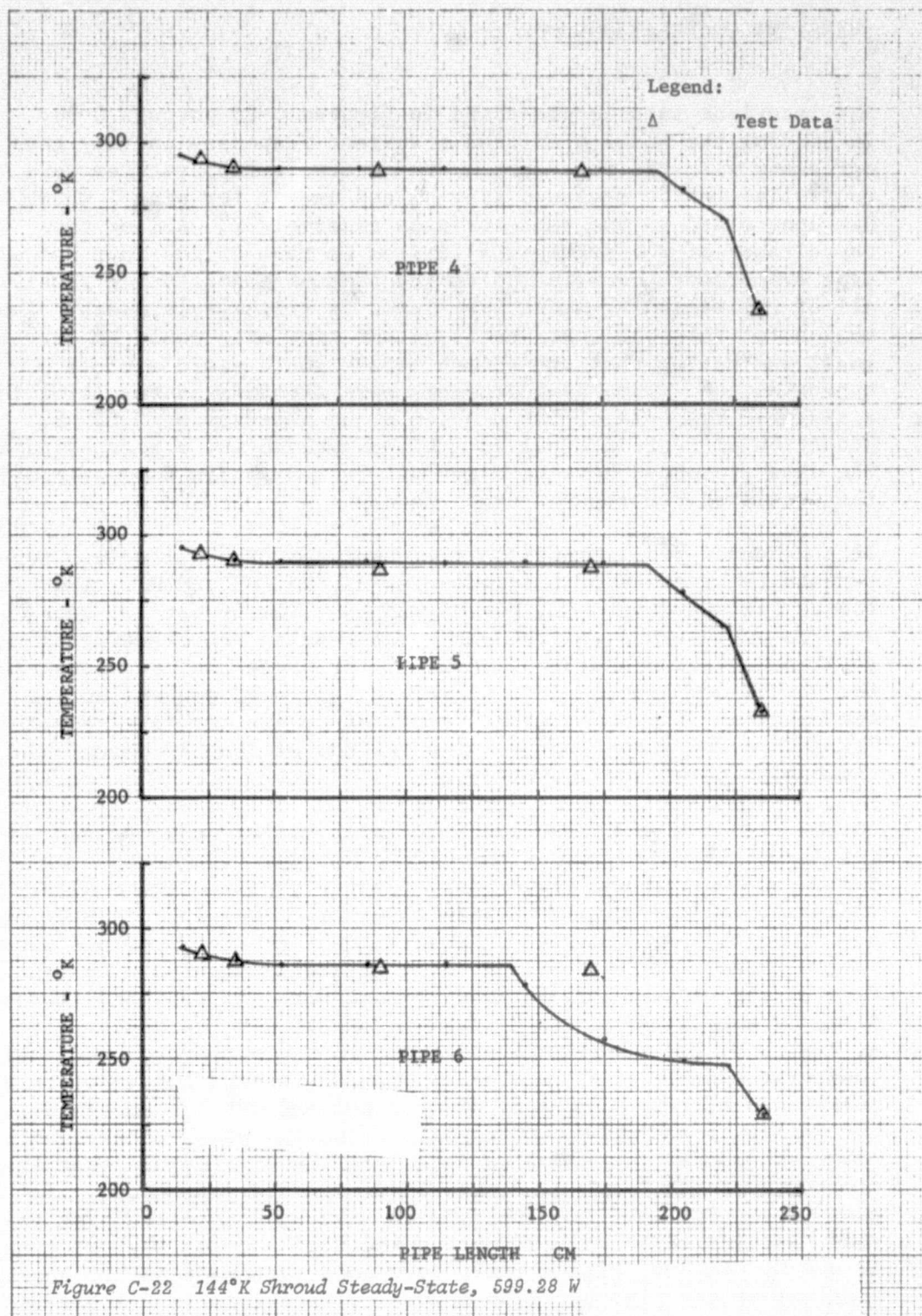


Figure C-22 144°K Shroud Steady-State, 599.28 W

B. TRANSIENT CORRELATIONS

The transient data is presented in Figures C-23 through C-29. In general the model predicted transient responses in very good agreement with the test data. The reservoir temperatures were controlled to the measured test values except for pipe 1 which was controlled to the same curve as reservoir 2. All of the capacitance of the system was limited to that of the four header pipe evaporator nodes including the thermal conditioning panel. All of the remaining nodes were input as arithmetic nodes. The reason for this was that the resultant time step would be extremely small indicating that the chosen method would yield a close approximation. Time step problems were encountered resulting in a sluggish response of the problem at an interval of 0.05 hr. Reduction of that interval to 0.02 hr yielded the presented data. The data presented here were derived from Appendix B superimposing the predicted results for comparison.

In the header pipe comparison the upper set of model points represents the average of thermocouples H1, H3, H5 and H7. The next cooler set represents H2, H4, H6 and H8. The lowest two sets are the hottest and coldest condenser results representing thermocouples H10 through H15. Figure C-23 presents the data comparison for the header pipe which resulted in very good comparison in temperature. The most severe transient conditions were chosen for this correlation representing the end of the 200 W run and the beginning of the 400 W run.

In the feeder pipe comparisons the upper set of model points represents the evaporator, the middle set the first condenser thermocouple from the evaporator. Feeder pipe 1, Figure C-24, yielded excellent agreement with the test. Pipe 2, Figure C-25, gave results approximately 2°K warmer on the evaporator and displayed faster response of the front movement compared with test. Pipe 3, Figure C-26, compared very well with the test and showed slightly faster response in front movement than the test. Pipe 4, Figure C-27, showed good agreement in the evaporator and active condenser section. The agreement with the second condenser thermocouple was mixed. The front did not respond out far enough during the initial front movement resulting from the power change and later showed the front moving back into the pipe beyond that indicated by test. Pipe 5, Figure C-28, yielded very good agreement except for the front tending to move back into the pipe beyond that indicated by test during the cold part of the orbit while at 400 W. Pipe 6, Figure C-29, gave good agreement in the active sections of the pipe but also showed a front location closer to the evaporator than indicated in the test result during the 400 W portion.

Figure C-23

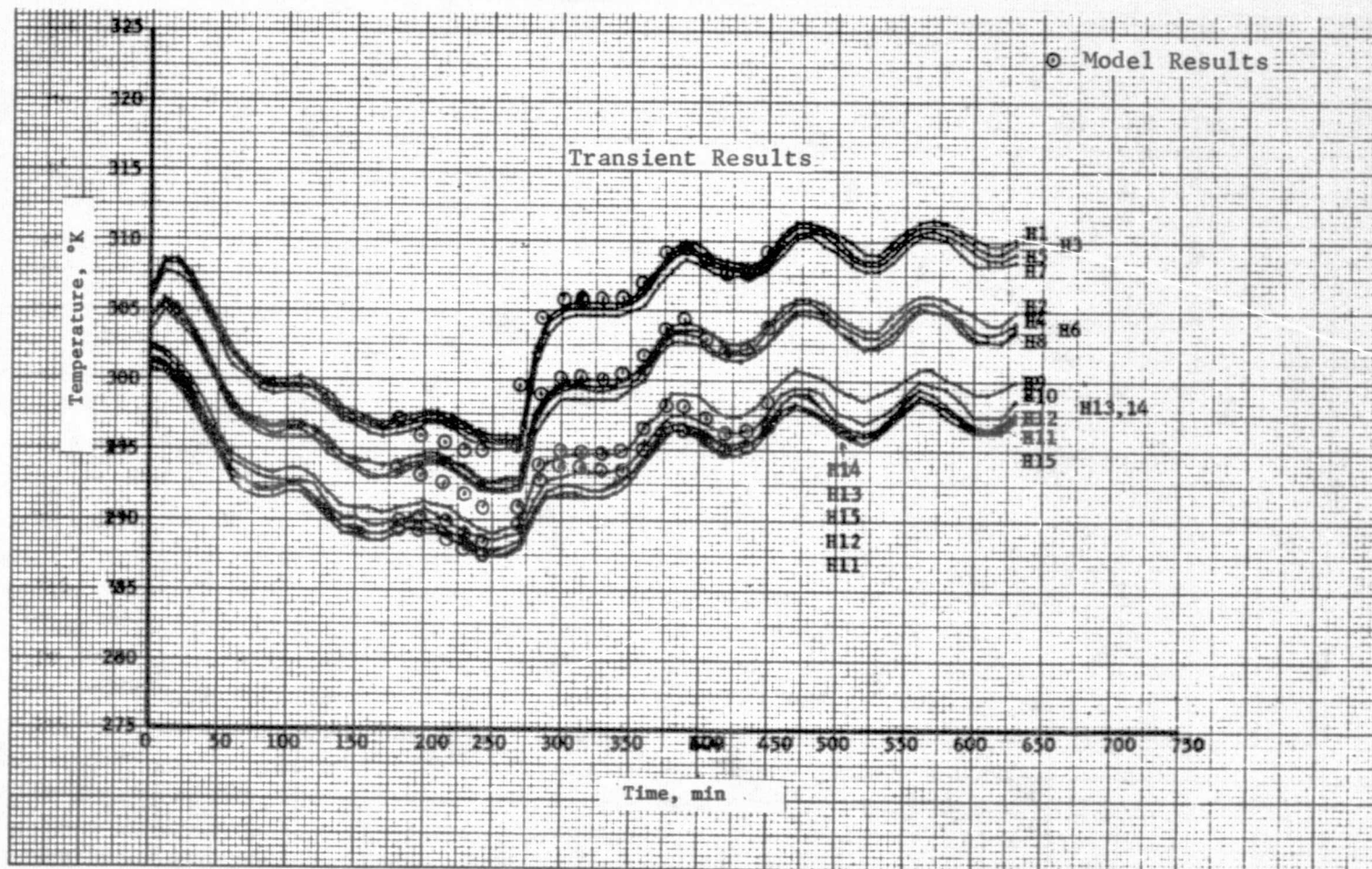


Figure C-23 Header Heat Pipe

Figure C-23

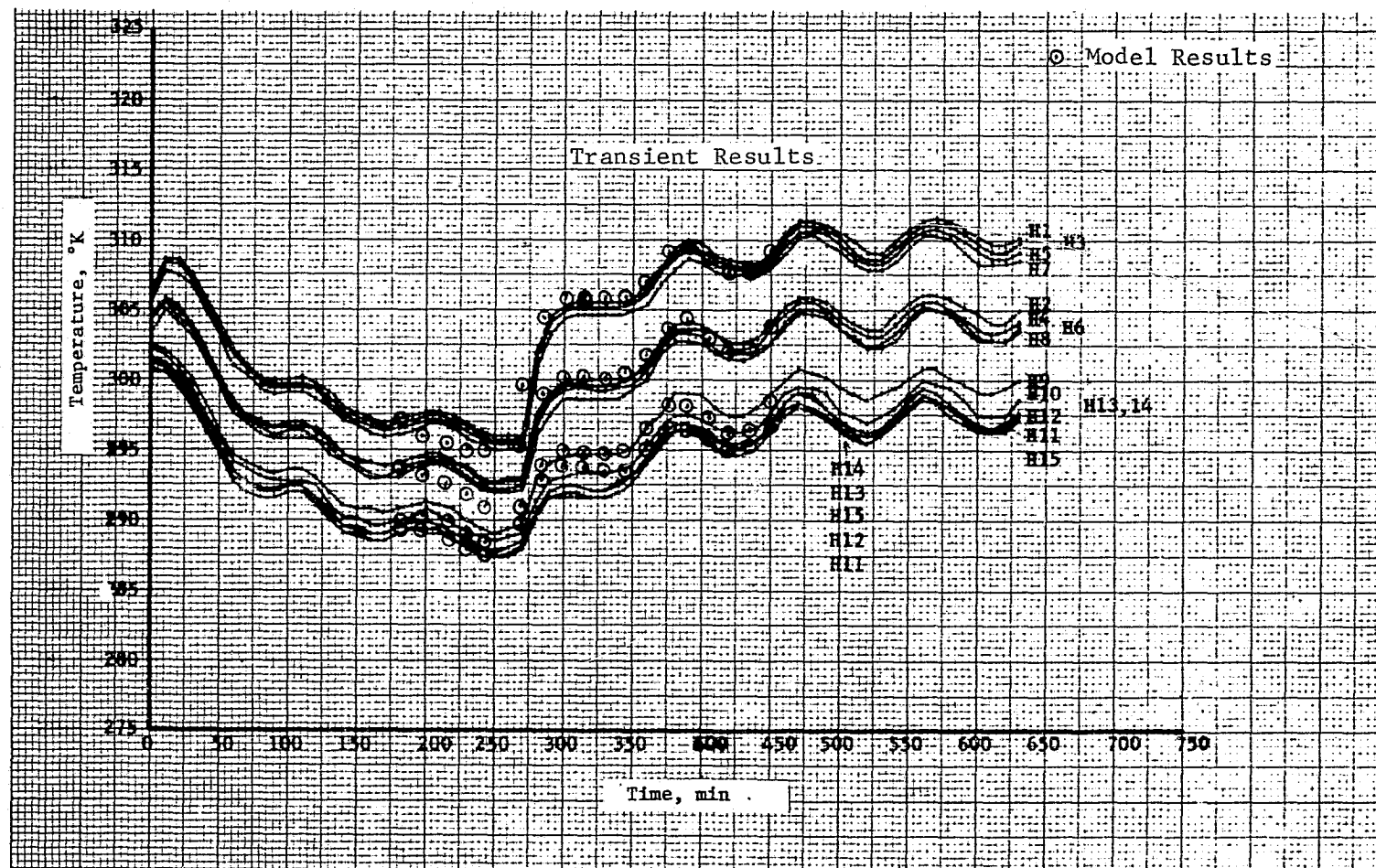


Figure C-23 Header Heat Pipe

Figure C-24

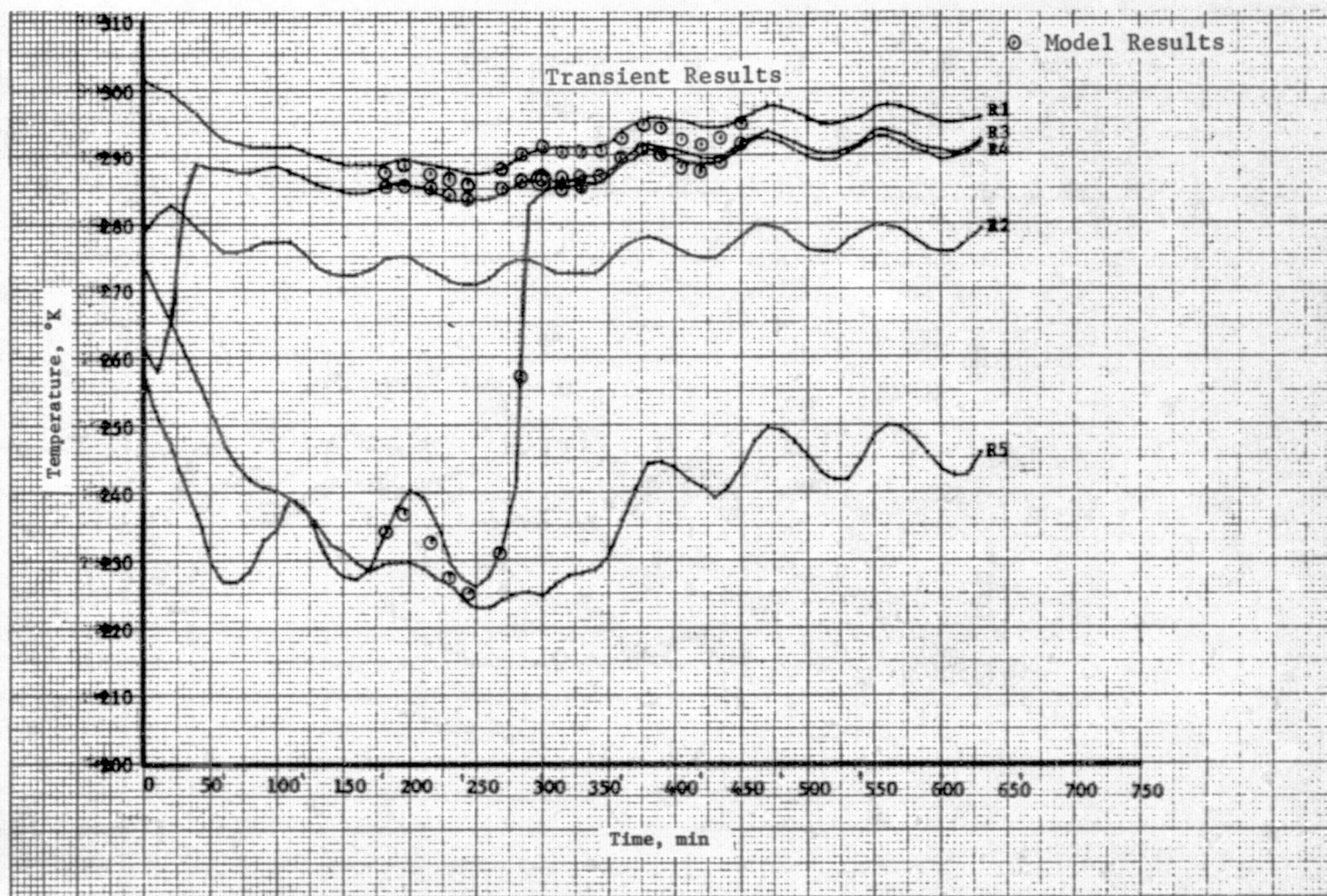


Figure C-24 Radiator Heat Pipe No. 1

Figure C-25

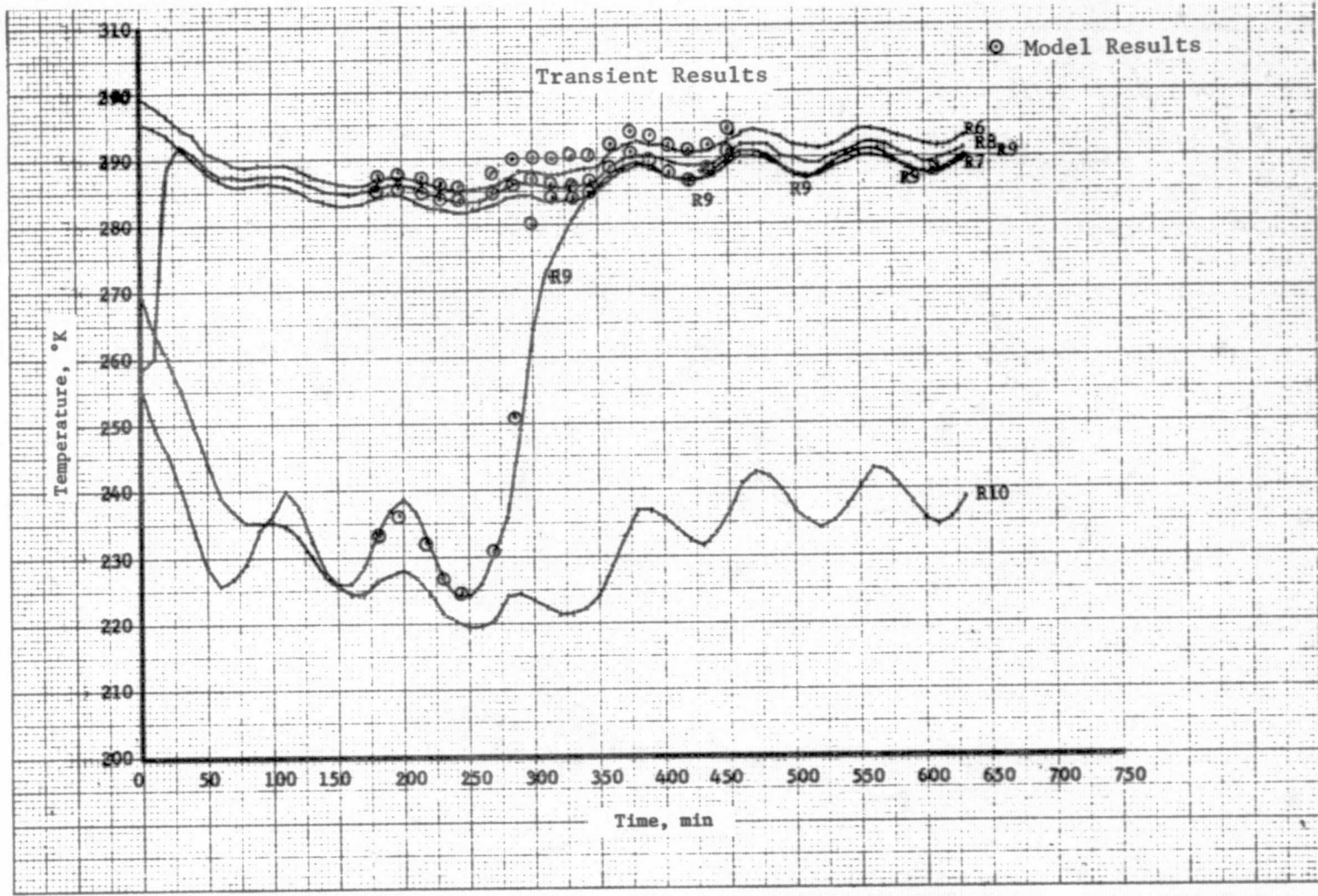


Figure C-25 Radiator Heat Pipe No. 2

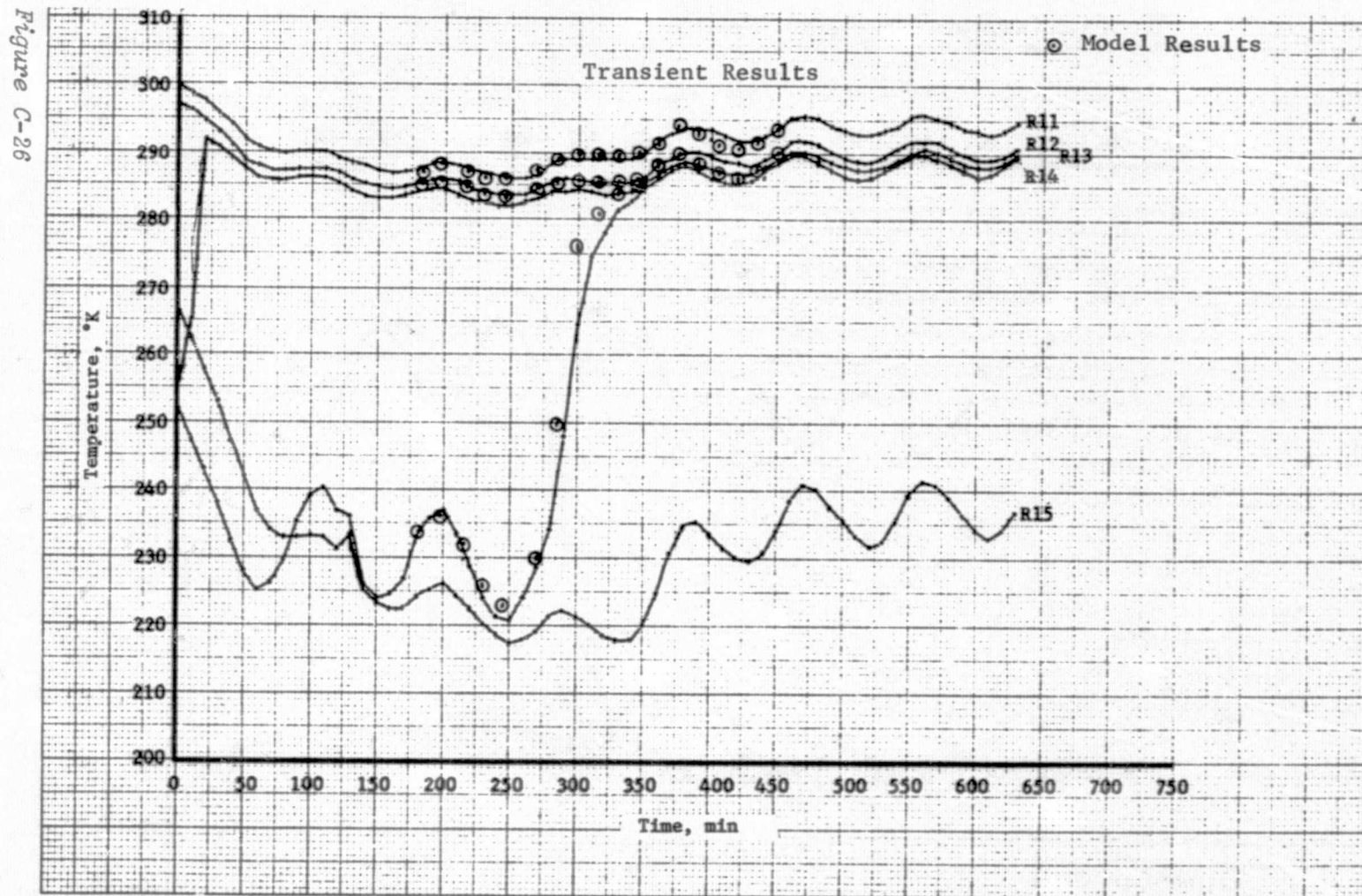


Figure C-26 Radiator Heat Pipe No. 3

Figure C-27

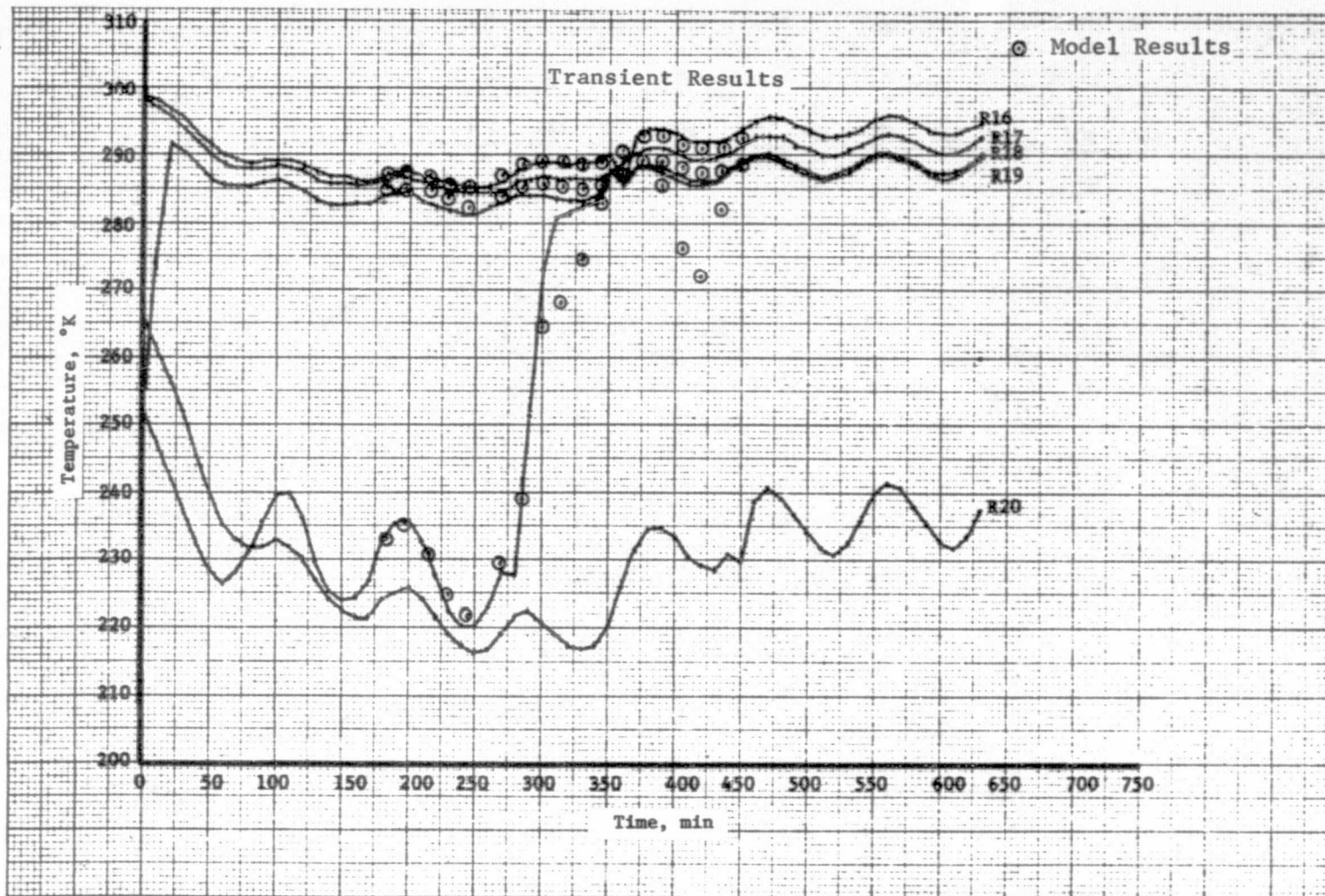


Figure C-27 Radiator Heat Pipe No. 4

Figure C-28

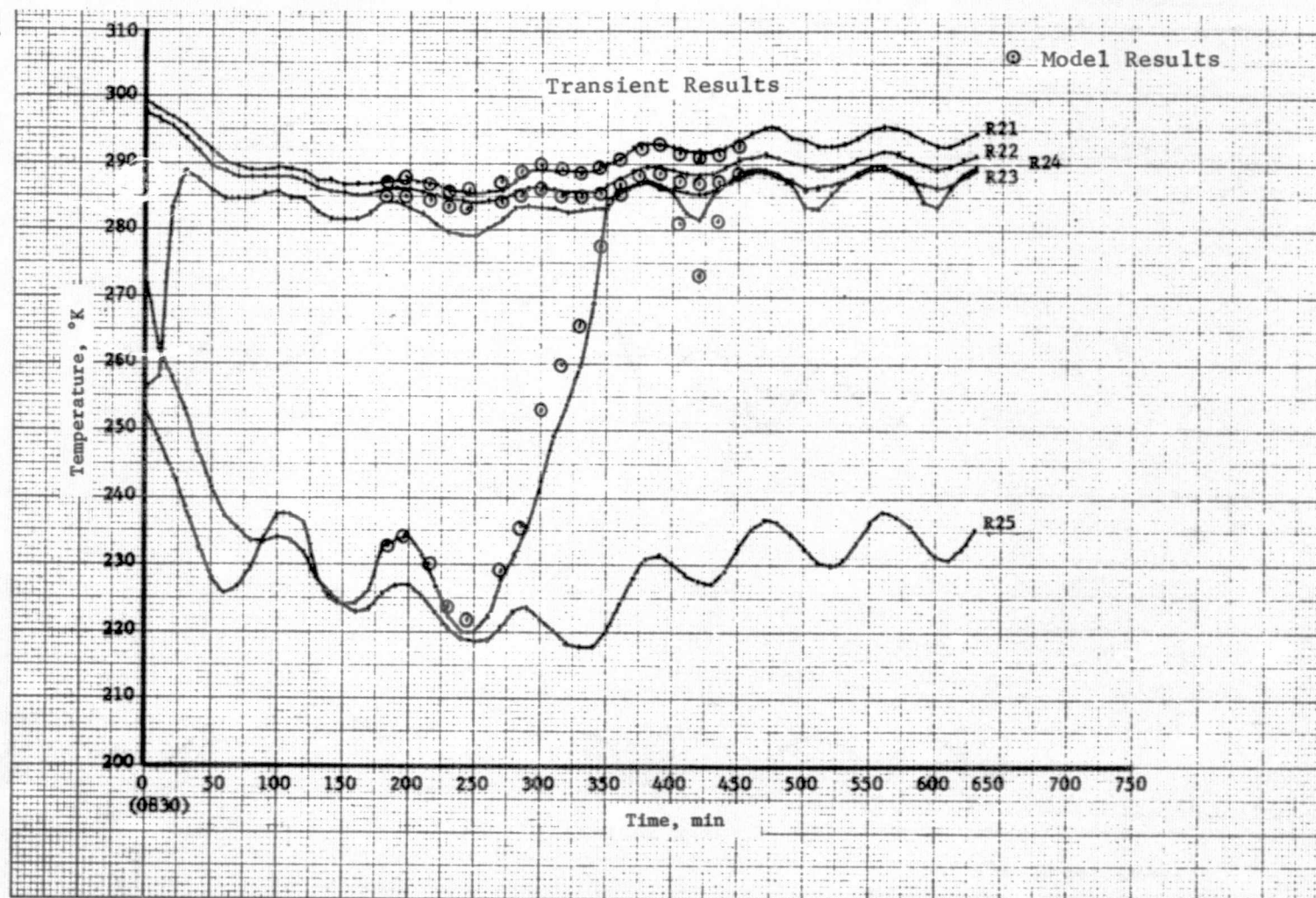


Figure C-28 Radiator Heat Pipe No. 5

Figure C-29

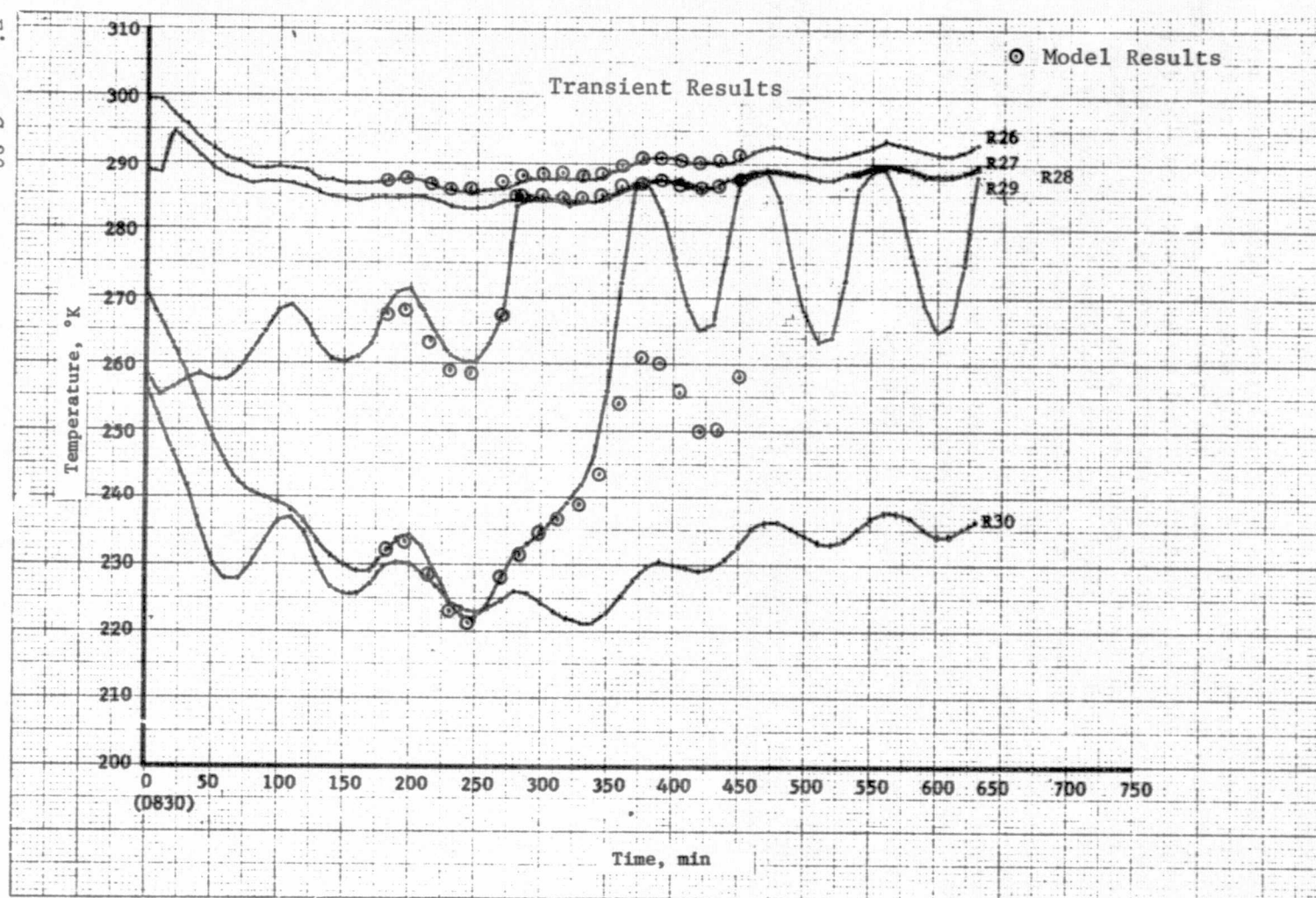


Figure C-29 Radiator Heat Pipe No. 6

1. Discussion

The transient results were in good agreement with the test data except for pipes 4 and 6. A slightly sluggish response to the load change in the model caused the front in pipe 4 to be too far toward the evaporator when the shroud temperature began to drop. Consequently, a much greater temperature excursion resulted in the model than in test. Preliminary runs in the 540 to 630-min region indicated that this excursion would be eliminated by that time. Pipe 6 showed the most inconsistent comparison with test throughout the analysis, and in the transient again a slightly further decrease in noncondensable mass would have resulted in better results. The error indicated in the evaporator of pipe 2 is uniform throughout the analysis and indicates an instrumentation problem especially since in some cases this thermocouple registered temperatures below the condenser temperatures of the same pipe.

Although the capacitance of the radiator was ignored in the transient analysis, the response rate results indicated that the thermal conditioning panel was the dominant mass in the system.

V. CONCLUSIONS

The model correlations with the test data indicate the techniques of analyzing heat pipe thermal control systems are maturing and can be incorporated into the design analyses of spacecraft. Since future spacecraft will very likely depend upon heat pipes for controlling the vehicle thermal balance and equipment temperatures, this analytical tool will become more useful and important to the thermal design.

Specific pipe configurations and designs still require empirical data for the model such as the determination of the characteristics of liquid layer in the axial groove pipe through which the heat is transferred. This can be evaluated through test and analysis yielding an effective $\frac{A}{\Delta X}$ for use in modelling. Mechanical joints are inherent problems in heat pipe systems and particularly in a radiator system. Considerable data is available for design applications, however the performance of a specific system is still dependent upon the values and the repeatability obtained.

The techniques employed in this analysis did not incorporate the front movement into the transition tube and reservoir. Generalized approaches to handle this problem would aid ones ability to predict the reservoir temperatures with more accuracy during full open pipe operations.

VI.

REFERENCES

1. N. Kosowski and R. Kosson: *Experimental Performance of Grooved Heat Pipes at Moderate Temperatures*. AIAA Paper 71-409, presented at AIAA 6th Thermophysics Conference, April 1971.
2. F. Edelstein: *Deployable Heat Pipe Radiator*. DHPR - 75 -3, Contract NAS8-29905. Grumman Aerospace Corporation, April 1975.

ATTACHMENT 1

MODEL LISTING

```

SEQ,ICJHP.
JOB,T600,CM70000.
CHARGE.  PG FD363  2040120012400000 0484 09952 T L WARD  X2972
REQUEST,RSTRTO,*PF.
REWIND,SEDI TN,SEDI TI.
COPY,SEDI TN,SEDI TI.
UNLOAD,SEDI TN.
REWIND,EDI TN,EDI TI.
COPY,EDI TN,EDI TI.
UNLOAD,EDI TN.
REWIND,RSTR TN,RSTR TI.
COPY,RSTR TN,RSTR TI.
UNLOAD,RSTR TN.
COMMENT.  LABEL,RSTRTO,W,O=PE,L=HTPIPE,VSN=FXXXX.
REWIND,SEDI TI,EDI TI,RSTR TI,EDITO,RSTRTO.
ATTACH,FD363CP,FD363COMPILER,ID=FD363,MR=1.
ATTACH,FD363I,FD363INFORMATION,ID=FD363,MR=1.
RFL(70000)
FD363CP.
UNLOAD,EDITO.
RETURN,FD363CP,FD363I.
REWIND,EXFOR.
RUN24(S,,,EXFOR,,MITAS,377777,,1,1)
RETURN,EXFOR.
REDUCE.
REWIND,FLCT,FILE1,FILE2.
ATTACH,FD363LB,FD363LIBRARY,ID=FD363,MR=1.
ATTACH,NSMARL,ID=DDCSYS.
MAP(ON)
LDSET(LIB=FD363LB/NSMARL/RUNLIB/MARLIB,PRESET=ZERO)
MITAS.
UNLOAD,FILE1,FILE2.
EXIT(S)
CATALOG,RSTRTO,RSTRTH1,ID=WARD.
DMP.
DMP(150000)
NOT RESTART

```

```

BCD 3TITLE DATA
RCO 9 HEAT PIPE RADIATOR TEST CORRELATION, 200 WATTS,
BCD 9 HOT CASE RESULTS, TS=-30
ENC

```

1. 凡在本行开立存款账户的客户，均可向本行申请开立支票。

```

C *** BCD 3NODE DATA
      EVAPORATOR NODES    FEEDER PIPES

```

101, 68., -1.

201, 67., -1.

301, 66., -1.

401, 66, -1.

501, 66.5, -1.

601, 65., -1.

C *** HEADER EVAPORATOR NODES

702, 79., -1.

704. 78. -1.

706, 76.5, -1.

708, 76., -1.

C *** ADIABATIC SECTION NODES FEEDER PIPES

102, 64., -1.

202, 64., -1.

302, 63., -1.

402, 64.5, -1.

502, 64.5, -1.

602, 61., -1.

C *** HEADER ADIABATIC SECTION

```

709, 72.5, -1.
C *** CONDENSER NODES      PIPES 1 THRU 6
GEN 103, 3, 1, 62., 1., 1., 1., 1.3
GEN 106, 3, 1, 4., 1., 1., 1., 1.3
GEN 203, 3, 1, 62.5, 1., 1., 1., 1.3
GEN 206, 3, 1, -5.5, 1., 1., 1., 1.3
GEN 303, 3, 1, 61., 1., 1., 1., 1.3
GEN 306, 3, 1, -9.5, 1., 1., 1., 1.3
GEN 403, 3, 1, 60., 1., 1., 1., 1.3
GEN 406, 3, 1, -11., 1., 1., 1., 1.3
GEN 503, 3, 1, 60., 1., 1., 1., 1.3
GEN 506, 3, 1, -14.5, 1., 1., 1., 1.3
GEN 603, 3, 1, 60.5, 1., 1., 1., 1.3
GEN 606, 3, 1, -13.5, 1., 1., 1., 1.3
CCONDENSER PIPE 1
CCONDENSER PIPE 1
CONDENSER PIPE 2
CCONDENSER PIPE 2
CCONDENSER PIPE 3
CCONDENSER PIPE 3
CCONDENSER PIPE 4
CONDENSER PIPE 4
CCONDENSER PIPE 5
CCONDENSER PIPE 5
CONDENSER PIPE 6
CONDENSER PIPE 6
C *** HEADER CONDENSER NODES
GEN 710, 6, 1, 70.5, 1., 1., 1., 1.3
C *** RESERVOIR NODES      PIPES 1 THRU 6
-119, -24.5, 0.
-219, -26., 0.
-319, -28., 0.
-419, -29., 0.
-519, -27., 0.
-619, -24., 0.
C *** VAPOR NODES          PIPES 1 THRU 6
123, 64., -1.
223, 64., -1.
323, 63., -1.
423, 64.5, -1.
523, 64.5, -1.
623, 61., -1.
716, 72.5, -1.3
C *** HEADER MOUNTING PLATE NODES
GEN 701, 84., -1.
GEN 703, 83.5, -1.
GEN 705, 83., -1.
GEN 707, 82., -1.
C *** EFFECTIVE SINK TEMPS
GEN -10, 6, 1, -30., 0., 1., 1., 1.
GEN -20, 6, 1, -30., 0., 1., 1., 1.
GEN -30, 6, 1, -30., 0., 1., 1., 1.
GEN -40, 6, 1, -30., 0., 1., 1., 1.
GEN -50, 6, 1, -30., 0., 1., 1., 1.
GEN -60, 6, 1, -30., 0., 1., 1., 1.
END
C *****
PCD 3CONDUCTOR DATA
C *** AXIAL FEEDER TUBE CONDUCTION PIPE 1
GEN 311, 7, 1, 101, 1, 102, 1, 1., 1., 1., 1.3
C *** AXIAL FEEDER TUBE CONDUCTION PIPE 2
GEN 321, 7, 1, 201, 1, 202, 1, 1., 1., 1., 1.3
C *** AXIAL FEEDER TUBE CONDUCTION PIPE 3
GEN 331, 7, 1, 301, 1, 302, 1, 1., 1., 1., 1.3
C *** AXIAL FEEDER TUBE CONDUCTION PIPE 4
GEN 341, 7, 1, 401, 1, 402, 1, 1., 1., 1., 1.3
C *** AXIAL FEEDER TUBE CONDUCTION PIPE 5
GEN 351, 7, 1, 501, 1, 502, 1, 1., 1., 1., 1.3
C *** AXIAL FEEDER TUBE CONDUCTION PIPE 6
GEN 361, 7, 1, 601, 1, 602, 1, 1., 1., 1., 1.3
C *** HEADER PIPE AXIAL CONDUCTION
501, 702, 704, 1.3
502, 704, 706, 1.3
503, 706, 708, 1.3
GEN 504, 7, 1, 708, 1, 709, 1, 1., 1., 1., 1.3
C *** CONDENSER TO RESERVOIR CONDUCTION
318, 100, 119, 1.3
328, 206, 219, 1.3

```

```

338, 308, 319, 1.3
348, 408, 419, 1.3
358, 508, 519, 1.3
368, 608, 619, 1.3
C *** FEEDER EVAPORATOR TO HEADER CONDENSER CONDUCTION
401, 101, 710, 19.45
402, 101, 711, 19.45
403, 201, 711, 20.35
404, 201, 712, 20.35
405, 301, 712, 17.78
406, 301, 713, 17.78
407, 401, 713, 13.40
408, 401, 714, 13.40
409, 501, 714, 16.47
410, 501, 715, 16.47
411, 601, 715, 13.83
C *** HEADER PIPE EVAPORATOR TO MOUNTING PLATE
511, 701, 702, 34.04
512, 703, 704, 34.04
513, 705, 706, 34.04
514, 707, 708, 34.04
C *** RADIAL CONDUCTION IN WALL, WICK, AND LIQUID
C *** EVAPORATORS
GEN 1001, 6, 1000, 101, 100, 120, 100, 1., 1., 1., 1.3 FEEDERS
GEN 7001, 4, 1, 702, 2, 716, 0, 1., 1., 1., 1.3 HEADER
C *** ADIABATIC SECTIONS
GEN 1002, 6, 1000, 102, 100, 120, 100, 1., 1., 1., 1.3 FEEDERS
7005, 719, 716, 1.3 HEADER
C *** CONDENSERS
GEN 1003, 6, 1, 103, 1, 120, 0, 1., 1., 1., 1.3 FEEDER 1
GEN 2003, 6, 1, 203, 1, 220, 0, 1., 1., 1., 1.3 FEEDER 2
GEN 3003, 6, 1, 303, 1, 320, 0, 1., 1., 1., 1.3 FEEDER 3
GEN 4003, 6, 1, 403, 1, 420, 0, 1., 1., 1., 1.3 FEEDER 4
GEN 5003, 6, 1, 503, 1, 520, 0, 1., 1., 1., 1.3 FEEDER 5
GEN 6003, 6, 1, 603, 1, 620, 0, 1., 1., 1., 1.3 FEEDER 6
GEN 7006, 6, 1, 710, 1, 716, 0, 1., 1., 1., 1.3 HEADER PIPE
C *** CONDUCTANCES TO EFFECTIVE SINK TEMPS (ARBITRARY)
GEN 10, 6, 1, 103, 1, 10, 1, 10., 1., 1., 1.
GEN 20, 6, 1, 203, 1, 20, 1, 10., 1., 1., 1.
GEN 30, 6, 1, 303, 1, 30, 1, 10., 1., 1., 1.
GEN 40, 6, 1, 403, 1, 40, 1, 10., 1., 1., 1.
GEN 50, 6, 1, 503, 1, 50, 1, 10., 1., 1., 1.
GEN 60, 6, 1, 603, 1, 60, 1, 10., 1., 1., 1.
END
C *****
RCO 3CONSTANTS DATA
C...CONVERSION CONSTANTS
1 = 3.14159 $ PI
2 = 32.174 $ GSUBC (LPM-FT/LRF-SEC**2)
3 = 778.156 $ MECHANICAL EQUIVALENT OF HEAT (FT-LBF/RTU)
4 = 57.29578 $ DEGREES/RADIAN
5 = .1714E-3 $ STEPHAN-BOLTZMANN CONSTANT (BTU/HR-FT**2-R**4)
6 = 1.296E+7 $ SEC**2/HR**2
7 = 1545. $ UNIVERSAL GAS CONSTANT (FT-LRF/LBMOLE-R)
C...COMPUTED CONSTANTS
11 = 0. $ TOTAL PANEL HEAT REJECTION (BTU/HP)
20 = -31.
C...LOGIC CONTROL CONSTANT
JTEST = 0 $ FLAG FOR STEADY STATE (0) OR TRANSIENT (1)
C...MITAS CONTROL CONSTANTS
ARLXCA = .01
ORLXCA = .01
EBALSA = 15.0
EBALNA = 5.0
ABSZRC = -460.
SBCNST = 1.

```



```

EXTLIM = 10.
ITERMX = 200
ITEROT = J
TSTEPI = .02
TSTEPO = .02
TIMEO = 0.0
TIMEND = 0.0
NDSTOR = 400
END
*****
BCD 3ARRAY DATA
C *** WALL PARAMETERS
C *** EVAPORATOR
500, 1, REPEAT, 6, 4, ENDS NUMBER OF NODES EACH PIPE (INTEGER)
501, 169., REPEAT, 6, 558., REPEAT, 4, ENDS DENSITY (LBM/FT**3)
502, .214, REPEAT, 6, .091, REPEAT, 4, ENDS SPECIFIC HEAT (BTU/LBM-F)
503, 111., REPEAT, 6, 224., REPEAT, 4, ENDS CONDUCTIVITY (BTU/HR-FT-F)
504, .0515884, REPEAT, 6, .08333, REPEAT, 4, ENDS TUBE OD (FT)
505, .0358333, REPEAT, 6, .07300, REPEAT, 4, ENDS TUBE ID (FT)
506, 1., REPEAT, 5, .5, .625, REPEAT, 4, ENDS NODAL LENGTH (FT)
507, 1., REPEAT, 5, .5, 2.50, ENDS TOTAL LENGTH (FT)
C *** ADIABATIC SECTION
510, 1, REPEAT, 7, ENDS
511, 169., REPEAT, 6, 558., ENDS
512, .214, REPEAT, 6, .091, ENDS
513, 111., REPEAT, 6, 224., ENDS
514, .0515884, REPEAT, 6, .08333, ENDS
515, .0358333, REPEAT, 6, .07300, ENDS
516, .25, REPEAT, 6, 1.500, ENDS
517, .25, REPEAT, 6, 1.500, ENDS
C *** CONDENSER SECTION
520, 6, REPEAT, 7, ENDS
521, 169., REPEAT, 36, 558., REPEAT, 6, ENDS
522, .214, REPEAT, 36, .091, REPEAT, 6, ENDS
523, 111., REPEAT, 36, 224., REPEAT, 6, ENDS
524, .0515884, REPEAT, 36, .08333, REPEAT, 6, ENDS
525, .0358333, REPEAT, 36, .07300, REPEAT, 6, ENDS
526, 1., REPEAT, 36, .66667, REPEAT, 6, ENDS
527, 6., REPEAT, 6, 4., ENDS
C *** WICK PARAMETERS
C *** EVAPORATOR
530, 2, REPEAT, 6, 2, REPEAT, 4, ENDS
C *** 1= WRAPPED SCREEN, SINTERED POWDER, FELT, OR FOAM
C *** 2= OPEN AXIAL GROOVES
C *** 3= SCREEN COVERED AXIAL GROOVES
C *** 4= SCREEN COVERED AXIAL SPACER WIPES
C *** 5= CIRCUMFERENCEAL GROOVES (THREADS)
531, 169., REPEAT, 6, 558., REPEAT, 4, ENDS DENSITY (LBM/FT**3)
532, .214, REPEAT, 6, .091, REPEAT, 4, ENDS SPECIFIC HEAT (BTU/LBM-F)
533, 111., REPEAT, 6, 224., REPEAT, 4, ENDS CONDUCTIVITY (BTU/HR-FT-F)
534, .035833, REPEAT, 6, .07300, REPEAT, 4, ENDS OD (FT)
535, .029167, REPEAT, 6, .07299, REPEAT, 4, ENDS ID (FT)
536, .001, REPEAT, 6, 1.00, REPEAT, 4, ENDS EFFECTIVE BUBBLE RADIUS
C *** FOR BOILING (FT)
537, 1., REPEAT, 5, .5, .625, REPEAT, 4, ENDS NODAL LENGTH (FT)
538, .62537, REPEAT, 6, .999, REPEAT, 4, ENDS POROSITY
C *** (LIQ VOL/ TOTAL VOL OF WICK ) DIMENSIONLESS
539, 0.001, REPEAT, 6, 1.0, REPEAT, 4, ENDS EFF. PORE RADIUS (FT)
540, J., REPEAT, 10, ENDS NOT USED BUT REQUIRED
541, 7.250, REPEAT, 6, 8.0, REPEAT, 4, ENDS ENTRAINMENT
C *** CHARACTERISTIC LENGTH
542, 27., REPEAT, 6, 2., REPEAT, 4, ENDS NUMBER OF AXIAL GROOVES OR
C *** SPACER WIRES OR NUMBER THREADS PER FT (FLOATING POINT NUMBER)
543, .002766, REPEAT, 6, .0355, REPEAT, 4, ENDS GROOVE OR THREAD MEAN
C *** WIDTH (FT)
544, .003333, REPEAT, 6, .00001, REPEAT, 4, ENDS GROOVE OR THREAD DEPT

```

```

***      OR SPACER WIRE DIAMETER (FT)
C ***    ADIABATIC SECTION
550, 2, REPEAT, 6, 2, ENDS
551, 169., REPEAT, 6, 558., ENDS
552, .214, REPEAT, 6, .091, ENDS
553, 111., REPEAT, 6, 224., ENDS
554, .035833, REPEAT, 6, .07300, ENDS
555, .029167, REPEAT, 6, .07299, ENDS
556, 0., REPEAT, 7, ENDS
557, .25, REPEAT, 6, 1.500, ENDS
558, .62537, REPEAT, 6, .999, ENDS
559, .001, REPEAT, 6, 1.0, ENDS
560, 0., REPEAT, 7, ENDS
561, 7.25, REPEAT, 6, 8.0, ENDS
562, 27., REPEAT, 6, 2., ENDS
563, .002365, REPEAT, 6, .0365, ENDS
564, .003333, REPEAT, 6, .00001, ENDS

C ***    CONDENSER SECTION
570, 2, REPEAT, 36, 2, REPEAT, 6, ENDS
571, 169., REPEAT, 36, 558., REPEAT, 6, ENDS
572, .214, REPEAT, 36, .091, REPEAT, 6, ENDS
573, 111., REPEAT, 36, 224., REPEAT, 6, ENDS
574, .035833, REPEAT, 36, .07300, REPEAT, 6, ENDS
575, .029167, REPEAT, 36, .07299, REPEAT, 6, ENDS
576, 0.00, REPEAT, 42, ENDS
577, 1.0, REPEAT, 36, .66667, REPEAT, 6, ENDS
578, .62537, REPEAT, 36, .999, REPEAT, 6, ENDS
579, .001, REPEAT, 36, 1.0, REPEAT, 6, ENDS
580, 0., REPEAT, 42, ENDS
581, 7.25, REPEAT, 36, 8.0, REPEAT, 6, ENDS
582, 27., REPEAT, 36, 2., REPEAT, 6, ENDS
583, .002365, REPEAT, 36, .0365, REPEAT, 6, ENDS
584, .003333, REPEAT, 36, .00001, REPEAT, 6, ENDS

C ***    FLUID PROPERTIES
591, 20., REPEAT, 6, 90., ENDS WETTING ANGLE (DEGREES)
592, 1.31, REPEAT, 6, 1.23, ENDS SPECIFIC HEAT RATIO

C ***    OPERATING CONDITIONS
602, 32.17, REPEAT, 7, ENDS BODY FORCE ACCELERATION (LBM-FT/LBF-SEC**2)
603, 90., REPEAT, 7, ENDS ANGLE BETWEEN BODY FORCE AND PIPE AXIS (DEG)
604, -1., REPEAT, 7, ENDS +1., IF EVAP HIGHER THAN CONDENSER
        -1., IF EVAP BELOW CONDENSER

C ***    CONDENSER FIN PARAMETERS
610, 0., REPEAT, 42, ENDS ABSORBED FLUX
611, .004167, .004167, .002667, .002667, .004167, .004167
        .004167, .004167, .002667, .002667, .004167, .004167
        .004167, .004167, .002667, .002667, .004167, .004167
        .004167, .004167, .002667, .002667, .004167, .004167
        .004167, .004167, .002667, .002667, .004167, .004167
        0., REPEAT, 6, ENDS FIN THICKNESS (FT)
612, .333333, REPEAT, 36, 0., REPEAT, 6, ENDS WIDTH (FT)
613, 70., REPEAT, 36, 0., REPEAT, 6, ENDS K (BTU/FT-HR-F)
614, .85, REPEAT, 36, 0., REPEAT, 6, ENDS EMISSIVITY
615, -26., -25., -24., -26., -28., -31.
        -26., -25., -24., -26., -28., -31.
        -26., -25., -25., -27., -28., -31.
        -27., -25., -25., -27., -29., -31.
        -27., -26., -26., -28., -29., -31.
        -27., -26., -26., -28., -29., -31.
        0., REPEAT, 6, ENDS
616, 169., REPEAT, 36, 0., REPEAT, 6, ENDS
617, .214, REPEAT, 36, 0., REPEAT, 6, ENDS
618, 1, REPEAT, 36, 0, REPEAT, 6, ENDS 0 = NO TIE TO ADJACENT FIN
        1 = FIN PERFECTLY TIED TO ADJACENT FIN

C ***
C...ARTERY PARAMETERS
C....EVAPORATOR

```

```

623, J      , REPEAT, 13, END$ TYPE OF ARTERY (INTEGER) --
C           1 = NONE
C           1 = PEDESTAL
C           2 = SPIRAL WITH SPACER WIRES
621, 0.      , REPEAT, 13, END$ OUTER DIAM (FT) -- USE EFF DIAM IF
C           NOT CIRCULAR: EFF D = (4.* X-S AREA / PI)**.5
622, 0.      , REPEAT, 10, END$ INNER DIAM (FT) -- USE EFF D
623, 0.      , REPEAT, 13, END$ DIAM OF SPACER WIRES IF M620+I = 2 (FT)
624, 0.      , REPEAT, 13, END$ ARTERY SPIRAL SCREEN THICKNESS (FT)
C           IF M620+I = 2 (FT)
625, C.      , REPEAT, 13, END$ ARTERY SCREEN POROSITY (DIMENSIONLESS)
626, J.      , REPEAT, 13, END$ NO OF SPIRAL TURNS IF M620+I=2 (REAL)
627, 0.      , REPEAT, 13, END$ ARTERY SCREEN DENSITY*CP PRODUCT (BTU/FT**3-F)
628, J.      , REPEAT, 13, END$ SPACER WIRES DENSITY*CP PRODUCT IF M620+I = 2
629, J.      , REPEAT, 13, END$ ARTERY SCREEN THERMAL CONDUCTIVITY (BTU/HR-FT-F)
630, 0.      , REPEAT, 13, END$ SPACER WIRE THERMAL CONDUCTIVITY IF M620+I = 2
631, 0.      , REPEAT, 13, END$ THICKNESS OF OUTER ARTERY WRAP IF
C           M620+I = 2 (FT)
632, 0.      , REPEAT, 13, END$ EFF RADIUS OF LARGEST ARTERY HOLE
C           EXCLUDING THE CONDENSER END OF THE ARTERY (FT)
C.....ADIABATIC SECTION
640, J.      , REPEAT, 7, END
641, 0.      , REPEAT, 7, END
642, 0.      , REPEAT, 7, END
643, 0.      , REPEAT, 7, END
644, 0.      , REPEAT, 7, END
645, 0.      , REPEAT, 7, END
646, J.      , REPEAT, 7, END
647, J.      , REPEAT, 7, END
648, J.      , REPEAT, 7, END
649, J.      , REPEAT, 7, END
650, J.      , REPEAT, 7, END
651, 0.      , REPEAT, 7, END
C.....CONDENSER
660, 0.      , REPEAT, 42, END
661, 0.      , REPEAT, 42, END
662, 0.      , REPEAT, 42, END
663, 0.      , REPEAT, 42, END
664, J.      , REPEAT, 42, END
665, 0.      , REPEAT, 42, END
666, 0.      , REPEAT, 42, END
667, 0.      , REPEAT, 42, END
668, 0.      , REPEAT, 42, END
669, 0.      , REPEAT, 42, END
670, J.      , REPEAT, 42, END
671, 0.      , REPEAT, 42, END
C *** RESERVOIR PARAMETERS
808, .01269/28.316, REPEAT, 6, 0., END$ MOLES NCG (LBMOL)
809, 33.4/1728., REPEAT, 6, 0., END$ RESERVOIR VOLUME (FT**3)
822, 6./12., REPEAT, 6, 0., END$ RESERVOIR LENGTH (FT)
823, 2.902/12., REPEAT, 6, 0., END$ RESERVOIR WICK OD AND RESERVOIR ID
824, 2.885/12., REPEAT, 6, 0., END$ RESERVOIR WICK ID (FT)
825, 3.30/12., REPEAT, 6, 0., END$ RESERVOIR OD (FT)
826, 2.85/12., REPEAT, 6, 0., END$ FEEDTUBE LENGTH (FT)
827, .381/12., REPEAT, 6, 0., END$ FEEDTUBE WICK OD AND FEEDTUBE ID
828, .380/12., REPEAT, 6, 0., END$ FEEDTUBE WICK ID (FT)
829, .437/12., REPEAT, 6, 0., END$ FEEDTUBE OD (FT)
830, 8., REPEAT, 6, 0., END$ FEEDTUBE THERMAL COND (BTU/HR-FT-F)
831, 0., REPEAT, 6, 0., END$ INSULATION COND (BTU/HR-FT-F)
837, 8., REPEAT, 6, 0., END$ RESERVOIR THERMAL COND (SAME)
838, J., REPEAT, 6, 0., END$ INSULATION THICKNESS (FT)
C *** ANGULAR WIDTHS OF EVAPORATOR SPIRAL ANNULI (DEGREES)
910, J, REPEAT, 7, END$ NUMBER OF ANNULI IN EACH PIPE
911, J., REPEAT, 7, END$ ANGULAR WIDTHS OF ALL ANNULI
C *** ANGULAR WIDTHS OF ADIABATIC SECTION SPIRAL ARTERY ANNULI (DEGREES)
912, J, REPEAT, 7, END$

```

```

913, J., REPEAT, 7, END$
C *** ANGULAR WIDTHS OF CONDENSER SPIRAL ARTERY ANNULI (DEGREES)
914, J, REPEAT, 7, END$
915, J., REPEAT, 7, END$
C...ARTERY CAPACITANCE (BTU/F) (COMPUTED IN SUB ARTERY)
681, SPACE, 10, END$ EVAP
682, SPACE, 7, END$ ADIA
683, SPACE, 42, END$ COND
C...ARTERY AXIAL CONDUCTANCE (BTU/HR-F) (COMPUTED IN SUB ARTERY)
684, 1.E-12, REPEAT, 10, END$ EVAP
685, 1.E-12, REPEAT, 7, END$ ADIA
686, 1.E-12, REPEAT, 42, END$ COND
C...EFFECTIVE VAPOR PASSAGE DIAMETER (FT) (COMPUTED IN SUB ARTERY)
687, SPACE, 10, END$ EVAP
688, SPACE, 7, END$ ADIA
689, SPACE, 42, END$ COND
C...(PERMEABILITY)*(X-SECTIONAL AREA) PRODUCT (FT**4) (COMPUTED IN SUB PERMAL)
690, SPACE, 10, END$ EVAP
691, SPACE, 7, END$ ADIA
692, SPACE, 42, END$ COND
C...WALL AXIAL CONDUCTANCE (BTU/HR-F) (COMPUTED IN SUB AXCOND)
693, 1.E-12, REPEAT, 10, END$ EVAP
694, 1.E-12, REPEAT, 7, END$ ADIA
695, 1.E-12, REPEAT, 42, END$ COND
C...WICK AXIAL CONDUCTANCE (BTU/HR-F) (COMPUTED IN SUB AXCOND)
696, 1.E-12, REPEAT, 10, END$ EVAP
697, 1.E-12, REPEAT, 7, END$ ADIA
698, 1.E-12, REPEAT, 42, END$ COND
C...EVAP WORKING FLUID LIQUID PROPERTIES (DETERMINED IN SUB LOOKUP)
701, SPACE, 10, END$ LIQUID DENSITY (LBM/FT**3)
702, SPACE, 10, END$ LIQUID SPECIFIC HEAT (BTU/LBM-F)
703, SPACE, 10, END$ LIQUID VISCOSITY (LBM/FT-HR)
704, SPACE, 10, END$ LIQUID THERMAL CONDUCTIVITY (BTU/HR-FT-F)
705, SPACE, 10, END$ SURFACE TENSION (LBF/FT)
706, SPACE, 10, END$ HEAT OF VAPORIZATION (BTU/LBM)
707, SPACE, 10, END$ HEAT OF FUSION (BTU/LBM)
C...ADIA WORKING FLUID LIQUID PROPERTIES (DETERMINED IN SUB LOOKUP)
711, SPACE, 7, END$ LIQUID DENSITY (LBM/FT**3)
712, SPACE, 7, END$ LIQUID SPECIFIC HEAT (BTU/LBM-F)
713, SPACE, 7, END$ LIQUID VISCOSITY (LBM/FT-HR)
714, SPACE, 7, END$ LIQUID THERMAL CONDUCTIVITY (BTU/HR-FT-F)
715, SPACE, 7, END$ SURFACE TENSION (LBF/FT)
716, SPACE, 7, END$ HEAT OF VAPORIZATION (BTU/LBM)
717, SPACE, 7, END$ HEAT OF FUSION (BTU/LBM)
C...COND WORKING FLUID LIQUID PROPERTIES (DETERMINED IN SUB LOOKUP)
721, SPACE, 42, END$ LIQUID DENSITY (LBM/FT**3)
722, SPACE, 42, END$ LIQUID SPECIFIC HEAT (BTU/LBM-F)
723, SPACE, 42, END$ LIQUID VISCOSITY (LBM/FT-HR)
724, SPACE, 42, END$ LIQUID THERMAL CONDUCTIVITY (BTU/HR-FT-F)
725, SPACE, 42, END$ SURFACE TENSION (LBF/FT)
726, SPACE, 42, END$ HEAT OF VAPORIZATION (BTU/LBM)
727, SPACE, 42, END$ HEAT OF FUSION (BTU/LBM)
C...WORKING FLUID VAPOR PROPERTIES (DETERMINED IN SUB C10EG1)
731, SPACE, 7, END$ VAPOR DENSITY (LBM/FT**3)
732, SPACE, 7, END$ VAPOR SPECIFIC HEAT (BTU/LBM-F)
733, SPACE, 7, END$ VAPOR VISCOSITY (LBM/FT-HR)
734, SPACE, 7, END$ VAPOR THERMAL CONDUCTIVITY (BTU/HR-FT-F)
C...OPERATING CONDITIONS (CALCULATED IN SUB LIMITS)
751, SPACE, 7, END$ MASS FLOWRATE (LBM/HR)
752, SPACE, 7, END$ LATENT HEAT TRANSFER (BTU/HR)
753, SPACE, 7, END$ WICKING LIMIT (BTU/HR)
754, SPACE, 7, END$ SONIC LIMIT (BTU/HR)
755, SPACE, 7, END$ ENTRAINMENT LIMIT (BTU/HR)
756, SPACE, 7, END$ BOILING LIMIT (BTU/HR)
757, SPACE, 7, END$ OVERALL LIMIT (LOWEST OF A253 THRU A256) (BTU/HR)
758, SPACE, 10, END$ EVAPORATOR VAPOR PRESSURE (PSIA)

```



```

759,SPACE,7,END$ ADIABATIC SECTION VAPOR PRESSURE (PSIA)
760,SPACE,42,END$ CONDENSER VAPOR PRESSURE (PSIA)
761,SPACE,7,END$ RESERVOIR VAPOR PRESSURE (PSIA)
763,SPACE,7,END$ INJECTION REYNOLDS NUMBER (DIMENSIONLESS)
764,SPACE,7,END$ SUCTION REYNOLDS NUMBER (DIMENSIONLESS)
C...LIQUID/WICK MATRIX EFFECTIVE RADIAL THERMAL CONDUCTIVITY (BTU/HR-FT-F)
C....(COMPUTED IN SUB EFFKWK)
765,SPACE,10,END$ EVAP
766,SPACE,7,END$ ADIA
767,SPACE,42,END$ COND
C...PANEL ENVIRONMENTAL PARAMETERS (COMPUTED IN SUB RADFIN)
768,SPACE,42,END$ NODAL ENVIRONMENTAL TEMPERATURE (F)
770,SPACE,42,END$ NODAL HEAT REJECTION (BTU/HR)
771,SPACE,7,END$ PIPE ENERGY BALANCE (BTU/HR)
811,SPACE,7,END$ PIPE HEAT REJECTION (BTU/HR)
C...FLAGS
781,SPACE,7,END$ NO OF ITERATIONS IN SUBROUTINE FRONT
783,SPACE,7,END$ BACKUP SWITCH IN SUBROUTINE FRONT
C...VCHP PARAMETERS
810,.6,.6,.5,.5,.4,.4,1,END$ ACTIVE/TOTAL CONDENSER LENGTH (C-LESS)
820,3.6,3.6,3.,3.,2.4,2.4,4,END$ NEW ACTIVE CONDENSER LENGTH (FT)
832,SPACE,7,END$ OLD ACTIVE CONDENSER LENGTH (FT)
836,SPACE,7,END$ NUMBER OF INACTIVE CONDENSER SECTIONS
841,SPACE,7,END$ OSCILLATION TEST
842,SPACE,7,END$ OSCILLATION TEST
843,SPACE,7,END$ OSCILLATION TEST
844.2.,REPEAT,7,END$ INITIAL DAMPING
C...FIN CAPACITANCE AND AXIAL CONDUCTANCE
850,SPACE,42,END$ CAPACITANCE (COMPUTED IN SUB CAPFIN)
851,SPACE,42,END$ AXIAL CONDUCTANCE (COMPUTED IN SUB RADFIN)
C...WORKING FLUID THERMOPHYSICAL DATA
1001$ LIQUID DENSITY (LBM/FT**3) VS TEMP (F) - AMMONIA
-107.9,46., -94.,45.3, -50.,43.5, 0.,41.34, 50.,39.1, 100.,36.4
150.,33.6, 200.,29.5, 270.3,16., END
1002$ VAPOR DENSITY (LBM/FT**3) VS TEMP (F) - AMMONIA
-107.9,.0037, -94.,.007, -50.,.0332, 0.,.1097, 50.,.3036
100.,.7048, 124.,1.01, 150.,1.54, 200.,3.45, 250.,9.1
270.3,16., END
1003$ LIQUID SPECIFIC HEAT (BTU/LBM-F) VS TEMP (F) - AMMONIA
-107.9,1.032, -75.,1.045, -50.,1.066, -22.,1.069, -4.,1.077
14.,1.09, 32.,1.107, 50.,1.126, 68.,1.146, 86.,1.168, 104.,1.194
122.,1.222, 150.,1.29, 175.,1.365, 200.,1.45, 225.,1.555, 250.,1.7
270.3,1.86, END
1004$ VAPOR SPECIFIC HEAT (BTU/LBM-F) VS TEMP (F) - AMMONIA
-107.9,., END$ UNNECESSARY
1005$ LIQUID VISCOSITY (LBM/FT-HR) VS TEMP (F) - AMMONIA
-107.9,1.415, -92.2,1.1484, -50.,.7668, -40.,.666, 20.,.3889
40.,.3384, 60.,.2916, 100.,.2197, 150.,.153, 200.,.098
250.,.0533, 270.3,.03384, END
1006$ VAPOR VISCOSITY (LBM/FT-HR) VS TEMP (F) - AMMONIA
-107.9,.01626, -50.,.01863, 32.,.02221, 68.,.02376, 122.,.02642
150.,.02755, 200.,.03025, 270.3,.03384, END
1007$ LIQUID THERMAL CONDUCTIVITY (BTU/HR-FT-F) VS TEMP (F) - AMMONIA
-107.9,.325, -20.,.317, 32.,.312, 50.,.307, 80.,.293, 120.,.275
150.,.254, 200.,.205, 225.,.171, 250.,.13, 270.3,.068, END
1008$ VAPOR THERMAL CONDUCTIVITY (BTU/HR-FT-F) VS TEMP (F) - AMMONIA
-107.9,.0092, -75.,.00955, -40.,.0105, 0.,.0117, 40.,.0129
80.,.0142, 100.,.0149, 120.,.0155, 150.,.0173, 200.,.0223
250.,.036, 270.3,.068, END
1009$ SURFACE TENSION (LBF/FT) VS TEMP (F) - AMMONIA
-107.9,.00346, -60.,.00278, -20.,.00201, 20.,.00189, 52.,.001576
93.4,.00124, 138.2,.000891, 150.,.00081, 175.,.000635, 200.,.00047
225.,.00029, 250.,.00013, 270.3,0., END
1010$ HEAT OF VAPORIZATION (BTU/LBM) VS TEMP (F) - AMMONIA
-107.9,639., -50.,604.3, 0.,568.9, 50.,527.3, 100.,477.8
124.,450.1, 150.,409., 175.,365., 200.,328., 225.,249.

```

250.,150., 270.3,J., END
 1J11S HEAT OF FUSION (BTU/LBM) VS TEMP (F) - AMMONIA
 -107.9,J., ENDS UNNECESSARY
 1J12S SATURATION PRESSURE (PSIA) VS TEMP (F) - AMMONIA
 -107.9.,.85, -75.,.3.6, -50.,.7.67, -25.,.15.5, 0.,.30.42, 25.,.53.2
 50.,.89.19, 75.,.143., 100.,.211.9, 124.,.303.4, 150.,.425., 175.,.580.
 200.,.765., 225.,.1008., 250.,.1330., 270.3,1650., END
 1J13S THERMAL CONDUCTIVITY (BTU/HR-FT-F) VS TEMP (F) - 6061 ALUMINUM
 -260.,.65., -160.,.76., -60.,.84., 40.,.91., 140.,.96., 240.,.101., END
 1J21S LIQUID DENSITY (LBM/FT**3) VS TEMP (F) - GENETRON 31/114
 -100.,.94.6, -50.,.90.6, 0.,.86.4, 50.,.81.9, 100.,.77.
 150.,.71.5, 200.,.64.8, END
 1J22S VAPOR DENSITY (LBM/FT**3) VS TEMP (F) - GENETRON 31/114
 -100.,.01224, -50.,.0647, 0.,.2298, 50.,.627, 100.,.1.4339
 150.,.2.9308, 200.,.5.6593, END
 1J23S LIQUID SPECIFIC HEAT (BTU/LBM-F) VS TEMP (F) - GENETRON 31/114
 -100.,.21, -50.,.22, 0.,.237, 50.,.256, 100.,.276, 150.,.303
 200.,.348, END
 1J24S VAPOR SPECIFIC HEAT (BTU/LBM-F) VS TEMP (F) - GENETRON 31/114
 -100.,.0., ENDS UNNECESSARY
 1J25S LIQUID VISCOSITY (LBM/FT-HR) VS TEMP (F) - GENETRON 31/114
 0.,.9676, 25.,.8346, 50.,.7257, 75.,.64, 100.,.5685, 125.,.5
 150.,.432, END
 1J26S VAPOR VISCOSITY (LBM/FT-HR) VS TEMP (F) - GENETRON 31/114
 -100.,.0195, 200.,.0345, END
 1J27S LIQUID THERMAL COND (BTU/HR-FT-F) VS TEMP (F) - GENETRON 31/114
 -100.,.0755, 200.,.0389, END
 1J28S VAPOR THERMAL COND (BTU/HR-FT-F) VS TEMP (F) - GENETRON 31/114
 -100.,.00356, 200.,.0123, END
 1J29S SURFACE TENSION (LBF/FT) VS TEMP (F) - GENETRON 31/114
 -100.,.003391, 200.,.006415, END
 1J30S HEAT OF VAPORIZATION (BTU/LBM) VS TEMP (F) - GENETRON 31/114
 -100.,.112.72, -50.,.108.77, 0.,.104., 50.,.98.06, 100.,.90.66
 150.,.81.22, 200.,.68.45, END
 1J31S HEAT OF FUSION (BTU/LBM) VS TEMP (F) - GENETRON 31/114
 -100.,.0., ENDS UNNECESSARY
 1J32S SATURATION PRESSURE (PSIA) VS TEMP (F) - GENETRON 31/114
 -100.,.503, -50.,.3.001, -20.,.7.065, 0.,.11.73, 20.,.18.55
 40.,.28.18, 60.,.41.35, 80.,.58.84, 100.,.81.52, 120.,.110.3
 140.,.146.2, 160.,.191.2, 180.,.243.5, 200.,.307.4, END

C...FIN GRADIENT TABLE

600S LTV DATA- DIMENSIONLESS TEMP GRADIENT FOR FLAT EXTENDED SURFACES
 10,12.,.00.,.6000.,.7000.,.8000.,.9000.,1.000,1.1000,1.2000,1.3000,1.4000,1.5000
 .00.,.2000.,.1500.,.1000.,.0500.,.0000.,-.0500.,-.1000.,-.1500.,-.2000.,-.2500
 .10.,.2566.,.2133.,.1700.,.1293.,.0890.,.0499.,.0120.,-.0247.,-.0597.,-.0939
 .25.,.3314.,.2948.,.2598.,.2265.,.1949.,.1649.,.1336.,.1100.,.0849.,.0613
 .50.,.4369.,.4079.,.3804.,.3552.,.3317.,.3099.,.2898.,.2713.,.2542.,.2385
 .75.,.5275.,.5032.,.4806.,.4599.,.4411.,.4239.,.4083.,.3940.,.3810.,.3692
 1.00.,.6074.,.5863.,.5671.,.5497.,.5340.,.5198.,.5070.,.4954.,.4849.,.4755
 1.50.,.7458.,.7292.,.7143.,.7011.,.6893.,.6789.,.6694.,.6610.,.6535.,.6468
 2.00.,.8650.,.8513.,.8392.,.8285.,.8191.,.8109.,.8034.,.7969.,.7911.,.7860
 2.50.,.9709.,.9593.,.9491.,.9402.,.9324.,.9255.,.9195.,.9142.,.9095.,.9054
 3.00.,1.067,1.057,1.048,1.041,1.034,1.028,1.023,1.019,1.015,1.011
 3.50,1.156,1.147,1.139,1.133,1.127,1.122,1.118,1.114,1.110,1.107
 4.00,1.239,1.231,1.224,1.218,1.213,1.208,1.205,1.201,1.198,1.196
 10,12.,.50.,.6000.,.7000.,.8000.,.9000.,1.000,1.1000,1.2000,1.3000,1.4000,1.5000
 .00.,.2000.,.1500.,.1000.,.0500.,.0000.,-.0500.,-.1000.,-.1500.,-.2000.,-.2500
 .10.,.2508.,.2075.,.1651.,.1237.,.0834.,.0443.,.0065.,-.0301.,-.0651.,-.0992
 .25.,.3180.,.2817.,.2467.,.2139.,.1824.,.1527.,.1246.,.0981.,.0732.,.0498
 .50.,.4135.,.3846.,.3578.,.3330.,.3099.,.2885.,.2687.,.2506.,.2338.,.2184
 .75.,.4950.,.4712.,.4495.,.4295.,.4112.,.3946.,.3793.,.3656.,.3530.,.3416
 1.00.,.5670.,.5469.,.5285.,.5120.,.4970.,.4834.,.4712.,.4601.,.4501.,.4411
 1.50.,.6916.,.6763.,.6626.,.6504.,.6395.,.6298.,.6210.,.6133.,.6064.,.6001
 2.00.,.7990.,.7868.,.7759.,.7664.,.7580.,.7505.,.7439.,.7381.,.7328.,.7282
 2.50.,.8941.,.8842.,.8754.,.8677.,.8609.,.8550.,.8498.,.8452.,.8411.,.8374
 3.00.,.9807.,.9723.,.9649.,.9586.,.9531.,.9482.,.9439.,.9402.,.9369.,.9339

3.50,1.060,1.053,1.047,1.042,1.037, 1.033, 1.029, 1.026, 1.024, 1.021
 4.00,1.135,1.128,1.123,1.119,1.115, 1.111, 1.108, 1.106, 1.103, 1.101
 10,12,.60,.6000,.7000,.8000,.9000,1.000,1.1000,1.2000,1.3000,1.4000,1.5000
 .00,.2000,.1500,.1000,.0500,.0000,-.0500,-.1000,-.1500,-.2000,-.2500
 .10,.2447,.2013,.1589,.1176,.0774,. 0384,.0006,-.0359,-.0709,-.1049
 .25,.3038,.2678,.2332,.2003,.1691,. 1396,.1117,.0854,.0607,.0375
 .50,.3882,.3598,.3337,.3092,.2864,. 2657,.2463,.2285,.2121,.1970
 .75,.4605,.4375,.4166,.3972,.3795,. 3635,.3488,.3355,.3232,.3122
 1.00,.5244,.5053,.4879,.4721,.4578,. 4449,.4333,.4227,.4133,.4046
 1.50,.6352,.6212,.6006,.5973,.5873,. 5784,.5703,.5632,.5567,.5509
 2.00,.7308,.7199,.7114,.7019,.6944,. 6878,.6819,.6766,.6720,.6678
 2.50,.8157,.8072,.7996,.7931,.7873,. 7821,.7776,.7736,.7700,.7669
 3.00,.8928,.8860,.8800,.8747,.8701,. 8660,.8625,.8593,.8565,.8540
 3.50,.9643,.9584,.9535,.9492,.9455,. 9422,.9393,.9368,.9345,.9326
 4.00,1.033,1.026,1.022,1.018,1.015, 1.012, 1.010, 1.008, 1.006, 1.005
 10,12,.70,.6000,.7000,.8000,.9000,1.000,1.1000,1.2000,1.3000,1.4000,1.5000
 .00,.2000,.1500,.1000,.0500,.0000,-.0500,-.1000,-.1500,-.2000,-.2500
 .10,.2343,.1912,.1489,.1076,.0675,. 0286,-.0090,-.0454,-.0804,-.1142
 .25,.2803,.2448,.2106,.1781,.1473,. 1181,.0905,.0646,.0402,.0175
 .50,.3471,.3197,.2943,.2706,.2485,. 2284,.2096,.1925,.1765,.1619
 .75,.4047,.3830,.3632,.3449,.3283,. 3130,.2992,.2866,.2751,.2645
 1.00,.4561,.4384,.4224,.4079,.3948,. 3829,.3721,.3624,.3536,.3455
 1.50,.5458,.5337,.5227,.5128,.5041,. 4963,.4892,.4830,.4772,.4721
 2.00,.6243,.6151,.6072,.6002,.5940,. 5884,.5836,.5791,.5752,.5717
 2.50,.6938,.6872,.6814,.6762,.6712,. 6676,.6640,.6608,.6579,.6554
 3.00,.7577,.7526,.7482,.7443,.7408,. 7378,.7350,.7327,.7305,.7286
 3.50,.8168,.8128,.8094,.8063,.8037,. 8013,.7993,.7974,.7958,.7943
 4.00,.8720,.8689,.8662,.8638,.8617,. 8599,.8583,.8568,.8556,.8544
 10,12,.80,.6000,.7000,.8000,.9000,1.000,1.1000,1.2000,1.3000,1.4000,1.5000
 .00,.2000,.1500,.1000,.0500,.0000,-.0500,-.1000,-.1500,-.2000,-.2500
 .10,.2186,.1756,.1335,.0924,.0524,. 0175,-.00238,-.0588,-.0950,-.1285
 .25,.2450,.2100,.1762,.1442,.1139,. 0853,.0583,.0329,.0091,-.0133
 .50,.2852,.2590,.2346,.2121,.1913,. 1721,.1543,.1380,.1228,.1089
 .75,.3215,.3016,.2835,.2667,.2514,. 2375,.2248,.2131,.2026,.1929
 1.00,.3552,.3397,.3256,.3128,.3011,. 2907,.2812,.2724,.2647,.2575
 1.50,.4164,.4064,.3974,.3895,.3823,. 3758,.3700,.3648,.3600,.3558
 2.00,.4713,.4646,.4586,.4533,.4486,. 4444,.4406,.4371,.4341,.4313
 2.50,.5214,.5167,.5126,.5090,.5057,. 5028,.5003,.4979,.4958,.4940
 3.00,.5677,.5644,.5615,.5589,.5566,. 5546,.5528,.5511,.5497,.5484
 3.50,.6110,.6086,.6065,.6046,.6030,. 6015,.6002,.5990,.5979,.5970
 4.00,.6517,.6499,.6484,.6470,.6458,. 6447,.6437,.6428,.6421,.6414
 10,12,.85,.6000,.7000,.8000,.9000,1.000,1.1000,1.2000,1.3000,1.4000,1.5000
 .00,.2000,.1500,.1000,.0500,.0000,-.0500,-.1000,-.1500,-.2000,-.2500
 .10,.2083,.1653,.1232,.0882,.0424,. 0038,-.0336,-.0697,-.1047,-.1379
 .25,.2213,.1867,.1535,.1219,.0920,. 0637,.0370,.0118,-.0117,-.0336
 .50,.2446,.2194,.1960,.1742,.1540,. 1353,.1182,.1024,.0877,.0743
 .75,.2703,.2491,.2319,.2161,.2017,. 1986,.1765,.1655,.1555,.1464
 1.00,.2938,.2765,.2635,.2517,.2410,. 2314,.2225,.2145,.2072,.2007
 1.50,.3348,.3262,.3183,.3112,.3049,. 2992,.2941,.2894,.2852,.2814
 2.00,.3760,.3705,.3655,.3610,.3570,. 3534,.3502,.3473,.3447,.3423
 2.50,.4145,.4128,.4105,.4075,.4045,. 3996,.3974,.3955,.3938,.3923
 3.00,.4505,.4480,.4457,.4437,.4419,. 4403,.4389,.4376,.4365,.4354
 3.50,.4844,.4826,.4811,.4797,.4784,. 4773,.4763,.4754,.4746,.4739
 4.00,.5164,.5151,.5140,.5130,.5121,. 5113,.5106,.5099,.5094,.5089
 10,12,.90,.6000,.7000,.8000,.9000,1.000,1.1000,1.2000,1.3000,1.4000,1.5000
 .00,.2000,.1500,.1000,.0500,.0000,-.0500,-.1000,-.1500,-.2000,-.2500
 .10,.1959,.1530,.1111,.0702,.0305,. 0081,-.0453,-.0812,-.1159,-.1492
 .25,.1938,.1594,.1266,.0955,.0660,. 0381,.0119,-.0129,-.0362,-.0577
 .50,.1971,.1730,.1533,.1293,.1100,. 0921,.0756,.0604,.0463,.0334
 .75,.2054,.1878,.1717,.1571,.1435,. 1312,.1200,.1098,.1003,.0918
 1.00,.2163,.2034,.1916,.1808,.1711,. 1623,.1543,.1469,.1403,.1342
 1.50,.2414,.2340,.2273,.2212,.2157,. 2108,.2063,.2023,.1986,.1953
 2.00,.2676,.2631,.2593,.2553,.2520,. 2491,.2464,.2440,.2418,.2398
 2.50,.2932,.2903,.2877,.2854,.2834,. 2815,.2798,.2783,.2769,.2757
 3.00,.3178,.3159,.3142,.3126,.3113,. 3101,.3093,.3080,.3071,.3063
 3.50,.3411,.3399,.3387,.3377,.3368,. 3360,.3352,.3346,.3340,.3334

REPRODUCIBILITY OF THE ORIGINAL PAGE IS POOR

```

4.00,.3634,.3625,.3617,.3610,.3604,.3598,.3593,.3589,.3585,.3581
10,12,.95,.6000,.7000,.8000,.9000,1.000,1.1000,1.2000,1.3000,1.4000,1.5000
.00,.2000,.1500,.1000,.0500,.0000,-.0500,-.1000,-.1500,-.2000,-.2500
.10,.1813,.1385,.0967,.0560,.0164,-.0219,-.0590,-.0948,-.1293,-.1625
.25,.1612,.1273,.0923,.0644,.0354,.0082,-.0178,-.0420,-.0646,-.0860
.50,.1419,.1187,.0973,.0773,.0588,.0418,.0260,.0115,-.0019,-.0143
.75,.1336,.1174,.1025,.0890,.0765,.0651,.0547,.0452,.0365,.0285
1.00,.1314,.1198,.1092,.0996,.0909,.0830,.0758,.0692,.0632,.0574
1.50,.1359,.1296,.1239,.1188,.1142,.1100,.1062,.1028,.0997,.0968
2.00,.1456,.1420,.1387,.1358,.1332,.1308,.1286,.1267,.1249,.1233
2.50,.1571,.1549,.1529,.1511,.1495,.1481,.1468,.1456,.1446,.1436
3.00,.1689,.1675,.1663,.1652,.1642,.1633,.1625,.1617,.1611,.1605
3.50,.1806,.1797,.1789,.1782,.1775,.1770,.1764,.1760,.1755,.1751
4.00,.1919,.1914,.1908,.1903,.1899,.1895,.1892,.1889,.1886,.1883
10,12,1.00,.6000,.7000,.8000,.9000,1.000,1.100,1.200,1.300,1.400,1.500
.00,.2000,.1500,.1000,.0500,0.000,-.050,-.100,-.150,-.200,-.250
.10,.1645,.1219,.0802,.0397,0.000,-.0379,-.0749,-.1104,-.1447,-.1777
.25,.1235,.0902,.0586,.0286,0.000,-.0266,-.0510,-.0755,-.0978,-.1187
.50,.0787,.0568,.0364,.0176,0.000,-.0160,-.0310,-.0447,-.0574,-.0691
.75,.0521,.0374,.0238,.0114,0.000,-.0103,-.0190,-.0285,-.0365,-.0439
1.00,.0356,.0254,.0162,.0077,0.000,-.0069,-.0134,-.0192,-.0245,-.0294
1.50,.0179,.0128,.0081,.0039,0.000,-.0035,-.0066,-.0095,-.0121,-.0145
2.00,.0097,.0069,.0044,.0021,0.000,-.0019,-.0036,-.0051,-.0065,-.0079
2.50,.0056,.0040,.0025,.0012,0.000,-.0011,-.0021,-.0029,-.0037,-.0045
3.00,.0034,.0024,.0015,.0007,0.000,-.0006,-.0012,-.0018,-.0022,-.0027
3.50,.0021,.0015,.0009,.0004,0.000,-.0004,-.0008,-.0011,-.0014,-.0017
4.00,.0013,.0009,.0006,.0003,0.000,-.0003,-.0005,-.0007,-.0009,-.0011
10,6,1.00,.6000,.7000,.8000,.9000,1.000,1.100,1.200,1.300,1.400,1.500
.00,.2000,.1500,.1000,.0500,0.000,-.0500,-.1000,-.1500,-.2000,-.2500
.10,.1213,.0797,.0384,-.0017,-.0407,-.0784,-.1149,-.1501,-.1840,-.2165
.25,.0295,-.0017,-.0318,-.0603,-.0872,-.1127,-.1366,-.1590,-.1800,-.1999
.50,-.0740,-.0929,-.1107,-.1273,-.1423,-.1563,-.1694,-.1814,-.1925,-.2028
.75,-.1413,-.1529,-.1637,-.1736,-.1827,-.1911,-.1987,-.2058,-.2124,-.2187
1.00,-.1892,-.1965,-.2034,-.2097,-.2154,-.2206,-.2253,-.2297,-.2337,-.2374
10,6,1.25,.6000,.7000,.8000,.9000,1.000,1.100,1.200,1.300,1.400,1.500
.00,.2000,.1500,.1000,.0500,0.000,-.0500,-.1000,-.1500,-.2000,-.2500
.10,.0322,-.0094,-.0494,-.0884,-.1263,-.1632,-.1989,-.2332,-.2659,-.2973
.25,-.1606,-.1890,-.2159,-.2414,-.2653,-.2880,-.3095,-.3293,-.3483,-.3659
.50,-.3710,-.3853,-.3986,-.4111,-.4226,-.4331,-.4431,-.4521,-.4607,-.4685
.75,-.5082,-.5157,-.5227,-.5291,-.5350,-.5404,-.5454,-.5501,-.5544,-.5584
1.00,-.6107,-.6148,-.6187,-.6222,-.6254,-.6284,-.6312,-.6337,-.6361,-.6383
10,4,1.00,.6000,.7000,.8000,.9000,1.000,1.100,1.200,1.300,1.400,1.500
.00,.2000,.1500,.1000,.0500,0.000,-.0500,-.1000,-.1500,-.2000,-.2500
.10,-.0941,-.1336,-.1726,-.2105,-.2471,-.2825,-.3165,-.3493,-.3808,-.4111
.25,-.4179,-.4421,-.4652,-.4868,-.5072,-.5264,-.5445,-.5615,-.5776,-.5925
.50,-.7517,-.7616,-.7705,-.7790,-.7869,-.7942,-.8013,-.8074,-.8133,-.8189
10,3,1.50,.6000,.7000,.8000,.9000,1.000,1.100,1.200,1.300,1.400,1.500
.00,.2000,.1500,.1000,.0500,0.000,-.0500,-.1000,-.1500,-.2000,-.2500
.10,-.2018,-.2409,-.2787,-.3152,-.3507,-.3848,-.4177,-.4494,-.4796,-.5087
.25,-.6292,-.6503,-.6705,-.6892,-.7069,-.7235,-.7391,-.7538,-.7676,-.7806
10,5,1.75,.6000,.7000,.8000,.9000,1.000,1.100,1.200,1.300,1.400,1.500
.00,.2000,.1500,.1000,.0500,0.000,-.0500,-.1000,-.1500,-.2000,-.2500
.10,-.5732,-.6074,-.6409,-.6732,-.7043,-.7341,-.7628,-.7903,-.8169,-.8421
.25,-1.295,-1.308,-1.320,-1.331,-1.342,-1.352,-1.362,-1.371,-1.380,-1.389
.50,-1.927,-1.931,-1.935,-1.938,-1.942,-1.945,-1.948,-1.951,-1.954,-1.957
.75,-2.384,-2.385,-2.387,-2.388,-2.389,-2.391,-2.391,-2.392,-2.393,-2.394
10,3,2.00,.6000,.7000,.8000,.9000,1.000,1.100,1.200,1.300,1.400,1.500
.00,.2000,.1500,.1000,.0500,0.000,-.0500,-.1000,-.1500,-.2000,-.2500
.10,-1.112,-1.131,-1.158,-1.184,-1.209,-1.233,-1.256,-1.277,-1.298,-1.318
.25,-2.147,-2.154,-2.160,-2.166,-2.171,-2.177,-2.182,-2.186,-2.191,-2.195
END
2000,SPACE,6,END
END
C*****
ACD 3EXECUTION
MTEST = J

```



```

      N      = M500
      DO 10 I=1,N
      IF(A808+I .NE. 0.)          MTEST = 1
10  CONTINUE                      GO TO 160
      IF(JTEST .EQ. 1)
C...SOLVE STEADY STATE PROBLEM
      VAPRL1
      IF(MTEST .EQ. 0)            GO TO 70
20  LTEST = MDUM = 0
      IDUM = JDUM = KDUM = 1
      DO 40 ITEST=1,N
      IF(A808+ITEST .EQ. 0.)      GO TO 30
      MDUM = MDUM + 1
      FRONT
      IF(M783+ITEST .EQ. 0)       LTEST = 1
30  IDUM = IDUM + (M500+ITEST)
      JDUM = JDUM + (M510+ITEST)
      KDUM = KDUM + (M520+ITEST)
40  CONTINUE
      IF(LTEST .EQ. 0)            GO TO 50
      STDSL
      GO TO 20
50  WRITE (6,51) (M781+J,J=1,N)
F 51  FORMAT(*J FRONT ITERATION COUNTERS -- *,20(I3,2X))
      WRITE (6,52) (A844+J,J=1,N)
F 52  FORMAT(* FRONT DAMPING FACTORS -- *,13(F6.0,2X))
      DO 60 I=1,N
      M781+I = 1.
60  A844+I = 1.
      GO TO 30
70  CONTINUE
      STDSL
80  CONTINUE
      LIMITS(A500,A500,G1001,T120,T101,R1,R2,P7,R4,R6,A1112,A1132)
C---  QMAP(5H07AH9)
      II=0
      DO 110 III=1,6
      A2000+III=(G318+III-1)*((T100+II)-(T119+III-1))/(T119+III-1+460.)
      ***4-(R20+460.)*4)
110  II=II+6
      PRINTA(6HSINCCN,C318,6,1)
      PRINTA(6HFASGMA,A2000+1,6,1)
      RETURN
C...SOLVE TRANSIENT PROBLEM
100  CONTINUE
C---  FWDCK
C---  NETDMP
      END
C*****
      BCO 3VARIABLES 1
      N      = M500
      P11    = 0.
      L      = LL = 0
      N1     = N2 = N3 = 1
      DO 1000 I=1,N
      IF(A808+I .NE. 0.)          L = L + 1
C...LIQUID PROPERTIES
      IF(I.GT. 5)                GO TO 100
      LOOKUP(M500+I,T101+N1-1,A1001,A701+N1) $ LIQUID DENSITY
      LOOKUP(M510+I,T102+N2-1,A1001,A711+N2)
      LOOKUP(M520+I,T103+N3-1,A1001,A721+N3)
      LOOKUP(M500+I,T101+N1-1,A1003,A702+N1) $ LIQUID SPECIFIC HEAT
      LOOKUP(M510+I,T102+N2-1,A1003,A712+N2)
      LOOKUP(M520+I,T103+N3-1,A1003,A722+N3)
      LOOKUP(M500+I,T101+N1-1,A1005,A703+N1) $ LIQUID VISCOSITY
      LOOKUP(M510+I,T102+N2-1,A1005,A713+N2)

```

```

LOOKUP(M520+I,T103+N3-1,A1005,A723+N3)
LOOKUP(M500+I,T101+N1-1,A1007,A704+N1)$ LIQUID THERMAL CONDUCTIVITY
LOOKUP(M510+I,T102+N2-1,A1007,A714+N2)
LOOKUP(M520+I,T103+N3-1,A1007,A724+N3)
LOOKUP(M500+I,T101+N1-1,A1009,A705+N1)$ SURFACE TENSION
LOOKUP(M510+I,T102+N2-1,A1009,A715+N2)
LOOKUP(M520+I,T103+N3-1,A1009,A725+N3)
LOOKUP(M500+I,T101+N1-1,A1010,A706+N1)$ HEAT OF VAPOFIZATION
LOOKUP(M510+I,T102+N2-1,A1010,A716+N2)
LOOKUP(M520+I,T103+N3-1,A1010,A726+N3)
C...VAPOR PROPERTIES
D10EG1( T120+I-1,A1002,A731+I)$ VAPOR DENSITY
D10EG1( T120+I-1,A1004,A732+I)$ VAPOR SPECIFIC HEAT
D10EG1( T120+I-1,A1006,A733+I)$ VAPOR VISCOSITY
D10EG1( T120+I-1,A1008,A734+I)$ VAPOR THERMAL CONDUCTIVITY
GO TO 101
C ... HEADER PIPE PROPERTIES
100 LOOKUP(M500+I,T101+N1-1,A1021,A701+N1)$ LIQUID DENSITY
LOOKUP(M510+I,T102+N2-1,A1021,A711+N2)
LOOKUP(M520+I,T103+N3-1,A1021,A721+N3)
LOOKUP(M500+I,T101+N1-1,A1023,A702+N1)$ LIQUID SPECIFIC HEAT
LOOKUP(M510+I,T102+N2-1,A1023,A712+N2)
LOOKUP(M520+I,T103+N3-1,A1023,A722+N3)
LOOKUP(M500+I,T101+N1-1,A1025,A703+N1)$ LIQUID VISCOSITY
LOOKUP(M510+I,T102+N2-1,A1025,A713+N2)
LOOKUP(M520+I,T103+N3-1,A1025,A723+N3)
LOOKUP(M500+I,T101+N1-1,A1027,A704+N1)$ LIQUID THERMAL CONDUCTIVITY
LOOKUP(M510+I,T102+N2-1,A1027,A714+N2)
LOOKUP(M520+I,T103+N3-1,A1027,A724+N3)
LOOKUP(M500+I,T101+N1-1,A1029,A705+N1)$ SURFACE TENSION
LOOKUP(M510+I,T102+N2-1,A1029,A715+N2)
LOOKUP(M520+I,T103+N3-1,A1029,A725+N3)
LOOKUP(M500+I,T101+N1-1,A1030,A706+N1)$ HEAT OF VAPORIZATION
LOOKUP(M510+I,T102+N2-1,A1030,A716+N2)
LOOKUP(M520+I,T103+N3-1,A1030,A726+N3)
C...VAPOR PROPERTIES
D10EG1( T120+I-1,A1022,A731+I)$ VAPOR DENSITY
D10EG1( T120+I-1,A1024,A732+I)$ VAPOR SPECIFIC HEAT
D10EG1( T120+I-1,A1026,A733+I)$ VAPOR VISCOSITY
D10EG1( T120+I-1,A1028,A734+I)$ VAPOR THERMAL CONDUCTIVITY
101 CONTINUE
C...COMPUTE ARTERY CAPACITANCES AND CONDUCTANCES
ARTERY(M500+I,M910+I,M620+N1,A621+N1,A622+N1,A631+N1,A623+N1,
* A624+N1,A625+N1,R1,A626+N1,A627+N1,A628+N1,A629+N1,
* A630+N1,A704+N1,A537+N1,A701+N1,A702+N1,A535+N1,
* A681+N1,A684+N1,A687+N1)
ARTERY(M510+I,M912+I,M640+N2,A641+N2,A642+N2,A651+N2,A643+N2,
* A644+N2,A645+N2,R1,A646+N2,A647+N2,A648+N2,A649+N2,
* A650+N2,A714+N2,A557+N2,A711+N2,A712+N2,A555+N2,
* A682+N2,A685+N2,A688+N2)
ARTERY(M520+I,M914+I,M660+N3,A661+N3,A662+N3,A671+N3,A663+N3,
* A664+N3,A665+N3,R1,A666+N3,A667+N3,A668+N3,A669+N3,
* A670+N3,A724+N3,A577+N3,A721+N3,A722+N3,A575+N3,
* A683+N3,A686+N3,A689+N3)
C...COMPUTE CAPACITANCES
CAPFIN(M521+N3,A612+N3,A611+N3,A526+N3,A616+N3,A617+N3,A850+N3)
CAPWCK(M500+I,A501+N1,A502+N1,R1,A504+N1,A505+N1,A506+N1,A538+N1,
* A701+N1,A702+N1,A531+N1,A532+N1,A534+N1,A535+N1,A537+N1,
* A681+N1,0.,CAPE)
CAPWCK(M510+I,A511+N2,A512+N2,R1,A514+N2,A515+N2,A516+N2,A558+N2,
* A711+N2,A712+N2,A551+N2,A552+N2,A554+N2,A555+N2,A557+N2,
* A682+N2,0.,CAPA)
CAPWCK(M520+I,A521+N3,A522+N3,R1,A524+N3,A525+N3,A526+N3,A578+N3,
* A721+N3,A722+N3,A571+N3,A572+N3,A574+N3,A575+N3,A577+N3,
* A683+N3,A850+N3,C103+N3-1)
C103+N3-1 = C103+N3-1 + CAPE + CAPA

```

C...COMPUTE AXIAL CONDUCTANCES

```

15  AXCOND(M500+I,A513+N1,A504+N1,A505+N1,A506+N1,R1,A537+N1,
    *      A538+N1,A533+N1,A534+N1,A535+N1,A693+N1,A696+N1)
    AXCOND(M510+I,A513+N2,A514+N2,A515+N2,A516+N2,R1,A557+N2,
    *      A558+N2,A553+N2,A554+N2,A555+N2,A594+N2,A697+N2)
    AXCOND(M520+I,A523+N3,A524+N3,A525+N3,A526+N3,R1,A577+N3,
    *      A578+N3,A573+N3,A574+N3,A575+N3,A595+N3,A698+N3)

```

C

```

50  GO TO (201,202,203,204,205,206,221), I
201  RADFIN(M520+I,T103,T103,T203,A613+N3,A612+N3,A611+N3,A526+N3,
    *      R5,A600,A614+N3,A615+N3,A768+N3,A610+N3,G10,A851+N3,
    *      T10,A770+N3,A811+I)
    GO TO 210
202  RADFIN(M520+I,T203,T103,T303,A613+N3,A612+N3,A611+N3,A526+N3,
    *      R5,A600,A614+N3,A615+N3,A768+N3,A610+N3,G20,A851+N3,
    *      T20,A770+N3,A811+I)
    GO TO 210
203  RADFIN(M520+I,T303,T203,T403,A613+N3,A612+N3,A611+N3,A526+N3,
    *      R5,A600,A614+N3,A615+N3,A768+N3,A610+N3,G30,A851+N3,
    *      T30,A770+N3,A811+I)
    GO TO 210
204  RADFIN(M520+I,T403,T303,T503,A613+N3,A612+N3,A611+N3,A526+N3,
    *      R5,A600,A614+N3,A615+N3,A768+N3,A610+N3,G40,A851+N3,
    *      T40,A770+N3,A811+I)
    GO TO 210
205  RADFIN(M520+I,T503,T403,T603,A613+N3,A612+N3,A611+N3,A526+N3,
    *      R5,A600,A614+N3,A615+N3,A768+N3,A610+N3,G50,A851+N3,
    *      T50,A770+N3,A811+I)
    GO TO 210
206  RADFIN(M520+I,T603,T503,T603,A613+N3,A612+N3,A611+N3,A526+N3,
    *      R5,A600,A614+N3,A615+N3,A768+N3,A610+N3,G60,A851+N3,
    *      T60,A770+N3,A811+I)
210  CONTINUE
221  CONTINUE

```

C

```

    AGCOMB(M500+I,M510+I,M520+I,A684+N1,A685+N2,A686+N3,A693+N1,
    *      A694+N2,A695+N3,A696+N1,A697+N2,A698+N3,A618+N3,
    *      A851+N3,G311+LL)

```

C...COMPUTE LIQUID/WICK EFFECTIVE RADIAL THERMAL CONDUCTIVITIES

```

    EFFKWK(M500+I,M530+N1,A533+N1,A704+N1,A503+N1,A538+N1,
    *      A534+N1,A535+N1,R1,A542+N1,A543+N1,A544+N1,A765+N1)
    EFFKWK(M510+I,M550+N2,A553+N2,A714+N2,A513+N2,A558+N2,
    *      A554+N2,A555+N2,R1,A562+N2,A563+N2,A564+N2,A766+N2)
    EFFKWK(M520+I,M570+N3,A573+N3,A724+N3,A523+N3,A578+N3,
    *      A574+N3,A575+N3,R1,A582+N3,A583+N3,A584+N3,A767+N3)

```

C...COMPUTE RADIAL CONDUCTANCES

```

    RACOND(M500+I,R1,A765+N1,A537+N1,A534+N1,A535+N1,A503+N1,
    *      A506+N1,A504+N1,A505+N1,G1001+N1-1)
    RACOND(M510+I,R1,A766+N2,A557+N2,A554+N2,A555+N2,A513+N2,
    *      A516+N2,A514+N2,A515+N2,G1002+N2-1)
    RACOND(M520+I,R1,A767+N3,A577+N3,A574+N3,A575+N3,A523+N3,
    *      A526+N3,A524+N3,A525+N3,G1003+N3-1)

```

GO TO(321,321,322,323,324,325,300),I

```

320  FAC = 18.6
    GO TO 330
321  FAC = 18.6
    GO TO 330
322  FAC = 18.6
    GO TO 330
323  FAC = 18.6
    GO TO 330
324  FAC = 18.6
    GO TO 330
325  FAC = 18.6
330  G1001+N1-1 = G1001+N1-1 / FAC
    G1002+N2-1 = G1002+N2-1 / FAC

```

REPRODUCIBILITY OF THE
ORIGINAL PAGE IS POOR

```

      DO 301 II=1,6
301  G1003+N3+II-2 = G1003+N3+II-2 / FAC
      GO TO 310
300  DO 303 II=1,4
303  G1001+N1+II-2 = G1001+N1+II-2 / 144.2
      G1002+N2-1 = G1002+N2-1 / 144.2
      DO 304 II=1,6
304  G1003+N3+II-2 = G1003+N3+II-2 / 144.2
310  CONTINUE
C...COMPUTE FEEDTURE CONDUCTANCES
      JJ      = M520+I
      RCOND(A808+I,R1,A526+JJ,A523+JJ,A524+JJ,A525+JJ,A826+I,
      *      A836+I,A825+I,A823+I,A822+I,A837+I,A829+I,A827+I,
      *      A577+JJ,A578+JJ,A573+JJ,A574+JJ,A575+JJ,A828+I,
      *      A824+I,G318+L-1)
C...ADJUST CONDENSER COUPLINGS BASED ON LA/LC
      ADJG(A808+I,M520+I,A526+N3,A829+I,G1003+N3-1)
C...COMPUTE HEAT LOADS
      R11      = R11 + A811+I
      N1        = N1 + (M500+I)
      N2        = N2 + (M510+I)
      N3        = N3 + (M520+I)
      LL        = LL + (M500+I) + (M510+I) + (M520+I) - 1
1000  CONTINUE
      Q701 = Q703 = Q705 = Q707 = 683.21/4.
      ENC
C*****
      RCD 3VARIABLES 2
      IF(JTEST .EQ. 0 .OR. MTEST .EQ. 0) RETURN
      N      = M500
      MDUM   = J
      IDUM   = JDUM = KDUM = 1
      DO 50 ITEST=1,N
      IF(A808+ITEST .EQ. 0)          GO TO 40
      MDUM   = MDUM + 1
      FRONT
      IF(M783+ITEST .EQ. 0)          BACKUP = 1.
40      IDUM   = IDUM + (M500+ITEST)
      JDUM   = JDUM + (M510+ITEST)
      KDUM   = KDUM + (M520+ITEST)
50      CONTINUE
      IF(BACKUP .NE. 0)              RETURN
100  WRITE (6,51) (M781+J,J=1,N)
F 51  FORMAT(*J FRONT ITERATION COUNTERS -- *,20(I3,2X))
      WRITE (6,52) (A844+J,J=1,N)
F 52  FORMAT(* FRONT DAMPING FACTORS -- *,13(F6.0,2X))
      DO 110 I=1,N
      M781+I = 1
110  A844+I = 1.
      STOREP
      ENC
C*****
      RCD 3OUTPUT CALLS
      TPRINT
      PRINTA(6HTENVIR,A768+1,M768,1)
      PRINTA(6HQLATNT,A752+1,M752,1)
      PRINTA(6HQRJCTN,A770+1,M770,1)
      PRINTA(6HQRJCTP,A811+1,M811,1)
      WRITE(6,10) F11
F 10  FORMAT(* TOTAL PANEL HEAT REJECTION =*,F15.3,* BTU/HR*)
      IF(JTEST .EQ. 1)              GO TO 20
      STOREP
      RETURN
C...COMPUTE HEAT TRANSFER LIMITS
20  LIMITS(A500,A500,G1001,T100,T101,R1,R2,R3,R4,R6,A1012,A1032)
      END

```



```

C*****
C      BCD 3SUBROUTINES
C...IN SEVERAL OF THE FOLLOWING SUBROUTINES, MULTIPLE CASES CAN BE CONSIDERED
C...WITH ONE CALL, SINCE ALL VARIABLES ARE SUBSCRIPTED. THIS OPTION IS USED
C...BY INPUTTING THE VARIABLES IN ARRAYS WHERE EACH ARRAY CONTAINS MULTIPLE
C...VALUES, REPRESENTING EITHER SEVERAL PIPES OR SEVERAL NODES IN ONE PIPE.
C...IF ONLY ONE CASE IS DESIRED, INPUT N=1 IN THE SUBROUTINE CALL. IF SEVERAL
C...CASES ARE DESIRED, ENTER THE INTEGER COUNT OF ONE OF THE ARRAYS. THE
C...SUBROUTINES CONTAINING THIS OPTION ARE EFFKWK, ARTERY, RACOND, AXCOND,
C...CAPWCK, CAPFIN, RADFIN, AND LOOKUP.
FSTART
      SUBROUTINE EFFKWK(N,NWICK,KWICK,KL,KWALL,POROS,CD,ID,PI,
      *      GNO,WIDTH,DEPTH,EFFK)
C-----
C      THIS SUBROUTINE COMPUTES THE EFFECTIVE RADIAL THERMAL CONDUCTIVITY
C      OF THE LIQUID-SATURATED WICK. IT ASSUMES THE CONTACT BETWEEN WICK
C      AND WALL IS GOOD, WITH THE EXCEPTION OF THE AXIAL SPACER WIRES
C      WHERE POOR CONTACT IS ASSUMED. EFFK IS USED IN SUBROUTINE
C      RACOND, THUS EFFKWK MUST BE CALLED BEFORE RACOND IN VARPL1.
C      N      = NUMBER OF CASES TO BE TREATED IN THIS CALL
C      NWICK   = TYPE OF WICK
C      KWICK   = THERMAL CONDUCTIVITY OF WICK MATERIAL
C      KL      = THERMAL CONDUCTIVITY OF LIQUID
C      KWALL   = THERMAL CONDUCTIVITY OF WALL MATERIAL
C      POROS   = WICK POROSITY
C      OD,ID   = WICK OUTER AND INNER DIAMETERS
C      GNO     = NUMBER OF GROOVES, WIRES, OR THREADS/FT
C      WIDTH   = GROOVE OR THREAD MEAN WIDTH
C      DEPTH   = GROOVE OR THREAD DEPTH, OR WIRE DIAM
C      EFFK    = EFFECTIVE THERMAL CONDUCTIVITY
C-----
      REAL KWICK, KL, KWALL, ID
      DIMENSION NWICK(1),KWICK(1),KL(1),KWALL(1),POROS(1),CD(1),ID(1)
      DIMENSION GNO(1),WIDTH(1),DEPTH(1),EFFK(1)
      DO 2000 I=1,N
      IF(NWICK(I) .LE. 3 .OR. NWICK(I) .GE. 6) GO TO 1000
      J      = NWICK(I)
      GO TO (100,200,300,400,500),J
C...WRAPPED SCREEN, SINTERED POWDER, FELT, OR FCAM ON IC OF PIPE
      100 EFFK(I)= KL(I)*(KL(I)+KWICK(I) - (1.-POROS(I))*(KL(I)-KWICK(I)))/
      *      (KL(I)+KWICK(I) + (1.-POROS(I))*(KL(I)-KWICK(I)))
      IF(NWICK(I) .EQ. 3) GO TO 310
      IF(NWICK(I) .EQ. 4) GO TO 410
      GO TO 2000
C...OPEN AXIAL GROOVES ON ID OF PIPE -- APPROXIMATE ODD-SHAPED
C...GROOVE X-SECTIONS WITH EQUIVALENT SQUARE LENGTH AND DEPTH
      200 EFFK(I)= GNO(I)*WIDTH(I)*(KL(I)-KWALL(I))/(PI*(CD(I)-DEPTH(I)))
      *      + KWALL(I)
      IF(NWICK(I) .EQ. 3) GO TO 320
      GO TO 2000
C...SCREEN-COVERED AXIAL GROOVES ON ID OF PIPE
      300 GO TO 100
      310 EFFK1 = EFFK(I)
      GO TO 200
      320 EFFK2 = EFFK(I)
      EFFK(I)= 1./(1./EFFK1 + 1./EFFK2)
      GO TO 2000
C...SCREEN-COVERED AXIAL SPACER WIRES
      400 GO TO 100
      410 EFFKW = EFFK(I) * 2.* PI * ID(I)/(OD(I) - ID(I) - 2.* DEPTH(I))
      EFFKL = KL(I) * (PI * (OD(I)/DEPTH(I)-1.) - GNO(I))
      EFFKS = KL(I) * KWALL(I)/(1.738 * KWALL(I) + .8262 * KL(I))
      EFFK(I)= 2.*(OD(I)-ID(I))/(PI*(OD(I)+ID(I))*(1./(EFFKS+EFFKL)
      *      + 1./EFFKW))
      GO TO 2000
C...CIRCUMFERENTIAL GROOVES ON ID OF PIPE (THREADS)

```

```

500 EFFK(I)= GNC(I) * WIDTH(I) * (KL(I)-K WALL(I)) + K WALL(I)
GO TO 2000
1000 WRITE(6,1001)
1001 FORMAT(*J *****ERROR***** INVALID WICK TYPE,*,
* * RACIAL WICK CONDUCTORS ERRONEOUS*)
2000 CONTINUE
RETURN
END

C*****
SUBROUTINE PERMBL(NWICK,OD,ID,GNC,WIDTH,DEPTH,NART,DOART,
* DIART,WT,AART,K,NT,SD,T,PERM,PERMTA,PI,DR)
C-----
C THIS SUBROUTINE COMPUTES THE PERMEABILITY * CROSS-SECTIONAL AREA
C PRODUCTS OF THE ARTERY (IF ANY) AND WICK. SINCE THE ARTERY AND
C WICK FORM PARALLEL LIQUID FLOW PATHS, THEIR PERMEABILITIES ARE
C SUMMED LINEARLY. PERMTA IS USED BY SUBROUTINE LIMITS AND PERMBL
C IS CALLED BY LIMITS INTERNALLY.
C NWICK = TYPE OF WICK
C OD,ID = WICK OUTER AND INNER DIAMETERS
C GNC = NUMBER OF GROOVES, WIRES, OR THREADS/FT
C WIDTH = GROOVE OR THREAD MEAN WIDTH
C DEPTH = GROOVE OR THREAD DEPTH, OR WIRE DIAM
C NART = TYPE OF ARTERY
C DOART = ARTERY OUTER DIAMETER
C DIART = ARTERY INNER DIAMETER
C WT = THICKNESS OF OUTER ARTERY WRAP
C AART = ARRAY OF ANGULAR WIDTHS OF SPIRAL ARTERY ANNULI
C K = NUMBER OF SPIRAL ARTERY ANNULI
C NT = NUMBER OF SPIRAL ARTERY TURNS
C SD = SPIRAL ARTERY SPACER WIRE DIAMETER
C T = SPIRAL ARTERY SCREEN THICKNESS
C PERM = HOMOGENEOUS WICK PERMEABILITY
C PERMTA = PERMEABILITY * CROSS-SECTIONAL AREA
C DR = DEGREES-RADIANS CONVERSION (57.3)
C-----
DIMENSION AART(1)
REAL ID, NT, KAC
PERMA = 0.
IF(NART .EQ. 0) GO TO 90
IF(NART .LT. 3 .OR. NART .GE. 3) GO TO 1002
GO TO (1,2,3),NART
C...PEDESTAL ARTERY
10 PERMA = PI * DIART**4 / 128.
GO TO 90
C...SPIRAL ARTERY WITH SPACER WIRES BETWEEN SPIRALS
20 DART = DOART - 2.* WT
PI = DIART/2. + T + (DART-DIART-2.*T) * AART(1) /
* (8.* PI * NT * DR)
RO = RI + SD
THETA = AART(1)/(2.*DR) - SD/(RO+RI)
CALL ANNSPC(RI,RC,THETA,KAC)
PERMA = KAC
DO 25 I=2,K
RI = RI + (DART-DIART-2.*T) * (AART(I-1) + AART(I)) /
* (8.* PI * NT * DR)
RO = RI + SD
THETA = AART(I)/(2.*DR) - SD/(RO+RI)
CALL ANNSPC(RI,RC,THETA,KAC)
PERMA = PERMA + KAC
25 CONTINUE
PERMA = PERMA + PI * (DIART/2.)**4 / 8.
90 IF(NWICK .LE. 0 .OR. NWICK .GE. 6) GO TO 1000
GO TO (100,200,300,400,500),NWICK
C...WRAPPED SCREEN, SINTERED POWDER, FELT, OR FOAM ON ID OF PIPE
100 PERMTA = PERM * PI * (OD**2 - ID**2) / 4. + PERMA
RETURN

```

```

C...OPEN AXIAL GROOVES ON ID OF PIPE -- APPROXIMATE COO-SHAPED
C...GROOVE X-SECTIONS WITH EQUIVALENT SQUARE LENGTH AND DEPTH
200 PERMTA = 5.* GNO * WIDTH**3 * DEPTH**3/(18.* (WIDTH**2
*
* 4.* DEPTH**2)) + PERMA
RETURN
C...SCREEN-COVERED AXIAL GROOVES ON ID OF PIPE
300 PERMTA = 5.* GNC * WIDTH**3 * DEPTH**3/(72.* (WIDTH**2
*
* DEPTH**2)) + PERMA
RETURN
C...SCREEN-COVERED AXIAL SPACER WIRES
400 RO = OR / 2.
PI = RO - DEPTH
THETA = (PI * (RO+PI) - GNO*DEPTH)/(GNO * (RO+PI))
CALL ANNSPC(RI,RC,THETA,KAC)
PERMTA = GNO * KAC + PERMA
RETURN
C...CIRCUMFERENTIAL GROOVES ON ID OF PIPE (THREADS)
500 PERMTA = 5.* WIDTH**3 * DEPTH**3/(GNC * PI * (CO+ID) *
*
* 9.* (WIDTH**2 + 4.* DEPTH**2)) + PERMA
RETURN
1000 WRITE(6,1001)
1001 FORMAT(*,+++++ERROR+++++ INVALID WICK TYPE,*,
*
* PERMEABILITY ERPONECUS*)
RETURN
1002 WRITE(6,1003)
1003 FORMAT(*,+++++CAUTION+++++ INVALID ARTERY TYPE,*,
*
* NO ARTERY ASSUMED*)
GO TO 90
END
C*****
SUBROUTINE ANNSPC(RI,RC,THETA,KAC)
C-----
C THIS SUBROUTINE COMPUTES THE PERMEABILITY * CROSS-SECTIONAL AREA
C PRODUCT OF AN ANNULAR SPACE. IT IS USED BY SUBROUTINE PERMBL AND
C IS CALLED BY PERMBL INTERNALLY.
C RI,RC = ANNULAR SPACE INNER AND OUTER RADII
C THETA = HALF-ANGLE WIDTH OF ANNULAR SPACE
C KAC = PERMEABILITY * CROSS-SECTIONAL AREA
C-----
PEAL KAC
KAC = 5.* THETA**3 * (RO**4 - PI**4 -
*
* 2.* (RC**3 * RI - RO * RI**3))**2 /
*
* (18.* ((4.* THETA**2 + 5.) * (RO**4 - RI**4) -
*
* 8.* (THETA**2 + 5.) * (RO**3 * RI - RC * RI**3) +
*
* 6.* RC**2 * RI**2 * ALOG(RO/RI)))
RETURN
END
C*****
SUBROUTINE ARTERY(N,NA1,NART,DOART,DIART,WT,SD,T,POPCS,PI,NT,
*
* RHCCFA,RHOCPS,KA,KS,KL,L,DENL,CPL,ID,CAP,
*
* COND,EFFVD)
C-----
C THIS SUBROUTINE COMPUTES THE CAPACITANCE AND AXIAL CONDUCTANCE
C OF AN ARTERY. RADIAL CONDUCTANCE IS UNNECESSARY. BOTH THE
C ARTERY MATERIAL AND THE LIQUID FILLING IT ARE CONSIDERED. THE
C CAPACITANCE AND THE CONDUCTANCE ARE ADDED TO THOSE OF THE WICK
C IN SUBROUTINES CAPWCK AND AXCCND, THUS ARTERY MUST BE CALLED
C BEFORE THOSE ROUTINES IN VAPRL1. THE EFFECTIVE VAPOR SPACE
C DIAMETER RESULTING FROM THE PRESENCE OF AN ARTERY IS ALSO COM-
C PUTED FOR USE IN SUBROUTINE LIMITS.
C N = NUMBER OF CASES TO BE TREATED IN THIS CALL
C NA1 = NUMBER OF SPIRAL ARTERY ANNULI
C NART = TYPE OF ARTERY
C DOART = ARTERY OUTER DIAMETER
C DIART = ARTERY INNER DIAMETER
C WT = THICKNESS OF OUTER ARTERY WRAP

```

REPRODUCIBILITY OF THE
ORIGINAL PAGE IS POOR

```

C      SD      = SPIRAL ARTERY SPACER WIRE DIAMETER
C      T      = SPIRAL ARTERY SCREEN THICKNESS
C      PCROS   = ARTERY SCREEN POROSITY
C      NT      = NUMBER OF SPIRAL ARTERY TURNS
C      RHOCPA  = ARTERY SCREEN DENSITY * SPECIFIC HEAT
C      RHOCPS  = SPACER WIRE DENSITY * SPECIFIC HEAT
C      KA      = ARTERY SCREEN THERMAL CONDUCTIVITY
C      KS      = SPACER WIRE THERMAL CONDUCTIVITY
C      KL      = LIQUID THERMAL CONDUCTIVITY
C      L      = NODAL LENGTH ALONG PIPE AXIS
C      DENL    = LIQUID DENSITY
C      CPL     = LIQUID SPECIFIC HEAT
C      ID      = WICK INNER DIAMETER
C      CAP     = ARTERY CAPACITANCE
C      COND    = ARTERY AXIAL CONDUCTANCE
C      EFFVD   = EFFECTIVE VAPOR SPACE DIAMETER IN PIPE
C-----
      REAL L, LSCRN, ID, KA, KS, KL, NT
      DIMENSION NART(1), DOART(1), DIART(1), WT(1), SD(1), T(1), PCROS(1)
      DIMENSION NT(1), RHOCPA(1), RHOCPS(1), KA(1), KS(1), KL(1), L(1)
      DIMENSION DENL(1), CPL(1), ID(1), CAP(1), COND(1), EFFVD(1)
      DO 2000 I=1,N
      IF(NART(I) .NE. 0)          GO TO 50
C...NO ARTERY
      10 CAP(I) = 0.
      COND(I) = 1.E-12
      ARTXSA = 0.
      EFFVD(I) = ID(I)
      GO TO 2000
      50 IF(NART(I) .LT. 0 .OR. NART(I) .GE. 3) GO TO 1000
      J = NART(I)
      GO TO (100,200),J
C...PEDESTAL ARTERY
      100 VSCRN = PI*(DOART(I)**2 - DIART(I)**2)*L(I)*(1.-PCROS(I))/4.
      VLIO = PI * DOART(I)**2 * L(I) / 4. - VSCRN
      CAP(I) = VSCRN * RHOCPA(I) + VLIO * DENL(I) * CPL(I)
      COND(I) = KA(I) * VSCRN / (2.* L(I)**2) +
      * KL(I) * PI * DIART(I)**2 / (4.* L(I))
      ARTXSA = PI * DOART(I)**2 / 4.
      EFFVD(I) = ((PI * ID(I)**2/4. - ARTXSA) * 4./ PI)**.5
      GO TO 2000
C...SPIRAL ARTERY WITH SPACER WIRES BETWEEN SPIRALS
      200 DART = DOART(I) - 2.* WT(I)
      A = (DART - DIART(I) - 2.*T(I)) / (4.* PI * NT(I))
      B = DIART(I)/2. + T(I)
      LSCRN = (2.*PI * NT(I) + B/A) * ((2.* PI * NT(I) * A + B)**2 +
      * A**2)**.5 - B/A * (B**2 + A**2)**.5 + A/2.*
      * ALOG(((2.* PI * NT(I) * A + B)**2 + A**2)**.5 +
      * 2.* PI * NT(I) * A + B) / ((B**2 + A**2)**.5 + B))
      VSCRN = LSCRN * T(I) * L(I) * (1.-PCROS(I)) + PI * (DOART(I)**2
      * - DART**2) * L(I) * (1.-PCROS(I)) / 4.
      VSPAC = FLCAT(NART(I)) * PI * SD(I)**2 * L(I) / 4.
      VLIO = PI * DOART(I)**2 * L(I) / 4. - VSCRN - VSPAC
      CAP(I) = VSCRN * RHOCPA(I) + VSPAC * RHOCPS(I) + VLIO * DENL(I)
      * CPL(I)
      COND(I) = (VSCRN/2.* KA(I) + VSPAC * KS(I) + (PI * DART**2/4. -
      * LSCRN * T(I)) * L(I) * KL(I)) / L(I)**2
      ARTXSA = PI * DOART(I)**2 / 4.
      EFFVD(I) = ((PI * ID(I)**2/4. - ARTXSA) * 4./ PI)**.5
      GO TO 2000
      1000 WRITE(6,1001)
      1001 FORMAT(*,++++CAUTION++++ INVALID ARTERY TYPE,*,
      * * NO ARTERY ASSUMED*)
      GO TO 10
      2000 CONTINUE
      RETURN

```



```

END
C*****
SUBROUTINE LOCKUP(N,T,A,P)
C-----
C      THIS SUBROUTINE OBTAINS PROPERTIES AS A FUNCTION OF TEMPERATURE
C      ON AN AUTOMATED BASIS. THE INDEPENDENT AND DEPENDENT VARIABLES
C      MUST BE INPUT SEQUENTIALLY.
C      N      = NUMBER OF LOOKUPS IN THIS CALL
C      T      = INDEPENDENT VARIABLE (TEMPERATURE)
C      A      = ARRAY OF T,P VALUES
C      P      = DEPENDENT VARIABLE (PROPERTY)
C-----
      DIMENSION T(1),P(1)
      DO 10 I=1,N
10  CALL D1DEG1(T(I),A,P(I))
      RETURN
      END
C*****
SUBROUTINE CAPWCK(N,RHWA,CPWA,PI,ODWA,IDWA,LWA,
*          POROS,RHOL,CPL,RHCK,CPWK,ODWK,IDWK,
*          LWK,CAPA,CAPF,CAP)
C-----
C      THIS SUBROUTINE COMPUTES THE CAPACITANCE OF THE LIQUID-SATURATED
C      WICK AND PIPE WALL. THEY ARE SUMMED ALONG WITH THE ARTERY CAPA-
C      CITANCE FROM SUBROUTINE ARTERY AND THE FIN CAPACITANCE FROM SUB-
C      ROUTINE CAPFIN (IF ANY) TO OBTAIN THE TOTAL CAPACITANCE OF EACH
C      PIPE NODE. THE CAPACITANCE OF THE VAPOR IS IGNORED.
C      N      = NUMBER OF CASES TO BE TREATED IN THIS CALL
C      RHWA   = PIPE WALL DENSITY
C      CPWA   = PIPE WALL SPECIFIC HEAT
C      ODWA,IDWA = PIPE WALL OUTER AND INNER DIAMETERS
C      LWA    = PIPE WALL NODAL LENGTH
C      POROS  = WICK POROSITY
C      RHOL   = LIQUID DENSITY
C      CPL    = LIQUID SPECIFIC HEAT
C      RHCK   = WICK DENSITY
C      CPWK   = WICK SPECIFIC HEAT
C      ODWK,IDWK = WICK OUTER AND INNER DIAMETERS
C      LWK    = WICK NODAL LENGTH
C      CAPA   = ARTERY CAPACITANCE
C      CAPF   = FIN CAPACITANCE
C      CAP    = TOTAL CAPACITANCE
C-----
      REAL IDWA,LWA,IDWK,LWK
      DIMENSION RHWA(1),CPWA(1),ODWA(1),IDWA(1),LWA(1),POROS(1)
      DIMENSION RHOL(1),CPL(1),RHCK(1),CPWK(1),ODWK(1),IDWK(1)
      DIMENSION LWK(1),CAPA(1),CAPF(1),CAP(1)
      DO 10 I=1,N
      CAPWA = RHWA(I) * CPWA(I) * PI * (ODWA(I)**2 - IDWA(I)**2)
      *      * LWA(I)/4.
      CAPWK = (POROS(I) * RHOL(I) * CPL(I) + (1.-POROS(I))
      *      * RHCK(I) * CPWK(I)) * PI * (ODWK(I)**2 - IDWK(I)**2)
      *      * LWK(I)/4.
10  CAP(I) = CAPWA + CAPWK + CAPA(I) + CAPF(I)
      RETURN
      END
C*****
SUBROUTINE CAPFIN(N,X,Y,Z,DEN,CP,CAP)
C-----
C      THIS SUBROUTINE COMPUTES THE CAPACITANCE OF A SPACE RADIATOR
C      FIN (IF ANY), ATTACHED TO A HEAT PIPE CONDENSER.
C      N      = NUMBER OF CASES TO BE TREATED IN THIS CALL
C      X      = FIN LENGTH (HALF PIPE-TO-PIPE DISTANCE)
C      Y      = FIN THICKNESS
C      Z      = FIN WIDTH (CONDENSER LENGTH)
C      DEN    = FIN DENSITY

```

```

C          CP          = FIN SPECIFIC HEAT
C          CAP          = FIN CAPACITANCE
C-----
C          DIMENSION X(1),Y(1),Z(1),DEN(1),CP(1),CAP(1)
C          DO 10 J=1,N
10 CAP(J) = 2.* X(J) * Y(J) * Z(J) * DEN(J) * CP(J)
C          RETURN
C          END
C*****
C          SUBROUTINE AXCOND(N,KWA,ODWA,IDWA,LWA,PI,LWK,POROS,KWK,ODWK,
C          * IDWK,CONDWA,CONDWK)
C-----
C          THIS SUBROUTINE COMPUTES THE TOTAL AXIAL CONDUCTANCE OF THE
C          WICK AND WALL. NEGLIGIBLE CONTACT CONDUCTANCE IS ASSUMED
C          BETWEEN CROSSED MEMBERS IN HOMOGENEOUS WICKS--THE WICK VOLUME
C          IS CONSEQUENTLY HALVED. THE CONDUCTANCES ARE COMBINED WITH
C          THOSE FROM SUBROUTINE ARTERY IN SUBROUTINE AGCOMB. THUS ARTERY
C          AND AXCOND MUST BE CALLED BEFORE AGCOMB IN VARBL1.
C          N          = NUMBER OF CASES TO BE TREATED IN THIS CALL
C          KWA          = WALL THERMAL CONDUCTIVITY
C          ODWA,IDWA    = WALL OUTER AND INNER DIAMETERS
C          LWA          = WALL NODAL LENGTH
C          LWK          = WICK NODAL LENGTH
C          POROS        = WICK POROSITY
C          KWK          = WICK THERMAL CONDUCTIVITY
C          ODWK,IDWK    = WICK OUTER AND INNER DIAMETERS
C          CONDWA       = WALL AXIAL CONDUCTANCE
C          CONDWK       = WICK/LIQUID AXIAL CONDUCTANCE
C-----
C          REAL KWA, IDWA, LWA, LWK, KWK, IDWK
C          DIMENSION KWA(1),ODWA(1),IDWA(1),LWA(1),LWK(1),POROS(1)
C          DIMENSION KWK(1),ODWK(1),IDWK(1),CONDWA(1),CONDWK(1)
C          DO 10 I=1,N
C          CONDWA(I) = KWA(I) * PI * (ODWA(I)**2 - IDWA(I)**2)/(4.*LWA(I))
10 CONDWK(I) = (1.-POROS(I)) * KWK(I) * PI * (ODWK(I)**2 -
C          * IDWK(I)**2)/(4.* LWK(I))
C          RETURN
C          END
C*****
C          SUBROUTINE RSCOND(NCG,PI,LWA,KWA,ODWA,IDWA,LFT,KFT,ODR,IDR,
C          * LR,KR,ODFT,IDFT,LWK,POROS,KWK,ODWK,IDWK,
C          * IDFTW,IDPW,GFTTOT)
C-----
C          THIS SUBROUTINE COMPUTES THE TOTAL AXIAL CONDUCTANCE FROM THE
C          CONDENSER TO THE RESERVOIR OF A VCHP. THE SAME ASSUMPTIONS
C          USED IN SUBROUTINE AXCOND APPLY. THE WICKS USED IN THE CON-
C          DENSER, FEEDTUBE, AND RESERVOIR ARE ASSUMED TO BE IDENTICAL.
C          NCG          = FLAG FOR VCHP
C          LWA          = CONDENSER WALL NODAL LENGTH
C          KWA          = CONDENSER WALL THERMAL CONDUCTIVITY
C          ODWA,IDWA    = CONDENSER WALL OUTER AND INNER DIAMETERS
C          LFT          = FEED TUBE NODAL LENGTH
C          KFT          = FEED TUBE THERMAL CONDUCTIVITY
C          ODR,IDR      = RESERVOIR OUTER AND INNER DIAMETERS
C          LR          = RESERVOIR LENGTH
C          KR          = RESERVOIR THERMAL CONDUCTIVITY
C          ODFT,IDFT    = FEED TUBE OUTER AND INNER DIAMETERS
C          LWK          = CONDENSER WICK NODAL LENGTH
C          POROS        = WICK POROSITY
C          KWK          = WICK THERMAL CONDUCTIVITY
C          ODWK,IDWK    = CONDENSER WICK OUTER AND INNER DIAMETERS
C          IDFTW        = FEED TUBE WICK INNER DIAMETER (ODFTW = IDFT)
C          IDRW        = RESERVOIR WICK INNER DIAMETER (ODRW = IDR)
C          GFTTOT       = TOTAL AXIAL FEED TUBE CONDUCTANCE
C-----
C          REAL NCG, LWA, KWA, LFT, KFT, IDWA, IDFT, IDR, LR, KR

```

```

      REAL LWK, KWK, ICWK, IDFTW, IDRW
      IF (NCG .EQ. 0.) RETURN
      GWA = PI * KWA * (ODWA**2 - IDWA**2)/(2.* LWA)
      GFT = PI * KFT * (ODFT**2 - IDFT**2)/(4.* LFT)
      GR = PI * KP * (ODR**2 - IDR**2)/(2.* LR)
      GWK = PI * KWK * (1.- POROS)*(ODWK**2 - IDWK**2)/(4.* LWK)
      GFTW = PI * KWK * (1.- POROS)*(IDFT**2 - IDFTW**2)/(8.* LFT)
      GRW = PI * KWK * (1.- POROS)*(IDR**2 - IDRW**2)/(4.* LR)
      GFTTOT = 1./(1./GWA + 1./GFT + 1./GR) +
      * 1./(1./GWK + 1./GFTW + 1./GRW)
      RETURN
      ENC
C*****
      SUBROUTINE AGCOMB(NE,NA,NC,GAE,GAA,GAC,GWAE,GWAA,GWAC,
      * GWKE,GWKA,GWKC,NCTRAP,GFIN,GTOT)
C-----
C      THIS SUBROUTINE COMPUTES THE TOTAL AXIAL CONDUCTANCE OF THE
C      ARTERY, LIQUID-SATURATED WICK, AND WALL. THE RESULTS OF
C      SUBROUTINES ARTERY, AXCOND, AND RADFIN ARE REQUIRED, THUS
C      THOSE ROUTINES MUST BE CALLED BEFORE AGCOMB IN VARBL1.
C      N = NUMBER OF NODES IN EACH PIPE SECTION
C      GA = ARTERY CONDUCTANCE IN EACH SECTION
C      GWA = WALL CONDUCTANCE IN EACH SECTION
C      GWK = WICK/LIQUID CONDUCTANCE IN EACH SECTION
C      NCTRAP = COLD TRAP FLAG
C      GFIN = AXIAL FIN CONDUCTANCE
C      GTOT = TOTAL AXIAL CONDUCTANCE
C      E,A,C = PIPE SECTION: EVAP, ADIA, OR COND
C-----
      DIMENSION GAE(1),GAA(1),GAC(1),GWAE(1),GWAA(1),GWAC(1)
      DIMENSION GWKE(1),GWKA(1),GWKC(1),NCTRAP(1),GFIN(1),GTOT(1)
      DO 10 I=1,NE
      IF(NE .EQ. 1) GO TO 20
      10 GTOT(I) = 2./(1./GAE(I)+1./GAE(I+1)) + 2./(1./GWAE(I)
      * +1./GWAE(I+1)) + 2./(1./GWKE(I)+1./GWKE(I+1))
      20 GTOT(I) = 2./(1./GAE(I)+1./GAA(1)) + 2./(1./GWAE(I)
      * +1./GWAA(1)) + 2./(1./GWKE(I)+1./GWKA(1))
      II = NE + 1
      III = NE + NA
      DO 30 I=II,III
      J = I - NE
      IF(III .EQ. I) GO TO 40
      30 GTOT(I) = 2./(1./GAA(J)+1./GAA(J+1)) + 2./(1./GWAA(J)
      * +1./GWAA(J+1)) + 2./(1./GWKA(J)+1./GWKA(J+1))
      40 GTCT(I) = 2./(1./GAA(J)+1./GAC(1)) + 2./(1./GWAA(J)
      * +1./GWAC(1)) + 2./(1./GWKA(J)+1./GWKC(1))
      II = NE + NA + 1
      III = NE + NA + NC
      DO 50 I=II,III
      J = I - NE - NA
      IF(III .EQ. I) RETURN
      GTCT(I) = 2./(1./GAC(J)+1./GAC(J+1)) + 2./(1./GWAC(J)
      * +1./GWAC(J+1)) + 2./(1./GWKC(J)+1./GWKC(J+1))
      IF(NCTRAP(J) .EQ. 1) GTOT(I) = GTOT(I) + 2./
      * (1./GFIN(J)+1./GFIN(J+1))
      50 CONTINUE
      RETURN
      END
C*****
      SUBROUTINE RACOND(N,PI,EFFKWK,LWK,ODWK,IDWK,KWL,LWL,
      * GDWL,IDWL,COND)
C-----
C      THIS SUBROUTINE COMPUTES THE TOTAL RADIAL CONDUCTANCE OF THE
C      LIQUID-SATURATED WICK AND THE PIPE WALL. THE EFFECTIVE
C      THERMAL CONDUCTIVITY OF THE LIQUID-SATURATED WICK FROM SUB-
C      ROUTINE EFFKWK IS REQUIRED, THUS EFFKWK MUST BE CALLED RE-

```

```

C      FORE RACOND IN VARBL1.
C      N          = NUMBER OF CASES TO BE TREATED IN THIS CALL
C      EFFKWK     = LIQUID/WICK EFFECTIVE THERMAL CONDUCTIVITY
C      LWK        = WICK NODAL LENGTH
C      ODWK,IDWK  = WICK OUTER AND INNER DIAMETERS
C      KWL        = WALL THERMAL CONDUCTIVITY
C      LWL        = WALL NODAL LENGTH
C      ODWL,IDWL  = WALL OUTER AND INNER DIAMETERS
C      COND       = TOTAL RADIAL CONDUCTANCE
C-----
      REAL LWK,IDWK,KWL,LWL,IDWL
      DIMENSION EFFKWK(1),LWK(1),ODWK(1),IDWK(1),KWL(1),LWL(1)
      DIMENSION ODWL(1),IDWL(1),COND(1)
      DO 10 I=1,N
      CONDKW = 2.* PI * EFFKWK(I) * LWK(I)/ALOG(ODWK(I)/IDWK(I))
      CONDWL = 2.* PI * KWL(I) * LWL(I)/ALOG(ODWL(I)/IDWL(I))
10    COND(I) = 1./(1./CONDKW + 1./CONDWL)
      RETURN
      END
C*****
      SUBROUTINE PSLEAK(NCG,KINS,PI,ODR,XINS,LR,GLEAK)
C-----
C      THIS SUBROUTINE COMPUTES THE RESERVOIR-TO-SINK HEAT LEAK CONDUCTANCES
C      NCG      = FLAG FOR VCHP
C      KINS     = INSULATION THERMAL CONDUCTIVITY
C      ODR      = RESERVOIR OUTER DIAMETER
C      XINS     = INSULATION THICKNESS
C      LR       = RESERVOIR LENGTH
C      GLEAK    = RESERVOIR HEAT LEAK CONDUCTANCE
C-----
      REAL NCG, KINS, LR
      IF(NCG.EQ.0. .OR. XINS.LE.0.) RETURN
      GLEAK = 2.* PI * KINS * LR / ALOG((ODR + 2.* XINS)/ODR)
      RETURN
      END
C*****
      SUBROUTINE RADFIN(N,TR,TRL,TRR,COND,X,Y,Z,SIG,ASLOPE,EMISS,TEX,
      * TENV,QABSA,GSINK,AXFING,TSINK,QNODE,QTOT)
C-----
C      THIS SUBROUTINE COMPUTES THE EFFECTIVE SINK TEMPERATURE (SECONDARY
C      NODE) FOR A SPACE RADIATOR, ACCOUNTING FOR FIN GEOMETRY, ABSORBED
C      EXTERNAL ENERGY, AND CONDUCTION TO ADJACENT RADIATOR PANELS. IT
C      CONSIDERS END EFFECTS--FIN ROOT TEMPERATURES MUST BE INPUT SE-
C      QUENTIALLY. RADFIN SHOULD BE CALLED FROM VARBL1.
C      N          = NUMBER OF CASES TO BE TREATED IN THIS CALL
C      TR         = FIN ROOT TEMPERATURE
C      TRL        = LEFT SIDE ADJACENT FIN ROOT TEMPERATURE
C      TRR        = RIGHT SIDE ADJACENT FIN ROOT TEMPERATURE
C      COND       = FIN THERMAL CONDUCTIVITY
C      X          = FIN LENGTH (HALF PIPE-TO-PIPE DISTANCE)
C      Y          = FIN THICKNESS
C      Z          = FIN WIDTH (CONDENSER NODAL LENGTH)
C      SIG        = STEPHAN-BOLTZMANN CONSTANT (.1713E-8)
C      ASLOPE     = ARRAY OF NONDIMENSIONAL FIN TEMPERATURE
C                  GRADIENTS AS A FUNCTION OF ENVIRONMENT, ADJA-
C                  CENT PANEL TEMPERATURE, AND FIN GEOMETRY
C      EMISS      = PANEL EMISSIVITY
C      TEX        = EXTERNAL SURROUNDINGS TEMPERATURE
C      TENV       = ENVIRONMENT TEMPERATURE
C      QABSA      = ABSORBED EXTERNAL FLUX
C      GSINK      = RADIATION CONDUCTOR FROM ROOT TO EFFECTIVE SINK
C      AXFING     = AXIAL FIN CONDUCTANCE
C      TSINK      = EFFECTIVE SINK TEMPERATURE
C      QNODE      = HEAT REJECTED FROM EACH HEAT PIPE NODE
C      QTOT       = TOTAL HEAT REJECTED FROM ALL NODES IN THIS CALL
C-----

```



```

      DIMENSION TP(1),TRL(1),TRR(1),COND(1),X(1),Y(1),Z(1),EMISS(1)
      DIMENSION TEX(1),TENV(1),QARSA(1),GSINK(1),AXFING(1),TSINK(1)
      DIMENSION QNODE(1)
      QTOT = 0.
      DO 10 I=1,N
      IF(X(I).EQ.0.) GO TO 10
      C...CONVERT TEMPERATURES TO RANKINE
      TEXT = TEX(I) + 460.
      TROOT = TR(I) + 460.
      TROOTL = TRL(I) + 460.
      TROOTR = TRR(I) + 460.
      C...COMPUTE FIN PROFILE NUMBER
      PROFNO = SIG * EMISS(I) * X(I)**2 * TROOT**3 / (COND(I) * Y(I))
      IF(PROFNO.LT.0.OR.PROFNO.GT.4.) WRITE(6,1) PROFNO
      1 FORMAT(*0+++++ERROR+++++ PROFNO (*E12.5*) EXCEEDS BOUNDS*)
      C...COMPUTE ADJACENT ROCT TEMPERATURE RATIOS
      THETAL = TROOTL/TROOT
      IF(THETAL.LT.0.6.OR.THETAL.GT.1.5) WRITE(6,2) THETAL
      2 FORMAT(*0+++++ERROR+++++ THETAL (*E12.5*) EXCEEDS BOUNDS*)
      THETAR = TROOTR/TROOT
      IF(THETAR.LT.0.6.OR.THETAR.GT.1.5) WRITE(6,3) THETAR
      3 FORMAT(*0+++++ERROR+++++ THETAR (*E12.5*) EXCEEDS BOUNDS*)
      C...COMPUTE EFFECTIVE ENVIRONMENT TEMPERATURE AND TENVIR RATIO
      TENVIR = ((.828 * TEXT**4 + .J22 * TROOT**4
      * + QARSA(I)/SIG)/EMISS(I))**.25
      THETAET = TENVIR/TROOT
      IF(THETAET.LT.0.0.OR.THETAET.GT.2.0) WRITE(6,4) THETAET
      4 FORMAT(*0+++++ERROR+++++ THETAET (*E12.5*) EXCEEDS BOUNDS*)
      C...LOOK UP FIN GRADIENT AT ROOT
      CALL D3DEG1(THETAL,PROFNO,THETAET,ASLOPE,DTDXL)
      CALL D3DEG1(THETAR,PROFNO,THETAET,ASLOPE,DTDXR)
      C...COMPUTE HEAT REJECTION FROM EACH SIDE OF ROCT, AND TOTAL
      QL = -COND(I) * Z(I) * Y(I) * TROOT * DTDXL / X(I)
      QR = -COND(I) * Z(I) * Y(I) * TROOT * DTDXR / X(I)
      QNODE(I) = QL + QR
      C...COMPUTE SINK TEMPERATURE REQUIRED TO GIVE QNODE
      TSINK(I) = QNODE(I)/GSINK(I) + TR(I)
      C...CONVERT ENVIRONMENT TEMPERATURE TO FAHRENHEIT
      TENV(I) = TENVIR - 460.
      C...SUM HEAT REJECTION FOR EACH NODE INTO TOTAL PIPE HEAT REJECTION
      QTOT = QTOT + QNODE(I)
      C...COMPUTE FIN AXIAL CONDUCTANCE
      AXFING(I) = COND(I) * 2. * X(I) * Y(I) / Z(I)
      10 CONTINUE
      RETURN
      END
      C*****
      SUBROUTINE D3DEG1 (X, Y, Z, A, W)
      DIMENSION A(1), V(5)
      NT = A(1).OR.0
      N1 = A(2).OR.0
      N2 = A(3).OR.0
      V(1) = 4.0R.0
      V(2) = A(4)
      M1 = 2
      IF(Z.GT.A(4)) GO TO 200
      100 X1 = A(M1+1)
      A(M1+1) = (N1*N2+N1+M2+1).OR.0
      X2 = A(M1+2)
      A(M1+2) = N1.OR.0
      CALL D2DEG1 (X, Y, A(M1+1), W)
      A(M1+1) = X1
      A(M1+2) = X2
      RETURN
      200 M2 = M1+N1*N2+N1+M2+3
      IF(M2.GT.NT) GO TO 100

```

```

N3          = A(M2).OR.0
N4          = A(M2+1).OR.0
V(4)       = A(M2+2)
IF (Z.NE.A(M2+2))      GO TO 400
N1          = N3
N2          = N4
M1          = M2
GO TO 100
400 IF (Z.GT.A(M2+2))    GO TO 500
X1          = A(M1+1)
A(M1+1)     = (N1*N2+N1+N2+1).OR.0
X2          = A(M1+2)
A(M1+2)     = N1.OR.0
X3          = A(M2+1)
A(M2+1)     = (N3*N4+N3+N4+1).OR.0
X4          = A(M2+2)
A(M2+2)     = N3.OR.0
CALL D2DEG1 (X, Y, A(M1+1), V(3))
CALL D2DEG1 (X, Y, A(M2+1), V(5))
CALL D1DEG1 (Z, V(1), W)
A(M1+1)     = X1
A(M1+2)     = X2
A(M2+1)     = X3
A(M2+2)     = X4
RETURN
500 M1       = M2
N1          = N3
N2          = N4
V(2)       = V(4)
GO TO 200
END

```

```

C*****
C-----
SUBROUTINE FLFRNT(PVA,PVR,R,TR,VP,VC,N,K,PVS,TS,NN,LALC)
C-----

```

```

C THIS SUBROUTINE COMPUTES THE LOCATION OF THE INTERFACE BETWEEN
C WORKING VAPOR AND NONCONDENSIBLE GAS IN A VARIABLE CONDUCTANCE
C HEAT PIPE. THE PRINCIPLES OF CONSERVATION OF MASS AND THE PER-
C FECT GAS LAWS ARE EMPLOYED. PRESSURES ARE DERIVED FROM TEMPERA-
C TURES ACCORDING TO THE CLAPEYRON EQUATION. DIFFUSION EFFECTS
C ARE IGNORED, WHILE AXIAL CONDUCTION EFFECTS ARE CONSIDERED. THE
C RATIO OF ACTIVE CONDENSER LENGTH TO TOTAL CONDENSER LENGTH IS
C USED TO MODIFY THE VAPOR-TO-CONDENSER COUPLINGS TO SIMULATE THE
C SHUT-OFF PORTION OF THE CONDENSER. FLFRNT IS CALLED BY FRONT
C INTERNALLY.
C PVA = VAPOR PRESSURE IN THE ACTIVE PORTION OF THE PIPE
C PVR = VAPOR PARTIAL PRESSURE IN THE RESERVOIR
C P = UNIVERSAL GAS CONSTANT (1545)
C TR = RESERVOIR TEMPERATURE
C VR = RESERVOIR VOLUME
C VC = TOTAL CONDENSER VOLUME
C N = NUMBER OF MOLES OF NONCONDENSIBLE GAS IN PIPE
C K = NUMBER OF INACTIVE NODES (NOT NECESSARILY AN INTEGER)
C PVS = VAPOR PARTIAL PRESSURE IN EACH INACTIVE CONDENSER NODE
C TS = TEMPERATURE IN EACH INACTIVE CONDENSER NODE
C NN = TOTAL NUMBER OF CONDENSER NODES
C LALC = RATIO OF ACTIVE TO TOTAL CONDENSER LENGTHS
C-----

```

```

REAL N, K, LALC, KNEW
DIMENSION PVS(1),TS(1)
IF(N.EQ.0) GO TO 30
C--- KNEW = K + .02
C...ITERATE ON FRONT LOCATION
C--- DO 25 J=1,15
C--- IF(ABS(K-KNEW).LT. .01) RETURN
C--- K = KNEW
C--- K = K + 1.E-10

```

```

      TRR = TR + 46J.
      KK = INT(K)
C...SUM GAS DENSITY OVER ALL INACTIVE NODES
      SUM = 0.
      IF(KK.EQ. J) GO TO 2C
      DO 1. I=1, KK
      TSR = TS(NN+1-I) + 46J.
C....NODE TOTALLY BLANKETED
      SUM = SUM + (PVA - PVS(NN+1-I))/(R * TSR)
      10 CONTINUE
C....NODE PARTIALLY BLANKETED
      20 SUM = SUM + (K-FLOAT(KK))*(PVA - PVS(NN-KK))/(R *
      * (TS(NN-KK)+46J.))
      IF(ABS(SUM) .LT. 1.E-50) GO TO 3J
C...COMPUTE FRONT LOCATION
      LALC = 1.+ (((PVA - PVR)/(R * TRR)) * (VR/VC) - N/(144.*VC))
      * K / SUM)
C...ADJUST TO BETWEEN 0 AND 1
      IF(LALC .GT. 1.) LALC = 1.
      IF(LALC .LT. 0.) LALC = 0.
C--- KNEW = (1.-LALC) * FLOAT(NN)
C---25 CONTINUE
C...WRITE MESSAGE IF CONVERGENCE IS NOT SATISFIED
C--- DELTA = K - KNEW
C--- WRITE(6,40) DELTA
C---40 FCPMAT(*3+++++ CAUTION ++++ NO LA/LC CONVERGENCE, DELTA =*,
C--- * F8.4,* ACTIVE NODES*)
      RETURN
      30 LALC = 1.
      RETURN
      END

```

```

C*****
      SUPROUTINE ADJG(NCG,NC,LC,LACT,GCOND)

```

```

C-----
C      THIS SUBROUTINE ADJUSTS THE CONDENSER COUPLINGS OF A VCHP
C      TO SIMULATE THE LOCATION OF THE VAPOR/GAS INTERFACE.
C      NCG = FLAG FOR VCHP
C      NC = NO OF CONDENSER NODES
C      LC = CONDENSER NODAL LENGTH
C      LACT = ACTIVE CONDENSER LENGTH
C      GCOND = FIRST CONDENSER WALL-TO-VAPOR COUPLING
C-----

```

```

      REAL NCG, LC, LACT
      DIMENSION LC(1),GCOND(1)
      IF(NCG.EQ. 0.) RETURN
      CL = 0.
      DO 30 I=1,NC
      CL = CL + LC(I)
      IF(CL .LE. LACT) GO TO 30
      10 IF(CL-LC(I) .GE. LACT) GO TO 20
      GCOND(I) = ((LACT - (CL-LC(I))) / LC(I)) * GCOND(I)
      GO TO 30
      20 GCOND(I) = 0.
      30 CONTINUE
      RETURN
      END

```

```

C*****
      SUBROUTINE LIMITS(A,M,G,TV,TE,PI,GC,H,DR,SH,APRSS1,APRSS2)

```

```

C-----
C      THIS SUBROUTINE COMPUTES THE MAXIMUM HEAT LOAD CAPABILITY
C      OF A HEAT PIPE. THIS MAXIMUM LOAD IS LIMITED BY THE CAPIL-
C      LARY RETURN MECHANISM (WICKING LIMIT), CHOKED VAPOR FLOW
C      (SONIC LIMIT), THE INTERACTION BETWEEN VAPOR AND LIQUID AT
C      THE WICK SURFACE (ENTRAINMENT LIMIT), AND THE TENDENCY TO
C      FORM BUBBLES IN THE EVAPORATOR WICK (POILING LIMIT). A
C      FIFTH LIMIT OCCURS WHEN AN ARTERY IS INTRODUCED, SINCE THE

```

C ABILITY OF CAPILLARY FORCES TO FILL THE ARTERY IS A FUNCTION
 C OF APPLIED HEAT LOAD (ARTERY SELF-PRIMING LIMIT). SUBROUTINE
 C LIMITS CALLS ON SUBROUTINE PERML. IF THE PIPE HEAT LOAD
 C EXCEEDS THE LOWEST LIMIT, THE PERCENT OVERLOAD IS PRINTED.
 C IF NO LIMITS ARE EXCEEDED, THE PERCENT UNDERLOAD IS PRINTED.
 C ALSO OUTPUT ARE VAPOR AND LIQUID PRESSURE DROPS, ABSOLUTE PRES-
 C SURES, AND MASS FLOWRATE. LIMITS SHOULD BE CALLED FROM VARBL2
 C FOR TRANSIENT ANALYSES, EXECUTION FOR STEADY-STATE.
 C A = INTEGER COUNT LOCATION OF FIRST HEAT PIPE ARRAY.
 C HEAT PIPE ARRAYS MUST BE INPUT AS A BLOCK
 C IN THE ORDER SHOWN IN THE ARRAY DATA.
 C M = SAME AS A. USED TO ALLOW ACCESS TO INTEGER
 C COUNTS AND INTEGER ARRAY DATA VALUES.
 C G = FIRST HEAT PIPE EVAPORATOR-TO-VAPOR COUPLING.
 C HEAT PIPE CONDUCTORS MUST BE INPUT AS A BLOCK
 C IN THE ORDER SHOWN IN THE CONDUCTOR DATA.
 C TV = FIRST HEAT PIPE VAPOR TEMPERATURE.
 C TE = FIRST HEAT PIPE EVAPORATOR WALL TEMPERATURE.
 C HEAT PIPE NODES MUST BE INPUT AS A BLOCK
 C IN THE ORDER SHOWN IN THE NODE DATA.
 C GC = CONSTANT RELATING MASS AND FORCE (G SURF)
 C H = MECHANICAL EQUIVALENT OF HEAT
 C DR = DEGREES/RADIAN
 C SH = NO OF SECONDS**2 PER HOUR**2
 C APRESS = SATURATION PRESSURE VS TEMPERATURE ARRAY
 C -----

DIMENSION A(1),M(1),G(1),TV(1),TE(1)
 REAL MUL, MUV, KL, KV, MDOT
 N = M(1)
 N1 = N2 = N3 = NN = 1
 I1 = I2 = I3 = 1
 DO 1000 I=1,N
 II = M(1) + 1
 J = M(II+1) + 1
 K = M(3*II+6*J+1) + 1
 L = M(5*II+6*J+6*K+1) + 1
 JJ = M(26*II+34*J+33*K+42*L+1) + 1
 KK = M(27*II+34*J+33*K+42*L+JJ+1) + 1
 LL = M(28*II+34*J+33*K+42*L+JJ+KK+1) + 1
 EVAPL = A(II+6*J+1+I)
 ADIAL = A(3*II+6*J+6*K+1+I)
 CONDL = A(5*II+6*J+6*K+6*L+1+I)
 QLAT = A(33*II+47*J+46*K+55*L+JJ+KK+LL+1+I) = G(NN) *
 * (TE(N1) - TV(II))
 ACTL = A(46*II+49*J+48*K+59*L+JJ+KK+LL+1+I) * CONDL
 DENL = A(28*II+47*J+39*K+48*L+JJ+KK+LL+1+N2)
 DENV = A(28*II+47*J+46*K+55*L+JJ+KK+LL+1+I)
 CPL = A(28*II+47*J+46*K+48*L+JJ+KK+LL+1+N2)
 CPV = A(29*II+47*J+46*K+55*L+JJ+KK+LL+1+I)
 MUL = A(28*II+47*J+41*K+48*L+JJ+KK+LL+1+N2)
 MUV = A(30*II+47*J+46*K+55*L+JJ+KK+LL+1+I)
 KL = A(28*II+47*J+42*K+48*L+JJ+KK+LL+1+N2)
 KV = A(31*II+47*J+46*K+55*L+JJ+KK+LL+1+I)
 SURFT = A(28*II+47*J+43*K+48*L+JJ+KK+LL+1+N2)
 HFG = A(28*II+47*J+44*K+48*L+JJ+KK+LL+1+N2)
 HFS = A(28*II+47*J+45*K+48*L+JJ+KK+LL+1+N2)
 IF(I.LE. 6) CALL D1DEG1(TE(NN),APRSS1,PEVAP)
 IF(I.GT. 6) CALL D1DEG1(TE(NN),APRSS2,PEVAP)
 A(39*II+47*J+46*K+55*L+JJ+KK+LL+1+N1) = PEVAP
 C....WICKING LIMIT
 IFLAG = 0
 DPCAP = 2.* SURFT * COS(A(6*II+21*J+21*K+21*L+1+I)/DR) /
 * A(6*II+15*J+6*K+6*L+1+N1)
 DPCAPI = DPCAP / 144.
 C
 DPROD = DENL * A(8*II+21*J+21*K+21*L+1+I) * (A(1J*II+21*J


```

*      +21*K+21*L+1+I)*(EVAPL+ADIAL+ACTL) * CCS(A(9*II
*      +21*J+21*K+21*L+1+I)/DP) + (A(II+4*J+1+N1)+A(3*II
*      +6*J+4*K+1+N2)+A(5*II+6*J+6*K+4*L+1+N3))/3.3
*      * SIN(A(9*II+21*J+21*K+21*L+1+I)/DR)) / GC

```

OP900I = OP8CD / 144.

C

```

CALL PERMPL(M(6*II+6*J+6*K+6*L+1+N1),A(6*II+10*J+6*K+6*L+1+N1),
* A(6*II+11*J+6*K+6*L+1+N1),A(6*II+18*J+6*K+6*L+1+N1),
* A(6*II+19*J+6*K+6*L+1+N1),A(6*II+20*J+6*K+6*L+1+N1),
* M(11*II+21*J+21*K+30*L+1+N1),A(11*II+22*J+21*K+30*L+1+N1),
* A(11*II+23*J+21*K+30*L+1+N1),A(11*II+32*J+21*K+30*L+1+N1),
* A(26*II+34*J+33*K+42*L+1+I),M(25*II+34*J+33*K+42*L+1+I),
* A(11*II+27*J+21*K+30*L+1+N1),A(11*II+24*J+21*K+30*L+1+N1),
* A(11*II+25*J+21*K+30*L+1+N1),A(6*II+16*J+6*K+6*L+1+N1),
* A(28*II+37*J+36*K+45*L+JJ+KK+LL+1+N1),PI,DR)
CALL PERMPL(M(6*II+21*J+6*K+6*L+1+N2),A(6*II+21*J+10*K+6*L+1+N2),
* A(6*II+21*J+11*K+6*L+1+N2),A(6*II+21*J+18*K+6*L+1+N2),
* A(6*II+21*J+19*K+6*L+1+N2),A(6*II+21*J+20*K+6*L+1+N2),
* M(11*II+34*J+21*K+30*L+1+N2),A(11*II+34*J+22*K+30*L+1+N2),
* A(11*II+34*J+23*K+30*L+1+N2),A(11*II+34*J+32*K+30*L+1+N2),
* A(27*II+34*J+33*K+42*L+JJ+1+I),M(26*II+34*J+33*K+42*L+JJ+1+I),
* A(11*II+34*J+27*K+30*L+1+N2),A(11*II+34*J+24*K+30*L+1+N2),
* A(11*II+34*J+25*K+30*L+1+N2),A(6*II+21*J+16*K+6*L+1+N2),
* A(28*II+38*J+36*K+45*L+JJ+KK+LL+1+N2),PI,DR)
CALL PERMPL(M(6*II+21*J+21*K+6*L+1+N3),A(6*II+21*J+21*K+10*L+1+
* N3),A(6*II+21*J+21*K+11*L+1+N3),A(6*II+21*J+21*K+18*L+1+N3),
* A(6*II+21*J+21*K+19*L+1+N3),A(6*II+21*J+21*K+20*L+1+N3),
* M(11*II+34*J+33*K+30*L+1+N3),A(11*II+34*J+33*K+31*L+1+N3),
* A(11*II+34*J+33*K+32*L+1+N3),A(11*II+34*J+33*K+41*L+1+N3),
* A(28*II+34*J+33*K+42*L+JJ+KK+1+I),M(27*II+34*J+33*K+42*L+
* JJ+KK+1+I),A(11*II+34*J+33*K+36*L+1+N3),A(11*II+34*J+33*K+33*L+
* 1+N3),A(11*II+34*J+33*K+34*L+1+N3),A(6*II+21*J+21*K+16*L+1+N3),
* A(28*II+38*J+37*K+45*L+JJ+KK+LL+1+N3),PI,DR)
SOPLIQ = .5* MUL * EVAPL / (SH * GC * DENL * HFG * A(28*II+
* 37*J+36*K+45*L+JJ+KK+LL+1+N1)) +
* MUL * ADIAL / (SH * GC * DENL * HFG * A(28*II+
* 38*J+36*K+45*L+JJ+KK+LL+1+N2)) +
* .5* MUL * ACTL / (SH * GC * DENL * HFG * A(28*II+
* 38*J+37*K+45*L+JJ+KK+LL+1+N3))
DPLIQI = SOPLIQ * GLAT / 144.

```

C

```

SOPVPA = 128.* MUV * ADIAL / (PI * SH * GC * HFG * DENL
* A(28*II+37*J+35*K+44*L+JJ+KK+LL+1+N2)**4)
OPVPAI = SOPVPA * GLAT / 144.

```

C

150 IF(OPBOD .GE. DPCAP) GO TO 230

C

```

ORWL = 0.
REI = 40.
RES = 40.
DO 220 M4M = 1,50
SDPVPE = 8.* MUV * EVAPL / (PI * SH * GC * HFG * DENL
* A(28*II+36*J+35*K+44*L+JJ+KK+LL+1+N1)**4
* (.J481+.J49+/(4.7+REI)**.8))
OPVPEI = SDPVPE * GLAT / 144.

```

C

```

IF(ARS(RES) .LT. 4.5975) GO TO 200
SOPVPC = 32./(PI**2 * SH * GC * DENL * HFG**2 * A(28*II+
* 37*J+36*K+44*L+JJ+KK+LL+1+N3)**4)
OPVPCI = SOPVPC * GLAT**2 / 144.

```

C

```

ORWL = (-(SOPLIQ+SOPVPA+SOPVPE) + SQRT((SOPLIQ
+ SOPVPA+SOPVPE)**2 - 4.*SOPVPC*(OPBOD-
DPCAP)))/(2.*SOPVPC)

```

C

GO TO 210

```

200 SDPVPC = 8.* MUV * ACTL / IPI * SH * GC * HFG * DENV
*      * A(28*II+37*J+36*K+44*L+JJ+KK+LL+1+N3)**4
*      * (.0481+.0494/(4.7-ARS(RES))**.8))
DPVPCI = SDPVPC * GLAT / 144.

C
QWL = (DPCAP-CPBOD)/(SDPLIQ+SDPVPE+SDPVPA+SDPVPC)

C
210 DQWL = ARS(QWL-DQWL)
IF(DQWL.LT..05) GO TO 260
DQWL = QWL
REI = A(40*II+48*J+47*K+56*L+JJ+KK+LL+1+I) = QWL /
*      (PI * HFG * EVAPL * MUV)
RES = A(41*II+48*J+47*K+56*L+JJ+KK+LL+1+I) = QWL /
*      (PI * HFG * ACTL * MUV)

220 CONTINUE
GO TO 240

230 QWL = 0.
GO TO 260

2 WRITE(6,250) I, DQWL, IFLAG
250 FORMAT(*0++++CAUTION++++ MORE THAN 50 ITERATIONS REQUIRED *
*      * TO COMPUTE QWL FOR PIPE*,I2,* --- DQWL = *,F10.3,
*      * STU/HR, IFLAG =*,I2)

260 IF(IFLAG.EQ.1) GO TO 261
QWLIM = A(34*II+47*J+46*K+55*L+JJ+KK+LL+1+I) = QWL
GO TO 262

261 QPRIM = QWL
GO TO 266

262 WRITE(6,265) I, DPCAPI, DPBODI, DPLIGI, DPVPAI, DPVPEI, DPVPCI
265 FORMAT(*0 PRESSURE ORCFS FOR PIPE*,I2,* ---*/ * DPCAP =*,
*      * E12.4,* PSID*/ * DPBOD =*,E12.4,* PSID*/ * DPLIQ =*,
*      * E12.4,* PSID*/ * DPVFA =*,E12.4,* PSID*/ * DPVPE =*,
*      * E12.4,* PSID*/ * DPVPC =*,E12.4,* PSID*)

C...ARTERY SELF-PRIMING LIMIT
IF(M(11*II+21*J+21*K+30*L+1+N1).EQ.0.AND.
*      M(11*II+34*J+21*K+30*L+1+N2).EQ.0.AND.
*      M(11*II+34*J+33*K+30*L+1+N3).EQ.0) GO TO 266
DPCAP = 2.* SURFT * COS(A(6*II+21*J+21*K+21*L+1+I)/DR) /
*      A(11*II+33*J+21*K+30*L+1+N1)
IFLAG = 1
GO TO 150

C....SONIC LIMIT
266 OSLIM = A(35*II+47*J+46*K+55*L+JJ+KK+LL+1+I) = DENV * HFG *
*      PI * A(28*II+36*J+35*K+44*L+JJ+KK+LL+1+N1)**2 * SQRT(A
*      (7*II+21*J+21*K+21*L+1+I) * A(39*II+47*J+46*K+55*L
*      +JJ+KK+LL+1+N1) * SH * GC * 144./(2.* DENV * (A
*      (7*II+21*J+21*K+21*L+1+I)+1.)))/4.

C....ENTRAINMENT LIMIT
QELV = PI * A(28*II+36*J+35*K+44*L+JJ+KK+LL+1+N1)**2
*      * HFG * SQRT(SURFT*SH*GC*DENV/A(6*II+17*J+6*K
*      +6*L+1+N1))/4.
QELAD = PI * A(28*II+37*J+35*K+44*L+JJ+KK+LL+1+N2)**2
*      * HFG * SQRT(SURFT*SH*GC*DENV/A(6*II+21*J+17*K
*      +6*L+1+N2))/4.
QELCO = PI * A(28*II+37*J+36*K+44*L+JJ+KK+LL+1+N3)**2
*      * HFG * SQRT(SURFT*SH*GC*DENV/A(6*II+21*J+21*K
*      +17*L+1+N3))/4.
QELIM = A(36*II+47*J+46*K+55*L+JJ+KK+LL+1+I) = AMIN1(QELV,
*      QELAD,QELCO)

C....BOILING LIMIT
QBLIM = A(37*II+47*J+46*K+55*L+JJ+KK+LL+1+I) = 2.* PI *
*      (TE(N1)+460.) * SURFT * EVAPL * (A(6*II+10*J+
*      6*K+6*L+1+N1)+A(6*II+11*J+6*K+6*L+1+N1)) * A(42*II
*      +48*J+47*K+56*L+JJ+KK+LL+1+N1) / (H * HFG * DENV *
*      A(6*II+12*J+6*K+6*L+1+N1) * (A(6*II+10*J+6*K+6*L+1
*      +N1)-A(6*II+11*J+6*K+6*L+1+N1)))
WRITE(6,270) I, QWLIM, OSLIM, QELIM, QBLIM

```

```

270 FORMAT(*G LIMITS FOR PIPE*,I2,* ---*/* WICKING LIMIT =*,
* F15.3,* BTU/HR*/* SCNIC LIMIT =*,F15.3,* BTU/HR*/
* * ENTRAINMENT LIMIT =*,F15.3,* BTU/HR*/* BOILING *,
* * LIMIT =*,F15.3,* BTU/HR*)
IF(IFLAG .EQ. 1) WRITE(6,275) GPRIM
275 FORMAT(* ARTERY SELF-*/7X,*PRIMING LIMIT =*,F15.3,
* * BTU/HR*)
C...COMPUTE MIN LIMIT AND OPERATING POINT OF PIPE
QMLIM = A(38*II+47*J+46*K+55*L+JJ+KK+LL+1+I) = AMIN1(QWLM,
* QSLIM,QELIM,QBLIM)
IF(QMLIM .EQ. 0) QMLIM = 1.E-10
PCTLM = QLAT / QMLIM * 100.
IF(QMLIM .GE. QLAT) WRITE(6,280) I, PCTLM
IF(QMLIM .LT. QLAT) WRITE(6,290) I, PCTLM
280 FORMAT(*G PIPE*,I2,* OPERATING AT*,F12.3,* PERCENT OF LIMIT*)
290 FORMAT(*J PIPE*,I2,* LOAD ABOVE CAPACITY BY*,F15.3* PERCENT*)
C...COMPUTE MASS FLOWRATE
MDOT = A(32*II+47*J+46*K+55*L+JJ+KK+LL+1+I) = QLAT / HFG
WRITE(6,300) I, MDOT
300 FORMAT(*J PIPE*,I2,* MASS FLOWRATE =*,E12.4,* LBM/HR*)
N1 = N1 + M(1+I)
N2 = N2 + M(2*II+6*J+1+I)
N3 = N3 + M(4*II+6*J+6*K+1+I)
NN = NN + M(1+I) + M(2*II+6*J+1+I) + M(4*II+6*J+6*K+1+I)
I1 = I1 + M(25*II+34*J+33*K+42*L+1+I)
I2 = I2 + M(26*II+34*J+33*K+42*L+JJ+1+I)
I3 = I3 + M(27*II+34*J+33*K+42*L+JJ+KK+1+I)
1000 CONTINUE
RETURN
END

FSTOP
C*****
F SURFOUTINE FRONT
C-----
C THIS SUBROUTINE PROVIDES THE LOGIC REQUIRED TO CONTROL THE
C ITERATIVE FRONT LOCATION SOLUTION. DUE TO THE VARIATIONS
C IN SENSITIVITY OF WORKING FLUID, NONCONDENSIBLE GAS, AND
C GEOMETRY COMBINATIONS, THIS ROUTINE WILL PROBABLY REQUIRE
C MODIFICATION TO ACHIEVE PROPER DAMPING AND CONTROL. FRONT
C CALLS FLFRNT INTERNALLY, AND REQUIRES PLACEMENT IN EJECTN
C FOR STEADY-STATE CASES, AND IN VARBL2 FOR TRANSIENT CASES.
C-----
FCALL COMMON
I = ITEST
N = M520+I
N1 = IDUM
N2 = JDUM
N3 = KDUM
L = MDUM
LOOKUP(M500+I,T101+N1-1,A1012,A758+N1)
LOOKUP(M510+I,T102+N2-1,A1012,A759+N2)
LOOKUP(M520+I,T103+N3-1,A1012,A760+N3)
D10EG1(T119+L-1,A1012,A761+I)
A832+I = A820+I
VC = 0.
DO 5 II=1,N
5 VC = VC + A526+N3+II-1 * R1 * A689+N3+II-1**2 / 4.
A836+I = (A527+I - A820+I) / A526+N3
IF(A836+I .GT. FLOAT(N)) A836+I = FLOAT(N)
IF(A836+I .LT. 0.) A836+I = 0.
FLFRNT(A759+N2,A761+I,R7,T119+L-1,A809+I,VC,A808+I,
* A836+I,A760+N3,T103+N3-1,M520+I,A810+I)
WRITE (6,98) I, A810+I
F 98 FORMAT(*C PIPE *,I2,* LA/LC (PRELIM) = *,F10.4)
A820+I = A527+I * A810+I
DELTA = A820+I - A832+I

```

```

IF (ABS(DELTA) .LT. .05 * A526+N3)      GO TO 100
IF (MOD(M781+I,2) .EQ. 0)                A841+I = DELTA
IF (MOD(M781+I,2) .EQ. 1)                A842+I = DELTA
C--- IF (MOD(M781+I,3) .EQ. 2)            A843+I = DELTA
      IF ((A841+I.GT.0..AND.A842+I.LT.0.) .OR.
          (A841+I.LT.0..AND.A842+I.GT.0.))
      *   A844+I = A844+I * 2.
      IF (DELTA .GT. A526+N3)      A820+I = A832+I + A526+N3/A844+I
      IF (DELTA .LT. -A526+N3)     A820+I = A832+I - A526+N3/A844+I
      IF (DELTA.GT.0. .AND. DELTA.LT.A526+N3)
      *   A820+I = A832+I + A526+N3 / A844+I / 4.
      IF (DELTA.LT.0. .AND. DELTA.GT.-A526+N3)
      *   A820+I = A832+I - A526+N3 / A844+I / 4.
      A810+I = A820+I / A527+I
      WRITE (6,99) I, A810+I
F 99  FORMAT(* PIPE *,I2,* LA/LC (FINAL) = *,F10.4)
      IF (ABS(A820+I-A832+I) .LT. .01 * A526+N3) GO TO 60
      IF (M781+I .GT. 40)      GO TO 50
      M781+I = (M781+I) + 1
      M783+I = 0
      RETURN
      50  WRITE (6,51)
F 51  FORMAT(*J++++CAUTION++++ FRONT LOCATION NOT SOLVED IN 40 *
F    * *ITERATIONS*)
      GO TO 100
      60  WRITE (6,61)
F 61  FORMAT(*G++++NOTE++++ FRONT LOCATION CHANGING LESS THAN*
F    * * 1 PERCENT OF NODE LENGTH EACH ITERATION, ACCEPTING*)
      100 M783+I = 1
      RETURN
F      END
      END
      RCD 3END OF DATA

```

```

*****      CJCJICJ  //// END OF LIST ////
*****      CJCJICJ  //// END OF LIST ////

```


ATTACHMENT 2
SUBROUTINES DISCUSSION

2. HEAT PIPE MODELING

A. GOVERNING EQUATIONS FOR FIXED-CONDUCTANCE NON-ARTERIAL PIPES

The heat pipe is a device which transfers heat nearly isothermally through the vaporization and condensation of a working fluid within a closed container. Referring to Figure 2-1, the processes occurring within the heat pipe are: 1) vaporization of the working fluid in the evaporator due to heat input, 2) flow of the resulting vapor toward the condenser due to the pressure difference created by the evaporator/condenser temperature difference, 3) condensation of the vapor in the condenser due to heat removal, and 4) flow of the condensate toward the evaporator due to the capillary pumping action of the wick material.

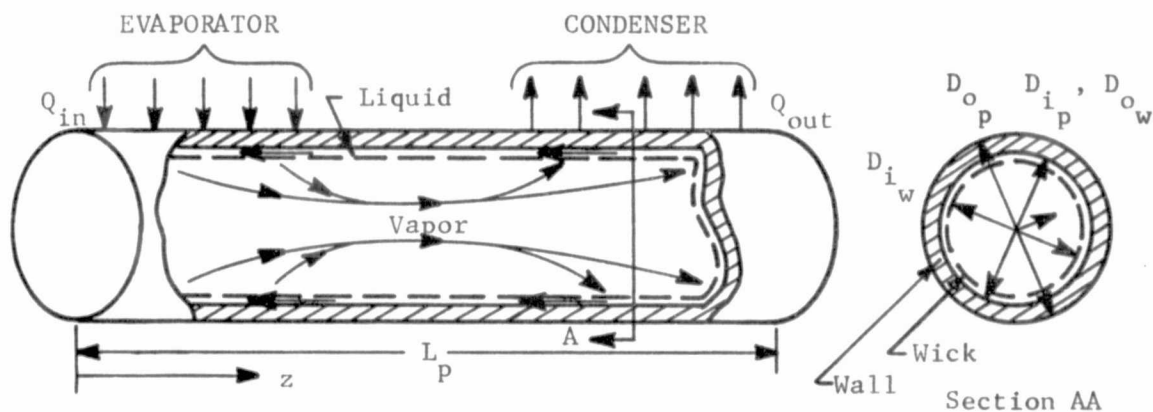


Figure 2-1 Heat Pipe Geometry

Each of these processes, as well as the more conventional heat transfer by axial and radial conduction, will be treated in this section. The limitations on heat pipe performance will also be briefly discussed.

1. Capacitance

The capacitances (mass x specific heat) of the basic part of the heat pipe are computed in subroutines CAPWCK and CAPFIN. The capacitance of the vapor is assumed to be negligible due to its low density and heat capacity. The pipe wall capacitance, C_p , is

$$C_p = \rho_p C_{p_p} \pi (D_o^2 - D_i^2) L_p / 4. \quad (2-1)$$

The capacitance of the liquid/wick combination matrix $C_{l/w}$ is equal to the sum of the liquid capacitance and the wick material capacitance:

$$\begin{aligned} C_{l/w} &= C_{\text{liquid}} + C_{\text{wick}} \\ &= \left[\phi_w \rho_l C_{p_l} + (1 - \phi_w) \rho_w C_{p_w} \right] \pi (D_o^2 - D_i^2) L_w / 4, \end{aligned} \quad (2-2)$$

where the porosity ϕ_w or void fraction of the wick is used to separate the liquid and wick material components of the liquid/wick matrix.

The inputs required for subroutine CAPWCK are ρ_p , C_{p_p} , π , D_{o_p} , D_{i_p} , L_p , ϕ_w , ρ_l , C_{p_l} , ρ_w , C_{p_w} , D_{o_w} , D_{i_w} , and L_w and the CAPFIN and ARTERY capacitances, from subroutines CAPFIN and ARTERY respectively if applicable. The capacitance of each pipe section is output. There are no restrictions to the use of CAPWCK. The subroutine has sufficient flexibility to allow various wick structures and dissimilar wick and wall materials.

The radiator fin capacitance is obtained by calling subroutine CAPFIN. This routine provides an automated means of updating the fin node capacitances in a "DO" loop by the equation

$$C_f = V_f \rho_f C_{p_f}.$$

The calling sequence is

CAPFIN (N, X, Y, Z, DEN, CP, CAP)

where N = number of fin nodes

X = fin length ($\frac{1}{2}$ distance between tubes)

Y = fin thickness

Z = fin width (condenser length)

DEN = fin density

CP = fin specific heat

CAP = fin capacitance of node

2. Axial Conductance

The conductances (thermal conductivity x cross-sectional area/ heat flow path length) of the heat pipe in the axial direction are computed in subroutines AXCOND and AGCØMB. The conductance of the vapor is assumed very small due to its low thermal conductivity. The pipe wall axial conductance $G_{p,ax}$ in any node is given by

$$G_{p,ax} = \frac{1}{\left[\frac{L_p/2}{k_p \pi (D_o^2 - D_i^2)/4} \right]_1 + \left[\frac{L_p/2}{k_p \pi (D_o^2 - D_i^2)/4} \right]_2},$$

or

$$G_{p,ax} = \frac{1}{\left[\frac{2L_p}{k_p \pi (D_o^2 - D_i^2)} \right]_1 + \left[\frac{2L_p}{k_p \pi (D_o^2 - D_i^2)} \right]_2}. \quad (2-3)$$

The axial conductance of the liquid/wick matrix $G_{l/w,ax}$ is equal to the sum of the liquid conductance and the wick material conductance. However, the liquid conductance is small compared with the wick when the axial distance is large compared with the wick thickness. Therefore

$$G_{l/w,ax} = G_{w,ax} = \frac{1}{\left[\frac{L_w/2}{k_w \pi \left(\frac{D_{o_w}^2 - D_{i_w}^2}{4} \right) \left(\frac{1-\phi_w}{2} \right)} \right]_1 + \left[\frac{L_w/2}{k_w \pi \left(\frac{D_{o_w}^2 - D_{i_w}^2}{4} \right) \left(\frac{1-\phi_w}{2} \right)} \right]_2}$$

or

$$G_{w,ax} = \frac{1}{\left[\frac{4L_w}{k_w \pi (D_{o_w}^2 - D_{i_w}^2) (1-\phi_w)} \right]_1 + \left[\frac{4L_w}{k_w \pi (D_{o_w}^2 - D_{i_w}^2) (1-\phi_w)} \right]_2} \quad (2-4)$$

Again the porosity ϕ_w is used to isolate the wick material. For symmetrical (screen-type) wicks, contact resistance between axial and circumferential wick components effectively removes the circumferential components' contribution to axial heat transfer. Therefore, the wick cross-sectional area

$$\pi \left(\frac{D_{o_w}^2 - D_{i_w}^2}{4} \right) (1-\phi_w)$$

is halved to isolate the axial wick components' contribution. For unsymmetrical wicks (grooves, axial wires, etc.), the appropriate effective porosity is used. Subroutine AXCOND is

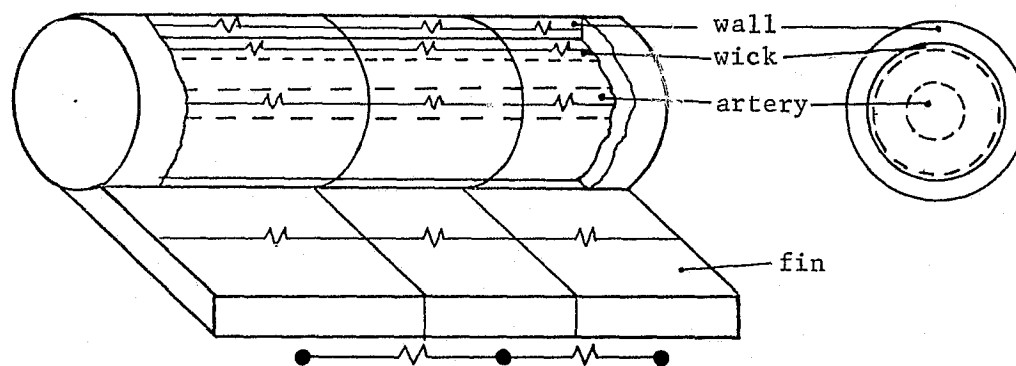
used to compute the axial conduction of each node; subroutine AGCOMB is used to combine the axial conductances of each node in a node center to node center overall conductance.

The inputs to subroutine AXCOND are π , k_p , D_{o_p} , D_{i_p} , L_p , k_w , D_{o_w} , D_{i_w} , L_w and ϕ_w . The wall and wick conductances are output. The

only restriction to the use of AXCOND is its assumption: small liquid conductance compared with the wick material. This subroutine is flexible enough to accommodate various wick structures and dissimilar wall and wick materials.

The total axial conductance of the pipe section is then evaluated by subroutine AGCOMB. This routine will treat all pipes including those containing arteries. The routine must be called after calls to ARTERY, AXCOND, and RADFIN in Variables 1.

The results of the above calls yield the following conductances which must be combined reducing to a single axial conductance between node centers.



The calling sequence is

AGCOMB(NE,NA,NC,GAE,GAA,GAC,GWAE,GWAA,GWAC,GWKE,GWKA,GWKC,NCTRAP,
GFIN,GTOT)

where

N	=	NUMBER OF NODES IN EACH PIPE SECTION
GA	=	ARTERY CONDUCTANCE IN EACH SECTION
GWA	=	WALL CONDUCTANCE IN EACH SECTION
GWK	=	WICK/LIQUID CONDUCTANCE IN EACH SECTION
NCTRAP	=	COLD TRAP FLAG
GFIN	=	AXIAL FIN CONDUCTANCE
GTOT	=	TOTAL AXIAL CONDUCTANCE
E,A,C,	=	PIPE SECTION: EVAP, ADIA, OR COND

3. Radial Conductance

The conductances of the heat pipe in the radial direction are computed in subroutine RACOND. The radial conductance of the pipe wall, $G_{p,r}$, is computed as

$$G_{p,r} = \frac{2\pi k_p L_p}{\ln(D_{o_p}/D_{i_p})} \quad (2-5)$$

The radial conductance of the liquid/wick matrix, $G_{\ell/w,r}$, is computed by

$$G_{\ell/w,r} = \frac{2\pi k_{\ell/w} L_w}{\ln(D_{o_w}/D_{i_w})} \quad (2-6)$$

where the effective thermal conductivity of the liquid/wick matrix $k_{\ell/w}$ is computed in subroutine EFKWK, using the methods of Gorring and Churchill for screen wicks (Ref. 1) as discussed in Section 2-A-6. $G_{p,r}$ and $G_{\ell/w,r}$ are combined into

$$G_r = \frac{1}{\frac{1}{G_{p,r}} + \frac{1}{G_{\ell/w,r}}} \quad ,$$

the total radial conductance.

The inputs to subroutine RACOND are π , k_p , L_p , D_{o_p} , D_{i_p} , $k_{\ell/w}$, L_w , D_{o_w} , and D_{i_w} . The conductance is output. No restrictions exist for this subroutine, and it can handle dissimilar wall and wick materials.

4. Flow Effects

The enthalpy change in the flowing liquid in the heat pipe G_{enth} is computed by

$$G_{enth} = \dot{m} C_p \quad (2-7)$$

$$\text{where the mass flow rate } \dot{m} = \frac{Q}{hfg} \quad (2-8)$$

The processes of evaporation and condensation occurring within the pipe are associated with small pressure drops. Since the vapor and liquid are in equilibrium with each other within the closed system, the Clausius-Clapeyron equation relating temperature and pressure at saturation conditions is applicable:

$$\frac{dT}{dP} = \frac{T_v}{\rho_v hfg} \quad (2-9)$$

Consequently, once a vapor pressure drop in the pipe is determined, a corresponding temperature drop can be computed. This temperature drop can, in turn, be translated into a "conductance" if the heat transfer rate is known. Derivations of the vapor pressure drops in a heat pipe, and the corresponding "conductances," follow.

For evaporation, conservation of axial momentum requires that

$$\frac{dP_{\text{evap}}}{dz} = - \frac{2c_f \rho_v U^2}{D_v (3600)^2 g_c} - \frac{8}{D_v^2 (3600)^2 g_c} \frac{d}{dz} \int_0^{D_v/2} \rho_v u_v^2 r dr, \quad (2-10)$$

or the axial pressure gradient $\frac{dP_{\text{evap}}}{dz}$ is equal to the sum of the friction loss and the momentum gradient (Ref. 2). Since $u_v = 0$ at $z = 0$ and $z = L$ (there is no velocity at the ends of the pipe), the momentum gradient term is zero. Therefore,

$$\frac{dP_{\text{evap}}}{dz} = \frac{-2c_f \rho_v U^2}{D_v (3600)^2 g_c}, \quad (2-11)$$

or

$$\Delta P_{\text{evap}} = \int_0^L \frac{2c_f \rho_v U^2}{D_v (3600)^2 g_c} dz = \frac{2c_f \rho_v U^2 L}{D_v (3600)^2 g_c} \quad (2-12)$$

The skin friction coefficient c_f can be computed from the following relation derived from Navier-Stokes with wall suction or injection, assuming laminar fully-developed flow (Ref. 3):

$$c_f = \frac{1}{\text{Re} \left(.0481 + \frac{.0494}{(4.7 + |Re_w|)^{.8}} \right)}, \quad (2-13)$$

which reduces to the Hagen-Poiseuille solution $c_f = \frac{16}{Re}$ at $Re_w = 0$ (no suction or injection). The Reynolds numbers Re and Re_w can be expressed as

$$Re = \frac{UD_v \rho_v}{\mu_v}, \quad (2-14)$$

and

$$Re_w = \frac{\dot{m}}{\pi \mu_v L} = \frac{Q}{\pi \mu_v L hfg}. \quad (2-15)$$

Substituting equations 2-13, 2-14, and 2-15 into 2-12 and using the result in equation 2-9, the temperature drop ΔT_{evap} associated with the evaporation process can be determined:

$$\Delta T_{\text{evap}} = \frac{8 T_v \mu_v L Q}{\pi (3600)^2 g_c H hfg^2 \rho_v^2 D_v^4 \left[.0481 + \frac{.0494}{(4.7 + |Re_w|)^{.8}} \right]}. \quad (2-16)$$

Converting this ΔT into a "conductance" using $G = Q / \Delta T$,

$$G_{\text{evap}} = \frac{1}{\frac{8 T_v \mu_v L}{\pi (3600)^2 g_c H hfg^2 \rho_v^2 D_v^4 \left[.0481 + \frac{.0494}{(4.7 + |Re_w|)^{.8}} \right]}}. \quad (2-17)$$

This conductance value is valid in the evaporator for all positive values of Re_w . It is also valid in the condenser when $Re_w > -4.5975$. At larger negative values of Re_w (higher suction rates), c_f drops to zero, and the following derivation is used.

Again, conservation of momentum requires that equation 2-10 be satisfied. In the case of zero c_f , however, the friction term is neglected. Therefore,

$$\frac{dP_{\text{cond}}}{dz} = - \frac{8}{D_v^2 (3600)^2 g_c} \frac{d}{dz} \int_0^{D_v/2} \rho_v u_v^2 r dr,$$

or

$$\Delta P_{\text{cond}} = \frac{2 \rho_v}{R_v^2 (3600)^2 g_c} \int_0^{R_v} u_v^2 r dr. \quad (2-18)$$

The velocity profile u_v can be expressed as

$$u_v = \frac{1}{\mu_v} \frac{dP}{dz} \frac{R_v^2}{4} \left[1 - \left(\frac{r}{R_v} \right)^2 \right] (3600)^2 g_c, \quad (2-19)$$

from Navier-Stokes for laminar flow in a circular tube of constant cross-section (Poiseuille flow) (Ref. 4). Substituting equation 2-19 into 2-18 and integrating,

$$\Delta P_{\text{cond}} = \frac{\rho_v}{8 \mu_v} \left(\frac{dP}{dz} \right)^2 \left(\frac{R_v^4}{4} \right) (3600)^2 g_c. \quad (2-20)$$

For Poiseuille flow,

$$\frac{dP}{dz} = \frac{8 \dot{m} \mu_v}{R_v^4 (3600)^2 g_c \rho_v \pi}, \quad (2-21)$$

from Appendix A. Substituting equations 2-21 and 2-8 into 2-20 and the result into 2-9.

$$\Delta T_{\text{cond}} = \frac{32 T_v Q^2}{\pi^2 (3600)^2 g_c H hfg^3 \rho_v^2 D_v^4}, \quad (2-22)$$

or, again converting to a "conductance,"

$$G_{\text{cond}} = \frac{1}{\frac{32 T_v Q}{\pi^2 (3600)^2 g_c H hfg^3 \rho_v^2 D_v^4}}. \quad (2-23)$$

This conductance is valid for the condenser when the wall Reynolds number $Re_w \leq -4.5975$. Since the adiabatic section can act as a condenser during transients (especially startup), the relationships derived for the condenser are applicable to the adiabatic section as well. When the vapor temperature exactly equals the

adiabatic section liquid/wick temperature, condensation will cease and the conductances will transfer no heat.

The remaining vapor pressure drop, and corresponding temperature drop, is due to the friction loss of the vapor flowing axially in the tube. Thus,

$$\frac{dP_v}{dz} = \frac{-2c_f \rho_v U^2}{(3600)^2 g_c D_v} \quad (2-24)$$

For this case, the skin friction coefficient $c_f = 16/Re$. Substituting c_f and equation 2-14 and integrating equation 2-24 over the pipe length gives

$$\Delta P_v = \frac{128 Q \mu_v L}{\pi (3600)^2 g_c hfg \rho_v D_v^4} \quad (2-25)$$

From equation 2-9,

$$\Delta T_v = \frac{128 Q \mu_v L T_v}{\pi (3600)^2 g_c H hfg^2 \rho_v^2 D_v^4} \quad (2-26)$$

or

$$G_v = \frac{1}{\frac{128 \mu_v L T_v}{\pi (3600)^2 g_c H hfg^2 \rho_v^2 D_v^4}} \quad (2-27)$$

The resultant network is shown in Figure 2-2.

The typically very large vaporization, condensation and vapor flow conductances G_{evap} , G_{cond} , and G_v ($\approx 10^3$ to 10^6 Btu/hr-°R), in combination with the typically very small axial conduction conductances $G_{p,a}$ and $G_{w,a}$ ($\approx 10^{-2}$ to 10^{-3} Btu/hr-°R), result in slow MITAS thermal analyzer solutions. Fortran logic to alleviate the problem in steady-state has been developed, but the transient case presents more difficulty because of the additional heat

REPRODUCIBILITY OF THE
ORIGINAL PAGE IS POOR

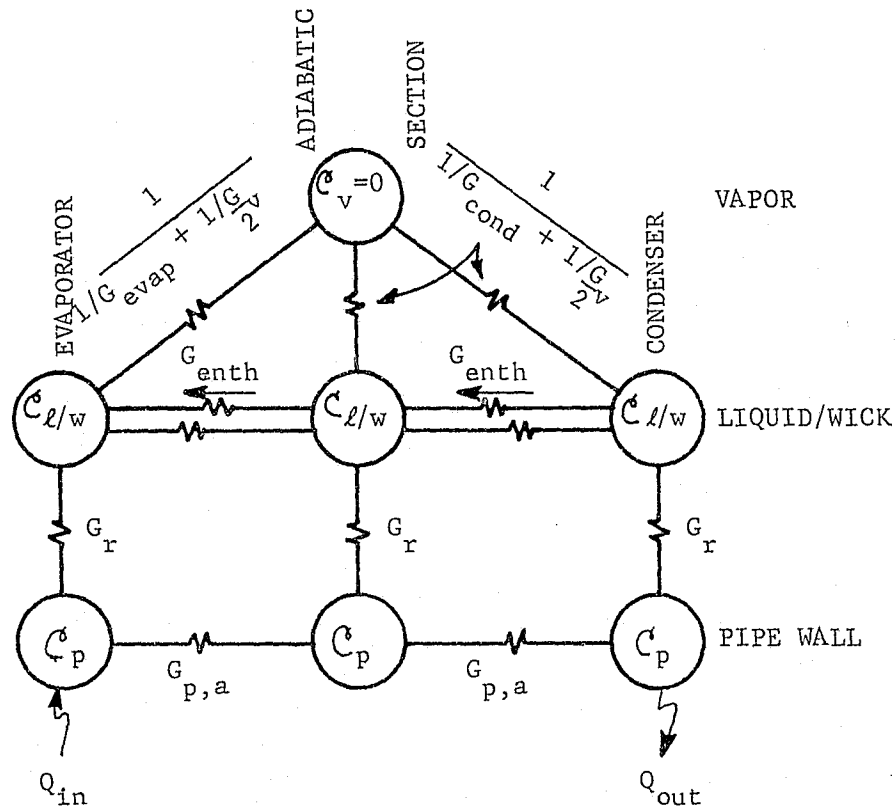


Figure 2-2 Network Schematic

storage term and the lack of an energy balance criterion. The more logical solution to the problem is to eliminate the large conductances, making the vapor and liquid in the pipe isothermal. This results in a loss in the capability to conveniently handle internal phenomena, such as liquid freezing or wick dryout. However, since these cases can be treated with suitable Fortran logic, the loss is minimal in most instances. When this compromise is made, the resultant simplified network becomes that shown in Figure 2-3.

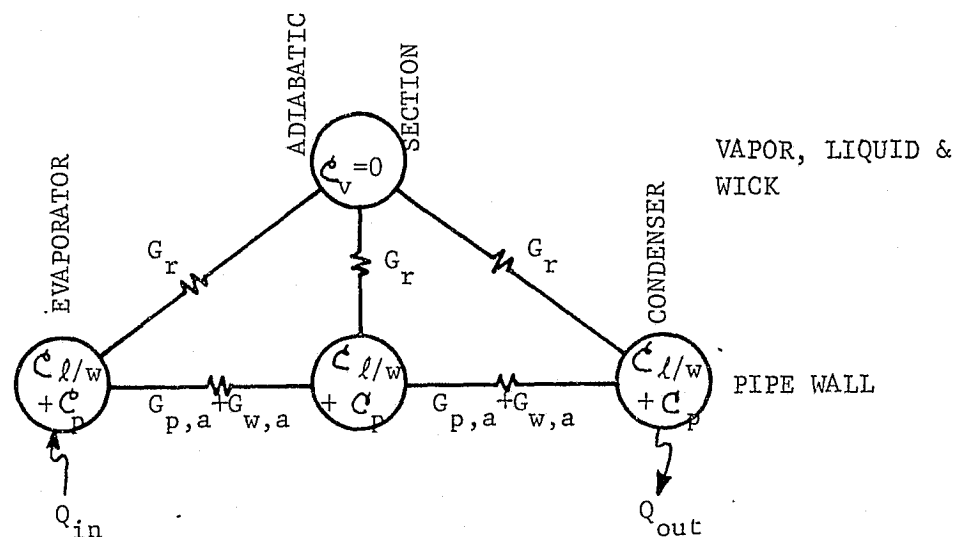


Figure 2-3 Simplified Network Schematic

5. Heat Pipe Limitations

Limitations on the heat transfer capability of heat pipes occur due to effects that inhibit vapor or liquid flow. The derivations of the relations governing these limits are covered adequately in the literature (Ref. 2,5) and will only be briefly summarized here. The effects to be dealt with include the hydrodynamic, sonic, entrainment and nucleation limits. The limitations discussed below are computed in subroutine LIMITS. The inputs to subroutine LIMITS consist of the first data array number, evaporation conductance and temperature required for the boiling limit calculation, physical constants, and working fluid pressure vs time array number. Several limitations are placed upon the use of MITAS constants and arrays, primarily that the arrays are input in a specific order in a block. This routine will be generalized in the future to remove the current limitations.

a. Hydrodynamic Limit

The hydrodynamic or "wicking" limit is a result of the pressure variations due to moving fluids within the heat pipe. A circulation is established in the pipe fluids due to the capillary pumping capability of the wick. When the pressure drops due to viscous and momentum effects become large enough to overcome the capillary pumping pressure rise plus the effects of body forces, the hydrodynamic limit has been reached. The liquid being vaporized cannot be replaced

through capillary action at a high enough rate, resulting in evaporator dryout (burnout) and a corresponding evaporator temperature increase. Thus

$$\Delta P_c \pm \Delta P_b = \Delta P_\ell + \Delta P_v$$

$$\left[\begin{array}{c} \text{Capillary} \\ \text{Head} \end{array} \right] \pm \left[\begin{array}{c} \text{Body} \\ \text{Force} \\ \text{Head} \end{array} \right] = \left[\begin{array}{c} \text{Liquid} \\ \text{Pressure} \\ \text{Drop} \end{array} \right] + \left[\begin{array}{c} \text{Vapor} \\ \text{Pressure} \\ \text{Drop} \end{array} \right] \quad (2-28)$$

Each of these contributions will be discussed in the following paragraphs.

The capillary pumping pressure rise is due to the difference in meniscus radius of curvature in the evaporator and condenser wicks. Vaporization in the evaporator results in a concave meniscus tending to recede into the wick. Condensation in the condenser results in a nearly flat meniscus at the wick surface. The surface tension forces attempt to flatten the evaporator meniscus, creating a pressure difference which pumps liquid toward the evaporator. The maximum ΔP which can be generated due to capillary action is

$$\Delta P_c = \frac{2 \sigma \cos \psi}{R_{\text{pore}}}, \quad (2-29)$$

where R_{pore} is a minimum effective pore radius which corresponds to a minimum evaporator meniscus radius, and is usually experimentally determined. ψ is the wetting angle as defined in Figure 2-4.

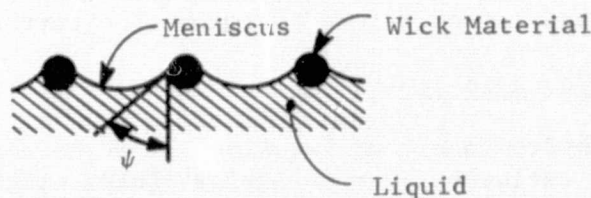


Figure 2-4 Definition of Wetting Angle ψ

The body force contribution is a result of acceleration fields in the pipe environment, such as gravity, thrust, or rotation. These fields may either augment or diminish the performance of the pipe, depending on its orientation with respect to the field. The body force pressure drop ΔP_b can be expressed as

$$\Delta P_b = \rho_f \frac{a}{g_c} (\pm L \cos \beta + D_{i_p} \sin \beta), \quad (2-30)$$

where a is the body force acceleration and β is the angle between the body force vector and the pipe axis, as defined in Figure 2-5.

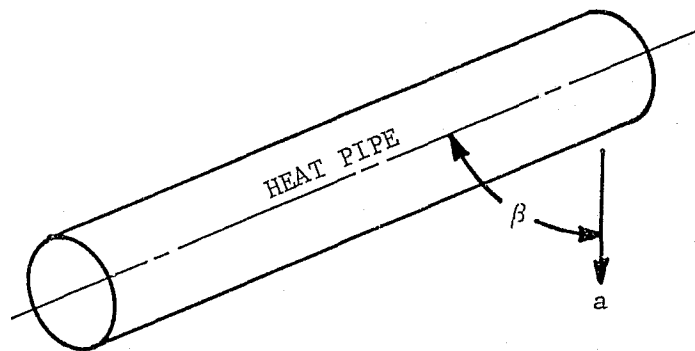


Figure 2-5 Definition of Pipe Orientation Angle β

Equation 2-30 indicates that the body force pressure drop is made up of two components, that of the pipe length parallel to the body force vector, and that of the internal pipe diameter parallel to the body force vector. That is, the capillary action must raise the fluid a height equivalent to the diameter of the pipe if the pipe is horizontal in a vertical acceleration field, the height of the pipe if it is vertical (and the evaporator is at the top), or some intermediate distance if the orientation is other than horizontal or vertical. The $(+)$ in equation 2-30 indicates that the length component can be positive or negative depending on whether the evaporator or the condenser is raised. A positive length component indicates a pressure drop; negative indicates a pressure rise aiding the capillary action.

The third contribution to the pressure balance is the pressure drop due to liquid viscous flow losses, ΔP_ℓ . From Navier-Stokes for steady, incompressible, fully-developed laminar flow in a rectangular cross-section passage, the axial pressure gradient dP_ℓ/dz is

$$\frac{dP_\ell}{dz} = \mu_\ell \left[\frac{\partial^2 u_\ell}{\partial x^2} + \frac{\partial^2 u_\ell}{\partial y^2} \right], \quad (2-31)$$

or, in cylindrical coordinates,

$$\frac{dP_\ell}{dz} = \mu_\ell \left[\frac{1}{r} \frac{\partial}{\partial r} \left(r \frac{\partial u_\ell}{\partial r} \right) + \frac{1}{r^2} \frac{\partial^2 u_\ell}{\partial \theta^2} \right]. \quad (2-32)$$

These equations must be solved individually for each geometry involved. The solutions for five cases — open grooves, closed grooves, closed cylinders, full annuli, and partial annuli — have been derived for the model. The solutions of equations 2-31 and 2-32 are all of the following form:

$$\Delta P_\ell = \frac{\mu_\ell \dot{m} L}{(3600)^2 g_c \rho_\ell K A_{xs}}, \quad (2-33)$$

which, after substituting equation 2-8, becomes

$$\Delta P_\ell = \frac{\mu_\ell L Q}{(3600)^2 g_c \rho_\ell hfg K A_{xs}}, \quad (2-34)$$

where KA_{xs} is the (permeability x cross-sectional area) product obtained from the solution of Navier-Stokes for the appropriate geometry. These KA_{xs} relations have been programmed into subroutine PERMBL, which computes KA_{xs} for the input geometry. PERMBL is discussed in Section 2-A-6.

The fourth contribution to the pressure balance in equation 2-28 is the vapor pressure drop due to evaporation, condensation and flow losses detailed in the conductor derivations of Section 2-4. The evaporation ΔP , and the con-

densation ΔP at low suction rates, is given by equation 2-12 with 2-13 used to eliminate c_f . The condensation ΔP at high suction rates is given by 2-20 with 2-21 used to eliminate dP/dz . The vapor pressure drop due to flow losses is given by equation 2-25.

These four contributions to the heat pipe pressure balance are inserted into equation 2-28, which is then solved for Q_h , the maximum hydrodynamic latent heat transfer capability. Since the suction or injection Reynolds number, Re_w , is dependent upon Q (equation 2-15), an iterative solution is the most convenient method of solving 2-28.

b. Sonic Limit

The second limitation on heat transfer capability in a heat pipe is the sonic limit. This limit arises since constant-area flow with suction and injection is analogous to constant mass flow in a converging-diverging nozzle (Ref. 5). The end of the injection (evaporator) section of a heat pipe is analogous to the throat of the nozzle, and consequently, there is a flow velocity limit at the evaporator exit analogous to choked flow (Mach 1) in the nozzle throat. As the heat input is increased above the sonic limit, an evaporator temperature increase results since no more axial heat transfer can occur. The definition of the Mach number gives

$$M = \frac{U}{c} = \frac{U}{\sqrt{\gamma P_v (3600)^2 g_c (144) / \rho_v}}, \quad (2-35)$$

where U is the bulk vapor velocity and c is the sonic vapor velocity. Using

$$U = \frac{\dot{m}_v}{\rho_v A_{xs}} \quad (2-36)$$

and equation 2-8, and solving for Q , equation 2-35 becomes

$$Q = \rho_v hfg A_{xs} M \sqrt{\gamma P_v (3600)^2 g_c (144) / \rho_v}, \quad (2-37)$$

where the cross-sectional vapor flow area A_{xs} is equal to

$$\frac{\pi D_i^2}{4} \cdot \text{The maximum velocity through the "throat," or}$$

evaporator exit, occurs at $M = 1$. Therefore the maximum sonic latent heat transfer capability Q_s is

$$Q_s = \rho_v hfg \frac{\pi D_w^2}{4} \sqrt{\gamma P_v (3600)^2 g_c (144) / \rho_v} \quad (2-38)$$

c. Entrainment Limit

The third heat transfer limit is the entrainment limit and results from a high velocity vapor stream entraining the liquid in the wick, preventing it from returning to the evaporator, resulting in evaporator dryout and a temperature increase. The capability of the vapor to entrain liquid is a function of the wick geometry, e.g., open axial grooves are far more subject to entrainment than a tight mesh screen.

The force F_e required to tear a particle of liquid from the wick is proportional to the product of the dynamic pressure and a characteristic length X (representing wick geometry) squared:

$$F_e \propto \frac{\rho_v U^2}{(3600)^2 g_c} X^2 \quad (2-39)$$

The restoring force F_R required to retain that particle is proportional to the surface tension and the characteristic length:

$$F_R \propto \sigma X \quad (2-40)$$

The ratio of these two forces is the Weber number

$$Wb = \frac{\rho_v U^2 X}{(3600)^2 g_c \sigma} \quad (2-41)$$

When the Weber number exceeds unity, entrainment will occur and pipe performance degradation will begin. Although the entrainment limit has not actually been reached at $Wb = 1$, the true limit is difficult to compute. Therefore, the conservative approach is to assume it has and to set $Wb = 1$ in equation 2-41. Using 2-8 and 2-36 to eliminate U and solving for Q , equation 2-41 becomes

REPRODUCIBILITY OF THE
ORIGINAL PAGE IS POOR

$$Q_e = hfg \frac{\pi D_{i_w}^2}{4} \sqrt{\frac{\sigma \rho_v (3600)^2 g_c}{X}} \quad (2-42)$$

d. Nucleation Limit

The fourth heat transfer limit is the nucleation or boiling limit and is caused by superheating of the liquid at the pipe wall. Since the liquid and vapor are at equilibrium at the wick surface, a temperature drop must exist across the wick if any heat is to be transferred, and this ΔT increases with increasing load. At some critical ΔT , nucleation will occur near the point of highest superheat, the pipe wall. This bubble inhibits replacement of the evaporating liquid, causing dryout and a temperature increase.

For a bubble of radius R_n at equilibrium, the expansion force must equal the restoring force, i.e.,

$$\pi R_n^2 (P_v - P_\ell) = 2 \pi R_n \sigma \quad (2-43)$$

where P_v is the saturation pressure at the wall temperature, P_{wall} , and P_ℓ is the saturation pressure at the wick surface temperature, P_{wick} .

Solving equation 2-43 for $P_{wall} - P_{wick}$,

$$P_{wall} - P_{wick} = \frac{2\sigma}{R_n} \quad (2-44)$$

For small $P_{wall} - P_{wick}$,

$$\frac{P_{wall} - P_{wick}}{T_{wall} - T_{wick}} \approx \frac{dP}{dT} = \frac{hfg \rho_v M}{T_v} \quad (2-45)$$

from equation 2-9. Substituting 2-45 into 2-44,

$$T_{wall} - T_{wick} = \frac{2 \sigma T_v}{hfg \rho_v R_n M} \quad (2-46)$$

If this critical ΔT is reached, the bubble will grow and nucleation failure will result. The corresponding maximum nucleation latent heat transfer capability Q_n is

$$Q_n = \frac{k \ell/w A}{\Delta x} (T_{\text{wall}} - T_{\text{wick}}), \quad (2-47)$$

where

$$A = \frac{\pi (D_{i_p} + D_{i_w}) L}{2}, \quad (2-48)$$

and

$$\Delta x = \frac{D_{i_p} - D_{i_w}}{2}. \quad (2-49)$$

Substituting equations 2-46, 2-48 and 2-49 into 2-47.

$$Q_n = \frac{2\pi T_v \sigma L (D_{i_p} + D_{i_w}) k \ell/w}{H hfg \rho_v R_n (D_{i_p} - D_{i_w})}. \quad (2-50)$$

These four limits are computed in LIMITS, and a message is printed if any one of the limits is reached.

6. Auxiliary Subroutines

Several auxiliary subroutines are used to supplement that above. The liquid/wick conductivity $k_{\ell/w}$ is calculated in subroutine

EFFKWK for the following five wick geometries, shown in Figure 2-6.

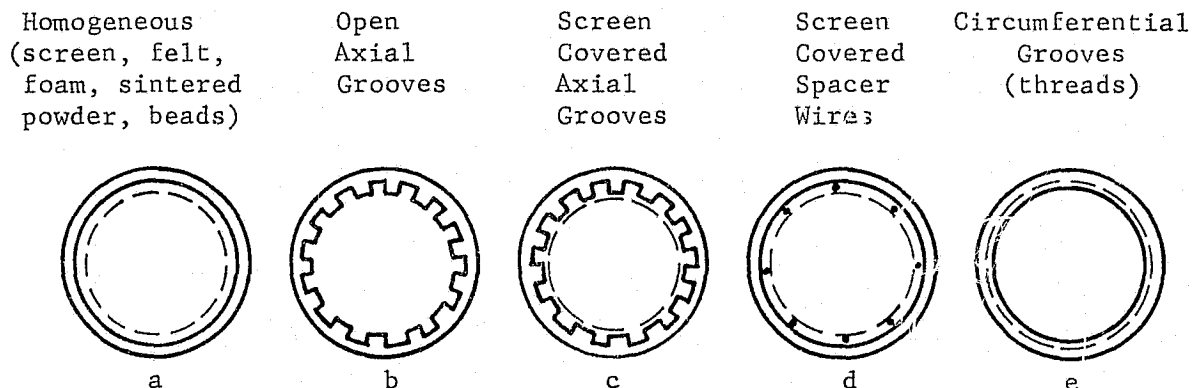


Figure 2-6 Available Wick Geometries

For homogenous wicks, Figure IV-6a,

$$k_{\ell/w} = k_{\ell} \frac{k_{\ell} + k_w - (1 - \phi_w)(k_{\ell} - k_w)}{k_{\ell} + k_w + (1 - \phi_w)(k_{\ell} - k_w)}, \quad (2-51)$$

from Reference 1. For open axial grooves, Figure 2-6b, $k_{\ell/w}$ is computed assuming two parallel heat flow paths, one through the liquid and one through the lands between grooves. The lands are assumed to be composed of wall material.

$$k_{\ell/w} = \frac{(kA)_{\text{wall}} + (kA)_{\ell}}{A_{\text{wall}} + A_{\ell}}, \quad (2-52)$$

where

$$A_{\text{wall}} = \left(\pi (D_{ow} - d) - N_g W \right) L, \quad (2-53)$$

or the total mean circumference less the total width of the grooves multiplied by the pipe length, and

$$A_{\ell} = N_g W L. \quad (2-54)$$

Substituting equations 2-53 and 2-54 into 2-52,

$$k_{\ell/w} = \frac{N_g W (k_{\ell} - k_{\text{wall}})}{\pi (D_{ow} - d)} + k_{\text{wall}}. \quad (2-55)$$

Screen-covered axial grooves are treated as a homogenous wick (equation 2-51) and open grooves (equation 2-55) in series, see Figure 2-6c:

$$k_{\ell/w} = \frac{1}{\left(\frac{1}{k_{\ell/w}} \right)_{\text{homogenous wick}} + \left(\frac{1}{k_{\ell/w}} \right)_{\text{open grooves}}} \quad (2-56)$$

The fourth wick type is screen-covered axial spacer wires as shown in Figure 2-6d. This type is treated similarly to screen-covered axial grooves, except the path corresponding to the wall equation 2-52 must be handled differently to account for the

poor contacts between wire and pipe wall and between wire and screen. The method chosen to simulate this poor contact is to treat the wire as three materials in series: a layer of liquid, one of wire and another of liquid as shown in Figure 2-7.

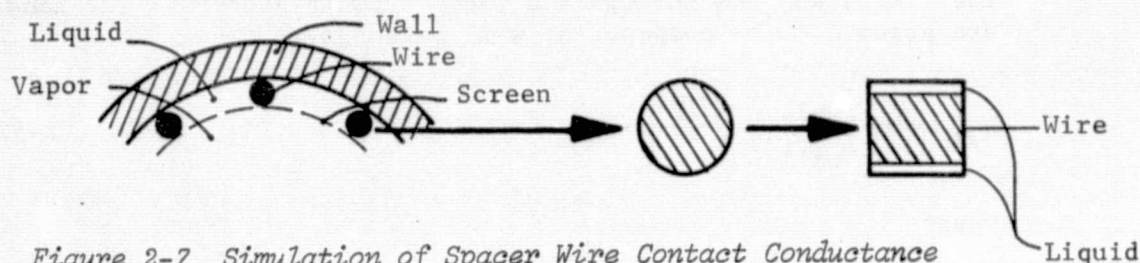


Figure 2-7 Simulation of Spacer Wire Contact Conductance

The liquid layer thicknesses are analytically determined as a first approximation, but test data is probably necessary for an accurate $k_{\ell/w}$. The assumption made in computing the liquid layer thickness is that the volume of liquid under the spacer wire to the left of line C-C is equal to that to the right of C-C in Figure 2-8.

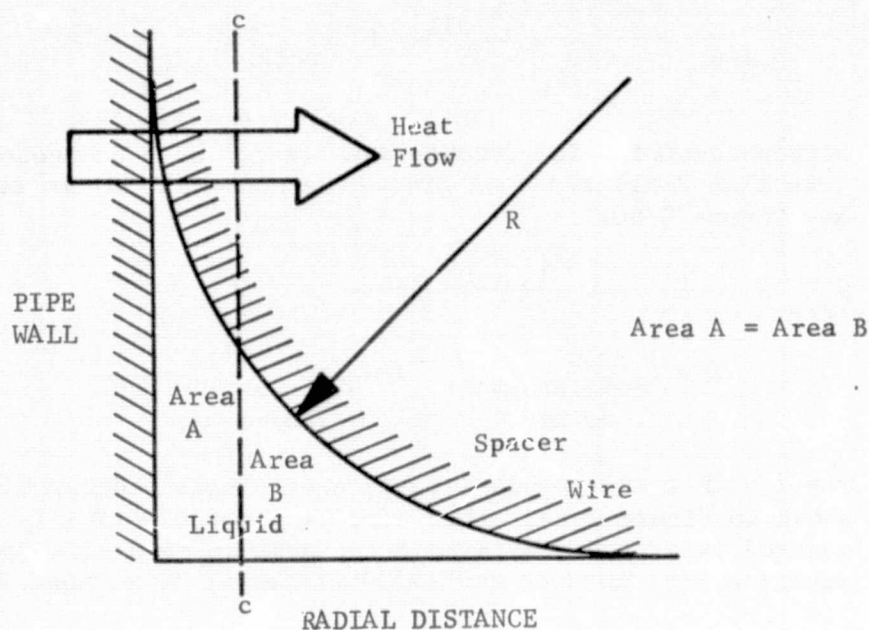


Figure 2-8 Liquid Layer Equivalent Thickness

This is analogous to assuming that the same amount of heat that has a less difficult path through the thin portions of the liquid layer, has a more difficult path through the thicker portions of the liquid layer. The liquid layer thickness is obtained in Appendix B and is equal to $.1738 R_{\text{spacer}}$, where R_{spacer} is the spacer wire radius. The conductance through the spacer wire is then

$$G_{\text{spacer}} = \frac{1}{\frac{.1738}{2 k_{\ell} L} + \frac{(.8262)}{k_{\text{spacer}} L} + \frac{.1738}{2 k_{\ell} L}},$$

$$= \frac{k_{\ell} k_{\text{spacer}} L}{.1738 k_{\text{spacer}} + .8262 k_{\ell}} \quad (2-57)$$

The conductance through the liquid between spacer wires is

$$G_{\ell} = \frac{k_{\ell}}{D_{\text{spacer}}} \left\{ \pi (D_{o_w} - D_{\text{spacer}}) - (N_{\text{spacer}} D_{\text{spacer}}) \right\} L \quad (2-58)$$

The conductance through the screen covering is

$$G_{\text{screen}} = \frac{k_{\text{screen}} \pi D_{i_w} L}{D_{o_w} - \frac{D_{i_w}}{2} - D_{\text{spacer}}} = \frac{2k_{\text{screen}} \pi D_{i_w} L}{D_{o_w} - D_{i_w} - 2D_{\text{spacer}}}, \quad (2-59)$$

where k_{screen} is the homogeneous wick effective thermal conductivity from equation 2-51. The three contributions are combined as follows:

$$G_{\text{total}} = \frac{1}{\frac{1}{G_{\text{spacer}}} + \frac{1}{G_{\ell}} + \frac{1}{G_{\text{screen}}}}, \quad (2-60)$$

and the corresponding $k_{\ell/w}$ is computed from

$$k_{\ell/w} = G_{\text{total}} \frac{\Delta x}{A} = G_{\text{total}} \left[\frac{D_{o_w} - D_{i_w}}{D_{o_w} + D_{i_w}} \right] \pi \left(\frac{D_{o_w} + D_{i_w}}{2} \right) L$$

or

$$k_{\ell/w} = \frac{2 (D_{o_w} - D_{i_w})}{\pi (D_{o_w} + D_{i_w}) \left\{ \frac{1}{G_{\text{spacer}}} + \frac{1}{G_{\ell}} + \frac{1}{G_{\text{screen}}} \right\}} \quad (2-61)$$

The fifth wick type is the circumferential groove (or threaded pipe) as shown in Figure 2-6e. This case is treated as one continuous groove and equation 2-52 is used with the following values for A.

$$A_{\text{wall}} = (L - N_g W) \pi (D_{o_w} - d), \quad (2-62)$$

$$A_{\ell} = N_g W \pi (D_{o_w} - d). \quad (2-63)$$

Thus

$$k_{\ell/w} = \frac{\left\{ k_{\text{wall}} (L - N_g W) + k_{\ell} N_g W \right\} \pi (D_{o_w} - d)}{L \pi (D_{o_w} - d)},$$

or

$$k_{\ell/w} = \frac{N_g W (k_{\ell} - k_{\text{wall}})}{L} + k_{\text{wall}}. \quad (2-64)$$

The inputs to subroutine EFFKWK are the type of wick, k_{ℓ} , k_{wall} , k_w , ϕ_w , D_{o_w} , D_{i_w} , π , N_g , N_{spacer} , W , d , D_{spacer} , and L . Its use is restricted by the assumptions made above for each wick.

The second auxiliary subroutine is called PERMBL and is used to compute the product of permeability and cross-sectional area for liquid flow for the five wick types in Figure 2-6. These KA_{xs} values are obtained from Appendix A by comparing the specific liquid pressure drop solutions contained there to the general form of the pressure drop

$$\frac{dP_{\ell}}{dz} = \frac{\mu_{\ell} Q L}{KA_{\text{xs}} \rho_{\ell} h_{\text{fg}}} \quad (2-65)$$

The KA_{xs} values needed to satisfy equation 2-65 for each wick type are as follows. For homogeneous wicks (Figure 2-6a):

$$KA_{xs} = K \frac{\pi (D_{ow}^2 - D_{iw}^2)}{4}, \quad (2-66)$$

since the permeability of a homogeneous wick is generally known. For open axial grooves (Figure 2-6b),

$$KA_{xs} = N_g \left[\frac{5W^3 d^3}{18 (W^2 + 4d^2)} \right]. \quad (2-67)$$

For screen-covered axial grooves (Figure 2-6c),

$$KA_{xs} = N_g \left[\frac{5W^3 d^3}{72 (W^2 + d^2)} \right]. \quad (2-68)$$

Screen-covered axial spacer wires (Figure 2-6d), are treated as annular spaces:

$$KA_{xs} = \frac{5 \delta^3 B}{18}, \quad (2-69)$$

for each annular space, where

$$B = \frac{\left\{ R_{oa}^4 - R_{ia}^4 - 2 (R_{oa}^3 R_{ia} - R_{oa} R_{ia}^3) \right\}^2}{(4 \delta^2 + 5) (R_{oa}^4 - R_{ia}^4) - 8 (\delta^3 + 5) (R_{oa}^3 R_{ia} - R_{oa} R_{ia}^3)} + 60 \left[R_{oa}^2 R_{ia}^2 \ln \frac{R_{oa}}{R_{ia}} \right]. \quad (2-70)$$

Utility subroutine ANNSPC is used to compute B.

The values of the outer annulus radius R_{oa} , the inner annulus radius R_{ia} , and the half-angle between spacer wires are computed as follows:

$$\begin{aligned}
 R_{o_a} &= D_{o_w} / 2, \\
 R_{i_a} &= R_{o_a} - D_{\text{spacer}}, \\
 \text{and} \\
 \delta &= \frac{\pi (R_{o_a} + R_{i_a}) - N_{\text{spacer}} D_{\text{spacer}}}{2 N_{\text{spacer}} \left(\frac{R_{o_a} + R_{i_a}}{2} \right)}.
 \end{aligned}
 \tag{2-71}$$

The half angle between spacer wires δ is derived from $\frac{1}{2} \left[\frac{\text{arc length}}{\text{radius}} \right] /$ number of spaces as expressed in equation 2-71. The total KA_{xs} is then the number of annular spaces N_a multiplied by the KA_{xs} in equation 2-69.

Circumferential grooves are treated as one long open groove and equation 2-67 applies with the number of grooves $N_g = 1$. However, the pipe length L in equation 2-65 must now be replaced by the actual length of the groove

$$L_{\text{groove}} = \pi \left(\frac{D_{o_w} + D_{i_w}}{2} \right) N_g \tag{2-72}$$

such that KA_{xs} is expressed as

$$KA_{xs} = \frac{5W^3 d^3}{18 (W^2 + 4d^2)} \left(\frac{L}{L_{\text{groove}}} \right),$$

or

$$KA_{xs} = \frac{5W^3 d^3 L}{9 (W^2 + 4d^2) \pi (D_{o_w} + D_{i_w}) N_g} \tag{2-73}$$

The inputs to subroutine PERMBL are the type of wick, D_{o_w} , D_{i_w} , N_g , W , d , K , π , D_{spacer} and N_{spacer} . Its restrictions correspond to the assumptions made for each wick type.

Another utility routine was written to automate the evaluation of specific properties which are mono-variant. Subroutine LOOKUP provides a "DO" loop table lookup using the library routine DIDEGL.

The calling sequence is

LOOKUP (N,T,A,P)

where

N = number of lookups in this call

T = independent variable

A = Array of T, P values

P = Dependent variable (property)

B. GOVERNING EQUATIONS FOR FIXED-CONDUCTANCE ARTERIAL PIPES

An artery is inserted in the vapor flow passage of a heat pipe to provide an auxiliary flow passage for the liquid returning to the evaporator. By removing most of the liquid flow from the pipe wall vicinity, large radial conductances can be achieved, minimizing the temperature drops across the wick. At the same time, the artery can be designed for minimum pressure drop, maximizing the hydrodynamic limit. The result is a decoupling of hydrodynamics and heat transfer in the pipe, with corresponding performance increases. Typical geometries are the pedestal artery and its high performance derivative, the spiral artery, shown in Figure 2-9.

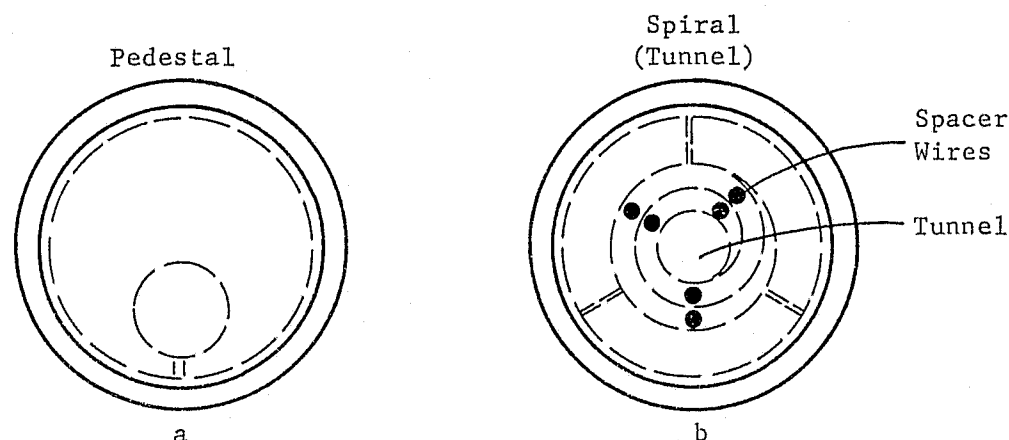


Figure 2-9 Available Artery Geometries

1. Capacitance

Artery capacitance is computed in subroutine ARTERY and is added to the liquid/wick capacitance calculated in equation 2-2. Artery supports are ignored. The pedestal artery shown in

Figure 2-9a has a capacitance equal to the sum of the screen capacitance and the liquid capacitance:

$$C_{\text{screen}} = \pi \left(\frac{D_{\text{o art}}^2 - D_{\text{i art}}^2}{4} \right) L (1 - \phi_{\text{art}}) \rho_{\text{art}} C_{\text{p art}} \quad (2-74)$$

$$C_{\ell} = \left\{ \pi \left(\frac{D_{\text{o art}}^2}{4} \right) L - \pi \left[\frac{D_{\text{o art}}^2 - D_{\text{i art}}^2}{4} \right] L (1 - \phi_{\text{art}}) \right\} \rho_{\ell} C_{\text{p } \ell} \quad (2-75)$$

The liquid volume is the total artery volume less the screen volume. Summing equations 2-74 and 2-75, the total artery capacitance C_{art} is given by

$$C_{\text{art}} = C_{\text{screen}} + C_{\ell} \quad (2-76)$$

The second artery configuration is the spiral type, shown in Figure 2-9b. Its capacitance is the sum of the screen, spacer wires, and liquid capacitances. The screen length is obtained from an integration of the equation of a spiral over the total angular displacement of the spiral, see Appendix C. The screen length is thus

$$L_{\text{screen}} = (2 \pi N_t + \frac{w}{v}) (v^2 + (2 \pi N_t v + w)^2)^{\frac{1}{2}} - \frac{w}{v} (v^2 + w^2)^{\frac{1}{2}} + \frac{v}{2} \left(\ln \left[\frac{(v^2 + (2 \pi N_t v + w)^2)^{\frac{1}{2}} + 2 \pi N_t v + w}{(v^2 + w^2)^{\frac{1}{2}} + w} \right] \right) \quad (2-77)$$

where

$$v = \frac{D_{\text{art}} - D_{\text{i art}} - 2t}{4 \pi N_t},$$

and

$$w = \frac{D_{\text{i art}}}{2} + t.$$

(2-78)

The screen capacitance C_{screen} is then the sum of the spiral screen volume and the wrapping screen volume, all multiplied by the density and specific heat:

$$C_{\text{screen}} = \left\{ L_{\text{screen}} tL (1 - \phi_{\text{art}}) + \pi \left(\frac{D_{\text{o art}}^2 - D_{\text{art}}^2}{4} \right) L (1 - \phi_{\text{art}}) \right\} \rho_{\text{art}} C_{\text{p art}}. \quad (2-79)$$

The spacer wire capacitance is

$$C_{\text{spacer}} = (N_a + 1) \pi \frac{D_{\text{spacer}}^2}{4} L \rho_{\text{spacer}} C_{\text{p spacer}}, \quad (2-80)$$

since there is one more spacer wire than there are annular spaces. The liquid capacitance is

$$= \left\{ \pi \left(\frac{D_{\text{o art}}^2}{4} \right) L - \left[L_{\text{screen}} tL (1 - \phi_{\text{art}}) + \pi \left(\frac{D_{\text{o art}}^2 - D_{\text{art}}^2}{4} \right) L (1 - \phi_{\text{art}}) \right] - (N_a + 1) \pi \left(\frac{D_{\text{spacer}}^2}{4} \right) L \right\} \rho_{\ell} C_{\text{p } \ell}, \quad (2-81)$$

since the liquid volume is the total artery volume less the screen and spacer volumes. The total spiral artery capacitance C_{art} is then

$$C_{\text{art}} = C_{\text{screen}} + C_{\text{spacer}} + C_{\ell}. \quad (2-82)$$

2. Axial Conductance

The artery contributes to the total axial heat transfer capability of the pipe. Its axial conductance is calculated in subroutine ARTERY and is added to the liquid/wick conductance from equation 2-4. The pedestal artery conductance is equal to the sum of the screen conductance and the liquid conductance. The screen conductance is

$$G_{\text{screen}} = \frac{k_{\text{art}} \pi \left(\frac{D_{\text{o art}}^2 - D_{\text{i art}}^2}{4} \right) \left(\frac{1 - \phi_{\text{art}}}{2} \right)}{L}, \quad (2-83)$$

where the screen volume fraction $(1 - \phi_{art})$ is halved since contact resistance between axial and circumferential results in only the axial members of the screen conducting heat. The liquid conductance is

$$G_{\ell} = \frac{k_{\ell} \pi \left[\frac{D_{i,art}^2}{4} \right]}{L} . \quad (2-84)$$

The total conductance of the pedestal artery is then

$$G_{art} = \frac{k_{art} \pi \left(\frac{D_{o,art}^2 - D_{i,art}^2}{4} \right) \left(\frac{1 - \phi_{art}}{2} \right) + k_{\ell} \pi \left[\frac{D_{i,art}^2}{4} \right]}{L} . \quad (2-85)$$

The spiral artery conductance is equal to the sum of the screen, spacer wire, and liquid conductances. The screen conductance is

$$G_{screen} = \frac{k_{art}}{L} \left[L_{screen} t \left(\frac{1 - \phi_{art}}{2} \right) + \pi \left(\frac{D_{o,art}^2 - D_{i,art}^2}{4} \right) \left(\frac{1 - \phi_{art}}{2} \right) \right] , \quad (2-86)$$

where the screen volume fraction $(1 - \phi_{art})$ is again halved since only the axial screen members carry heat. The spacer wire conductance is

$$G_{spacer} = \frac{k_{spacer}}{L} (N_a + 1) \pi \left(\frac{D_{spacer}^2}{4} \right) . \quad (2-87)$$

and the liquid conductance is

$$G_{\ell} = \frac{k_{\ell}}{L} \left[\pi \left(\frac{D_{art}^2}{4} \right) - L_{screen} t - (N_a + 1) \pi \left(\frac{D_{spacer}^2}{4} \right) \right] . \quad (2-88)$$

The total conductance is thus

$$G_{art} = G_{screen} + G_{spacer} + G_{\ell} , \quad (2-89)$$

for the spiral artery configuration. These artery conductances are computed for each pipe section. When they are combined with

the liquid/wick axial conductance, they are converted to a node center-to-center conductance by

$$G_{art} = \frac{1}{\frac{1}{G_{art_1}} + \frac{1}{G_{art_2}}} , \quad (2-90)$$

and then added to the liquid/wick axial conductance linearly.

3. Radial Conductance

The arterial radial conductance is not considered since no radial heat transfer occurs across an artery.

4. Arterial Effects on Hydrodynamics

Since the purpose of an artery is to improve the hydrodynamic limit of the heat pipe, the liquid pressure drop computation of Section 2-A-5 must be revised. The (permeability x cross-sectional area) KA_{xs} must be computed for the artery and added to that of the wick. This calculation is performed in subroutine PERMBL, using KA_{xs} relations derived in Appendix A and summarized here.

The pedestal artery contains simple Poiseuille flow and the permeability cross-sectional flow area product is thus

$$KA_{xs} = \frac{\pi R_i^4}{8} \text{pedestal} . \quad (2-91)$$

The spiral artery is extremely complex and must be treated as multiple annular spaces with varying internal and external radii (R_{i_a} and R_{o_a}) and differing angular widths (δ). The basic relations for the KA_{xs} of an annular space are equations IV-69 and IV-70. The values of R_{o_a} , R_{i_a} , and δ , however, require modification for use in a spiraling configuration. The method used is a "DO" loop with initialized values of R_{o_a} , R_{i_a} , and δ corresponding to the innermost annular passage. The radii are incremented using the equation of a spiral to the values corresponding to the next outward space, and δ is adjusted if the wire spacing changes. KA_{xs} values are computed for each space and summed.

EXTENSION OF THE
OF THE WICK

The general equation of a spiral in polar coordinates is

$$r = m\theta + b. \quad (2-92)$$

Referring to Figure 2-10, at $\theta = 0$, $r = \frac{D_{i\text{art}}}{2} + t$, and at $\theta = 2\pi N_t$,
 $r = \frac{D_{\text{art}}}{2}$.

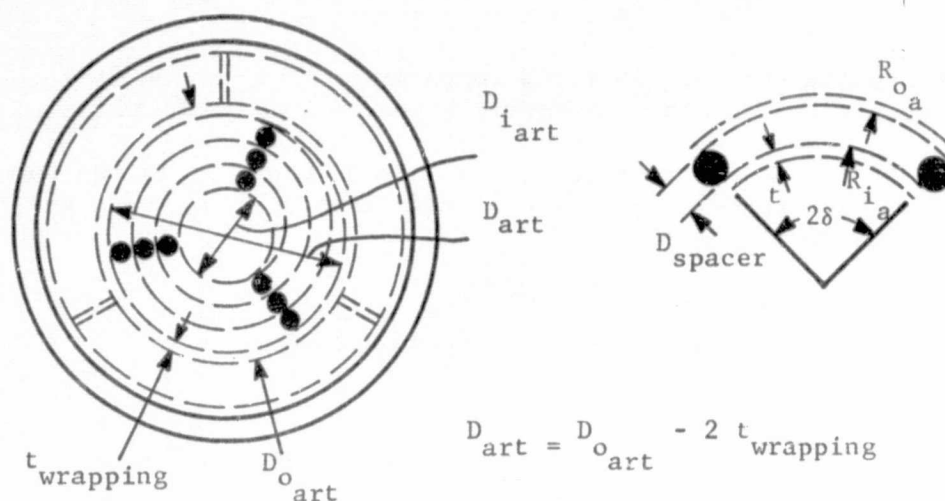


Figure 2-10 Detailed Spiral Artery Geometry

Therefore, the equation of the spiral artery is

$$r = \frac{D_{\text{art}} - D_{i\text{art}} - 2t}{4\pi N_t} \theta + \frac{D_{i\text{art}}}{2} + t. \quad (2-93)$$

The initial values of R_{oa} , R_{ia} , and δ are

C-4

$$\begin{aligned}
 R_{i_a} &= \frac{D_{art} - D_{i_{art}} - 2t}{4 \pi N_t} \frac{\delta_{j=1}}{2} + \frac{D_{i_{art}}}{2} + t, \\
 R_{o_a} &= R_{i_a} + D_{spacer}, \\
 \text{and} \\
 \delta &= \frac{\delta_{j=1}}{2} - \frac{D_{spacer}}{(R_{o_a} + R_{i_a})}.
 \end{aligned}
 \tag{2-94}$$

The subtracted term in the δ computation of equation 2-94 accounts for the angular contribution of the spacer wire.

The "DO" loop iterates on j from 2 to N_a where N_a is the number of annular spaces. The general relations for R_{o_a} , R_{i_a} , and δ in the "DO" loop are

$$\begin{aligned}
 R_{i_a} &= R'_{i_a} + \frac{D_{art} - D_{i_{art}} - 2t}{4 \pi N_t} \left(\frac{\delta_{j-1} + \delta_j}{2} \right), \\
 R_{o_a} &= R_{i_a} + D_{spacer}, \\
 \text{and} \\
 \delta &= \frac{\delta_j}{2} \frac{D_{spacer}}{(R_{o_a} + R_{i_a})},
 \end{aligned}
 \tag{2-95}$$

where R'_{i_a} is the R_{i_a} from the previous iteration and the additive term in the R_{i_a} computation of equation 2-95 represents the ΔR_{i_a} to convert R'_{i_a} to the new R_{i_a} . Utility subroutine ANNSPC is called in each iteration of the loop, and the resulting KA_{xs} values for each space are summed into a total KA_{xs} .

There is an additional passage in the center of the spiral which is treated as Poiseuille flow:

$$KA_{xs} = \frac{\pi}{8} \left(\frac{D_{iart}}{2} \right)^4 \quad (2-96)$$

This contribution is added to the summed annular KA_{xs} values for a total spiral artery KA_{xs} , which in turn is added to the wick KA_{xs} to compute the total liquid pressure drop. The additional inputs to PERMBL to account for arteries are artery type, D_{oart} , D_{iart} , $t_{wrapping}$, an array of δ values, N_a , N_t , D_{spacer} , t , and L .

The second major effect of the artery on the hydrodynamic limit is a reduction in the vapor flow cross-sectional area. A revised effective vapor flow passage diameter D_{veff} is computed in subroutine ARTERY as:

$$D_{veff} = \left\{ \left[\pi \left(\frac{D_{ip}^2}{4} \right) - \pi \left(\frac{D_{oart}^2}{4} \right) \right] \frac{4}{\pi} \right\}^{\frac{1}{2}},$$

or

$$D_{veff} = \left(D_{ip}^2 - D_{oart}^2 \right)^{\frac{1}{2}}, \quad (2-97)$$

and this value is used in place of D_v in the vapor pressure drop equations 2-12, 2-20 and 2-25 when an artery is present.

Subroutine ARTERY requires the artery type, N_a , D_{oart} , D_{iart} , $t_{wrapping}$, D_{spacer} , t , \emptyset_{art} , π , N_t , ρC_{part} , $\rho C_{pspacer}$, k_{art} , k_{spacer} , k_ℓ , L , ρ_ℓ , $C_{p\ell}$, and $D_{ip_{pedestal}}$.

The third effect on heat pipe hydrodynamics concerns the fact that the largest pore in the wick/artery system determines the capillary pumping capability. If the artery contains a pore with a radius larger than R_{pore} in equation 2-29, the artery R_{pore} must be substituted. A decrease in the hydrodynamic limit results.

5. Artery Self-Priming Limit

A new pipe heat transfer limit arises when an artery is introduced. Since an artery can be depleted of liquid by forces arising from acceleration fields, its design must allow repriming. The artery will reprime if the capillary head generated by the

largest gap in the artery exceeds the body force head, under zero load. The existence of a load, however, introduces the additional head losses due to flow which must be accounted for. The maximum load under which the artery will reprime can be computed using equation 2-28, where ΔP_c is calculated using the maximum artery gap width (excluding the end of the condenser since no liquid/vapor pressure difference exists there) instead of the wick pore size R_{pore} in equation 2-29. This is accomplished by repeating the hydrodynamic limit logic in subroutine LIMITS with the artery gap size replacing the wick pore size.

C. GOVERNING EQUATIONS FOR VARIABLE-CONDUCTANCE PIPES

The variable-conductance heat pipe (VCHP) utilizes a charge of non-condensable gas added to the working fluid to achieve a relatively constant heat pipe temperature regardless of heat load. This gas is swept to the condenser end of the heat pipe and forms a plug which blocks the flow of vapor. (Note the distinction between non-condensable gas and working fluid vapor.) As the pipe temperature drops, the vapor pressure of the working fluid drops, causing an expansion of the non-condensable gas plug. This expanded plug effectively shuts off a portion of the condenser to vapor flow, decreasing the area available for condenser heat rejection. This, in turn, increases the pipe temperature. In a properly designed VCHP, the pipe temperature can thus be made nearly independent of heat load. A reservoir for the non-condensable gas at the condenser end of the heat pipe provides closer temperature control since a greater vapor/gas interface movement can be achieved for a given temperature (and pressure) change. Temperature control of the reservoir through a heater can be used to actively control pipe temperatures by a feedback loop. A schematic of the variable-conductance heat pipe is given in Figure 2-11.

The simulation of non-condensable gas control of the operating temperature of a heat pipe regardless of load requires more sophisticated modeling techniques. The location of the vapor/gas interface ("front") in a variable-conductance heat pipe must be computed based on ideal gas relations. The presence of a gas reservoir to provide improved control adds complexity to the problem, as does the popular use of a reservoir heater to achieve even more precise control.

The basic assumption in the following analysis is that the effect of the diffusion of vapor into the gas plug on the temperature gradient is negligible compared to the effect of axial conduction in the pipe wall on the temperature gradient. This is generally

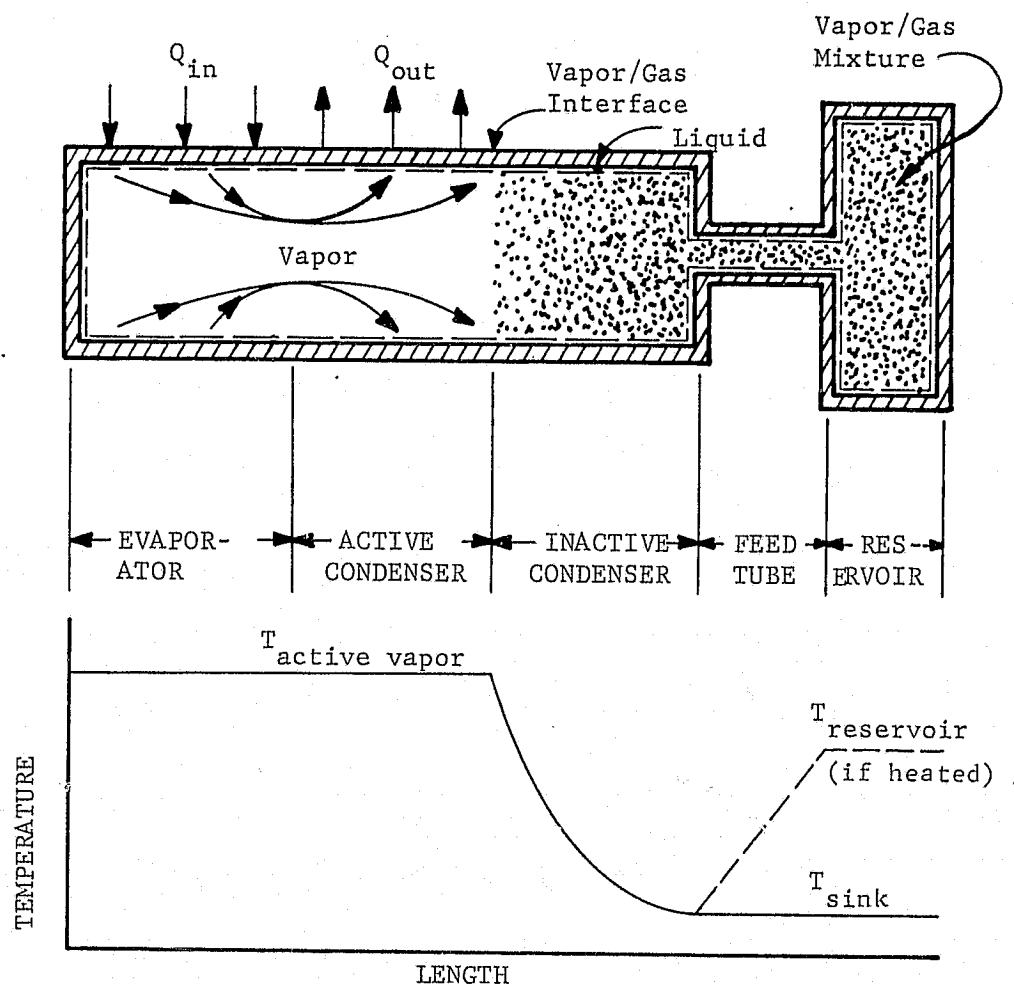


Figure 2-11 Variable Conductance Heat Pipe Geometry

a good assumption for high thermal conductivity pipe walls. The number of moles of non-condensable gas is a constant n :

$$n = \sum_i \frac{P_{\text{gas}} V_i}{R T_{\text{gas}}}, \quad (2-98)$$

summed over the volume elements of the reservoir and inactive condenser. There is no gas in the active section of the condenser, the adiabatic section, or the evaporator due to the tendency of the moving vapor to sweep it towards the condenser. In the reservoir,

$$\left. \begin{aligned} T_{\text{gas}} &= T_{\text{res}}, \\ \text{and} \\ P_{\text{gas}} &= P_{\text{vact}} - P_{\text{vres}}, \end{aligned} \right\} \quad (2-99)$$

since P_{vact} is the total pipe pressure, and the sum of the vapor and gas partial pressures in the reservoir must equal the total pressure.

Equation 2-99 assumes a negligible pressure gradient in the pipe. It also assumes the reservoir vapor temperature is equal to the reservoir temperature, and that the vapor partial pressure is that of saturated vapor at the reservoir temperature. In the j th element of the inactive condenser,

$$\left. \begin{aligned} T_{\text{gas}_j} &= T_{\text{wall}_j}, \\ \text{and} \\ P_{\text{gas}_j} &= P_{\text{vact}} - P_{\text{vwall}_j}. \end{aligned} \right\} \quad (2-100)$$

The assumptions for equation 2-99 are used in 2-100 also, substituting the condenser wall temperature for the reservoir temperature. Inserting equations 2-99 and 2-100 into 2-98,

$$n = \frac{(P_{v_{act}} - P_{v_{res}}) V_{res}}{\bar{R} T_{res}} + \sum_{j=1}^J \frac{(P_{v_{act}} - P_{v_{wall,j}})}{\bar{R} T_{wall,j}}$$

$$\frac{V_{cond} - V_{act}}{J}, \quad (2-101)$$

where the volume of the jth element of inactive condenser is the total condenser volume less the active condenser volume, divided by the number of inactive elements J. Dividing by V_{cond} , using the fact that V_{act}/V_{cond} is equal to L_{act}/L_{cond} for a constant-diameter condenser, and solving for L_{act}/L_{cond} ,

$$\frac{L_{act}}{L_{cond}} = 1 + \frac{\left(\frac{P_{v_{act}} - P_{v_{res}}}{\bar{R} T_{res}} \right) \left(\frac{V_{res}}{V_{cond}} \right) - \frac{n}{V_{cond}}}{\frac{1}{J} \sum_{j=1}^J \left(\frac{P_{v_{act}} - P_{v_{wall,j}}}{\bar{R} T_{wall,j}} \right)} \quad (2-102)$$

Multiple vapor-wall couplings are needed to simulate a variable-conductance heat pipe. The couplings in the inactive region are zeroed according to the vapor/gas interface position determined in equation 2-102, to simulate no heat pipe action in that region.

This is accomplished by a call to subroutine ADJG. Condenser nodes which are within the active length are left alone while the conductances are set to zero for those nodes which are totally beyond the active length. The conductance of the node in which the front is located is adjusted based upon the proportion of active length calculated.

The calling sequence is

ADJG (NCG,NC,LC,LACT,GCOND)

where

NCG = number of moles of control gas for a VCHP.
0.0 for a fixed conduction pipe

NC = number of condenser nodes

LC = condenser nodal length

LACT = active condenser length

GCOND = first condenser wall-to-vapor coupling

Since L_{act}/L_{cond} is dependent on pipe temperatures and pressures and since the temperatures and pressures are dependent on the front, an iterative solution is necessary to achieve a satisfactory result. In steady-state problems, the iterative solution is handled by multiple calls to STDSTL from EXECTN since VARBL1 is called each iteration of the network solution. In transient problems, VARBL1 is entered only once for each time step; consequently, the BACKUP option is used in VARBL2 to force a recomputation of temperatures if the L_{act}/L_{cond} based on the most recent network solution does not match the L_{act}/L_{cond} from the previous solution. L_{act}/L_{cond} is computed in subroutine FLFRNT, using Pv_{act} , Pv_{res} , R , T_{res} , V_{res} , V_{cond} , n , J , Pv_{wall} , and T_{wall} as inputs.

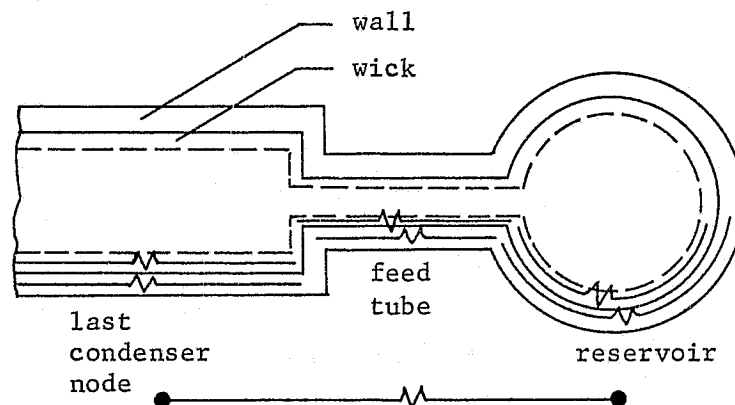
Subroutine FRONT controls and dampens the movement of the vapor/control gas interface location resulting from subroutine FLFRNT. The results of FLFRNT predict the new front location based upon temperatures resulting from the present time step and the previous front location. The maximum front movement allowed is one condenser node length. Since the new front location will result in new temperatures, and since FLFRNT will predict a new front location based on these new temperatures, an iterative process is required. This iterative process is repeated until the front location change is reduced to 1% of the condenser node length or less. At that point the iteration is completed and the time step is advanced. Additional logic is required in the execution block for steady state runs and in the variables 2 block for transient runs to support subroutine FRONT. Refer to the program listing for the supporting logic.

The calling sequence is

FRONT

No argument list is included for this subroutine.

Computation of the last condenser node axial conductance to the reservoir is obtained by calling subroutine RSCOND for a VCHP. The same assumptions used in subroutine AXCOND also apply. The wicks used in the condenser, feedtube and reservoir are assumed to be identical. The following network is reduced to a single conductor.



Each of the three parallel combinations are summed and are then add by the series combination rule. The artery is not considered in this calculation since it does not extend beyond the condenser.

The calling sequence is

RSCOND (NCG, PI, LWA, KWA, ODWA, IDWA, LFT, KFT, ODR, IDR, LR, KR, ODFT, LWK, POROS, KWK, ODWK, IDWK, IDFTW, IDRW, GFTTOT)

NCG	=	FLAG FOR VCHP
LWA	=	CONDENSER WALL NODAL LENGTH
KWA	=	CONDENSER WALL THERMAL CONDUCTIVITY
ODWA, IDWA	=	CONDENSER WALL OUTER AND INNER DIAMETERS
LFT	=	FEED TUBE NODAL LENGTH
KFT	=	FEED TUBE THERMAL CONDUCTIVITY
ODR, IDR	=	RESERVOIR OUTER AND INNER DIAMETERS
LR	=	RESERVOIR LENGTH
KR	=	RESERVOIR THERMAL CONDUCTIVITY
ODFT, IDFT	=	FEED TUBE OUTER AND INNER DIAMETERS
LWK	=	CONDENSER WICK NODAL LENGTH
POROS	=	WICK POROSITY
KWK	=	WICK THERMAL CONDUCTIVITY
ODWK, IDWK	=	CONDENSER WICK OUTER AND INNER DIAMETERS
IDFTW	=	FEED TUBE WICK INNER DIAMETER (ODFTW = IDFT)
IDRW	=	RESERVOIR WICK INNER DIAMETER (ODRW = IDR)
GFTTOT	=	TOTAL AXIAL FEED TUBE CONDUCTANCE

GLOSSARY

A	area $[\text{ft}^2]$
B	defined by equation IV-70 $[\text{ft}^4]$
C	capacitance (mass x specific heat) $[\text{Btu}/^{\circ}\text{F}]$
C_p	specific heat $[\text{Btu}/\text{lbm}-^{\circ}\text{F}]$
D	diameter $[\text{ft}]$
F	force $[\text{lbf}]$
G	conductance $[\text{Btu}/\text{hr}-^{\circ}\text{F}]$
H	mechanical equivalent of heat $[\text{ft}-\text{lbf}/\text{Btu}]$
J	number of inactive condenser sections [dimensionless]
K	wick permeability $[\text{ft}^2]$
L	pipe length $[\text{ft}]$
M	Mach number [dimensionless]
N	number of grooves, turns, spacers, etc. (depending on subscript) [dimensionless]
P	absolute pressure $[\text{lbf}/\text{ft}^2]$
Q	latent heat transfer rate $[\text{Btu}/\text{hr}]$
R	radius $[\text{ft}]$
\bar{R}	universal gas constant $[1545 \text{ ft}-\text{lbf}/\text{lbmole}-^{\circ}\text{R}]$
Re	Reynolds number along tube [dimensionless]
Re_w	Reynolds number for suction (-) or injection (+) at wick surface [dimensionless]
T	temperature $[^{\circ}\text{R}]$
U	bulk average vapor velocity $[\text{ft}/\text{hr}]$

V	volume [ft ³]
W	groove width [ft]
Wb	Weber number [dimensionless]
X	entrainment characteristic length [ft]
a	body force acceleration [ft/sec ²]
c	sonic velocity [ft/hr]
c _f	skin friction coefficient [dimensionless]
d	groove depth [ft]
g _c	conversion constant relating force and mass [32.2 lbm-ft/lbf-sec ²]
hfg	heat of vaporization of working fluid [Btu/lbm]
k	thermal conductivity [Btu/hr-ft-°F]
l	distance along fin length [ft]
\dot{m}	mass flow rate [lbm/hr]
n	number of moles of non-condensable gas [lbmole]
r, θ	polar coordinates
t	spiral artery screen thickness [ft]
u	local velocity [ft/hr]
v, w	defined by equation IV-78 [ft]
x, y	rectangular coordinates
z	axial distance along pipe [ft]
β	pipe orientation angle [degrees]
γ	specific heats ratio (Cp/Cv) [dimensionless]
Δ	difference

δ	half-angle width of annular space [radians]
μ	dynamic viscosity [lbm/ft-hr]
π	3.14159
ρ	density [lbm/ft ³]
σ	surface tension [lbf/ft]
ϕ	wick porosity (void fraction) [dimensionless]
ψ	wetting angle [degrees]

Subscripts

a	annular spaces
act	active
art	artery
ax	axial
b	body force
c	capillary
cond	condenser
e	entrainment limit
eff	effective
enth	enthalpy
evap	evaporator
f	fin
g	grooves
h	hydrodynamic limit
i	inner

j	iteration counter
l	liquid
n	nucleation limit
o	outer
p	pipe
R	restoring
r	radial
rej	rejection
res	reservoir
root	fin root
s	sonic limit
t	turns of spiral artery
v	vapor
w	wick
xs	cross-sectional
1, 2	pipe sections

REFERENCES

1. R. L. Gorrington and S. W. Churchill: "Thermal Conductivity of Heterogeneous Materials," Chemical Engineering Progress, Volume 57, July 1961, p. 53 through 59.
2. S. W. Chi: Mathematical Modeling of High and Low Temperature Heat Pipes. Final Report to Goddard Space Flight Center, NASA. NASA-CR-122419. December 1971.
3. G. Raithby: "Laminar Heat Transfer in the Thermal Entrance Region of Circular Tubes and Two-Dimensional Rectangular Ducts with Wall Suction and Injection." Int. J. Heat Mass Transfer, Volume 14, 1971, p. 223 through 243.
4. J. W. Daily and D. R. F. Harleman: Fluid Dynamics. Addison-Wesley Publishing Company, Reading, Massachusetts, 1966.
5. B. D. Marcus: Theory and Design of Variable Conductance Heat Pipes. NASA-CR-2018. April 1972.
6. G. L. Fleischman and D. J. Wanous: Active Control Heat Pipe Performance for Long Life Battery Cooling. TRW Systems Group, Redondo Beach, California. Paper presented at ASME Meeting, New York, New York, November 1972.
7. B. Swerdling and J. Alario: Heat Pipe Radiator. Final Report to Johnson Space Center, NASA under contract NAS9-12848. Grumman Aerospace Corporation, Bethpage, New York, October 1973.
8. J. P. Sellers, Jr.: Steady State Operation of a Heat Pipe Radiator System: Analytical and Experimental. Report to Johnson Space Center, NASA, under Grant NGR-01-005-017. Tuskegee Institute, Tuskegee, Alabama, December 1973.

All references unclassified.

ATTACHMENT 3

MARTIN MARIETTA CORPORATION
SPACE RADIATOR PROGRAM
FIN GRADIENT TECHNIQUE

As illustrated in Figure 3-1, there are essentially three types of gradients which are possible in a space radiator. These are:

- a) The classical condition where the adjacent fin root temperatures are equal giving a symmetrical temperature distribution between nodes. The point where the temperature gradient, dT/dX , is equal to zero exists at the midpoint. This condition could have been analyzed by the fin effectiveness technique which is commonly used. (Ref. 3-1)
- b) The condition where adjacent fin root temperatures are not equal giving a nonsymmetrical temperature distribution and the point where the temperature gradient dT/dX is equal to zero exists at some point other than the midpoint.
- c) The condition where the difference between the adjacent fin root temperatures is so large that no point exists between nodes where the temperature gradient dT/dX is equal to zero.

The fin gradient technique used in the MMC radiator program has the capability to evaluate all three types of gradients.

Referring to Figure D-2, the heat which is radiated from an element of the fin surface is as follows:

$$dq_{\text{rad}} = \epsilon \sigma W dX (T^4 - T_e^4) \quad (1)$$

and the heat which is transferred in the fin by conduction is:

$$q_{\text{cond}} = -Ka \frac{dT}{dX} \quad (2)$$

Differentiating equation (2) with respect to X ,

$$\frac{dq_{\text{cond}}}{dX} = -Ka \frac{d}{dX} \left(\frac{dT}{dX} \right) dX \quad (3)$$

and since the heat lost by radiation represents the difference in heat passing across the two internal faces of the element, then equations (1) and (2) can be equated as follows:

$$dq_{\text{RAD}} = -dq_{\text{cond}}$$

Performing the required substitutions and differentiating yields the following differential equation:

$$\frac{d^2\theta}{dZ^2} = N_R (\theta^4 - \theta_e^4) \quad (4)$$

with the boundary conditions $\theta = 1 @ Z = 0$
 $\theta = \theta_R @ Z = 2$

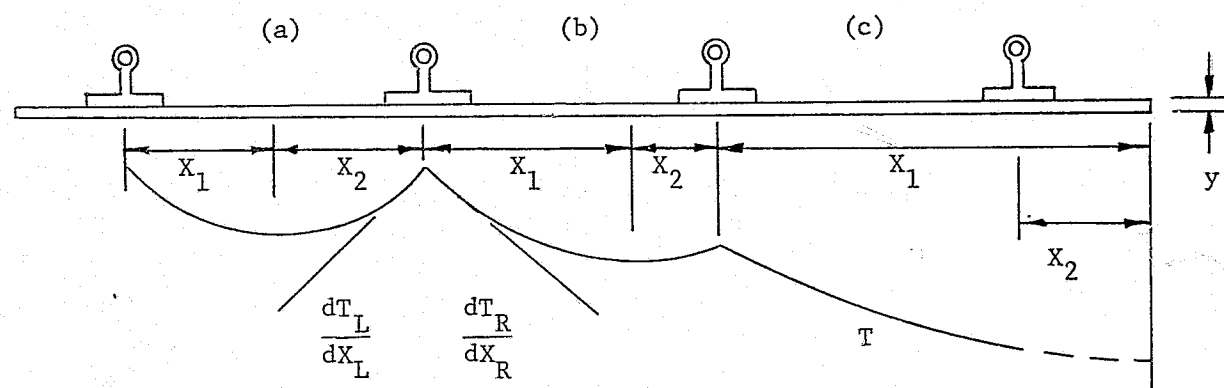


Figure 3-1 Martin Marietta Radiator Program Fin Gradient Technique

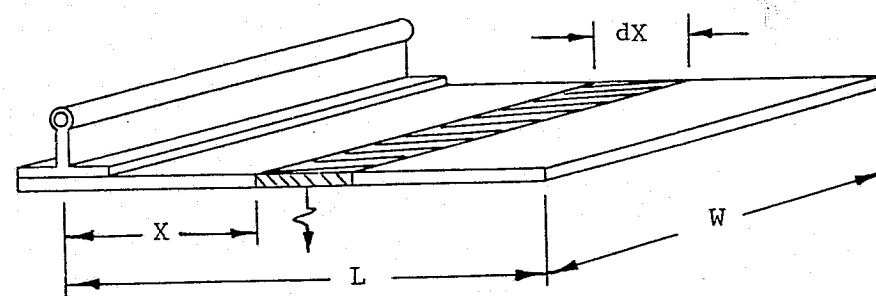


Figure 3-2 Fin/Tube Configuration - AM Radiator

where:

$$N_R = \frac{\epsilon \sigma T_r^3 L^2}{Ky} \quad (\text{sometimes referred to as the fin profile number})$$

$$\theta_R = T_{r+1}/T_r \quad \text{Ratio of adjacent fin root temperature to the root temperature}$$

$$\theta_e = T_e/T_r \quad \text{Ratio of equivalent temperature of surrounding space to root temperature}$$

$$T_e = \left[\frac{\sum F_n A_n T_n^4 + Q_{abs}}{\epsilon \sigma A_R} \right]^{1/4} \quad \text{Environmental temperature}$$

$$\theta = T/T_r$$

$$Z = X/L$$

$$d\theta/dZ = d(T/T_r)/d(X/L)$$

a = Fin cross sectional area

T = Fin Temperature

σ = Stephan Boltzmann constant

ϵ = Radiator surface node emissivity

T_r = Fin root temperature

T_{r+1} = Root temperature of adjacent fin

X_R = Fin length to right side of fin

X_L = Fin length on left side of fin

K = Fin thermal conductivity

y = Fin thickness

L = Half the distance between tubes

A_R = Area of radiator surface node

F_n = Gray Body view factor from other external surface to the radiator skin node

A_n = Area of other external surface

T_n = Temperature of other external surface

Q_{abs} = Absorbed flux from solar, albedo, and earth IR sources

W = Fin width

A set of tables was available (Ref. D-2) which expressed the dimensionless temperature gradient $d\theta/dZ$ as a function of the three variables N_R , θ_R , and θ_e . These tables were expanded by MMC to also include the condition where the equivalent temperature of surrounding space was hotter than the root temperature ($\theta_e > 1$). This was required for the AM radiator since the segments of the radiator which were exposed to the sun actually reheated the coolant as it flowed through the radiator.

The net heat loss from the skin node was determined in the radiator model for each time step by a table look-up for the $d\theta/dZ$ on the right side and the left side of the fin root. Then by multiplying these dimensionless gradients by T_r/L , the temperature gradients dT_R/dX_R and dT_L/dX_L were then determined for the right and left side. The net heat loss from the root of the radiator fin taken at the stringer was then determined by performing the following energy balance on the fin root.

$$q_{\text{net}} = -KA_L \frac{dT_L}{dX_L} - KA_R \frac{dT_R}{dX_R} \quad (5)$$

This technique was included in the subroutine RADFIN which calculated the total heat loss for each radiator skin node. The heat loss was first calculated on both sides of the tube by using the node temperature at the stringer attach points as the root temperatures. The heat loss was then calculated for both ends of the node by assuming that the temperature gradient at the edge was nearly adiabatic with $\theta_R \approx 1.0$ and the root temperature was the node temperature at the stringer attach point. The subroutine also computed the environmental temperature which was printed later for reference.

To determine the significance of the circumferential conduction, a comparison was made between the two cases, with and without circumferential conduction. As a result, neglecting circumferential conduction gave approximately 10% better performance than the more accurate method. A side conclusion would be that the radiator performance could be improved if the hot side of the radiator were isolated from the cold side. Because of the nonlinear nature of radiant interchange, this would result in a higher heat rejection from the surface.

References:

- D-1 Mackay, D. B., "Design of Space Power Plants," Prentice-Hall, Inc., Englewood Cliffs, N. J., 1963.
- D-2 French, R. J., "Computer Program for Space Radiator Analysis." Technical Report No. 00.716, NASA Contract NAS9-2772, LTV Aerospace Corp., Dallas, Texas, 17 Nov. 1965.